EVALUATION OF MULTIPLE CORROSION PROTECTION SYSTEMS FOR REINFORCED CONCRETE BRIDGE DECKS

By
Pooya Vosough Grayli
Matthew O'Reilly
David Darwin

A Report on Research Sponsored by

OKLAHOMA DEPARTMENT OF TRANSPORTATION

ODOT SP&R Item Number 2281

Structural Engineering and Engineering Materials
SM Report No. 152
July 2023

THE UNIVERSITY OF KANSAS CENTER FOR RESEARCH, INC.
2385 Irving Hill Road, Lawrence, Kansas 66045-7563

EVALUATION OF MULTIPLE CORROSION PROTECTION SYSTEMS FOR REINFORCED CONCRETE BRIDGE DECKS

By

Pooya Vosough Grayli

Matt O'Reilly

David Darwin

A Report on Research Sponsored by

Oklahoma Department of Transportation (ODOT)

ODOT SP&R Item Number 2281

Structural Engineering and Engineering Materials

SM Report No. 152

THE UNIVERSITY OF KANSAS CENTER FOR RESEARCH, INC.

LAWRENCE, KANSAS

July 2023

ABSTRACT

This study evaluated the corrosion resistance of epoxy-coated (ASTM A775), hot-dip galvanized (ASTM A767), and continuously galvanized (ASTM A1094) reinforcement, and the conventional reinforcement (ASTM A615) used to produce them, as well as ChromX reinforcement (ASTM A1035 Type CS) under the rapid macrocell, Southern Exposure, and cracked beam tests. To simulate the effects of handling, placing, and construction practices in the field, epoxy-coated and galvanized bars were tested in the as-received condition, with intentional damage to the coating, and after bending. To simulate the effects of outdoor exposure on epoxy-coated reinforcement, selected epoxy-coated reinforcing bars were tested under accelerated ultraviolet exposure cycles, both without and with physical damage. The corrosion performance of conventional and ChromX reinforcement was also evaluated in conjunction with IPANEX and Xypex, two waterproofing admixtures. Additionally, a 100-year life cost analysis was conducted to compare the cost-effectiveness of the reinforcing bars and admixtures evaluated in providing corrosion resistance based on construction costs in the states of Oklahoma and Kansas. Finally, the effect of variability in corrosion on the predicted service life is investigated using a Monte Carlo simulation using data from conventional, ECR, and ChromX reinforcement from the current study and previous studies.

Epoxy-coated reinforcement exhibited much greater corrosion resistance than conventional reinforcement, even after damage; however, ultraviolet exposure equivalent to as low as 1.2 months of outdoor exposure reduced the effectiveness of the coating resulting in increased corrosion rates. Both A767 and A1094 reinforcement exhibited better corrosion resistance than conventional reinforcement, but corrosion rates on both types of galvanized reinforcement increased when the bars were bent. Xypex was generally effective at reducing the corrosion rate

of conventional reinforcement, but not ChromX reinforcement; further study is recommended on the effects of Xypex on the corrosion resistance of reinforced concrete. IPANEX did not affect the corrosion resistance of either type of reinforcement. Over a 100-year design life, epoxy-coated, galvanized, and ChromX reinforcement are all cost-effective solutions.

Keywords: chlorides, concrete, corrosion, ChromX, epoxy-coated reinforcement, galvanized reinforcement, IPANEX, Xypex

ACKNOWLEDGMENTS

This report is based on a thesis presented by Pooya Vosough Grayli in partial fulfillment of the requirements for the Ph.D. degree from the University of Kansas. This study was supported by the Oklahoma Department of Transportation (ODOT SP&R Item Number 2281). Additional material support was provided by Commercial Metals Company, the Concrete Reinforcing Steel Institute, Midwest Concrete Materials, Cement Chemistry Systems LP, and Xypex Chemical Corporation. Walter Peters, P.E. of ODOT provided data bridge construction costs in Oklahoma.

TABLE OF CONTENTS

LIST OF FIGURES

LIST OF TABLES

CHAPTER 1: INTRODUCTION

1.1 GENERAL

The increasing use of deicing salts in the United States over the past 65 years has caused deterioration of bridge decks due to corrosion of the steel reinforcement. Two decades ago, the direct annual cost of corrosion damage in highway bridges was estimated at $8.3 billion; indirect costs were estimated to be more than ten times this value (Koch et al. 2002). Bridge decks are exposed to chlorides from deicing salts, which increase the corrosion rate in the reinforcing steel. This problem is worsened by the inevitable development of cracks in concrete, which allows chlorides to quickly penetrate to the level of reinforcing bars, initiating corrosion on conventional steel bars as early as the first year of service (Lindquist, Darwin, and Browning 2005). Alternative non-chloride deicing chemicals exist, but their use is not economically viable compared to conventional deicing salts (National Research Council 1991). Therefore, corrosion control typically involves preventing or slowing down the penetration of water, oxygen, and chlorides into concrete as well as using reinforcement that is more resistant to corrosion.

The corrosion resistance of epoxy-coated, galvanized (ASTM A767 and A1094), and ChromX (ASTM A1035 Type CS) reinforcement is evaluated in this study using bench-scale and rapid macrocell tests, as described in Chapter 2. The epoxy-coated and galvanized reinforcing bars are tested with and without intentional damage in their coating. The coated reinforcing bars are also tested in the bent condition; the coating on the bent specimens is not intentionally damaged. The corrosion performance of epoxy-coated reinforcement is also evaluated after exposure to ultraviolet (UV) light. Furthermore, potential improvement in the corrosion performance by decreasing concrete permeability using two waterproofing admixtures, commercially available

under brand names IPANEX and Xypex, is evaluated in concrete with conventional and ChromX reinforcement.

1.2 CORROSION MECHANISM OF STEEL IN REINFORCED CONCRETE

The corrosion process of steel in reinforced concrete requires four components to occur: an anode, a cathode, an electrical connection, and an ionic connection (electrolyte). The anode is a location on the steel where material loss due to oxidation occurs:

$$Fe \rightarrow Fe^{2+} + 2e^{-} \tag{1.1}$$

The electrons from the anode move to the cathode via the reinforcing bars or other metallic contacts, and are used in a reduction reaction that typically occurs in the presence of oxygen and water:

$$2H_2O + O_2 + 4e^{-} \rightarrow 4OH^{-} \tag{1.2}$$

This reaction releases hydroxyl ions (OH^-) that travel to the anode through concrete and lead to the formation of ferrous hydroxide after reacting with ferrous ions:

$$Fe^{2+} + 2OH^{-} \rightarrow Fe(OH)_2 \tag{1.3}$$

In addition to ferrous hydroxide, iron oxides and other hydroxides can form at the anode with oxidation states of +2 and +3 (Fe (II) and Fe (III)). In highly alkaline environments such as concrete, corrosion products, such as $Fe(OH)_2$, FeOOH, and $FeCO_3$, form on the surface of the reinforcing steel and protect it from further corrosion (Torbati-Sarraf and Poursaee 2018). The corrosion products that form on the steel embedded in concrete (pH of 13 and higher) are composed of two layers. The inner layer, which serves as a protective film, is compact and adhering, while the outer layer is porous and does not offer protection against corrosion. The inner (passive) layer is mainly non-stoichiometric magnetite (Fe_3O_4) along with Ca and Al substituted magnetite firmly

adhered to the substrate, and the outer layer is composed of mostly α- and γ-iron oxyhydroxides, which are non-protective corrosion products (Duffo et al. 2004); the magnetite layer and iron oxyhydroxide crystals are shown in Figure 1.1.

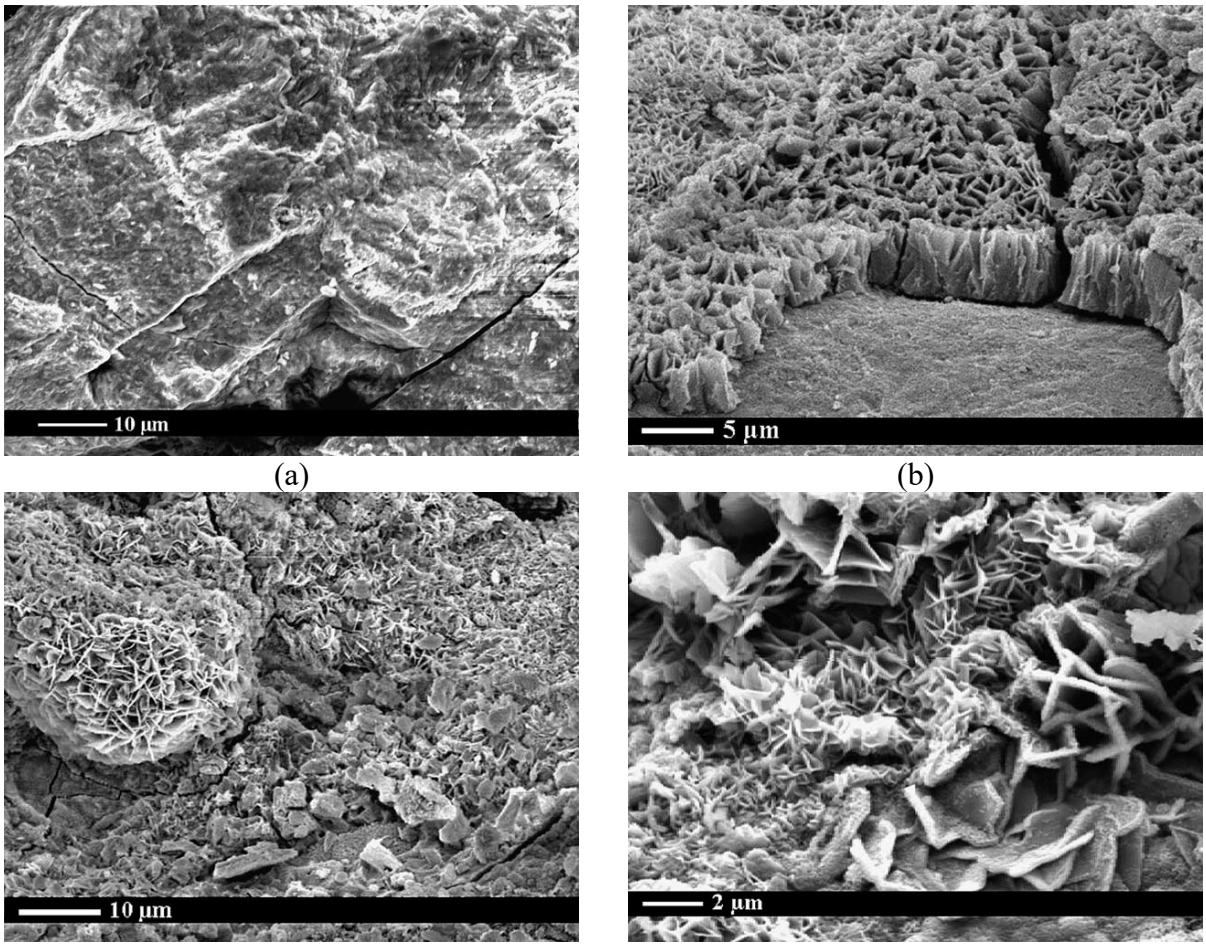

Figure 1.1: a) Magnetite layer, b) α-FeOOH crystals grown on a flat surface of magnetite, c) α-FeOOH crystals, d) Crystals of α- and γ-FeOOH and powdery rust on a corroded steel reinforcing bar (Duffo et al. 2004)

Ghods et al. (2011) performed a depth profile analysis to study the characteristics of oxides on carbon steel passivated in a saturated calcium hydroxide (CH) solution with a pH of 12.5. The saturated CH solution was selected to serve as a surrogate for concrete pore solution–the alkaline solution in the pores of hardened concrete (Elsener and Rossi 2018). Ghods et al. reported that the oxide film (approximately 4 nm thick) was mainly composed of protective Fe (II) oxides near the

substrate and Fe (III) oxides near the free surface. Longer exposure to the saturated CH solution increased the ratio of the Fe (II) to Fe (III) oxides near the substrate (Ghods et al. 2011).

Ghods et al. (2012) questioned whether the saturated CH solution used by Ghods et al. (2011) was truly suitable to serve as a surrogate for concrete pore solution. Ghods et al. (2012) argued that even though the pore solution of portland cement concrete is saturated with calcium hydroxide (Ca^{2+} and OH^-), it also contains other ions. Therefore, Ghods et al. (2012) prepared a simulated pore solution (CP) with calcium hydroxide, sodium hydroxide, potassium hydroxide, and calcium sulfate, with a pH of 13.3. Ghods et al. (2012) obtained the ratio between the concentration of Fe_3O_4/FeO, in which iron exists as a combination of Fe (II) and Fe (III), and Fe_2O_3/FeOOH, in which iron exists solely as Fe (III). They confirmed the previous findings that showed the oxide film is mainly Fe (II) oxides near the substrate and mostly Fe (III) oxides near the surface of the film. These findings are comparable to the results of a previous study by Duffo et al. (2004) that indicated the pronounced presence of Fe_3O_4 (ionic compounds with oxidation states of +2 and +3) in the inner passive layer and the presence of Fe (III) oxyhydroxides in the outer layer. Ghods et al. (2012) discovered that the thickness of the iron oxide film formed in the CP solution was approximately 5 nm, 1 nm greater than that of the iron oxide formed in the saturated CH solution; also, the ratio of protective Fe (II) oxides to Fe (III) oxides was larger in the film formed in the CP solution. They attributed these findings to the composition of the CP solution, its higher alkalinity, or both.

The passive layer on reinforcing steel can be disrupted via carbonation or exposure to chlorides. Carbonation disrupts the formation of the passive layer on steel reinforcing bars embedded in concrete by decreasing the pH of concrete pore solution. Carbon dioxide reacts with

water and calcium hydroxide, neutralizing hydroxides in concrete pore solution (Broomfield 2003):

$$CO_2 + H_2O \rightarrow H_2CO_3 \tag{1.4}$$

$$H_2CO_3 + Ca(OH)_2 \rightarrow CaCO_3 + 2H_2O \tag{1.5}$$

The depth of carbonation increases gradually at a rate depending on the concrete quality and relative humidity. The decrease in the pH of concrete causes the following reactions to form rust on reinforcing steel in the presence of water and oxygen:

$$4Fe(OH)_2 + 2H_2O + O_2 \rightarrow 4Fe(OH)_3 \tag{1.6}$$

$$4Fe(OH)_3 \rightarrow 4Fe_2O_3 \cdot H_2O + 4H_2O \tag{1.7}$$

No exact cutoff pH value where the passive layer destabilizes is agreed upon in the literature; however, a pH below 11.5 seems to negatively affect the passive layer (Verbeck 1975, Poursaee 2016).

As shown in Eq. (1.4), the carbonation reaction requires water; however, the rate of diffusion of carbon dioxide in fully-saturated concrete is insignificant. Carbon dioxide diffuses through saturated concrete much more slowly than it does through concrete that is partially dry. Concrete structures are the most prone to carbonation at internal relative humidities ranging from 50% to 75%; the degree of carbonation is insignificant below 25% internal relative humidity, and the moisture in the pores restricts CO_2 penetration in concrete with above 75% internal relative humidity (ACI Committee 201 2016). Figure 1.2 shows that longer periods of wetting and drying increase the depth of carbonation compared to more frequent wetting and drying. Other environmental factors such as temperature and concentrations of carbon dioxide along with concrete properties also affect the carbonation depth (Bertolini et al. 2014).

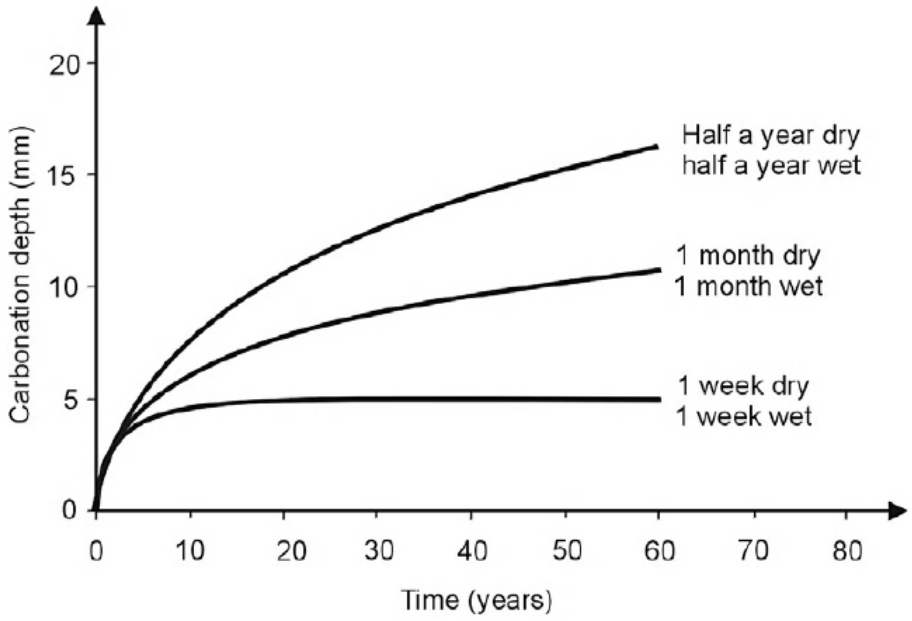

Figure 1.2: Influence of frequency of wet and dry cycles on carbonation depth (Bertolini et al. 2014)

Chlorides can also destroy the passive layer on reinforcing steel, either when cast into fresh concrete or diffused from an external source. The use of chloride-laden components, seawater, or set accelerators that contain chlorides (such as $CaCl_2$) contaminate concrete; chlorides can also penetrate concrete from external sources, such as deicing salts or exposure to sea salt spray. These chlorides are either dissolved in the pore solution (free), which is the usual case for chlorides from an external source, or chemically bound to the cement hydrates, which occurs for a portion of chlorides from chloride-laden components. Free (water-soluble) chlorides in concrete are of primary concern when it comes to corrosion; nevertheless, the effects of chemically-bound chlorides should not be ignored as the bound chlorides may be freed due to a local drop in the pH (Ann and Song 2007). Both free and chemically-bound chlorides can be cast-in or from an external source.

The chloride concentration in concrete is typically measured by performing chemical analysis using a chloride specific ion electrode on samples taken from concrete specimens. The

samples are obtained by drilling into concrete specimens or crushing cores taken from concrete specimens. The concentration of chloride ions is reported in terms of either free (water-soluble) or total (acid-soluble) chloride content. Water-soluble chlorides are the main contributor to corrosion even though the binding of chlorides in the cement matrix can be reversible. Results obtained from acid-soluble chloride testing are more reproducible than water-soluble testing (Broomfield 2003, O'Reilly et al. 2011, Bertolini et al. 2014).

Chlorides break down the passive layer, even in highly alkaline concrete, by reacting with the iron in the passive layer and forming a Fe-Cl complex. The Fe-Cl complex reacts with water to form ferric oxides, releasing chloride ions to react with other ferrous ions, a process which causes depletion of the passive layer known as depassivation (Zhao and Jin 2016):

$$Fe^{2+} + 2Cl^{-} + 4H_2O \rightarrow FeCl_2 \cdot 4H_2O \tag{1.8}$$

$$FeCl_2 \cdot 4H_2O \rightarrow Fe(OH)_2 + 2Cl^{-} + 2H^{+} + 2H_2O \tag{1.9}$$

Ghods et al. (2012) confirmed that the oxide layer close to the steel substrate, which is mainly composed of protective Fe (II) oxides, becomes disrupted (thinner) after exposure to chlorides, while the surface rust, mainly consisting of Fe (III) oxides, increases in thickness after exposure to chlorides. Accordingly, they attributed the breakdown of the passive layer in the presence of chlorides to further oxidation of inner Fe (II) oxides to Fe (III) oxides (Ghods et al. 2010, 2012).

Ghods et al. (2010) compared the chloride concentrations that caused depassivation of conventional steel reinforcing bars in a simulated CP solution (pH of 13.3) and a saturated CH solution (pH of 12.5), and found that the chloride concentration required to initiate corrosion in the specimens in the simulated CP solution was two to three times greater than that for specimens in the saturated CH solution. The minimum concentration of chloride ions required to initiate

corrosion of steel reinforcing bars is defined as the critical chloride corrosion threshold, which is discussed in more detail in Section 1.3.

The buildup of corrosion products around corroding reinforcing bars induces tensile stresses in the surrounding concrete, as these corrosion products have a much larger volume than the original steel (Figure 1.3). These tensile stresses, in turn, lead to the generation and propagation of cracks in concrete, allowing greater access to oxygen, moisture, and corrosive chemicals.

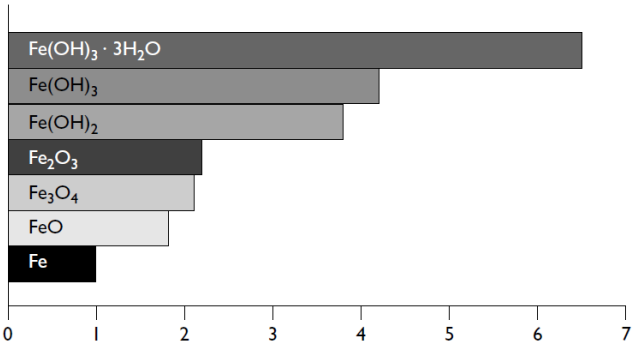

Figure 1.3: Volume of steel versus its corrosion products in concrete (Broomfield 2003)

1.2.1 Service Life of Reinforced Concrete Structures

The service life of a reinforced concrete structure is divided into two stages: the initiation stage with no corrosion activity, followed by the corrosion propagation stage, during which corrosion products accumulate, leading to cracking and spalling of the concrete cover. A limit state marks the end of the functional life of structures when the concrete deteriorates beyond repair, as shown in Figure 1.4 (Bertolini et al. 2014). The time required for each phase depends on the concrete properties, the environment, and the reinforcing steel itself. Increasing the concrete cover, improving concrete quality, and using corrosion resistant bars can extend the service life of reinforced concrete structures (O'Reilly et al. 2011, Farshadfar et al. 2017).

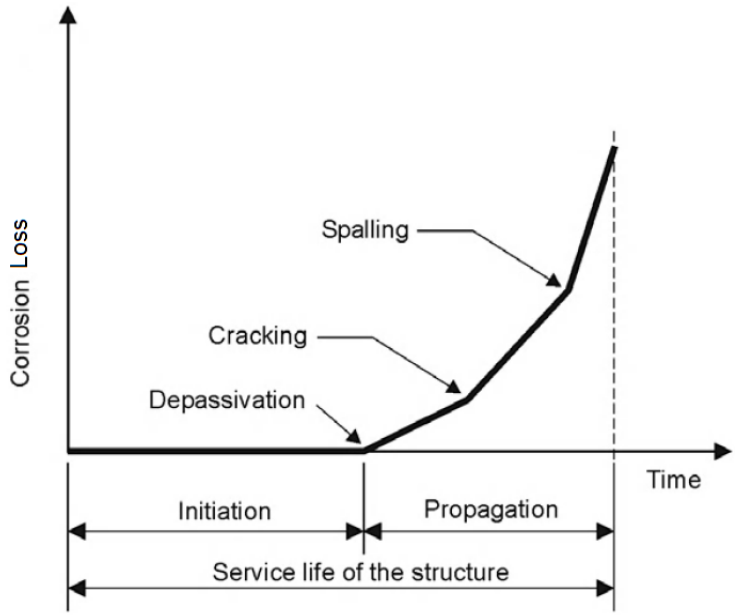

Figure 1.4: Initiation and propagation stages of corrosion in reinforced concrete (Bertolini et al. 2014)

1.3 CHLORIDE INGRESS AND CRITICAL CHLORIDE CORROSION THRESHOLD

Fick's second law of diffusion approximates the chloride ingress profile through uncracked concrete, with a high chloride content near the exposed surface and decreasing chloride content at greater depths:

$$\frac{\partial[Cl^-]}{\partial t} = D_c \frac{\partial^2[Cl^-]}{\partial x^2} \tag{1.10}$$

where D_c is the diffusion coefficient and $[Cl^-]$ is the chloride concentration at depth 'x' and time 't' (Broomfield 2003, Bertolini et al. 2014). The usual form of the diffusion equation in Fick's second law is at best applicable only for permanently fully-saturated concrete where chloride ions penetrate concrete through pure diffusion. This equation, however, neglects other factors affecting chloride content in concrete, such as absorption, chloride binding, temperature, and most importantly, cracking (Broomfield 2003). The sequence and duration of wetting and drying cycles in concrete influence chloride ingress strongly through absorption, where drying to greater depths allows for subsequent wetting to take the chlorides deeper into the concrete. Evaporation and

capillary suction help absorb the chlorides in dry or partially dry concrete to create reservoirs of chlorides carried into concrete by subsequent wetting. Chloride ingress is slower at greater depths where chlorides penetrate mostly through diffusion since concrete is less likely to dry out at greater depths (Hong and Hooton 1999).

The minimum concentration of chloride ions required to initiate corrosion of reinforcing bars is known as the critical chloride corrosion threshold, which depends on many factors related to both the concrete and the composition of the reinforcing steel. The critical chloride corrosion threshold of conventional reinforcing bars usually ranges between 1 and 2 lb/yd^3 (0.59 and 1.19 kg/m^3) (Lindquist et al. 2006). There are many, often interrelated, factors affecting the critical chloride corrosion threshold such as (O'Reilly et al. 2011, Bertolini et al. 2014, Farshadfar, O'Reilly, and Darwin 2017):

- reinforcing bar type,
- electrochemical potential of reinforcing bars,
- cement content (water/cement ratio) and type (chlorides bind with tricalcium aluminate),
- pH of the concrete (the concentration of hydroxyl ions in the pore solution),
- the use of supplementary cementitious materials (they affect the permeability and resistivity of concrete or may bind with hydroxyl ions),
- availability of oxygen and moisture,
- presence of voids adjacent to the reinforcing bars in concrete.

Major factors affecting the critical chloride corrosion threshold, among the factors mentioned above, are the pH of the concrete, the electrochemical potential of reinforcing bars, the type of reinforcement, and the presence of voids at the bar-concrete interface. The electrochemical potential of the reinforcing bars mainly depends on the pH of the pore solution, availability of

oxygen at the surface of the reinforcing bar, and the moisture content of the concrete; a decrease in the electrochemical potential of steel may increase the critical chloride corrosion threshold by more than an order of magnitude (Bertolini et al. 2014). The critical chloride corrosion threshold and time to corrosion initiation are best treated as probability functions or ranges, rather than as fixed numbers due to various and often interrelated factors with significant uncertainty (Broomfield 2003, Hartt and Nam 2008). For example, concrete with different types of cement can exhibit different values of pH, which significantly affects the critical chloride corrosion threshold; chlorides may temporarily or permanently form chemical bonds in concrete; concrete that is very dry, fully-saturated, or sealed may limit the oxygen availability or moisture content required for the corrosion process in concrete (Broomfield 2003).

Different methods of measuring and reporting the critical chloride corrosion threshold exist. The methods used affect both the value obtained and its consistency since the local chloride content at a given depth in concrete is not constant. For example, the fineness of the concrete sample, sample size, and existence of large pieces of aggregate in the sampling volume may affect the results; furthermore, impermeable aggregate particles will hinder chloride ingress forcing the chlorides to move around the aggregate (Yu, Himiob, and Hartt 2007). Chloride concentrations in samples taken directly over reinforcing bars may be 1.9 to 3.8 times greater than the concentration at the same level (depth) away from the bars, as the bars act as a barrier to chloride ingress (Yu and Hartt 2007). Also, the chloride content of samples taken close to the surface is highly dependent on recent weather history; rain or other water sources may temporarily reduce the chloride content (Broomfield 2003). Direct comparison of critical chloride corrosion threshold results reported in the literature is challenging due to varied experimental conditions and corrosion initiation assessment methods in different studies (Ann and Song 2007); furthermore, the variables

affecting the critical chloride corrosion threshold are often interrelated, which makes the comparison between these results even more complicated (Hui Yu and Hartt 2007). The critical chloride corrosion threshold is commonly expressed as total or free chloride content relative to the weight of cementitious material or concrete, total or free chloride content relative to the volume of concrete, or chloride ion concentration relative to the pH of the pore solution ($[Cl^-]/[OH^-]$) (Ann and Song 2007, Angst et al. 2009).

Hausmann (1967) was among the first to introduce thresholds for the effects of chlorides on the corrosion of steel in concrete. Hausmann (1967) found a $[Cl^-]/[OH^-]$ ratio of 0.6 in the presence of oxygen is required for corrosion initiation at the steel surface. However, a change in the pH may be accompanied by a change in the $[Cl^-]/[OH^-]$ at a fixed level of total chlorides. Also, the capacity of concrete to inhibit corrosion cannot be expressed solely through the OH^- content in the pore solution due to factors such as the buffering capacity of concrete (alkaline reserves) and the presence of relatively denser hydration products at the steel-concrete interface (Ann and Song 2007, Angst et al. 2009).

Tables 1.1 and 1.2 summarize the range of the critical chloride corrosion threshold for reinforcing bars in ordinary portland cement concrete in terms of total chlorides by weight of the binder. Table 1.1 presents results obtained from studies with reinforced concrete specimens under outdoor exposure, and Table 1.2 presents results obtained from studies with laboratory specimens with the reinforcement embedded in cement-based materials (concrete or mortar). Critical chloride corrosion threshold in terms of total (acid-soluble) chloride content by weight of the binder for structures with outdoor exposure were as low as 0.1% and as high as 1.96%, as shown in Table 1.1, while they were as low as 0.1% and as high as 3.08% in laboratory studies with the reinforcement embedded in cement-based materials, as shown in Table 1.2. Assuming that the

majority of chlorides in concrete are from external sources, studies involving chlorides mixed (admixed chlorides) in concrete and studies using a simulated pore solution may provide less-realistic values for free chloride content at corrosion initiation than studies where the concrete is subjected to an external source of chlorides; chlorides more readily bind with tricalcium aluminate in plastic concrete, whereas they bind with chlorides in hardened concrete gradually. Furthermore, acid-soluble chloride contents may include chlorides internally bound in the aggregate, which are not available to the cement paste (Broomfield 2003).

Table 1.1: Critical chloride corrosion threshold in terms of total (acid-soluble) chloride content by weight of the binder (ordinary portland cement) for reinforced concrete structures with outdoor exposure (Angst et al. 2009)

Study	Total Cl^- (%)	Chloride Introduction
(Hope and Ip 1987)	0.1–0.19	Added to the mix
(Treadaway, Cox, and Brown 1989)	0.96–1.96	Added to the mix
(Thomas, Matthews, and Haynes 1990, Thomas 1996)	0.7	Diffusion and capillary suction
(Morris et al. 2002, Morris, Vico, and Vázquez 2004)	0.4–1.3	Added to the mix, Diffusion, and capillary suction

Table 1.2: Critical chloride corrosion threshold in terms of total (acid-soluble) chloride content by weight of the binder obtained in laboratory studies with the reinforcement embedded in cement-based materials (with ordinary portland cement) (Angst et al. 2009)

Study	Total Cl^- (%)	Chloride Introduction	Cement-Based Specimen
(Locke and Siman 1980)	0.4–0.8	Added to the mix	Concrete
(Elsener and Böhni 1986)	0.25–0.5	Added to the mix	Mortar
(Hope and Ip 1987)	0.1–0.19	Added to the mix	Concrete
(Schiessl and Breit 1996)	0.5–1.0	Added to the mix and diffusion	Concrete
(Alonso et al. 2000)	1.24–3.08	Added to the mix	Mortar
(Zimmermann, Elsener, and Böhni 1999, Zimmermann 2000)	0.25–1.25	Diffusion and capillary suction	Mortar
(Morris et al. 2002, Morris et al. 2004)	0.4–1.3	Added to the mix, diffusion, and capillary suction	Concrete
(Manera, Vennesland, and Bertolini 2008)	1.1–2.0	Added to the mix	Concrete

1.4 CONCRETE CRACKING AND CORROSION

In general, the corrosion of reinforcing bars in bridge decks, which results in significant costs across the United States each year (Yunovich and Thompson 2003), is aggravated by cracking and the subsequent rapid ingress of chlorides from deicing chemicals. These cracks provide a path for moisture, oxygen, and chlorides to reach the reinforcing bars and lead to corrosion that, in turn, may cause more cracking (O'Reilly et al. 2011). Rodriguez and Hooton (2003) observed that the rate of chloride diffusion is independent of crack width or roughness in wall cracks ranging from 0.08 mm to 0.68 mm (0.003 in. to 0.027 in.), indicating that even narrow cracks are problematic. Concrete bridge decks crack due to several causes, including plastic shrinkage, settlement, drying shrinkage, thermal changes, loading, and corrosion. Drying shrinkage and settlement cracking generally have the greatest impact on generating cracks (Lindquist et al. 2006). Lindquist et al. (2006) studied the effect of cracking on the chloride content of reinforced monolithic bridge decks and bridge decks with conventional and silica fume overlays by measuring chloride concentrations in the field. Lindquist et al. discovered that the chloride concentration in uncracked concrete on bridge decks that were up to twelve years old was lower than the most conservative estimates of critical chloride corrosion threshold for conventional reinforcing bars, 1.0 lb/yd^3 (0.6 kg/m^3), at the depth of the reinforcement. At cracks, however, the chloride content at the depth of the reinforcement frequently exceeded the critical chloride corrosion threshold of conventional reinforcement by the end of the first year (Lindquist et al. 2006).

The factors affecting the influence of cracks on the corrosion of reinforcing bars include the environment and the structure type as well as the orientation, intensity, origin, width, depth, and shape of the cracks. Wider cracks cause greater corrosion loss in the reinforcement at early

stages; the supply of oxygen and moisture to a cathode site, which is electrically connected to the anode, is required for the corrosion process to continue. Unlike longitudinal cracks over the reinforcement, cracks meeting the reinforcement perpendicular to the bar typically cause local corrosion that eventually slows down and may stop in concrete with low permeability. Furthermore, the crack width at the surface does not indicate the crack width at the depth of the bar. The crack width at the bar is a function of crack origin (flexural, settlement, etc.), concrete cover, steel stress, bar diameter, reinforcement ratio, and depth of the tensile zone (Darwin et al. 1985).

The tensile stress that causes concrete to crack is a function of corrosion product buildup surrounding the reinforcement. The corrosion loss required to crack the concrete cover on a reinforcing bar, or simply the corrosion loss to crack concrete, is useful for predicting the service life of reinforced concrete structures. The value of this corrosion loss depends on the concrete cover depth, the reinforcing bar diameter, bar spacing, area, and the length of the anode, as well as concrete properties and the existence of voids around the concrete-bar interface. These factors affect crack initiation, crack propagation, or both to different degrees (Vidal, Castel, and Francois 2004, O'Reilly et al. 2011, Farshadfar et al. 2017).

Several studies have attempted to experimentally determine the corrosion loss required to crack concrete. Alonso et al. (1998) studied prismatic 6 × 6 × 15 in. (150 × 150 × 380 mm) specimens in which bar diameters ranged from 0.125 to 0.625 in. (3 to 16 mm) and cover ranged from 0.4 to 2.75 in. (10 to 70 mm). The splitting tensile strength of the concrete ranged from 348 psi to 558 psi (2.40 to 3.85 MPa). Calcium chloride (3% by weight of cement) was added to the mix water to initiate corrosion, and corrosion was driven by the application of a current density of

100 μA/cm^2 to the bars. Alonso et al. proposed the following model for the corrosion loss to crack concrete:

$$x_{crit} = 7.53 + 9.32\,{}^{c}\!/_{d} \tag{1.11}$$

where:

x_{crit} = corrosion loss required to crack concrete, μm

${}^{c}\!/_{d}$ = concrete-cover-to-bar-diameter ratio

At a cover-to-diameter (*c/d*) ratio of 4, representative of that expected for a bridge deck, this equation yields a value of x_{crit} of 44.8 μm (1.76 mils). Alonso et al. also found that the rate of crack growth decreases as the water/cement ratio increases; this decrease was attributed to the greater available space for corrosion products due to the higher porosity of concrete with greater water/cement ratios. Moreover, the lower modulus of elasticity in concrete with higher water/cement ratios enables greater local deformations before cracking occurs (Alonso et al. 1998).

Torres-Acosta and Sagues (2004) studied corrosion loss required to crack concrete when only a fraction of the steel bar length is corroding using prismatic and cylindrical specimens with varied exposed reinforcement lengths under an applied current density of 100 μA/cm^2. A bar with a diameter of 0.875 in. (21 mm) was centered in the cylindrical specimens with the concrete cover ranging from 1.1 to 2.6 in. (27.6 to 65.7 mm). The exposed length of the bar in cylindrical specimens ranged from 0.75 to 13.5 in. (19.1 to 346 mm). The prismatic specimens measured 5.5 × 5.5 × 16 in. (140 × 140 × 406 mm), with a concrete cover ranging from 0.5 to 1.75 in. (13 to 45 mm). The bars in the prismatic specimens were 0.25 and 0.5 in. (6 and 13 mm) in diameter with exposed lengths ranging from 0.3 to 15.4 in. (8 to 390 mm). The 30-day compressive strength of the concrete ranged from 5800 psi to 7690 psi (40 to 53 MPa). Torres-Acosta and Sagues proposed the following relationship to calculate the corrosion loss to crack concrete:

$$x_{crit} = 11.0 \frac{c}{d}\left(\frac{c}{l}+1\right)^2 \tag{1.12}$$

where:

x_{crit} = corrosion loss required to crack concrete, μm

c = concrete cover, mm (in.)

d= bar diameter, mm (in.)

l = length of exposed steel, mm (in.)

When corrosion occurs over a limited region of a bar, higher local losses are required to crack the concrete cover than in the case of uniform corrosion spread evenly over the full length of a bar. Equation (1.12) can be simplified for uniform corrosion, which is corrosion spread evenly over the surface, along the full length of a bar to:

$$x_{crit} = 11.0 \frac{c}{d} \tag{1.13}$$

Under uniform corrosion and for a *c/d* ratio of 4, this model predicts a corrosion loss required to crack concrete of 44 μm (1.73 mils), which is close to the value of 44.8 μm (1.76 mils) based on the model introduced by Alonso et al.

O'Reilly et al. (2011) generated finite element models for bare and damaged epoxy-coated bars with different concrete cover thicknesses and compared the results to those from laboratory specimens. The finite element models represented uniform and local corrosion of steel in concrete to develop a relationship between corrosion loss required to crack concrete, bar diameter, and the corroding area of the bar using ABAQUS. The corroding area was expressed as a fraction of the total area of the bar that was corroding. O'Reilly et al. modeled the buildup of corrosion products by applying deflection normal to the reinforcing bar surface and used a series of springs, defined based on the fracture energy of concrete, to represent the nonlinear behavior of concrete during

cracking. The lab specimens consisted of conventional, galvanized, and intentionally damaged epoxy-coated reinforcement cast in concrete with 2% chloride by weight of cement, under a current density of 100-500 μA/cm^2. Accordingly, O'Reilly et al. proposed the following equation for predicting the corrosion loss required to crack concrete in conventional and epoxy-coated reinforcement:

$$x_{crit} = 0.53\left(\frac{c^{2-A_f}}{d^{0.38}L_f^{0.1}A_f^{0.6}} + 0.6\right) \times 3^{A_f - 1} \tag{1.14}$$

where:

x_{crit} = corrosion loss required to crack concrete, mils (0.001 in.)

c = cover, in.

d = bar diameter, in.

L_f = fractional length of bar corroding, $L_{\text{corroding}}/L_{\text{bar}}$

A_f = fractional area of bar corroding, $A_{\text{corroding}}/A_{\text{bar}}$

The fractional area and length of the bar corroding are equal to 1 (A_f =1, L_f =1) in the case of uniform corrosion, which simplifies Eq. (1.14) to (O'Reilly et al. 2011):

$$x_{crit} = 0.53\left(\frac{c}{d^{0.38}} + 0.6\right) \tag{1.15}$$

Equation (1.15) predicts a corrosion loss of 1.90 mils (48 μm) to crack a 2.5 in. (64 mm) concrete cover for a bar diameter of 0.625 in. (16 mm) (c/d ratio of 4), which is close to the values of 44.8 and 44 μm (1.76 and 1.73 mils) based on the models introduced by Alonso et al. and Torres-Acosta and Sagues, respectively. O'Reilly et al. also found that galvanized reinforcement requires twice the corrosion loss of conventional reinforcement to crack concrete for covers of 1 in. and 2 in. (25 mm and 51 mm).

1.5 CORROSION PROTECTION

The main approaches to control corrosion in reinforced concrete are decreasing the chloride penetration rate through concrete, increasing the critical chloride corrosion threshold of the reinforcement, and decreasing the rate of corrosion after initiation. Increasing concrete cover, lowering the water/cementitious material ratio, and using corrosion inhibiting admixtures can improve corrosion resistance by hindering the diffusion of chlorides through concrete. Epoxy-coated bars have a barrier preventing chloride exposure of the steel. ASTM A1035 bars show delayed initiation because of a greater critical chloride corrosion threshold as well as lower corrosion rates upon corrosion initiation. The zinc coating on galvanized reinforcement acts as a barrier to chlorides; furthermore, zinc acts as a sacrificial anode and provides cathodic protection to steel (O'Reilly et al. 2011). Multiple methods can be combined to further improve corrosion resistance.

1.5.1 Epoxy-Coated Reinforcement

Epoxy-coated reinforcement (ECR) is the most commonly used corrosion-resistant reinforcement due to its availability and long service life. Epoxy-coated bars were first used in bridge decks in the mid-1970s (Poursaee 2016). Epoxy coatings are nonconductive and isolate the bars from the surrounding concrete, preventing the electrical connection required for macrocell corrosion between bars; furthermore, the epoxy coating acts as a barrier to oxygen and moisture and protects the steel from chlorides. Darwin et al. (2002) recommended the use of epoxy-coated reinforcement for corrosion protection in bridge decks until a superior corrosion protection system becomes available. While epoxy-coated bars are an effective solution to corrosion, they come with their own set of challenges. Epoxy-coated bars must be handled, stored, and placed with care; they should be stored away from moisture and ultraviolet (UV) light exposure from sunlight. Moreover,

epoxy-coated reinforcement is prone to damage and, thus, may require patching and repair. The corrosion mechanism for bare bars is usually pitting or uniform corrosion, while for epoxy-coated bars the mechanism is underfilm or crevice corrosion (Weyers, Pyc, and Sprinkel 1998).

Water has detrimental effects on the durability of epoxy coatings. Water can affect the mechanical properties of coatings and result in their swelling or shrinkage. Penetration of water into the coating reduces adhesion and can cause cracking, which may lead to corrosion of the metallic substrate. This degradation occurs more quickly as temperature increases, and is also accelerated under cycles of wetting and drying (Shi, Hinderliter, and Croll 2010).

Loss of adhesion (disbondment) of the epoxy coating to the steel under long-term exposure to harsh environments is one concern regarding the long-term durability of ECR. The loss of adhesion in the presence of defects in the coating, such as holes, lowers the corrosion performance of ECR (Manning 1996). Oxygen is required to form a passive film on the metal surface; the oxygen supply is limited under a disbonded coating (Ahmad 2006, Iversen and Leffler 2010, Popov 2015). The lack of oxygen under the coating can lead to breakdown of the passive layer and may cause the local pH to drop as low as 5, leading to underfilm and crevice corrosion (Weyers, Pyc, and Sprinkel 1998). Chlorides can also destabilize the passive layer under the disbonded coating in the presence of water in the absence of oxygen:

$$\left[Fe^{2+}Cl_2^{2-}\right] + 2H_2O \rightarrow Fe(OH)_2 + 2\left[H^+Cl^-\right] \quad (1.16)$$

The hydrogen ions released in this process decrease the pH in the crevice environment and further destabilize the passive layer (Weyers, Pyc, and Sprinkel 1998, O'Reilly et al. 2011).

Overall, ECR has provided good corrosion resistance. Coating damage during transportation and construction occurs over a limited region of a bar and higher losses are required to crack the concrete cover than in the case of uniform corrosion spread evenly over the full length

of a conventional bar, as discussed in Section 1.4. Laboratory studies have shown that the average total corrosion losses of ECR are less than 5% of the corrosion losses of conventional reinforcement (Weyers, Pyc, and Sprinkel 1998, Draper et al. 2006, O'Reilly et al. 2011, Poursaee 2016). In the past, reports of poor performance of epoxy-coated reinforcement in the field have usually involved bars with low-quality or low-thickness coatings and high amounts of damage. For example, in the late 1980s, cracking and spalling was observed as early as five to seven years in bridges constructed in the Florida Keys using the first generation of epoxy-coated reinforcement. This first-generation coating, which had poor flexibility in bending, readily disbonded, resulting in significant corrosion in four out of the five major bridges it was used on (Broomfield 2003, Poursaee 2016). The flexibility and disbondment resistance of epoxy-coated reinforcement has improved since the first generation; these improvements have made ECR more reliable and effective in protecting reinforcing bars from corrosion. Other cases of poor corrosion performance of ECR were due to poor quality concrete or the simultaneous use of ECR and conventional bars forming a corrosion cell where the conventional bars served as the cathode. Reports of poor ECR performance do not represent the current corrosion protection provided by ECR available today. Research into higher-quality epoxy coatings for reinforcing bars has progressed into studying self-healing and organic coatings (Bymark et al. 1995, Correll and Berstler 1997, Selvaraj, Selvaraj, and Iyer 2009, Weishaar et al. 2018).

UV light from sunlight is also known to cause degradation in epoxy coatings; cracks formed in epoxy coatings due to UV-induced degradation are known as silver cracks (Kotnarowska 1999, Cetiner et al. 2000). UV light has enough energy to break the covalent bonds of organic molecules, including those in epoxy. Even if the epoxy itself does not absorb the radiation energy, it may be susceptible to attack by free radicals produced as a result of UV light absorption by other

materials in the coating, such as additives blended with the epoxy (Hare 1992). Aging-induced changes in the coating affect its mechanical properties, such as hardness, along with its static and dynamic strength. Longer UV light exposure results in deeper and more numerous silver cracks and causes the coating structure to become more coarse-grained. Prior UV light exposure worsens the effects of moisture/heat-induced aging of epoxy coatings in the presence of chlorides (Kotnarowska 1999, Ramniceanu et al. 2008).

Cetiner et al. (2000) evaluated the effects of UV light on the degradation of epoxy coatings used on pipelines at periodic exposure intervals, up to two years. The pipes were not rotated, allowing for the underside of the pipe to serve as a low-UV exposure control. After 15 to 21 months of exposure, the portions of the coating subjected to full sunlight exposure suffered from chalking, which is polymer degradation resulting in the formation of a loose chalky layer on the coating surface (Hare 1992), along with loss of thickness, flexibility, and gloss; there were no significant differences in the disbondment, adhesion, and impact properties compared to the coating on the underside of the pipe. UV light exposure had the most pronounced effect on the loss of flexibility of the coating. Furthermore, approximately 1 to 2 mils of coating thickness loss and a visible reduction in the coating gloss were observed for pipes subjected to full sunlight. Cetiner et al. (2000) recommended that pipes stored outside for longer than a year should be protected from UV light.

Kumar et al. (2002) observed that cyclic exposure to both UV radiation and condensation with a duration of 1000 hours resulted in a 29% decrease in the tensile strength of an epoxy coating. Nikafshar et al. (2017) exposed an epoxy coating to 800 hours of UV radiation and observed a 30% decrease in the tensile strength. Al-Turaif (2013) found that longer UV radiation exposure increased oxygen bonds and decreased carbon bonds in the coating up to 250 hours; they detected

no further changes in the chemical composition of epoxy coating samples due to oxidation degradation after 250 hours of UV light exposure. Accordingly, Al-Turaif concluded that the changes in the chemical composition in the top thin layers (reaching or exceeding 10 nm) occur during the early stages of UV light exposure. Al-Turaif ‘s findings indicate that the changes in the chemical composition on the surface of epoxy coatings may stop after a specific duration of UV light exposure, giving rise to the idea of a UV-induced surface oxidation degradation time limit, after which changes in the chemical composition are not substantial (Al-Turaif 2013).

Kamde and Pillai (2020) used steel-mortar specimens to study the corrosion performance of epoxy-coated reinforcing bars that had been subjected to prolonged sunlight during storage. They found that that UV light exposure resulted in shrinkage-induced cracking of the coating and decreased the chloride threshold for corrosion initiation. They concluded that exposure to sunlight can decrease the service life of epoxy-coated reinforcing bars by about 70%. Kamde and Pillai recommended that exposure of epoxy-coated reinforcing bars to sunlight be limited to less than one month.

Currently, ASTM A775 and ASTM D3963 require coated bars to be covered with opaque polyethylene or other suitable protective material if cumulative environmental exposure of epoxy-coated bars is expected to be greater than two months before concrete embedment; this two-month period includes all periods during which bars are uncovered. The material used to protect the bars must allow for air circulation around the bars to minimize condensation.

1.5.2 ChromX (A1035 Type CS) Reinforcement

ASTM 1035 reinforcing steel, produced under the brand name ChromX by Commercial Metals Company (CMC), is a chromium alloy reinforcing steel. The steel has nominal chromium contents of 2% (Type CL), 4% (Type CM), or 9% (Type CS) (see Table 1.3). Other than corrosion

protection benefits, ASTM A1035 reinforcement can be used to reduce the amount of reinforcement because it is produced with yield strength of 100 to 120 ksi (689 to 827 MPa), which is higher than that of conventional reinforcement, with a typical yield strength of 60 ksi (414 MPa) (Darwin et al. 2002, Kahl 2007). Farshadfar et al. (2018) found that the critical chloride corrosion threshold of A1035 reinforcement Type CS and Type CM to be 4.25 and 4.54 lb/yd^3, respectively, which is approximately four times higher than that of conventional reinforcing steel. Darwin et al. (2002) found that A1035 Type CS reinforcing bars exhibit corrosion rates one-third to two-thirds that of conventional bars; however, they also found that A1035 Type CS reinforcing bars have a lower corrosion resistance than damaged epoxy-coated bars. They did not recommend the use of A1035 reinforcement Type CS unless used along with a supplementary corrosion protection system. Darwin et al. found that A1035 Type CS reinforcement was less cost-effective than epoxy-coated reinforcement for use in bridge decks. The service life model used by Darwin et al. predicted that bridge decks containing A1035 Type CS reinforcing steel would require repair approximately 30 years after construction compared to 10 to 25 years after construction for conventional steel and 40 years for epoxy-coated reinforcement.

Table 1.3: Nominal chromium content in ASTM A1035 reinforcement

A1035 Alloy Type	Chromium Content (%)
CL	2.0–3.9
CM	4.0–7.9
CS	8.0–10.9

1.5.3 Galvanized Reinforcement

The hot-dip galvanizing process forms an outer layer of pure zinc with several layers of underlying intermetallic iron-zinc alloys. The outer zinc layer on galvanized reinforcement protects the steel from corrosion by acting as a barrier to moisture, oxygen, and chloride, raising the critical chloride corrosion threshold as well as serving as a sacrificial anode (Darwin et al.

2009, O'Reilly et al. 2018). Zinc coatings can also sacrificially protect steel reinforcing bars since zinc is thermodynamically more active than iron. Zinc coatings, which are tough, provide cathodic protection to steel bars during storage and construction even when damaged, as long as the coating is not substantially consumed. Galvanized steel exhibits a greater critical chloride corrosion threshold than conventional reinforcement and delays the onset of cracking and spalling since zinc corrosion products are not as expansive as those of iron. Mixing galvanized and non-galvanized reinforcement can result in the accelerated depletion of the zinc coating on the galvanized reinforcement; therefore, maintaining complete electrical isolation between galvanized and non-galvanized reinforcement is necessary (Broomfield 2003, Yeomans 2018).

The zinc coating on galvanized bars reacts with water in concrete in a calcium-rich alkaline solution to form calcium hydroxyzincate (Andrade and Macias 1988):

$$Zn + 2H_2O \rightarrow Zn\left(OH\right)_2 + H_2 \uparrow \tag{1.17}$$

$$2Zn\left(OH\right)_2 + 2H_2O + Ca(OH)_2 \rightarrow Ca(Zn(OH_3)_2) \cdot 2H_2O \tag{1.18}$$

At a pH of about 12.6, the zinc surface is fully covered with a compact layer of calcium hydroxyzincate (Yeomans 2016). ZnO and $Zn(OH)_2$ are also formed during the corrosion of zinc in concrete. Pokorný, Kouřil, and Kučera (2019) questioned the extent to which calcium hydroxyzincate passivated the surface of galvanized reinforcement. Rather, they suggested that the passivation of galvanized reinforcement is due to the presence of ZnO and $Zn(OH)_2$ in the pores between crystals of calcium hydroxyzincate, especially in the presence of oxygen. The stability of the zinc passive layer is highly dependent on the pH of the environment (alkali content). The passive layer is stable below a pH of 13.3; above 13.3, zinc tends to form large non-protective crystals (Andrade and Macias 1988). Initially, the new concrete pore solution with saturated calcium hydroxide has a pH of about 12.2; as hydration continues, the pH rises as high as 14,

depending on the alkali content of the cement, which is dominated by NaOH and KOH. When galvanized coatings come in contact with wet concrete, about 10 μm (0.39 mils) of zinc from the outer layer of the coating is consumed (Yeomans 2016).

Most galvanized bars are treated with chromate or an organic coating to protect the zinc in high pH environments and prevent the formation of hydrogen. Hydrogen evolution occurs during passivation and active corrosion of zinc in concrete, as shown in Eq. (1.17). The hydrogen bubbles can remain at the concrete-bar interface and decrease the effective area of contact between the reinforcement and concrete; bond between reinforcing bars and concrete is essential for load transfer in reinforced concrete. Kayali and Yeomans (1995) found no significant loss of bond between galvanized bars and concrete. Darwin et al. (2009) observed that the average critical chloride corrosion threshold for hot-dip galvanized reinforcement without chromate treatment was about 1.6 times higher than that of conventional steel. Furthermore, they examined the concrete from the specimens after the tests to determine signs of increased porosity due to hydrogen formation; for all specimens (conventional and galvanized steel), the concrete below the bars exhibited higher porosity than the concrete above the bars. The increased porosity near the galvanized bars was comparable to that of conventional bars in similar air-entrained concrete, indicating that the increased porosity in concrete observed below the bars was likely due to entrapped air, not hydrogen formation.

Studies of the corrosion performance of galvanized reinforcing bars show mixed results, especially when highly alkaline pore solutions are used as a surrogate for the concrete pore solution. Macias and Andrade (1987) studied the corrosion behavior of galvanized reinforcement in 0.001–1.5M KOH and NaOH solutions, as a surrogate for concrete pore solution. They found that they could establish pH ranges where localized corrosion (pH < 12), stability (pH of 12 to

13.4), and complete dissolution of the galvanic coating (pH > 13.4) occur. Saraswathy and Song (2005) tested chromated and non-chromated galvanized and conventional (non-galvanized) cold twisted deformed and thermo mechanically treated (CTD and TMT) reinforcement using concrete specimens ponded with NaCl solution following ASTM G109 and found only non-chromated galvanized TMT bars performed better than the corresponding conventional reinforcement. CTD conventional bars generally showed lower total integrated macrocell currents (in coulombs) than chromated and non-chromated galvanized CTD bars during testing; over most of the testing duration, conventional TMT bars showed lower total integrated macrocell currents than the chromated galvanized TMT bars, but higher than non-chromated galvanized TMT bars.

The range of critical chloride corrosion threshold values obtained by Darwin et al. (2009) was greater than that of conventional bars, and on the low side, some galvanized specimens showed critical chloride corrosion threshold values of the same magnitude as conventional bars. Darwin et al. attributed signs of corrosion, including loss of the pure zinc layer and exposure of the intermetallic layer, to either a lack of a chromate treatment in the bars tested or the high pH of concrete. Swamy et al. (1988) studied the corrosion performance of galvanized bars in a corrosive tidal zone and under an accelerated wetting and drying cyclic regime in seawater; they concluded that galvanized bars exhibit better corrosion performance than conventional reinforcement.

Hot-dip galvanizing (HDG), covered under ASTM A767, is the most common galvanizing method for reinforcing steel. HDG involves immersing treated steel in a bath of molten zinc at a temperature of 440 °C to 460 °C where metallurgical reactions occur between the steel and the zinc. The coating that remains on the steel after it cools has an external bright layer of pure zinc and internal layers of iron-zinc alloys linked to the base steel, as shown in Figure 1.5. The thickness of the layers depends on the composition of the base steel, the temperature of the bath, the time of

immersion, and the composition of the zinc bath. The iron-zinc alloys formed in the HDG process are brittle and may crack upon bending, causing preferential sites for corrosion (Wilson et al. 1988, Poursaee 2016, Yeomans 2016). ASTM A767 prescribes coating thickness and weight requirements, which are given in Table 1.4.

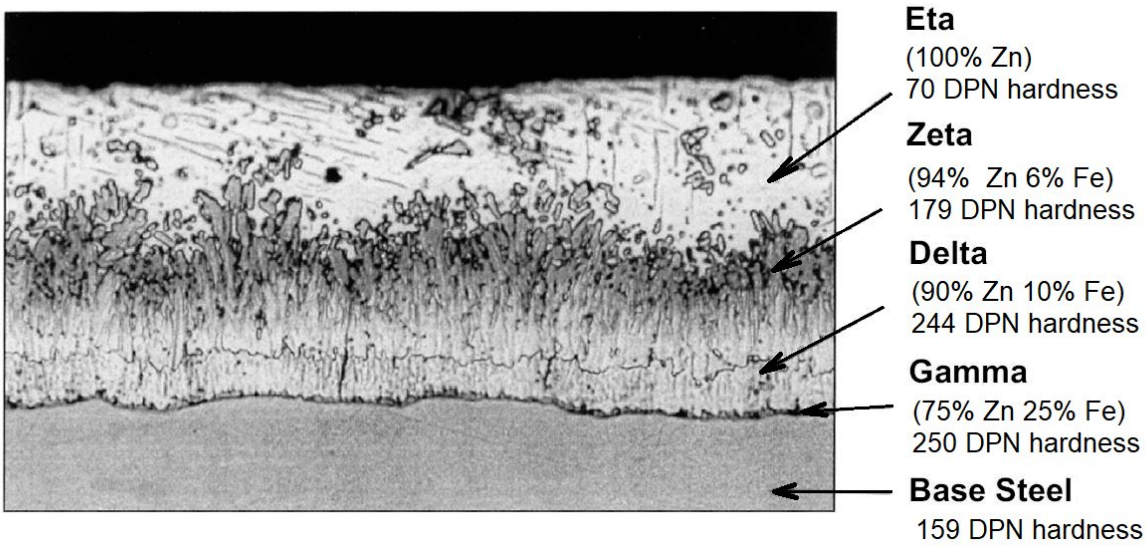

Figure 1.5: Microstructure of HDG steel bar (Poursaee 2016)

Table 1.4: Minimum coating thickness and weight requirements for galvanized reinforcement as per ASTM A767

Bar Size	Thickness in mils (µm)	Weight in oz/ft^2 (mg/cm^2)
Class 1 No. 3	5.1 (129)	3.0 (92)
Class 1 No. 4 and larger	5.9 (150)	3.5 (107)
Class 2 No. 3 and larger	3.4 (86)	2.0 (62)

O'Reilly et al. (2018) compared the corrosion loss required to crack concrete for galvanized A767 galvanized bars without chromate treatment with that of conventional reinforcement. Specimens had concrete cover ranging from 0.5 to 2 in. (12.7 to 51 mm). For most specimens, the top and bottom bars were connected across a 30 V power supply to provide an impressed current that drove corrosion on the top bars. Companion specimens with no impressed current were also evaluated; it was found that the use of impressed current did not appreciably alter the relative performance of the bars tested (O'Reilly et al. 2018). Galvanized reinforcement required twice the

corrosion loss required to crack concrete compared to conventional reinforcement in this study. O'Reilly et al. (2011) and (2018) suggested that cracking due to corrosion of galvanized reinforcement involved the buildup of corrosion products from the underlying intermetallic layers or the base steel, as opposed to the corrosion products of the zinc. Darwin et al. (2009) also found the intermetallic layers in galvanized reinforcement were exposed due to corrosion.

Continuous galvanizing (CG), covered under ASTM A1094, was introduced in 2015; the continuous galvanizing process was designed to achieve thinner zinc coatings through addition of low amounts of aluminum (a concentration of less than 1%) to the zinc bath. The coating thickness and weight requirements prescribed by ASTM A1094 are given in Table 1.5. The added aluminum forms a thin Fe-Al-Zn layer on the base steel that inhibits extensive dissolution of zinc to form intermetallic phases; the majority of the coating thickness consists of almost pure zinc (shown in Figure 1.6). Intermetallic layers that form on HDG bars do not significantly contribute to the corrosion protection compared to the outer pure zinc layer. The outer pure zinc layer remaining on the surface of the HDG is generally about 40 to 50 μm (1.57 to 1.97 mils) thick. The zinc layer on CG bars provides a reserve (a minimum of about 50 μm, 2.0 mils) of pure zinc to achieve better corrosion protection; this zinc reserve is beneficial because some of the zinc coating is consumed during passivation of galvanized bars in concrete. It has also been claimed that continuous galvanizing will yield galvanized reinforcement that can be bent without damage to the coating (Yeomans 2018), a particular point of interest in the current study. Limited research on A1094 coatings is available. A recent study by Ogunsanya and Hansson (2018) found that HDG bars showed lower corrosion rates than CG bars. The CG coating evaluated in that study, however, was an early prototype and had a non-uniform coating thickness and bare spots.

Table 1.5: Minimum average coating thickness and weight for galvanized reinforcement as per ASTM A1094

Coating Grade	Thickness in mils (µm)	Weight in oz/ft^2 (mg/cm^2)
50	2.0 (50)	1.2 (36)

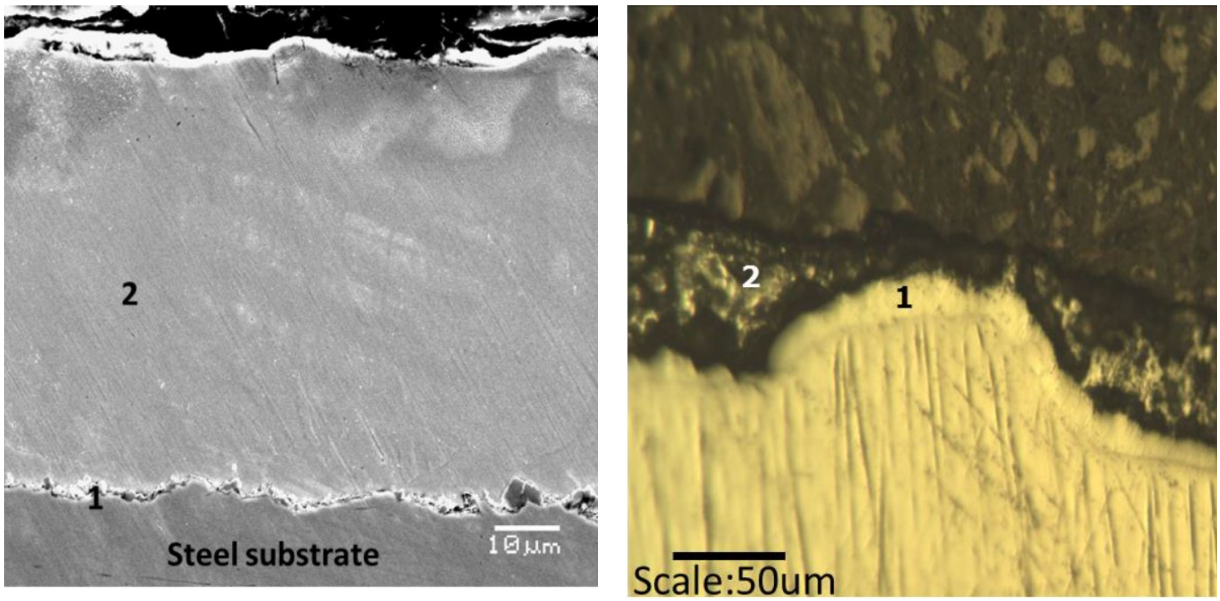

Figure 1.6: Microstructure of CG steel bar: 1 and 2 are Fe-Al-Zn and pure zinc layers, respectively (Ogunsanya 2016).

1.5.4 Corrosion Inhibitors

A corrosion inhibitor is defined as a substance that decreases the corrosion rate when present in the system in an appropriate concentration without significantly changing the concentration of any other corrosion agents (Broomfield 2003); this definition excludes coatings, pore blockers (decreases permeability), and chemicals that bind with chlorides. Corrosion inhibitors are divided into three categories based on the corrosion inhibition process (Broomfield 2003, Poursaee 2016):

1. Anodic inhibitors suppressing the anodic corrosion reaction; these include chromates, nitrites, molybdates, alkali phosphates, silicates, and carbonates
2. Cathodic inhibitors suppressing the cathodic reaction; these include zinc and salts of magnesium, manganese, and nickel

3. Ambiodic inhibitors suppressing both anodic and cathodic reactions; these include amines, esters, and sulfonates.

Anodic inhibitors passivate the metal by forming an insoluble protective film on anodic surfaces or by adsorption on the metal, while cathodic inhibitors form an insoluble or adsorbed film on the cathode surfaces; adsorption forms an insoluble protective film on the reinforcement. Cathodic inhibitors are generally less effective. Ambiodic inhibitors block both anodic and cathodic reactions by adsorption on the surface of the reinforcement. Some corrosion inhibitors may have negative effects on concrete, such as decreasing the concrete strength, affecting setting time, and exacerbating alkali aggregate reaction (Broomfield 2003, Xing et al. 2010, Darwin et al., O'Reilly et al. 2011, Poursaee 2016). Despite the potential side effects of adding corrosion inhibitors to concrete, their use has increased in recent years (Broomfield 2003, O'Reilly et al. 2011, Poursaee 2016).

1.5.5 Waterproofing Chemical Admixtures

Waterproofing chemical admixtures, such as commercially available IPANEX and Xypex, are used in concrete to decrease permeability and, thus, improve the corrosion resistance of reinforcing steel by decreasing the penetration of chlorides and limiting the supply of oxygen required for the corrosion process. Of the two example products, IPANEX is an inorganic admixture composed of calcium silicate hydrate compounds (C-S-H), which give the C-S-H produced in the cement hydration process a finer microstructure (Cement Chemistry Systems 2016). Xypex reacts with byproducts of cement hydration process to form "non-soluble crystalline structures" in concrete pores in the presence of water and is claimed to improve concrete durability and resistance to sulfate attack (XYPEX 2020). Overall, few studies have evaluated the corrosion performance of either product. Hisey (2004) found that IPANEX affected neither hardened

concrete properties nor the corrosion performance of reinforcing bars in the concrete. Hisey did not investigate the effect of IPANEX on the permeability of concrete. Engle (1999) found that IPANEX had no significant benefits on the permeability, chloride resistance, or strength of concrete.

1.6 DISCUSSION

The corrosion performance of epoxy-coated (ASTM A775), hot-dip and continuously galvanized (HDG and CG, respectively covered in ASTM A767 and ASTM A1094), and ChromX (ASTM A1035 Type CS) reinforcing bars, which are of interest to the Oklahoma Department of Transportation (ODOT), are evaluated in this study. ODOT is also interested in evaluating the effectiveness of the waterproofing admixtures IPANEX and Xypex in providing corrosion protection to bridge decks. The work includes a study on the effect of ultraviolet (UV) light on the corrosion resistance of ECR, the paired behavior of the waterproofing admixtures and ChromX reinforcement, and the corrosion resistance of continuously galvanized bars. This brief discussion establishes the need for this work to bridge the gap between the literature review and the objectives of this study. Accordingly, a case is made for specimen type and conditions of testing for each corrosion protection system evaluated.

Reinforcing bars are commonly bent for use in reinforced concrete members, for example in stirrups and hooks. Bending reinforcing bars may damage coated bars and cause preferential corrosion sites and, therefore, affect corrosion performance. Coated reinforcing bars are tested in both the bent condition and straight in this study to investigate if bending has a statistically significant effect on corrosion performance. Furthermore, coated reinforcing bars may be damaged during handling and construction, which can also reduce corrosion resistance. Therefore, coated

reinforcing bars are tested both with and without damage in the coating to establish more realistic testing conditions.

The amount of damage on the surface of the bars in specimens in this study does not exceed 1% of their surface area in contact with concrete or pore solution. As mentioned before, the testing conditions are described in Chapter 2.

Epoxy-coated reinforcement (ECR) has been in use for the past 50 years (Poursaee 2016). The use of ECR is the recommended corrosion protection method for bridge decks and will likely remain so until a superior corrosion protection system becomes available (Darwin et al. 2002). The literature on both the corrosion resistance of ECR and the effects of UV light on epoxy coatings is rich, but adequate research is not available on the effect of prolonged UV exposure on the corrosion performance of epoxy-coated reinforcement. In the current study, ECR specimens are tested both without and after exposure to accelerated weathering under UV light and moisture exposure cycles following ASTM G154 to investigate the effect of improper transportation and storage on the corrosion performance of ECR. Epoxy-coated reinforcing bars are likely to be damaged during transportation, storage, and construction. The detrimental effect of this damage on corrosion performance is expected to be worsened by the exposure to UV light and humidity. Additionally, bent ECR specimens were included in the testing program since bending can affect the coating. Accordingly, ECR (ASTM A775) specimens are tested in as-received, intentionally damaged, and bent conditions; the bent bars were not damaged or exposed to UV light.

Epoxy-coated reinforcing bars must be protected from sunlight, salt spray, and weather exposure if outside storage is required. It is well known that epoxies are vulnerable to UV light exposure, and limiting outside storage of epoxy-coated reinforcing bars under sunlight is

recommended to minimize the detrimental effect of UV light on corrosion resistance (Kotnarowska 1999, Cetiner et al. 2000, Ramniceanu et al. 2008).

Currently, ASTM D3963 limits unprotected outdoor exposure of epoxy-coated reinforcing bars to two months. This study investigates if this established limit is sufficient to maintain the corrosion resistance of epoxy-coated reinforcement and further evaluates the combined effects of damage in the coating and UV light exposure on the corrosion resistance.

ASTM A775 sets the maximum allowable damage to an epoxy-coated bar as 2% of the surface area in any 1-ft (0.3-m) length of the bar and requires all damaged coating discernible with normal or corrected vision to be repaired with patching material. Also, cracking or disbonding visible with normal or corrected vision after the bend test, specified in ASTM A775, is cause for rejection of the epoxy-coated reinforcing bar.

Hot-dip galvanized reinforcement has been used for over 80 years (Yeomans 2016). Continuous galvanization for reinforcement is a new development that facilitates the production of galvanized bars with a thinner zinc coating (Ogunsanya and Hansson 2018) that can decrease production costs. Studies examining the effectiveness of hot-dip galvanized reinforcement in preventing corrosion have shown mixed results over the years (O'Reilly et al. 2011). Evaluating the corrosion resistance of CG reinforcement is unique to this study since these bars have been developed only recently. Furthermore, only a prototype version of CG reinforcement was used in the single available peer-reviewed study by Ogunsanya and Hansson (2018) that compared the corrosion resistance of HDG and CG bars. To achieve a fair comparison between galvanized reinforcement and ECR, the galvanized reinforcement is tested in as-received, bent, and intentionally damaged conditions similar to ECR. Bent specimens provide insight into the extent that the corrosion resistance of galvanized reinforcement is affected by any preferential corrosion

sites created due to bending; damaged specimens are also useful since reinforcement is typically handled roughly. Incorporating HDG bars in this study sets a reference point for evaluating the corrosion performance of CG bars and enables this study to compare the corrosion resistance of HDG and CG reinforcement.

It has been claimed that ASTM A1094 reinforcement has a more flexible coating and, therefore, is less likely to lead to corrosion on bent reinforcing bars than ASTM A767 reinforcement; this study evaluates that claim.

Both ASTM A767 and A1094 require that the maximum amount of repaired damaged coating not exceed 1 % of the total surface area in each 1-ft (0.3-m) length of the galvanized bar; this limit does not include patching the cut ends of the bar. The zinc coating on A1094 and Class 2 A767 galvanized reinforcing bars must not flake off or be removed by any reasonable handling process. The coating of both ASTM A767 and A1094 galvanized bars must be adherent and meet the requirements of the bend test specified in ASTM A615 and ASTM A706.

The corrosion performance of conventional and ASTM A1035 reinforcement has been evaluated in previous studies. This study includes three heats of conventional steel reinforcement, corresponding to the three heats of steel used to produce the epoxy-coated and galvanized steel reinforcement evaluated, as a benchmark for comparing the corrosion performance of these bars. In prior studies, ASTM A1035 Type CS reinforcement was not recommended for use unless it was combined with a supplementary corrosion protection system (Darwin et al. 2002). Therefore, the corrosion protection provided by the combined use of ChromX (ASTM A1035 Type CS) reinforcement and waterproofing admixtures IPANEX or Xypex is studied and compared with that of ChromX reinforcement alone, and with conventional reinforcement with IPANEX and Xypex.

1.7 OBJECTIVE AND SCOPE

The purpose of this study is to evaluate and compare the performance and cost-effectiveness of multiple corrosion protection systems. The following systems are included in this study:

1. Three heats of conventional steel reinforcement (ASTM A615), corresponding to the steel used to produce the epoxy-coated and galvanized steel reinforcement.
2. Epoxy-coated reinforcement (ASTM A775).
3. Hot-dip galvanized (HDG) bars (ASTM A767) and continuously galvanized (CG) bars (ASTM A1094).
4. ChromX reinforcement (ASTM A1035 Type CS).
5. Xypex and IPANEX waterproofing admixtures paired with conventional and ChromX reinforcement.

Only a single study by Kamde and Pillai (2020) has evaluated the effect of UV light on the corrosion resistance of ECR in concrete. The effects of damage and bending on the corrosion resistance of epoxy-coated reinforcement are studied in this study. Moreover, this study evaluates the effect of ultraviolet (UV) light exposure on the ECR corrosion resistance; studying the effect of UV on ECR is necessary to evaluate the effectiveness of the current UV exposure limits for ECR in maintaining the corrosion resistance.

There is limited research on the evaluation of corrosion resistance of continuously galvanized (CG) bars (Ogunsanya and Hansson 2018); the cost-effectiveness of CG bars, especially compared to hot-dip galvanized (HDG) reinforcement needs to be investigated. The corrosion resistance of HDG (ASTM A767) and CG (ASTM A1094) bars are compared both without and with damage. Furthermore, the effect of bending on the corrosion resistance of

galvanized bars is studied; studying the effect of bending is necessary to evaluate the claim, by the manufacture, that the coating on A1094 bars is more flexible than A767 and, therefore, less likely to lead to corrosion when bent. There are only two studies that evaluate the corrosion resistance of IPANEX admixture (Engle 1998, Hisey 2004), and no studies evaluate that of Xypex for use in reinforced concrete bridge decks. In this study, conventional and ChromX reinforcement are evaluated in conjunction with IPANEX and Xypex.

The corrosion resistance of the reinforcement is evaluated using the rapid macrocell test and two bench-scale tests: the Southern Exposure and cracked beam. The test methods are described in Chapter 2. Corrosion activity is monitored using macrocell corrosion rate, corrosion potential, and linear polarization resistance (LPR); Southern Exposure specimens are sampled for chloride content upon corrosion initiation.

A 100-year service life cost analysis of the corrosion protection systems under study is conducted to establish their life expectancy and cost-effectiveness compared to the use of conventional bars. This analysis is based on the construction and maintenance costs of these systems in the states of Oklahoma and Kansas, and is based on the mean chloride thresholds and corrosion rates obtained in this study. This approach is commonly used in life expectancy prediction, but it fails to account for the variability in corrosion. Therefore, a Monte Carlo simulation is also used to predict service life using the results from this study and previous studies at the University of Kansas (Ji et al. (2005), Draper (2009), Darwin et al. (2011), O'Reilly et al. (2011), Darwin et al. (2013), Farshadfar et al. (2017), O'Reilly et al. (2021)). The Monte Carlo simulation is used to treat service life for corrosion protection systems as a range, as opposed to a fixed number, since the critical chloride corrosion threshold and time to corrosion initiation values used to calculate it are highly varied.

CHAPTER 2: EXPERIMENTAL WORK

2.1 GENERAL

This chapter describes the experimental methods used in this study. The gradual nature of corrosion requires experimental methods to induce corrosion at a faster pace. One way to address the time issue is to use methods that accelerate chloride exposure. ASTM International provides standard accelerated testing procedures, such as the cracked beam and rapid macrocell tests (Annexes A1 and A2 of ASTM A955-19), that expedite the corrosion of steel bars to evaluate their corrosion resistance. In this study, the Southern Exposure test is used in addition to the cracked beam and rapid macrocell tests. The two bench-scale tests, cracked beam and Southern Exposure, use reinforcement cast in concrete to evaluate the corrosion resistance, while the rapid macrocell test exposes reinforcement to a simulated pore solution with and without NaCl.

2.1.1 Overview

The corrosion protection systems evaluated in this study employ epoxy-coated (ASTM A775), hot-dip and continuously galvanized (ASTM A767 and A1094 or HDG and CG) respectively), and ChromX (ASTM A1035 Type CS) reinforcement, as well as IPANEX and Xypex waterproofing chemical admixtures. Cracked beam and Southern Exposure are ponded with a 15% (6.04 molal ion) NaCl solution and are subjected to cyclic wetting and drying for 96 weeks. The rapid macrocell tests take 15 weeks. Corrosion rates and potentials are measured in all specimens, and concrete samples are taken from Southern Exposure specimens to measure the chloride content at the level of the anode upon corrosion initiation; cracked beam specimens are not sampled for chloride content as they allow chlorides to reach the anode at the start of testing.

2.2 MATERIALS AND AGGREGATE PROPERTIES

Tests were performed on No. 5 ASTM A775 epoxy-coated, ASTM A767 and A1094 galvanized bars, and ChromX (ASTM A1035 Type CS) bars, the latter with a nominal 9% chromium content (under the trade name ChromX) in the as-received condition, as well as with intentional perforations in the coated bars. Three heats of ASTM A615 conventional reinforcement (Conv) were also evaluated; Conv-A, B, and C bars are the conventional bars used to produce the ECR, A767, and A1094 reinforcing bars, respectively. A second heat of epoxy-coated bars (ECR 2) was used for additional rapid macrocell tests that were beyond the original scope in the study. The chemical compositions of the reinforcing bars are listed in Table 2.1. Mill certificates for Conv-B and Conv-C were not provided.

Table 2.1: Chemical composition of reinforcing steels (provided by manufacturers)

Material	C%	Mn%	P%	S%	Si%	Cu%	Ni%	Cr%	V%	Mo%	Sn%	N_2%	Al
ECR 1, Conv-A	0.42	0.72	0.011	0.039	0.21	0.22	0.13	0.3	0.001	0.021	0.006	-	0.003
ECR 2	0.03	1.23	0.012	0.038	0.26	0.33	0.09	0.17	-	0.023	0.009	0.013	-
A1035 (ChromX)	0.09	0.59	0.012	0.017	0.39	0.18	0.09	9.36	0.019	0.02	0.008	0.01	-

The materials used in the concrete mixtures were:

Water – Municipal tap water from the city of Lawrence.

Cement – Type I/II Ash Grove portland cement.

Coarse Aggregate – Crushed limestone from Midwest Concrete Materials.

Nominal maximum size = 0.75 in. (19 mm), bulk specific gravity (SSD) = 2.58, absorption = 2.3%, unit weight = 95.9 lb/ft^3 (1534 kg/m^3).

Fine Aggregate – Kansas River sand. Bulk specific gravity (SSD) = 2.62, absorption = 0.8%, fineness modulus = 2.51.

Air-Entraining Agent – Daravair 1400, a saponified rosin-based air-entraining agent manufactured by W. R. Grace.

Corrosion inhibitors – IPANEX and Xypex are waterproofing chemical admixtures. IPANEX is an inorganic admixture composed of calcium silicate hydrate (C-S-H) compounds (Cement Chemistry Systems 2016), and Xypex (C-500NF Admixture used in this study) reacts with byproducts of cement hydration process to form "non-soluble crystalline structures" in concrete pores in the presence of water (XYPEX 2020).

The concrete mixture proportions are shown in Table 2.2. The mixtures have a water-cement ratio of 0.45 and are targeted to have a slump of 3 ± 0.5 in. (75 ± 13 mm), air content of 6 ± 1%, and a 28-day compressive strength of 4000 psi (27.6 MPa).

For mixtures containing IPANEX and Xypex, the corrosion inhibitors were added at a dosage rate of 75 oz/yd^3 (2901 ml/m^3) and 6 lb/yd^3 (3.56 kg/m^3), respectively.

Table 2.2: Mixture proportions for lab specimens based on SSD aggregate

Cement **lb/yd^3 (kg/m^3)**	**Water** **lb/yd^3 (kg/m^3)**	**Coarse Aggregate** **lb/yd^3 (kg/m^3)**	**Fine Aggregate** **lb/yd^3 (kg/m^3)**	**Air-Entraining Agent** **oz/yd^3 (mL/m^3)**
598 (355)	269 (160)	1484 (880)	1435 (851)	8.5-9.5 (329-367)

2.3 CORROSION MONITORING AND MEASUREMENTS

Monitoring the corrosion of steel reinforcing bars is particularly challenging since the steel is cast inside the concrete, which renders visual inspection of the reinforcing bars impossible. By the time there are visible signs of staining and spalling at the surface, significant damage has occurred (O'Reilly et al. 2011). Methods other than visual inspection are, therefore, required to monitor corrosion in reinforced concrete. The corrosion measurement and monitoring methods used in this study are described below.

2.3.1 Corrosion Potential

Corrosion potential is the tendency of a metal to be oxidized to its ions. The corrosion potential signifies the relative thermodynamic stability of a metal, which depends on environmental conditions. The corrosion potential only indicates the likelihood of corrosion and does not indicate the corrosion rate. Corrosion potential is measured with respect to a reference electrode with known properties, such as the Copper-Copper Sulfate Electrode (CSE). The CSE consists of a copper rod immersed in a saturated copper sulfate solution. ASTM C876 specifies guidelines for taking and interpreting corrosion potential measurements on uncoated reinforcing bars. The guidelines for evaluating corrosion behavior based on the corrosion potential with reference to a CSE are given in Table 2.3 (ASTM C876). These guidelines only apply to uncoated conventional reinforcing bars.

Table 2.3: CSE corrosion potential interpretation according to ASTM C876

Measured Potential: CSE (mV)	Corrosion Activity
Greater than –200	Greater than 90% probability corrosion is not occurring
–200 to –350	The corrosion activity is uncertain
More negative than –350	Greater than 90% probability corrosion is occurring

2.3.2 Macrocell Corrosion Rate

Macrocell corrosion in reinforced concrete occurs when the anode and the cathode are on different bars, forming a corrosion circuit through electrical connections between the bars, while corrosion occurring locally on the same bar is called microcell corrosion. The electric current flowing from the anode to the cathode required for the corrosion process can be measured to

determine the corrosion rate, which may be expressed in terms of current density ($\mu A/cm^2$) or converted to material loss at the surface over time (μm/year) as follows:

$$r = k\frac{ia}{nF\rho} \tag{2.1}$$

where

r = corrosion rate, μm/year

k = conversion factor, $315360\frac{A \cdot \mu m \cdot s}{\mu A \cdot cm \cdot yr}$

i = current density, $\mu A/cm^2$

a = atomic weight of the corroding metal, g/mol

n = number of electrons lost per atom of metal oxidized

F = Faraday's constant, 96,485 Coulombs/equivalent

ρ = density of metal, g/cm^3

For iron, a = 55.85 g/mol, n = 2, and ρ = 7.87 g/cm^3: Equation (2.1) simplifies to:

$$r = 11.6i \tag{2.2}$$

For zinc, a = 65.38 g/mol, n = 2, and ρ = 7.13 g/cm^3: Equation (2.1) simplifies to:

$$r = 15.0i \tag{2.3}$$

Faraday's law is used to determine corrosion rate in the rapid macrocell, Southern Exposure, and cracked beam tests (described in Section 2.4) where the anode is exposed to a corrosion-inducing environment. The rapid macrocell test involves an anode and a cathode immersed in concrete pore solution in separate containers. The Southern Exposure and cracked beam tests use specimens with top and bottom mats of steel reinforcing bars, which serve as the anode and the cathode, respectively, in a concrete slab where chlorides are applied to the surface

to reach the anode. In each case, the anode and cathode are electrically connected across a resistor, which enables measuring the corrosion current using Ohm's law.

$$i = 10^6 \times \frac{V}{RA} \tag{2.4}$$

i = current density, μA/cm^2

V = measured voltage drop across resistor, volts

R = resistance, ohms

A = surface area of the anode, cm^2

The current density calculated from Eq. (2.4) is used in Eq. (2.1) to calculate corrosion rate.

2.3.3 Linear Polarization Resistance

Linear polarization resistance (LPR) is used to measure the total corrosion rate, which includes both macrocell and microcell corrosion of a metal by measuring the metal's response to an applied voltage. The polarization resistance curve is populated by measuring the potential shifts after applying a range of currents to the sample or measuring the current shifts after applying a range of potentials (Figure 2.1). The polarization resistance is defined as the slope of the potential-current curve as follows (Jones 1996):

$$R_p = \left[\frac{\Delta\varepsilon}{\Delta i}\right]_{\varepsilon \to 0} \tag{2.5}$$

where

R_p = polarization resistance

$\Delta\varepsilon$ = imposed potential change

Δi = current density change caused by $\Delta\varepsilon$

As shown in Figure 2.1, a corroding metal exhibits a potential E_{corr} and a current density i_{corr} with no externally applied voltage; the potential and current density are shifted by Δi and, in

turn, $\Delta\varepsilon$ under the applied voltage used for determining the LPR, respectively. Polarization resistance is inversely proportional to corrosion current density for small changes in the potential where the polarization curve is linear:

$$i = \frac{\beta_a \beta_c}{2.3 R_p (\beta_a + \beta_c)} \tag{2.6}$$

where

β_a, β_c = anodic and cathodic Tafel constants, V/decade

R_p = polarization resistance

Accordingly, assuming anodic and cathodic Tafel constants of 0.12 V/decade yields a curve with the following slope over a region of approximately ± 20 mV with respect to E_{corr}:

$$i = \frac{0.026}{R_p} \tag{2.7}$$

Equation (2.7) is used to determine the corrosion current densities based on LPR data.

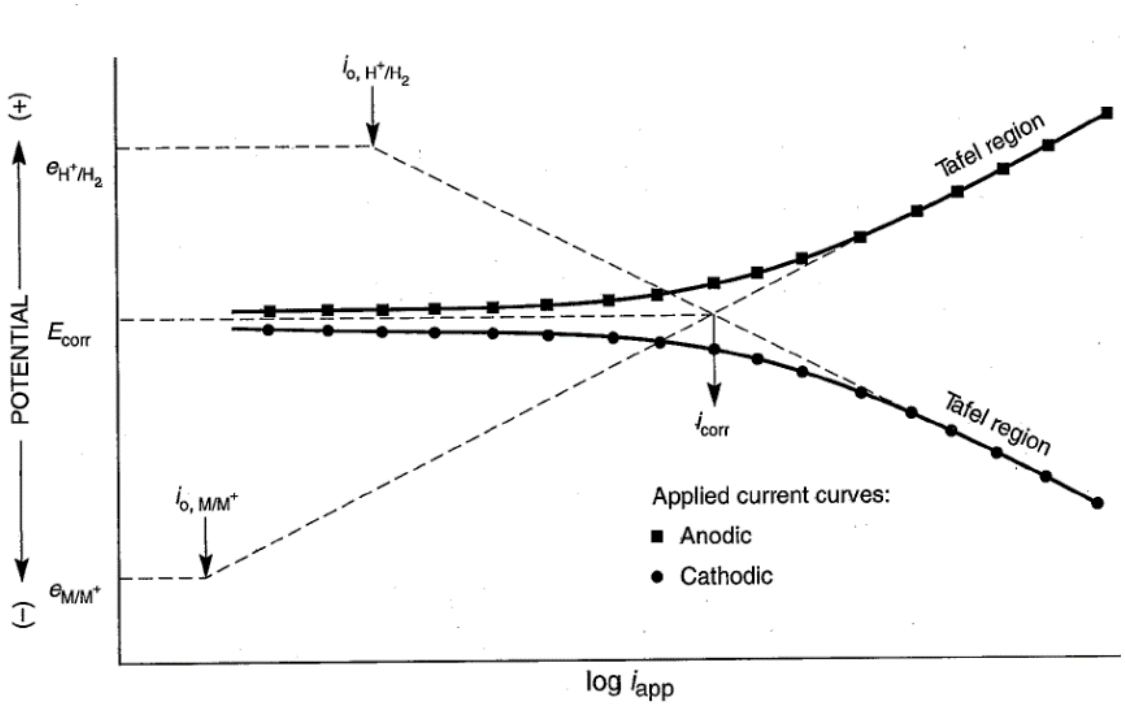

Figure 2.1: Linear polarization resistance curves (Jones 1996)

2.4 TEST METHODS

Comparisons of the corrosion behavior of steel reinforcing bars are made using the rapid macrocell, the Southern Exposure (SE), and the cracked beam (CB) tests. A description of each of these test methods follows.

2.4.1 Rapid Macrocell Test

The rapid macrocell test was originally developed at the University of Kansas under the SHRP program (Martinez et al. 1990, Chappelow et al. 1992) and updated under the NCHRP-IDEA program (Darwin 1995, Senecal, Darwin, and Locke Jr 1995), work for the South Dakota Department of Transportation (Darwin et al. 2002), and an NSF-KDOT study at KU (Ji, Darwin, and Browning 2005). The test has been incorporated in ASTM A955 as a qualification test for stainless steel reinforcing bars but is used as a method of comparison for all reinforcing steel types (Sturgeon et al. 2010). The rapid macrocell test is used to measure the comparative performance of corrosion protection systems in a short time.

The rapid macrocell test consists of an anode and a cathode, as shown in Figure 2.2 and outlined in Annex A2 of ASTM A955/A955M-19. In the rapid macrocell test, the reinforcement is exposed to chlorides added to a pore solution; one liter of the pore solution consists of 974.8g of distilled water, 18.81g of potassium hydroxide (KOH), and 17.87g of sodium hydroxide (NaOH). The anode consists of one bar immersed upright in the pore solution with 15% NaCl (6.04 molal ion concentration) added, and the cathode consists of two bars immersed upright in the pore solution. At the anode and the cathode, the containers are filled with the solution to a depth of 3 in. (75 mm). The solution is changed every five weeks; the test takes 15 weeks to complete. Air, scrubbed to remove CO_2, is bubbled into the pore solution at the cathode to ensure

an adequate supply of oxygen for the cathodic reaction. Deionized water is added to the containers, as needed, to maintain a constant depth of the solution in the containers. The anode and cathode are electrically connected across a 10-ohm resistor. A salt bridge, made from potassium chloride (KCl) and agar, provides ionic connection between the anode and the cathode. In accordance with ASTM A955/A955M-19, at least five rapid macrocell specimens are required to evaluate a reinforcing steel type.

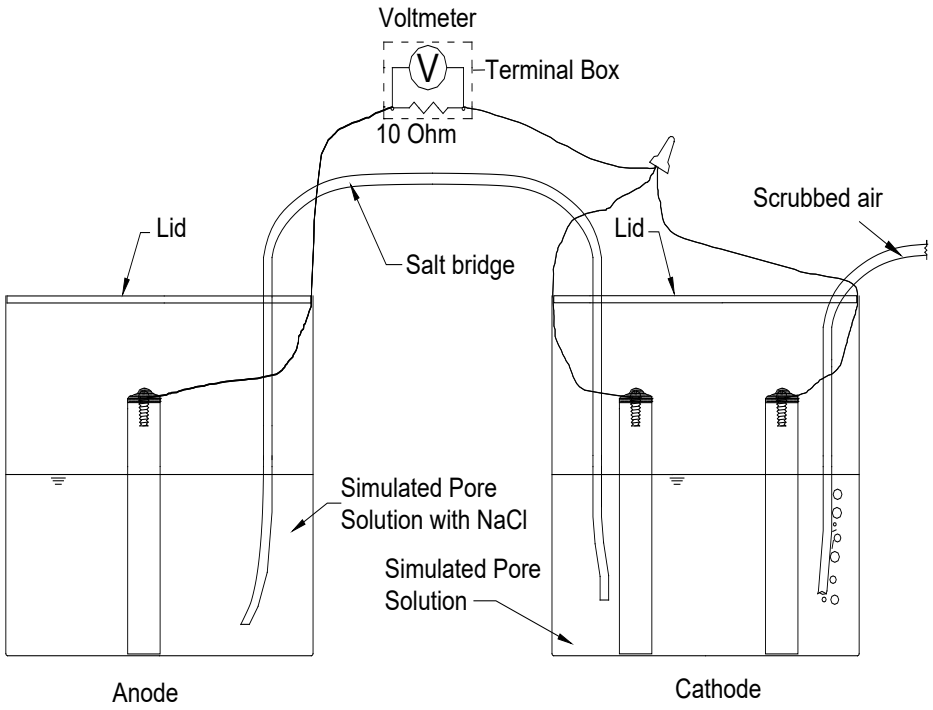

Figure 2.2: Rapid macrocell test

2.4.1.1 Fabrication

Fabrication of rapid macrocell specimens proceeds as follows:

Reinforcing bars are cut to a length of 5 in. (127 mm) with a band saw. One end of each bar is drilled and tapped to receive a 3/8-in. (10-mm) long stainless steel screw with 10-24 threads. For coated reinforcing bars (ECR or galvanized) with intentional damage, the coating is penetrated to a depth of 15 mils (0.4 mm) with a 0.125-in. (3-mm) diameter four-flute drill bit using a milling machine. Two holes are machined on each side of the bar approximately 1 in. (25 mm) and 2 in.

(50 mm) from the bottom. Bare and galvanized bars are soaked in acetone for a minimum of two hours and cleaned to remove any oil. Epoxy-coated bars are cleaned with warm soapy water, rinsed, and allowed to dry. 16-gauge (1.5 mm^2) wire leads are connected to the test bars using a 10-24 × 3/8-in. (10-mm) stainless steel screw. Multiple coats of epoxy (3M Scotchkote rebar liquid patch) are applied to the electrical connection to protect it from corrosion. Vinyl caps filled with epoxy (3M Scotchkote rebar liquid patch) are applied to the end of coated specimens to protect the cut end from corrosion. Bars are placed upright in the plastic containers and the pore solution is added to a depth of 3 in. (76 mm). Bars are connected to a terminal box at the start of testing. In addition to the coated bars, the matching conventional bars were also capped to maintain a consistent testing condition across all these specimens; ChromX bars were not capped.

A modified rapid macrocell specimen is used for bent anode bars to determine the effects of field fabrication on the corrosion resistance of coated reinforcement as shown in Figure 2.3. The modified test uses a single anode bar cut to a length of 12 in. (305 mm), bent around a 3.75-in. (95-mm) diameter pin, and submerged to a depth of 1.75 in. (64 mm) in a simulated pore solution with a 15% (6.04 molal ion) sodium chloride content. The coating is not penetrated on bent bars. The cathode consists of four No. 5 reinforcing bars submerged to a depth of 3 in. (76 mm). The change in the solution depth at the anode and the number of cathode bars is used to keep the ratio of the anode bar area to the cathode bar area the same as in the standard macrocell test. The test is otherwise identical to the standard macrocell test. Damage caused on the coating of epoxy-coated reinforcement due to bending is repaired with 3M Scotchkote rebar liquid patch before testing.

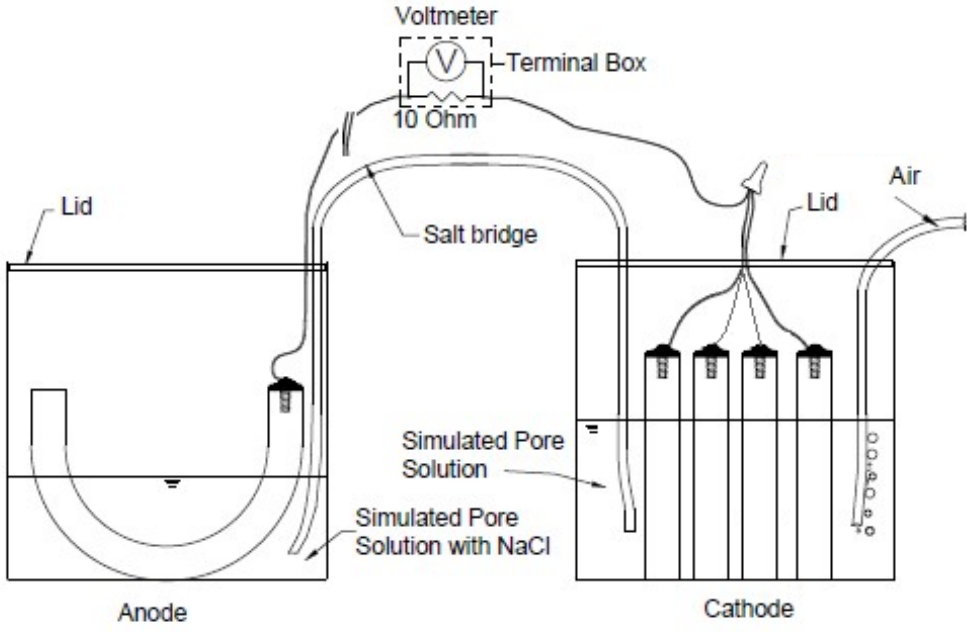

Figure 2.3: Rapid macrocell test with a bent bar

2.4.1.2 Rapid Macrocell Test Procedure

The rapid macrocell test is a 15-week test. The corrosion rate and corrosion potential measurements are taken daily for the first week and weekly thereafter. The area on the anode bar in contact with the solution is used to calculate the corrosion rate, which is calculated based on the voltage drop measured across a 10-ohm resistor using Faraday's equation:

$$\text{Rate} = K \frac{V\ m}{n\ F\ D\ R\ A} \tag{2.8}$$

where the rate is given in μm/yr,

K = conversion factor = $31.5 \cdot 10^4$ amp·μm·sec/μA·cm·yr

V = measured voltage drop across a resistor, millivolts

m = atomic weight of the metal (for iron, m = 55.8 g/mol; for zinc, m = 65.4 g/mol)

n = number of ion equivalents exchanged (for iron and zinc, n = 2 equivalents)

F = Faraday's constant = 96485 coulombs/equivalent

D = density of the metal, g/cm^3 (for iron, D = 7.87 g/cm^3; for zinc, D = 7.14 g/cm^3)

R = resistance of the resistor, ohms = 10 ohms for the test

A = surface area of anode exposed to the solution

In some cases, the corrosion rate may appear to be negative, especially when low corrosion rates are observed. The negative corrosion rate does not indicate negative corrosion; it is rather caused by minor differences in the oxidation rate between the single anode bar and the cathode bars. The negative corrosion rates usually occur when corrosion resistant bars, such as stainless steel or epoxy-coated bars, are tested since these bars exhibit very low corrosion rates. Negative corrosion rates can also occur in specimens with galvanized bars since the cathode may also corrode rapidly in the alkaline pore solution used in the rapid macrocell test. As discussed in Chapter 1, zinc can corrode rapidly in high-pH environments.

In addition to determining the corrosion rate by taking voltage readings across a 10-ohm resistor, the corrosion potential is measured at both the anode and cathode using a silver-silver chloride electrode. Linear polarization resistance (LPR) measurements, as discussed in Section 2.3.3, are performed every 3 weeks.

The specimens are photographed upon completion of the test. Protective caps on the coated bars are removed and the specimens are inspected for under-the-cap corrosion; the test is invalid if under-the-cap corrosion is found; under-the-cap corrosion did not occur in any of the specimens in this study. A disbondment test is conducted on ECR specimens with intentional damage. A sharp utility knife is used to cut through the epoxy at 45° forming an “X” at the intentional hole. The coating is then peeled back as far as possible. If the disbondment extends more than 0.5 in. (12 mm) beyond the hole, the coating is considered to have undergone total disbondment. A transparent sheet with a 0.01-in. (0.254-mm) grid is used to measure the disbonded area.

The pH of the pore solution in the rapid macrocell test is about 13.8, which is somewhat higher than that of ordinary portland cement concrete, which ranges from 12.5 to 13.0 (Behnood et al. 2016). As mentioned in Chapter 1, the stability of the zinc passive layer is highly dependent on the pH of the environment; the passive layer is stable below a pH of 13.3; above 13.3, zinc tends to form large non-protective crystals (Andrade and Macias 1988). Exposing galvanized reinforcement to a high-pH liquid environment is, therefore, not conducive to the formation of a protective passive layer on the zinc coating, and the zinc coating rapidly corrodes in highly alkaline pore solution. Therefore, rapid macrocell test results are not representative of the behavior of galvanized reinforcement in concrete. The bars in Figures 2.4 and 2.5 are representative of the anode and cathode of A767 and A1094 specimens, respectively, after 15 weeks of exposure to the test. Figures 2.4 and 2.5 show that the zinc coating immersed in the pore solution is lost and bare steel is visible. Since the zinc rapidly corrodes regardless of the presence of chlorides, corrosion occurs at both anode and cathode of rapid macrocell test specimens. Cathode bars have twice the surface area of anode bars; this greater area in the cathode can frequently result in apparent negative corrosion rates for galvanized reinforcement. Accordingly, results of galvanized reinforcement in the rapid macrocell test are not presented in Chapter 3.

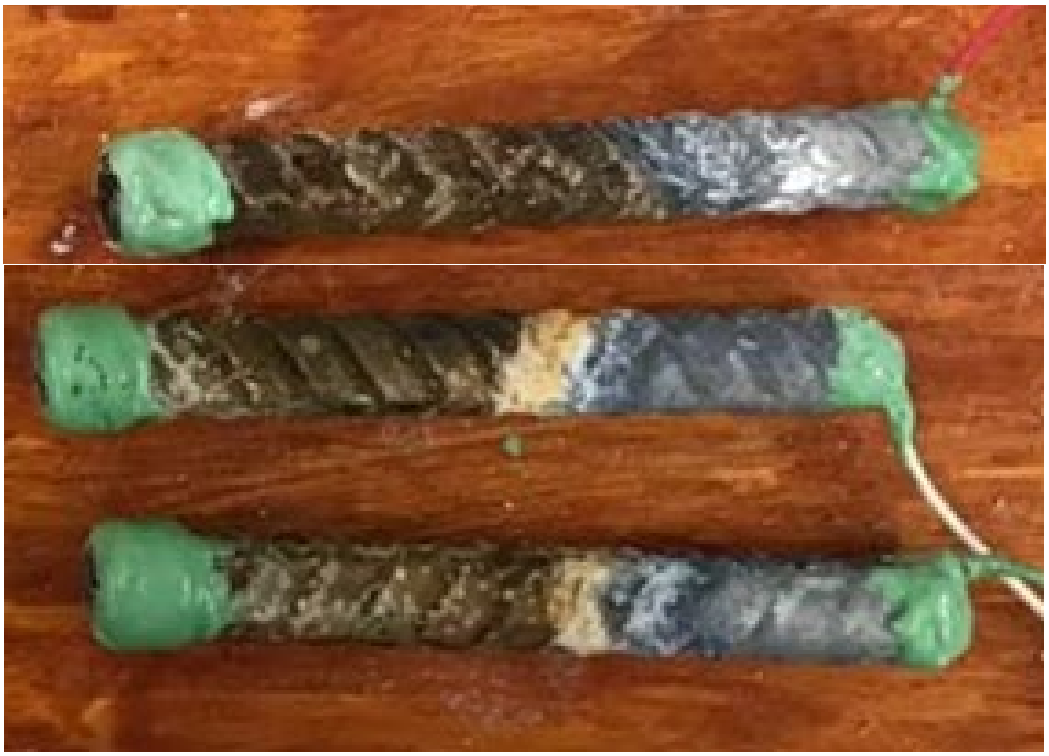

Figure 2.4: Specimen A767-1 anode bar (top) and cathode bars (bottom) after 15 weeks of rapid macrocell testing

Figure 2.5: Specimen A1094-4 anode bar (top) and cathode bars (bottom) after 15 weeks of rapid macrocell testing

2.4.2 Bench-Scale Tests

Bench-scale tests, such as the Southern Exposure, ASTM G109, and cracked beam tests, have been frequently used to evaluate the corrosion performance of steel reinforcing bars. Although these tests typically require one to two years to complete, they qualify as accelerated tests. Of these tests, the Southern Exposure and cracked beam tests have been found to give useful data (Darwin et al. 2014).

The Southern Exposure (SE) and cracked beam (CB) test specimens are shown in Figure 2.6. These specimens are cast in an inverted position. The specimens are subjected to alternative cycles of wetting (exposure to 15% by weight NaCl solution) and drying. Southern Exposure specimens (Figure 2.6a) are 12 × 12 × 7 in. (305 × 305 × 178 mm). Twelve-inch (305 mm) long No. 5 (No. 16) reinforcing bars are placed inside the formwork in two mats before casting. The top and bottom mats have two and four bars, respectively, each with 1-in. (25.4-mm) clear cover. The bars in the top and bottom mats are electrically connected through a terminal box across a 10-ohm resistor to allow for the macrocell corrosion rate measurements. A 0.75-in. (19-mm) deep concrete dam is integrally cast with the specimen to contain the ponded salt solution. Southern Exposure tests represent conditions in uncracked reinforced concrete.

Cracked beam specimens (Figure 2.6b), measuring 12 × 6 × 7 in. (305 × 152 × 178 mm), are half the width of the Southern Exposure specimens. The top mat is a single No. 5 (No. 16) bar; the bottom mat has two No. 5 (No. 16) bars. Before fabrication, a 12-mil (0.3-mm) thick × 6-in. (152-mm) long stainless steel shim is placed in the formwork; the shim is in direct contact with the reinforcing bar serving as the anode. Since the specimens are cast upside down, the shim is placed on the bottom of the form. The shim is removed 12-24 hours after casting. The simulated

crack formed by the shim removal results in direct infiltration of chlorides at the beginning of the test. Cracked beam tests represent conditions in cracked reinforced concrete.

Both the Southern Exposure and cracked beam tests have a duration of 96 weeks. With conventional uncoated reinforcement, SE specimens typically exhibit corrosion initiation after 8 to 16 weeks of testing while CB specimens exhibit corrosion initiation during the first week. As in the rapid macrocell tests, epoxy-coated and galvanized bars are evaluated using specimens with the epoxy or zinc intact or penetrated. Coatings are milled to a depth of 15 mils (0.4 mm) to cut ten 0.125-in. (3-mm) diameter holes (5 on each side) on the coating surface to simulate defects or damage. In the current study, the galvanized and epoxy-coated bars were also evaluated in the Southern Exposure test with a bent anode bar to determine the effects of field fabrication on corrosion resistance (Figure 2.7).

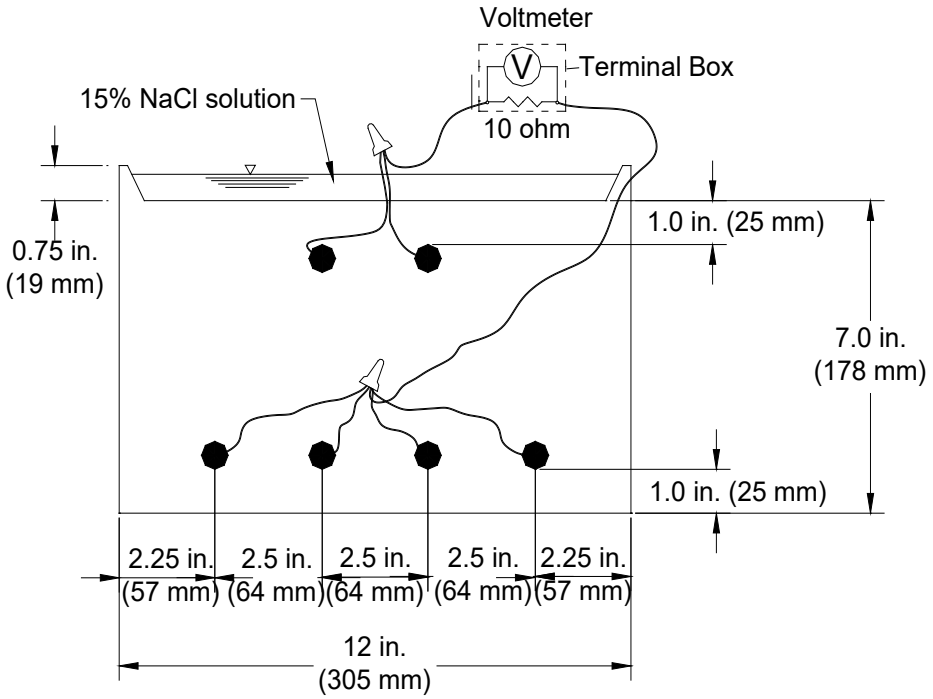

Figure 2.6a: End view of Southern Exposure (SE) specimen

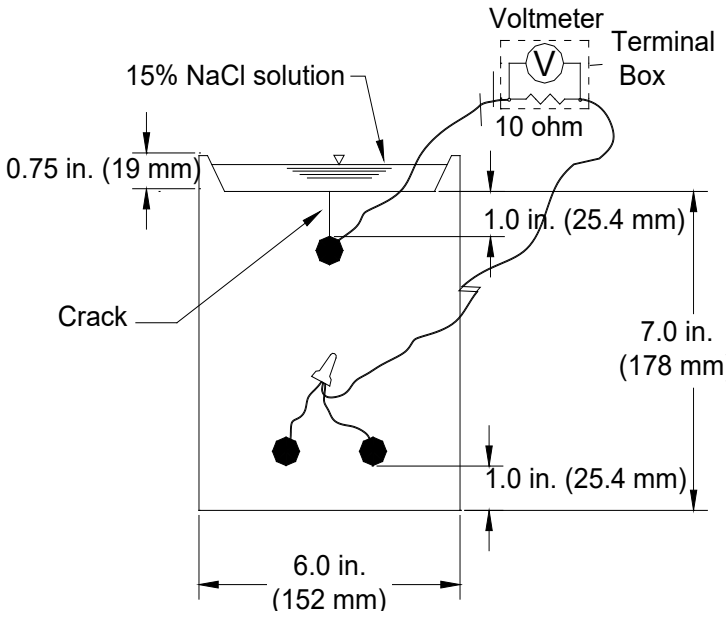

Figure 2.6b: End view of cracked beam (CB) specimen

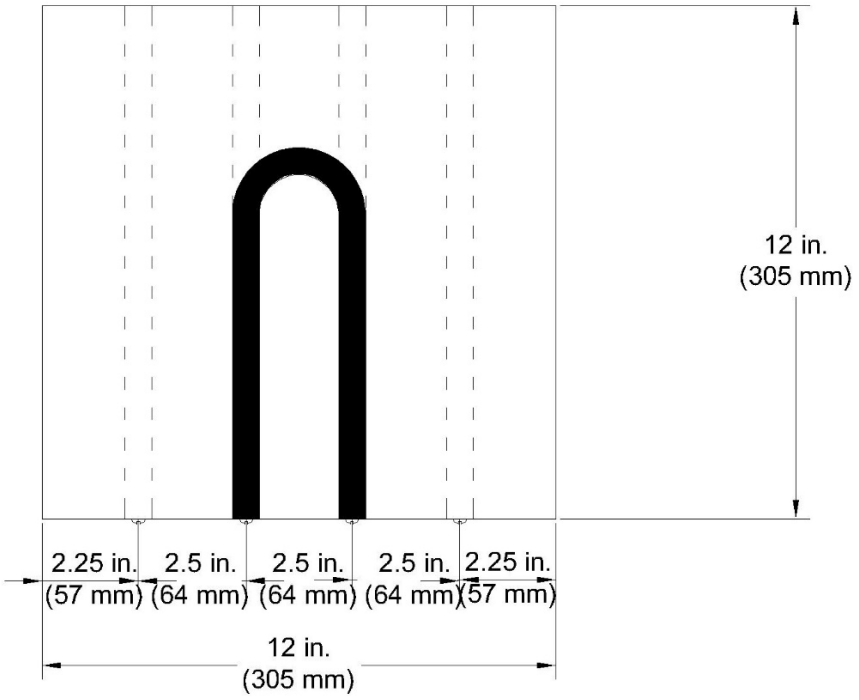

Figure 2.7: Top view of Southern Exposure specimen with a bent anode bar

2.4.2.1 Fabrication

The Southern Exposure and cracked beam specimens are fabricated as follows:

Reinforcing bars are cut to 12 in. (305 mm) with a band saw. Bars that are to be bent and placed at the top mat in the Southern Exposure specimens are cut to a length of 15 in (381 mm).

Epoxy-coated bars are covered with padding for protection against unintentional damage during machining. Both ends of the bars are drilled and tapped to a depth of 3/8 in. (10 mm) with 10-24 threading. When appropriate, epoxy-coated or galvanized bars are intentionally damaged, as described in Section 2.2.2. The coating is not penetrated on bent bars. Epoxy-coated bars are cleaned with warm soapy water, rinsed, and allowed to dry. Conventional, galvanized, and ChromX reinforcing bars are soaked in acetone for a minimum of two hours and cleaned to remove any oil. The forms are assembled, and the reinforcement is attached. Reinforcing bars with penetrations in the coating are aligned so that the holes face the top and bottom of the specimen. The formwork and reinforcement are held in place using 10-24 threaded stainless-steel machine screws. Specimens are cast using concrete with the mixture proportions shown in Table 2.2. Specimens are cast in an inverted position and filled in two layers, with each layer consolidated using a 0.75- in. (19-mm) diameter vibrator. The free surface of the concrete (the bottom of the specimen as they are cast upside-down) is finished with a trowel. Specimens are cured for 24 hours at 72 ± 3° F (22 °C). Plastic sheets are used to limit evaporation. Stainless steel shims are removed from cracked beam specimens 12 to 24 hours after casting, when the concrete has set. Forms are removed after 24 hours. Specimens are cured for an additional two days in a plastic bag containing deionized water, then air-cured for 25 days. Before starting the test, wire leads are connected to the test bars using 10-24 × 3/8-in. (10-mm) stainless steel screws. Epoxy (Pond Shield Non Toxic Epoxy) is applied to the vertical sides of the specimens and the top surface of the dams, while the top and bottom surfaces of the specimens are left uncoated. The two mats of steel are connected to the terminal box. Specimens are left connected across the 10-ohm resistor, except when potential and LPR (as described in Section 2.3) readings are taken. Specimens are placed on 1.5 × 1.5 in. (38 × 38 mm) lumber to allow airflow under the specimens. Tests begin 28 days after casting.

2.4.2.2 Test Procedure

The Southern Exposure and cracked beam tests begin with 12 weeks of ponding and drying, followed by 12 weeks of ponding, for a total of 24 weeks. This exposure regime is then repeated for the duration of the test. The tests conclude after 96 weeks. The procedures are described below.

Ponding and Drying Cycles:

A 15% by weight NaCl solution (450 g of NaCl dissolved in 2550 g of deionized water) is ponded on the surface of the specimens. The temperature is maintained at 72 ± 3° F (22 °C). CB specimens receive 300 mL of solution, and SE specimens receive 600 mL of solution. The specimens are covered with plastic sheets during ponding to limit evaporation. Readings are taken on day 4. After the readings are completed, the specimens are vacuumed to remove the NaCl solution, and a heating tent is placed over the specimens. The tent maintains the specimens at 100 ± 3 °F (38 °C) for three days. The tent is then removed, and the specimens are again ponded at 72 ± 3 °F (22 °C) with the NaCl solution to start the second week of testing. Ponding and drying cycles continue for 12 weeks.

Ponding Cycle:

After 12 weeks of ponding and drying, specimens are ponded for 12 weeks with the 15% NaCl solution and covered with plastic sheets. The NaCl solution remains on the specimens throughout the 12 weeks at 72 ± 3 °F (22 °C). Readings continue to be taken weekly. Deionized water is added to maintain the solution depth on the specimens during this time. After 12 weeks, the specimens are again subjected to the weekly ponding and drying cycles.

Corrosion rate and corrosion potential measurements are taken weekly; linear polarization resistance (LPR) measurements are taken every four weeks. The voltage drop between the anode and the cathode is recorded and used to calculate the corrosion rate using Faraday's equation and

Ohm's law, as described in Section 2.3.2. Following the measurement of the voltage drop, the electrical connection is switched off to measure corrosion potentials. The specimens remain disconnected for a minimum of two hours before measuring corrosion potentials and LPR readings. Potentials are measured with respect to a silver-silver chloride electrode.

A schematic of a heating tent is shown in Figure 2.8. The tents are 8 ft (2.44 m) long by 4 ft (1.22 m) wide by 3.5 ft (1.07 m) high. The tents are fabricated using 0.5-in. (13 mm) plywood with six 1.5 × 1.5 in. (38 × 38 mm) pieces of dimension lumber. Two sheets of plastic cover the space between the lumber. Three 250-watt heating lamps are spaced along the inside roof of the tent. The lamps are 1.5 ft above the surface of the bench-scale specimens. Temperature is controlled with a thermostat.

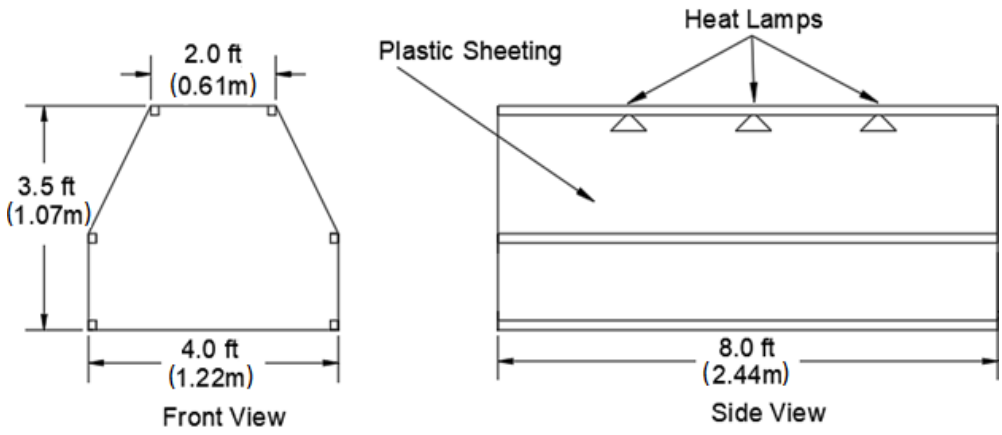

Figure 2.8: Heating tent dimensions

In the study, some epoxy-coated bars were exposed to accelerated weathering following ASTM G154 Cycle 1. ASTM G154 uses a combination of elevated temperatures (50–60ºC), ultraviolet (UV) light exposure, and moisture to simulate accelerated weathering of plastics and epoxies. Epoxies are susceptible to degradation when exposed to UV light and moisture (Kumar, Singh, and Nakamura 2002, Rezig et al. 2006). ASTM D3963 limits outdoor exposure without protection to a maximum of two months. Exposure for 1000 hours in accordance with ASTM G154

Cycle 1 is, on average, equivalent to one year of natural weathering due to outdoor storage (Fedor and Brennan 1996). To characterize the average outdoor exposure from different locations, the sites chosen by Fedor and Brennan, where samples of different polymers were exposed to natural weathering, were in a subtropical climate (Florida), a desert climate (Arizona), and a northern industrial climate (Ohio). In ASTM G154 Cycle 1, 8 hours of UV light at 60 ± 3° C are followed by 5 hours of condensation at 50 ± 3° C.

Figure 2.9a compares an epoxy-coated bar after exposure to accelerated weathering following ASTM G154 Cycle 1 before corrosion testing with an epoxy-coated bar in the as-received condition. Figure 2.9b highlights the extent of discoloration of the epoxy coating after the accelerated weathering by comparing the end of the bars, which was protected.

(a) (b)

Figure 2.9: (a) Epoxy-coated bar without (top) and after (bottom) exposure to ASTM G154 Cycle 1, (b) close up of the damaged epoxy-coated bar after exposure to ASTM G154 Cycle 1 before corrosion testing

2.5 CHLORIDE SAMPLING FOR SOUTHERN EXPOSURE SPECIMENS

Upon the initiation of corrosion, Southern Exposure specimens are drilled to obtain chloride samples at the level of the top mat of steel (anode). Cracked beam specimens are not sampled for chlorides because the crack allows direct infiltration of the salt solution. For conventional reinforcement, corrosion initiation is marked by voltage drops that signify macrocell corrosion rates above 0.3 µm/yr and top-mat corrosion potentials more negative than -0.350 V

with respect to a CSE in accordance with ASTM C876. For coated bars, corrosion initiation is marked by sudden voltage drops, which are often smaller than those signifying corrosion in conventional reinforcement.

Chloride Sampling Procedure

Chloride sampling is performed once corrosion has initiated, as determined when the weekly corrosion measurements are taken. Before sampling, the specimen is cleaned on all four sides with tap water and soap. Afterward, the specimens are rinsed with deionized water. After drying, the specimens are marked for drilling so that the top of the drill bit is level with the top of the top mat of steel (Figure 2.10). Samples are obtained from the sides of the specimen, perpendicular to the steel bars, using a 0.25-in. (6.4-mm) masonry drill bit. Three samples are taken from each side of the specimen for a total of six samples. Sample sites are taken along the side of the specimen, with no samples within 1 in. (25 mm) of the edge of the specimen.

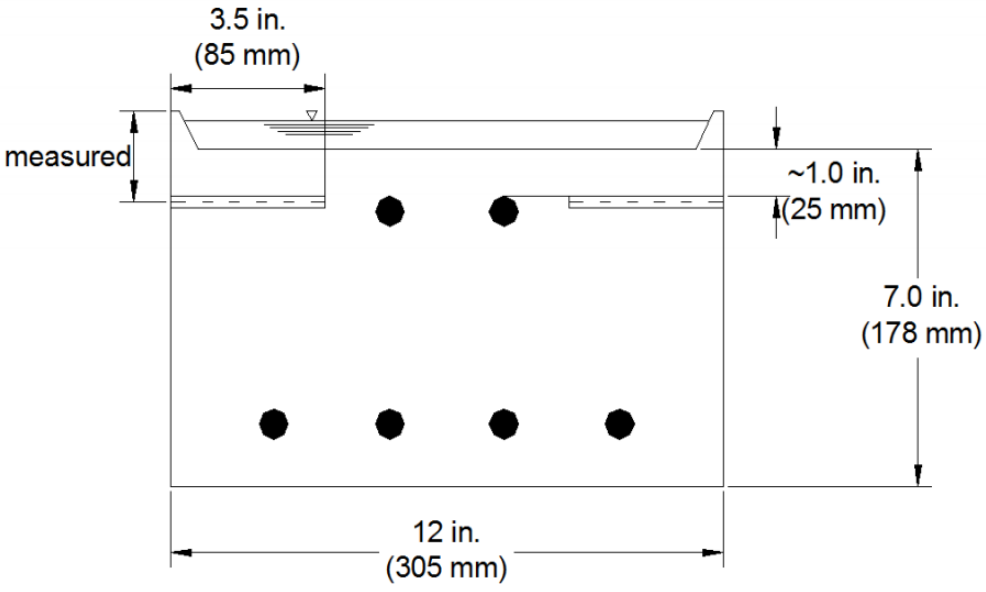

Figure 2.10: Southern Exposure chloride sampling

A 0.5-in. (12.7-mm) deep hole is initially drilled at each sample site. The collected powder is then removed and discarded. The drill bit is then rinsed with distilled water, re-inserted, and

used to penetrate to a depth of 3.5 in. (89 mm). This sample is collected in a plastic bag and labeled for analysis. Each sample provides approximately four grams of material. The drill bit is rinsed with distilled water before obtaining the next sample. The holes left from drilling are filled with clay, and the specimen is reconnected for continued testing.

Chloride Analysis

The concrete was sampled in accordance with ASTM C1218 and analyzed for water-soluble chlorides in accordance with AASHTO T 260-97. The potential with respect to a chloride sensitive electrode (Oakton by Cole-Parmer Combination Ion-Selective Electrode (ISE), Chloride (Cl)) is measured throughout the titration. The procedure gives the chloride concentration in terms of percent chloride by mass of the sample. In this study, values are presented in lb/yd^3 using the unit weight of concrete, taken as 3786 lb/yd^3.

2.6 TEST PROGRAM

The objectives of this study are highlighted in Section 1.6. They cover studying the effects of exposure to ultraviolet (UV) light on the corrosion resistance of epoxy-coated reinforcement (ECR), comparing the corrosion resistance of continuously galvanized reinforcement (ASTM 1094) to that of hot-dip galvanized reinforcement (ASTM A767), and investigating the paired behavior of the waterproofing admixtures and conventional and ChromX reinforcement. Table 2.4 shows the test program, including the corrosion test methods used. The table indicates the number of specimens of each type that were tested for each reinforcement type. The designations in Table 2.4 indicate whether the coating was damaged or undamaged, and if the bar was bent or exposed to UV light. The "ND" designation indicates the coating was undamaged, and the "Bent" designation indicates the bar was bent; there are no designations for damaged bars. The "UV" designation indicates exposure to UV light. The Conv-A, B, and C bars are the conventional bars

used to produce the ECR, A767, and A1094 reinforcing bars evaluated in this study, respectively. Some of the ECR bars exposed to UV light came from a second heat of steel; ECR specimens in Table 2.4 are labeled to reflect the two heats of reinforcement used (ECR1 and ECR2). ECR1-UV-1000 and ECR1-ND-UV-1000 bars were exposed to 1000 hours of an accelerated UV light exposure according to ASTM G154, equivalent to one year of natural weathering due to outdoor exposure. As described in Section 2.4.2.2, outdoor exposure corresponded to the average of sites chosen by Fedor and Brennan (1996) for the natural weathering: Subtropical climate (Florida), a desert climate (Arizona), and a northern industrial climate (Ohio). ECR1-UV-500, ECR1-UV-250, ECR2-UV-200, and ECR2-UV-100 bars were exposed to 500, 250, 200, and 100 hours of UV light exposure, respectively, as their designations indicate. The cut ends of coated bars in the rapid macrocell test were sealed with epoxy and capped to protect the ends, as described in Section 2.4.1.1; the matching conventional bars were also capped to maintain a consistent testing condition across all these specimens; ChromX bars were not capped. Cracked beam and Southern Exposure specimens containing ChromX and Conv-B reinforcing bars were also used to study the effects of waterproofing admixtures IPANEX and Xypex. The casting order and concrete properties for each batch are given in Appendices A and B, respectively. Each batch contained single specimen type (SE or CB) for each reinforcement type, except for batches with waterproofing admixtures or batches containing additional conventional, ChromX, and ECR-UV specimens to validate the repeatability of results (recast batches).

Table 2.4: Number of rapid macrocell, SE, and CB specimens for each reinforcement type in the test program

Reinforcement*	Test Method		
	Macrocell	Southern Exposure (SE)	Cracked Beam (CB)
Conv-A	6	7	6
Conv-B	6	7	7
Conv-C	6	6	3
ECR1	6	4	4
ECR2	5	-	-
ECR1-ND	6	3	3
ECR2-ND	6	-	-
ECR1-UV-1000	12	3	7
ECR1-UV-500	6	-	-
ECR1-UV-250	6	-	-
ECR2-UV-1000	5	-	-
ECR2-UV-200	6	-	-
ECR2-UV-100	6	-	-
ECR1-ND-UV-1000	6	3	3
ECR1-Bent	6	-	-
A767	6**	6	6
A767-ND	6**	6	6
A767-Bent	6**	6	-
A1094	6**	6	6
A1094-ND	6**	6	6
A1094-Bent	6**	6	-
ChromX	6	6	6
Conv-B-IPANEX	-	6	6
ChromX-IPANEX	-	6	6
Conv-B-Xypex	-	6	6
ChromX-Xypex	-	6	6

*Damaged bars in rapid macrocell specimens have four $^{1}/_{8}$ in. diameter holes in the coating (two on each side). Damaged bars in the Southern Exposure and cracked beam specimens have 10 $^{1}/_{8}$-in. diameter holes (5 on each side).

**Results are not presented in Chapter 3.

CHAPTER 3: CORROSION TEST RESULTS

This chapter presents the results of the rapid macrocell, Southern Exposure (SE), and cracked beam (CB) tests for conventional, epoxy-coated (ECR), and ChromX (ASTM A1035 Type CS) reinforcement. The chapter also presents the results of the Southern Exposure and cracked beam tests for galvanized (A767 and A1094) reinforcement. ASTM A1094 reinforcement is marketed as having a more flexible coating that is less likely to lead to corrosion on bent reinforcing bars than A767 reinforcement; this claim is evaluated. The effects of fabrication and construction practices on the corrosion performance of coated reinforcement were investigated by incorporating intentionally damaged or bent specimens in the tests. The coating was not otherwise damaged on the bent specimens. Conventional and ChromX reinforcing bars were also evaluated in conjunction with the waterproofing admixtures IPANEX and Xypex. Furthermore, the effect of ultraviolet (UV) exposure on the corrosion performance of epoxy-coated reinforcement was studied. Corrosion rate, corrosion loss, and corrosion potential were measured for each specimen using the procedures described in Chapter 2. The results given in this chapter are presented in terms of the average values for a given corrosion protection system. Results for individual specimens are presented in Appendix C.

3.1 RAPID MACROCELL TESTS

The rapid macrocell test was used to evaluate conventional, epoxy-coated, and ChromX (ASTM A1035 Type CS) bars. Epoxy-coated bars were evaluated both in the undamaged (as-received) and damaged conditions. On the damaged specimens, the coating was penetrated to a depth of 15 mils (0.4 mm) with four 0.125-in. (3-mm) diameter holes (two on each side) to simulate damage that occurs during handling and placement of reinforcement in the field, as described in Chapter 2. The corrosion performance of ECR specimens was also evaluated after different periods

of ultraviolet (UV) exposure in accordance with ASTM G154 Cycle 1 to simulate unprotected outdoor storage. Furthermore, epoxy-coated reinforcement was evaluated with a 180-degree bend to simulate field fabrication; bending reinforcing bars can create preferential sites for corrosion.

A corrosion rate or corrosion loss may appear to be negative in some cases. These negative values, however, do not mean that there is "negative" corrosion; they are artifacts of the testing method. Negative corrosion rates may occur when specimens are otherwise exhibiting very low or no corrosion activity, where minor differences in the oxidation rate between the anode and cathode bars dominate the behavior of the specimen.

This section describes the corrosion rate, corrosion potential, macrocell corrosion loss, and total corrosion loss based on linear polarization resistance (LPR). A summary of total corrosion losses is given first, followed by the test details. Finally, corrosion losses are compared to those observed in previous research.

Overall, conventional reinforcement exhibited the highest average total corrosion losses among the reinforcement evaluated using the rapid macrocell test. Epoxy-coated reinforcement exhibited corrosion losses close to zero when undamaged; damaged epoxy-coated reinforcement exhibited an average total corrosion loss about 4% of the value for the matching conventional reinforcement. The difference between the total corrosion loss of bent ECR and the value for the matching damaged ECR is not statistically significant. The damaged epoxy-coated reinforcement exposed to any amount of UV exhibited average total losses ranging from 1.3 to 10.6 times the values for the matching ECR not exposed to UV. As described in Chapter 2, rapid macrocell results are not representative of the behavior of galvanized reinforcement in concrete and are not summarized in this chapter. ChromX reinforcement exhibited an average total macrocell loss lower

than the values for the three heats of conventional reinforcement, but higher than those of the epoxy-coated reinforcement. Details of the tests follow.

3.1.1 Average Macrocell Corrosion Rates and Potentials

3.1.1.1 Conventional Reinforcement

Figure 3.1 shows the average macrocell corrosion rate for the three heats of conventional reinforcement evaluated in the rapid macrocell test, with each data point representing the average of six specimens (8.5 to 39.5 μm/yr); the corrosion rate is based on the total area of conventional reinforcement exposed to the pore solution. Conv-A, Conv-B, and Conv-C (ASTM A615) are the conventional reinforcing bars used to produce the epoxy-coated (ASTM A775), hot-dip galvanized (ASTM A767), and continuously galvanized (ASTM A1094) reinforcement, respectively. For the first 10 weeks of testing, Conv-A reinforcement exhibited corrosion rates lower than those of Conv-B or Conv-C. During the last five weeks of testing, the three heats exhibited similar corrosion rates dropping for Conv-B and Conv-C and increasing for Conv-A. As will be discussed in Section 3.1.2, the relative performance of the three heats of steel differs somewhat based on LPR measurements.

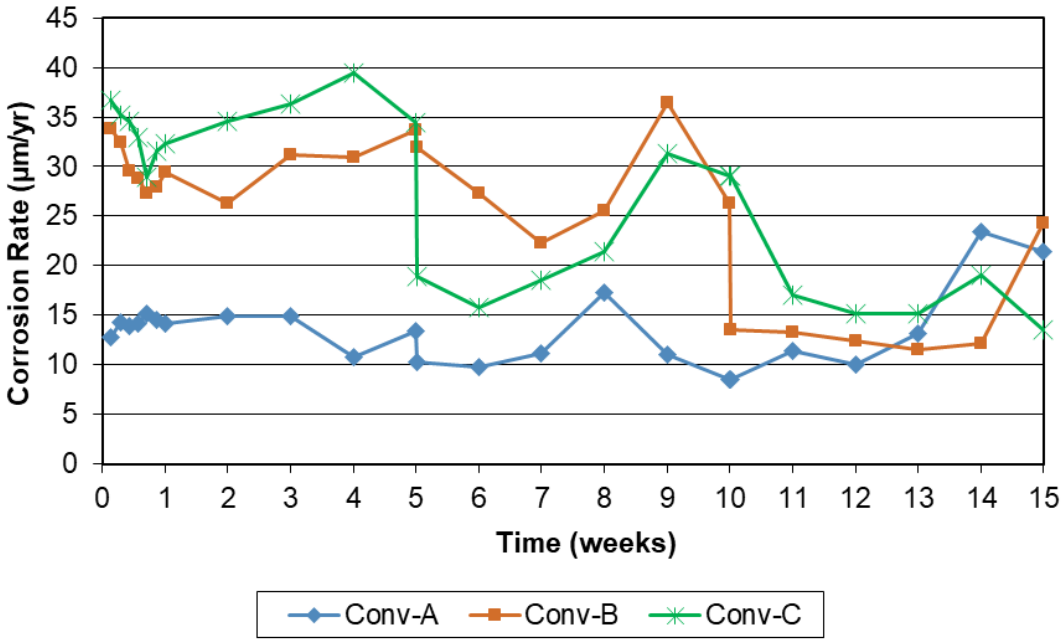

Figure 3.1: Average corrosion rate (µm/yr) for conventional reinforcement in the rapid macrocell test

The corrosion rates of Conv-A were lower than those observed for conventional reinforcement in previous research, where corrosion rates ranged from about 10 to 60 µm/yr over 15 weeks of testing; the corrosion rates of Conv-B and Conv-C are, however, similar to those observed in previous research (Guo et al. 2006, Darwin et al. 2011, O'Reilly et al. 2011, Darwin et al. 2013).

Figure 3.2 shows the average corrosion potential of the anode for the three heats of conventional reinforcement with respect to a copper/copper sulfate electrode (CSE). The three heats exhibited a potential of approximately –0.60 V with respect to CSE throughout the test. A corrosion potential more negative than –0.35 V indicates a greater than 90% probability of active corrosion according to ASTM C876.

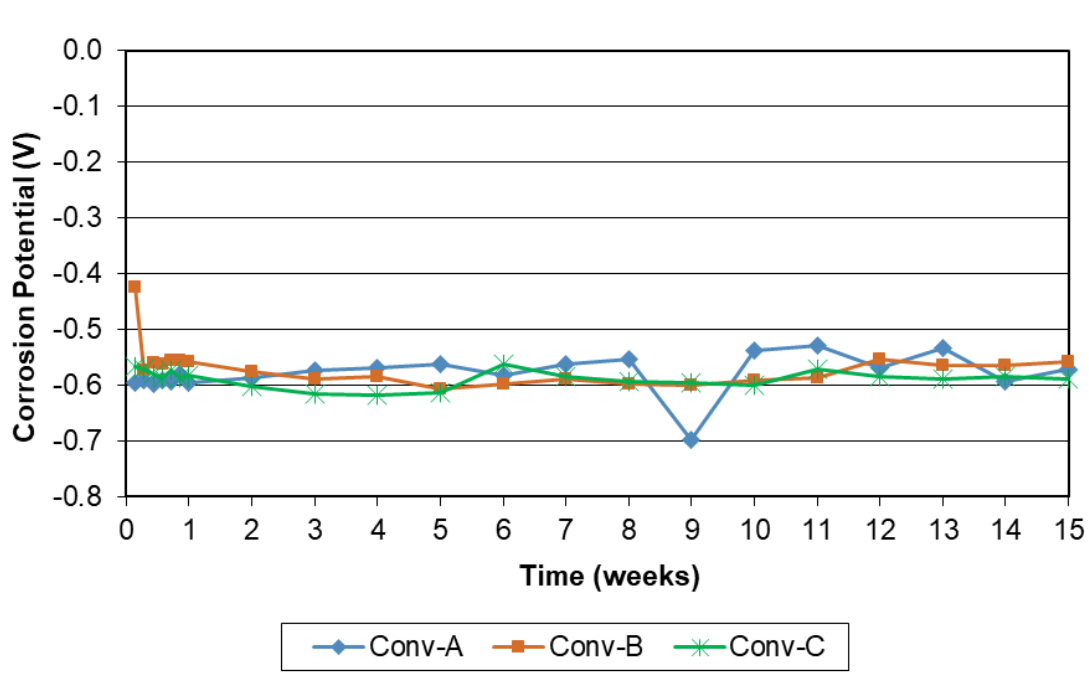

Figure 3.2: Average corrosion potential (vs. CSE) of the anode for conventional reinforcement in the rapid macrocell test

3.1.1.2 Epoxy-Coated Reinforcement (ECR)

3.1.1.2.1 Epoxy-Coated Reinforcement (ECR)-with and without UV Exposure

Figure 3.3 shows the average macrocell corrosion rate based on total bar area[1] for two heats of ECR without and with damage, as well as with 1000 hours of UV exposure in accordance with ASTM G154, simulating one year of outdoor exposure. Initial test results led to an expansion of the scope of work to further investigate the effect of the length of UV exposure. To validate the results for the ECR specimens with 1000 hours of UV exposure (ECR1-UV-1000), the rapid macrocell test was repeated (ECR1-UV-1000(b)). As insufficient ECR remained from the original heat of steel, a second heat of epoxy-coated bars (ECR2) was used for some of the additional rapid macrocell tests. The ECR1 and ECR2 specimens exhibited average corrosion rates below 1.1

[1] Specifically describing the results in terms of "total bar area" for ECR, and later galvanized reinforcement, is meant to distinguish the results from those presented later in this report where corrosion loss is expressed based on both the total bar area in contact with concrete/pore solution and the area of bare steel exposed by penetrations in the epoxy or zinc coating.

μm/yr. ECR1-ND and ECR2-ND, undamaged ECR without UV exposure, did not exhibit corrosion activity, but corrosion rates fluctuated around zero due to the nature of the test. Throughout the test, ECR1-UV-1000 specimens exhibited average corrosion rates from 1 to 4.8 μm/yr; ECR1-UV-1000(b) specimens exhibited average corrosion rates from 1 to 5.5 μm/yr, and ECR2-UV-1000 specimens exhibited average corrosion rates from 1 to 5.8 μm/yr. Even undamaged ECR exposed to UV (ECR1-UV-1000-ND) exhibited small but positive average corrosion rates greater than 0.1 μm/yr during six out of 15 weeks, in contrast to the undamaged ECR without UV exposure.

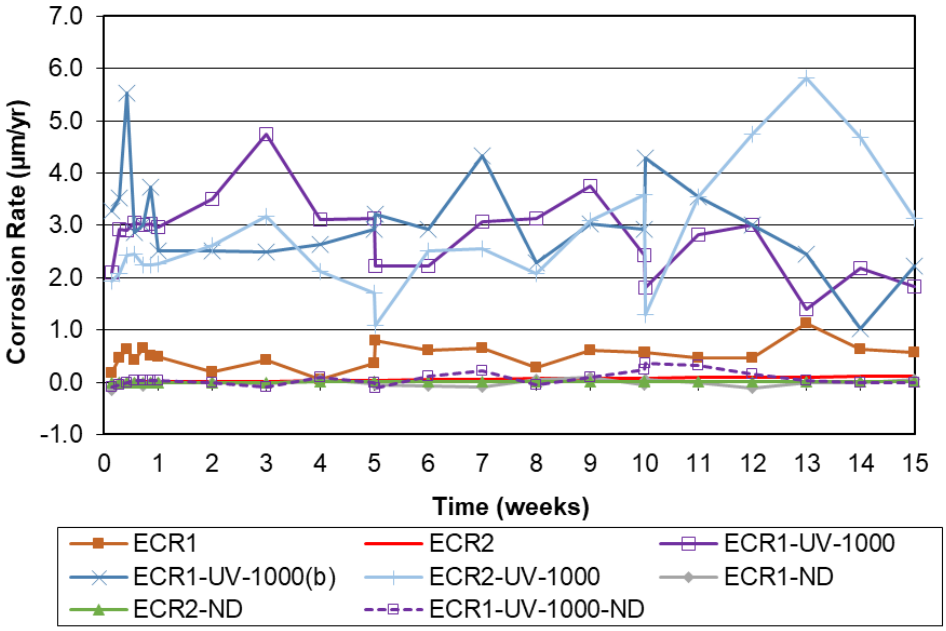

Figure 3.3: Average corrosion rate (μm/yr) based on total area in the rapid macrocell test: ECR, ECR-ND, ECR-UV-1000, and ECR1-UV-1000-ND

Additional rapid macrocell tests were performed on damaged ECR bars with 100 to 500 hours of UV exposure to investigate the effects of shorter periods of UV exposure. Figure 3.4 shows the average corrosion rate based on total area for all damaged epoxy-coated reinforcement with different periods of UV exposure; Figures 3.5 and 3.6 show the average corrosion rates for damaged ECR1 and ECR2, respectively, without and with different durations of UV exposure.

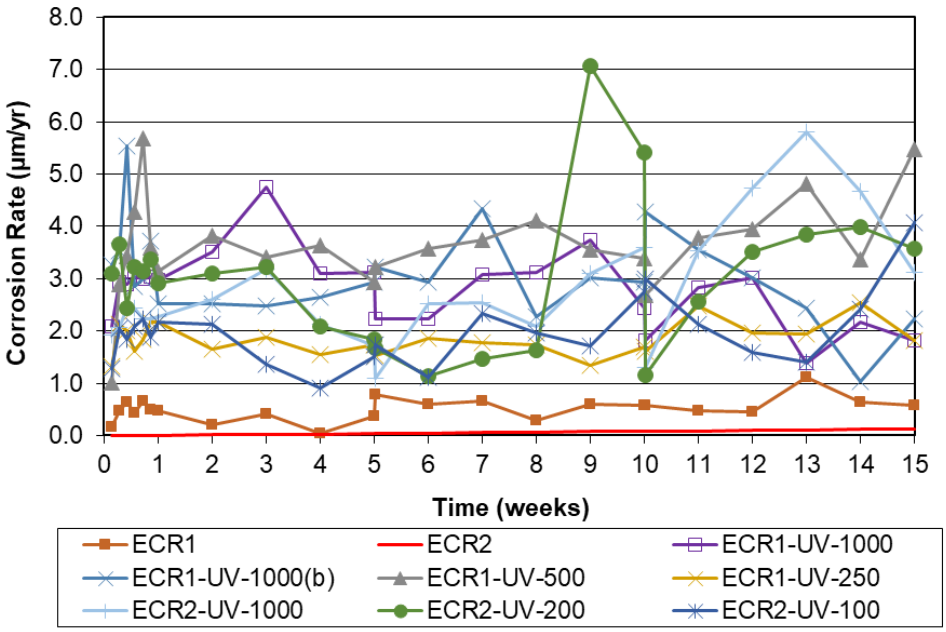

Figure 3.4: Average corrosion rate (µm/yr) based on total bar area in the rapid macrocell test: damaged ECR without and with UV exposure

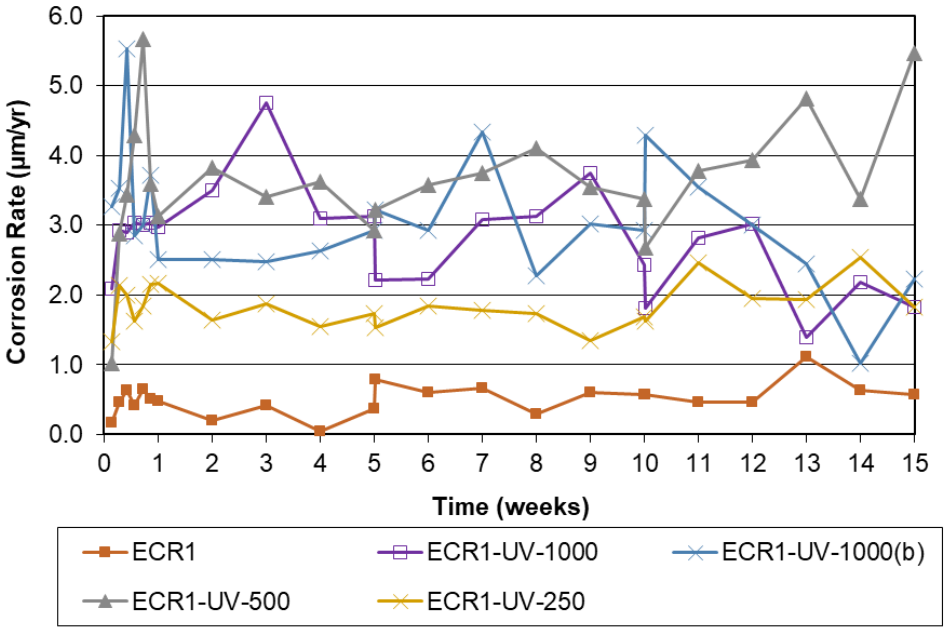

Figure 3.5: Average corrosion rate (µm/yr) based on total bar area in the rapid macrocell test: damaged ECR1 without and with different durations of UV exposure

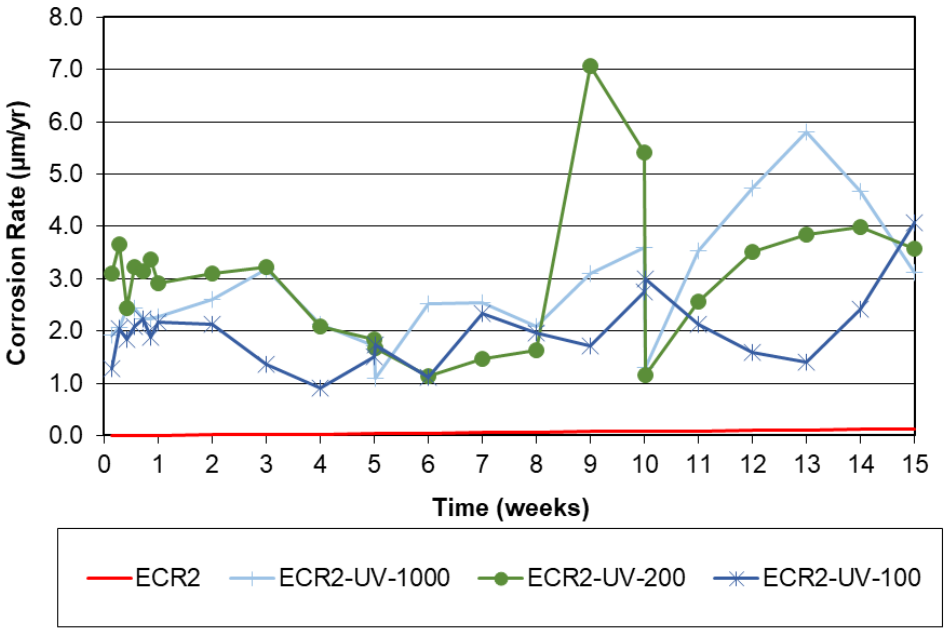

Figure 3.6: Average corrosion rate (µm/yr) based on total bar area in the rapid macrocell test: damaged ECR2 without and with different durations of UV exposure

For most of the test duration, ECR1-UV-1000, ECR1-UV-1000(b), and ECR1-UV-500 exhibited average macrocell corrosion rates of close to 3 µm/yr based on the total bar area in contact with the pore solution (Figure 3.5). ECR1-UV-250, ECR1 exposed to 250 hours of UV, exhibited average corrosion rates close to 2 µm/yr, lower than the rates for ECR specimens with 500 or 1000 hours of UV exposure.

Figure 3.6, which shows average corrosion rates for ECR2 specimens, indicates that any amount of UV exposure increases the corrosion rate. ECR2-UV-100, ECR2-UV-200, and ECR-2-UV-1000 had corrosion rates in the 1 to 3 µm/yr range in the first five weeks of testing. ECR2-UV-1000 exhibited corrosion rates as high as 6 µm/yr. ECR2-UV-100 and ECR2-UV-200 exhibited spikes of 4.1 and 7.1 µm/yr at weeks 15 and 9, respectively. ECR2-UV-100, ECR2-UV-200, and ECR-2-UV-1000 exhibited corrosion rates in the 3.5 to 4.1 µm/yr range at the end of the test.

Figures 3.7 and 3.8 show the average anode corrosion potential for ECR1 and ECR2, respectively, without and with damage, as well as with different periods of UV exposure. Corrosion potentials could not be obtained on undamaged ECR not exposed to UV (ECR1-ND and ECR2-ND), likely due to the undamaged coating preventing an ionic connection between the reference electrode and the steel. Damaged ECR without UV exposure (ECR1) exhibited average corrosion potentials between –0.40 V and –0.60 V throughout the test. During the first six weeks of testing, ECR with 1000 hours of UV exposure (ECR1-UV-1000) exhibited average corrosion potentials between –0.60 and –0.75 V, more negative than the values for ECR1 specimens; afterward, ECR1-UV-1000 exhibited corrosion potentials of –0.40 V to –0.60 V, in the same range as ECR1. The ECR1-UV-1000(b) and ECR1-UV-500 specimens exhibited average corrosion potentials between –0.55 and –0.70 V; the ECR1-UV-250 specimens exhibited average corrosion potentials between –0.50 and –0.75 V throughout the test, except for a spike to –0.40 V at week 2. While no correlation was observed between the amount of UV exposure and corrosion potential, ECR1 (damaged ECR) specimens with any amount of UV exposure exhibited average corrosion potentials more negative than ECR1 without UV exposure, except for the ECR1-UV-250 specimens at week 2 and the ECR1-UV-1000 specimens at week 15, which exhibited a corrosion potential of –0.40 V and –0.45 V, respectively, more positive than the value for ECR1. ECR1-UV-1000-ND, undamaged ECR with 1000 hours of UV exposure, exhibited average corrosion potentials between –0.30 and –0.65 V, which were nearly identical to the corrosion potentials of ECR1 through most of the testing. The fact that the ECR1-UV-1000-ND bars exhibited corrosion activity and a measurable corrosion potential shows that UV exposure exposed the underlying metal to the pore solution.

ECR2-UV-1000, ECR2-UV-200, ECR2-UV-100 exhibited average corrosion potentials from –0.50 to –0.75 V. The effect of UV on corrosion potential follows the same general trend as it does for corrosion rate, in that the exposure to UV causes more negative corrosion potentials, indicating increased corrosion activity.

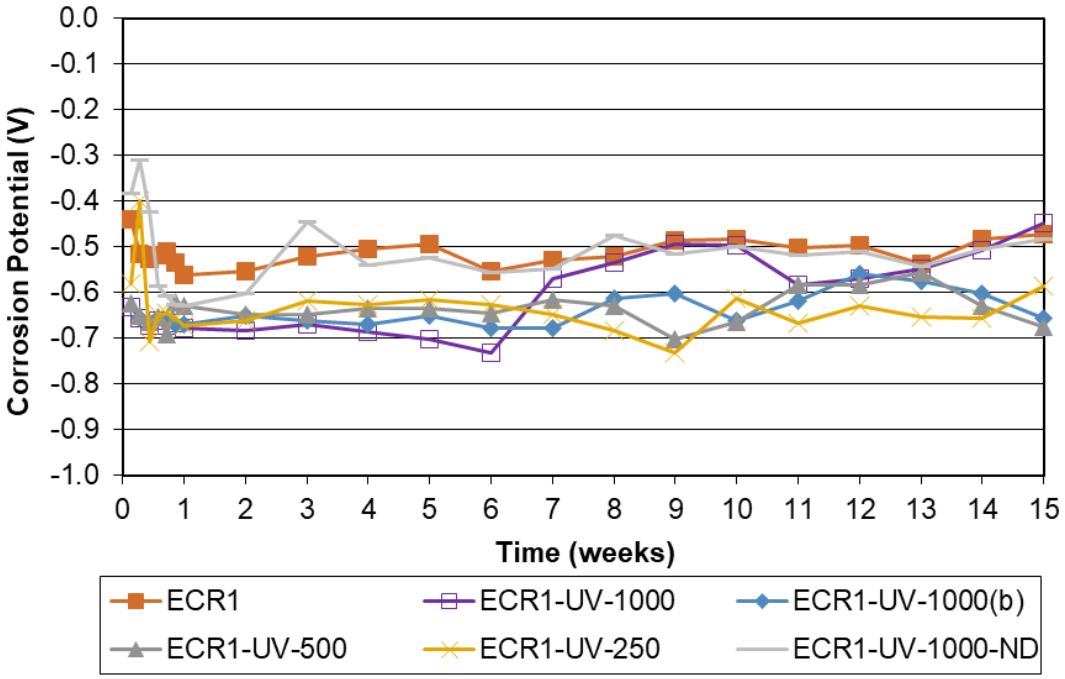

Figure 3.7: Average corrosion potential (vs. CSE) of the anode of damaged and undamaged ECR1 without and with UV exposure in the rapid macrocell test

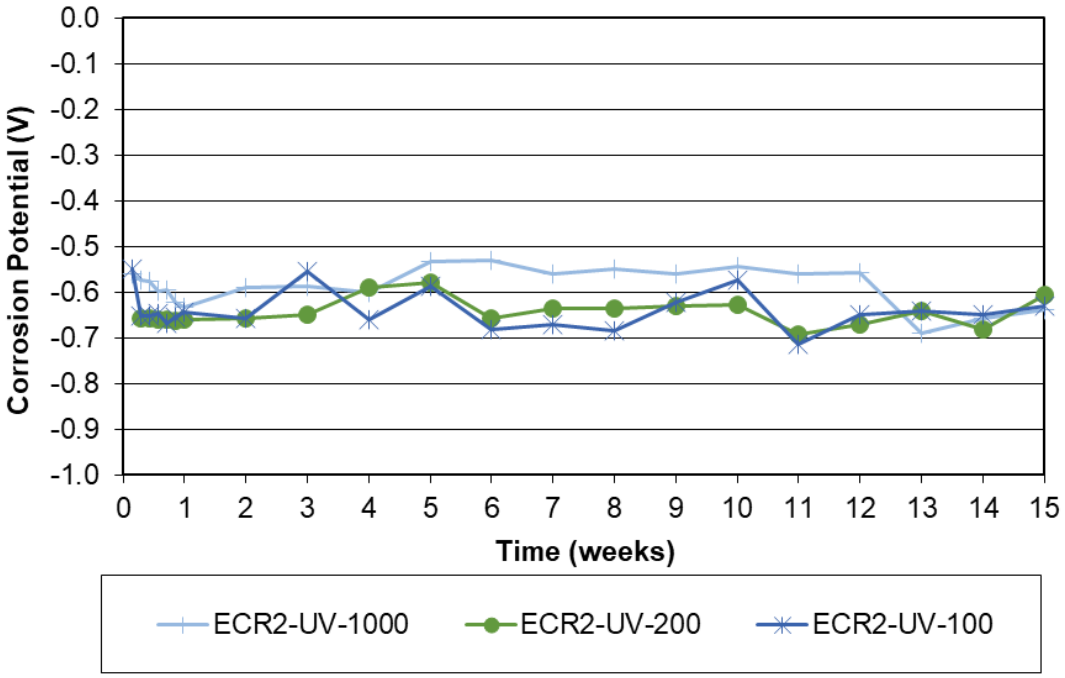

Figure 3.8: Average corrosion potential (vs. CSE) of the anode of damaged ECR2 with UV exposure in the rapid macrocell test

3.1.1.2.1 Epoxy-Coated Reinforcement (ECR)-Bent Specimens

Figure 3.9 shows the average macrocell corrosion rate for bent ECR (ECR1-Bent) and straight ECR without and with damage (ECR1-ND and ECR1). Bent ECR, which has no intentional penetrations in the coating, exhibited average corrosion rates of less than 0.2 μm/yr, below the value for damaged straight ECR (ECR1). Figure 3.10 shows the average anode corrosion potentials for the damaged ECR (ECR1) and bent ECR (ECR1-Bent). The ECR1-Bent specimens had average corrosion potentials more negative than –0.50 V, more negative than those of ECR1, except for a single reading of –0.35 V at week 12. The fact that the bent bars exhibited corrosion activity and a measurable corrosion potential shows that bending exposed the underlying metal to the pore solution.

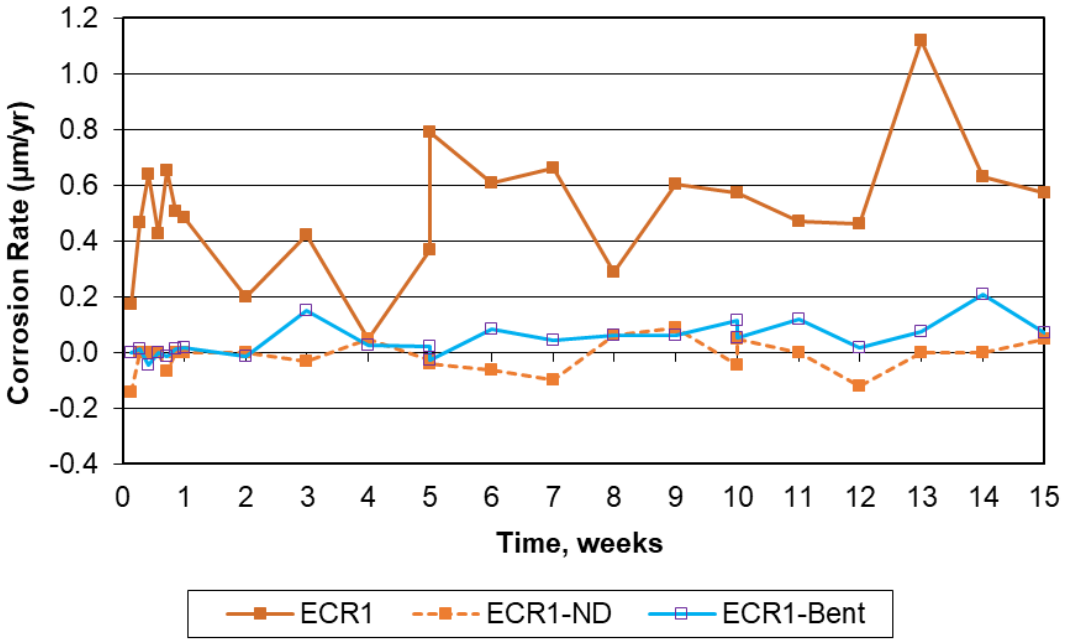

Figure 3.9: Average corrosion rate (µm/yr) based on total bar area in the rapid macrocell test: ECR1, ECR1-ND, and ECR1-Bent

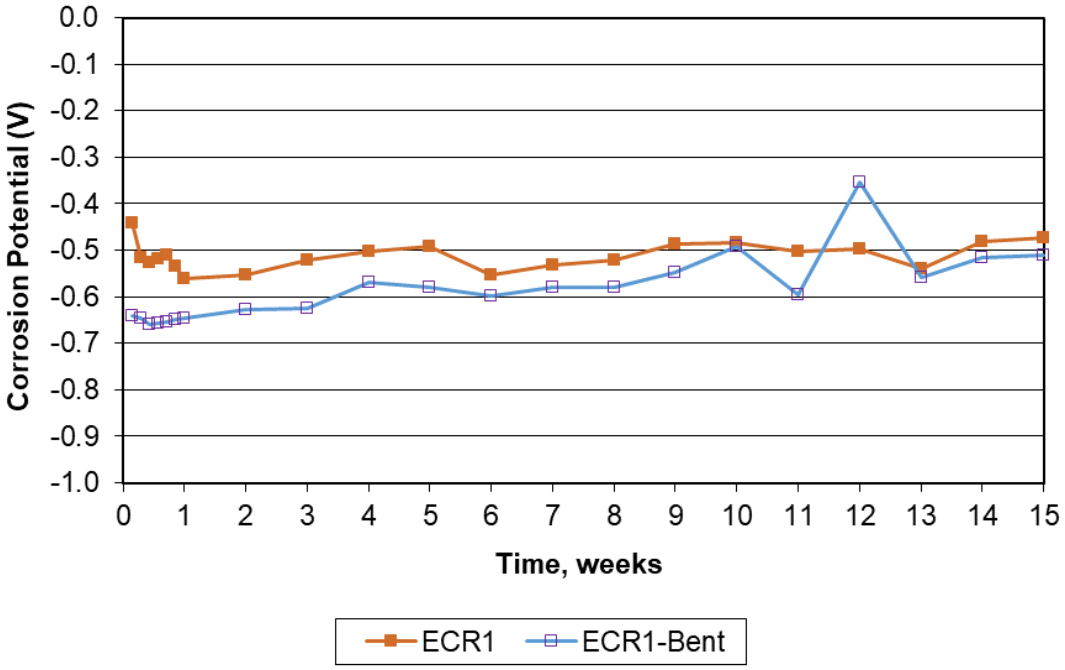

Figure 3.10: Average corrosion potential (vs. CSE) of the anode in the rapid macrocell: ECR1 and ECR1-Bent

3.1.1.3 ChromX (ASTM A1035 Type CS) Reinforcement

Figure 3.11 shows the average macrocell corrosion rate for ChromX (ASTM A1035 Type CS) along with Conv-B and Conv-C reinforcement. The rates for Conv-A are not shown because they are unusually low for conventional reinforcement. ChromX reinforcement exhibited corrosion rates of 9 to 24 µm/yr, below the rates for Conv-B and Conv-C during the first 10 weeks, except for a spike at week 5 corresponding to the solution change. After week 10, ChromX exhibited average corrosion rates somewhat greater than those of Conv-B and Conv-C. The corrosion rates exhibited by ChromX are similar to those in previous research (Ji et al. 2005, Farshadfar et al. 2017) Figure 3.12 shows the average corrosion potentials for ChromX along with Conv-B and Conv-C reinforcement. The average corrosion potentials of ChromX reinforcement ranged between –0.40 V and –0.55 V, compared to values between –0.40 V and –0.65 V for conventional reinforcement.

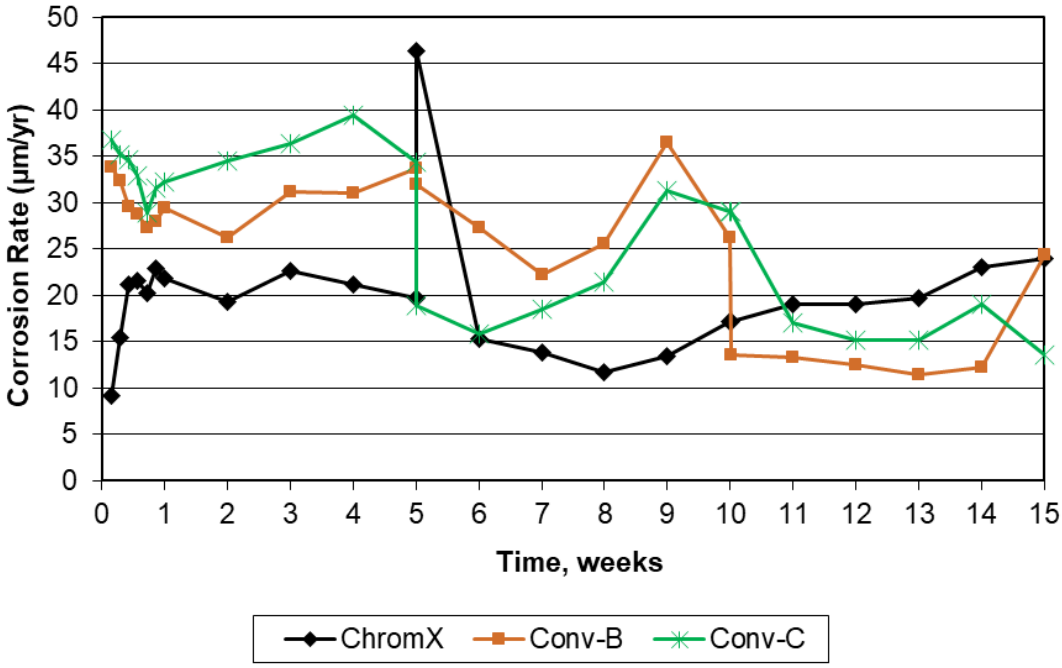

Figure 3.11: Average corrosion rate (µm/yr) for conventional and ChromX reinforcement in the rapid macrocell test

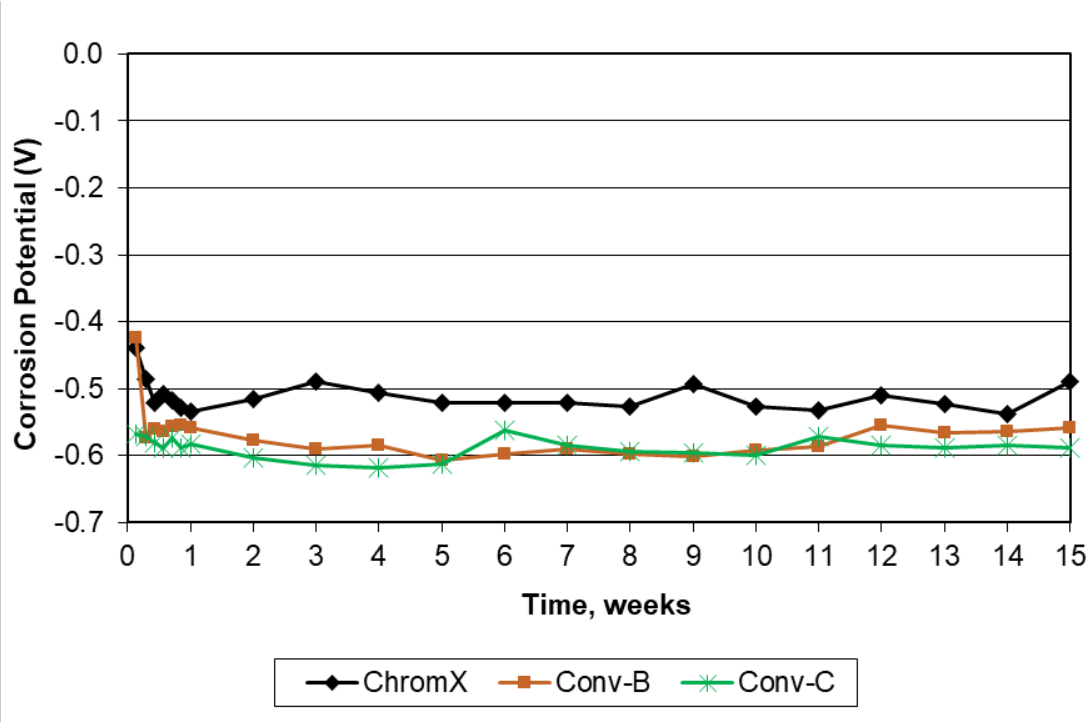

Figure 3.12: Average corrosion potential (vs. CSE) of the anode for conventional and ChromX reinforcement in the rapid macrocell test

3.1.2 Corrosion Losses at End of Testing

The individual macrocell and total corrosion losses based on total area of the specimens exposed to the pore solution, as well as the average and standard deviation for each set are given in this section. Due to the nature of corrosion of reinforcement in concrete, the standard deviations are very high, sometimes greater than the corresponding average values. To determine if the differences between corrosion protection systems are statistically significant, a two-tailed Student's t-test was performed. Student's t-test is a statistical analysis method used to investigate if the difference between two data sets is due to a difference between the means of the populations from which they are taken or only due to variations among data sets in the same population (due to chance). A null hypothesis, which states that any difference in the means of two data sets is due to chance, is introduced. Student's t-test may be one or two-tailed. In the two-tailed t-test, the mean of one data set can be greater or lower than that of the other one. The results of Student's t-test are

expressed as p values, which is the probability that the differences between two data sets are due to chance. The null hypothesis can be rejected when its probability (p) is lower than the threshold set for statistical significance. Rejecting the null hypothesis indicates that the differences in the means of two data sets are statistically significant (not due to chance). $p = 0.20$ is considered as the threshold for statistical significance in this study. Therefore, values of p greater than 0.20 indicate the difference between two mean values is not statistically significant. Results for all Student's t-test analyses are given in Appendix D.

3.1.2.1 Macrocell Losses at End of Testing

Table 3.1 shows the macrocell corrosion losses after 15 weeks of testing. Individual specimens with conventional reinforcement exhibited corrosion losses between 1.77 and 9.49 μm at the end of the test. Conv-A bars exhibited an average corrosion loss of 3.97 μm, lower than Conv-B or Conv-C bars (6.98 and 7.17 μm, respectively); the differences are statistically significant ($p \leq 0.02$). The average for the three heats of conventional reinforcement is 6.04 μm. As pointed out before, the corrosion loss of Conv-A is unusually low for conventional reinforcement. The difference in the corrosion losses between Conv-B and Conv-C is not statistically significant. For the purpose of calculating the average macrocell losses, negative corrosion losses are treated as zero.

Table 3.1: Macrocell corrosion losses (μm) based on total area at 15 weeks for rapid macrocell specimens

Specimen	Corrosion Loss						Average Loss[1]	Std. Dev.
	1	2	3	4	5	6		
Conv-A	2.64	6.52	3.48	1.77	4.53	4.88	3.97	1.70
Conv-B	7.20	6.60	8.60	9.47	6.25	3.73	6.98	2.01
Conv-C	9.49	7.28	5.74	6.14	6.42	7.96	7.17	1.39
ECR1	0.110	0.430	0.060	0.010	0.280	0.010	0.150	0.170
ECR2	0.080	0.170	0.270	0.100	0.110	-	0.146	0.077
ECR1-ND	0.000	-0.010	0.010	-0.010	0.020	-0.020	0.005	0.015
ECR1-UV-1000	0.580	0.690	0.820	1.21	0.870	0.800	0.828	0.214
ECR1-UV-1000(b)	1.06	0.48	0.75	1.04	0.71	0.77	0.802	0.219
ECR2-UV-1000	2.65	0.26	0.33	0.2	0.53	-	0.794	1.05
ECR1-UV-500	1.32	1.15	0.930	1.06	1.30	0.790	1.09	0.219
ECR1-UV-250	0.730	0.530	0.890	0.240	0.430	0.390	0.535	0.238
ECR2-UV-200	0.970	0.560	0.670	0.720	2.02	0.540	0.913	0.564
ECR2-UV-100	0.910	0.540	0.440	0.400	0.570	0.510	0.562	0.182
ECR1-UV-1000-ND	-0.010	-0.010	0.000	0.060	0.090	-0.010	0.050	0.044
ECR1-Bent	0.020	0.020	0.020	0.030	0.020	0.010	0.020	0.006
ChromX	5.47	4.42	6.04	5.27	3.68	7.05	5.32	1.19

- No specimen

[1] Negative values are taken zero for calculating the average

Damaged ECR without UV exposure, ECR1 and ECR2, exhibited average corrosion losses of 0.150 and 0.146 μm, respectively, equal to about 4% of the value for Conv-A, the reinforcement used to produce ECR1. The corrosion losses observed in undamaged ECR without UV exposure and bent ECR were equal to about 3% and 13% of the value for damaged ECR without UV exposure. Damaged ECR with any amount of UV exposure had average corrosion losses between 0.535 and 1.09 μm, equal to 3.6 to 7.3 times those of the matching ECR not exposed to UV. The differences in the corrosion losses between the UV-exposed ECR and unexposed ECR are statistically significant ($p \leq 0.20$). The difference in losses between undamaged ECR without and with UV exposure is not statistically significant.

ChromX (ASTM A1035 Type CS) reinforcement exhibited an average corrosion loss of 5.32 μm, greater than that observed for Conv-A and lower than the values for Conv-B or Conv-C.

The differences are statistically significant ($p \leq 0.14$). Again, the corrosion loss for Conv-A is unusually low for conventional reinforcement.

The assumption made in Table 3.1 is that corrosion loss is uniformly distributed over the total surface area of the bar in the pore solution with NaCl; therefore, the corrosion losses for epoxy-coated reinforcement in Table 3.1 do not accurately represent the localized nature of corrosion of epoxy-coated reinforcement at damaged sites. Corrosion loss based on the damaged area is calculated based on the assumption that corrosion only occurs at the damaged areas, as opposed to the total area of the bar. Multiplying the corrosion rate based on total area by the ratio of immersed area of the anode (total area) to the damaged area yields the corrosion loss based on exposed area. Table 3.2 presents the macrocell corrosion losses based on exposed area for damaged ECR; this table does not include undamaged specimens because there was no intentional damage on these specimens. The average corrosion loss based on exposed area for ECR1 is five times the loss exhibited by the matching conventional reinforcement (Conv-A) based on total area ($p = 0.13$). The average corrosion loss based on exposed area for both ECR1 and ECR2 without UV exposure (18.7 and 18.6 μm, respectively) was about 3 times the value for the average of the losses exhibited by Conv-A, Conv-B, and Conv-C (6.04 μm). Any amount of UV exposure resulted in corrosion losses 3.6 to 7.3 times the values for the matching ECR without UV exposure ($p \leq 0.02$), with average losses ranging from 67.4 to 138 μm.

Table 3.2: Macrocell corrosion losses (μm) based on exposed area at 15 weeks for ECR rapid macrocell specimens

Specimen	Corrosion Loss						Average Loss	Std. Dev.
	1	2	3	4	5	6		
ECR1	13.4	54.7	7.45	0.76	35.1	0.76	18.7	21.7
ECR2	10.4	21.5	34.6	12.6	14.0	-	18.6	9.9
ECR1-UV-1000	73.7	87.0	103	153	110	101	105	26.9
ECR1-UV-1000(b)	134	61	94.9	131	89.9	97.2	101	27.5
ECR2-UV-1000	335	32.5	41.1	25.4	67.2	-	100	132
ECR1-UV-500	167	145	118	134	164	99.2	138	26.4
ECR1-UV-250	91.9	66.5	112	30.7	53.7	49.4	67.4	29.9
ECR2-UV-200	122	70.3	85.1	90.5	255	68.4	115	71.2
ECR2-UV-100	115	67.7	55.6	50.9	72.3	63.8	70.9	23.1

- No specimen

3.1.2.2 Total Losses at End of Testing

Table 3.3 shows the total corrosion losses based on total area obtained from LPR measurements at 15 weeks. The LPR corrosion losses capture total corrosion by incorporating both the macrocell corrosion losses and localized corrosion on the bar, often described as microcell corrosion. Individual LPR rates for each specimen are presented in Appendix E. Total corrosion losses were two to three times the values for macrocell corrosion losses for conventional reinforcement. The relative losses differ from those observed based on macrocell corrosion where Conv-B and Conv-C exhibited nearly the same values, higher than those of Conv-A (about 60% of Conv-B and C). Conv-A, Conv-B, and Conv-C exhibited total average corrosion losses of 9.77, 19.8, and 12.5 μm, respectively. The average corrosion loss for the three heats is 14.0 μm. The differences in total loss between the three heats of conventional reinforcement are statistically significant ($p \leq 0.16$).

Table 3.3: LPR corrosion losses (μm) based on total area at 15 weeks for rapid macrocell specimens

Specimen	Corrosion Loss						Avg. Loss	Std. Dev.
	1	2	3	4	5	6		
Conv-A	7.71	12.9	7.90	9.42	11.8	8.89	9.77	2.13
Conv-B	12.4	11.0	12.0	38.7	14.0	30.4	19.8	11.8
Conv-C	15.2	13.9	10.6	11.3	11.3	12.4	12.5	1.76
ECR1	0.149	1.00	0.054	0.257	0.606	-	0.413	0.388
ECR2	0.109	0.39	-	2.01	0.482	0.146	0.637	0.785
ECR1-ND	0.000	0.000	0.000	0.081	0.000	0.000	0.014	0.033
ECR2-ND	0.000	0.000	0.000	0.000	0.000	0.000	0.000	0.000
ECR1-UV-1000	1.87	15.3	1.37	2.85	2.83	2.04	4.38	5.39
ECR1-UV-1000(b)	2.54	1.91	2.00	2.78	1.64	2.06	2.15	0.424
ECR2-UV-1000	0.782	0.916	0.951	1.59	1.17	-	1.08	0.317
ECR1-UV-500	1.92	1.81	3.03	3.81	0.573	1.41	2.09	1.16
ECR1-UV-250	0.65	1.14	2.56	0.691	0.691	0.45	1.03	0.781
ECR2-UV-200	0.78	0.353	1.08	0.454	0.462	1.85	0.830	0.568
ECR2-UV-100	2.29	0.187	0.113	0.887	0.520	0.801	0.800	0.796
ECR1-UV-1000-ND	0.005	0.663	0.020	0.313	0.573	0.052	0.271	0.293
ECR1-Bent	0.053	0.124	0.284	0.069	0.098	1.615	0.374	0.614
ChromX	2.79	2.45	3.84	3.73	4.41	5.82	3.84	1.21

- No specimen

The average corrosion loss of damaged ECR not exposed to UV (ECR1) is 0.413 μm, equal to about 4% of the value for Conv-A, the reinforcement used to produce ECR1; damaged ECR2 exhibited average corrosion loss of 0.637 μm. Undamaged ECR (ECR1-ND and ECR2-ND) showed no corrosion losses. Damaged ECR with UV exposure had corrosion losses between 1.3 and 10.6 times the value for the matching ECR not exposed to UV. With 1000 hours of UV exposure, the average corrosion losses of damaged ECR increased to 4.38, 2.15, and 1.08 μm for ECR1-UV-1000, ECR1-UV-1000(b), and ECR2-UV-1000, respectively. ECR1-UV-500, ECR1-UV-250, ECR1-UV-200, and ECR1-UV-100 exhibited average corrosion losses of 2.09, 1.03, 0.830, and 0.800 μm, respectively. The differences in losses between ECR1 without and with UV exposure is statistically significant ($p \leq 0.14$); the differences between ECR2 without and with exposure to UV are not statistically significant. The total losses were greater than the macrocell

losses for all ECR, except for ECR2-UV-200. Undamaged ECR exposed to UV (ECR1-UV-1000-ND) and bent ECR1 had total corrosion losses of 0.271 and 0.374 μm, respectively. The difference between the total corrosion losses of bent ECR1 and damaged ECR1 is not statistically significant.

ChromX (ASTM A1035 Type CS) reinforcement exhibited an average total corrosion loss of 3.84 μm, much lower than the losses observed on conventional reinforcement and lower than average macrocell losses observed for ChromX. The latter observation is unusual; total corrosion losses are, theoretically, greater than macrocell losses. The differences between the total corrosion loss of ChromX and those of conventional reinforcement are statistically significant ($p \leq 0.01$).

Table 3.4 shows the total corrosion losses at 15 weeks based on exposed area for ECR reinforcement obtained from LPR measurements. Damaged ECR (ECR1 and ECR2) exhibited average total corrosion losses of 52.1 and 80.5 μm, respectively, based on exposed area, compared to 9.77 μm in Conv-A based on total area. ECR with any amount of UV exposure exhibited average total losses between 101 to 553 μm based on exposed area. ECR with UV exposure (ECR1-UV-1000) exhibited an average total corrosion loss of 553 μm, with individual losses as high as 1940 μm; ECR1-UV-1000(b) and ECR2-UV-1000 exhibited average losses of 272 and 137 μm based on exposed area, respectively. As mentioned before, the standard deviations are very high, sometimes greater than the corresponding average values.

Table 3.4: LPR corrosion losses (μm) based on exposed area at 15 weeks for ECR rapid macrocell specimens

Specimen	Corrosion Loss						Average Loss	Std. Dev.
	1	2	3	4	5	6		
ECR1	18.8	126	6.82	32.5	76.5	-	52.1	49.0
ECR2	13.8	55.5	254	60.8	18.5	-	80.5	99.1
ECR1-UV-1000	237	1940	173	360	357	257	553	681
ECR1-UV-1000(b)	320	241	252	351	207	260	272	53.5
ECR2-UV-1000	99.3	116	120	201	148	-	137	40.0
ECR1-UV-500	242	228	383	481	71.7	178	264	146
ECR1-UV-250	82.3	143	323	87.2	87.2	56.9	130	98.6
ECR2-UV-200	98.7	44.6	136	57.4	58.3	234	105	71.7
ECR2-UV-100	290	23.6	14.2	112	65.7	101	101	100.5

- No specimen

The macrocell and total corrosion losses of conventional, epoxy-coated, and ChromX (ASTM A1035 Type CS) reinforcement at the end of rapid macrocell test from previous studies are summarized in Table 3.5. Total corrosion losses are available in only four out of the 14 cases in the table. When more than one result is reported for the same type of reinforcement in an individual reference, more than one heat of that type of reinforcement was tested. In terms of macrocell losses, from Guo et al. (2006) and Gong et al. (2004) had the lowest and highest macrocell corrosion losses for conventional reinforcement, 6.03 and 12.6 μm, respectively. Conventional reinforcement evaluated by Darwin et. al (2013) had an average macrocell corrosion loss of 10.9 μm. Conv-A, Conv-B, and Conv-C exhibited average macrocell corrosion losses of 3.97, 6.98, and 7.17 μm, respectively. In terms of total losses, conventional reinforcement evaluated by Darwin et. al (2013) had an average total corrosion loss of 13.6 μm compared to average total corrosion losses of 9.77, 19.8, and 12.5 μm, for Conv-A, Conv-B, and Conv-C, respectively.

ECR1 and ECR2 exhibited average macrocell corrosion losses of 0.150 and 0.146 μm, comparable to those observed by Guo et al. (0.340 μm) and Darwin et al. (2013) (0.107 μm).

(2006). ECR1 and ECR2 exhibited average total corrosion losses of 0.413 and 0.637 μm, comparable to those observed by Darwin et al. (2013) (0.322 μm). O'Reilly et al. (2011) found average corrosion losses an order of magnitude higher than the ECR from this study.

ChromX exhibited an average macrocell corrosion loss of 5.32 μm, in line with the values from previous studies, except for those of Gong et al (2004) (2.49 μm).

Table 3.5: Corrosion losses (μm) at 15 weeks for rapid macrocell specimens from previous research

Reinforcement	Study	Macrocell Corrosion loss	Total Corrosion loss
Conventional	Gong et al. (2004)	9.02	-
Conventional	Gong et al. (2004)	12.6	-
Conventional	Balma et al. (2005)	11	-
Conventional	Balma et al. (2005)	9.03	-
Conventional	Ji et al. (2005)	8.88	-
Conventional	Guo et al. (2006)	6.03	-
Conventional	Darwin et al. (2013)	10.9	13.6
Conv-A	Current Study	3.97	9.77
Conv-B	Current Study	6.98	19.8
Conv-C	Current Study	7.17	12.5
ECR	Guo et al. (2006)	0.340	-
ECR	O'Reilly et al. (2011)	1.95	2.83
ECR	Darwin et al. (2013)	0.107	0.322
ECR1	Current Study	0.150	0.413
ECR2	Current Study	0.146	0.637
ChromX	Gong et al. (2004)	5.53	-
ChromX	Gong et al. (2004)	2.49	-
ChromX	Ji et al. (2005)	5.83	-
ChromX	Farshadfar et al. (2017)	4.63	4.08
ChromX	Current Study	5.32	3.84

3.1.3 End of Test Photos and Disbondment Results

Figure 3.13 shows specimen Conv-B-5 after 15 weeks of testing and is representative of all conventional specimens in the rapid macrocell test; corrosion products are visible on the anode bar (the bar in the container with the added NaCl), particularly at and above the 3-in. pore solution

level. The corrosion above 3 in. is due to more oxygen availability above the solution surface. Also, corrosion products tend to separate from the surface of the bar in the pore solution, reducing the amount of corrosion products remaining on the bar in this region. No corrosion products were found on the cathode bars (the bars immersed in the pore solution without NaCl).

Figure 3.13: Specimen Conv-B-5 anode bar (top) and cathode bars (bottom) after 15 weeks of rapid macrocell testing

Figure 3.14 shows specimen ECR1-2 after 15 weeks of testing. Some of the intentional damage sites on the anode bars had rust, while others appeared clean. No blistering was visible on the undamaged portions of the coating. No signs of corrosion were visible on undamaged bars; Figure 3.15 shows specimen ECR1-Bent-5 after testing; no signs of corrosion are visible. The darkened area in the figure is the area patched after being damaged due to bending.

A disbondment test, as described in Chapter 2, was performed on the anodes of all damaged ECR after testing. Figure 3.16 shows the anode bar for specimen ECR1-2 after the disbondment

test; a portion of the coating disbonded from the underlying metal both at sites without and with visible corrosion at the hole. Figures 3.17 and 3.18 show the anode bar for specimen ECR1-UV-1000-4 before and after the disbondment test, respectively. Figures 3.19 through 3.21 show the anode bars for ECR specimens with 500, 200, and 100 hours of UV exposure, respectively, after the disbondment test; corrosion products were visible at all damage sites and the coating peeled back readily; UV caused discoloration on the coating of ECR specimens, even on bars with lower periods of exposure. Figure 3.22 shows specimen ECR-UV-1000-ND-6 after the test; no disbondment occurred on any of the undamaged bars.

Figure 3.14: Specimen ECR1-2 anode bar (top) and cathode bars (bottom) after 15 weeks of rapid macrocell testing

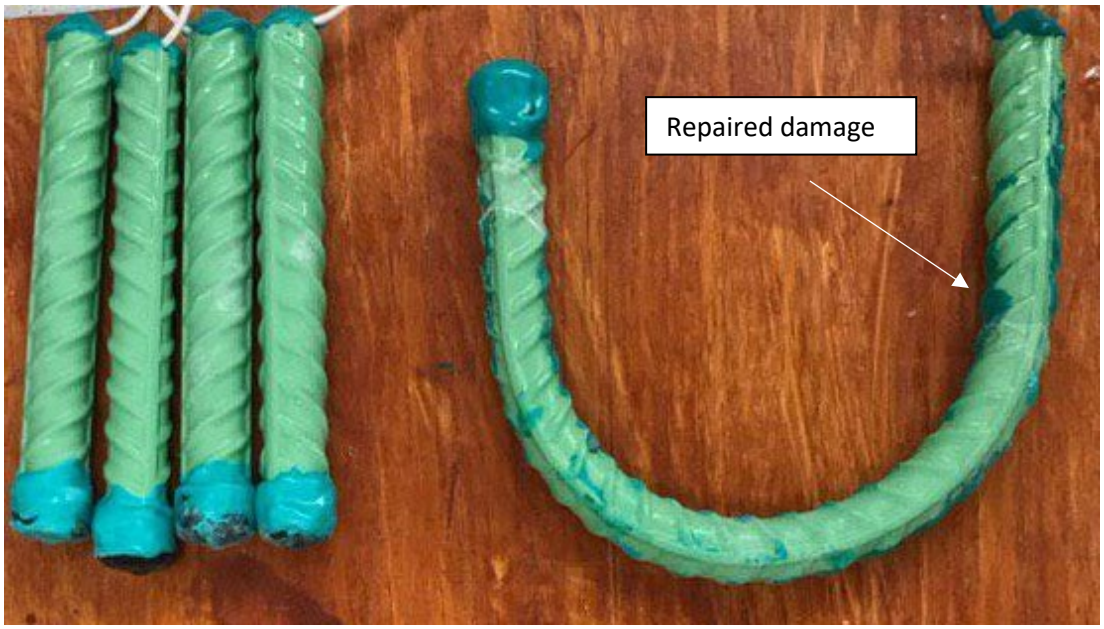

Figure 3.15: Specimen ECR1-5 anode bar (right) and cathode bars (left) after 15 weeks of rapid macrocell testing. Arrow identfying area with repaired damage

Figure 3.16: Specimen ECR1-2 anode bar after disbondment test

Figure 3.17: Specimen ECR1-UV-1000-4 anode bar (top) and cathode bars (bottom) after 15 weeks of rapid macrocell testing

Figure 3.18: Specimen ECR1-UV-1000-4 anode after disbondment test

Figure 3.19: Specimen ECR1-UV-500-5 anode bar after disbondment test

Figure 3.20: Specimen ECR2-UV-200-3 anode bar after disbondment test

Figure 3.21: Specimen ECR2-UV-100-4 anode bar after disbondment test

Figure 3.22: Specimen ECR-UV-1000-ND-6 anode bar after 15 weeks of rapid macrocell testing

Table 3.6 summarizes the measured disbonded area on the anodes of damaged ECR specimens at the end of testing. Disbondment that extended more than 0.5 in. from the intentional damage site in all directions is considered total disbondment and was assigned a disbonded area of 1.05 in.^{2}, as described in Chapter 2. Table 3.6 shows damaged ECR1 and ECR2 not exposed to

UV exhibited relatively low amounts of disbondment, with an average value of 0.06 and 0.13 in.^{2}, respectively, while any amount of UV exposure increased disbondment to values between 0.27 and 0.99 in.^{2}. The differences in the disbondment values between ECR1 without and with any amount of UV exposure (1000, 500, and 250 hours) are statistically significant ($p \leq 0.003$). The differences in the disbondment values between ECR2 without UV exposure and ECR2 with 1000 or 200 hours of UV exposure are also statistically significant ($p \leq 0.03$); the difference between ECR2 without and with 100 hours of UV exposure is not statistically significant. For the ECR2 specimens, disbondment increased as the amount of UV exposure increased; this trend was not observed for the ECR1 bars. Undamaged ECR, both without and with UV exposure, did not exhibit disbondment.

Table 3.6: Measured disbondment at end of rapid macrocell testing of anode bars in damaged ECR specimens without and with UV exposure

Specimen	Disbonded Area (in.^{2})							
	Specimen						Average	Std. Dev.
	1	2	3	4	5	6		
ECR1	0.05	0.10	0.04	0.00	0.16	0.00	0.06	0.06
ECR2	0.57	0.01	0.00	0.05	0.00	-	0.13	0.25
ECR1-UV-1000	0.17	0.25	0.39	0.29	0.30	0.24	0.27	0.07
ECR1-UV-1000 (b)	0.30	0.43	0.73	0.31	0.25	0.30	0.39	0.18
ECR1-UV-500	0.64	0.30	0.24	0.67	0.21	0.32	0.39	0.20
ECR1-UV-250	0.61	0.50	0.84	0.57	0.20	0.19	0.48	0.25
ECR2-UV-1000	1.05	1.05	0.71	1.05	1.05	1.05	0.99	0.14
ECR2-UV-200	0.59	0.23	1.05	0.59	0.24	1.05	0.62	0.37
ECR2-UV-100	0.64	0.06	0.07	0.61	0.16	0.18	0.29	0.27

Figure 3.23 shows specimen ChromX-6 after 15 weeks of testing and is representative of the ChromX specimens in the rapid macrocell test; corrosion products are visible on the anode bar, particularly at and above the 3-in. pore solution level. No corrosion products were observed on the cathode bars.

Figure 3.23: Specimen ChromX-6 anode bar (top) and cathode bars (bottom) after 15 weeks of rapid macrocell testing

3.2 SOUTHERN EXPOSURE AND CRACKED BEAM TESTS

The Southern Exposure and cracked beam tests were used to evaluate conventional, epoxy-coated, galvanized (A767 and A1094), and ChromX (A1035 Type CS) reinforcement; conventional and ChromX reinforcement was also evaluated in conjunction with the waterproofing admixtures IPANEX and Xypex. Coated bars were evaluated in both the undamaged (as-received) condition and with ten 0.125-in. holes in the coating, simulating damage that occurs during handling and placement of reinforcement. Epoxy-coated reinforcement was also evaluated after 1000 hours of UV exposure in accordance with ASTM G154 Cycle 1, which simulates outdoor storage, and galvanized bars were evaluated with a 180-degree bend, as shown in Figure 2.5.

This section describes the macrocell corrosion rate and loss, corrosion potential, and total corrosion rate and loss based on linear polarization resistance (LPR). A summary of total corrosion losses and critical chloride corrosion thresholds is given first, followed by a detailed description of the results. Finally, corrosion losses are compared to those observed in previous research.

At the end of the Southern Exposure test, the average of total corrosion losses for the three heats of conventional reinforcement was greater than the values for any other reinforcement evaluated. Epoxy-coated reinforcement not exposed to UV exhibited average total corrosion losses about 1% of the value for the matching conventional reinforcement based on total area of the bars in contact with concrete. Damaged epoxy-coated reinforcement exposed to 1000 hours of UV had a total average corrosion loss 13 times greater than the value for epoxy-coated reinforcement not exposed to UV. A767 and A1094 specimens exhibited average total corrosion losses lower than conventional reinforcement in damaged and undamaged conditions. ChromX reinforcement exhibited an average total corrosion loss lower than the average for the three heats of conventional reinforcement but higher than the value for epoxy-coated reinforcement. The addition of either IPANEX or Xypex did not result in a statistically significant difference in the total corrosion loss for conventional or ChromX reinforcement.

The results in the cracked beam test parallel those in the Southern Exposure test in most but not all cases. At the end of the cracked beam test, Conv-A, Conv-B, and Conv-C reinforcement exhibited average total corrosion losses greater than any other reinforcement evaluated. Epoxy-coated reinforcement exhibited an average total corrosion loss of 1% the value for conventional reinforcement based on total area of the bars in contact with concrete. Damaged epoxy-coated reinforcement exposed to 1000 hours of UV had an average total corrosion loss of 14 times the value for epoxy-coated reinforcement not exposed to UV. Undamaged ECR exposed to UV exhibited corrosion losses in the same range as damaged ECR not exposed to UV. A767 and A1094 specimens exhibited average total corrosion losses lower than conventional reinforcement in damaged and undamaged conditions. ChromX reinforcement exhibited an average total corrosion loss lower than that of conventional reinforcement but higher than the value for epoxy-coated

reinforcement; ChromX reinforcement exhibited average total corrosion losses greater than those of galvanized reinforcement. The addition of either IPANEX or Xypex did not result in a statistically significant difference in the total corrosion loss for ChromX reinforcement. The addition of IPANEX did not have a statistically significant effect on the total corrosion loss for conventional reinforcement, but the addition of Xypex resulted in a 45% reduction in total loss for conventional reinforcement.

Conv-A, Conv-B, and Conv-C reinforcement exhibited average critical chloride corrosion thresholds of 1.36, 0.655, and 1.54 lb/yd^3, respectively. The average critical chloride corrosion threshold for the three conventional reinforcement was 1.19 lb/yd^3. Epoxy-coated reinforcement had an average critical chloride corrosion threshold of 2.58 lb/yd^3. The critical chloride corrosion threshold for ECR with UV exposure was not determined. A767 and A1094 exhibited average critical chloride corrosion thresholds of 1.37 and 1.58 lb/yd^3, respectively, and ChromX reinforcement 3.37 lb/yd^3, higher than those of conventional, epoxy-coated, and galvanized reinforcement. Details of the tests follow.

3.2.1 Macrocell Corrosion Rates and Potentials

3.2.1.1 Conventional Reinforcement

Figure 3.24 shows the average macrocell corrosion rate of the three heats of conventional reinforcement evaluated in the Southern Exposure test. For the three heats of steel, the average corrosion rates gradually increased through the first 30 weeks before leveling off. After about 24 weeks, Conv-A exhibited an average corrosion rate of about 2 to 4 μm/yr most of the weeks, lower than those observed on Conv-B or Conv-C (4 to 10 μm/yr over most of the testing period). The average corrosion rates in the Southern Exposure test were approximately one-third to one-fifth of the average corrosion rates in the rapid macrocell test.

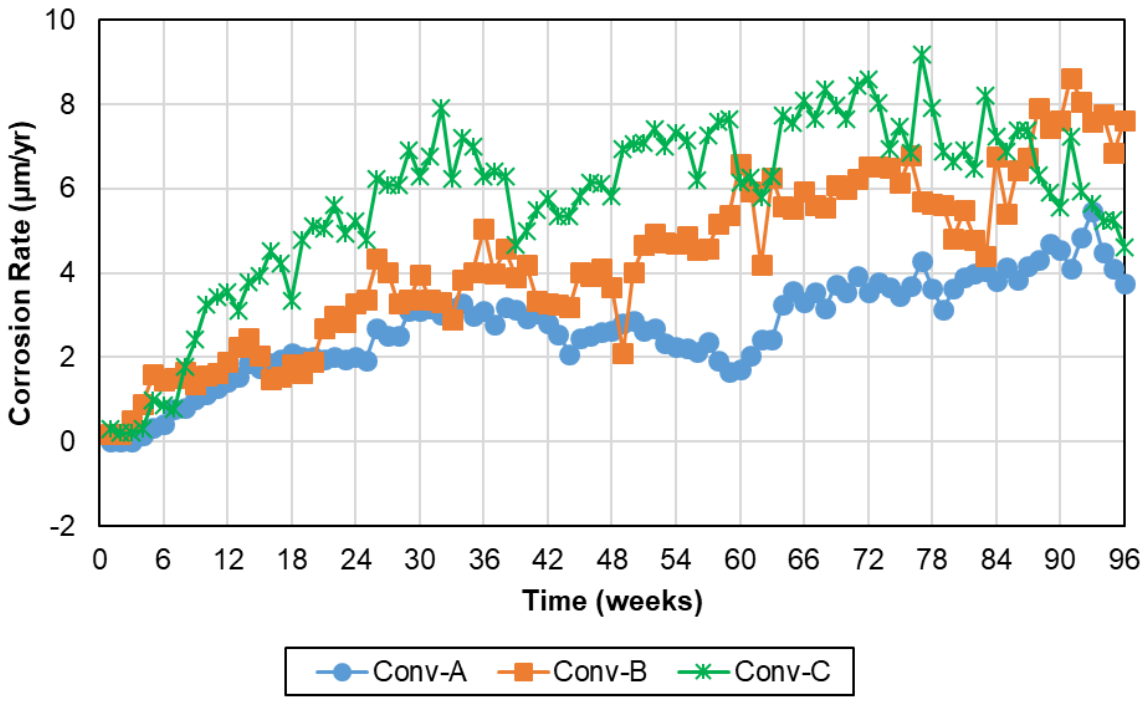

Figure 3.24: Average macrocell corrosion rate (µm/yr) of conventional reinforcement in the Southern Exposure test

Figure 3.25 shows the average macrocell corrosion rate based on total area in the cracked beam test; the three heats of steel exhibited the greatest corrosion rates at the start of testing, after which the corrosion rates gradually decreased over time. Both Conv-A and Conv-C exhibited average corrosion rates of about 15 µm/yr at the start of testing; the corrosion rates dropped to about 5 µm/yr by week 40 and fluctuated in the 3.5 to 11 µm/yr range for the remainder of testing. Conv-B exhibited greater average corrosion rates, starting near 25 µm/yr, dropping to 12 µm/yr by week 40 and fluctuating between 7.5 and 21 µm/yr after week 40. Conv-B showed average corrosion rates approximately twice those of Conv-A and Conv-C through the test. This is not consistent with the results from the rapid macrocell test where both Conv-B and Conv-C exhibited average corrosion rates close to twice that of Conv-A. However, Conv-A exhibited the lowest average corrosion rates among the three heats of conventional reinforcement in the rapid macrocell, Southern Exposure, and cracked beam tests.

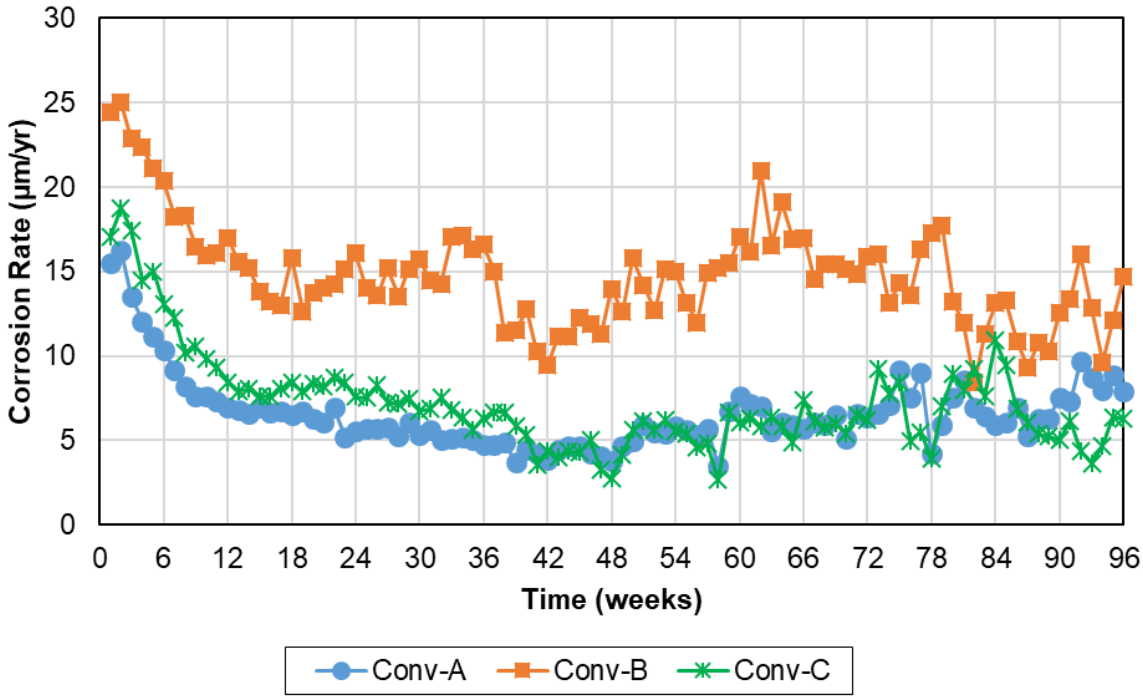

Figure 3.25: Average macrocell corrosion rate (µm/yr) of conventional reinforcement in the cracked beam test

Figures 3.26 and 3.27 show the average corrosion potential of the anodes for the three heats of conventional reinforcement with respect to a copper/copper sulfate electrode (CSE) in the Southern Exposure and cracked beam tests, respectively. In the Southern Exposure test, the three heats of steel exhibited corrosion potentials of about –0.20 V vs. CSE at the start of testing. Conv-A and Conv-C reached an average corrosion potential of –0.35 V by week 12, while Conv-B did so by week 27. The corrosion potentials of the three heats became more negative and reached values between –0.45 V and –0.60 V by week 54 and stayed there for the remainder of the test. A corrosion potential more negative than –0.35 V indicates a greater than 90% probability of active corrosion according to ASTM C876. Throughout the cracked beam test, the three heats of steel exhibited average corrosion potentials more negative than –0.40 V (between –0.45 V and –0.65 V during most of the test).

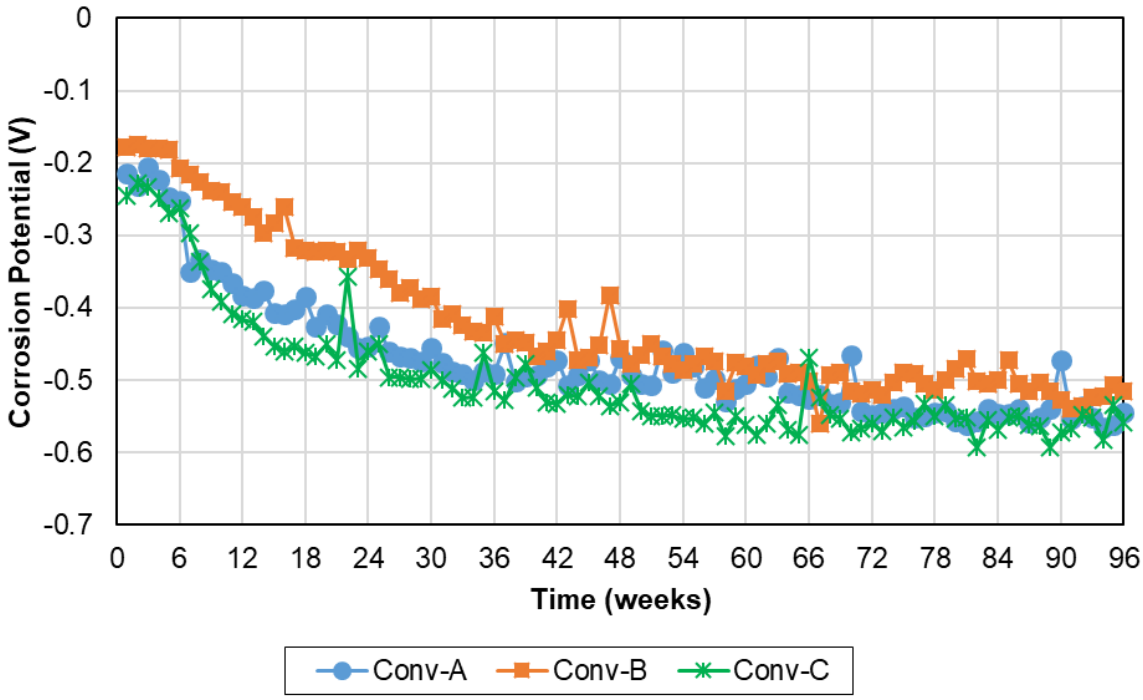

Figure 3.26: Average corrosion potential (vs. CSE) of the anode of conventional reinforcement in the Southern Exposure test

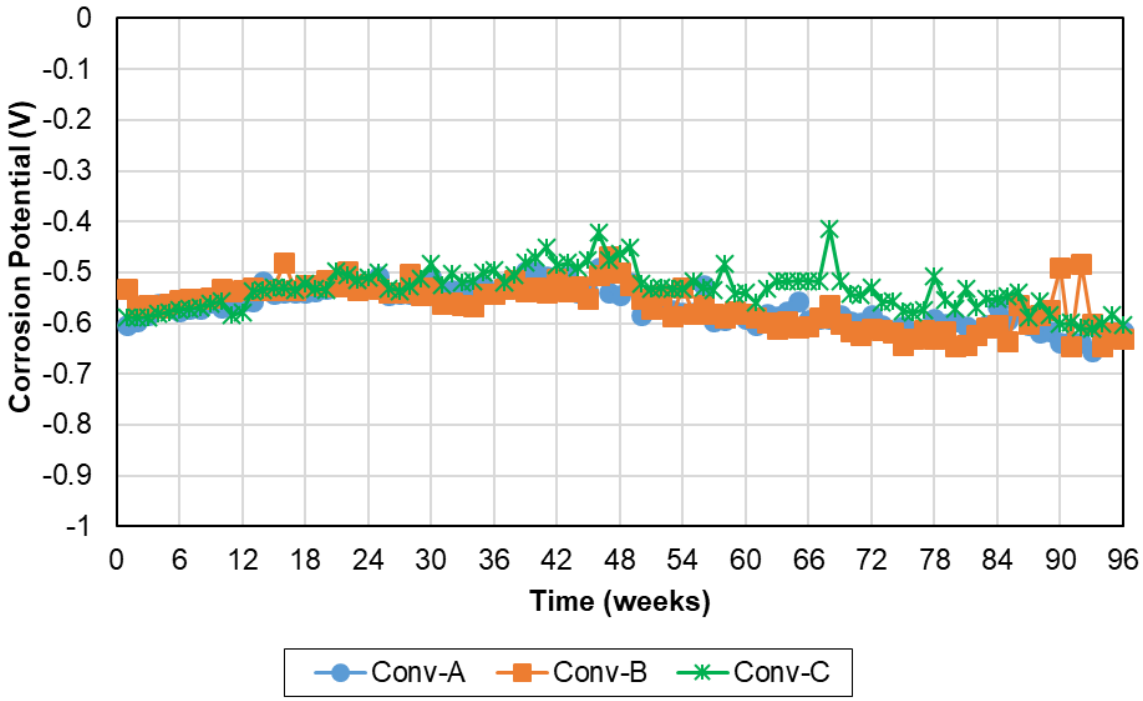

Figure 3.27: Average corrosion potential (vs. CSE) of the anode of conventional reinforcement in the cracked beam test

Five out of the seven cracked beam specimens with Conv-B reinforcement (Conv-B-3 through Conv-B-7) exhibited enough corrosion to crack the concrete (Figure 3.28). These specimens were removed from testing at weeks 49, 67, 77, 83, and 84 (Table 3.11).

Figure 3.28: Cracking of the concrete in specimen Conv-B-3 during the cracked beam test

3.2.1.2 Epoxy-Coated Reinforcement (ECR)

Figure 3.29 shows the average macrocell corrosion rate based on total bar area for specimens with epoxy-coated reinforcement in the Southern Exposure test. Damaged ECR with no UV exposure (ECR1) exhibited no corrosion activity through the first 30 weeks; after 30 weeks, the average corrosion rates peaked at 0.2 μm/yr for limited periods and returned to zero or exhibited negative rates. Damaged ECR1 with 1000 hours of UV exposure (ECR1-UV-1000) initiated corrosion at an earlier age (24 weeks) than ECR1. After week 48, average corrosion rates for ECR1-UV-1000 were consistently above 0.3 μm/yr, peaking at over 0.6 μm/yr at week 68. After peaking, the corrosion rates decreased to about 0.3 μm/yr by the end of the test. Undamaged ECR1

without and with UV exposure (ECR1-ND and ECR1-UV-1000-ND) exhibited corrosion rates of about 0.55 and 0.70 µm/yr at weeks 69 and 76, respectively. During most of the testing, however, they exhibited corrosion activity below 0.2 µm/yr.

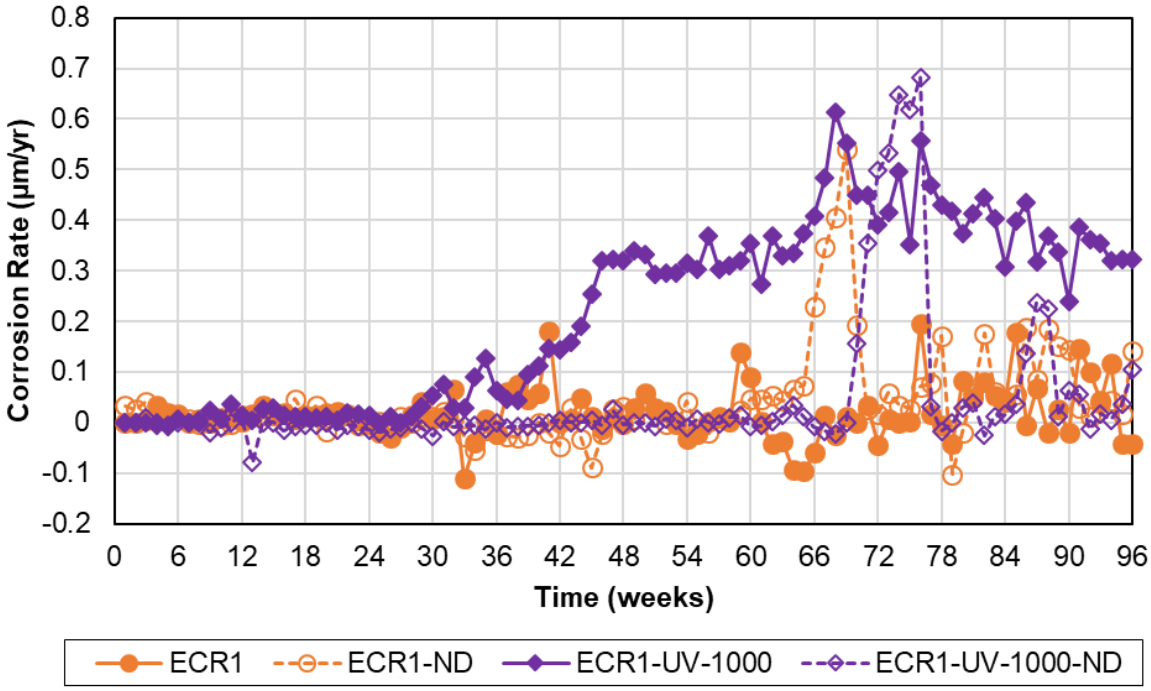

Figure 3.29: Average macrocell corrosion rate (µm/yr) based on total bar area of ECR1 in the Southern Exposure test

Figure 3.30 shows the average macrocell corrosion rate based on total bar area for specimens with epoxy-coated reinforcement in the cracked beam test. Damaged ECR without UV exposure (ECR1) exhibited corrosion rates in the range of 0.1 to 0.3 µm/yr with a spike to 0.6 µm/yr at the end of the test. Damaged ECR with UV exposure (ECR1-UV-1000) exhibited high corrosion activity at the start of the test, exceeding an average of 2 µm/yr. The corrosion activity of ECR1-UV-1000 gradually decreased to approximately 1 µm/yr by week 32; afterward, it increased to about 2 µm/yr by week 50 and then dropped again and reached 1 µm/yr by week 72 again, where it remained for the rest of the test. Undamaged ECR1 with UV exposure (ECR1-UV-1000-ND) exhibited corrosion activity from the start of the test, with corrosion rates in the range

of 0.1 to 0.2 µm/yr for the first 72 weeks of the test. After week 72, however, the corrosion rate of ECR1-UV-1000-ND began to increase, with spikes in the corrosion rates peaking at 0.8 µm/yr. Undamaged ECR1 without UV exposure (ECR1-ND) exhibited corrosion rates near zero with isolated spikes of corrosion activity as high as 0.6 µm/yr.

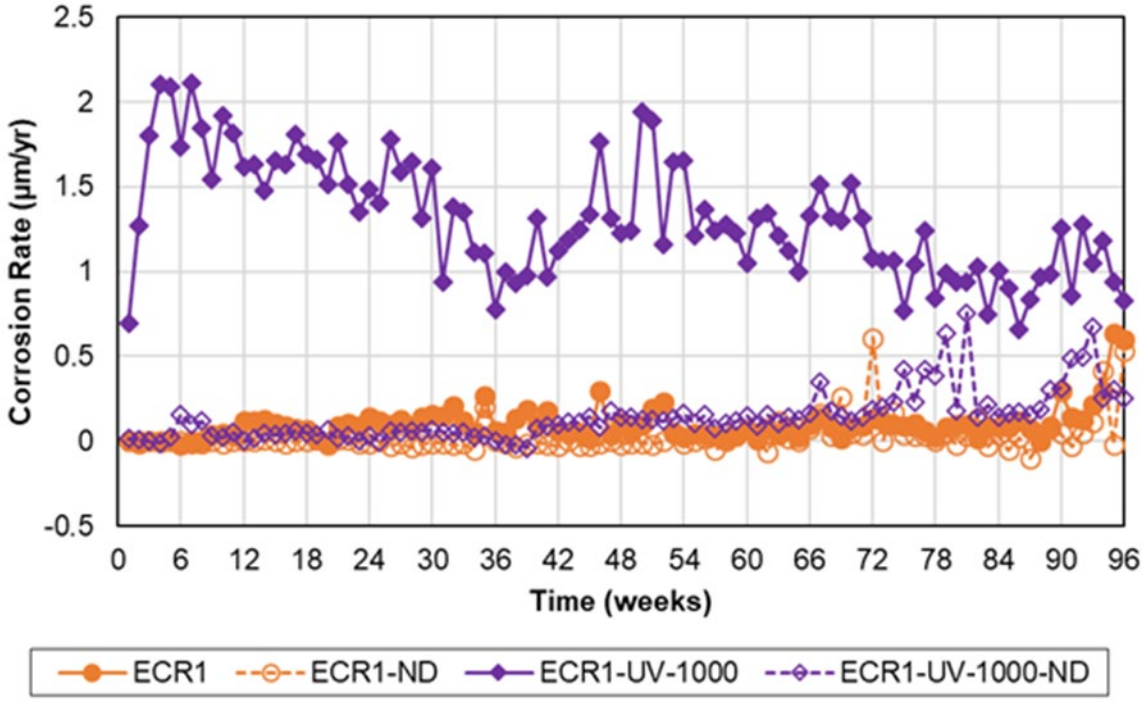

Figure 3.30: Average macrocell corrosion rate (µm/yr) based on total bar area of ECR in the cracked beam test

Figure 3.31 shows the average corrosion potential of the anode of specimens with epoxy-coated reinforcement with respect to CSE in the Southern Exposure test. At the start of testing, ECR1 and ECR1-ND exhibited average corrosion potentials of –0.25 and –0.35 V, respectively. Potentials for both series of specimens approached about –0.30 V by week 30 and remained there for the rest of the test. Damaged ECR1 with UV exposure, ECR1-UV-1000, exhibited potentials between –0.20 V and –0.10 V for the first 18 weeks and between –0.15 V and –0.35 V from week 18 to 42. The corrosion rates of ECR1-UV-1000 dropped around week 42 consistent with the time of corrosion initiation in these specimens. Afterward, ECR1-UV-1000 exhibited an average corrosion potential more negative than –0.40 V gradually decreasing to –0.55 V by the end of the

test. ECR1-UV-1000-ND exhibited average corrosion potentials identical to those of ECR1-UV-1000 in the first 42 weeks of testing; after week 42, the rates gradually became more negative with some fluctuations, approaching –0.30 V by the end of the test.

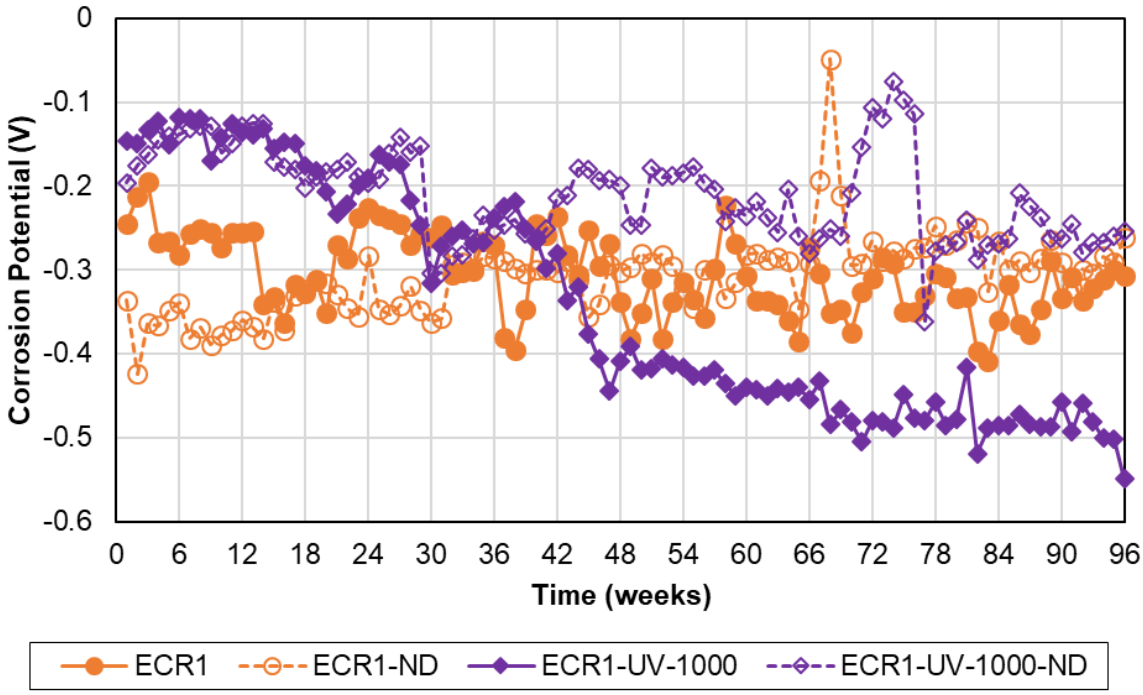

Figure 3.31: Average corrosion potential (vs. CSE) of the anode of ECR1 in the Southern Exposure test

Figure 3.32 shows the average corrosion potential for the anode of epoxy-coated reinforcement with respect to CSE for specimens in the cracked beam test. The specimens exhibited corrosion potentials that remained approximately constant after the first few weeks of testing. Specimens with UV exposure consistently exhibited more negative potentials than specimens without UV exposure. Damaged ECR without UV exposure (ECR1) exhibited potentials around –0.20 V at the beginning of the test dropping to about –0.50 V after week 6 before rising to –0.30 and –0.40 V by week 45. Damaged ECR with 1000 hours of UV exposure (ECR1-UV-1000) exhibited a corrosion potential of approximately –0.60 V, the most negative of any ECR specimens. Undamaged ECR with UV exposure (ECR1-UV-1000-ND) exhibited

average corrosion potentials between –0.29 and –0.52 V, while undamaged ECR1 without UV exposure (ECR1-ND) exhibited potentials between –0.17 and –0.36 V.

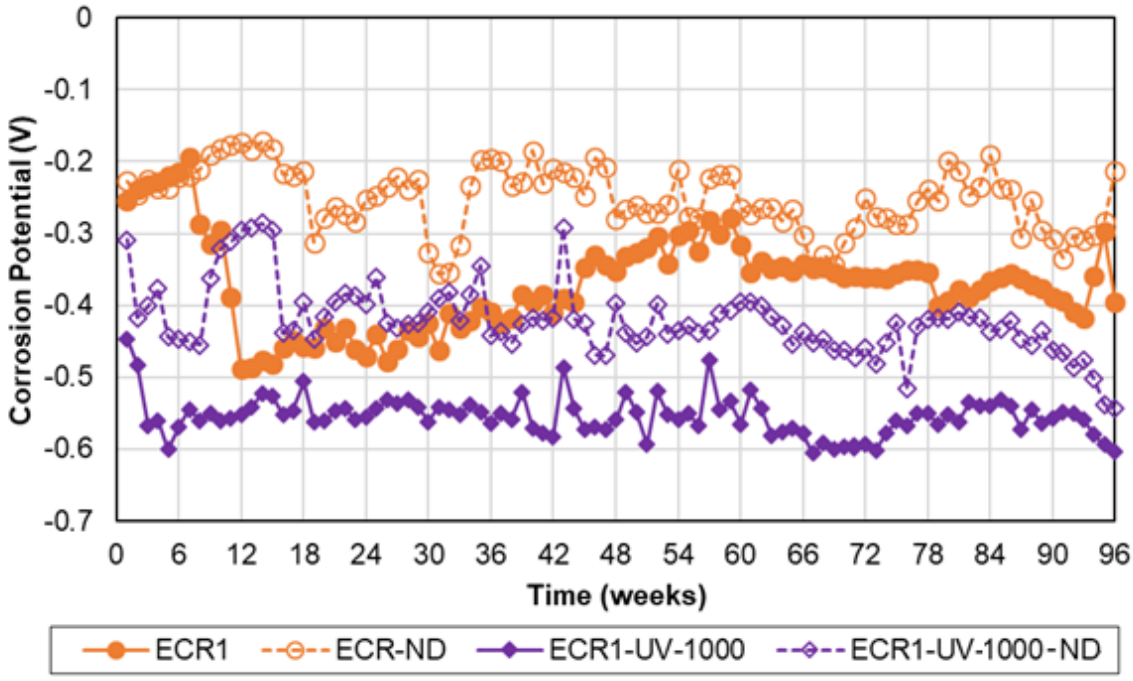

Figure 3.32: Average corrosion potential (vs. CSE) of the anode of ECR1 in the cracked beam test

3.2.1.3 Galvanized Reinforcement

Figures 3.33 and 3.34 show the average macrocell corrosion rates of A767 and A1094 galvanized reinforcement, as well as the matching conventional reinforcement used to produce them (Conv-B and Conv-C, respectively) in the Southern Exposure test. No difference in behavior was noted between damaged, undamaged, and bent galvanized specimens. A767 (A767, A767-ND, A767-Bent) reinforcement exhibited some corrosion activity at the beginning of the test, with average corrosion rates in the range of 1 to 2.5 µm/yr. The corrosion rates of damaged A767, peaking just below 2.5 µm/yr, were near zero most of the testing period and only dropped well below zero at week 72. Undamaged A767 exhibited corrosion rates similar to damaged A767 in the first 30 weeks. The corrosion rates of A767-Bent increased to 4 µm/yr by week 12 and remained between 2.5 to 4 µm/yr for about 12 weeks before dropping. By week 30, the average

corrosion rates of all A767 galvanized specimens dropped to near zero or became negative, which can indicate corrosion activity on both the bottom and top bars. Undamaged and bent A767 reinforcement began exhibiting positive corrosion activity again around week 54, fluctuating and peaking at 4 μm/yr.

A1094 (A1094, A1094-ND, A1094-Bent) reinforcement exhibited some corrosion activity at the beginning of the test, with average corrosion rates in the range of 0 to 2.5 μm/yr. Like A767 reinforcement, by week 30, the average corrosion rates of 1094 galvanized specimens dropped to near zero or became negative. The corrosion rates of A1094 reinforcement returned to near zero by week 48. Afterward, the corrosion rates remained lower than 1 μm/yr and near zero except for another drop to negative rates at around week 70.

The corrosion rates for all galvanized bars after week 20 were much lower than conventional reinforcement. The Conv-B corrosion rate increased gradually throughout the test from about zero to about 9.5 μm/yr. The Conv-C corrosion rates increased gradually throughout the test from about zero to about 9 μm/yr by week 91 and, afterward, decreased to about 7.5 μm/yr at the end of the test.

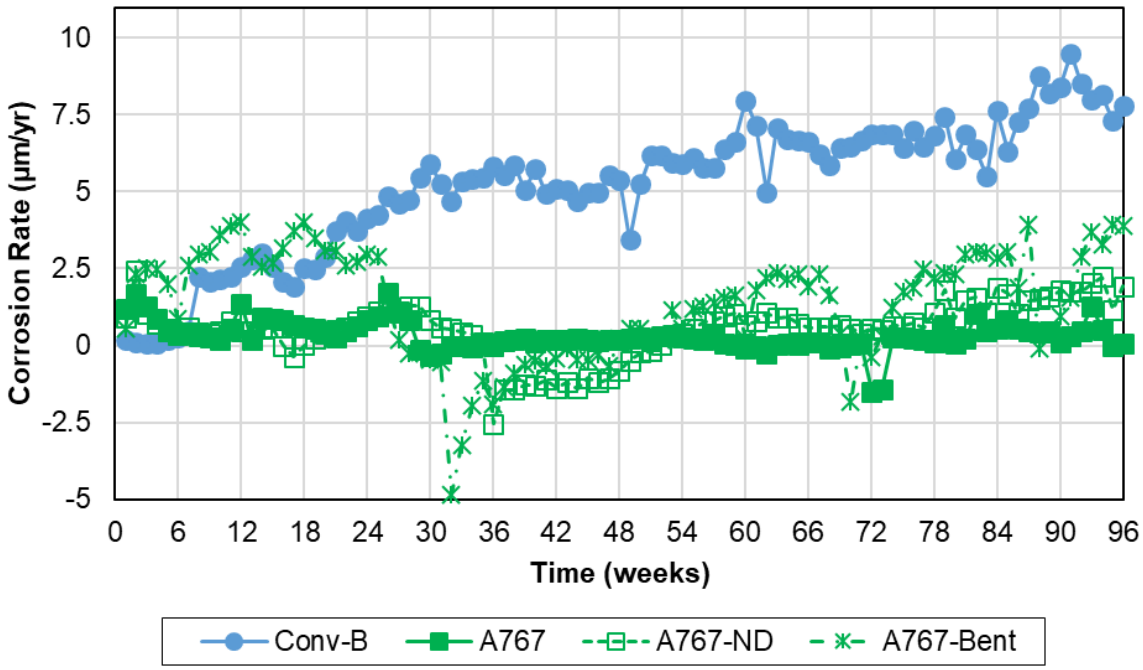

Figure 3.33: Average macrocell corrosion rate (µm/yr) of A767 galvanized and Conv-B reinforcement in the Southern Exposure test

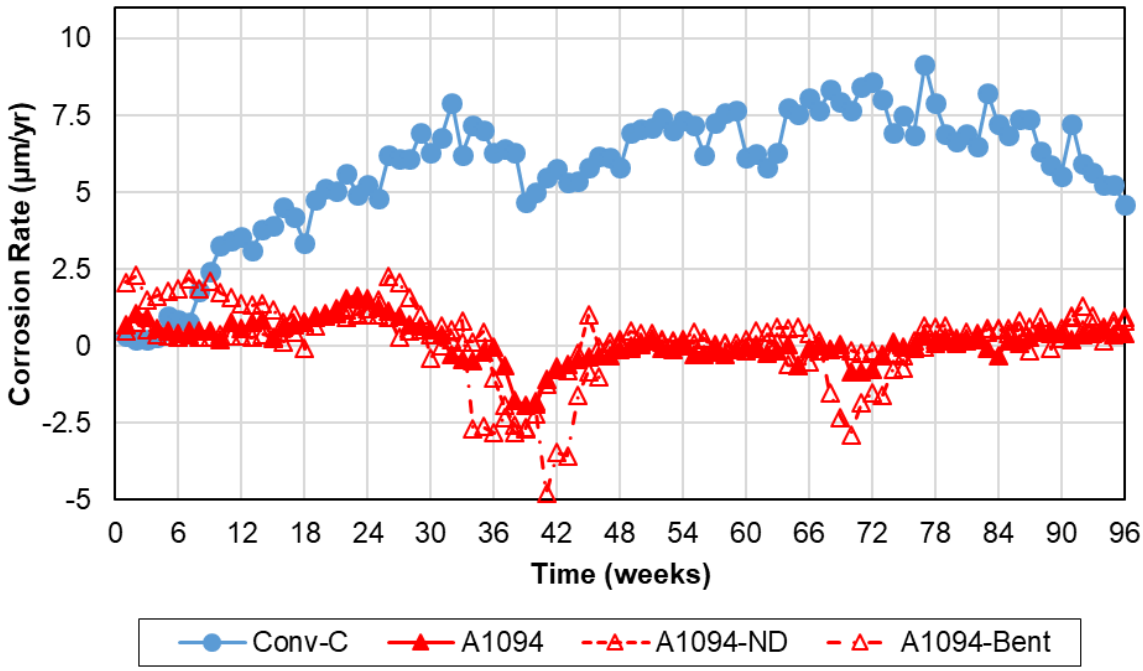

Figure 3.34: Average macrocell corrosion rate (µm/yr) of A1094 galvanized reinforcement and Conv-C in the Southern Exposure test

Figures 3.35 and 3.36 show the average macrocell corrosion rates of A767 and A1094 galvanized reinforcement, as well as the matching conventional reinforcement used to produce

them (Conv-B and Conv-C, respectively) in the cracked beam test. All specimens exhibited very high corrosion rates, between 15 and 25 μm/yr, during the first few weeks of testing. The corrosion rates for the galvanized bars dropped rapidly to values less than 4 μm/yr by week 10, and gradually decreased to 1 to 2 μm/yr by week 18. The corrosion rates for damaged and undamaged A767 began to increase after week 18, reaching 5 μm/yr, with the corrosion rates of damaged A767 gradually decreasing to zero during the last 24 weeks of testing. Average corrosion rates on A1094 reinforcement increased after a drop to negative rates at week 70 but remained lower than 3 μm/yr.

The corrosion rates for galvanized bars were one-third to one-fourth that of conventional reinforcement, except for the beginning of the testing. Conv-B and Conv-C had corrosion rates of about 25 and 20 μm/yr at the beginning of the test; these corrosion rates decreased to about 15 and 5 μm/yr at the end of the test, respectively. It should be noted, however, that Conv-B reinforcement was used to produce the A767 reinforcement and Conv-C reinforcement to produce the A1094 reinforcement. Therefore, the differences in the behavior between the two types of galvanized reinforcement may not be solely due to differences in the coating; differences in the corrosion performance of the conventional core may have affected the results, particularly for the damaged bars where the underlying steel was exposed.

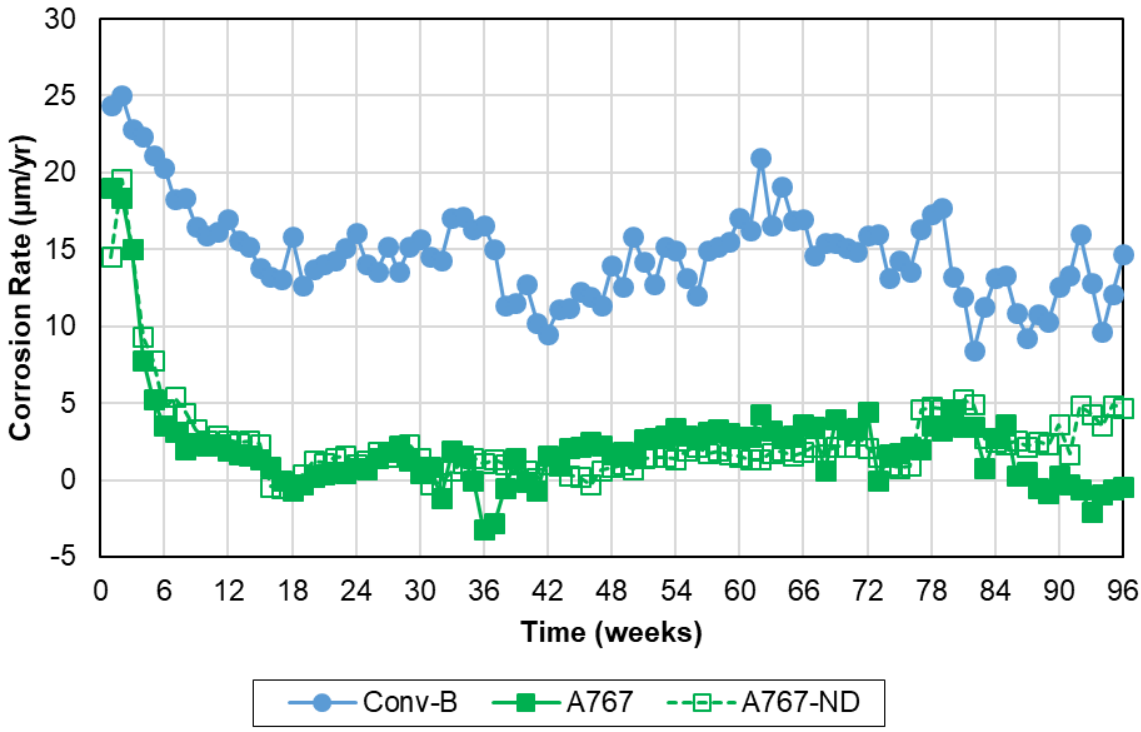

Figure 3.35: Average macrocell corrosion rate (µm/yr) of A767 galvanized and Conv-B reinforcement in the cracked beam test

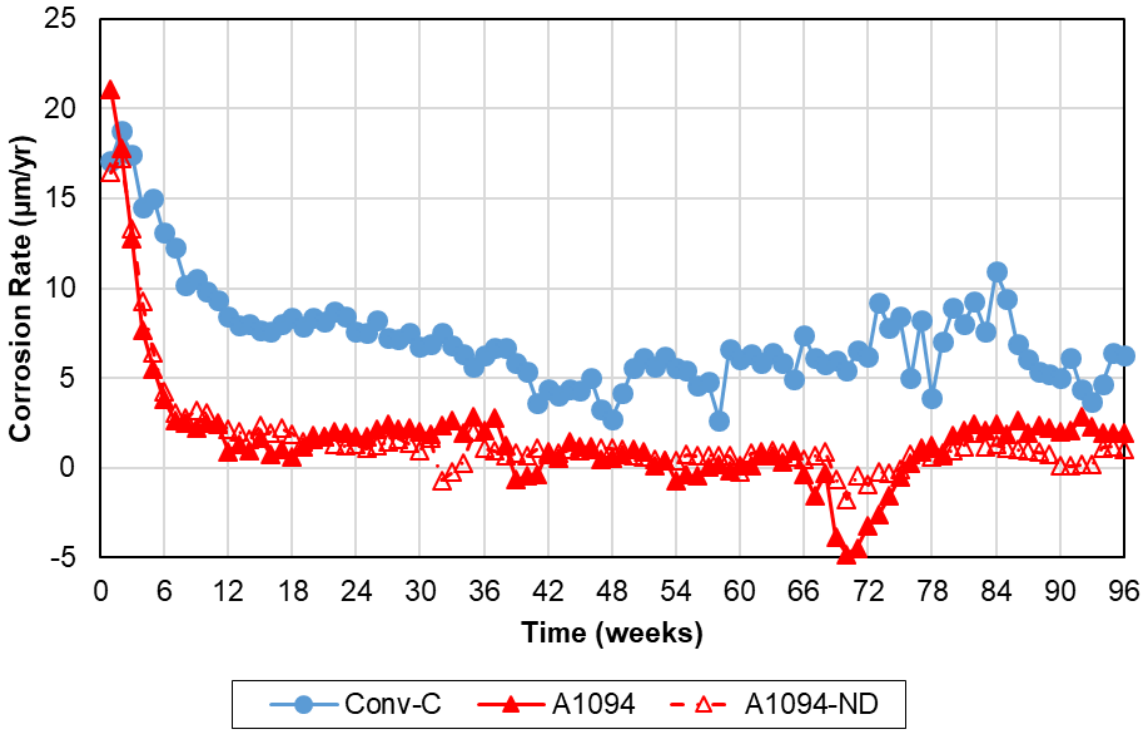

Figure 3.36: Average macrocell corrosion rate (µm/yr) of A1094 galvanized and Conv-C reinforcement in the cracked beam test

Figures 3.37 and 3.38 show the average corrosion potential of the anode for the ASTM

A767 and A1094 galvanized reinforcement and the matching conventional reinforcement used to produce them (Conv-B and Conv-C) versus CSE in the Southern Exposure test. At the beginning of the test, damaged, bent, and undamaged A767 had an average potential of about –0.50 V. The potentials for damaged A767 gradually became more positive over the first 12 weeks, reaching –0.40, before fluctuating until week 30. After week 30, the corrosion potentials of damaged A767 remained between –0.30 to –0.40 V until week 72 with some fluctuations. After week 72, they dropped to about –0.50 V except for some spikes. The corrosion potentials of undamaged A767 fluctuated near –0.40 V in the first 30 weeks and remained between –0.40 to –0.50 V after week 30. The potentials of bent A767 dropped to –0.40 V in the first 12 weeks and remained there for 12 weeks before gradually becoming more positive and reaching –0.30 V by week 66; Afterward, they remained there before a spike to –0.20 V at the end of the test.

At the beginning of the test, damaged, undamaged, bent, and undamaged A1094 had an average potential close to –0.70 V; they gradually became more positive and reached –0.50 V at week 30. Afterward, the corrosion potentials of A1094 remained approximately at about –0.50 V with spikes to about –0.40 V.

Conv-B and Conv-C had corrosion potentials near –0.20 V at the beginning of the test, more positive than those of galvanized reinforcement. Corrosion potentials of Conv-B and Conv-C gradually became more negative during the test, reaching about –0.60 V; more negative than those of galvanized reinforcement.

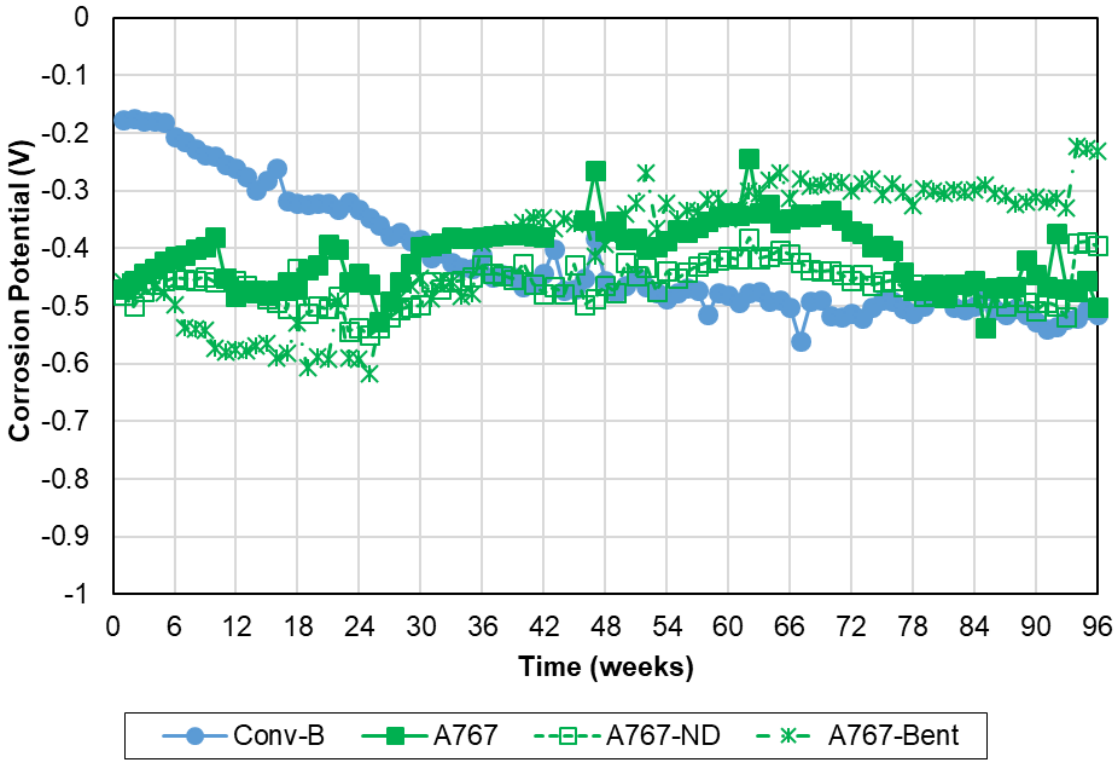

Figure 3.37: Average corrosion potential (vs. CSE) of the anode of A767 galvanized and Conv-B reinforcement in the Southern Exposure test

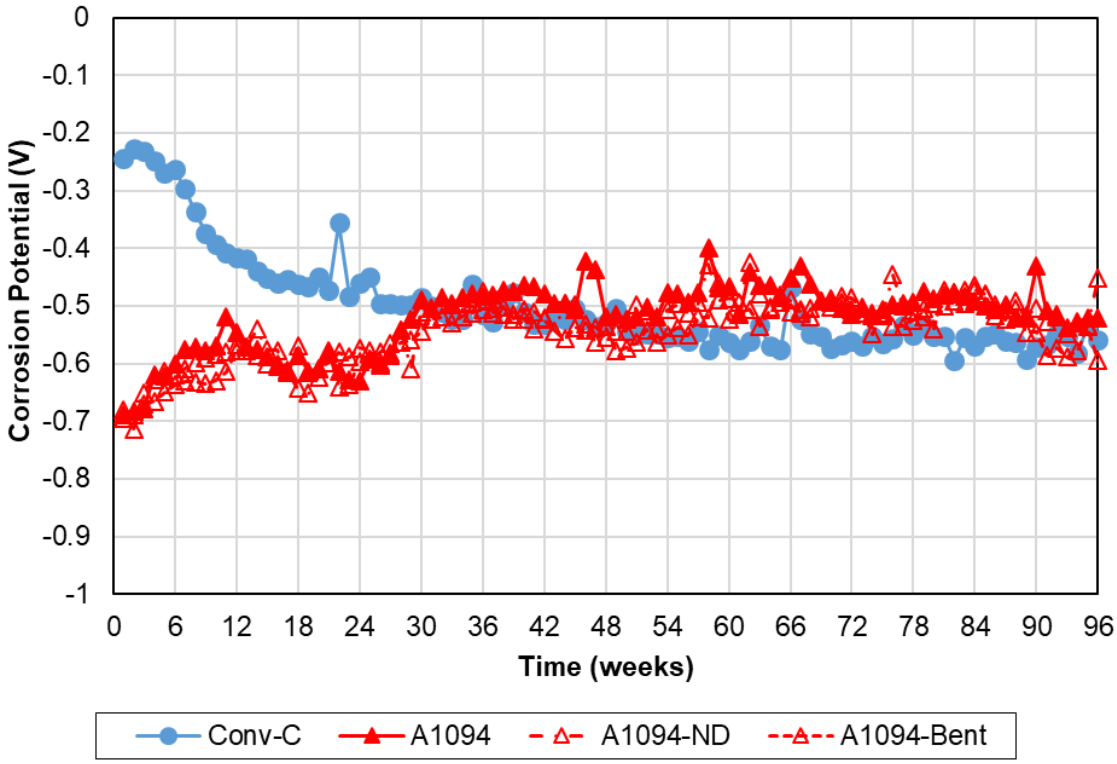

Figure 3.38: Average corrosion potential (vs. CSE) of the anode of A1094 galvanized and Conv-C reinforcement in the Southern Exposure test

Figures 3.39 and 3.40 show the average corrosion potential of the anode for the ASTM A767 and A1094 galvanized reinforcement and the matching conventional reinforcement used to produce them (Conv-B and Conv-C) versus CSE in the cracked beam test. At the beginning of the test, the damaged and undamaged A767 had an average potential of about –0.80 V, while the damaged and undamaged A1094 had an average potential of about –1.0 V. Over the first 18 weeks of the test, the potentials of the A767 and A1094 steel gradually became more positive, reaching values between –0.50 and –0.60 V, and then remained approximately constant for the remainder of the test.

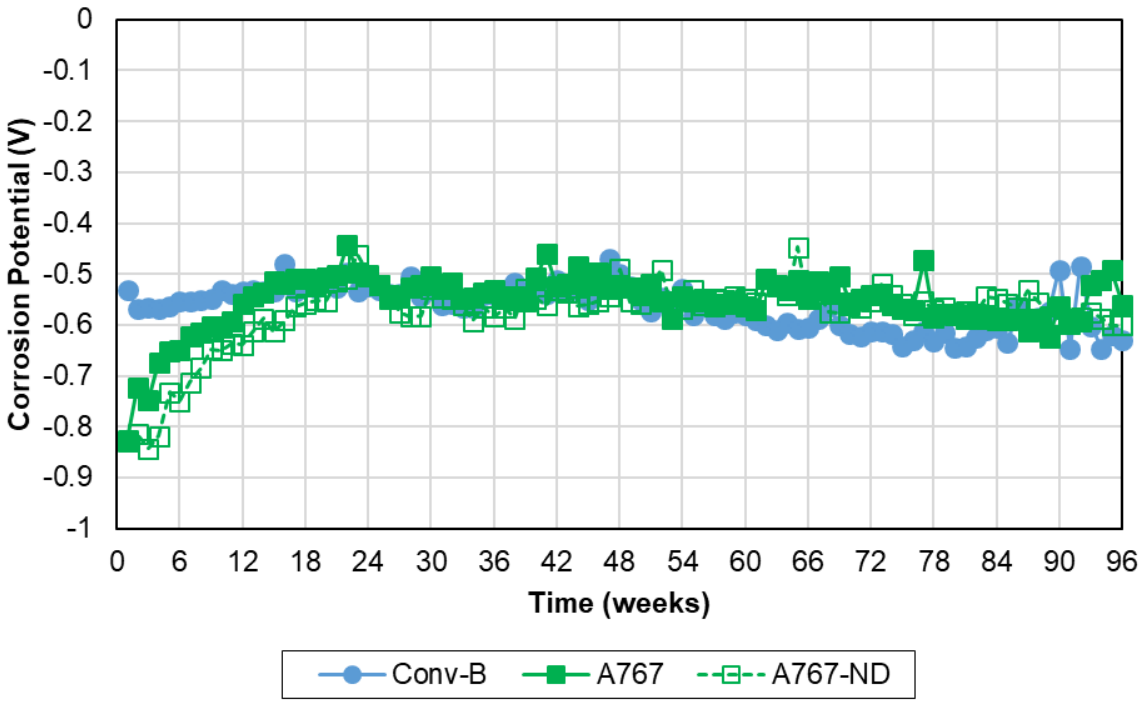

Figure 3.39: Average corrosion potential (vs. CSE) of the anode of A767 galvanized and Conv-B reinforcement in the cracked beam test

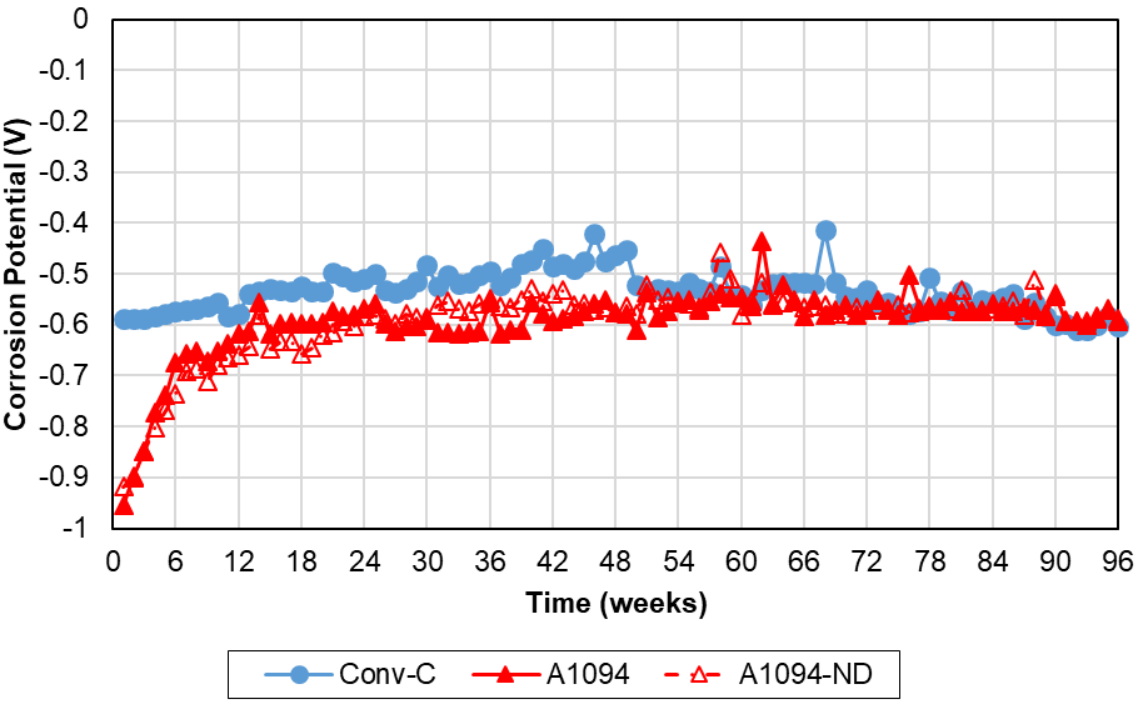

Figure 3.40: Average corrosion potential (vs. CSE) of the anode of A1094 galvanized and Conv-C reinforcement in the cracked beam test

3.2.1.4 ChromX (A1035 Type CS) and Conventional Reinforcement, IPANEX, and Xypex

Figure 3.41 shows the average macrocell corrosion rates for conventional and ChromX (A1035 Type CS) reinforcement in the Southern Exposure test. Results are presented for bars in concrete without and with the IPANEX and Xypex admixtures. Conv-B was the only conventional reinforcement evaluated with the two admixtures. The addition of IPANEX did not decrease the corrosion rate of either conventional or ChromX reinforcement. IPANEX even appeared to increase the corrosion rates. Xypex had no impact on corrosion performance early in the test but reduced the corrosion rate of Conv-B after week 54. Specimens with Conv-B reinforcement paired with Xypex exhibited a peak rate about 6 μm/yr, lower than Conv-B without Xypex (which peaked at about 8 μm/yr). The addition of Xypex did not alter the corrosion rate of ChromX reinforcement; both ChromX reinforcement alone and ChromX reinforcement paired with an admixture exhibited average corrosion rates below 2 μm/yr throughout the test. Xypex admixture gradually forms a non-soluble structure that decreases the permeability of concrete and, therefore, increases its electrical resistance, which will in turn decrease the macrocell corrosion rate. The decrease in permeability also slows down penetration of chlorides into concrete. Xypex is less effective paired with ChromX than conventional reinforcement since ChromX already exhibits a low corrosion rate.

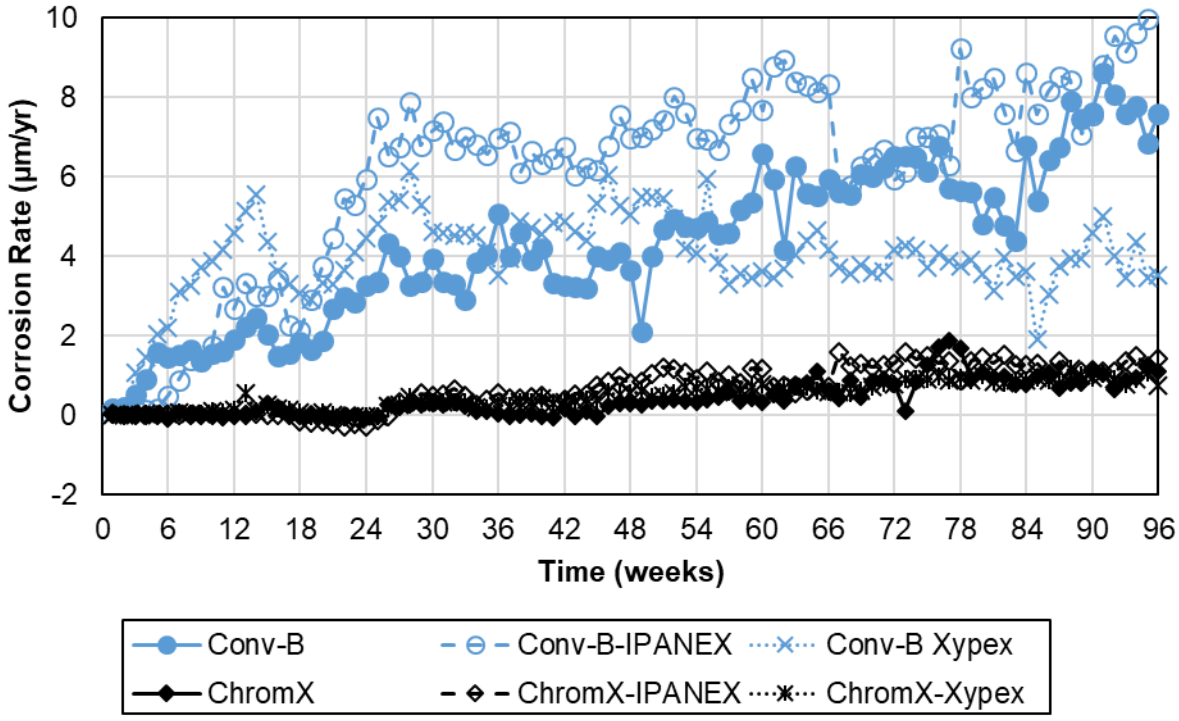

Figure 3.41: Average macrocell corrosion rate (µm/yr) of Conv-B and ChromX reinforcement without and with IPANEX and Xypex in the Southern Exposure test

Figure 3.42 shows the average macrocell corrosion rates for conventional and ChromX (A1035 Type CS) reinforcement in the cracked beam test. Results are presented for bars in concrete without and with IPANEX and Xypex. ChromX reinforcement without and with Xypex exhibited average corrosion rates between 2.5 and 5 µm/yr through most of the test. Conv-B reinforcement exhibited rates as high as 25 µm/yr early in the testing, with rates mostly in the 10 to 20 µm/yr range later. The addition of IPANEX did not alter the corrosion rate of either Conv-B or ChromX reinforcement and appeared to increase the corrosion rates of Conv-B in the beginning and at the end of testing. The corrosion rates of Conv-B without and with Xypex match in the beginning of testing. As observed in the Southern Exposure test, specimens with Conv-B reinforcement and Xypex exhibited lower corrosion rates than Conv-B without Xypex, particularly after 18 weeks of testing. After week 18, Conv-B reinforcement exhibited a peak corrosion rate of around 11 µm/yr with Xypex, lower than a peak of around 20 µm/yr without Xypex.

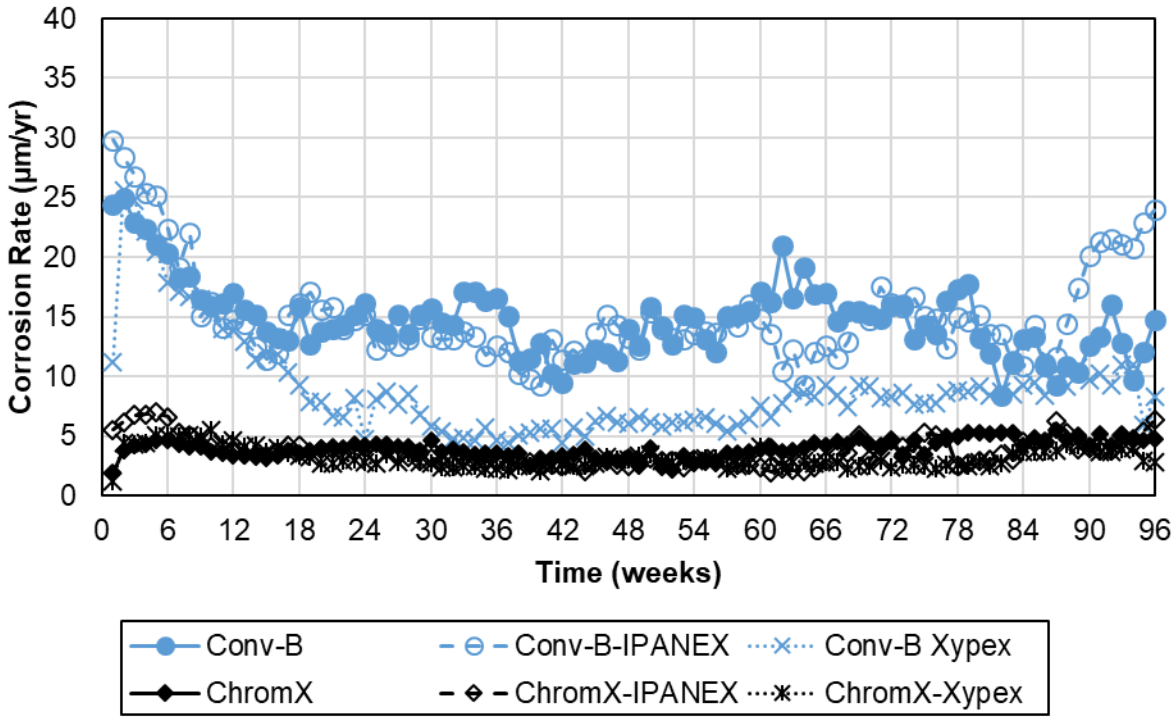

Figure 3.42: Average macrocell corrosion rate (µm/yr) of Conv-B and ChromX reinforcement without and with IPANEX and Xypex in the cracked beam test

Figures 3.43 and 3.44 show the average corrosion potential of the anode of conventional (Conv-B) and ChromX (A1035 Type CS) reinforcement in the Southern Exposure and cracked beam tests, respectively, for bars in concrete without and with IPANEX and Xypex. In both tests, ChromX reinforcement exhibited a potential about 0.10 V more positive than Conv-B reinforcement for most of the testing. In the Southern Exposure test, all specimens started with an average corrosion potential of about –0.20 V; potentials dropped as specimens initiated corrosion, and Conv-B and ChromX reinforcement reached potentials of –0.40 and –0.30 V by week 30, respectively. Potentials for Conv-B and ChromX became –0.10 V more negative by week 96. In the cracked beam test, specimens exhibited a consistent average corrosion potential throughout the test, with ChromX and Conv-B reinforcement exhibiting a potential around –0.50 and –0.60 V, respectively. Neither admixture affected corrosion potential.

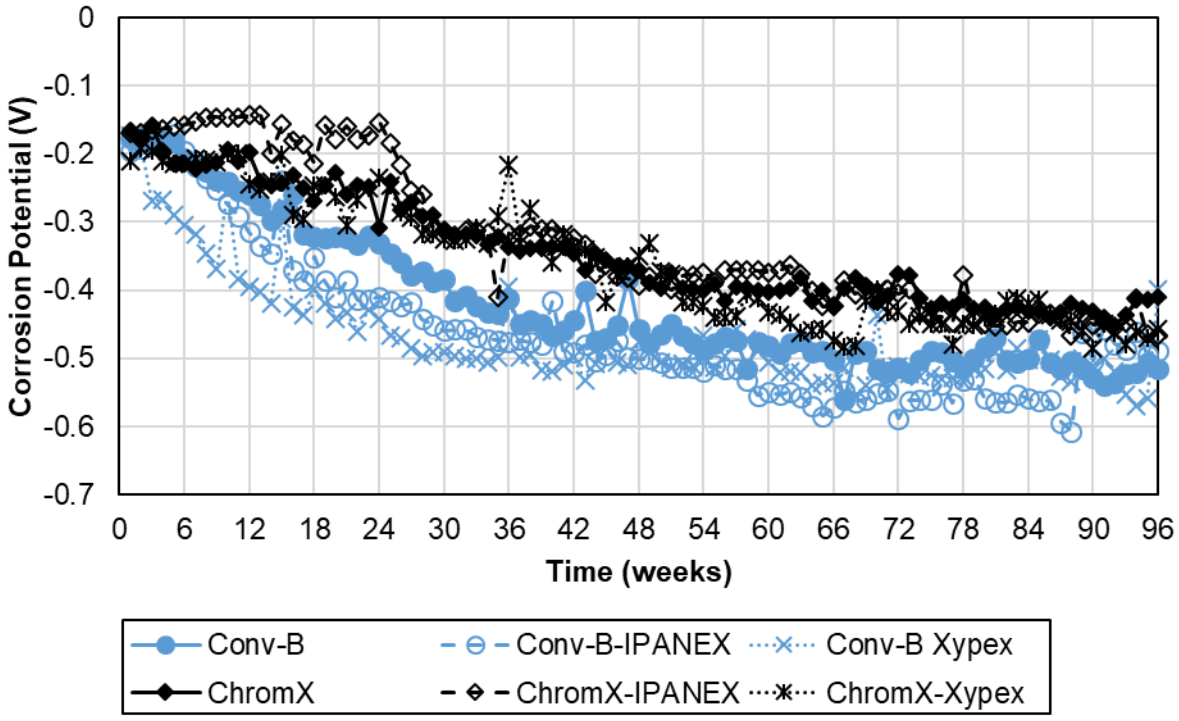

Figure 3.43: Average corrosion potential (vs. CSE) of Conv-B and ChromX reinforcement without and with IPANEX and Xypex in the Southern Exposure test

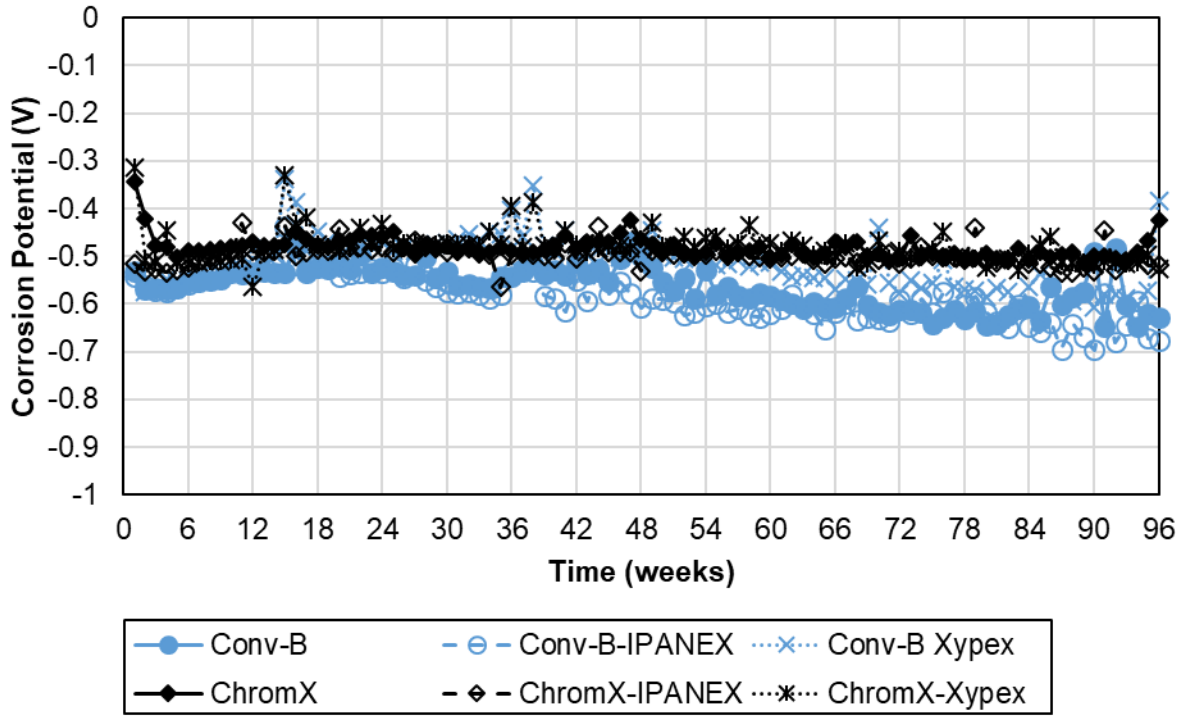

Figure 3.44: Average corrosion potential (vs. CSE) of Conv-B and ChromX reinforcement without and with IPANEX and Xypex in the cracked beam test

Four cracked beam specimens with conventional reinforcement and IPANEX cracked due

to excessive corrosion and were removed from testing before 96 weeks (Conv-B IPANEX-1 at week 55, Conv-B IPANEX-2 at week 77, Conv-B IPANEX-4 at week 81, and Conv-B IPANEX-5 at week 80) (Table 3.11).

3.2.2 LPR Corrosion Rates

3.2.2.1 Conventional Reinforcement

Figure 3.45 shows the average corrosion rate based on LPR for conventional reinforcement in the Southern Exposure test. At week four, both Conv-A and Conv-C exhibited corrosion rates near 1 μm/yr, while Conv-B exhibited rates near 4 μm/yr. As shown in Figure 3.24, at week 4, Conv-B exhibited a macrocell corrosion rate of 0.90 μm/yr, also greater than the values for Conv-A and Conv-B (0.16 and 0.30 μm/yr, respectively). The relative values of LPR rates are somewhat similar to those of macrocell rates. The corrosion rates for the three heats gradually increased in the first 40 weeks, and then fluctuated without major increases through weeks 84 to 92 depending on the reinforcement. All corrosion rates for the three heats dropped during the final weeks of the test. Conv-A, Conv-B, and Conv-C exhibited peak corrosion rates of 11, 14, and 15 μm/yr at weeks 92, 44, and 60, respectively. These rates are higher than the values for macrocell corrosion rates, which did not exceed 10 μm/yr (Figure 3.24). Conv-A had lower corrosion rates than Conv-B and Conv-C during most of the test.

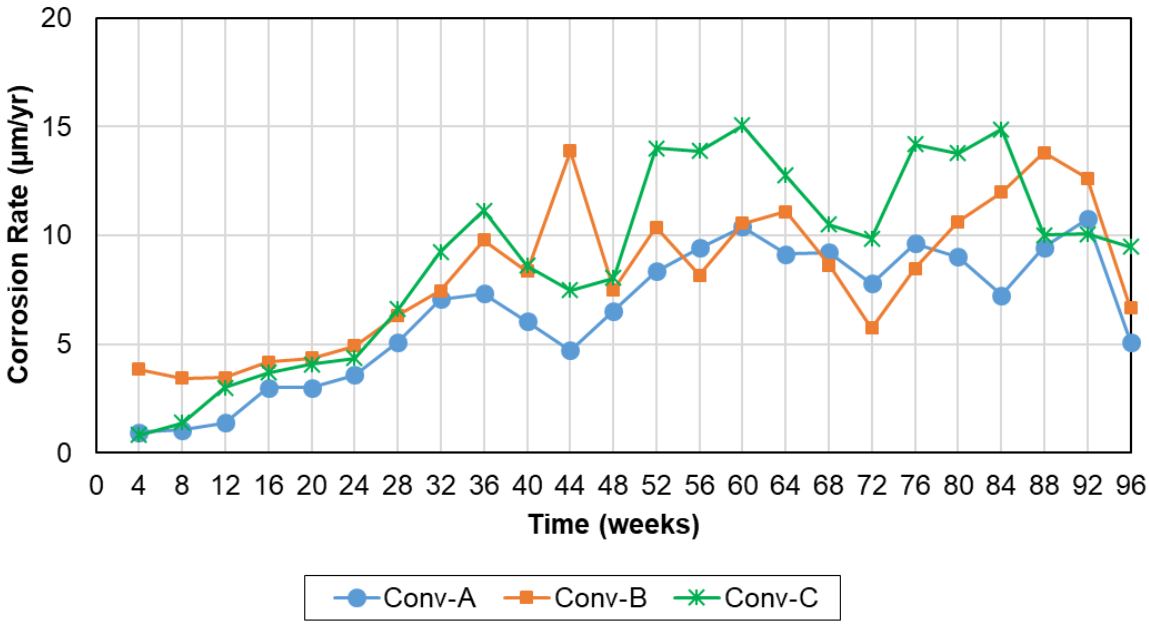

Figure 3.45: Average LPR corrosion rate (µm/yr) of conventional reinforcement in the Southern Exposure test

Figure 3.46 shows the average LPR corrosion rate for conventional reinforcement in the cracked beam test. At week four, Conv-A, Conv-B, and Conv-C exhibited LPR corrosion rates near 14, 22, 11.5 µm/yr, compared to their macrocell rates near 12, 22, and 15 µm/yr, respectively (Figure 3.25); the total corrosion rates are dominated by macrocell corrosion rates at the start of testing. Unlike macrocell rates, LPR corrosion rates for the three heats fluctuated in the same approximate range with macrocell corrosion rates gradually decreasing during the first half of the test, and remaining approximately constant afterward, as shown in Figure 3.25. This could be due to the gradual increase in concrete's resistance as it cures; this increased resistance affects macrocell corrosion rates. Conv-A, Conv-B, and Conv-C exhibited peak LPR corrosion rates of 35, 57, and 24 µm/yr at weeks 96, 84, and 84, respectively. Conv-C exhibited corrosion rates lower than Conv-A and Conv-B during most of the test, unlike in the Southern Exposure test.

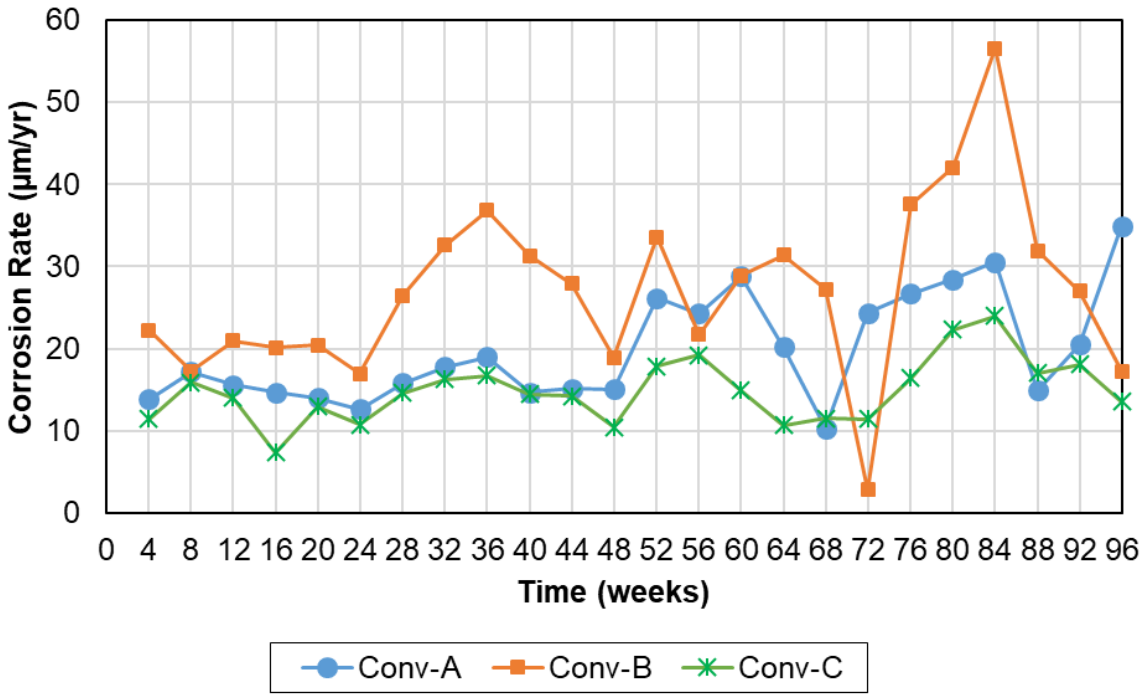

Figure 3.46: Average LPR corrosion rate (µm/yr) of conventional reinforcement in the cracked beam test

3.2.2.2 Epoxy-coated Reinforcement (ECR)

Figure 3.47 shows the average LPR corrosion rate for damaged and undamaged epoxy-coated reinforcement without and with 1000 hours of UV exposure in the Southern Exposure test. The LPR rates approximately match with the macrocell rates at week 4. ECR1 and ECR1-ND exhibited average LPR corrosion rates consistently below 0.15 µm/yr. Except for two isolated spikes to 0.45 µm/yr at weeks 20 and 32, ECR1-UV-1000-ND had LPR rates lower than 0.15 µm/yr. The LPR rates for ECR1-UV-1000 remained below 0.20 µm/yr until week 36, about the time the macrocell corrosion rates started increasing (Figure 3.29), and then gradually increased with some fluctuations and reached 1.3 µm/yr at the end of test. Unlike the macrocell corrosion rate, which peaked at about week 66 (Figure 3.29), the LPR rates of ECR1-UV-1000 did not gradually decrease at the end of testing but had two isolated drops to about 0.3 µm/yr at weeks 56 and 88.

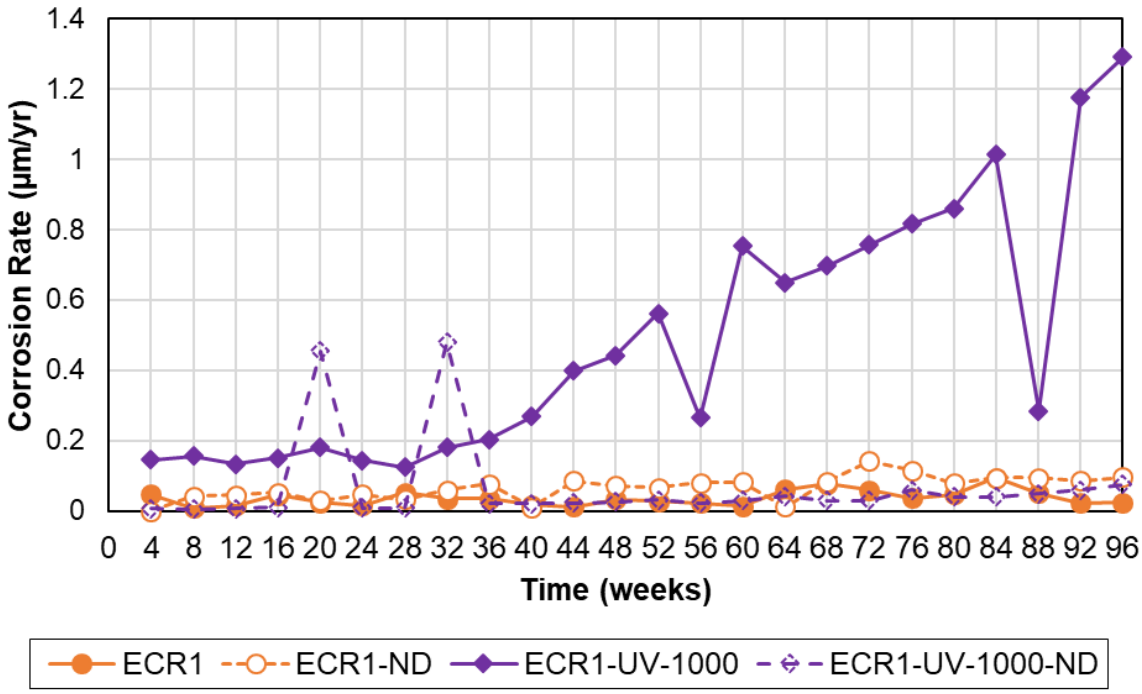

Figure 3.47: Average LPR corrosion rate (µm/yr) of damaged and undamaged ECR without and with 1000 hours of UV exposure in the Southern Exposure test

Figure 3.48 shows the average LPR corrosion rate for damaged and undamaged epoxy-coated reinforcement without and with 1000 hours of UV exposure in the cracked beam test. The LPR corrosion rates match the macrocell rates at week 4 (Figure 3.30). ECR1, ECR1-ND, ECR1-UV-1000-ND exhibited an average LPR corrosion rate consistently well below 1 µm/yr, similar to the macrocell corrosion rate (Figure 3.30). The LPR rate for ECR1-UV-1000 gradually increased with some fluctuations and reached 7 µm/yr at week 92 followed by a decrease to about 5 µm/yr at week 96; the largest fluctuations (to below 1 µm/yr) occurred at weeks 84 and 88. Similar to the Southern Exposure test, this is in contrast to the macrocell corrosion rates for ECR1-UV-1000, which gradually decreased after reaching the highest value in the first six weeks (Figure 3.30).

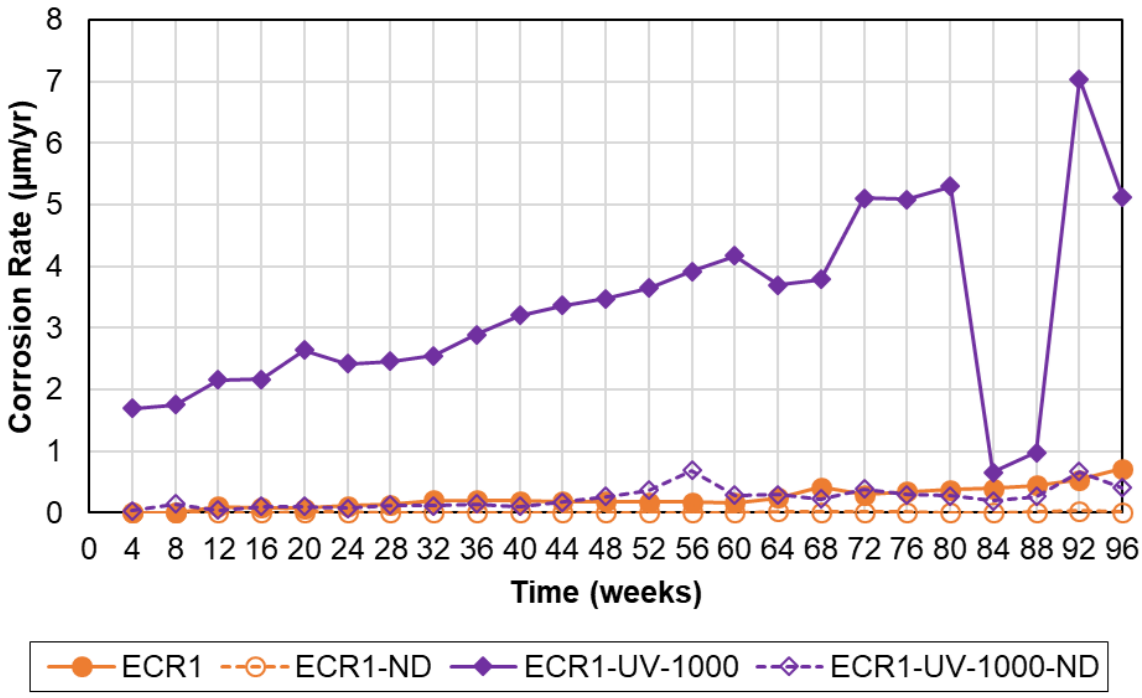

Figure 3.48: Average LPR corrosion rate (µm/yr) of damaged and undamaged ECR without and with 1000 hours of UV exposure in the cracked beam test

3.2.2.3 Galvanized Reinforcement

Figure 3.49 shows the average LPR corrosion rates for damaged, undamaged, and bent A767 galvanized reinforcement as well as the reinforcement used to produce them (Conv-B) in the Southern Exposure test. The LPR corrosion rates of Conv-B were described in Section 3.2.2.1. The LPR corrosion rates of damaged A767 (A767) started just below 2 µm/yr and gradually increased to about 5 µm/yr, less than half the rates for Conv-B through the first 64 weeks of testing. After week 64, the corrosion rates of damaged A767 increased to about the same range as Conv-B (between 5 to 15 µm/yr). The corrosion rates of undamaged A767 (A767-ND) were almost identical to those of damaged A767 during the first 60 weeks. After week 60, the LPR corrosion rates of undamaged A767 were about half the values of damaged A767. Unlike damaged and undamaged A767, bent A767 had LPR corrosion rates comparable to Conv-B.

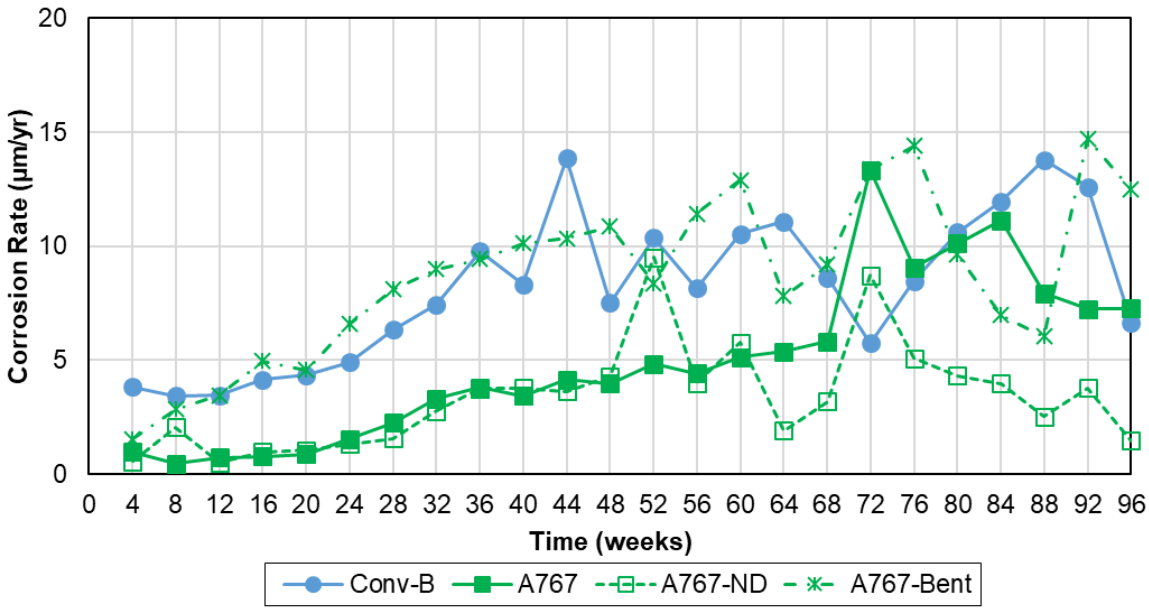

Figure 3.49: Average LPR corrosion rate (µm/yr) of A767 and Conv-B reinforcement in the Southern Exposure test

Figure 3.50 show the average LPR corrosion rates for damaged, undamaged, and bent A1094 galvanized reinforcement as well as the reinforcement used to produce them (Conv-C) in the Southern Exposure test. The corrosion rates of damaged and undamaged A1094 exhibited LPR corrosion rates in the same range throughout the test. Through most of the testing, damaged and undamaged A1094, A1094 and A1094-ND respectively, had LPR rates about half the rates for Conv-C. After week 84, the difference between the corrosion rates of damaged and undamaged A1094 and those of Conv-C decreased. During the first 60 weeks of testing, bent A1094 exhibited rates in the same range as Conv-C; after week 60, bent A1094 had rates generally in the same range as damaged and undamaged A1094.

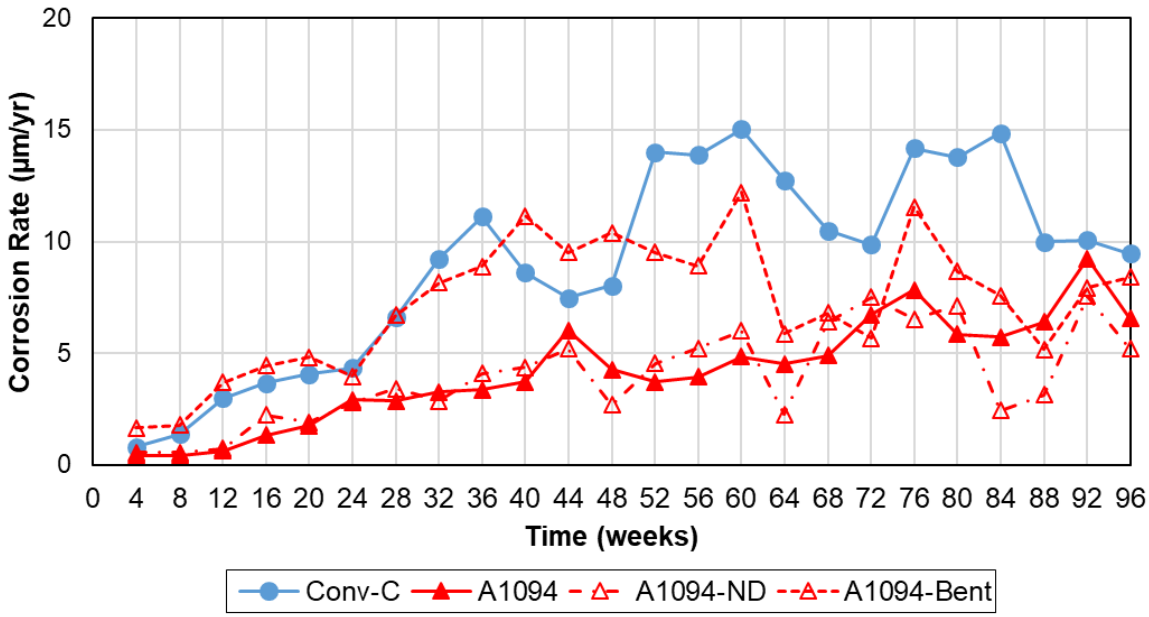

Figure 3.50: Average LPR corrosion rate (µm/yr) of A1094 and Conv-C reinforcement in the Southern Exposure test

The fact that bent galvanized bars exhibited LPR corrosion rates in the same range as the rates for conventional reinforcement indicates high local corrosion at the preferential sites created by the bending. This is in contrast with the macrocell rates for the Southern Exposure test in which both A767 and A1094 bent bars performed comparably to straight galvanized bars (Figures 3.33 and 3.34). This indicates that microcell corrosion plays an important role in the corrosion at the preferential sites created by bending.

Figures 3.51 and 3.52 show the average LPR corrosion rates for damaged and undamaged A767 and A1094 galvanized reinforcement as well as the reinforcement used to produce them (Conv-B and Conv-C), respectively, in the cracked beam test. The LPR corrosion rates of Conv-B and Conv-C were described in Section 3.2.2.1. Through most of the test, the LPR corrosion rates of both types of galvanized reinforcement remained in the 5 to 15 µm/yr range. This is in contrast to the macrocell corrosion rates (Figures 3.35 and 3.36), which gradually decreased during the first 48 weeks of testing, and remained approximately constant afterward. Through most of the test,

damaged and undamaged A767 exhibited corrosion rates less than half the rates for Conv-B. Damaged and undamaged A1094 exhibited corrosion rates just slightly less than those of Conv-C from week 16 to 76.

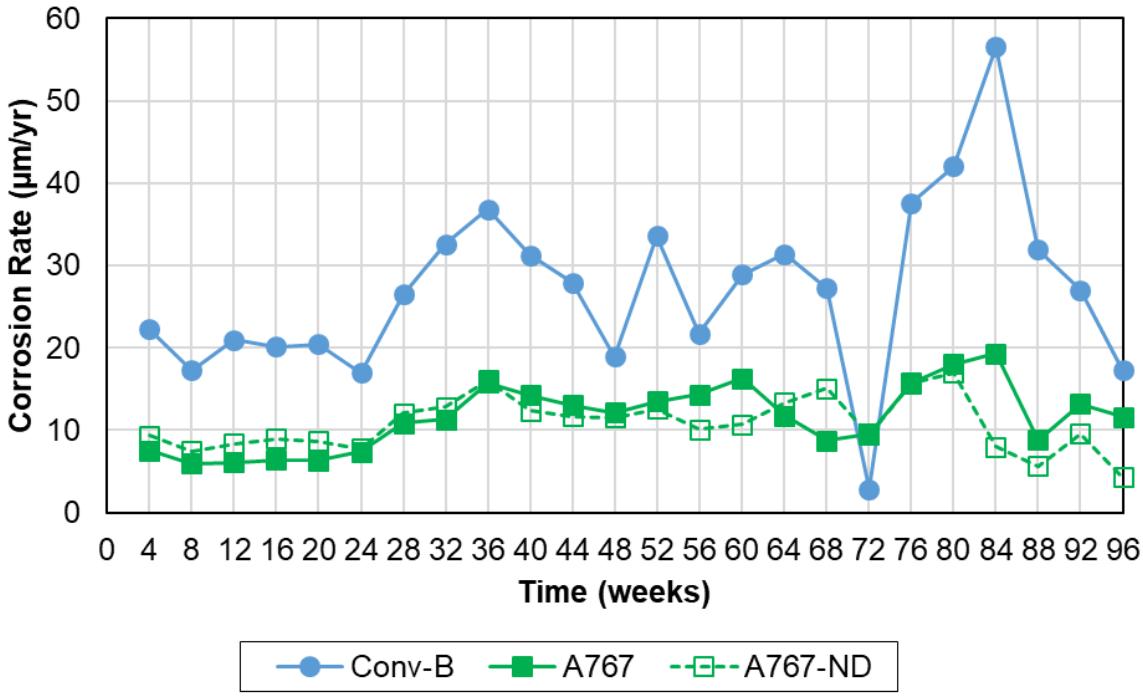

Figure 3.51: Average LPR corrosion rate (µm/yr) of A767 and Conv-B reinforcement in the cracked beam test

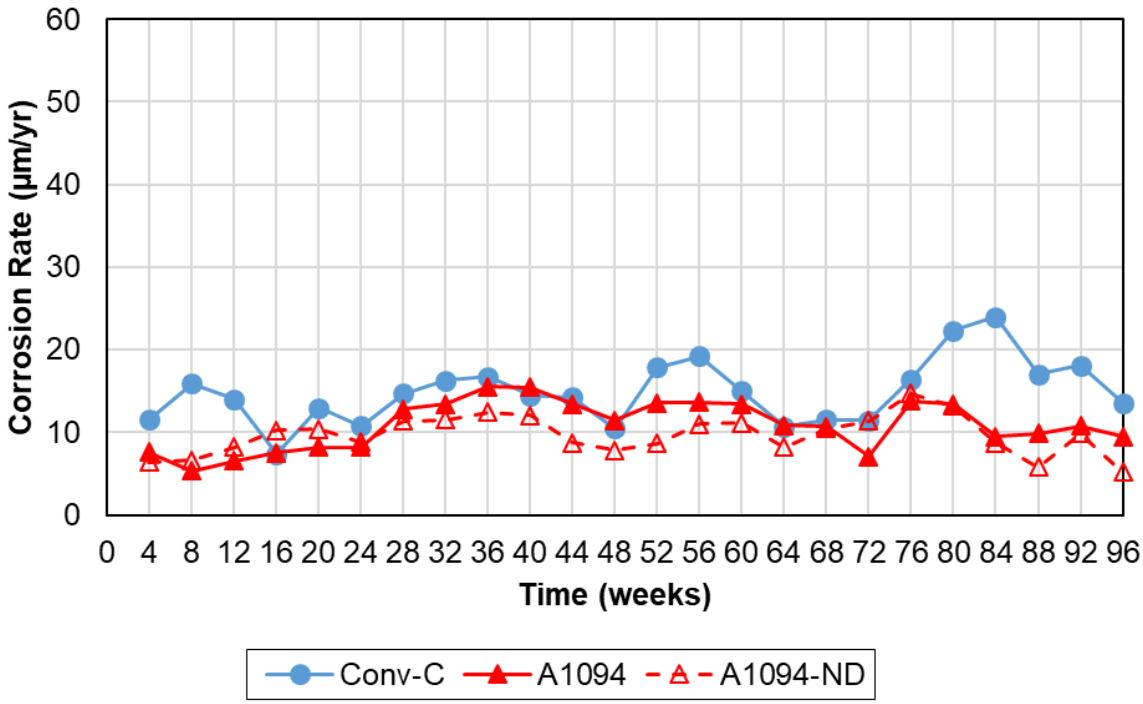

Figure 3.52: Average LPR corrosion rate (µm/yr) of A1094 and Conv-C reinforcement in the cracked beam test

3.2.2.4 ChromX (A1035 Type CS) and Conventional Reinforcement, IPANEX, and Xypex

Figures 3.53 and 3.54 show the average LPR corrosion rates for Conv-B and ChromX reinforcement without and with the IPANEX and Xypex admixtures in the Southern Exposure and cracked beam tests, respectively. The LPR corrosion rates of Conv-B were described in Section 3.2.2.1. The LPR corrosion rates are close to the values for macrocell rates at week 4 in both tests (Figures 3.43 and 3.44). IPANEX was not effective in decreasing the corrosion rates of Conv-B in either test. Neither IPANEX nor Xypex were effective in decreasing the corrosion rates for ChromX in either test.

In the Southern Exposure test, the corrosion rates of ChromX, without any admixture, gradually increased from zero the but did not exceed 6 µm; the use of Xypex did not decrease the LPR corrosion rates of Conv-B and even resulted in LPR rates greater than those of Conv-B alone

over many weeks; in contrast, it did decrease the macrocell corrosion rates of Conv-B after week 18 (Figure 3.43).

In the cracked beam test, ChromX in concrete without any admixture maintained rates between 6.5 and 13 µm/yr. IPANEX appeared to increase the corrosion rates of ChromX in the cracked beam test. Xypex did decrease the LPR corrosion rates of Conv-B by about 50% in the cracked beam test after week 20, except for some fluctuations, as it did for the macrocell corrosion rates (Figure 3.44).

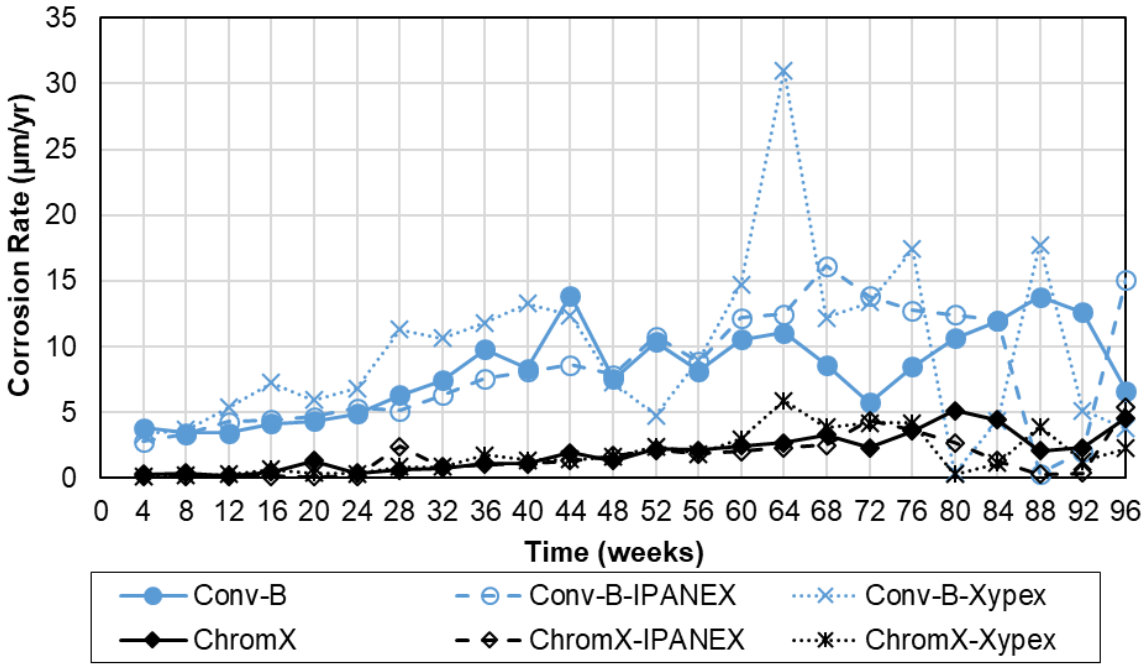

Figure 3.53: Average LPR corrosion rate (µm/yr) of Conv-B and ChromX reinforcement without and with IPANEX and Xypex admixtures in the Southern Exposure test

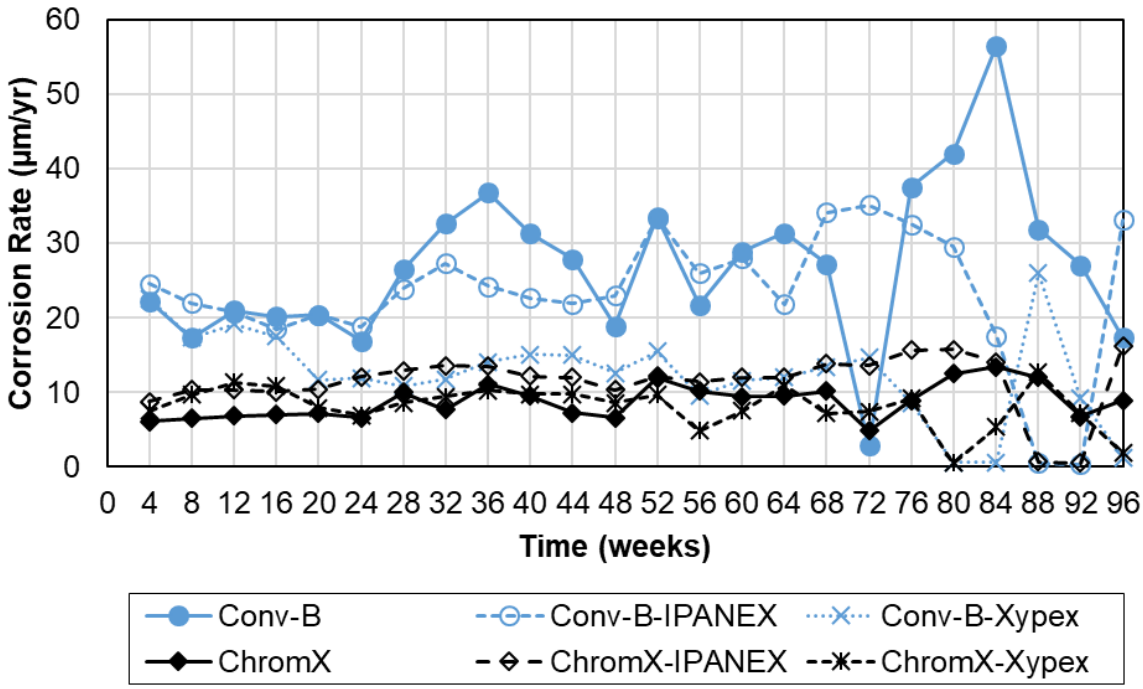

Figure 3.54: Average LPR corrosion rate (µm/yr) of Conv-B and ChromX reinforcement without and with IPANEX and Xypex admixtures in the cracked beam test

3.2.3 Initiation Age and Chloride Thresholds

Table 3.7 shows the age at corrosion initiation and average critical chloride corrosion threshold for specimens in the Southern Exposure test; initiation was not tracked in the cracked beam test because the crack provides a direct path for chlorides to reach the reinforcing steel, causing immediate corrosion initiation (Figures 3.25 to 3.44). Most specimens with conventional reinforcement initiated corrosion within the first 10 weeks of testing. The average times to corrosion initiation for Conv-A, Conv-B, and Conv-C are 9.8, 8.5, and 6 weeks, respectively. Conv-A, Conv-B, and Conv-C exhibited average critical chloride corrosion thresholds of 1.36, 0.655, and 1.54 lb/yd^3, respectively.

Table 3.7: Average age and chloride content at corrosion initiation in the Southern Exposure test

	Initiation Age, Weeks							Cl Cont.	
	1	**2**	**3**	**4**	**5**	**6**	**Avg. Age**	**lb/yd^3**	**Std. Dev.**
Conv-A	8	13	5	23	6	4	9.8	1.36	0.880
Conv-B	5	7	12	10	***	***	8.5	0.655	0.198
Conv-C	8	5	5	***	***	***	6	1.54	0.088
ECR1	55	-	40	40	***	***	45	2.58	0.958
ECR1-ND	-	-	-	***	***	***	-	-	-
ECR1-UV-1000	24*	48*	28*	***	***	***	33	*	*
ECR1-UV-1000-ND	68*	-	-	***	***	***	68	*	*
A767	23✓	26	62	82	17✓	64	46	1.37	0.092
A767-ND	56	76	26	48	64	47	52		
A767-Bent	57	80	79	40✓	56✓	37	58		
A1094	67	81	-	43	45✓	40	55	1.58	0.686
A1094-ND	18✓	83	37✓	23✓	62	72	45		
A1094-Bent	-	-	17✓	59	35	57	42		
ChromX	28	18	46	47	28	**	33	3.37	1.857
ChromX-IPANEX	74	28	32	44	26	28	39	2.00	0.497
ChromX-Xypex	46	52	16	15	37	26	32	3.42	2.26
Conv-B-IPANEX	11	15	8	12	8	7	10	0.859	1.26
Conv-B-Xypex	10	5	7	4	4	5	5.8	0.821	0.649

* Initiation in the specimen was missed: the specimen was not timely drilled for chlorides
** Specimen excluded due to corrosion at the electrical connection
*** No specimen
- No initiation
✓ Galvanized specimen used for critical chloride threshold value

Damaged epoxy-coated reinforcement initiated corrosion at 45 weeks on average, longer than conventional reinforcement, at an average critical chloride corrosion threshold of 2.58 lb/yd^3. With 1000 hours of UV exposure, ECR (ECR1-UV-1000) exhibited an average time to corrosion initiation of 33 weeks, which is still more than three times the value for the conventional reinforcement used to produce it (Conv-A) (p = 0.008). The critical chloride corrosion threshold for ECR1-UV-1000 was not determined as the specimens were not drilled timely. Undamaged ECR (ECR1-ND) did not exhibit corrosion, and only one specimen with undamaged ECR and UV

exposure (ECR1-UV-1000-ND) initiated corrosion (at 68 weeks).

Corrosion occurred on both the top and bottom bars of galvanized reinforcement (both A767 and A1094), resulting in individual corrosion rate readings that jumped erratically from week to week depending on the relative activity of the top and bottom bars, shown in Figures 3.33 and 3.34. Therefore, the time to corrosion initiation had to be determined retroactively because timely detection of corrosion initiation is difficult for galvanized reinforcement, and many of the specimens could not be sampled at the time of initiation. Galvanized specimens were sampled when corrosion rates did not fluctuate and decrease back for three weeks following a drastic increase. Due to the fact that many specimens were not sampled for chlorides in a timely manner, an average critical chloride corrosion threshold for each type (A767 and A1094) is presented; these critical chloride corrosion thresholds represent the average of all samples obtained for damaged, undamaged, and bent bars (indicated in Table 3.7). A767 and A1094 reinforcement exhibited average initiation ages ranging from 42 to 58 weeks. The differences between the initiation age of damaged, undamaged, and bent A767 are not statistically significant; similarly, the differences between the corresponding values for A1094 are not statistically significant. Bending the bar or damaging the coating did not appear to have an effect on the initiation age of a given bar type. Also, the differences between the initiation age of all A767 specimens grouped together in a data set versus all A1094 specimens grouped together are not statistically significant. The critical chloride corrosion thresholds for the two bar types are 1.37 and 1.58 lb/yd^3 for A767 and A1094 reinforcement, respectively; the difference is not statistically significant ($p = 0.995$).

ChromX (A1035 Type CS) reinforcement in concrete without any admixture exhibited an average initiation age of 33 weeks, more than three times the initiation age for conventional reinforcement ($p < 0.11$), and close to that of damaged ECR. The critical chloride corrosion

threshold, 3.37 lb/yd^3, was greater than that of conventional reinforcement ($p < 0.14$). The addition of IPANEX or Xypex did not affect the initiation age or the critical chloride corrosion threshold of either conventional or ChromX reinforcement.

As discussed in Chapter 1, the critical chloride corrosion threshold and time to corrosion initiation are best treated as probability functions or ranges, rather than as fixed numbers.

3.2.4 Corrosion Losses at End of Testing

3.2.4.1 Macrocell Corrosion Losses at End of Testing

Table 3.8 shows the macrocell corrosion losses for specimens based on the total area of the bars in contact with concrete in the Southern Exposure test after 96 weeks of testing. Table 3.9 shows the macrocell corrosion losses based on exposed area for ECR specimens in the Southern Exposure test. The corrosion losses were obtained by integrating the weekly corrosion rates over time. For calculating the average macrocell losses, negative values are treated as zero. Among specimens with conventional reinforcement, Conv-A exhibited the lowest average macrocell loss (4.94 μm at 96 weeks). The differences between Conv-A and the other two heats of steel is statistically significant ($p \leq 0.03$). Both Conv-B and Conv-C exhibited an average corrosion loss of 10.6 μm at 96 weeks. In the rapid macrocell test, Conv-B and Conv-C exhibited nearly the same average losses as well (Table 3.1). The average corrosion loss of the three heats is 8.71 μm.

Table 3.8: Macrocell corrosion loss based on total area at end of Southern Exposure testing

Specimen	Corrosion Loss (µm)-Total Area							Average Loss[1]	Std. Dev.
	1	2	3	4	5	6	7		
Conv-A	7.95	4.06	2.90	2.51	4.58	3.72	8.85	4.94	2.48
Conv-B	10.5	17.8	5.44	12.5	13.73	*	3.28	10.6	5.40
Conv-C	9.90	10.1	13.5	10.1	12.20	7.88	-	10.6	1.97
ECR1	0.034	-0.090	0.020	0.160	-	-	-	0.071	0.102
ECR1-ND	0.155	0.106	-0.013	-	-	-	-	0.131	0.086
ECR1-UV-1000	0.573	0.214	0.425	-	-	-	-	0.404	0.181
ECR1-UV-1000-ND	0.272	-0.031	0.003	-	-	-	-	0.138	0.166
A767	-0.109	-0.405	1.31	0.598	-0.010	0.893	-	0.944	0.674
A767-ND	2.11	0.405	1.27	-0.599	1.12	1.55	-	1.29	0.953
A767-Bent	1.90	-0.76	-0.077	4.01	3.68	6.56	-	4.04	2.75
A1094	-0.565	0.309	0.319	-0.759	-0.229	1.02	-	0.549	0.661
A1094-ND	0.504	-1.83	0.84	0.27	0.84	1.13	-	0.717	1.08
A1094-Bent	2.21	-4.78	-1.41	2.28	1.42	1.88	-	1.95	2.83
ChromX	0.05	1.11	1.37	-0.06	1.98	*	*	1.13	0.877
ChromX-IPANEX	0.10	1.99	0.72	1.07	2.27	1.39	-	1.26	0.805
ChromX-Xypex	0.45	0.79	0.34	0.53	0.94	2.46	-	0.916	0.789
Conv-B-IPANEX	15.8	10.1	6.03**	11.3	13.9	9.70	-	12.2	2.58
Conv-B-Xypex	6.65	6.53	7.35	2.46	9.16	8.30	-	6.74	2.32

*Specimen exhibited corrosion at the electrical connection with the bar

**Terminated early due to cracking of concrete (week 90)

-No specimen

[1] Negative values are taken as zero for calculating the average

Table 3.9: Macrocell corrosion loss based on exposed area at end of Southern Exposure testing

Specimen	Corrosion Loss (µm)-Exposed Area				Average Loss[1]	Std. Dev.
	1	2	3	4		
ECR1	6.61	-17.3	3.77	30.6	13.6	19.6
ECR1-UV-1000	110	41.0	81.7	-	77.6	34.7

-No specimen

[1] Negative values are taken zero for calculating the average

Damaged ECR without UV exposure (ECR1) had macrocell corrosion losses of 0.071 µm based on total bar area in contact with concrete, about 1% the value for the matching conventional reinforcement (Conv-A). ECR1 had a corrosion loss of 13.6 µm based on exposed area. ECR1-ND and ECR1-UV-1000-ND exhibited losses of 0.131 and 0.138 µm, respectively. Damaged ECR

with UV exposure (ECR1-UV-1000) exhibited losses of 0.404 μm (77.6 μm based on exposed area), 6 times the value for ECR1; the differences between ECR1-UV-1000 and with ECR1 is statistically significant ($p = 0.02$).

Specimens with galvanized reinforcement exhibited a wide variation in losses. As mentioned earlier, the corrosion of both top and bottom bars of steel resulted in fluctuations in the macrocell corrosion. Specimens with bent A767 bars exhibited an average loss of 4.04 μm, much greater than the other A767 specimens (0.944 and 1.29 μm for damaged and undamaged A767, respectively) and all A1094 specimens (0.549, 0.717, and 1.29 μm for damaged, undamaged, and bent A1094). The difference in the corrosion loss between bent and damaged A767 specimens is statistically significant ($p = 0.09$); the differences between bent and undamaged (A767-ND) specimens ($p = 0.23$) or between bent A1094 and other A1094 specimens are not statistically significant.

ChromX (A1035 Type CS) reinforcement exhibited average macrocell losses of 1.13 μm at the end of testing, 10 to 23% that of conventional reinforcement, and much greater than those of ECR1, ECR1-ND, and ECR1-UV-1000-ND specimens; the differences between average losses are statistically significant ($p \leq 0.18$).

The addition of IPANEX or Xypex had little effect on the average macrocell corrosion loss of ChromX reinforcement. The addition of IPANEX also had little effect on the average corrosion loss for Conv-B reinforcement, although the addition of Xypex resulted in a 36% reduction, from 10.6 to 6.74 μm, for Conv-B reinforcement with a statistically significant difference ($p = 0.14$).

Table 3.10 shows the macrocell corrosion losses based on total area for specimens in the cracked beam test after 96 weeks of testing. The average corrosion loss for Conv-B specimens only includes those specimens that reached 96 weeks; several specimens with Conv-B

reinforcement and Conv-B with IPANEX cracked due to excessive corrosion. The specimens that did not complete 96 weeks of testing are not included in the average in the body of the table; the averages of all specimens are shown in the footnote to the table. Table 3.11 shows the termination week for cracked beam specimens that were terminated before reaching 96 weeks. Table 3.12 shows average macrocell corrosion losses based on exposed area at the end of cracked beam test for damaged ECR specimens.

Among specimens with conventional reinforcement, Conv-A and Conv-C exhibited losses of 12.2 and 12.9 μm, respectively; Conv-B exhibited a higher average loss, 18.6 μm, based on specimens that completed 96 weeks of testing and 22.7 μm including all specimens. The differences, however, are not statistically significant. The average for the three heats is 14.5 μm.

Table 3.10: Macrocell corrosion losses based on total area at end of cracked beam testing

Specimen	Corrosion Loss (μm)-Total Area							Average Loss[1]	Std. Dev.
	1	2	3	4	5	6	7		
Conv-A	14.9	14.1	13.1	16.8	5.90	8.21	-	12.2	4.20
Conv-B	9.69	27.4	15.6*	28.7*	31.9*	29.5*	16.2*	18.6[2]	12.5
Conv-C	9.21	15.2	14.4	-	-	-	-	12.9	3.24
ECR1	0.000	0.292	0.467	-0.028	-	-	-	0.253	0.238
ECR1-ND	-0.135	0.025	0.101	-	-	-	-	0.063	0.121
ECR1-UV-1000	3.49	2.18	1.75	2.17	2.54	3.4	1.35	2.41	0.800
ECR1-UV-1000-ND	0.080	0.717	-0.002	-	-	-	-	0.399	0.39
A767	0.64	4.21	2.71	-1.18	9.35	8.18	-	5.02	4.15
A767-ND	1.32	8.81	2.20	6.98	6.51	2.29	-	4.69	3.13
A1094	3.60	6.12	3.10	-2.65	3.71	4.04	-	4.11	2.95
A1094-ND	2.78	4.59	2.36	1.99	2.02	4.00	-	2.96	1.09
ChromX	13.0	3.79	7.36	3.19	5.98	5.57	11.6	7.21	3.75
ChromX-IPANEX	6.24	6.16	4.88	5.98	10.2	6.99	-	6.74	1.84
ChromX-Xypex	5.05	5.92	5.81	9.07	2.98	7.09	-	5.99	2.04
Conv-B-IPANEX	16.8*	25.2*	32.2	18.8*	24.9*	19.0	-	25.6[3]	9.34
Conv-B-Xypex	5.92	5.81	9.07	2.98	7.09	5.99	-	6.14	1.98

*Terminated early due to cracking of concrete (see Table 3.10)

-No specimen

[1] Negative values are taken zero for calculating the average

[2] 22.7 μm including all specimens

[3] 22.8 μm including all specimens

Table 3.11: Early termination in the cracked beam test

Specimen	Termination Age (weeks)
Conv-B-3	49
Conv-B-4	67
Conv-B-5	84
Conv-B-6	77
Conv-B-7	83
Conv-B-IPANEX-1	55
Conv-B-IPANEX-2	77
Conv-B-IPANEX-4	81
Conv-B-IPANEX-5	80

Table 3.12: Macrocell corrosion losses based on exposed area at end of cracked beam testing

Specimen	Corrosion Loss (μm)-Exposed Area							Average Loss[1]	Std. Dev.
	1	2	3	4	5	6	7		
ECR1	0.028	56.1	89.6	-5.5	-	-	-	48.6	45.8
ECR1-UV-1000	669	418	335	415	487	652	258	459	144

-No specimen

[1] Negative values are taken zero for calculating the average

Damaged ECR without UV exposure (ECR1) exhibited a loss of 0.253 μm based on total area, equal to about 2% the value for Conv-A, and 48.6 μm based on exposed area. The variation between specimens is very large as evidenced by the standard deviations of 0.238 and 45.8 for macrocell and total losses of ECR1. Very low losses were observed on the ECR1-ND specimens (0.063 μm). Damaged ECR with UV exposure (ECR1-UV-1000) exhibited an average corrosion loss of 2.41 μm based on total area and 459 μm based on exposed area, equal to about 10 times the value for ECR1 ($p \leq 0.01$). ECR1-UV-1000-ND exhibited an average corrosion loss of 0.399 μm based on total bar area.

A wide variation in corrosion losses was observed on the specimens with galvanized reinforcement, similar to those observed in the Southern Exposure test. The damaged and undamaged A767 specimens exhibited respective corrosion losses of 5.02 and 4.69 μm based on total area, somewhat greater than the values for the A1094 specimens, 4.11 and 2.96 μm. The

differences, however, are not statistically significant.

ChromX reinforcement in concrete without an admixture exhibited average corrosion losses of 7.21 μm at the end of the test, 39 to 59% of the values for conventional reinforcement ($p \leq 0.05$), much greater than ECR not exposed to UV ($p \leq 0.02$). As observed in the Southern Exposure test, the addition of IPANEX or Xypex did not improve the corrosion resistance of ChromX reinforcement. The addition of IPANEX had little effect on the average corrosion loss; the difference is not statistically significant. In contrast, the addition of Xypex resulted in a 67% reduction in the average corrosion loss for Conv-B reinforcement ($p \leq 0.03$). The percentage reduction observed in the cracked beam test was greater than in the Southern Exposure test (Table 3.8).

3.2.4.2 Total Corrosion Losses at End of Testing

Table 3.13 shows the total corrosion losses based on LPR for specimens in the Southern Exposure test after 96 weeks of testing based on the total area of the bar in contact with concrete. Among the conventional reinforcement, Conv-A exhibited average corrosion losses of 9.98 μm, lower than Conv-B at 15.8 μm and Conv-C at 16.2 μm; the differences between Conv-A and Conv-B as well as Conv-A and Conv-C are statistically significant ($p \leq 0.01$). The difference in losses between Conv-B and Conv-C is not statistically significant. The average corrosion loss for the three heats is 14.0 μm.

Table 3.13: LPR corrosion losses based on total area at end of Southern Exposure testing

Specimen	Corrosion Loss (µm)-Total Area							Average Loss	Std. Dev.
	1	2	3	4	5	6	7		
Conv-A	9.50	13.0	11.3	3.76	11.5	10.2	10.6	9.98	2.96
Conv-B	11.8	17.8	11.7	15.8	20.8	*	16.8	15.8	3.53
Conv-C	18.5	15.8	19.6	16.3	19.1	7.55	-	16.2	4.49
ECR1	0.094	0.050	0.086	0.037	-	-	-	0.067	0.028
ECR1-ND	0.305	0.050	0.016	-	-	-	-	0.122	0.159
ECR1-UV-1000	1.502	0.586	0.602	-	-	-	-	0.897	0.524
ECR1-UV-1000-ND	0.031	0.172	0.161	-	-	-	-	0.121	0.078
A767	19.7	4.11	8.70	5.68	2.72	13.5	-	9.06	6.46
A767-ND	5.41	5.08	5.84	2.50	10.3	8.02	-	6.20	2.69
A767-Bent	16.3	9.19	4.66	16.1	30.1	20.0	-	16.1	8.81
A1094	15.4	6.13	5.17	3.11	2.72	14.2	-	7.79	5.59
A1094-ND	6.45	7.44	3.43	2.01	17.5	7.17	-	7.33	5.42
A1094-Bent	18.3	4.13	5.50	15.5	19.0	17.5	-	13.3	6.72
ChromX	2.54	3.03	0.352	1.93	8.86	*	*	3.34	3.24
ChromX- IPANEX	1.06	5.44	3.24	1.95	4.13	1.81	-	2.94	1.65
ChromX-Xypex	2.73	2.79	1.98	2.34	2.54	7.97	-	3.39	2.26
Conv-B IPANEX	19.2	12.1	10.1	15.3	18.3	11.9	-	14.5	3.74
Conv-B-Xypex	17.6	18.4	8.33	22.5	17.5	23.3	-	17.9	5.33

*Specimen exhibited corrosion at the electrical connection with the bar
-No specimen

Damaged ECR without UV exposure (ECR1) exhibited an average LPR corrosion loss of 0.067 µm based on total area, about 1% the value for Conv-A, similar to the macrocell losses. The undamaged ECR without UV exposure (ECR1-ND) exhibited an average corrosion loss of 0.122 µm, about twice the value for ECR1; the higher average corrosion loss of ECR1-ND is dominated by a single specimen with a corrosion loss of 0.305 µm. Undamaged ECR with UV exposure (ECR1-UV-1000-ND) exhibited an average loss of 0.121 µm; the difference in corrosion losses between ECR1-UV-1000-ND and ECR1-ND is not statistically significant. The difference between corrosion loss of ECR1 and the value for either ECR1-ND or ECR1-UV-1000-ND is not statistically significant. Damaged ECR with UV exposure (ECR1-UV-1000) exhibited an average corrosion loss of 0.897 µm based on total area, the greatest average loss among ECR specimens, about 13 times the value for ECR1 ($p = 0.02$).

A767 and A1094 reinforcement in both damaged and undamaged conditions exhibited average total corrosion losses lower than conventional reinforcement; the differences between corrosion losses of damaged and undamaged galvanized reinforcement and the matching conventional reinforcement is statistically significant ($p \leq 0.05$). Damaged A767 and A1094 specimens exhibited average corrosion losses of 9.06 and 7.79 μm, and undamaged A767 and A1094 specimens (A767-ND and A1094-ND) exhibited average losses of 6.20 and 7.33 μm, respectively. A767 and A1094 bent galvanized specimens exhibited average corrosion losses of 16.1 and 13.3 μm, respectively, in the same range as those of conventional reinforcement. The difference between losses of bent A767 and A1094 is not statistically significant. For both types of galvanized bars, however, bent bars exhibited higher total losses than straight bars. The differences are statistically significant ($p \leq 0.15$). Using total losses, as opposed to macrocell losses, is useful because it removes the effect of corrosion of the bars in the bottom bars that tends to reduce the apparent losses.

ChromX reinforcement in concrete without an admixture exhibited total average corrosion losses of 3.34 μm, 21 to 33% of the values for conventional reinforcement ($p \leq 0.01$). The addition of Xypex had no effect on total corrosion losses when paired with ChromX reinforcement and unlike the macrocell corrosion losses in the Southern Exposure test (Table 3.8), the addition of Xypex did not result in a reduction in corrosion loss for Conv-B. The addition of Xypex apparently increased the corrosion loss to 17.9 μm for Conv-B; the difference is not statistically significant. IPANEX was not effective in reducing corrosion losses.

Table 3.14 shows the total corrosion losses based on LPR for specimens in the cracked beam test after 96 weeks of testing based on total area of bar in contact with concrete. Conv-B had an average corrosion loss of 42.0 μm (36.7 μm including specimens terminated prior to 96 weeks),

the highest average loss of the three heats of steel, with Conv-A and Conv-C exhibiting average total losses of 36.6 and 27.4 μm, respectively; only the difference in loss between Conv-B and Conv-C is statistically significant ($p = 0.15$). The average for the three heats is 35.3 μm.

Table 3.14: LPR corrosion losses based on total area at end of cracked beam testing

Specimen	Corrosion Loss (μm)-Total Area							Average Loss	Std. Dev.
	1	2	3	4	5	6	7		
Conv-A	47.6	38.9	44.3	27.3	38.2	23.4	-	36.6	9.49
Conv-B	39.9	44.1	27.7*	28.3*	52.7*	37.2*	23.3*	42.0[1]	2.95
Conv-C	22.6	38.9	20.8	-	-	-	-	27.4	10.0
ECR1	0.034	0.611	1.01	0.107	-	-	-	0.439	0.456
ECR1-ND	0.007	0.024	0.007	-	-	-	-	0.013	0.010
ECR1-UV-1000	4.94	6.76	6.58	-	-	-	-	6.09	1.00
ECR1-UV-1000-ND	0.244	0.917	0.163	-	-	-	-	0.441	0.414
A767	15.2	23.4	28.3	8.74	18.2	34.0	-	21.3	9.14
A767-ND	19.8	21.4	6.28	21.8	27.4	24.2	-	20.2	7.29
A1094	14.2	33.5	12.7	13.0	19.1	26.9	-	19.9	8.55
A1094-ND	17.6	19.5	14.3	12.6	25.0	18.3	-	17.9	4.34
ChromX	16.8	14.8	14.5	11.2	18.0	16.9	26.5	17.0	4.75
ChromX-IPANEX	22.1	21.9	18.7	17.5	25.6	20.8	-	21.1	2.84
ChromX-Xypex	12.5	18.8	15.3	15.2	15.3	12.9	-	15.0	2.25
Conv-B- IPANEX	22.4*	48.8*	50.6	28.8*	30.6*	40.9	-	45.8[2]	6.87
Conv-B-Xypex	23.2	22.7	24.5	22.3	22.7	24.2	-	23.3	0.91

*Terminated early due to cracking of concrete (see Table 3.11)
-No specimen

[1] 36.7 μm including all specimens

[2] 37.0 μm including all specimens

Damaged ECR without UV exposure (ECR1) exhibited an average LPR loss of 0.439 μm, about 1% the value for Conv-A, similar to macorcell losses. Undamaged ECR without UV exposure (ECR1-ND) exhibited very small corrosion losses (average of 0.013 μm); the difference in the total corrosion losses between ECR1 and ECR1-ND is statistically significant ($p = 0.18$). Damaged ECR with UV exposure (ECR1-UV-1000) exhibited an average total corrosion loss of 6.09 μm, about 14 times the value for ECR1 ($p < 0.01$). Undamaged ECR UV exposure (ECR1-UV-1000-ND) exhibited an average total corrosion loss of 0.441 μm.

Average total corrosion losses for all galvanized reinforcement were close to 20 μm at the end of the test, compared to between 6.20 to 13.3 μm for macrocell losses. The differences between total corrosion losses of A767 and A1094 specimens are not statistically significant.

ChromX (A1035 Type CS) reinforcement in concrete without an admixture exhibited total losses of 17.0 μm, lower than those of conventional reinforcement without any admixture with differences that are statistically significant ($p \leq 0.05$). ChromX with Xypex and IPANEX exhibited losses of 15.0 and 21.1 μm, respectively; the addition of Xypex or IPANEX did not result in a statistically significant change in the corrosion losses for ChromX reinforcement. The difference between the total corrosion loss of Conv-B without IPANEX (42.0 μm) and with IPANEX (45.8 μm and 37.0 μm including the terminated specimens) was not statistically significant. The addition of Xypex, however, resulted in a 45% reduction in total losses of Conv-B from 42.0 to 23.3 μm ($p < 0.01$).

The corrosion losses of conventional, epoxy-coated, and ChromX (ASTM A1035 Type CS) reinforcement at the end of Southern Exposure and cracked beam tests from previous studies (and this study) are summarized in Table 3.15. The macrocell corrosion losses for conventional reinforcement range from 2.1 to 16.4 μm and 7.51 to 30.1 μm in Southern Exposure and cracked beam tests, respectively. The average macrocell and total corrosion losses, respectively, for the three heats of conventional reinforcement in this study are 8.71 and 14.0 μm in the Southern Exposure test and 14.5 and 35.3 μm in the cracked beam test. Balma et al. (2005) and Ji et al. (2005) found macrocell corrosion losses higher than those of Conv-A in the Southern Exposure test and close to those of Conv-A and Conv-C in the cracked beam test. The macrocell corrosion loss of Draper (2009) for conventional reinforcement in the Southern Exposure test (2.1 μm) is lower than those of other previous studies and this study; their corrosion loss in the cracked beam

test (13.1 μm) is, however, close to those of Conv-A and Conv-C. O'Reilly et al. (2011) and Darwin et al. (2013) found macrocell corrosion losses of 14.4 and 16.4 μm in the Southern Exposure test and 29.9 and 30.1 μm in the cracked beam test, respectively, greater than the values for conventional reinforcement in this study. Darwin et al. (2013) found total corrosion losses of 16.6 and 56.4 μm in the Southern Exposure and cracked beam tests, respectively, greater than those of this study for conventional reinforcement in both tests.

In this study, the average macrocell and total corrosion losses, respectively, for ECR are 0.071 and 0.067 μm in the Southern Exposure test and 0.253 and 0.439 μm in the cracked beam test. For epoxy-coated reinforcement, Draper (2009) found macrocell corrosion losses of 0.017 and 0.047 μm in the Southern Exposure and cracked beam tests, respectively, lower than this study, while Darwin et al. (2013) found respective macrocell and total corrosion losses of 0.342 and 1.05 μm in the Southern Exposure test and 0.453 and 3.71 μm in the cracked beam test, greater than this study.

For ChromX reinforcement, Farshadfar et al. (2017) found macrocell and total corrosion losses of 8.73 and 9.05 μm in the Southern Exposure test, greater than those of this study (1.13 and 3.34 μm, respectively). Similarly, they found macrocell and total corrosion losses of 16.4 and 20.4 μm in the cracked beam test, greater than the values for this study (7.21 and 17.0 μm, respectively).

Table 3.15: Corrosion losses (μm) at 96 weeks for Southern Exposure and cracked beam specimens from previous research

		Southern Exposure		Cracked beam	
Reinforcement	Research	Macrocell Corrosion loss	Total Corrosion loss	Macrocell Corrosion loss	Total Corrosion loss
Conventional	Ji et al. (2005)	7.64	-	10.1	-
Conventional	Ji et al. (2005)	12	-	13.9	-
Conventional	Balma et al. (2005)	5.78	-	7.51	-
Conventional	Balma et al. (2005)	7.3	-	11.6	-
Conventional	Draper (2009)	2.1	-	13.1	-
Conventional	O'Reilly et al. (2011)	14.4	-	29.9	-
Conventional	Darwin et al. (2013)	16.4	16.6	30.1	56.4
Conv-A	Current Study	4.94	9.98	12.2	36.6
Conv-B	Current Study	10.6	15.8	18.6	42.0
Conv-C	Current Study	10.6	16.2	12.9	27.4
ECR	Draper (2009)	0.017	-	0.047	-
ECR	Darwin et al. (2013)	0.342	1.05	0.453	3.71
ECR1	Current Study	0.071	0.067	0.253	0.439
ChromX	Farshadfar et al. (2017)	8.73	9.05	16.4	20.4
ChromX	Current Study	1.13	3.34	7.21	17.0

3.2.5 End of Test Photos and Disbondment Results

3.2.5.1 Conventional Reinforcement

Figure 3.55 shows the bars from specimen SE-Conv-C-1 after 96 weeks of testing and is representative of all conventional reinforcement in the Southern Exposure test. A moderate amount of corrosion was visible on both top bars, although corrosion did not cover the entire surface of the bars. Corrosion caused staining on the surface of the specimens, as shown in Figure 3.56. A small amount of corrosion was visible on the bottom bars.

Figure 3.55: Top bars (top) and bottom bars (bottom) of specimen SE-Conv-C-1 after 96 weeks of testing

Figure 3.56: Surface staining on Southern Exposure specimen with conventional reinforcement

Figure 3.57 shows the bars from specimen CB-Conv-B-4 after 96 weeks of testing and is representative of all conventional reinforcement in the cracked beam test. A heavy amount of corrosion was visible on the top bar, with some pitting and deeper localized corrosion occurring,

particularly in the region directly under the 6-in. simulated crack. Similar to the Southern Exposure specimens, most cracked beam specimens with conventional reinforcement exhibited staining on the surface, as shown in Figure 3.58. Light or no corrosion products were visible on the bottom bars.

Figure 3.57: Top bar (top) and bottom bars (bottom) of specimen CB-Conv-B-4 after 96 weeks of testing

Figure 3.58: Surface staining on the cracked beam specimen with conventional reinforcement

3.2.5.2 Epoxy-Coated Reinforcement

Figure 3.59 shows the bars from specimen SE-ECR1-2 after 96 weeks of testing and is representative of all damaged ECR in the Southern Exposure test. A minimal amount of corrosion damage was visible; corrosion was typically limited to small amounts at the damage sites. Figure

3.60 shows the top bar of specimen SE-ECR1-1 after the disbondment test; no disbondment was observed on any Southern Exposure specimens. Figure 3.61 shows undamaged ECR specimen SE-ECR1-ND-2 after 96 weeks of testing. No corrosion was observed on any ECR1-ND specimens.

Figure 3.59: Top bars (top) and bottom bars (bottom) of specimen SE-ECR1-2 after 96 weeks of testing

Figure 3.60: Top bar of specimen SE-ECR1-1 after disbondment test

Figure 3.61: Top bars (top) and bottom bars (bottom) of specimen SE-ECR1-ND-2 after 96 weeks of testing

Figure 3.62 shows the bars from specimen CB-ECR-3 after 96 weeks of testing and is representative of all damaged ECR in the cracked beam test. A minimal amount of corrosion damage was visible on the bars, limited to the damage sites in the top bar. Figure 3.63 shows the top bar of CB-ECR1-2 after the disbondment test. Unlike the damaged bars in the Southern Exposure test, damaged ECR bars without UV exposure exhibited disbondment in the cracked beam test, with corrosion underneath the undamaged portions of the coating.

Figure 3.62: Top bar (top) and bottom bars (bottom) of specimen CB-ECR1-3 after 96 weeks of testing

Figure 3.63: Top bar of specimen CB-ECR1-2 after disbondment test

Figures 3.64 and 3.65 show undamaged ECR after 96 weeks of testing in the cracked beam test. Two out of three of the undamaged ECR specimens showed no visible corrosion (Figure 3.64); specimen CB-ECR1-ND-1, however, showed some rust buildup at a previously unnoticed damage site in the coating (Figure 3.65). Disbondment tests were not performed on the undamaged bars.

Figure 3.64: Top bars (top) and bottom bars (bottom) of specimen CB-ECR1-ND-2 after 96 weeks of testing

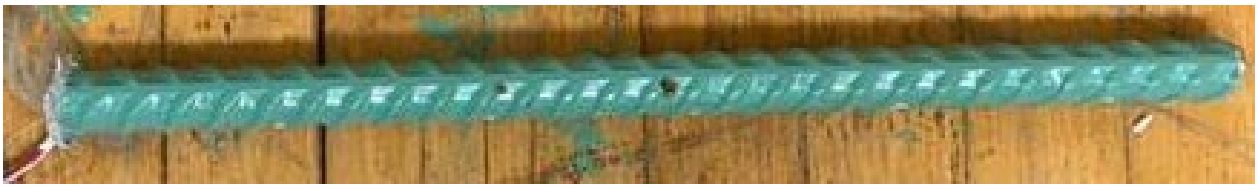

Figure 3.65: Top bar of specimen CB-ECR1-ND-1 after 96 weeks of testing

Figure 3.66 shows the bars from specimen SE-ECR1-UV-1000-1 after 96 weeks of testing and is representative of all ECR-UV-1000 Southern Exposure specimens on which much larger amounts of corrosion damage were visible than on damaged ECR specimens without UV exposure. Figure 3.67 shows a top bar of specimen SE-ECR1-UV-1000-1, which exhibited total disbondment; damaged ECR bars exhibited disbondment after exposure, and the entire coating easily peeled back for most of the bars. This is in contrast to the specimens without UV exposure that did not show any disbondment (Figure 3.61).

Figure 3.66: Top bars (top) and bottom bars (bottom) of specimen SE-ECR1-UV-1000-1 after 96 weeks of testing

Figure 3.67: Top bar of specimen SE-ECR1-UV-1000-1 after disbondment test

Figure 3.68 shows the bars from specimen SE-ECR1-UV-1000-ND-1 after 96 weeks of testing and is representative of all ECR1-UV-1000-ND specimens in the Southern Exposure test. Minimal to no corrosion damage was observed on the bars, but discoloration from the UV exposure was visible.

Figure 3.68: Top bars (top) and bottom bars (bottom) of specimen SE-ECR1-UV-1000-ND-1 after 96 weeks of testing

Figure 3.69 shows the bars from specimen CB-ECR1-UV-1000-1 after 96 weeks of testing and is representative of all ECR1-UV-1000 cracked beam specimens on which larger amounts of corrosion damage were visible than for the damaged ECR specimens without UV exposure. Blistering and cracking of the coating were observed on all top bars. Figure 3.70 shows the top bar of specimen CB-ECR1-UV-1000-2 after the disbondment test; damaged ECR bars with UV exposure exhibited disbondment after exposure, and the entire coating easily peeled back on every bar tested.

Figure 3.69: Top bar (top) and bottom bars (bottom) of specimen CB-ECR1-UV-1000-2 after 96 weeks of testing

Figure 3.70: Top bar of specimen CB-ECR1-UV-1000-2 after disbondment test

Figure 3.71 shows the bars from specimen CB-ECR1-UV-1000-ND-1 after 96 weeks of testing and is representative of all ECR1-UV-1000-ND specimens in the cracked beam test. Similar to the undamaged cracked beam without UV exposure, minimal to no corrosion damage was observed on the bars, but discoloration from the UV exposure was visible. No disbondment was observed.

Figure 3.71: Top bar (top) and bottom bars (bottom) of specimen CB-ECR1-UV-1000-ND-1 after 96 weeks of testing

Tables 3.16 and 3.17 summarize the measured disbondment for the damaged ECR specimen in the Southern Exposure and cracked beam tests at the end of testing, respectively. Disbondment tests were not performed on the undamaged bars; the coating on undamaged bars did not peel back. When disbondment test was attempted on undamaged bars, no coating was removed. As described in Chapter 2, disbondment that extended more than 0.5 in. from the intentional damage site in all directions is classified as total disbondment and is assigned a disbonded area of 1.05 in.^{2}. In the Southern Exposure test (Table 3.16), damaged ECR without UV exposure exhibited no disbondment, while ECR with UV exposure exhibited total disbondment on two out of the three specimens and 0.61 in.^{2} disbondment on the third specimen; the average disbonded area was 0.90 in.^{2} for ECR with UV exposure. In the cracked beam test (Table 3.17),

both the ECR1 and ECR1-UV-1000 bars exhibited greater disbondment than in the Southern Exposure test, and two out of four ECR1 bars and all of the ECR1-UV-1000 bars exhibited total disbondment. Average disbonded areas for ECR1 and ECR1-UV-1000 bars were 0.83 in.^{2} and 1.05 in.^{2}, respectively.

Table 3.16: Measured disbondment in the Southern Exposure test

Specimen	Disbonded Area (in.^{2})					
	1	2	3	4	Average	Std. Dev.
ECR1	0	0	0	0	0	0
ECR1-UV-1000	1.05	1.05	0.61	-	0.90	0.25

-No specimen

Table 3.17: Measured disbondment in the cracked beam test

Specimen	Disbonded Area (in.^{2})								
	1	2	3	4	5	6	7	Average	Std. Dev.
ECR1	0.38	1.05	1.05	0.63	-	-	-	0.83	0.24
ECR1-UV-1000	1.05	1.05	1.05	1.05	1.05	1.05	1.05	1.05	0.00

-No specimen

3.2.5.3 Galvanized Reinforcement

Figure 3.72 shows the bars from specimen SE-A767-2 after 96 weeks of testing and is representative of most of the A767 specimens in the Southern Exposure test. The top bars exhibited moderate to heavy amounts of corrosion with both zinc corrosion products (white) and steel corrosion products (orange-brown) visible. Corrosion was uneven; the zinc coating was intact in several places. Corrosion was present on the bottom as well the as top bars (Figure 3.72), explaining the "negative" corrosion loss observed. This also occurred on two out of six A767 Southern Exposure specimens.

Figure 3.72: Top bars (top) and bottom bars (bottom) of specimen SE-A767-2 after 96 weeks of testing. Oval indentifying rusted region

Figure 3.73 shows the bars from specimen CB-A767-3 after 96 weeks of testing, representative of all A767 bars in the cracked beam test. Similar to the Southern Exposure specimens, the top bar exhibited moderate to heavy amounts of corrosion with both zinc corrosion products (white) and steel corrosion products (orange-brown) visible. Fewer white zinc corrosion products were visible on the bottom bars, with isolated areas of steel corrosion products visible.

Figure 3.73: Top bar (top) and bottom bars (bottom) of specimen CB-A767-3 after 96 weeks of testing

Figure 3.74 shows the bars from specimen SE-A1094-4 after 96 weeks of testing,

representative of all A1094 specimens in the Southern Exposure test. One of the top bars exhibited moderate to heavy corrosion with both zinc corrosion products (white) and steel corrosion products (orange-brown) visible and the other one had a light amount of corrosion. Similar to the A767 specimens, corrosion was uneven, and there were parts on the bar with no corrosion products. Also similar to the A767 specimens, corrosion was also present on the bottom bars on some specimens, explaining the "negative" corrosion losses observed.

Figure 3.74: Top bars (top) and bottom bars (bottom) of specimen SE-A1094-4 after 96 weeks of testing

Figure 3.75 shows the bars from specimen CB-A1094-6 after 96 weeks of testing, representative of all A1094 specimens in the cracked beam test. The top bar exhibited a moderate amount of corrosion with both zinc corrosion products (white) and steel corrosion products (orange-brown) visible. Limited amounts of zinc corrosion products were observed on the bottom bars.

Figure 3.75: Top bar (top) and bottom bars (bottom) of specimen CB-A1094-6 after 96 weeks of testing

Figures 3.76 and 3.77 show the bars from specimens with bent A767 and A1094 bars, respectively, from the Southern Exposure test and are representative of all specimens with bent galvanized bars. Corrosion products are visible on the top bar both at and away from the bend on both types of bar. As discussed in Section 3.2.4 (total corrosion losses), the presence of the bend resulted in a statistically significant increase in corrosion when compared to straight bars. Limited amounts of zinc corrosion products were observed on the bottom bars of the A767 specimens. A moderate amount of corrosion with both zinc and steel corrosion products were visible on the bottom bars of the A1094 specimens. The greater amounts of steel corrosion products on the bottom A1094 bars are a result of the lower thickness of A1094 compared to A767 steel.

Figure 3.76: Top bar (top) and bottom bars (bottom) of specimen SE-Bent-A767-2 after 96 weeks of testing

Figure 3.77: Top bar (top) and bottom bars (bottom) of specimen SE-Bent-A1094-2 after 96 weeks of testing

3.2.5.4 ChromX Reinforcement

Figure 3.78 shows the bars from specimen SE-ChromX-5 after 96 weeks of testing, representative of all ChromX reinforcement with no admixture in the Southern Exposure Test. Light to moderate amounts of corrosion were visible on portions of both top bars. No corrosion products were visible on the bottom bars. Figures 3.79 and 3.80 show top and bottom bars of specimen SE-ChromX-IPANEX-2 and SE-ChromX-Xypex-1 after 96 weeks of testing, respectively. ChromX bars in concrete with IPANEX, shown in Figure 3.79, and Xypex, shown in Figure 3.80, are representative of all ChromX reinforcement paired with waterproofing admixtures in the Southern Exposure test. ChromX reinforcement with an admixture showed corrosion products similar to ChromX bars without an admixture.

Figure 3.78: Top bars (top) and bottom bars (bottom) of specimen SE-ChromX-5 after 96 weeks of testing

Figure 3.79: Top bars (top) and bottom bars (bottom) of specimen SE-ChromX-IPANEX-2 after 96 weeks of testing

Figure 3.80: Top bars (top) and bottom bars (bottom) of specimen SE-ChromX-Xypex-1 after 96 weeks of testing

Figure 3.81 shows the bars from specimen CB-ChromX-1 after 96 weeks of testing and is representative of all ChromX reinforcement with no admixtures in the cracked beam test. Light to moderate amounts of corrosion were visible on the steel, less than observed on conventional reinforcement in the cracked beam test. Corrosion was concentrated in the region immediately under the 6-in. simulated crack in the specimen. ChromX bars in concrete with IPANEX (shown in Figure 3.82) and Xypex (shown in Figure 3.83), representative of ChromX reinforcement paired

with waterproofing admixtures in the cracked beam test, exhibited similar behavior, with the corrosion products predominantly in the region under the simulated crack.

Figure 3.81: Top bar (top) and bottom bars (bottom) of specimen CB-ChromX-1 after 96 weeks of testing

Figure 3.82: Top bar (top) and bottom bars (bottom) of specimen CB-ChromX-IPANEX-6 after 96 weeks of testing

Figure 3.83: Top bar (top) and bottom bars (bottom) of specimen CB-ChromX-Xypex-2 after 96 weeks of testing

Figure 3.84 shows the bars from specimen SE-Conv-B-IPANEX-2, and Figure 3.85 the bars from specimen CB-Conv-B-IPANEX-1 after 96 weeks of testing. Moderate to heavy amounts of corrosion were visible on the bars from the top bars, no different than that observed on conventional reinforcement without IPANEX (Figures 3.55 and 3.57). Figure 3.86 shows the bars from specimen SE-Conv-B-Xypex-1, and Figure 3.87 the bars from specimen CB-Conv-B-Xypex-2 after 96 weeks of testing. A moderate amount of corrosion was visible on the bars from the top bar, but less than that observed on conventional reinforcement without Xypex; this is in line with the reduction observed in the corrosion loss in the conventional reinforcement with Xypex admixture. A light amount of corrosion was visible on the bottom conventional bars paired with both IPANEX and Xypex.

Figure 3.84: Top bar (top) and bottom bars (bottom) of specimen SE-Conv-B-IPANEX-2 after 96 weeks of testing

Figure 3.85: Top bar (top) and bottom bars (bottom) of specimen CB-Conv-B-IPANEX-1 after 96 weeks of testing

Figure 3.86: Top bars (top) and bottom bars (bottom) of specimen SE-Conv-B-Xypex-1 after 96 weeks of testing

Figure 3.87: Top bar (top) and bottom bars (bottom) of specimen CB-Conv-B-Xypex-2 after 96 weeks of testing

3.3 Comparison of Losses in Conv-A, Conv-B, and Conv-C

In this section, the ratio of total to macrocell corrosion loss for each heat of conventional reinforcement is given for the rapid macrocell, Southern Exposure, and cracked beam tests. Table 3.18 shows the average total and macrocell corrosion losses and the ratio of total to macrocell loss for Conv-A, Conv-B, and Conv-C at the end of the rapid macrocell (15 weeks), Southern Exposure (96 weeks), and cracked beam (96 weeks) tests. At the end of each test, each of the three heats of conventional reinforcing bars exhibited greater total corrosion losses than macrocell losses; the differences are statistically significant ($p < 0.07$). For each heat of reinforcement, the ratio of total to macrocell losses were lower in the Southern Exposure test (1.5 – 2) than in the cracked beam (2.1 – 3) or rapid macrocell tests (1.7 – 3), indicating that relatively more microcell corrosion occurred in the cracked beam and rapid macrocell tests than in the Southern Exposure test.

Table 3.18: Ratio of average total to macrocell losses on conventional reinforcement at end of rapid macrocell, Southern Exposure, and cracked beam tests

		Average Loss*		
	Type of loss	Rapid Macrocell	Southern Exposure	Cracked Beam
Conv-A	Macrocell (μm)	3.97	4.94	12.2
	Total (μm)	9.77	9.98	36.6
	Total/Macrocell	2.5	2	3
Conv-B	Macrocell (μm)	6.68	10.6	18.6
	Total (μm)	19.8	15.8	42.2
	Total/Macrocell	3	1.5	2.3
Conv-C	Macrocell (μm)	7.17	10.6	12.9
	Total (μm)	12.5	16.2	27.4
	Total/Macrocell	1.7	1.5	2.1

*At week 15 for rapid macrocell and at week 96 for Southern Exposure and cracked beam tests

3.4 DISCUSSION

Epoxy-coated reinforcement (ECR) without UV exposure exhibited greater corrosion resistance than conventional reinforcement across all laboratory tests. Undamaged ECR exhibited little corrosion activity under any test conditions (with or without UV exposure). Undamaged ECR, however, does not represent ECR in the field where damage is expected.

The corrosion resistance of damaged ECR was drastically reduced after as few as 100 hours of UV exposure under ASTM G154 Cycle 1 conditions (equivalent to approximately 1.2 months of outdoor exposure) with the damaged UV-exposed ECR exhibiting corrosion rates several times greater than damaged ECR without UV exposure. These results strongly suggest that the existing guidelines in ASTM D3963, which limit unprotected outdoor exposure to two months, are insufficient to protect epoxy coatings from damage. For practical reasons, it may not be possible to prohibit outdoor exposure of epoxy-coated bars, but limiting exposure to one month or less would be advantageous to maintain corrosion resistance. The bent ECR bars were patched before the rapid macrocell test, and the average corrosion rates did not exceed 0.2 μm/yr during the test.

More research is recommended on the effects of bending on the corrosion performance of ECR. Also, it would be interesting to evaluate the simultaneous effects of bending and UV exposure on the corrosion performance of ECR in future studies.

ASTM A767 and A1094 reinforcement exhibited similar performance in terms of corrosion resistance and can be used interchangeably. The corrosion losses were slightly less than the values for conventional reinforcement, both without and with damage on the coating; however, corrosion losses increased for both bar types when the bars were bent. Prior research suggests that A767 reinforcement can sustain greater corrosion losses than conventional reinforcement before the corrosion losses cause concrete to crack (O'Reilly et al. 2011). Similar research is needed on the corrosion loss to crack concrete with A1094 reinforcement, for which there is no data. It has been claimed that A1094 galvanized reinforcement has a more flexible coating than A767 reinforcement; the results of this study do not support that claim. The results show that the bent A767 and A1094 bars exhibit greater corrosion losses in the Southern Exposure test than straight bars. The observations suggest a potential need to patch or repair any damage that may occur after bending galvanized reinforcement. More research is recommended on the effect of bending on the corrosion performance of both types of galvanized reinforcement and the types of repairs required if bending is shown to consistently reduce the corrosion performance of either bar type.

In the tests described in this report, ChromX (ASTM A1035 Type CS) reinforcement exhibited corrosion losses lower than conventional reinforcement but higher than ECR.

It was excepted that the combined use of a waterproofing admixture and a reinforcement would result in lower corrosion rates compared to the reinforcement alone due to a potential decrease in permeability, and in turn, a decrease in the penetration of chlorides and oxygen. The corrosion resistance of ChromX reinforcement, however, was not improved by the addition of

either IPANEX or Xypex, which can be attributed to ChromX bars' inherently lower corrosion rates compared to conventional reinforcement resulting in less demand for oxygen at the cathode. IPANEX was not effective in improving the corrosion resistance of conventional reinforcement, but Xypex was, resulting in reductions in corrosion losses in both uncracked and cracked concrete.

LPR corrosion rates, including both macrocell and microcell rates, matched the macrocell corrosion rates at the beginning of the cracked beam test. As the test continued, macrocell rates decreased whereas LPR corrosion rates remained constant, indicating a relative increase in microcell rates.

In this study, epoxy-coated bars had a critical chloride corrosion threshold greater than those of conventional and galvanized reinforcing bars. Both A767 and A1094 galvanized reinforcing bars exhibited critical chloride corrosion thresholds greater than the average for Conv-A, Conv-B, and Conv-C. ChromX bars exhibited critical chloride corrosion thresholds greater than conventional, epoxy-coated, and galvanized reinforcing bar types, in agreement with the findings of Darwin et al. (2007).

CHAPTER 4: LIFE EXPECTANCY AND COST-EFFECTIVENESS OF CORROSION PROTECTION SYSTEMS FOR REINFORCED CONCRETE

4.1 GENERAL

This chapter describes an estimation of the life expectancy and cost-effectiveness of bridge decks with the corrosion protection systems evaluated in this study, which are conventional (ASTM A615), epoxy-coated (ASTM A775), hot-dip galvanized (ASTM A767), continuously galvanized (ASTM A1094), and ChromX (ASTM A1035 Type CS) reinforcing bars, and conventional and ChromX reinforcement cast in concrete containing the waterproofing admixtures IPANEX and Xypex. Three heats of conventional steel are included to demonstrate the variability in what may be expected in the field due to the differences in the properties of even this "standard" product. The time to corrosion initiation and the time from initiation to cracking of concrete cover is calculated based on experimental results and are used to estimate the time to first repair. A cost analysis is performed to determine the total cost (present value cost) of each system over a 100-year service life. Finally, the corrosion rates and critical chloride corrosion thresholds from previous studies are used to establish the variability inherent in corrosion.

4.2 LIFE EXPECTANCY

The life expectancy of reinforced concrete bridge decks is assessed by dividing the service life into two stages: the time between placing a structure into service to the point of corrosion initiation and the time for propagation of corrosion following initiation (Tutti 1982). The first stage, initiation, represents the time it takes for chlorides to reach the reinforcement and initiate corrosion. The second stage, propagation, is the time for corrosion to cause cracking of the concrete cover. The length of the two stages is estimated as described in the following sections.

4.2.1 Time to Corrosion Initiation

Corrosion initiation occurs when the chloride content in the concrete adjacent to reinforcing bars reaches the critical chloride corrosion threshold, as discussed in Chapter 1. The critical chloride corrosion thresholds obtained in this study are compared with the chloride concentrations at the depth of reinforcing bars in reinforced concrete bridge decks to determine the time of corrosion initiation for each corrosion protection system. Lindquist et al. (2006) measured the chloride concentrations in 57 bridge decks (mainly in northern-eastern Kansas) with an annual average daily traffic (AADT) greater than 7500; the bridge deck types included monolithic decks, decks with a conventional high-density overlay, and decks with 5 and 7% replacements of cement by silica fume. Powdered concrete samples were obtained from these bridge decks using a ¾-in. vacuum drill at ¾-in. (19 mm) depth intervals up to a depth of 3¾ in. (95 mm) both on and away from cracks. Chloride concentrations at specific depths were obtained by interpolation using the results of the five samples obtained at each location. Figure 4.1 shows the chloride concentrations versus the age for the bridge decks at crack locations at a depth of 3 in. (76 mm), equal to the concrete cover used in bridge decks in Kansas. Cracks are common on reinforced concrete bridge decks; cracks often form over the reinforcement due to settlement of plastic concrete and shrinkage of the hardened concrete. These cracks facilitate penetration of oxygen and chlorides to the level of the reinforcing steel. The trend line equation in Figure 4.1, obtained by Lindquist et al., is used to estimate the time to corrosion initiation in bridge decks with 3-in. (76-mm) cover:

$$t_1 = (C_{crit} - 0.4414) / 0.0187 \tag{4.1}$$

where,

C_{crit} = critical chloride corrosion threshold for reinforcing steel in question, kg/m^3

t_1 = time to reach the critical chloride corrosion threshold, months

In terms of pounds per cubic yard, Eq (4.1) is:

$$t_1 = (C_{crit} - 0.7444) / 0.0315 \tag{4.2}$$

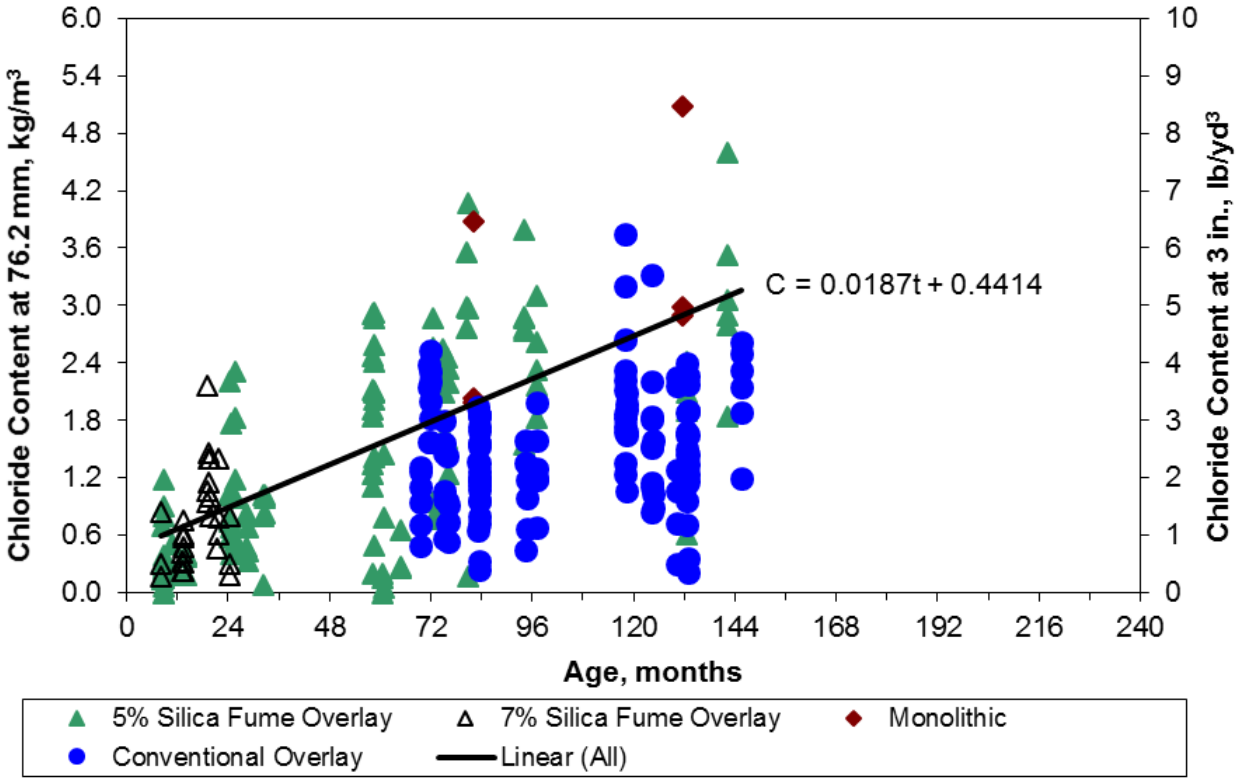

Figure 4.1: Chloride concentration on cracks interpolated at a depth of 3 in. (76 mm) versus time since placement for bridges with an AADT > 7500 (Lindquist et al. 2006)

Equations (4.1) and (4.2) will also be used for concrete with waterproofing admixtures IPANEX and Xypex since Figure 4.1 shows a direct linear relationship between the chloride concentration at crack locations and time, independent of concrete permeability.

The time to reach a given chloride concentration (C_{crit}) at cracks for 2.5-in. (64-mm) concrete cover (common in the state of Oklahoma) in terms of pounds per cubic yard is (Lindquist et al. 2005):

$$t_1 = (C_{crit} - 0.8215) / 0.0372 \tag{4.3}$$

For this study, critical chloride corrosion thresholds were obtained using the samples collected from Southern Exposure specimens at the level of the top bars upon corrosion initiation, as discussed in Chapter 2. Table 4.1 shows the average critical chloride corrosion thresholds in lb/yd^3 and kg/m^3 and the average times to corrosion initiation in months for bridge decks with 3-in. and 2.5-in. covers using Eq (4.2) and Eq (4.3), respectively. A minimum initiation age of one year is adopted in cases where a low critical chloride corrosion threshold results in negative or very low corrosion initiation times based on the equations; the 12-month minimum is assumed because deicing salts are not immediately applied to bridge decks after construction. The difference in critical chloride corrosion thresholds between Conv-A (1.36 lb/yd^3) and Conv-C (1.54 lb/yd^3) are not statistically significant (Table 3.7); the differences between those heats and Conv-B, however, are statistically significant ($p \leq 0.16$). Therefore, a value of 1.45 lb/yd^3 (average of 1.36 and 1.54 lb/yd^3) is used as the average critical chloride threshold for both Conv-A and Conv-C; 0.65 lb/yd^3 is used for Conv-B because the differences in the critical chloride corrosion thresholds between Conv-B and both Conv-A and Conv-C are statistically significant ($p \leq 0.16$). For decks with 3-in. cover, conventional reinforcement had initiation times of 22 months or less, while ECR had an initiation time of 58 months. The difference in critical chloride corrosion thresholds between ASTM A767 and A1094 is not statistically significant (Table 3.7). With a critical corrosion threshold of 1.48 lb/yd^3 (average of 1.37 and 1.58 lb/yd^3), both forms of galvanized reinforcement are estimated to initiate corrosion in 23 months, and ChromX reinforcement, with a critical corrosion threshold of 3.37 lb/yd^3, is estimated to have the highest corrosion initiation time among the reinforcement experimentally evaluated in this study, 83 months. For decks with 2.5-in. cover, the conventional reinforcement has calculated initiation times of 17 months or less, while ECR had a calculated initiation time of 47 months. The

galvanized reinforcement is estimated to initiate corrosion in 18 months, and ChromX reinforcement in 69 months. The average critical chloride corrosion threshold for ECR is used for ECR-UV as an insufficient number of samples were taken from ECR-UV specimens. Waterproofing admixtures did not alter the critical chloride corrosion thresholds for conventional or ChromX reinforcement. Therefore, the same initiation time is assumed for specimens without and with admixtures in Table 4.1.

Table 4.1: Critical chloride corrosion threshold and estimated time to corrosion initiation

Corrosion Protection System	Average Critical Chloride Corrosion Threshold		Initiation Time	
			(2.5-in. Cover)	(3-in. Cover)
	lb/yd^3	kg/m^3	Months	Months
Conv-A	1.45	0.856	17	22
Conv-B	0.65	0.384	12*	12*
Conv-C	1.45	0.856	17	22
ECR	2.58	1.52	47	58
ECR-UV	2.58	1.52	47	58
A767	1.48	0.873	18	23
A1094	1.48	0.873	18	23
ChromX	3.37	1.99	69	83
IPANEX-ChromX	3.37	1.99	69	83
Xypex-ChromX	3.37	1.99	69	83
IPANEX-Conv-B	0.65	0.384	12*	12*
Xypex-Conv-B	0.65	0.384	12*	12*

* Initiation time is assumed to be not less than 12 months as bridges are not immediately exposed to deciding salts after construction.

The estimated times to corrosion initiation found in this study differ from those calculated in previous studies. Farshadfar et al. (2017) estimated corrosion initiation times of 23, 197, and 120 months for bridge decks with conventional, epoxy-coated, and ChromX (ASTM A1035 Type CS reinforcement, with 3-in. cover, respectively. Farshadfar et al. adopted a critical chloride threshold of 2.57 lb/yd^3 (Darwin et al. (2009)) to estimate an initiation time of 58 months for

galvanized reinforcement. Darwin et al. (2013) estimated corrosion initiation times of 32 and 122 months for conventional and epoxy-coated reinforcement in bridge decks with 3-in. cover, respectively. They estimated corrosion initiation times of 25 and 101 months for conventional and epoxy-coated reinforcement for bridge decks with 2.5-in. cover, respectively. O'Reilly et al. (2011) calculated corrosion initiation times of 26 and 244 months for conventional and epoxy-coated reinforcement in bridge decks with 3-in. cover, respectively. As discussed in Chapter 1, the critical chloride corrosion threshold and time to corrosion initiation are best treated as ranges, rather than as fixed numbers; this is in line with the differences between the results, as discussed in Section 4.4.

4.2.2 Time from Corrosion Initiation to Cracking

The rate at which corrosion occurs after initiation (average corrosion rate) and the corrosion products needed to crack the concrete (discussed in Chapter 1, also referred to as critical corrosion loss in this chapter), are required to calculate the time to cracking of the concrete after corrosion has initiated. The time for concrete to crack after corrosion initiation is calculated by dividing the critical corrosion loss by the average corrosion rate. These calculations are discussed in more detail below.

4.2.2.1 Critical Corrosion Loss

The concrete cover on bridge decks cracks when the buildup of corrosion products on the steel reinforcement reaches the critical corrosion loss. This study uses the equation developed by O'Reilly et al. (2011) to estimate the critical corrosion loss in cases of both uniform corrosion, occurring in laboratory specimens, and local corrosion, occurring on the reinforcement in bridge decks:

$$x_{crit} = 0.53\left(\frac{c^{2-A_f}}{d^{0.38}L_f^{0.1}A_f^{0.6}} + 0.6\right)\times 3^{A_f-1} \tag{4.4}$$

x_{crit} = critical corrosion loss at crack initiation, mil (one-thousandth of an in.)

c = cover, in.

d = bar diameter, in.

L_f = fractional length of bar corroding, $L_{\text{corroding}}/L_{\text{bar}}$

A_f = fractional area of bar corroding, $A_{\text{corroding}}/A_{\text{bar}}$ (O'Reilly et al. 2011).

Equation (4.4) can be converted to the following equation to estimate the critical corrosion loss in μm:

$$x_{crit} = 13.46\left(\frac{c^{2-A_f}}{d^{0.38}L_f^{0.1}A_f^{0.6}} + 0.6\right)\times 3^{A_f-1} \tag{4.5}$$

Using field test specimens representing Kansas bridge decks, Darwin et al. (2011) and O'Reilly et al. (2011) found that corrosion occurs over only about 40% of the uncoated bar area. Therefore, a value of 0.4 is used for L_f and A_f to calculate the critical corrosion loss of conventional bars. Accordingly, the critical corrosion losses for a No. 5 bar with 3-in. and 2.5-in. (76-mm and 64-mm) covers in a bridge deck are, respectively, 96 μm and 73 μm, as shown in Eq. (4.6) and (4.7):

$$x_{crit} = 13.46\left(\frac{3^{2-0.4}}{0.625^{0.38}0.4^{0.1}0.4^{0.6}} + 0.6\right)\times 3^{0.4-1} = 96\ \mu\text{m} \tag{4.6}$$

$$x_{crit} = 13.46\left(\frac{2.5^{2-0.4}}{0.625^{0.38}0.4^{0.1}0.4^{0.6}} + 0.6\right)\times 3^{0.33-1} = 73\ \mu\text{m} \tag{4.7}$$

ChromX reinforcing bars are assumed to have the same critical corrosion loss as conventional bars in this study. Also, previous comparisons of the corrosion loss required to crack concrete for conventional and galvanized reinforcement indicated that galvanized reinforcement

requires about twice as much corrosion loss compared to steel reinforcement to crack concrete cover (O'Reilly et al. 2018). Therefore, the critical corrosion loss of galvanized bars is assumed to be twice that of conventional bars–194 μm and 146 μm for 3-in. and 2.5-in. concrete covers, respectively. For a No. 5 epoxy-coated bar with damage similar to those used in the field test specimens by O'Reilly et al. (2011) (0.125-in. diameter holes spaced at about 4.9 in. on each side of the bar), L_f is 0.024, A_f is 0.0023, and the value of x_{crit} is 2627 μm for 3-in. cover. For the same bar with 2.5-in. cover, x_{crit} is 1826 μm.

4.2.2.2 Average Corrosion Rate After Initiation

The average corrosion rate after initiation for each specimen is determined based on total (LPR) losses using the reported corrosion loss at corrosion initiation and at the end of testing. The corrosion losses were obtained by integrating the weekly corrosion rates of each specimen over time. Figure 4.2 schematically illustrates how the average corrosion rate is derived from the LPR corrosion loss for a given Southern Exposure specimen. As shown in the figure, the points representing corrosion initiation and end of testing are marked, and corresponding corrosion losses (L_i and L_f) and duration in weeks (based on W_i and W_f) for the two points are determined. Individual corrosion loss graphs for Southern Exposure and cracked beam specimens are shown in Appendix F. The average corrosion rate, R, after initiation, expressed in μm/yr, is calculated as follows:

$$R = \frac{L_f - L_i}{W_f - W_i} \times 52 \tag{4.8}$$

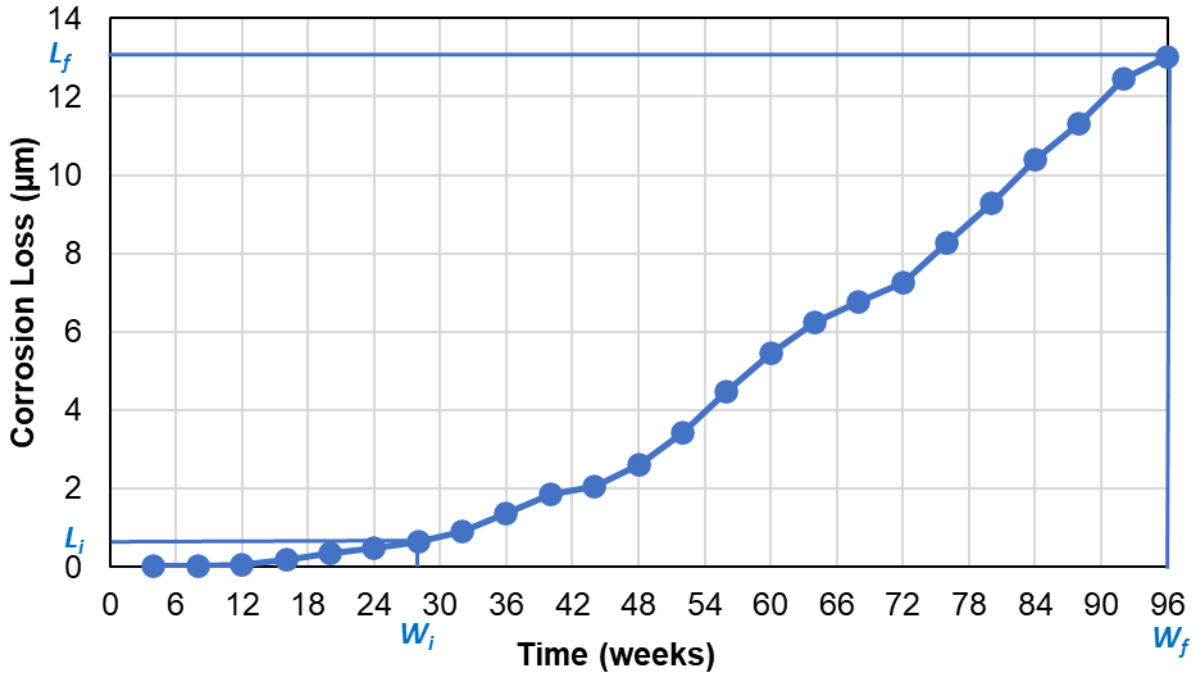

Figure 4.2: LPR corrosion loss for a conventional steel bar in a Southern Exposure specimen (Conv-A-2) with W_f equal to 96

The average corrosion rate is calculated for specimens that initiated corrosion during 96 weeks of testing. Tables 4.2 and 4.3 show the individual and average corrosion rates for the specimens in the Southern Exposure and cracked beam tests based on total (LPR) corrosion loss. The average LPR rates in the cracked beam specimens are used to determine life expectancy because cracks are commonplace on reinforced concrete bridge decks. The corrosion rates based on LPR results in the Southern Exposure test in Table 4.3 are presented for information and are not used to determine life expectancy.

Table 4.2: Average corrosion rate (µm/yr) of Southern Exposure specimens after corrosion initiation based on LPR (total area)

Corrosion Protection System	Average Corrosion Rate (µm/yr) Based on Losses (LPR)							Avg.	Std. Dev
	1.0	2.0	3.0	4.0	5.0	6.0	7.0		
Conv-A	5.26	8.33	6.33	2.49	6.64	6.50	6.30	5.98	1.79
Conv-B	6.55	9.90	6.70	8.80	6.21	11.2	4.38	7.68	2.38
Conv-C	10.9	9.20	11.0	-	-	-	-	10.4	1.02
ECR	0.047	0.028	0.049	0.021	-	-	-	0.036	0.014
ECR-UV	1.27	0.466	0.357	-	-	-	-	0.70	0.498
A767	11.6	2.36	6.12	3.45	1.59	7.51	-	5.43	3.75
A1094	9.91	3.71	3.11	2.17	1.69	8.67	-	4.88	3.51
ChromX	1.56	1.84	0.223	1.32	4.74	-	-	1.94	1.68
IPANEX-ChromX	10.7	6.73	5.58	8.52	10.2	6.58	-	8.07	2.11
Xypex-ChromX	1.04	4.08	2.51	1.83	2.34	1.30	-	2.18	1.09
IPANEX-Conv-B	9.83	10.2	4.58	12.6	9.72	13.0	-	10.0	3.01
Xypex-Conv-B	2.57	1.82	1.15	1.40	1.33	5.87	-	2.36	1.79

- No specimen

Table 4.3: Average corrosion rate (µm/yr) of cracked beam specimens after corrosion initiation based on LPR (total area)

Corrosion Protection System	Average Corrosion Rate (µm/yr) Based on Losses (LPR)								Avg.	Std. Dev
	1	2	3	4	5	6	7	8		
Conv-A	25.8	21.1	24.0	14.8	20.7	12.7	-	-	19.9	5.13
Conv-B	21.6	23.9	30.0	23.1	32.6	26.9	15.1	-	24.7	5.77
Conv-C	12.4	21.1	11.2	-	-	-	-	-	14.9	5.40
ECR	0.037	0.536	0.683	0.063	-	-	-	-	0.330	0.329
ECR-UV	2.68	3.66	3.56	1.78	2.97	3.30	1.24	-	2.74	0.918
A767	8.25	12.7	15.3	4.73	9.84	18.4	-	-	11.5	4.95
A1094	7.70	18.1	6.89	7.05	10.3	14.6	-	-	10.8	4.62
ChromX	9.10	8.03	7.88	6.09	9.73	3.66	9.14	14.4	9.19	2.57
IPANEX-ChromX	12.0	11.9	10.1	9.50	13.9	11.2	-	-	11.4	1.56
Xypex-ChromX	6.76	10.2	8.26	8.25	8.31	6.96	-	-	8.12	1.23
IPANEX-Conv-B	22.4	33.3	27.4	18.7	20.9	22.2	-	-	24.2	5.32
Xypex-Conv-B	12.6	12.3	13.3	12.1	12.3	13.1	-	-	12.6	0.483

- No specimen

The average corrosion rates based on exposed area are used for damaged epoxy-coated reinforcement because the exposed area is used to determine the critical corrosion loss for epoxy-coated reinforcement in Section 4.2.2.1. Tables 4.4 and 4.5 show the individual and average

corrosion rates for the ECR specimens in the Southern Exposure and cracked beam tests using LPR corrosion loss based on exposed area. The corrosion rate based on exposed area is calculated by multiplying the corrosion rates in Tables 4.2 and 4.3 by 192, the ratio of the bar surface area to the exposed area. The corrosion rates based on LPR results in the Southern Exposure test in Table 4.4 are presented for information and are not used to determine life expectancy.

Table 4.4: Average corrosion rate (µm/yr) of Southern Exposure specimens after corrosion initiation for epoxy-coated reinforcement based on LPR (exposed area)

Corrosion Protection System	Average Corrosion Rate (µm/yr) Based on Losses (LPR)				Avg.	Std. Dev
	1	2	3	4		
ECR	9.02	5.38	9.41	4.03	6.96	2.67
ECR-UV	244	89.5	68.5	-	134	95.7

Table 4.5: Average corrosion rate (µm/yr) of cracked beam specimens after corrosion initiation for epoxy-coated reinforcement based on LPR (exposed area)

Corrosion Protection System	Average Corrosion Rate (µm/yr) Based on Losses (LPR)							Avg.	Std. Dev
	1	2	3	4	5	6	7		
ECR	7.10	103	131	12.1	-	-	-	63.3	63.1
ECR-UV	515	703	684	342	570	634	239	526	176

Conventional reinforcement has the highest corrosion rate among the reinforcement evaluated in this study. In the cracked beam test, Conv-B specimens had the highest average corrosion rate among all specimens, with an average of 24.7 µm/yr, greater than the values for Conv-A and Conv-C, 19.9 and 14.9, respectively ($p \leq 0.14$). The difference between the average corrosion rates of Conv-A and Conv-C specimens in the cracked beam is not small; it is, however, not statistically significant ($p = 0.22$). Conv-A and Conv-C are analyzed separately to represent the inherent variability in the reinforcement used in conventional bridge decks. Epoxy-coated bars not exposed to ultraviolet (UV) light had average corrosion rates two orders of magnitude less than conventional bars (based on total area) in the cracked beam test; UV exposure increased the average corrosion rate in ECR from 0.330 µm/yr to 2.74 µm/yr ($p < 0.01$). The corrosion rates of

the two types of galvanized reinforcement are close, and the difference between them is not statistically significant; therefore, an average corrosion rate of 11.2 μm/yr based on total area (average of the values for A767 and A1094 reinforcement, 11.5 and 10.8 μm/yr, respectively) is used for both types of galvanized reinforcement. Specimens with galvanized bars exhibited average corrosion rates about half those of conventional bars. Corrosion of the galvanized bars can be attributed, in part, to sacrificial protection provided by the zinc coating; a key point, however, is that zinc corrosion products are not as voluminous as those of iron (Yeomans 2018), and, therefore, more corrosion losses are required to crack concrete. ChromX specimens exhibited an average corrosion rate of 9.18 μm/yr.

As described in Section 3.2.4.2, IPANEX did not decrease the corrosion LPR loss of Conv-B reinforcement in a statistically significant manner; the use of Xypex, however, resulted in a 45% reduction in the LPR corrosion loss of Conv-B reinforcement compared to Conv-B alone in the cracked beam test ($p < 0.01$) (Table 3.14). As shown in Table 4.3, Conv-B reinforcement paired with Xypex exhibited an average LPR corrosion rate of about 50% the value for Conv-B alone.

It was expected that the combined use of a waterproofing admixture and ChromX reinforcement would result in lower corrosion rates compared to the use of ChromX reinforcement alone. Specimens with ChromX reinforcement paired with IPANEX, however, exhibited an average corrosion rate higher than ChromX reinforcement without an admixture; the difference in corrosion rates of IPANEX paired with ChromX and ChromX without an admixture is statistically significant ($p = 0.05$). Because the difference between corrosion rates of ChromX paired with IPANEX (11.4 μm/yr) and ChromX without an admixture (9.18 μm/yr) is statistically significant and IPANEX increased the corrosion rates, combining ChromX and IPANEX is not considered further. ChromX reinforcement paired with Xypex had an average corrosion rate of 8.12 μm/yr,

lower than that of ChromX reinforcement without any admixture (9.18 μm/yr). The difference is, however, not statistically significant; therefore, the average corrosion rate for ChromX without any admixture is adopted for Xypex paired with ChromX reinforcement (Xypex-ChromX), conservatively.

IPANEX and Xypex were evaluated paired with Conv-B reinforcement. Conv-B exhibited average corrosion rates higher than Conv-A or Conv-C in the cracked beam test, and the differences are statistically significant ($p \leq 0.14$). Therefore, to achieve a fairer cost analysis when Xypex admixture is used, the same percentage reduction observed in the corrosion rate of Conv-B specimens when paired with Xypex is applied to the average corrosion rates of Conv-A and Conv-C when paired with Xypex (Xypex-Conv-A and Xypex-Conv-C).

The corrosion rates measured in the laboratory must be modified before they can be used for cost analysis of corrosion protection systems in bridge decks because laboratory specimens are exposed to more severe conditions than bridge decks, including more severe wetting and drying cycles and high chloride concentrations. Also, cracks in bridge decks, often formed as the result of the settlement of plastic concrete and shrinkage of hardened concrete, do not match the 12-mil-wide intentional crack in cracked beam specimens.

O'Reilly et al. (2011) and Darwin et al. (2011) found that conventional reinforcement exhibited a corrosion rate in their field specimens equal to 0.134 times the value in the lab. They also noted that corrosion occurred over only 40% of the uncoated bar surface area in the field, as opposed to nearly 100% of the bar area in the cracked beam test. It seems apparent, then, that a conversion factor (0.134/0.4) should be applied to account for the corrosion rate and percentage of area of corrosion on the bars; that is, these factors are used to convert the cracked beam corrosion rate to an equivalent field corrosion rate. Therefore, for uncoated bars, the average corrosion rates

based on corrosion losses from the LPR results in the cracked beam test are multiplied by 0.335 (0.134/0.4) to approximate the equivalent field corrosion rates.

As mentioned, the time to cracking of the concrete after corrosion has initiated is calculated using the average corrosion rate and critical chloride corrosion threshold. Therefore, these values work together, and both should be kept in mind when applying factors. It is noteworthy that a 0.4 factor is also included in Eq. (4.4) through (4.7) to calculate the critical corrosion loss of concrete in Section 4.2.2.1. Also, the average corrosion rates based on exposed area are used for damaged epoxy-coated reinforcement as equivalent field corrosion rates because the exposed area is used to determine their critical corrosion loss for concrete in Section 4.2.2.1.

The average LPR corrosion rates based on total area in the cracked beam test (laboratory corrosion rates), discussed earlier (see Table 4.3), and equivalent field corrosion rates are summarized in Table 4.6. As shown in the table, the equivalent field corrosion rates for Conv-A, Conv-B, and Conv-C are 6.65, 8.29, and 4.99 μm/yr, respectively; the values for conventional reinforcement with an admixture range from 2.55 to 8.09 μm/yr. ECR had an equivalent field corrosion rate of 63.3 μm/yr compared to 526 μm/yr for ECR-UV, which will be further discussed in this section. Both galvanized reinforcements had an equivalent field rate of 3.75 μm/yr. The equivalent field corrosion rate for ChromX without and with an admixture is 3.08 μm/yr.

Table 4.6: Laboratory and equivalent field corrosion rates for bridge decks in µm/yr

Corrosion Protection System	Laboratory Corrosion Rate (µm/yr)[1]	Equivalent Field Corrosion Rate (µm/yr)
Conv-A	19.9	6.65
Conv-B	24.7	8.29
Conv-C	14.9	4.99
ECR	0.330	63.3
ECR-UV	2.74	526
A767	11.2	3.75
A1094	11.2	3.75
ChromX	9.18	3.08
Xypex-ChromX	9.19	3.08
IPANEX-Conv-B	24.2	8.09
Xypex-Conv-B	12.6	4.23
XYPEX-Conv-A*	10.1	3.39
XYPEX-Conv-C*	7.60	2.55

*Assumed value

[1] LPR rate based on total area in the cracked beam test

Dividing the critical corrosion loss obtained in Section 4.2.2.1 by the appropriate equivalent corrosion rates in Table 4.6 yields the time from corrosion initiation to cracking for the systems evaluated. The estimated time to first cracking after corrosion initiation is given in Table 4.7.

Table 4.7: Estimated times to first cracking after corrosion initiation (years) based on equivalent corrosion rates

Corrosion Protection System	Equivalent Corrosion Rate (µm/yr)	Critical Corrosion Loss (µm)		Time from Initiation to Cracking (yr)	
		3-in. Cover	2.5-in. Cover	3-in. Cover	2.5-in. Cover
Conv-A	6.65	96	73	14.4	11.0
Conv-B	8.29	96	73	11.6	8.81
Conv-C	4.99	96	73	19.2	14.6
ECR	63.3	2627	1826	41.5	28.8
ECR-UV	526	2627	1826	4.99	3.47
A767	3.75	192	146	51.2	38.9
A1094	3.75	192	146	51.2	38.9
ChromX	3.08	96	73	31.2	23.7
Xypex-ChromX	3.08	96	73	31.2	23.7
IPANEX-Conv-B	8.09	96	73	11.9	9.02
Xypex-Conv-B	4.23	96	73	22.7	17.3
Xypex-Conv-A*	3.39	96	73	28.3	21.5
Xypex-Conv-C*	2.55	96	73	37.7	28.7

*Assumed value

As shown in Table 4.7, ECR-UV specimens have the lowest calculated time from initiation to cracking, as low as 3.47 years for a bridge deck with 2.5-in. cover. The precision of this extremely low time to cracking based on intentional damage area is debatable; this is because the corroding area of the ECR-UV bars was greater than just the intentional damage on the coating due to the blistering and cracking, and a greater corroding area results in a lower effective field rate. Therefore, 3.47 years is a conservative estimate for the initiation to cracking time for epoxy-coated bars exposed to UV light in the field. The detrimental effect of prolonged UV light exposure on the ECR reinforcement, however, is undeniable. That is, ECR-UV exhibited a higher time from initiation to cracking than ECR not exposed to UV; however, this time for ECR exposed to UV is likely to be not as low as 3.47 years in the field.

4.2.3 Time to the First Repair

Because bridge decks remain functional, they are not usually repaired immediately after the development of the first cracks. The time from the first cracking to the first repair of a bridge deck is assumed to be 10 years based on the experience of the Kansas Department of Transportation. Tables 4.8 and 4.9 summarize the total time to first repair for the corrosion protection systems evaluated in this study in cracked concrete for bridge decks with 3-in. and 2.5-in. covers, respectively. No corrosion protection systems achieved a 100-year design life without repair. A bridge deck with Conv-A, Conv-B, and Conv-C reinforcement and 3-in. cover needed repair in 26.3, 22.6, 31.1 years, respectively; the paired use of Xypex and ChromX or ChromX alone yields a first repair time of 48.2 years. ECR, if protected from prolonged UV light and humidity exposure, provides a service life of 56.3 years in bridge decks with 3-in. concrete cover. Galvanized reinforcement had the highest service life of 63.1 years in bridge decks with 3-in. concrete cover, owing to the assumption that their critical corrosion loss is twice that of conventional reinforcement. As shown in Tables 4.8 and 4.9, bridge decks with 3-in. cover exhibited greater times to corrosion initiation and greater times from initiation to cracking than bridge decks with 2.5-in. cover, resulting in a longer time to repair.

Table 4.8: Time (years) to first repair for corrosion protection systems (3-in. cover)

Corrosion Protection System	Initiation Time	Initiation to Cracking Time	Time from Cracking to Repair	Predicted Service Life
Conv-A	1.9	14.4	10.0	26.3
Conv-B	1.0	11.6	10.0	22.6
Conv-C	1.9	19.2	10.0	31.1
ECR	4.9	41.5	10.0	56.3
ECR-UV	4.9	4.99	10.0	19.8
A767	1.9	51.2	10.0	63.1
A1094	1.9	51.2	10.0	63.1
ChromX	6.9	31.2	10.0	48.2
Xypex-ChromX	6.9	31.2	10.0	48.2
IPANEX-Conv-B	1.0	11.9	10.0	22.9
Xypex-Conv-B	1.0	22.7	10.0	33.7
Xypex-Conv-A*	1.9	28.3	10.0	40.2
Xypex-Conv-C*	1.9	37.7	10.0	49.6

*Assumed value

Table 4.9: Time (years) to first repair for corrosion protection systems (2.5-in. cover)

Corrosion Protection System	Initiation Time	Initiation to Cracking Time	Time from Cracking to Repair	Predicted Service Life
Conv-A	1.4	11.0	10.0	22.4
Conv-B	1.0	8.81	10.0	19.8
Conv-C	1.4	14.6	10.0	26.0
ECR	3.9	28.8	10.0	42.8
ECR-UV	3.9	3.47	10.0	17.4
A767	1.5	38.9	10.0	50.4
A1094	1.5	38.9	10.0	50.4
ChromX	5.7	23.7	10.0	39.4
Xypex-ChromX	5.7	23.7	10.0	39.4
IPANEX-Conv-B	1.0	9.02	10.0	20.0
Xypex-Conv-B	1.0	17.3	10.0	28.3
Xypex-Conv-A*	1.4	21.5	10.0	32.9
Xypex-Conv-C*	1.4	28.7	10.0	40.1

*Assumed value

4.3 COST-EFFECTIVENESS

The expected costs of the corrosion protection systems evaluated in this study are compared in this section. The cost analyses are based on a 150 ft (46 m) long, 44.2 ft (13 m) wide bridge deck, and decks with thicknesses of both 8.5-in. (216-mm), with 3-in. (76-mm) cover, and 8.0-in. (203-mm), with 2.5-in. (64-mm) cover. The estimated costs include both the initial construction and the repair required to achieve a 100-year service life. Two approaches are taken to calculate the time repaired bridge decks last before repair is needed again. In the first approach, the bridge deck is demolished and a new bridge deck is cast (full deck replacement); the replacement deck is assumed to last for the same period as a new bridge deck for that corrosion protection system, except for ECR-UV where full deck replacements are assumed to be performed with ECR not exposed to UV. In the second approach, based on the experience from the Kanas Department of Transportation, the repair consists of applying a silica fume or polymer overlay to the deck after exposing the top mat of reinforcement (Darwin et al. 2011). Since coated reinforcement is likely to sustain damage during handling and placement, the 100-year service life of ECR and galvanized reinforcement is based on results from damaged specimens. Reinforcing steel costs were obtained from manufacturers; other costs are based on successful bids for new bridge decks and deck replacements in the states of Oklahoma and Kansas in 2020.

4.3.1 New Bridge Deck Construction Costs

An average reinforcing steel quantity of 54.4 lb/yd^2 is used for estimating bridge deck costs in Oklahoma (Darwin et al. 2013). Table 4.10 summarizes the in-place cost of each type of reinforcement. In-place costs per pound of conventional and epoxy-coated reinforcement are obtained from successful bids for new bridge decks. The free on board (FOB) cost of steel is obtained from Commercial Metals Company (CMC). The difference between the FOB and in-

place costs of conventional steel in Oklahoma is added to the FOB cost of ChromX and galvanized reinforcement to calculate the in-place cost. The cost of reinforcement per unit area for a bridge deck using the reinforcement evaluated in this study is given in Table 4.11.

Table 4.10: In-place cost of reinforcement per pound

Steel Type	FOB Cost $/lb	Placement Cost $/lb	In-place Cost $/lb
Conv-A, B, and C	0.28	0.69	0.97
ECR	0.36	0.89	1.25
ChromX	1.03	0.69	1.72
A767	0.71	0.69	1.40
A1094	0.58	0.69	1.27

Table 4.11: In-place cost of reinforcement in 8-in. and 8.5-in. bridge decks per square yard

Steel Type	Steel Quantity lb/yd^2	In-Place Cost $/yd^2$
Conv-A, B, and C	54.4	52.5
ECR	54.4	68.0
ChromX	54.4	93.3
A767	54.4	75.9
A1094	54.4	68.8

The in-place cost of concrete is taken to be $\$508/yd^3$ based on the average concrete cost in the state of Oklahoma in 2020; this includes delivery of concrete to the construction site and labor charges by the contractor. This value yields $\$120/yd^2$ and $113/yd^2$ for the in-place cost of concrete in 8.5-in. and 8-in. bridge decks, respectively. The price of Xypex (C-500NF Admixture) is $3.24 a pound, not including any freight cost (in August of 2020). Using 6 pounds of this admixture per cubic yard of concrete yields an additional cost of $4.59 and $4.32 per square yard of concrete (total of $\$125/yd^2$ and $\$117/yd^2$) for 8.5-in and 8-in. bridge decks, respectively. Similar costs are assumed for IPANEX, as the manufacturer did not provide a cost. Tables 4.12 and 4.13 summarize the total in-place cost for reinforced concrete per square yard for 8.5-in. and 8-in. thick bridge decks using the corrosion protection systems evaluated in this study. For an 8.5-in. thick bridge

deck, conventional reinforcement has the lowest initial cost, $173/yd^2, and the combination of a waterproofing admixture and ChromX reinforcement has the highest cost, $218/yd^2.

Table 4.12: Total in-place cost for reinforced concrete per square yard in an 8.5-in. bridge deck

Corrosion Protection System	In-Place Cost ($/yd^2)	Concrete Cost ($/yd^2)	Total Cost ($/yd^2)
Conv-A, B, and C	52.5	120	173
ECR	68.0	120	188
A767	75.9	120	196
A1094	68.8	120	189
ChromX	93.3	120	213
Xypex-ChromX	93.3	125	218
IPANEX-Conv-B	52.5	125	177
Xypex-Conv*	52.5	125	177

*Same cost for Conv-A, Conv-B, and Conv-C

Table 4.13: Total in-place cost for reinforced concrete per unit area in an 8-in. bridge deck

Corrosion Protection System	In-Place Cost ($/yd^2)	Concrete Cost ($/yd^2)	Total Cost ($/yd^2)
Conv-A, B, and C	52.5	113	166
ECR	68.0	113	181
A767	75.9	113	189
A1094	68.8	113	182
ChromX	93.3	113	206
Xypex-ChromX	93.3	117	211
IPANEX-Conv-B	52.5	117	170
Xypex-Conv*	52.5	117	170

* Same cost for Conv-A, Conv-B, and Conv-C

4.3.2 Repair Costs

A service life of 100 years is used for bridge decks in the 100-year design life cost analysis. Two approaches to bridge deck repair are analyzed in this study. In the first approach, the existing bridge deck is replaced with a new deck identical to the old deck (full deck replacement). For this

approach, a value of $323/yd^2 is assumed for the cost of mobilization, traffic control, removal of the existing deck, and other miscellaneous repair work (Darwin et al. 2020). This value is added to the cost of new deck construction to obtain repair costs, shown in Table 4.14.

Table 4.14: Repair cost for full deck replacement in bridge decks

Corrosion Protection System	Repair Cost ($/yd^2)	
	3-in. Cover	2.5-in. Cover
Conv-A, B, and C	496	489
ECR	511	504
A767	519	512
A1094	512	505
ChromX	537	530
Xypex-ChromX	541	534
IPANEX-Conv-B	500	493
Xypex-Conv*	500	493

* Same cost for Conv-A, Conv-B, and Conv-C

In the second approach, the bridge deck is repaired with an overlay after exposing the top mat of reinforcement; based on experience in Kansas, this partial depth repair is assumed to last 25 years before another repair is needed. The repair cost includes the costs of overlay, machine preparation, mobilization, traffic control, and patching. The repair cost of bridge decks with epoxy-coated reinforcement is assumed similar to that of conventional reinforcement (Darwin et al. 2011). The cost of bridge deck concrete overlay is taken $368/yd^2 based on the winning bids in the state of Kansas in 2020.

4.3.3 100-Year Design Life Cost Estimates

4.3.3.1 Present Value Cost

To establish a fair comparison of the cost-effectiveness of the corrosion protection systems, repair costs are converted to their present value using a 2% discount rate as follows:

$$P = F \times (1+i)^{-n} \tag{4.7}$$

where:

P = present value cost

F = future cost

i = discount rate

n = time to repair

4.3.3.2 Cost Estimates for Full Deck Replacement

Tables 4.15 and 4.16 give the times to repair and present value costs for corrosion protection systems in 8.5-in. (3-in. cover) and 8-in. (2.5-in. cover) bridge decks, respectively, based on a 100-year service life and repairs with a full deck replacement. Xypex-ChromX, IPANEX-ChromX, and IPANEX-Conv-B are not included in the results because they cost more than the matching reinforcement without an admixture.

Table 4.15: Present value cost based on initial cost and full deck replacement repair cost for an 8.5-in. bridge deck with different corrosion protection systems using a 2% discount rate

Corrosion Protection System	Initial Cost ($/yd^2)	Time to Repair (yr)					Repair Cost ($/yd^2)	Present Value Cost ($/yd^2)
		1	2	3	4	5		
Conv-A	173	26.3	52.6	78.9	-	-	496	746
Conv-B	173	22.6	45.2	67.7	90.3	-	496	905
Conv-C	173	31.1	62.2	93.3	-	-	496	663
ECR	188	56.3	-	-	-	-	511	356
ECR-UV	188	19.8	76.2**	-	-	-	511	458
A767	196	63.1	-	-	-	-	519	345
A1094	189	63.1	-	-	-	-	512	336
ChromX	213	48.2	-	-	-	-	537	420
Xypex-Conv-B	177	33.7	67.4	-	-	-	500	565
Xypex-Conv-A*	177	40.2	80.4	-	-	-	500	505
Xypex-Conv-C*	177	49.6	-	-	-	-	500	365

*Assumed value
** Repairs are done with ECR not exposed to UV
- No repair

Table 4.16: Present value cost based on initial cost and full deck replacement repair cost of an 8-in. bridge deck with different corrosion protection systems using a 2% discount rate

Corrosion Protection System	Initial Cost ($/yd^2)	Time to Repair (yr)					Repair Cost ($/yd^2)	Present Value Cost ($/yd^2)
		1	2	3	4	5		
Conv-A	166	22.4	44.8	67.2	89.5	-	489	893
Conv-B	166	19.8	39.6	59.4	79.2	-	489	971
Conv-C	166	26.0	52.1	78.1	-	-	489	736
ECR	181	42.8	85.6	-	-	-	504	490
ECR-UV	181	17.4	60.2**	-	-	-	504	691
A767	189	50.4	-	-	-	-	512	378
A1094	182	50.4	-	-	-	-	505	368
ChromX	206	39.4	78.9	-	-	-	530	560
Xypex-Conv-B	170	28.3	56.5	84.8	-	-	493	704
Xypex-Conv-A*	170	32.9	65.9	-	-	-	493	560
Xypex-Conv-C*	170	40.1	80.2	-	-	-	493	493

*Assumed value
** Repairs are done with ECR not exposed to UV
- No repair

The different times to repair for the three conventional reinforcement types evaluated represent the inherent variability in the reinforcement used in conventional bridge decks. Also, repairs with 2.5-in and 3-in concrete covers, customary in the states of Oklahoma and Kansas, respectively, led to a different number of repairs for Conv-A; Conv-A with 3-in. concrete cover needed repair three times compared to four times with 2.5-in. cover. With Conv-B reinforcement, the poorest performing reinforcement in this study, a bridge deck must be repaired 22.6, 45.2, 67.7, and 90.3 years after construction for an 8.5-in. bridge deck with full deck replacement (Table 4.15); the present value cost of this conventional bridge deck at a 2% discount rate is estimated at $905/yd^2; Conv-C, the best performing of the three heats of conventional reinforcement, needs repair at 31.1, 62.2, and 93.3 years with a present value cost of $663/yd^2. The major differences in the present value costs for the conventional bars show that minor changes in production or

chemistry can lead to large differences in corrosion resistance, even among conventional bars. ChromX reinforcement costs \$420/yd^2 with repair at 48.2 years; ChromX reinforcement is more cost-effective than conventional reinforcement but less so than ECR, which costs \$356/yd^2, with repair at 56.3 years. Table 4.15 shows that improper storage of ECR can increase the present value cost per square yard of a bridge deck from \$356/yd^2, one of the most cost-effective alternatives, to \$458/yd^2 because UV exposure decreases the time to first repair. The galvanized reinforcement had the lowest present value cost; bridge decks with ASTM A767 and A1094 bars have a present value cost of \$345/yd^2 and \$336/yd^2, respectively, requiring repair at 63.1 years. While the galvanized bars showed promising corrosion performance, the autopsy performed on the specimens at the end of testing revealed corrosion in both top and bottom mats; the underlying steel was occasionally exposed indicating total loss of the zinc coating and corrosion of steel Therefore, further research is recommended to evaluate the corrosion resistance of galvanized bars, as well as to compare the performance of hot-dip and continuously galvanized bars.

Xypex waterproofing admixture is claimed by the manufacturer to improve corrosion resistance by hindering the penetration of oxygen and moisture, needed for the cathodic reaction, by decreasing the permeability of the concrete. Lower permeability will limit corrosion, especially on conventional reinforcement, which exhibits high corrosion rates after corrosion initiation. For an 8.5-in. bridge deck, paired use of Xypex with Conv-B reinforcement costs \$565/yd^2, while Conv-B alone costs \$905/yd^2. Xypex paired with Conv-A and Conv-C costs \$505/yd^2 and \$365/yd^2, respectively; Conv-A and Conv-C alone cost \$746/yd^2 and \$663/yd^2, respectively.

The pairing of Xypex with conventional reinforcement decreased the present value cost of bridge decks over a 100-year design life by 32 to 45% in an 8.5-in. bridge deck and 27 to 37% in an 8-in. bridge deck.

For all systems with full deck replacement, the 2.5-in. cover (8-in. deck) resulted in earlier times to repair and higher present value costs over a 100-year design life than decks with 3-in. cover (8.5-in. deck). Conv-A, ECR, ChromX, Xypex-Conv-B, and Xypex-Conv-C systems needed one more repair when 2.5-in cover was used compared to 3-in. cover. The use of the higher cover resulted in an 11% decrease in the present value cost of decks with conventional reinforcement based on the average decrease in value for Conv-A, Conv-B, and Conv-C, and 27 and 33% decreases in the present value cost for decks with ECR and ECR-UV, respectively. The present value cost of a bridge deck with galvanized reinforcement and 3-in. cover is on average 9% lower than the deck with 2.5-in. cover. The present value cost of a bridge deck with ChromX reinforcement is 25% lower in a bridge deck with 3-in. cover than for the deck with 2.5-in. cover. When Conv-B reinforcement is paired with Xypex, a bridge deck with 3-in. cover costs 20% lower than the deck with 2.5-in. cover; the present value cost of a bridge deck with Conv-B reinforcement decreases 7% when 3-in. cover is used instead of 2.5-in. cover.

4.3.3.3 Cost Estimates for Partial Deck Repair

Tables 4.17 and 4.18 give the times to repair and present value costs for the corrosion protection systems in 8.5-in. (3-in. cover) and 8-in. (2.5-in. cover) bridge decks, respectively, based on a 100-year service life and partial deck repair with an overlay that lasts 25 years.

Table 4.17: Present value cost based on initial cost and partial deck repair cost for an 8.5-in. bridge deck with different corrosion protection systems using a 2% discount rate

Corrosion Protection System	Initial Cost ($/yd^2)	Time to Repair (yr)					Repair Cost ($/yd^2)	Present Value Cost ($/yd^2)
		1	2	3	4	5		
Conv-A	173	26.3	51.3	76.3	-	-	368	606
Conv-B	173	22.6	47.6	72.6	97.6	-	368	692
Conv-C	173	31.1	56.1	81.1	-	-	368	566
ECR	188	56.3	81.3	-	-	-	368	382
ECR-UV	188	19.8	44.8	69.8	94.8	-	368	736
A767	196	63.1	88.1	-	-	-	368	366
A1094	189	63.1	88.1	-	-	-	368	359
ChromX	213	48.2	73.2	-	-	-	368	442
Xypex-Conv-B	177	33.7	58.7	83.7	-	-	368	551
Xypex-Conv-A*	177	40.2	65.2	90.2	-	-	368	506
Xypex-Conv-C*	177	49.6	74.6	-	-	-	368	399

*Assumed value
- No repair

Table 4.18: Present value cost based on initial cost and partial deck repair cost for an 8-in. bridge deck with different corrosion protection systems using a 2% discount rate

Corrosion Protection System	Initial Cost ($/yd^2)	Time to Repair (yr)					Repair Cost ($/yd^2)	Present Value Cost ($/yd^2)
		1	2	3	4	5		
Conv-A	166	22.4	47.4	72.4	97.4	-	368	687
Conv-B	166	19.8	44.8	69.8	94.8	-	368	714
Conv-C	166	26.0	51.0	76.0	-	-	368	601
ECR	181	42.8	67.8	92.8	-	-	368	494
ECR-UV	181	17.4	42.4	67.4	92.4	-	368	757
A767	189	50.4	75.4	-	-	-	368	407
A1094	182	50.4	75.4	-	-	-	368	400
ChromX	206	39.4	64.4	89.4	-	-	368	540
Xypex-Conv-B	170	28.3	53.3	78.3	-	-	368	586
Xypex-Conv-A*	170	32.9	57.9	82.9	-	-	368	550
Xypex-Conv-C*	170	40.1	65.1	90.1	-	-	368	499

*Assumed value
- No repair

With Conv-B reinforcement, the poorest performing reinforcement evaluated in this study, a bridge deck must be repaired 22.6, 47.6, 72.6, and 97.6 years after construction for an 8.5-in. bridge deck with partial repairs using an overlay; the present value cost of this conventional bridge deck at a 2% discount rate is estimated at $692/yd^2; Conv-C, the best performing of the heats of conventional reinforcement, needs repair at 31.1, 56.1, and 81.1 years with a present value cost of $566/yd^2. ChromX reinforcement costs $442/yd^2 with repairs at 48.2 and 73.2 years; ChromX reinforcement is more cost-effective than conventional reinforcement but not more cost-effective than ECR, which costs $382/yd^2, with repairs at 56.3 and 81.3 years. Exposing ECR to UV increases the present value cost per square yard from $382/yd^2 to $736/yd^2. The galvanized reinforcement had the lowest present value cost; bridge decks with ASTM A767 and A1094 bars have a present value costs of $366/yd^2 and $359/yd^2, respectively, requiring repair at 63.1 and 88.1 years. Paired use of Xypex with Conv-B reinforcement costs $551/yd^2 in bridge decks, while Conv-B alone costs $692/yd^2. Xypex paired with Conv-A and Conv-C costs $506/yd^2 and $399/yd^2, respectively; Conv-A and Conv-C alone cost $606 yd^2 and $566/yd^2, respectively.

Pairing Xypex with conventional reinforcement (Conv-A, Conv-B, and Conv-C) compared to the use of the matching conventional reinforcement without an admixture, reduces the present value cost over a 100-year design life by 16 to 29% in an 8.5-in. bridge deck and 17 to 20% in an 8-in. bridge deck. Xypex waterproofing admixture is less effective in decreasing the present value cost when the bridge deck is partially repaired with an overlay (without Xypex in the overlay) than it is when the bridge deck with Xypex is fully replaced with an identical one. That is, the percentage of savings due to the use of Xypex are less when Xypex is only used in the initial construction of bridge decks and repairs are done with overlays than when full deck replacement (with concrete

containing Xypex) is performed. The effects of the addition of Xypex in overlays can be evaluated in future studies.

For all systems, the 2.5-in. (8-in. deck) cover resulted in earlier times to first repair with an overlay and higher costs over a 100-year design life than decks with 3-in. cover (8.5-in. deck). Overlay repairs with 2.5-in. concrete cover led to one extra repair compared to 3-in. for Conv-A, ECR, ChromX, and Xypex-Conv-C. The use of 3-in. compared to 2.5-in. cover resulted in a 7% decrease in the present value cost of conventional reinforcement, averaging the decrease in values for Conv-A, Conv-B, and Conv-C, and 23 and 3% decrease in the present value cost for ECR and ECR-UV, respectively. The present value cost of a bridge deck with galvanized reinforcement is 10% lower for a bridge deck with 3-in cover than with 2.5-in. cover. The present value cost of a bridge deck with ChromX reinforcement is 18% lower for a bridge deck with 3-in. cover than a deck with 2.5-in. cover. When Conv-B reinforcement is paired with Xypex, a bridge deck with 3-in. cover costs 6% less than that with 2.5-in. cover; the present value cost of a bridge deck with Conv-B reinforcement decreases 3% when 3-in. cover is used instead of 2.5-in. cover.

No clear trends are apparent when comparing the costs of full deck replacement vs. partial deck repair. For conventional reinforcement, full deck replacement is costlier than partial repair. For epoxy-coated and galvanized reinforcement, however, partial repair is costlier. ChromX exhibited similar design life costs in both methods. It is noteworthy that the costs for the two repair approaches are from different states, as mentioned in Section 4.3.

4.4 Probabilistic Analysis of Service Life Using Monte Carlo Simulation

The wide variation in performance between the three heats of conventional reinforcement evaluated in this study demonstrates significant unpredictability in the service life of any given corrosion protection system. To capture this variability, a Monte Carlo simulation is performed on

the collected data from prior research for conventional, epoxy-coated, and ChromX reinforcement in an 8.5-in. deck with 3-in. cover per the procedure outlined in Section 4.2 (Ji et al. 2005, Darwin et al. 2007, Draper 2009, Darwin et al. 2011, O'Reilly et al. 2011, Darwin et al. 2013, Farshadfar et al. 2017, O'Reilly et al. 2021). Accordingly, the critical chloride corrosion threshold and corrosion rate are treated as distributions and the critical corrosion loss as a deterministic value. Prior research used to support the Monte Carlo is limited to that performed at the University of Kansas to remain consistent in terms of specimen type and testing methods. The prior research provides data on 70 conventional, 17 ECR, and 37 ChromX uncracked specimens, used to establish critical chloride corrosion threshold, and 14 conventional, 14 ECR, and 6 ChromX cracked beam specimens, used to establish corrosion rate after initiation. The mean and standard deviation of the individual specimen data for critical chloride corrosion threshold and equivalent field corrosion rate used for the Monte Carlo simulation are summarized in Table 4.19, with details given in Appendix G; Tables G1 through G7 give the individual LPR corrosion loss and derived average corrosion rate for conventional, epoxy-coated, and ChromX reinforcement in the cracked beam test for each study, and Table G8 the critical chloride corrosion threshold in uncracked concrete separated by study. Conv-A, Conv-B, Conv-C, ECR, and ChromX from this study exhibited critical chloride corrosion thresholds of 1.45, 0.65, 1.45, 2.58, and 3.37 (lb/yd^3), as shown in Table 4.1, and equivalent field corrosion rates of 6.65, 8.29, 4.00, 63.3, and 3.08 (μm/yr), as shown in Table 4.7, respectively. Conv-A, Conv-B, Conv-C, ECR, and ChromX from this study exhibited lower equivalent field corrosion rates and critical corrosion thresholds than the mean value from prior studies. The purpose of this section is to establish how the service life of a corrosion protection system should be addressed in terms of a range as opposed to a fixed number by comparing the results from this study (referred to as the deterministic analysis in this section) to

prior research. To determine the sensitivity of the Monte Carlo simulation to the initial dataset used, the analysis is performed twice-once with only data from prior studies and a second time including the data from this study with those from prior studies. The results from the second analysis are presented at the end of this section.

Table 4.19: The mean and standard deviation for critical chloride corrosion threshold (lb/yd^3) and equivalent field corrosion rate (μm/yr) used for Monte Carlo Simulation

		Critical Chloride Corrosion Threshold	**Equivalent Field Corrosion Rate**
Conventional	Mean	1.8	9.3
	Standard Deviation	0.9	8.1
ECR	Mean	7.8	201.6
	Standard Deviation	4.3	197.9
ChromX	Mean	5.3	3.7
	Standard Deviation	2.3	1.5

The Monte Carlo method is used to numerically estimate the outcome of uncertain events, especially those with factors that can be described using a normal distribution, using the mean and standard deviation. A randomly generated number between 0 and 1 was assumed to be a probability for each dataset, normally distributed with the means and standard deviations listed in Table 4.19. For example, in a normal distribution the probability that a given data point is less than the mean is 50%, and the probability that a given data point is less than one standard deviation below the mean is 16%. Thus, in a given trial of the Monte Carlo simulation, a randomly generated value of 0.5 corresponds to a chloride threshold (or corrosion rate) exactly equal to the mean value in Table 4.19, whereas a randomly generated value of 0.16 corresponds to a chloride threshold or rate exactly one standard deviation below the mean value. A Monte Carlo simulation uses a large number of trials to simulate the variability inherit in real-world systems. Using a Monte Carlo simulation with 10,000 trials, the time to corrosion initiation, time from initiation to cracking, and time to first repair were calculated for each type of reinforcement; with 10,000 trials, the

simulations converged (that is, the average of all trials did not change with continued iteration). The results of the Monte Carlo simulation, which involve both critical chloride and equivalent field corrosion rates, will not necessarily have a normal distribution.

Figures 4.3, 4.4, and 4.5 show the cumulative distributions of the critical chloride corrosion thresholds from prior research overlaid by a normal cumulative distribution function based on the corresponding averages and standard deviations for, respectively, conventional, epoxy-coated, and ChromX reinforcement. The vertical axes represent the cumulative probability that a value on the horizontal axis will be exceeded. Figures 4.6, 4.7, and 4.8 show the cumulative distributions of the equivalent field corrosion rates, as described in Section 4.2.2.2, from prior research overlaid by a normal cumulative distribution function based on the corresponding averages and standard deviations for, respectively, conventional, epoxy-coated, and ChromX reinforcement. Figures 4.3 through 4.8 show that the distributions of corrosion thresholds and rates are close to that obtained for a normal distribution; therefore, they are assumed to have a normal distribution in the Monte Carlo simulation performed. The data cumulative distribution was populated using discrete data points (so it is not smooth). The cumulative distribution for the lowest number in each dataset was calculated by dividing one by the number of data points; the more data points there are, the closer to zero the cumulative probability for the lowest number gets. For each data point going forward, one divided by the number of data points was added to the cumulative probability from the previous point. The normal cumulative probability was calculated using the mean and standard deviation of the corresponding dataset. The absolute values for the difference between the cumulative and normal cumulative probabilities at each data point were averaged to evaluate how closely the distributions match. For the critical chloride corrosion threshold and equivalent

corrosion rate, the averages of the differences between the corresponding cumulative probabilities for each data point did not exceed 0.09 and 0.12, respectively, for any reinforcement type.

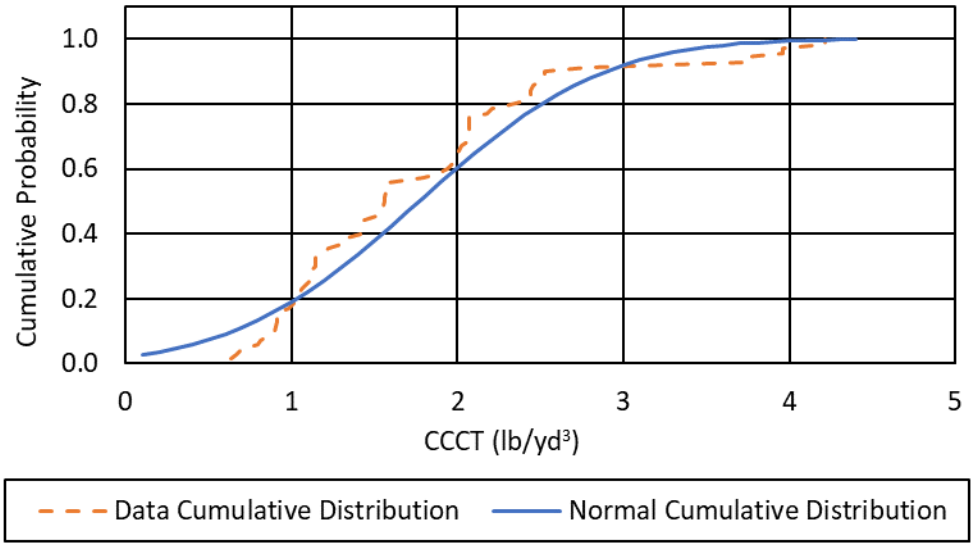

Figure 4.3: Cumulative distribution of critical chloride corrosion thresholds overlaid by normal cumulative distribution function for conventional reinforcement

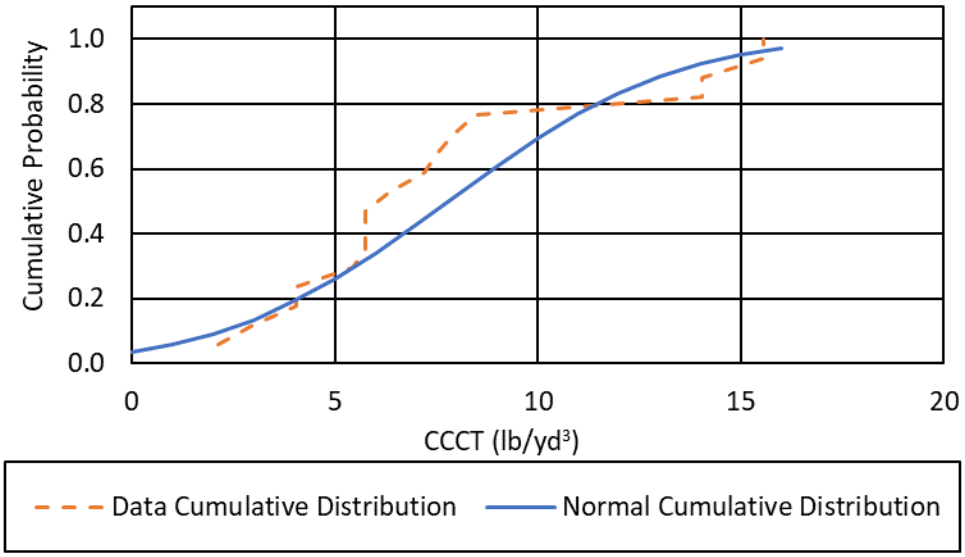

Figure 4.4: Cumulative distribution of critical chloride corrosion thresholds overplayed by normal cumulative distribution function for ECR

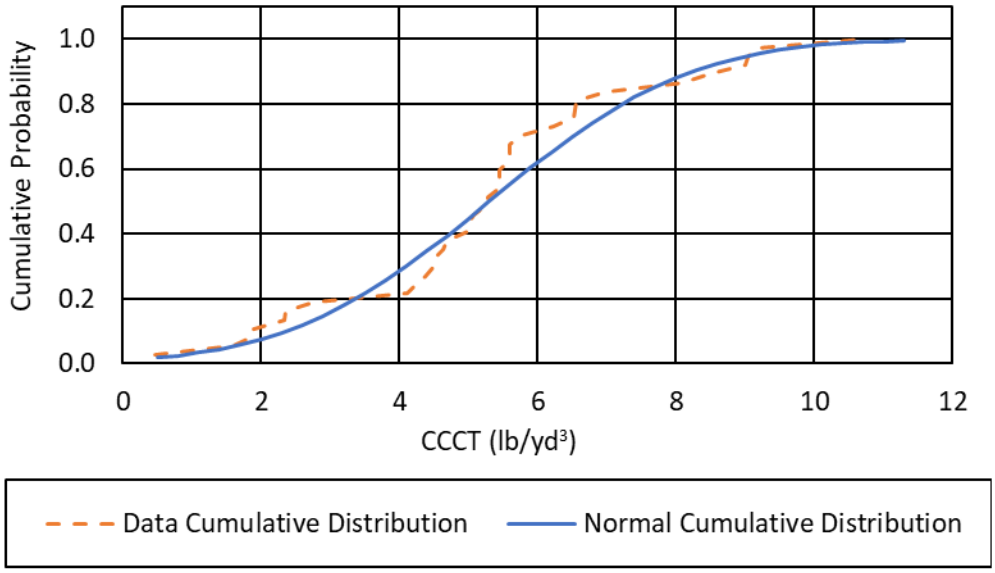

Figure 4.5: Cumulative distribution of critical chloride corrosion thresholds overlaid by normal cumulative distribution function for ChromX reinforcement

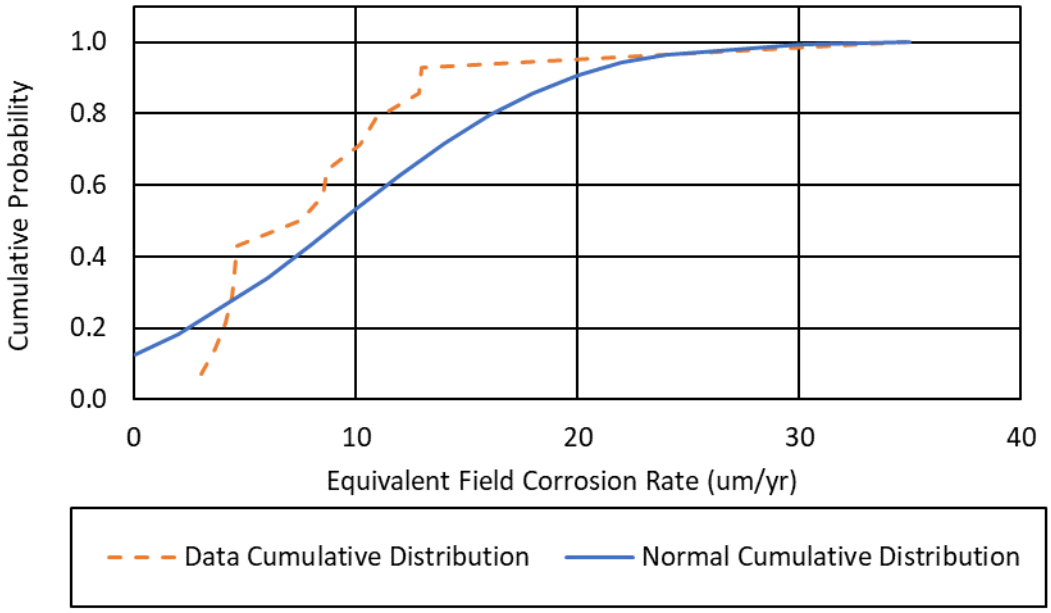

Figure 4.6: Cumulative distribution of equivalent field corrosion rates overplayed by normal cumulative distribution function for conventional reinforcement

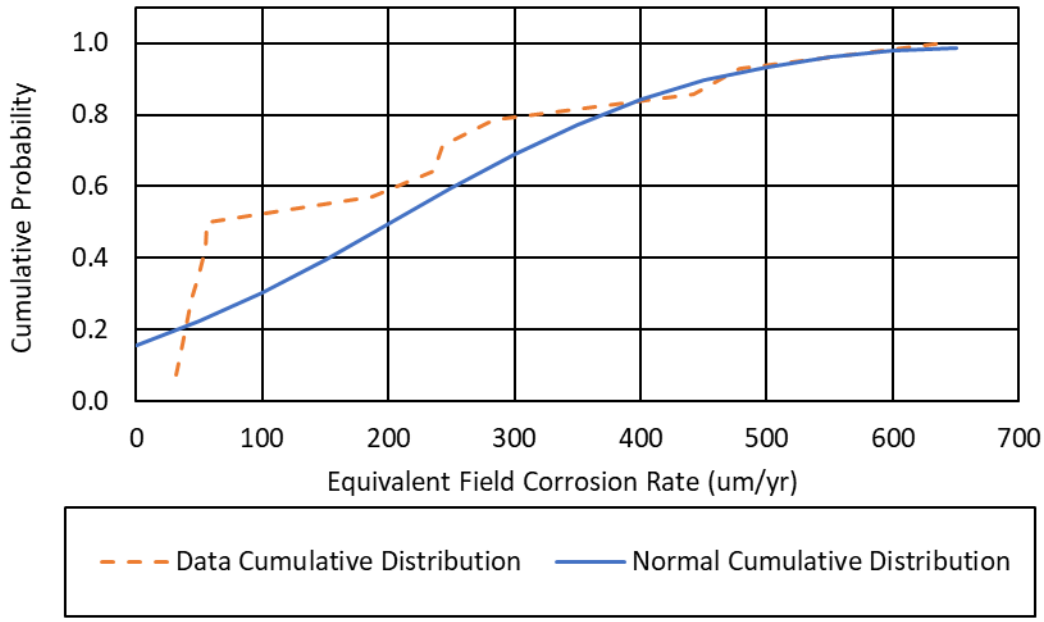

Figure 4.7: Cumulative distribution of equivalent field corrosion rates overlaid by normal cumulative distribution function for ECR

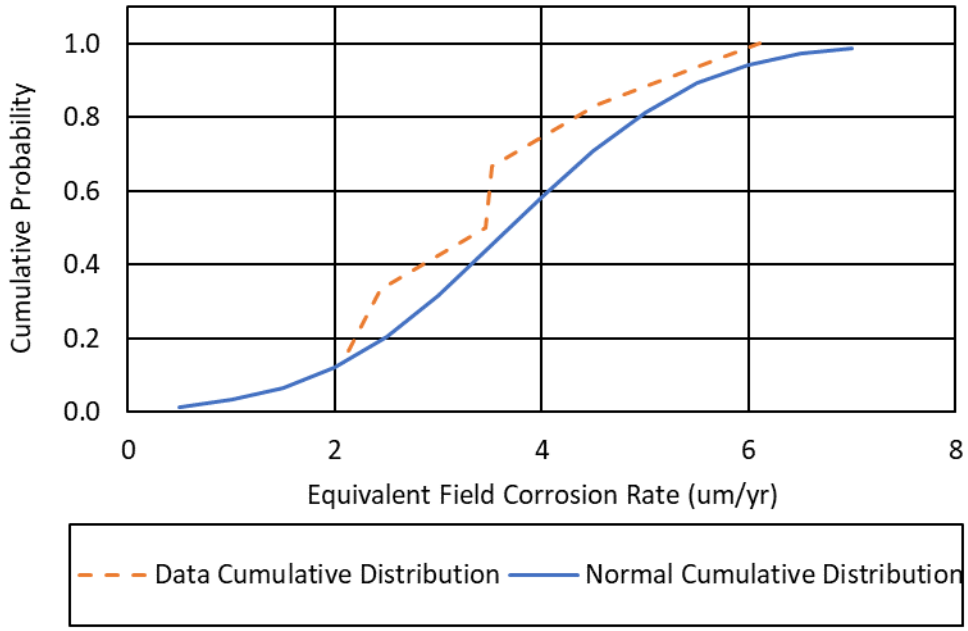

Figure 4.8: Cumulative distribution of equivalent field corrosion rates overlaid by normal cumulative distribution function for ChromX reinforcement

The combined corrosion rates from prior research have very high standard deviations, and a normal distribution generated based on their mean and standard deviation would result in some

negative values. Negative rates (resulting in negative time values) were interpreted as meaning the bridge deck is not corroding; therefore, it was assumed that any bridge deck with a negative corrosion rate in the Monte Carlo simulation lasts the entire service life, 100 years in this study. Also, any time to first repair exceeding the service life in each trial of the Monte Carlo simulation was treated as 100 years.

As described in Section 4.2, the time to corrosion initiation is assumed to be not less than 12 months as bridge decks are not immediately exposed to deciding salts after construction. A normal distribution is used for the critical chloride corrosion thresholds, and the calculations do not yield negative time values accordingly.

The time to corrosion initiation, the time from initiation to cracking, and the time to first repair based on the average test results from this study are summarized in Table 4.20. These results are compared to those of Monte Carlo simulation as follows.

Table 4.20: Time (years) to first repair for corrosion protection systems (3-in. cover) based on average test results from this study

Corrosion Protection System	Initiation Time	Initiation to Cracking Time	Time to First Repair
Conv-A	1.9	14.4	26.3
Conv-B	1.0	11.6	22.6
Conv-C	1.9	19.2	31.1
ECR	4.9	41.5	56.3
ChromX	6.9	31.2	48.2

Figures 4.9, 4.10, and 4.11 show the cumulative distributions for the time to corrosion initiation as a function of time based on Monte Carlo simulations for conventional, epoxy-coated, and ChromX reinforcement, respectively. The horizontal axis represents the time to corrosion initiation, and the vertical axis the cumulative probability (0 to 1). As mentioned, the minimum time to corrosion initiation was assumed to be not less than one year, which can be seen in the

figures; the maximum times to corrosion initiation for conventional, epoxy-coated, and ChromX reinforcement were 12, 64, and 37 years, respectively. The probability of corrosion initiation in one year or less was 0.23, 0.06, and 0.04 for conventional, epoxy-coated, and ChromX reinforcement, respectively. For conventional reinforcement, the average of all trials for time to corrosion initiation converged to three years with a median of three years; 70% of bridge decks initiated corrosion before reaching an age of four years. The deterministic analysis done earlier in this chapter indicated an initiation time between one and two years. The average time to corrosion initiation for ECR converged to 19 years with a median of 19 years, with 70% of bridge decks initiating before 25 years. The deterministic analysis indicated an initiation time of 5 years. For ChromX reinforcement, the average of all trials converged to 12 years (median of 12 years), with 70% of bridge decks initiating before 15 years. The deterministic analysis indicated an initiation time of 7 years for ChromX reinforcement.

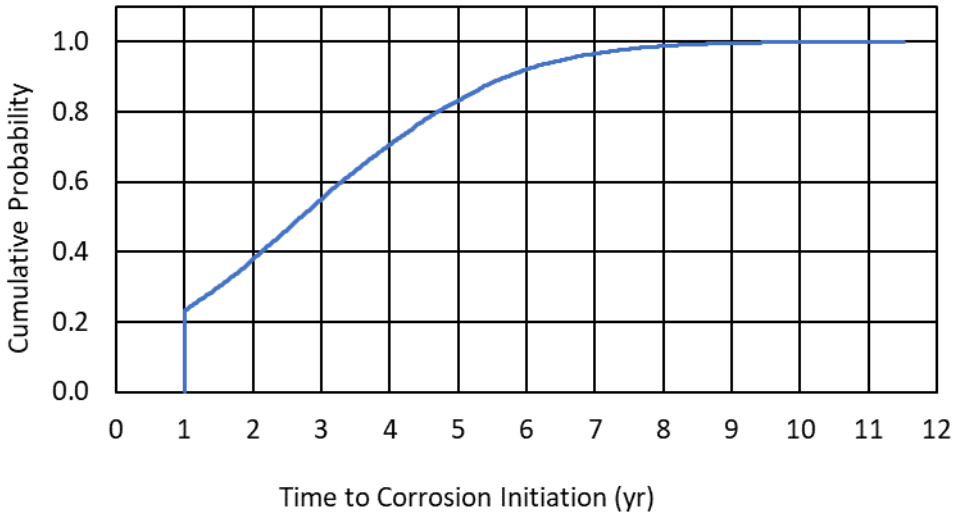

Figure 4.9: Cumulative distribution for the time to corrosion initiation using Monte Carlo simulation for conventional reinforcement

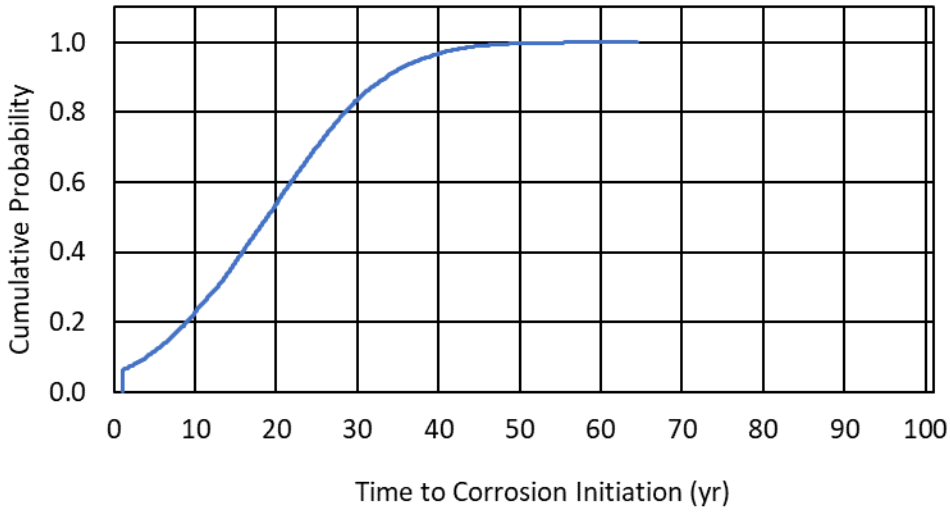

Figure 4.10: Cumulative distribution for the time to corrosion initiation using Monte Carlo simulation for ECR

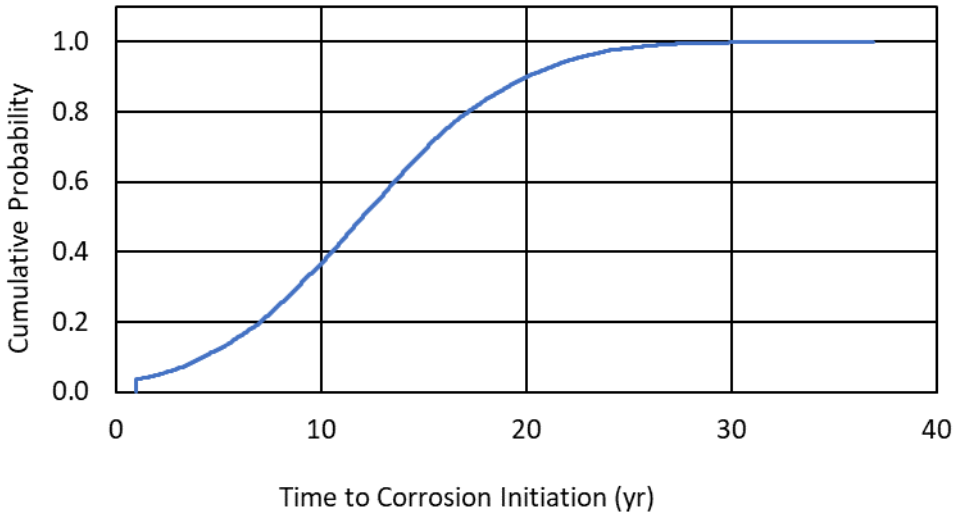

Figure 4.11: Cumulative distribution for the time to corrosion initiation using Monte Carlo simulation for ChromX reinforcement

Figures 4.12, 4.13, and 4.13 show cumulative distributions for the time to cracking after corrosion initiation as a function of time based on the Monte Carlo simulation for conventional, epoxy-coated, and ChromX reinforcement, respectively. The horizontal axis represents the time to cracking once corrosion has initiated, and the vertical axis represents the cumulative probability (0 to 1) for the number of results in the Monte Carlo simulation. The minimum times from corrosion initiation to cracking for conventional, epoxy-coated, and ChromX reinforcement were

2, 3, and 9 years, respectively, and the probability of bridge decks not initiating corrosion within the 100-year service life were 0.15, 0.19, and 0.03. For conventional reinforcement, the average of all trials converged to 26 years with a median of 10 years; 70% of bridge decks cracked before reaching 19 years after corrosion initiation. The deterministic analysis done in this chapter indicated a time from initiation to cracking of 14 to 19 years. For ECR, the average of all trials converged to 32 years with a median of 13 years, with 70% of bridge decks taking less than 28 years to crack after corrosion initiation. The deterministic analysis indicated a time from initiation to cracking of 42 years for ECR; this is because the ECR from this study had a corrosion rate equal to 31% of the mean value from prior studies. For ChromX reinforcement, the average of all trials converged to 32 years with a median of 26 years with 70% of bridge decks cracking before reaching 32 years after initiation. The deterministic analysis indicated a time from initiation to cracking of 31 years.

As seen above, the mean and median differ greatly, particularly for ECR. This is due to the greater scatter in the ECR results compared to conventional and ChromX reinforcement.

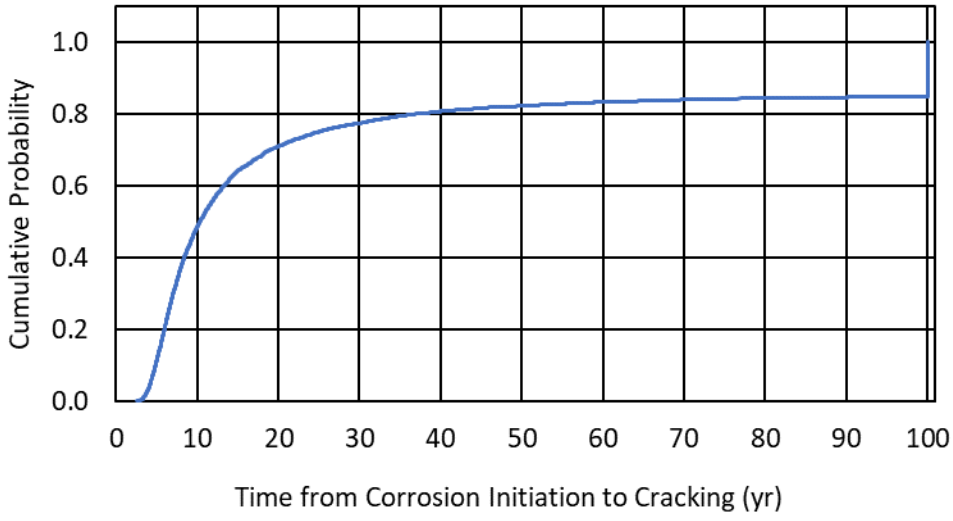

Figure 4.12: Cumulative distribution for the time to cracking once corrosion has initiated using Monte Carlo simulation for conventional reinforcement

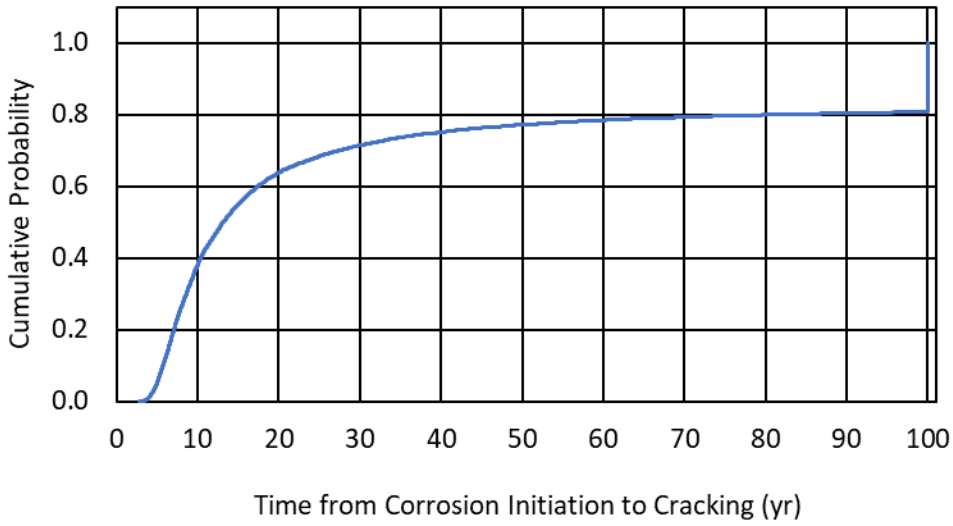

Figure 4.13: Cumulative distribution for the time to cracking once corrosion has initiated using Monte Carlo simulation for ECR

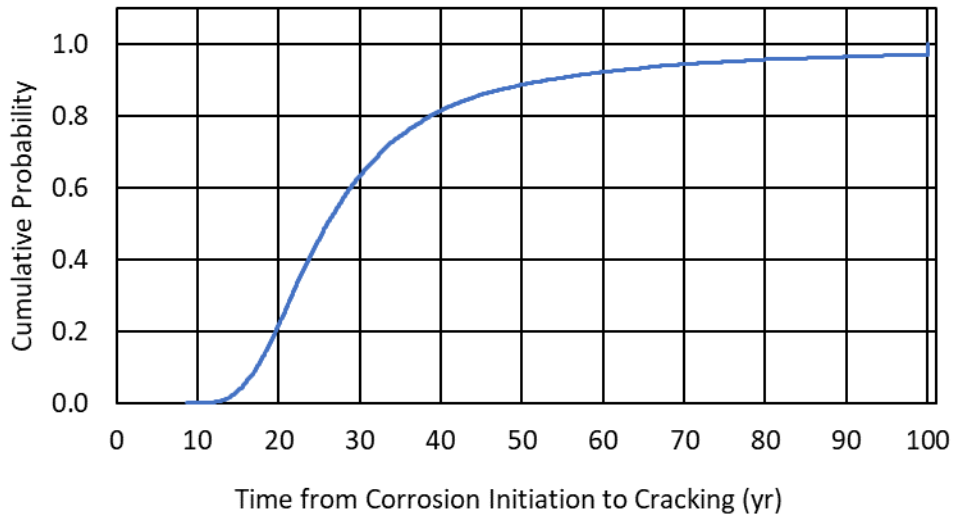

Figure 4.14: Cumulative distribution for the time to cracking once corrosion has initiated using Monte Carlo simulation for ChromX

The time to corrosion initiation and the time from initiation to cracking of concrete cover is used to calculate the time to first repair. The time from first cracking to repair of a bridge deck is assumed to be ten years, as mentioned in Section 4.2.3.

Figures 4.15, 4.16, and 4.17 show cumulative distribution for the time to first repair based on the Monte Carlo simulation described above for conventional, epoxy-coated, and ChromX

reinforcement, respectively. The horizontal axis represents the time to first repair, and the vertical axis the cumulative probability (0 to 1) for the number of results in the Monte Carlo simulation. For conventional, epoxy-coated, and ChromX reinforcement, the minimum times to first repair are 14, 14, and 21 years and the probabilities of not requiring repair within 100 years are 0.16, 0.20, and 0.04. For conventional reinforcement, the average of all trials converged to 37 years with a median of 24 years; 70% of bridge decks needed repair in less than 33 years after construction. The deterministic analysis done in this chapter indicated a time to first repair of 23 to 31 years. For ECR, the average of all trials converged to 55 years with a median of 46 years; 70% of bridge decks needed repair 62 years or less after construction. The deterministic analysis indicated a time to first repair of 56 years for ECR. For ChromX reinforcement, the average of all trials converged to 53 years with a median of 49 years; 70% of bridge decks requiring repair before reaching 56 years old. The deterministic analysis indicates a time to first repair of 48 years.

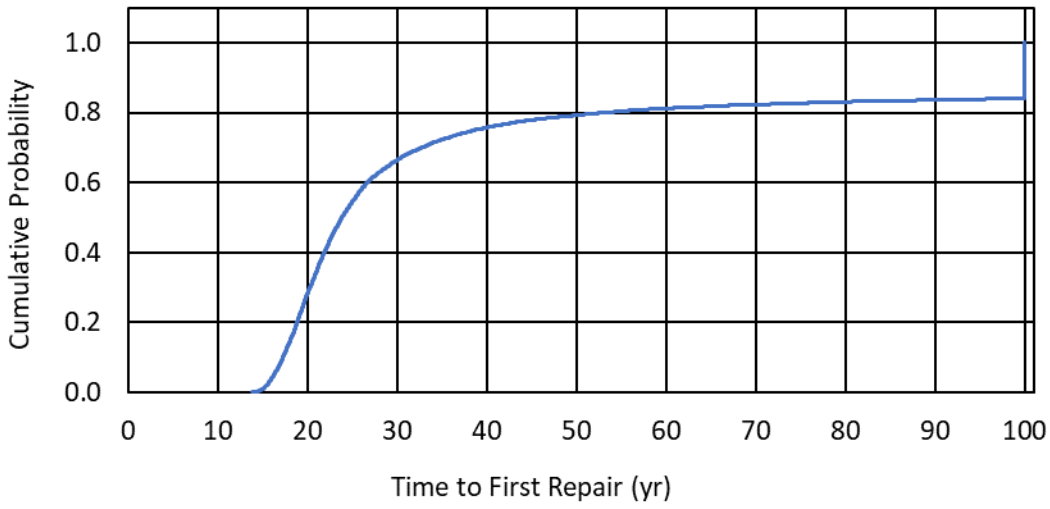

Figure 4.15: Cumulative distribution for the time to first repair using Monte Carlo simulation for conventional reinforcement

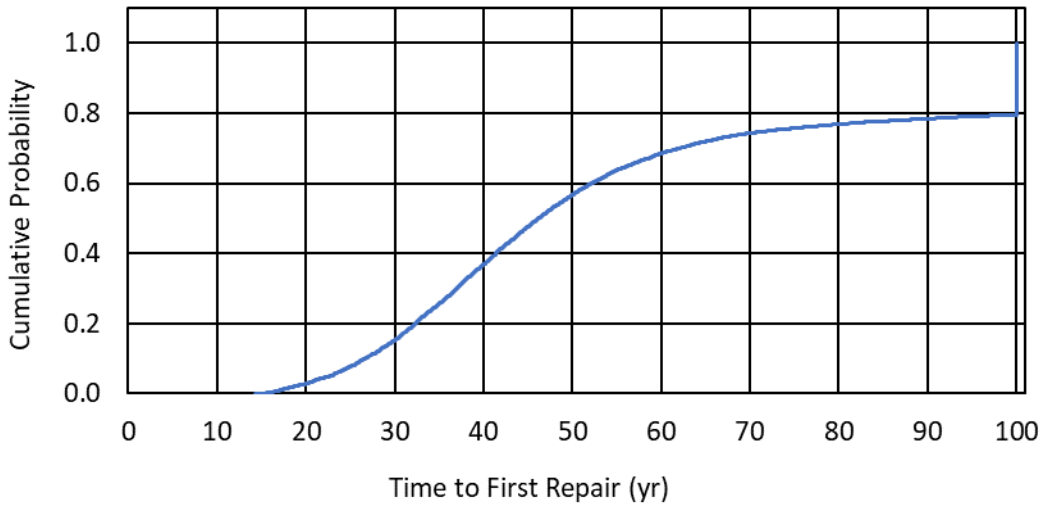

Figure 4.16: Cumulative distribution for the time to first repair using Monte Carlo simulation for ECR

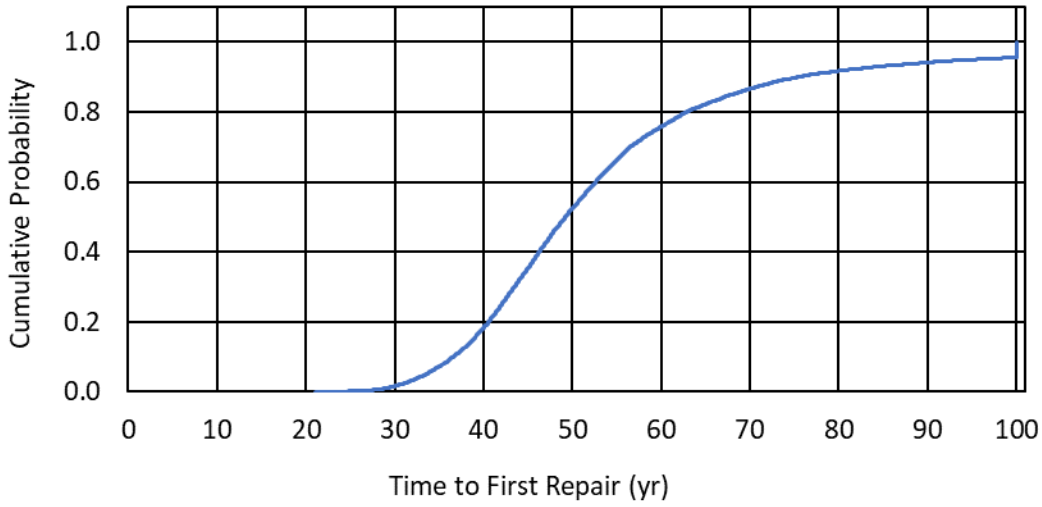

Figure 4.17: Cumulative distribution for the time to first repair using Monte Carlo simulation for ChromX reinforcement

Figure 4.18 compares the three cumulative distributions for the time to first repair based on the Monte Carlo simulation using the data from prior research.

Overall, the median values from the Monte Carlo simulation are in agreement with the results of the deterministic analyses described earlier in this chapter. In both analyses, conventional reinforcement exhibits the shortest median time to repair, and ECR exhibits the longest median

time to first repair. Inherently, there is more variability in the corrosion performance of ECR than for ChromX and conventional reinforcement. This variability is due to the fact that the chlorides penetrating concrete need to reach a damage site on the epoxy-coated bar to cause corrosion, as opposed to any point on uncoated bar. Furthermore, variability can result from differences in the coating quality from manufacturers (when comparing results of this research to older research) as well as transportation, storage, and construction practices. Overall, the time to first repair (service life) for corrosion protection systems is best treated as a range, rather than a fixed number, since the critical chloride corrosion threshold and time to corrosion initiation values used to calculate it can vary greatly.

It should be noted that the Monte Carlo model predicts that 17% of bridge decks with conventional reinforcement will last 100 years. This is likely erroneous, and is due to the wide amount of scatter between the numerous heats of conventional reinforcement used in this study. As seen in Table 4.19, the mean and standard deviation for conventional reinforcement are similar, meaning that Monte Carlo analysis will generate negative corrosion rates for a portion of the trials with conventional reinforcement. Negative corrosion rates automatically result in a 100-year design life in the model. Decades of practice have shown, however, that conventional reinforcement does not provide a long service life when exposed to chlorides. Future work should seek to refine the model and eliminate this discrepancy. A similar percentage of decks with ECR reinforcement lasted 100 years; as previously stated, the coating on ECR increases variability, making this result more plausible. The standard deviation for corrosion rates of ChromX reinforcement is lower than those of conventional and epoxy-coated reinforcement relative to their averages, and as a result yielded a lower percentage of negative values (ChromX corrosion rates

came from fewer studies than conventional and epoxy-coated reinforcement). ChromX reinforcement was therefore not affected by this discrepancy.

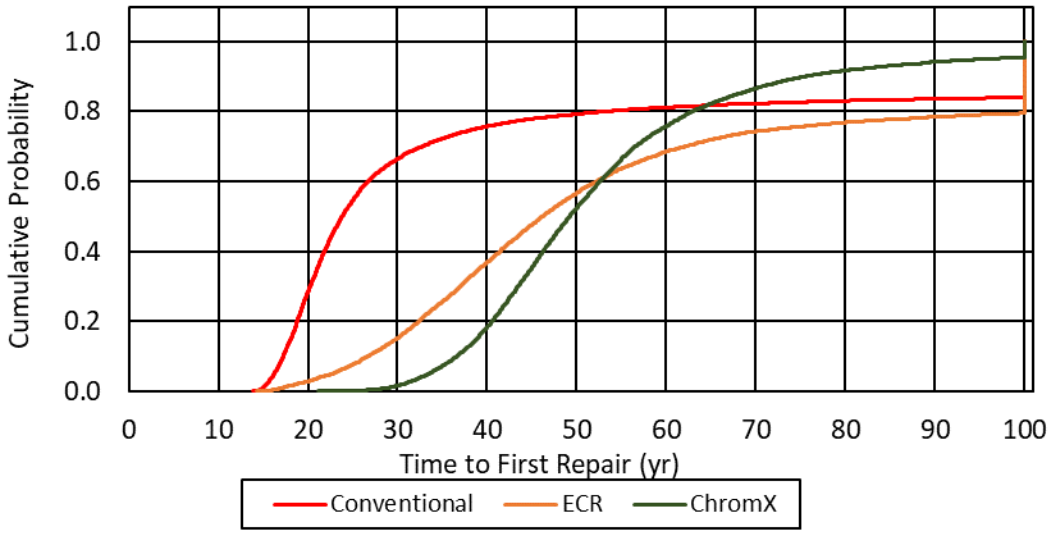

Figure 4.18: Cumulative distribution for the time to first repair using Monte Carlo simulation based on the data from prior research

To determine the sensitivity of the Monte Carlo simulation to the initial dataset, the analysis was performed a second time, including the data from the current study. Figure 4.19 shows the cumulative distributions for the time to first repair based on the Monte Carlo simulation including both the data from prior research and this study for conventional, epoxy-coated, and ChromX reinforcement. The cumulative probability curves for conventional, epoxy-coated, and ChromX reinforcement are similar to those in Figure 4.18, with the difference that the probability of the bridge deck lasting the entire service life without repair is 0.14, 0.22, and 0.07 for conventional. epoxy-coated, and ChromX reinforcement, respectively (compared to 0.16, 0.20, and 0.04 based solely on the prior research). It should be noted that the dataset for ChromX reinforcement in the first analysis was much smaller than those for conventional reinforcement or ECR, with the majority of corrosion rate data coming from a single study (Farshadfar et al. 2017).

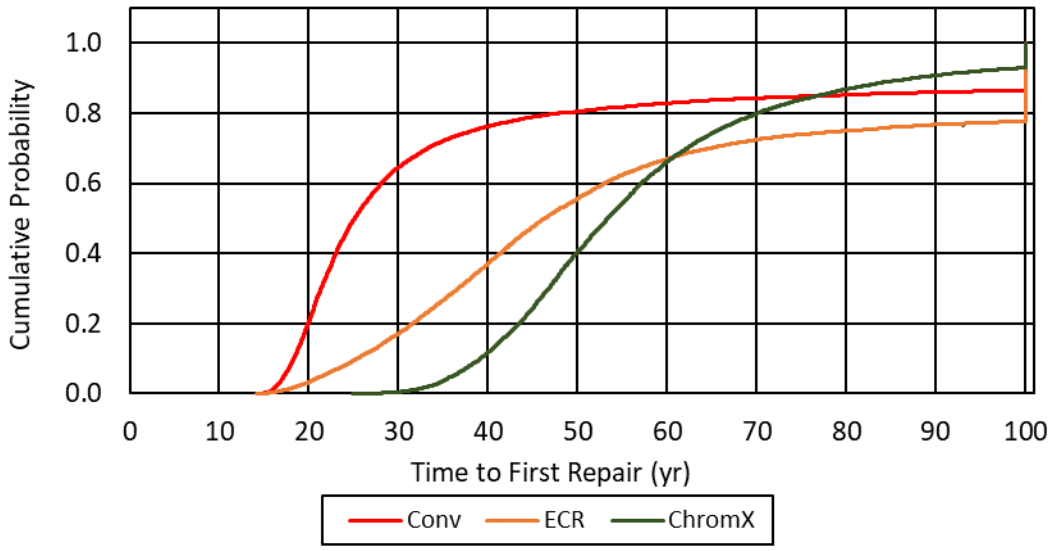

Figure 4.19: Cumulative distribution for the time to first repair using Monte Carlo simulation based on data from this study and prior studies

The discrepancy previously noted, with a large percentage of trials with conventional reinforcement lasting 100 years, was not altered by including the results from the current study. This outcome is not expected based on the laboratory results of this study and field experience (O'Reilly et al. 2011), and is an area in need of refinement for future models.

Despite the noted discrepancy at 100 years, the Monte Carlo simulation conducted in this study provides many benefits over the deterministic analysis used in previous analyses. Although both methods give similar mean times to first repair, the deterministic analysis fails to account for the variability in each system. This is particularly evident with ECR, where a large percentage of trials exhibited a service life of at least 100 years in the Monte Carlo simulation. The Monte Carlo simulation also further highlights the superiority of corrosion resistant materials to conventional reinforcement; as seen in Figures 4.18 and 4.19, the majority of bridge decks constructed with conventional reinforcement will require repair in 25 years or less, whereas less than 10% of bridge decks constructed with ECR or ChromX will require repair in this time. The probabilities from the

Monte Carlo simulation capture the effect of highly variable factors in play for service life of bridge decks more effectively than fixed numbers, proposed by prior studies.

CHAPTER 5: SUMMARY AND CONCLUSIONS

5.1 SUMMARY

This study evaluated the corrosion resistance of epoxy-coated (ASTM A775), hot-dip galvanized (ASTM A767), and continuously galvanized (ASTM A1094) reinforcement, and the conventional reinforcement (ASTM A615) used to produce them, as well as ChromX reinforcement (ASTM A1035 Type CS) using the rapid macrocell, Southern Exposure, and cracked beam tests. Coated bars were evaluated with coatings in both an undamaged condition and with damage simulating the effect of handling and placing. Some epoxy-coated bars were exposed to accelerated ultraviolet (UV) cycles, simulating outdoor exposure. Galvanized and epoxy-coated reinforcing bars were also evaluated after bending to simulate the effects of field fabrication. Conventional and ChromX reinforcement were also evaluated in conjunction with two waterproofing concrete admixtures, IPANEX and Xypex. Results from previous studies were used to convert the laboratory corrosion rates from this study into equivalent field rates to perform cost analysis. Construction costs and repair methods in the states of Oklahoma and Kansas were used to determine the cost of each system over a 100-year design life. Finally, the effect of variability of corrosion, specifically corrosion rates and critical chloride corrosion thresholds, on predicting the service life was investigated using results from previous studies on conventional, epoxy-coated reinforcement (ECR), and ChromX reinforcement performing Monte Carlo lation.

5.2 CONCLUSIONS

The following conclusions are based on this research:

1. ASTM A775 epoxy-coated reinforcement (ECR) without ultraviolet (UV) exposure exhibited a significantly greater corrosion resistance (lower corrosion loss) than conventional reinforcement across all laboratory tests. Damaged epoxy-coated

reinforcement exhibited average total corrosion losses of 4%, 1%, and 1% of the values for the matching conventional reinforcement in the rapid macrocell, Southern Exposure, and cracked beam tests based on total area of the bar.

2. Undamaged ECR exhibited no significant corrosion activity under any test conditions with corrosion losses close to zero.
3. After as few as 100 hours of UV exposure under ASTM G154 Cycle 1 conditions (equivalent to approximately 1.2 months of outdoor exposure) increased the total corrosion loss of ECR by 26% in the rapid macrocell test; the damaged epoxy-coated reinforcement exposed to any amount of UV exhibited average total losses ranging from 1.3 to 10.6 times the values for the matching (damaged) ECR not exposed to UV.
4. ASTM A767 and A1094 galvanized reinforcement exhibited similar corrosion resistance. The total corrosion losses were less than that of conventional reinforcement both with and without damage to the galvanized coating; the corrosion losses, however, increased when the bars were bent. In the Southern Exposure test, damaged A767 and A1094 specimens exhibited average total corrosion losses equal to 57% and 49% of the values for the matching conventional reinforcement, respectively, while undamaged A767 and A1094 specimens exhibited losses of 39% and 46% of the values for the matching conventional reinforcement. A767 and A1094 bent galvanized specimens exhibited losses in the same range as the matching conventional reinforcement. In the cracked beam test, average total corrosion losses for damaged and undamaged galvanized reinforcement were between 48% and 73% of the values for the matching conventional reinforcement.
5. ASTM 1035 ChromX reinforcement exhibited total corrosion losses between 21% and 33% of values for conventional reinforcement in the Southern Exposure test,

and 40% to 62%, in the cracked beam test, but between 39 and 50 times higher than damaged ECR (without UV exposure).

6. The addition of Xypex or IPANEX did not result in statistically significant improvements in the corrosion resistance of ChromX reinforcement in concrete.
7. IPANEX was not effective in improving the corrosion resistance of conventional reinforcement, exhibiting corrosion losses 92% and 109% the values for the matching conventional reinforcement in the Southern Exposure and cracked beam tests, respectively.
8. The use of Xypex admixture resulted in statistically significant reductions in total corrosion losses (as measured by LPR) of conventional reinforcement in some tests but not in others. Conventional reinforcement with Xypex showed a statistically significant reduction in total corrosion losses in cracked concrete (45%). However, the total corrosion losses in uncracked concrete increased by 13%, although the increase is not statistically significant. Unlike in the total corrosion losses, conventional reinforcement with Xypex showed reductions in macrocell corrosion losses in both cracked and uncracked concrete, 36% and 67%, respectively. Further study is recommended on the effects of Xypex on the corrosion resistance of reinforced concrete.
9. The cost analysis over a 100-year design life found that ECR, galvanized, and ChromX reinforcement were all cost-effective corrosion protection systems, with about half the average cost of conventional reinforcement in an 8.5- in. bridge deck with full deck replacement repairs.
10. 8.5-in bridge decks with 3-in cover have a lower cost over a 100-year design life

than 8-in. decks with 2.5-in. cover. Increasing the concrete cover from 2.5 in. (as is currently used in the state of Oklahoma) to 3.0 in. should be considered to reduce the present cost, the total life cost of bridge decks defined in Chapter 4, of bridge decks (see Tables 4.15 through 4.18).

11. Monte Carlo simulation provides mean times to first repair similar to those obtained from the deterministic analysis; however, the variability in time to first repair, particularly for ECR, can be represented by the Monte Carlo analysis but no the deterministic analysis based on average values.

5.3 RECOMMENDATIONS

1. Conventional reinforcement is not a cost-effective corrosion protection system and should not be used for bridge decks exposed to chlorides.
2. Improper storage of epoxy-coated reinforcement increases its cost for bridge decks over a 100-year design life. ECR should be protected from UV exposure. The existing guidelines in ASTM D3963, which limit unprotected exposure to two months, do not ensure adequate protection to epoxy coatings, and limiting exposure to one month or less should be required.
3. ASTM A767 and A1094 reinforcement exhibited similar corrosion resistance and can be used interchangeably.
4. Additional research is needed on the corrosion loss to crack concrete for ASTM A1094 reinforcement, for which there is no data.
5. Research is needed on the effect of bends on the corrosion performance of ASTM A767 and A1094 reinforcement and the type of repair needed if bends are shown to consistently reduce the corrosion performance of either reinforcement.

6. The simultaneous effect of bending and UV damage on ECR was not evaluated in this study, which should be investigated in future studies.

REFERENCES

AASHTO T 260-97. (2020). "Standard Method of Test for Sampling and Testing for Chloride Ion in Concrete and Concrete Raw Materials, American Association of State and Highway Transportation Officials, Washington, D.C, 15 pp.

ACI Committee 201. (2016). "Guide to Durable Concrete," *Technical Document* ACI 201.2R-16, American Concrete Institute, Farmington Hills, MI, 84 pp.

ACI Committee 318. (2019). "ACI CODE-318-19: Building Code Requirements for Structural Concrete and Commentary, American Concrete Institute, Farmington Hills, MI, 624 pp.

Ahmad, Z. (2006). "Chapter 4 - Types of Corrosion: Materials and Environments," In Z. Ahmad (Ed.), *Principles of Corrosion Engineering and Corrosion Control,* Butterworth-Heinemann, Oxford, UK, pp. 120-270.

Alonso, C., Andrade, C., Castellote, M., and Castro, P. (2000). "Chloride Threshold Values to Depassivate Reinforcing Bars Embedded in a Standardized OPC Mortar," *Cement and Concrete Research,* Vol. 30, No. 7, pp. 1047-1055.

Alonso, C., Andrade, C., Rodriguez, J., and Diez, J. M. (1998). "Factors Controlling Cracking of Concrete Affected by Reinforcement Corrosion," *Materials and Structures,* Vol. 31, No. 7, pp. 435-441.

Al-Turaif, H. A. (2013). "Surface Morphology and Chemistry of Epoxy-Based Coatings After Exposure to Ultraviolet Radiation," *Progress in Organic Coatings*, Vol. 76, No. 4, pp. 677-681.

Andrade, M., and Macias, A. (1988). "Galvanized Reinforcements in Concrete," In *Surface Coatings—2*, *Springer*, pp. 137-182.

Angst, U., Elsener, B., Larsen, C. K., and Vennesland, Ø. (2009). "Critical Chloride Content in Reinforced Concrete—A Review," *Cement and Concrete Research,* Vol. 39, No. 12, pp. 1122-1138.

Ann, K. Y., and Song, H.-W. (2007). "Chloride Threshold Level for Corrosion of Steel in Concrete," *Corrosion Science,* Vol. 49, No. 11, pp. 4113-4133.

ASTM A1035/A1035M-20 (2020). "Standard Specification for Deformed and Plain, Low-Carbon, Chromium, Steel Bars for Concrete Reinforcement," ASTM International, West Conshohocken, PA, 7 pp.

ASTM A1094/A1094M-20 (2020). "Standard Specification for Continuous Hot-Dip Galvanized Steel Bars for Concrete Reinforcement," ASTM International, West Conshohocken, PA, 5 pp.

ASTM A615/A615M-20 (2020). "Standard Specification for Deformed and Plain Carbon-Steel Bars for Concrete Reinforcement," ASTM International, West Conshohocken, PA, 8 pp.

ASTM A767/A767M-19 (2019). "Standard Specification for Zinc-Coated (Galvanized) Steel Bars for Concrete Reinforcement," ASTM International, West Conshohocken, PA, 6 pp.

ASTM A775/A775M-19 (2019). "Standard Specification for Epoxy-Coated Steel Reinforcing Bars," ASTM International, West Conshohcken, PA, 11 pp.

ASTM D3963/D3963M-15 (2015). "Standard Specification for Fabrication and Jobsite Handling of Epoxy-Coated Steel Reinforcing Bars," ASTM International, West Conshohocken, PA, 3 pp.

ASTM G109-07 (2013). "Standard Test Method for Determining Effects of Chemical Admixtures on Corrosion of Embedded Steel Reinforcement in Concrete Exposed to Chloride Environments," ASTM International, West Conshohocken, PA, 6 pp.

Behnood, A., Tittelboom, K. V., and De Belie, N. (2016). "Methods for Measuring pH in Concrete: A Review." *Construction and Building Materials,* Vol. 105, pp. 176-188.

Bertolini, L., Elsener, B., Pedeferri, P., Redaelli, E., and Polder, R. (2014). Corrosion of Steel in Concrete: Prevention, Diagnosis, Repair, Second Edition, Wiley Online Library, 434 pp.

Broomfield, J. P. (2003). Corrosion of Steel in Concrete: Understanding, Investigation and Repair, Second Edition, CRC Press, London, UK, 296 pp.

Bymark, R. M., Griggs, A. L., McHattie, J. S., and McKenzie, T. L. (1995). "Rapid Curing Powder Epoxy Coating Compositions Having Increased Flexibility, Incorporating Minor Amounts of Aliphatic Triepoxides", *U.S. Patent* No. 5,407,978.

Cement Chemistry Systems. (2016). Retrieved from https://www.ipanex.com Accessed on 3/29/2020.

Cetiner, M., Singh, P., Abes, J., and Gilroy-Scott, A. (2000). "UV Degradation of Fusion Bonded Epoxy Coating in Stockpiled Pipes," *The International Pipeline Conference*, Calgary, Alberta, Canada, pp. 691-702.

Chappelow, C. C., McElroy, A. D., Blackburn, R. R., Darwin, D., de Noyelles, F. G., and Locke Jr, C. E. (1992). "Handbook of Test Methods for Evaluating Chemical Deicers," *Report* No. SHRP-H-332, Strategic Highway Research Program, Washington DC, 283 pp.

Correll, G. D., and Berstler, R. M. (1997). "Disbondment Resistant Epoxy Powder Coating Composition," *U.S. Patent* No. 5,686,185.

Darwin, D., Browning, J., Balma, J., Ji, J., Gong, L., Nguyen, T., and Locke, C. (1995). "Corrosion-Resistant Reinforcing Steel," *SL Report* No. 95-2*,* University of Kansas Center for Research, Inc., Lawrence, KS, 25 pp.

Darwin, D., Browning, J., Nguyen, T., and Locke, C. (2002). "Mechanical and Corrosion Properties of a High-Strength, High Chromium Reinforcing Steel for Concrete," *SM Report* No. 66*,* University of Kansas Center for Research, Lawrence, KS, 142 pp.

Darwin, D., Browning, J., Nguyen, T., and Locke, C. (2007). "Evaluation of Metallized Stainless Steel Clad Reinforcement," *SM Report* No. 90*,* University of Kansas Center for Research, Inc., Lawrence, Kansas, 156 pp.

Darwin, D., Browning, J., Nguyen, T.V., and Locke, C. (2002). "Mechanical and Corrosion Properties of a High-Strength, High Chromium Reinforcing Steel for Concrete," *SM Report* No. 66, University of Kansas Center for Research, Inc., Lawrence, KS, 142 pp.

Darwin, D., Browning, J., O'Reilly, M., Locke, C. E., and Virmani, Y. P., "Multiple Corrosion Protection Systems for Reinforced Concrete Bridge Components," Publication No. FHWA-HRT-11-060, Federal Highway Administration, November 2011, 255 pp., also SM Report No. 101, University of Kansas Center for Research, Lawrence, KS

Darwin, D., Browning, J., O'Reilly, M., Xing, L., and Ji, J. (2009). "Critical Chloride Corrosion Threshold of Galvanized Reinforcing Bars," *ACI Materials Journal,* Vol. 106, No. 2, pp. 176-183.

Darwin, D., Manning, D. G., Hognestad, E., Beeby, A. W., Rice, P. F., and Ghowrwal, A. Q. (1985). "Debate Crack Width, Cover, and Corrosion," *Concrete International*, Vol. 7, No. 5, pp. 20-32.

Darwin, D., O'Reilly, M., Browning, J., Locke, C., Virmani, Y. P., Ji, J., Gong, L., Guo, G., Draper, G., Xing, L. (2014). "Multiple Corrosion-Protection Systems for Reinforced-Concrete Bridge Components: Laboratory Tests," *Journal of Materials in Civil Engineering,* Vol. 26, No. 11.

Darwin, D., O'Reilly, M., Somogie, I., Sperry, J., Lafikes, J., Storm, S., and Browning, J. (2013). "Stainless Steel Reinforcement as a Replacement for Epoxy Coated Steel in Bridge Decks," *SM Report* No. 105*,* University of Kansas Center for Research, Lawrence, KS, 205 pp.

Darwin, D., O'Reilly, M., Vosough Grayli, P., and Hartell, J. A. (2020). "Evaluating the Performance of Existing Reinforcement for Oklahoma Bridges," *SM Report* No. 146, University of Kansas Center for Research, Inc., Lawrence, KS, 194 pp.

Dasar, A., Hamada, H., Sagawa, Y., and Yamamoto, D. (2017). "Deterioration Progress and Performance Reduction of 40-Year-Old Reinforced Concrete Beams in Natural Corrosion Environments," *Construction and Building Materials,* Vol. 149, No. 15, pp. 690-704.

Draper, J., Darwin, D., Browning, J. P., Locke, C. E. (2009). "Evaluation of Multiple Corrosion Protection Systems for Reinforced Concrete Bridge Decks," *SM Report* No. 96*,* University of Kansas Center for Research, Lawrence, KS, 429 pp.

Duffo, G. S., Morris, W., Raspini, I., and Saragovi, C. (2004). "A Study of Steel Rebars Embedded in Concrete During 65 Years," *Corrosion Science,* Vol. 46, No. 9, pp. 2143-2157.

Elsener, B., and Böhni, H. (1986). "Corrosion of Steel in Mortar Studied by Impedance Measurements", *Materials Science Forum*, Vol. 8, pp. 363-372.

Elsener, B., and Rossi, A. (2018). "Passivation of Steel and Stainless Steel in Alkaline Media Simulating Concrete," In K. Wandelt (Ed.), *Encyclopedia of Interfacial Chemistry*, Elsevier, pp. 365-375.

Engle, E. (1999). "Effect of Waterproofing Admixture IPANEX on Concrete Durability," *Final Report* No. MLR-98-2, Iowa Department of Transportation, Ames, IA, 22 pp.

Farshadfar, O., O'Reilly, M., and Darwin, D. (2017). "Performance Evaluation of Corrosion Protection Systems for Reinforced Concrete," *SM Report* No. 122*,* University of Kansas Center for Research, Lawrence, KS, 350 pp.

Farshadfar, O., O'Reilly, M., and Darwin, D. (2018). "Corrosion Performance of Plain and Epoxy-Coated MMFX Bars," *SL Report* No. 18-4, University of Kansas Center for Research, Lawrence, KS, 114 pp

Fedor, G. R., and Brennan, P. J. (2011). "Comparison Between Natural Weathering and Fluorescent UV Exposures," *Durability Testing of Nonmetallic Materials,* ASTM International, West Conshohocken, PA, 15 pp.

García-Alonso, M. C., Escudero, M. L., Miranda, J. M., Vega, M. I., Capilla, F., Correia, M. J., Salata, M., Bennani, A., González, J. A. (2007). "Corrosion Behaviour of New Stainless Steels Reinforcing Bars Embedded in Concrete," Cement and Concrete Research, Vol. 37, No. 10, pp. 1463-1471.

Ghods, P., Isgor, O. Burkan, McRae, G.A., and Gu, G.P. (2010). "Electrochemical Investigation of Chloride-Induced Depassivation of Black Steel Rebar Under Simulated Service Conditions," *Corrosion Science,* Vol. 52, No. 5, pp. 1649-1659.

Ghods, P., Isgor, O.B., Bensebaa, F., and Kingston, D. (2012). "Angle-Resolved XPS Study of Carbon Steel Passivity and Chloride-Induced Depassivation in Simulated Concrete Pore Solution," *Corrosion Science,* Vol. 58, pp. 159-167.

Ghods, P., Isgor, O.B., Brown, J.R., Bensebaa, F., and Kingston, D. (2011). "XPS Depth Profiling Study on The Passive Oxide Film of Carbon Steel in Saturated Calcium Hydroxide Solution And The Effect of Chloride on The Film Properties," *Applied Surface Science,* Vol. 257, No. 10, pp. 4669-4677.

Hare, C. H. (1992). "The Degradation of Coatings by Ultraviolet Light And Electromagnetic Radiation," *Journal of Protective Coatings and Linings*.

Hartt, W. H., and Nam, J. (2008). "Effect of Cement Alkalinity on Chloride Threshold and Time-to-Corrosion of Reinforcing Steel in Concrete," *Corrosion,* Vol. 64, No. 8, pp. 671-680.
Hausmann, D. (1967). "Steel Corrosion in Concrete," *Materials Protection*, Vol. 6, No. 11, pp. 19-22.
Hisey, J. (2004). "Investigation of MMFX Reinforcing Steel and the Admixture IPANEX for Use in Bridge Decks," Oklahoma State University, 130 pp.
Hong, K., and Hooton, R. (1999). "Effects of Cyclic Chloride Exposure on Penetration of Concrete Cover," *Cement and Concrete Research,* Vol. 29, No. 9, pp. 1379-1386.
Hope, B. B., and Ip, A. K. (1987). "Chloride Corrosion Threshold in Concrete," *ACI Materials Journal,* Vol. 84, No. 4, pp. 306-314.
Iversen, A., and Leffler, B. (2010). "3.04 - Aqueous Corrosion of Stainless Steels," In B. Cottis, M. Graham, R. Lindsay, S. Lyon, T. Richardson, D. Scantlebury, and H. Stott (Eds.), *Shreir's Corrosion*, Elsevier, Oxford, UK, pp. 1802-1878.
Ji, J., Darwin, D., and Browning, J. (2005). "Corrosion Resistance of Duplex Stainless Steels and MMFX Microcomposite Steel for Reinforced Concrete Bridge Decks," *SM Report* No. 80*,* University of Kansas Center for Research, Inc., Lawrence, KS, 507 pp.
Jones, D. A. (1996). *Principles and Prevention of Corrosion*, Second Edition, Prentice Hall, Upper Saddle River, NJ, 572 pp.
Kahl, S. (2007). "Corrosion Resistant Alloy Steel (MMFX) Reinforcing Bar in Bridge Decks," *Report* No. R-1499, Michigan Department of Transportation, Lansing, MI, 22 pp.
Kamde, D. K., and Pillai, R. G. (2020). "Effect of Sunlight/Ultraviolet Exposure on the Corrosion of Fusion-Bonded Epoxy (FBE) Coated Steel Rebars in Concrete," *Corrosion,* Vol. 76, No. 9, pp. 843-860.
Kayali, O., and Yeomans, S. (1995). "Bond and Slip of Coated Reinforcement in Concrete," *Construction and Building Materials,* Vol. 9, No. 4, pp. 219-226.
Koch, G. H., Brongers, M. P., Thompson, N. G., Virmani, Y. P., and Payer, J. H. (2002). "Corrosion Cost and Preventive Strategies in the United States," *Final Report* FHWA-RD-01-156, Federal Highway Administration, United States, 773 pp.
Kotnarowska, D. (1999). "Influence of Ultraviolet Radiation And Aggressive Media on Epoxy Coating Degradation," *Progress in Organic Coatings,* Vol. 37, No. 3-4, pp. 149-159.
Kumar, B. G., Singh, R. P., and Nakamura, T. (2002). "Degradation of Carbon Fiber-Reinforced Epoxy Composites By Ultraviolet Radiation And Condensation," *Journal of Composite Materials,* Vol. 36, No. 24, pp. 2713-2733.
Lindquist, W. D., Darwin, D., and Browning, J. (2005). "Cracking and Chloride Contents in Reinforced Concrete Bridge Decks," *SM Report* No. 78*,* University of Kansas Center for Research, Lawrence, KS, 453 pp.
Lindquist, W. D., Darwin, D., Browning, J., and Miller, G. G. (2006). "Effect of Cracking on Chloride Content in Concrete Bridge Decks," *ACI Materials Journal,* Vol. 103, No. 6, pp. 467-473.
Locke, C., and Siman, A. (1980). "Electrochemistry of Reinforcing Steel in Salt-Contaminated Concrete," In D. Tonini and J. Gaidis (Ed.), *Corrosion of Reinforcing Steel in Concrete*, ASTM International, pp. 3-16.
Macias, A., and Andrade, C. (1987). "Corrosion of Galvanized Steel Reinforcements in Alkaline Solutions: Part 1: Electrochemical Results, " *British Corrosion Journal,* Vol. 22, No. 2, pp. 113-118.
Manera, M., Vennesland, Ø., and Bertolini, L. (2008). "Chloride Threshold for Rebar Corrosion in Concrete with Addition of Silica Fume," *Corrosion Science,* Vol. 50, No. 2, pp. 554-560.

Manning, D. G. (1996). “Corrosion Performance of Epoxy-Coated Reinforcing Steel: North American Experience,” *Construction and Building Materials,* Vol. 10, No. 5, pp. 349-365.

Martinez, S. L., Darwin, D., McCabe, S. L., and Locke Jr, C. E. (1990). “Rapid Test for Corrosion Effects of Deicing Chemicals in Reinforced Concrete,” *SL Report* No. 90-4*,* University of Kansas Center for Research, Inc., Lawrence, KS, 63 pp.

Morris, W., Vico, A., and Vázquez, M. (2004). “Chloride Induced Corrosion of Reinforcing Steel Evaluated by Concrete Resistivity Measurements,” *Electrochimica Acta,* Vol. 49, No. 25, pp. 4447-4453.

Morris, W., Vico, A., Vazquez, M., and De Sanchez, S. (2002). “Corrosion of Reinforcing Steel Evaluated by Means of Concrete Resistivity Measurements,” *Corrosion Science,* Vol. 44, No. 1, pp. 81-99.

National Research Council. (1991). “Highway Deicing: Comparing Salt and Calcium Magnesium Acetate,” *Special Report* No. 235, Transportation Research Board, Washington, DC, 170 pp.

Nikafshar, S., Zabihi, O., Ahmadi, M., Mirmohseni, A., Taseidifar, M., and Naebe, M. (2017). “The Effects of UV Light on The Chemical And Mechanical Properties of a Transparent Epoxy-Diamine System in The Presence of An Organic UV Absorber,” *Materials*, Vol. 10, No. 2.

O’Reilly, M., Darwin, D., Browning, J., and Locke, C. (2011). “Evaluation of Multiple Corrosion Protection Systems for Reinforced Concrete Bridge Decks,”, *SM Report* No. 100, University of Kansas Center for Research, Lawrence, KS, 535 pp.

O’Reilly, M., Vosough-Grayli, P., and Darwin, D. (2021). “Corrosion Performance of ChromX 2100, 4100, and 9100 Bars,” *SL Report* 21-1, The University of Kansas Center for Research, Inc., Lawrence, KS, 34 pp.

Ogunsanya, I. (2016). “Evaluation of the Behaviour of Continuously Galvanized Rebar,” University of Waterloo, 94 pp.

Ogunsanya, I. G., and Hansson, C. M. (2018). “The Influence of Coating Thickness and Composition on the Corrosion Propagation Rates of Galvanized Rebar in Cracked Concrete,” *Corrosion,* Vol. 74, No. 1, pp. 134-143.

Oklahoma Department of Transportation (2020). “Item Price History From January 1, 2019 to June 30, 2020.” Retrieved from https://www.odot.org/contracts/avgprices/index.php

O'Reilly, M., Farshadfar, O., Darwin, D., Browning, J., and Locke C. (2018). “Corrosion-Induced Concrete Cracking for Uncoated and Galvanized Reinforcing Bars,” *ACI Materials Journal*, Vol. 115, No. 6, pp. 825-832.

Pokorný, P., Kouřil, M., and Kučera, V. (2019). “Kinetics of Zinc Corrosion in Concrete as A Function of Water and Oxygen Availability,” *Materials,* Vol. 12, No. 17.

Popov, B. N. (2015). "Chapter 7 - Pitting and Crevice Corrosion," In B. N. Popov (Ed.), *Corrosion Engineering*, Elsevier, Amsterdam, Netherlands, pp. 289-325.

Poursaee, A. (2016). *Corrosion of Steel in Concrete Structures*, Woodhead Publishing., Sawston, UK, 312 pp.

Ramniceanu, A., Weyers, R. E., Riffle, J. S., and Sprinkel, M. M. (2008). “Parameters Governing Corrosion Protection Efficacy of Fusion-Bonded Epoxy Coatings on Reinforcing Bar,” *ACI Materials Journal,* Vol. 105, No. 5, pp. 459-467.

Rezig, A., Nguyen, T., Martin, D., Sung, L., Gu, X., Jasmin, J., and Martin, J. W. (2006). “Relationship Between Chemical Degradation and Thickness Loss of an Amine-Cured

Epoxy Coating Exposed to Different UV Conditions," *Journal of Coatings Technology Research,* Vol. 3, No. 3, pp. 173-184.

Rodriguez, O. G., and Hooton, R. D. (2003). "Influence of Cracks on Chloride Ingress into Concrete," *ACI Materials Journal,* Vol. 100, No. 2, pp. 120-126.

Saraswathy, V., and Song, H.-W. (2005). "Performance of Galvanized and Stainless Steel Rebars in Concrete under Macrocell Corrosion Conditions, " *Materials and Corrosion,* Vol. 56, No. 10, pp. 685-691.

Schiessl, P., and Breit, W. (1996). "Local Repair Measures at Concrete Structures Damaged by Reinforcement Corrosion-Aspects of Durability," *Royal Society of Chemistry,* Vol. 183, No. 1, pp. 525-534.

Selvaraj, R., Selvaraj, M., and Iyer, S. (2009). "Studies on the Evaluation of the Performance of Organic Coatings Used for the Prevention of Corrosion of Steel Rebars in Concrete Structures," *Progress in Organic Coatings,* Vol. 64, No. 4, pp. 454-459.

Senecal, M. R., Darwin, D., and Locke Jr, C. E. (1995). "Evaluation of Corrosion-Resistant Steel Reinforcing Bars," *SM Report* No. 40*,* University of Kansas Center for Research, Inc., Lawrence, KS, 153 pp.

Shi, X., Hinderliter, B. R., and Croll, S. G. (2010). "Environmental and time dependence of moisture transportation in an epoxy coating and its significance for accelerated weathering," *Journal of Coatings Technology and Research,* Vol. 7, No. 4, pp. 419-430.

Sturgeon, W. J., O'Reilly, M., Darwin, D., and Browning, J. (2010). "Rapid Macrocell Tests of ASTM A775, A615, and A1035 Reinforcing Bars," *SL Report* No. 10-4*,* University of Kansas Center for Research, Inc., Lawrence, KS, 46 pp.

Swamy, R. N., Koyama, S., Arai T., and Mikami N. (1998). "Durability of Steel Reinforcement in Marine Environment," *ACI Symposium Publication,* Vol. 109, pp. 147-162.

Thomas, M. (1996). "Chloride Thresholds in Marine Concrete," *Cement and Concrete Research,* Vol. 26, No. 4, pp. 513-519.

Thomas, M., Matthews, J., and Haynes, C. (1990). "Chloride Diffusion and Reinforcement Corrosion in Marine Exposed Concrete Containing Pulverized-Fuel Ash. Corrosion of Reinforcement in Concrete", *Third International Symposium on Corrosion of Reinforcement In Concrete Construction*, Wishaw, Warwickshire, UK, pp. 198-212.

Torbati-Sarraf, H., and Poursaee, A. (2018). "Study of the Passivation of Carbon Steel in Simulated Concrete Pore Solution Using Scanning Electrochemical Microscope (SECM)," *Materialia,* Vol. 2, pp. 19-22.

Torres-Acosta, A. A., and Sagues, A. A. (2004). "Concrete Cracking by Localized Steel Corrosion--Geometric Effects," *Materials Journal,* Vol. 101, No. 6, pp. 501-507.

Treadaway, K. W. J., Cox, R. N., and Brown, B. L. (1989). "Durability of Corrosion Resisting Steels in Concrete," *Proceedings of the Institution of Civil Engineers,* Vol. 86, No. 2, pp. 305-331.

Tuutti, K. (1982). "Corrosion of Steel in Concrete," Swedish Cement and Concrete Research Institute, Stockholm, Sweden, 473 pp

Verbeck, G. J. (1975). "Mechanisms of Corrosion of Steel in Concrete," *ACI Symposium Paper,* Vol. 49, pp. 21-38.

Vidal, T., Castel, A., and Francois, R. (2004). "Analyzing Crack Width to Predict Corrosion in Reinforced Concrete," *Cement and Concrete Research,* Vol. 34, No. 1, pp. 165-174.

Weishaar, A., Carpenter, M., Loucks, R., Sakulich, A., and Peterson, A. M. (2018). "Evaluation of Self-Healing Epoxy Coatings for Steel Reinforcement," *Construction and Building Materials,* Vol. 191, No. 10, pp. 125-135.

Weyers, R. E., Pyc, W., and Sprinkel, M. M. (1998). "Estimating the Service Life of Epoxy Coated Reinforcing Steel," *ACI Materials Journal,* Vol. 95, No. 5, pp. 546-557.

Wilson, A. D., Nicholson, J. W., and Prosser, H. J. (1988). *Surface Coatings-2*, Springer, Dordrecht, Netherlands, 230 pp.

Xing, L., Darwin, D., and Browning, J. (2010). "Evaluation of Multiple Corrosion Protection Systems and Corrosion Inhibitors for Reinforced Concrete Bridge Decks," *SM Report* No. 99*,* University of Kansas Center for Research, Lawrence, KS, 507 pp.

Xypex. (2020). Retrieved from https://www.xypex.com/ Accessed on 3/29/2020

Yeomans, S. R. (2016). "Galvanized Steel Reinforcement," In A. Poursaee (Ed.), *Corrosion of Steel in Concrete Structures*, Woodhead Publishing, Sawston, UK, pp. 111-129.

Yeomans, S. R. (2018). "Galvanized Steel Reinforcement: Recent Developments and New Opportunities," *Proceedings of 5th International Federation for Structural Concrete*, Melbourne, Australia, 16 pp.

Yu, H., and Hartt, W. H. (2007). "Effects of Reinforcement and Coarse Aggregates on Chloride Ingress Into Concrete and Time-to-Corrosion: Part 1—Spatial Chloride Distribution and Implications," *Corrosion,* Vol. 63, No. 9, pp. 843-849.

Yu, H., Himiob, R., and Hartt, W. (2007). "Effects of Reinforcement and Coarse Aggregates on Chloride Ingress into Concrete and Time-to-Corrosion: Part 2—Spatial Distribution of Coarse Aggregates," *Corrosion,* Vol. 63, No. 10, pp. 924-931.

Yunovich, M., and Thompson, N. G. (2003). "Corrosion of Highway Bridges: Economic Impact and Control Methodologies," *ACI Concrete International*, Vol. 25, No. 1, pp. 52-57.

Zhao, Y., and Jin, W. (2016). "Steel Corrosion in Concrete," In *Steel Corrosion-Induced Concrete Cracking*, Butterworth-Heinemann, Oxford, UK, pp. 19-29.

Zimmermann, L. (2000). Korrosionsinitiierender Chloridgehalt von Stahl in Beton, ETH Zurich, Zurich, Switzerland, 139 pp.

Zimmermann, L., Elsener, B., and Böhni, H. (1999). "Critical Factors for the Initiation of Rebar Corrosion", *International Congress EUROCORR'99*, European Federation of Corrosion, Aachen, Germany.

APPENDIX A: CASTING ORDER OF SPECIMENS

Table A.1: Casting order of specimens

Specimen			1	2	3	4	5	6	7	9	10	11	12	13	14	15	8	Recast	Recast UV
Conv-A	SE	3	1	1	1				1				1	1				1	
	CB	3	1	1	1				1				1	1					
Conv-B	SE	3	1	1	1			1									3		
	CB	3	1	1	1			1									3		
Conv-C	SE	3	1	1		1												3	
	CB	3	1	1		1													
ECR1	SE	6	1	1		1		1											
	CB	6	1	1		1		1											
ECR1-ND	SE	3			1	1		1											
	CB	3			1	1		1											
ECR1-UV-1000	SE	3										1	1	1					
	CB	3										1	1	1					4
ECR1-UV-1000-ND	SE	3										1	1	1					
	CB	3										1	1	1					
A767-D	SE	6	1	1	1		1	1				1							
	CB	6	1	1	1		1	1				1							
A767 -ND	SE	6			1		1	1	1			1		1					
	CB	6			1		1	1	1			1		1					
A767-bent	SE	6			1		1		1			1	1	1					
A1094-D	SE	6	1	1		1	1		1				1						
	CB	6	1	1		1	1		1				1						
A1094-ND	SE	6				1	1	1	1				1	1					
	CB	6				1	1	1	1				1	1					
A1094-bent	SE	6				1	1		1			1	1	1					
ChromX	SE	6				1	1	1	1			1					3		
	CB	6				1	1	1	1			1					2		
Conv-B-IPANEX	SE	6								3	3								
	CB	6								3	3								
ChromX-IPANEX	SE	6								3	3								
	CB	6								3	3								
Conv-B-Xypex	SE	6													3	3			
	CB	6													3	3			
ChromX-Xypex	SE	6													3	3			
	CB	6													3	3			

APPENDIX B: CONCRETE PROPERTIES

Table B.1: Concrete properties

	Batch 1	Batch 2	Batch 3	Batch 4	Batch 5	Batch 6	Batch 7	Batch 8	Batch 9	Batch 10	Batch 11
Slump (in.)	4.5	3.5	4.5	4	2.75	2.25	2.5	4.5	4.5	4.75	4
Temp (°F)	58	68	60	69	62	60	65	80	70	78	80
Air (%)	5.7	5.25	6.3	6.5	6	5	5	5	5.5	7	5.5
Unit wt. (lb/ft^3)	141.1	144.2	143.6	148.8	143.8	144.1	146.1	142.7	139.3	138.0	140.5
Compressive Strength (psi):	3966	4702	5033	4173	4744	4515	4720	4675	4186	3806	4051
7 day	2970	4230	2910	3600	3810	-	3490	3820	2960	2790	2970
28 day	3970	4700	5030	4170	4740	4520	4720	4680	4190	3810	4050
Cast date	2/16/2018	2/26/2018	3/12/2018	3/22/2018	4/2/2018	4/19/2018	4/30/2018	5/18/2018	5/21/2018	5/24/2018	5/31/2018

	Batch 12	Batch 13	Batch 14	Batch 15	Recast 1	Recast ECR-UV
Slump (in.)	4.75	4.75	4.5	5	4.75	4.5
Temp (°F)	70	80	80	66	78	62
Air (%)	5.5	6.5	6.5	5	5	6.1
Unit weight (lb/ft^3)	138.2	139.3	139.9	142.6	141.8	141.2
Compressive Strength (psi):	3327	3794	4351	3921	3767	4826
7 day	2800	3140	3150	2980	2970	4220
28 day	3330	3790	4350	3920	3770	4830
Cast date	6/19/2018	6/26/2018	7/16/2018	7/19/2018	8/13/2018	3/14/2019

APPENDIX C: INDIVIDUAL SPECIMEN CORROSION RATES AND CORROSION POTENTIALS

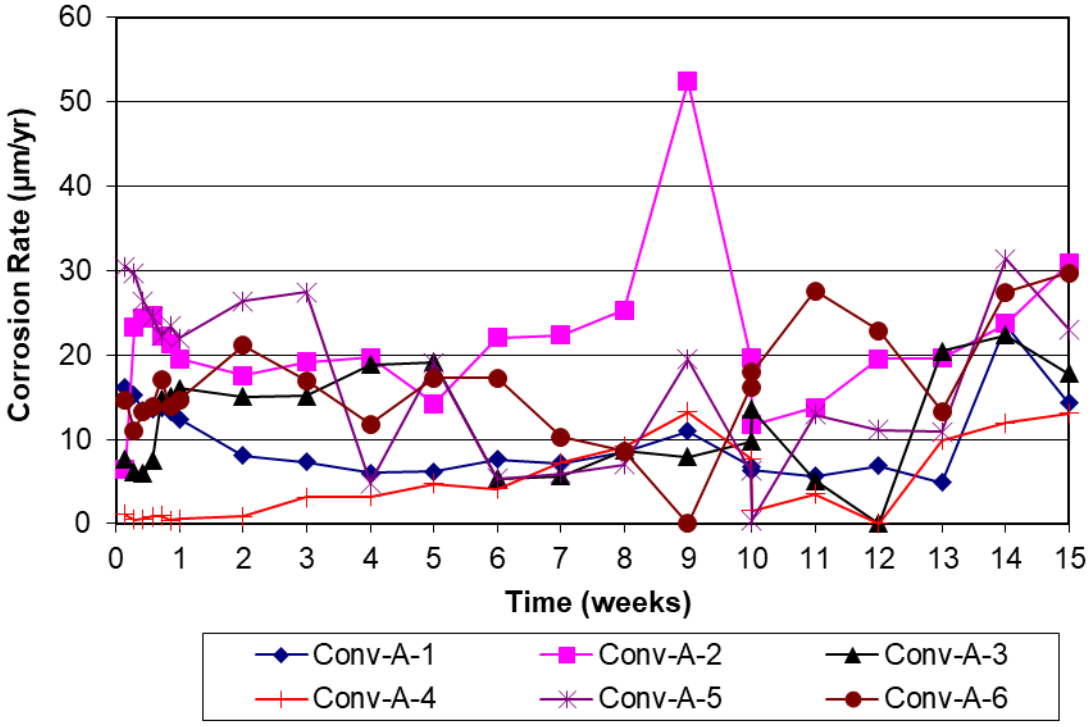

Figure C.1: Corrosion rate of Conv-A reinforcement in the rapid macrocell test

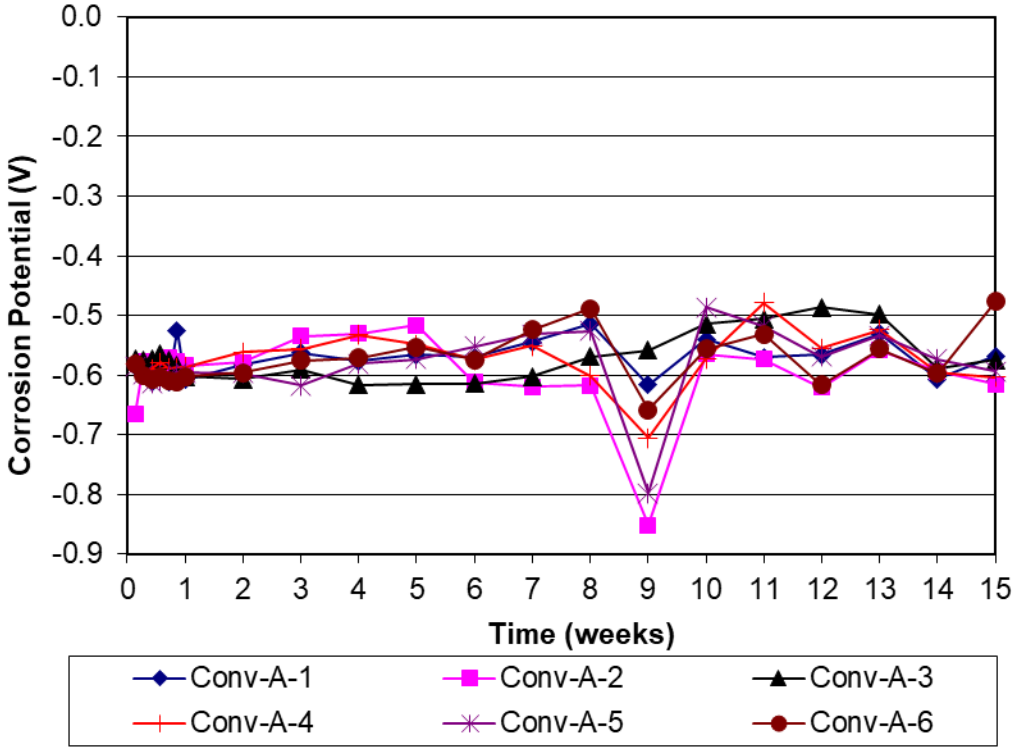

Figure C.2: Corrosion potential of Conv-A reinforcement in the rapid macrocell test

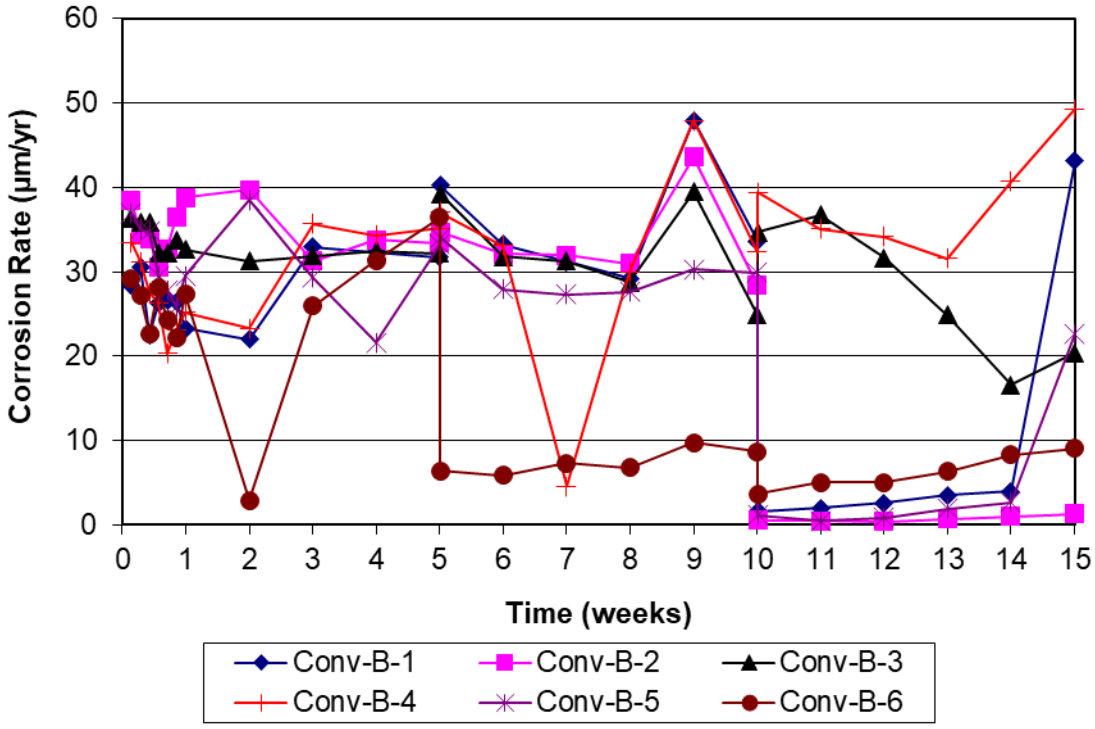

Figure C.3: Corrosion rate of Conv-B reinforcement in the rapid macrocell test

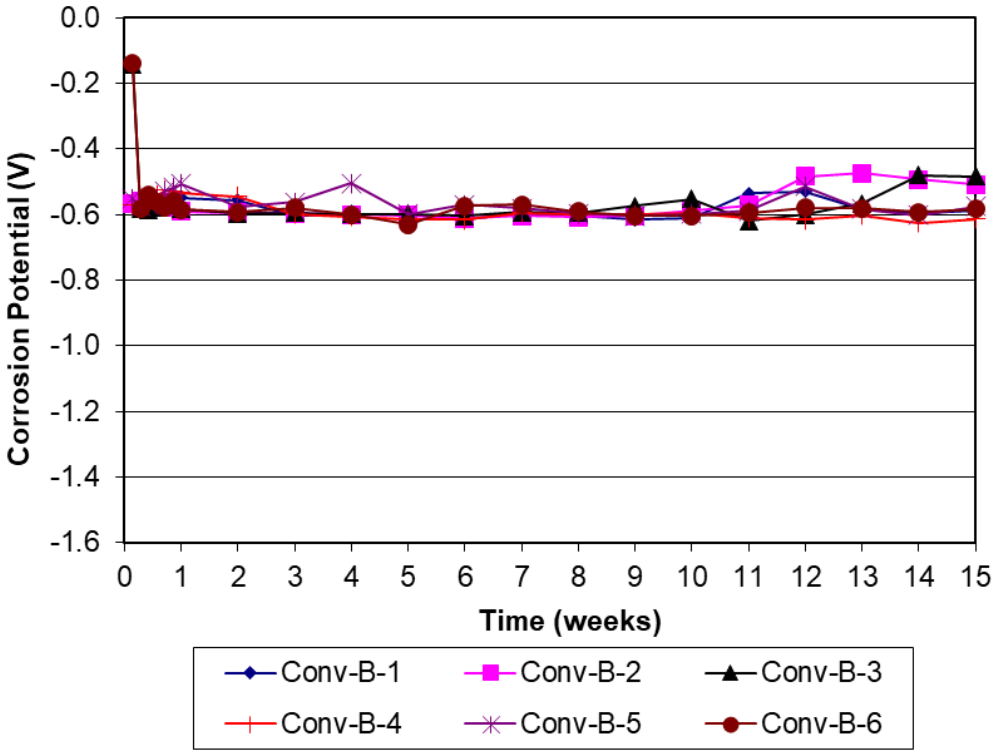

Figure C.4: Corrosion potential of Conv-B reinforcement in the rapid macrocell test

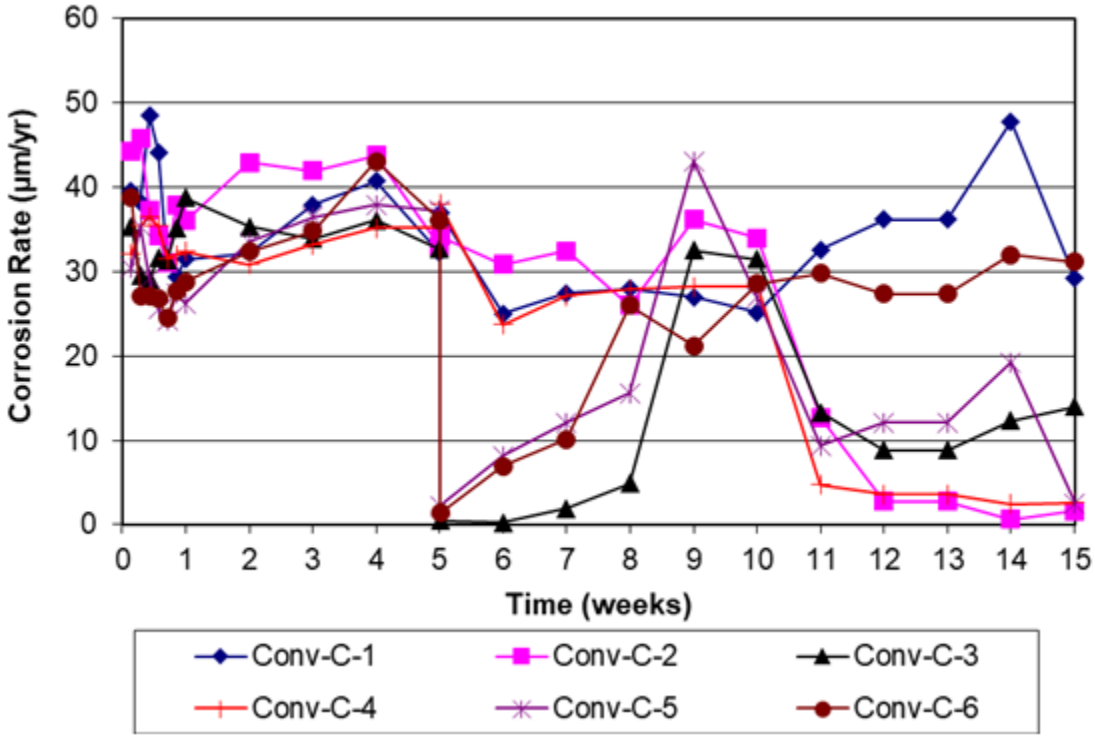

Figure C.5: Corrosion rate of Conv-C reinforcement in the rapid macrocell test

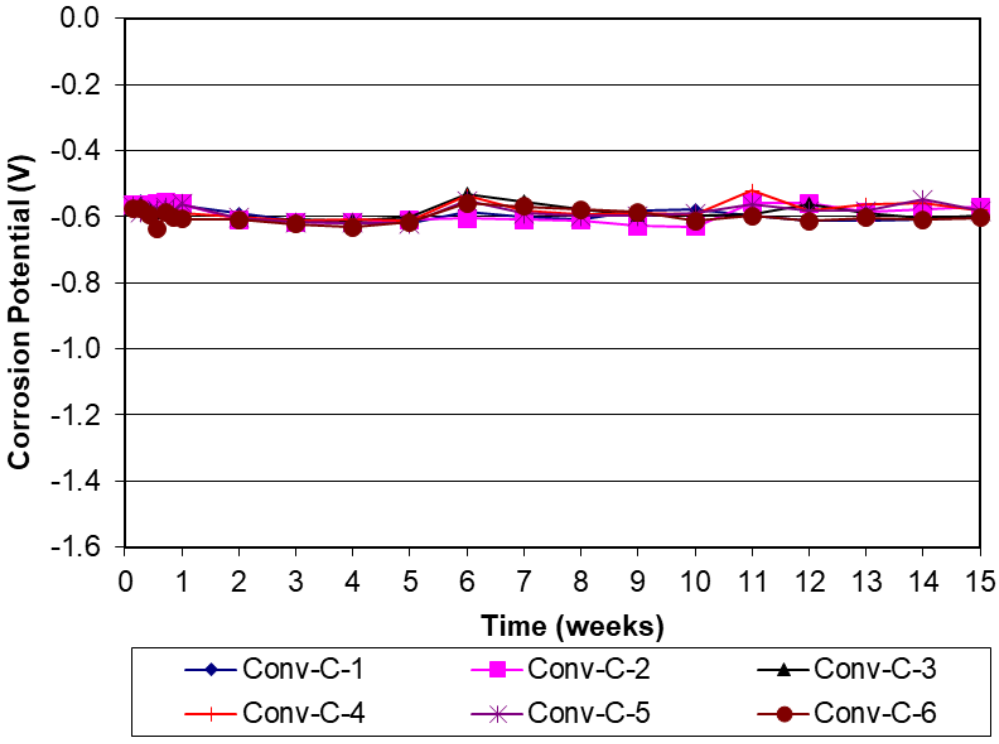

Figure C.6: Corrosion potential of Conv-C reinforcement in the rapid macrocell test

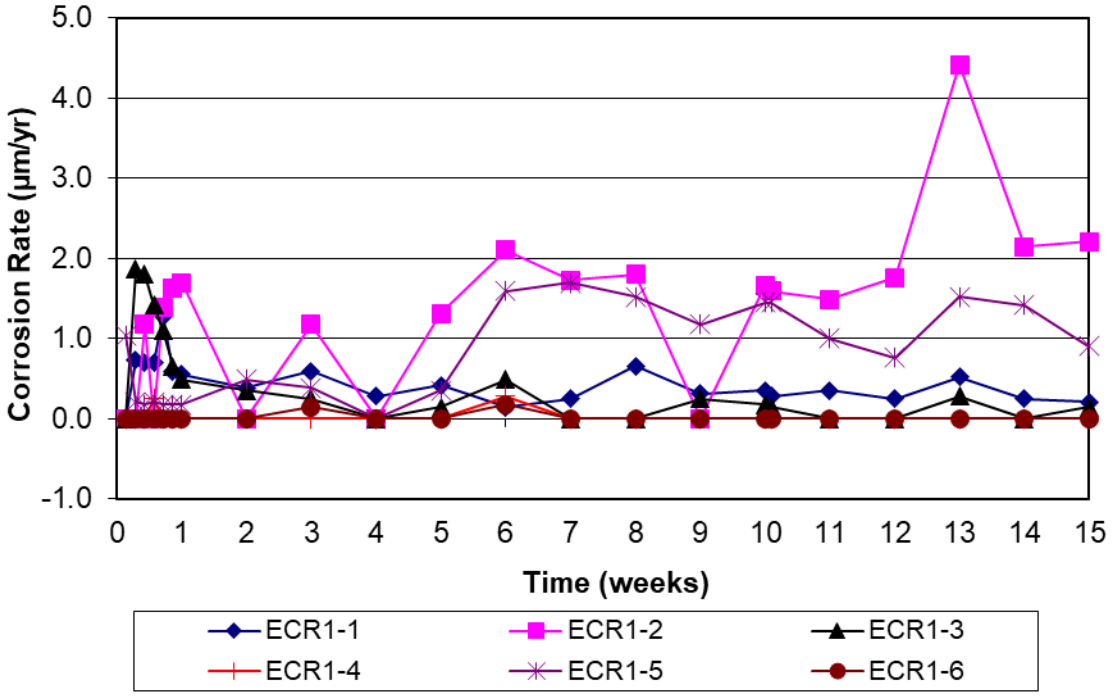

Figure C.7: Corrosion rate of ECR1 reinforcement in the rapid macrocell test

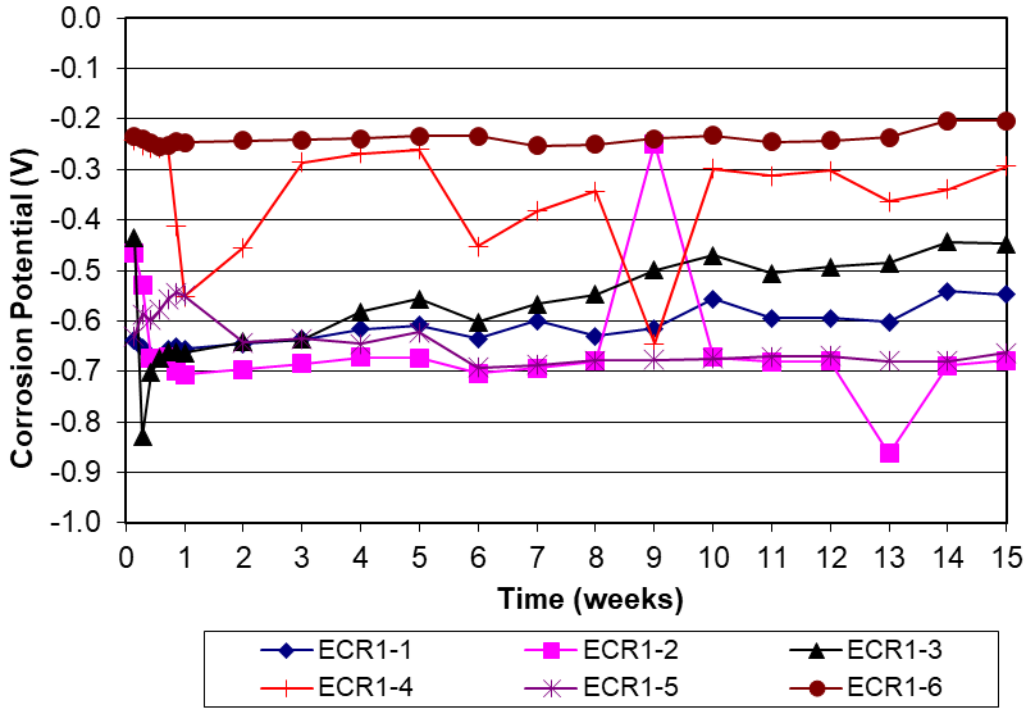

Figure C.8: Corrosion potential of ECR1 reinforcement in the rapid macrocell test

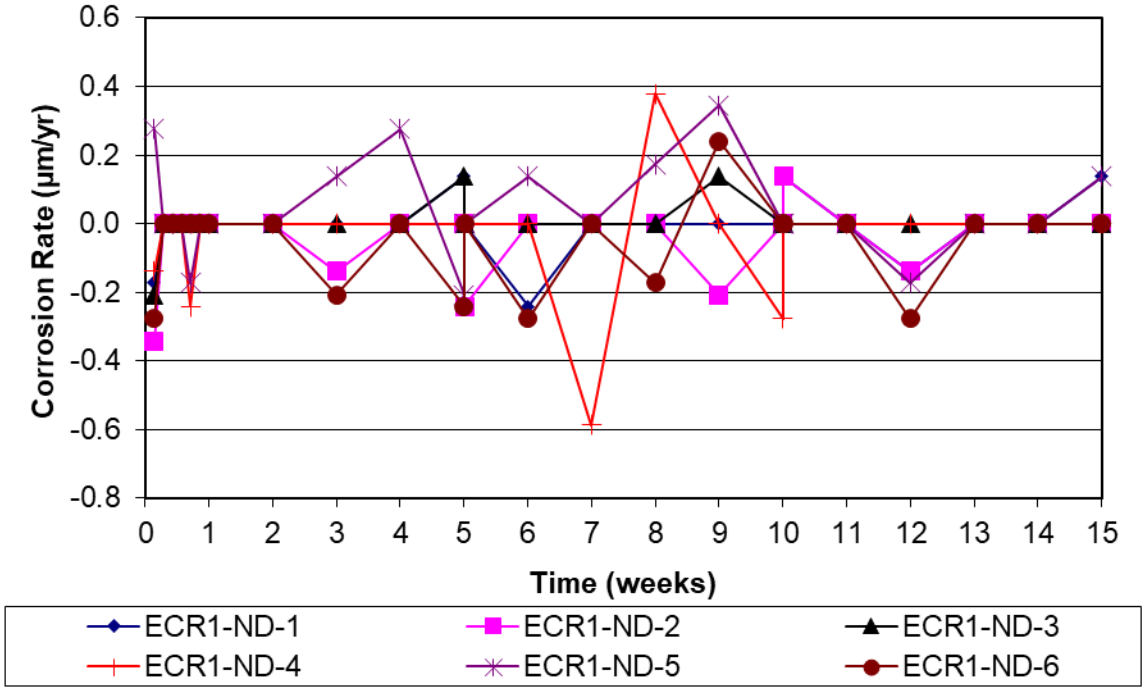

Figure C.9: Corrosion rate of ECR1-ND reinforcement in the rapid macrocell test

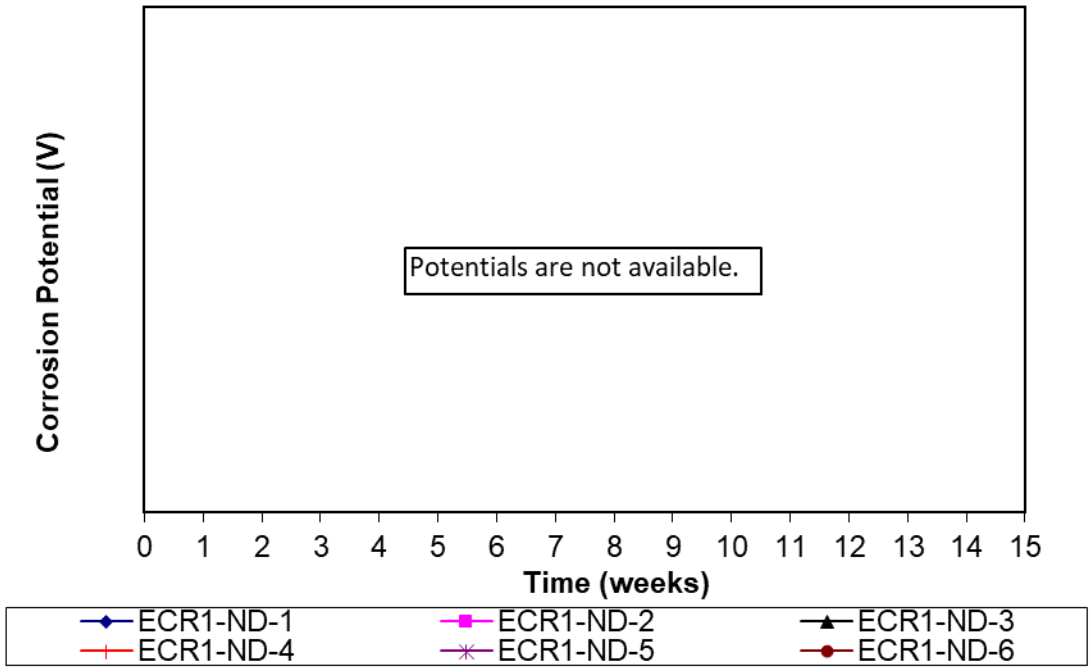

Figure C.10: Corrosion potential of ECR1-ND reinforcement in the rapid macrocell test

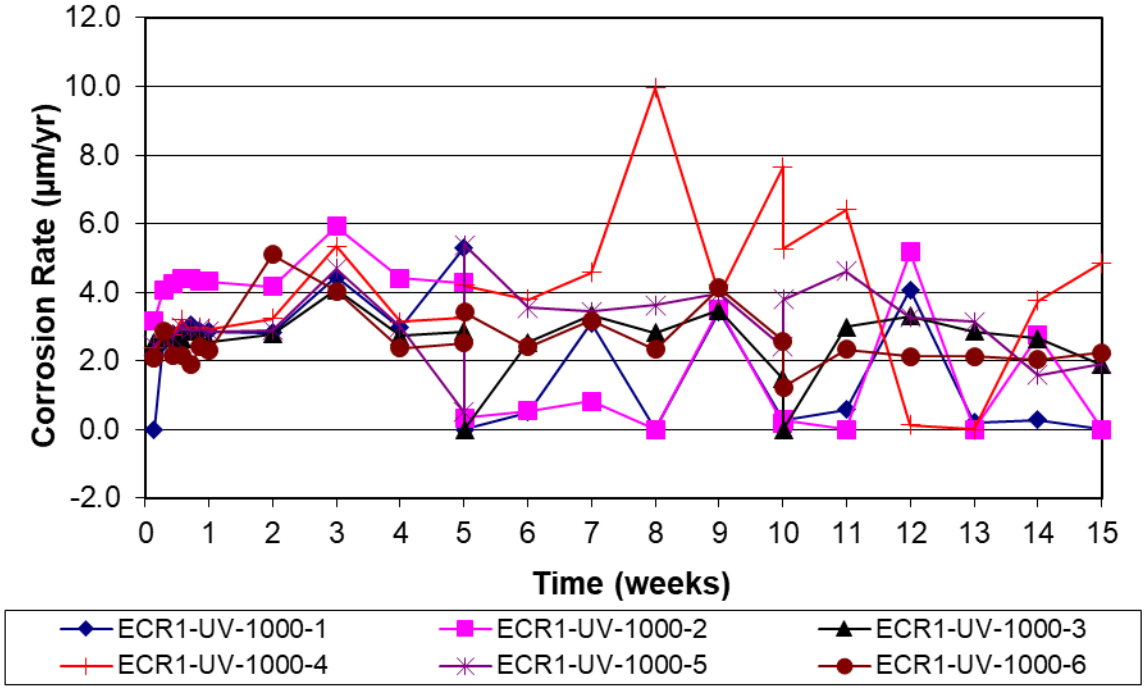

Figure C.11: Corrosion rate of ECR1-UV-1000 reinforcement in the rapid macrocell test

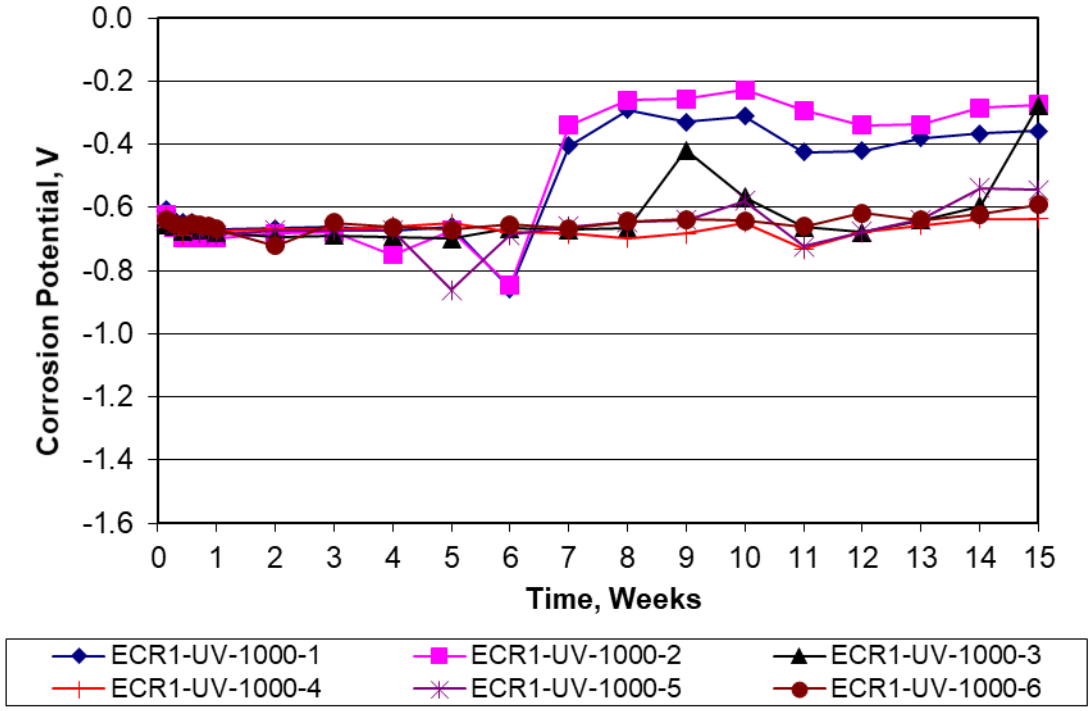

Figure C.12: Corrosion potential of ECR1-UV-1000 reinforcement in the rapid macrocell test

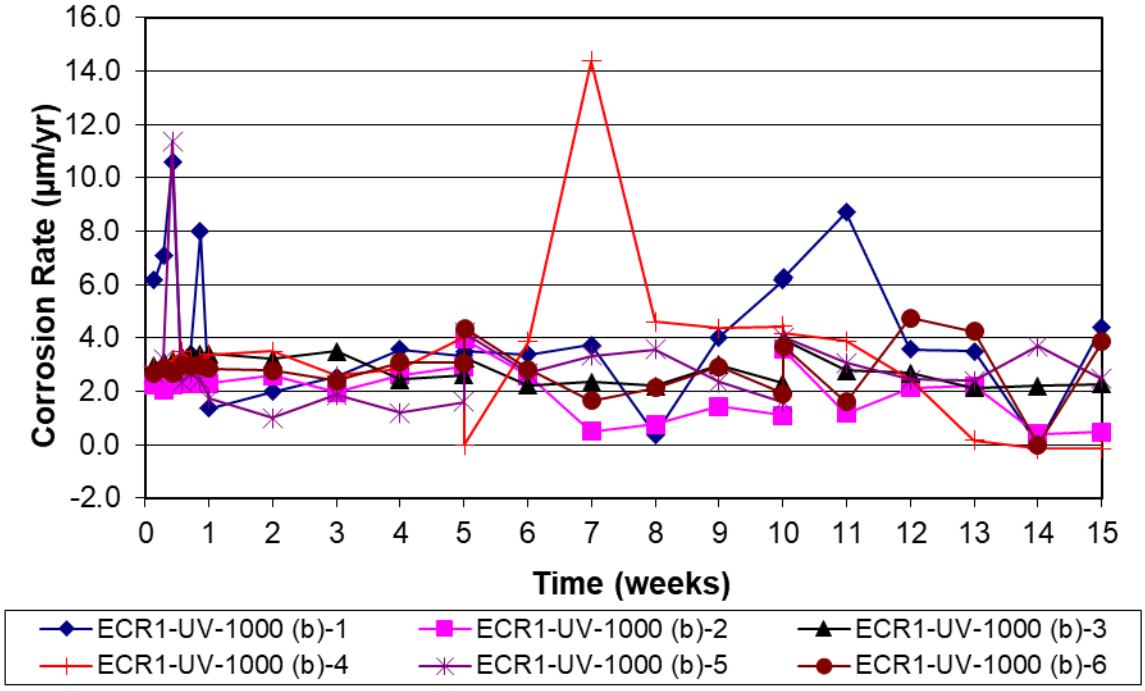

Figure C.13: Corrosion rate of ECR1-UV-1000(b) reinforcement in the rapid macrocell test

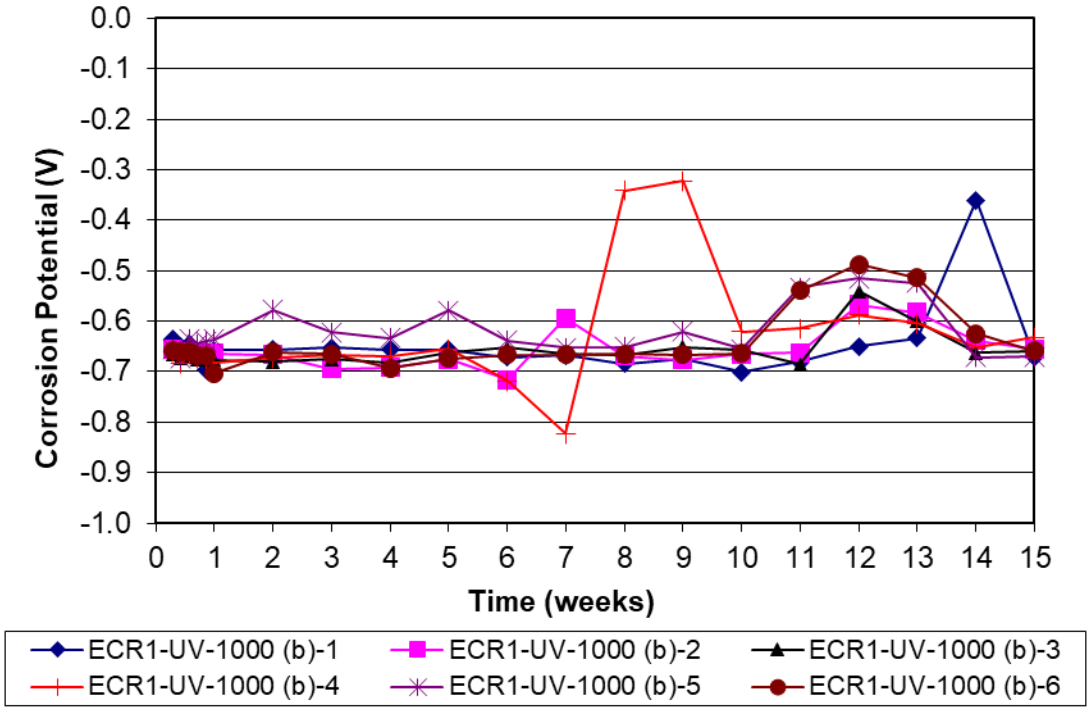

Figure C.14: Corrosion rate of ECR1-UV-1000(b) reinforcement in the rapid macrocell test

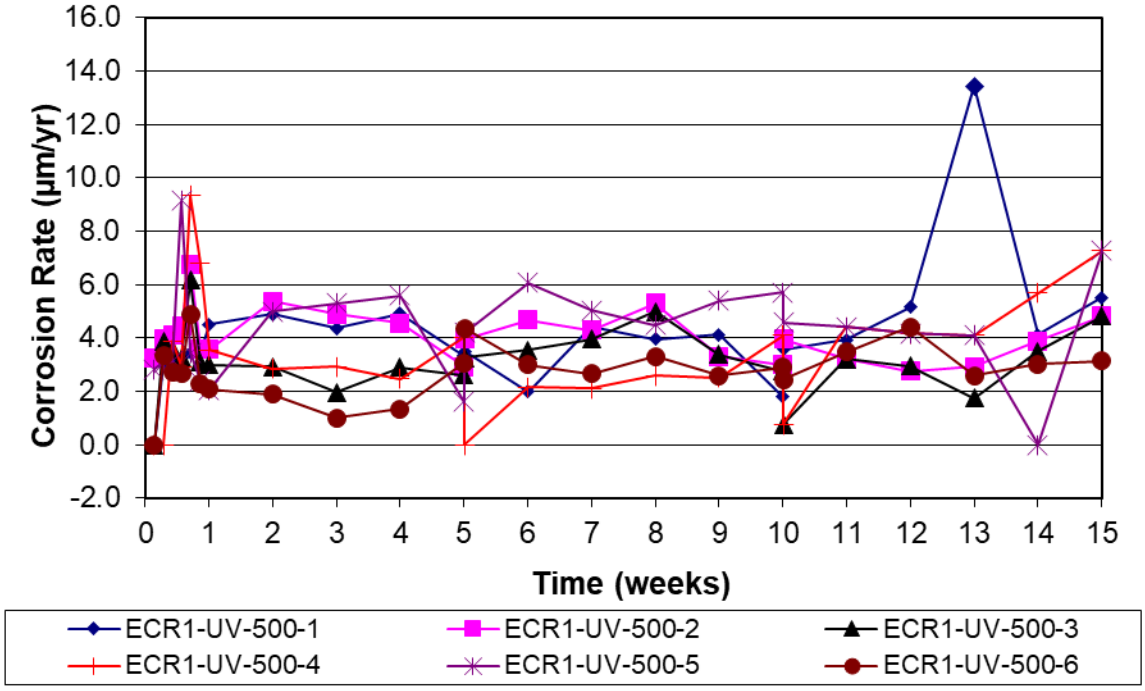

Figure C.15: Corrosion rate of ECR1-UV-500 reinforcement in the rapid macrocell test

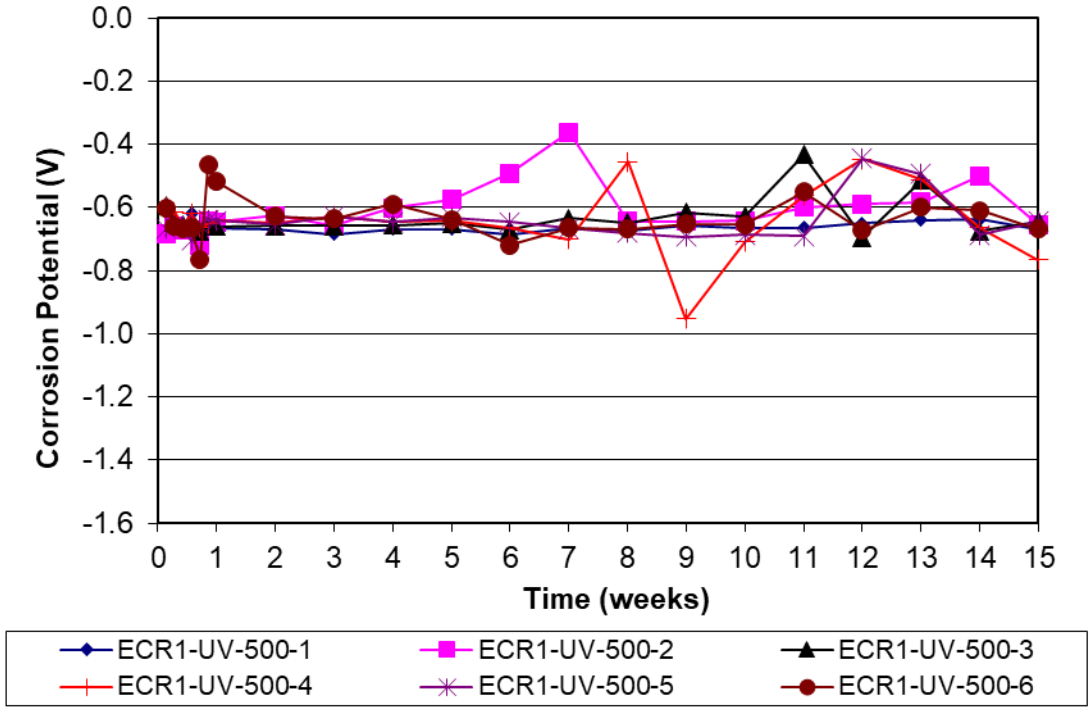

Figure C.16: Corrosion potential of ECR1-UV-500 reinforcement in the rapid macrocell test

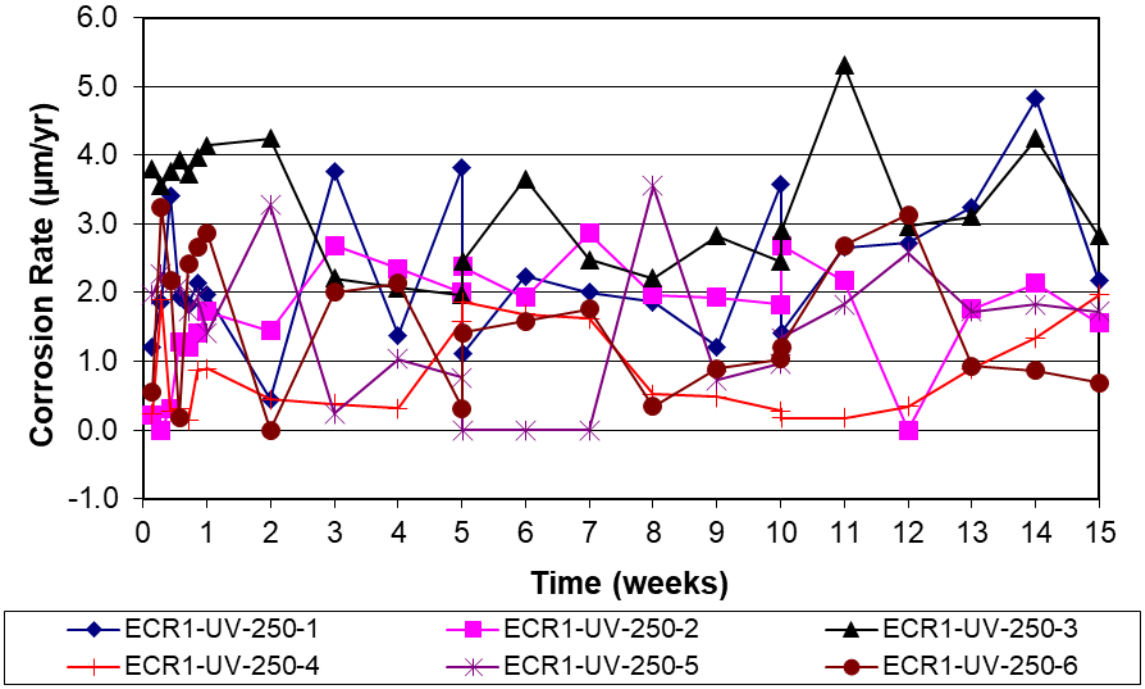

Figure C.17: Corrosion rate of ECR1-UV-250 reinforcement in the rapid macrocell test

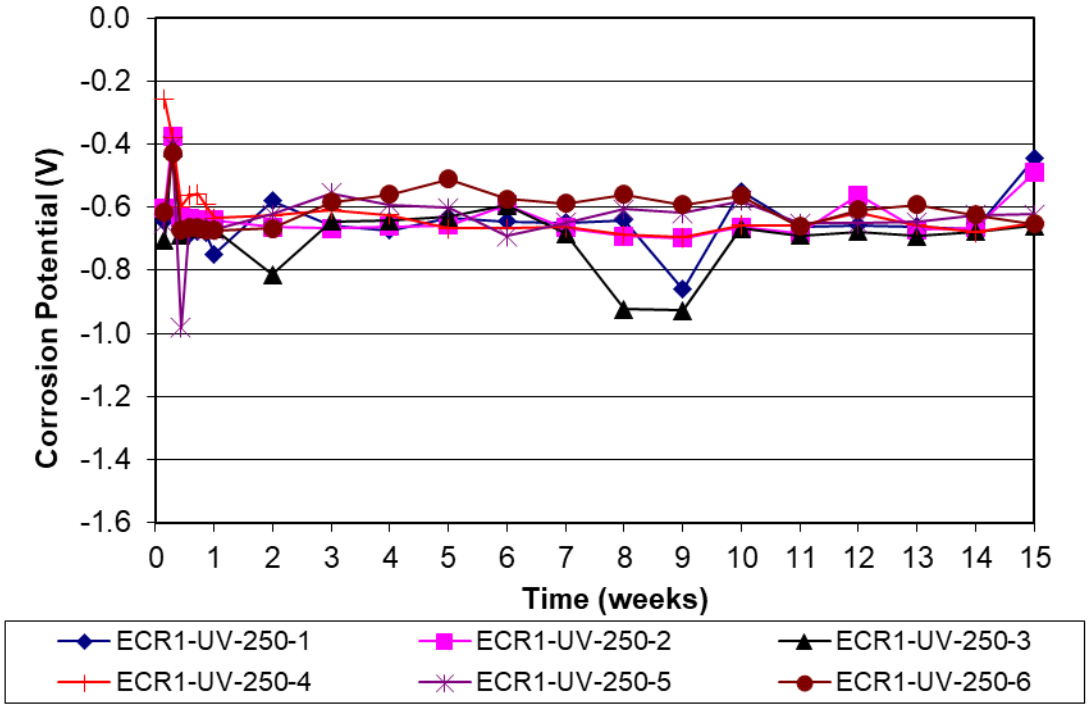

Figure C.18: Corrosion potential of ECR1-UV-250 reinforcement in the rapid macrocell test

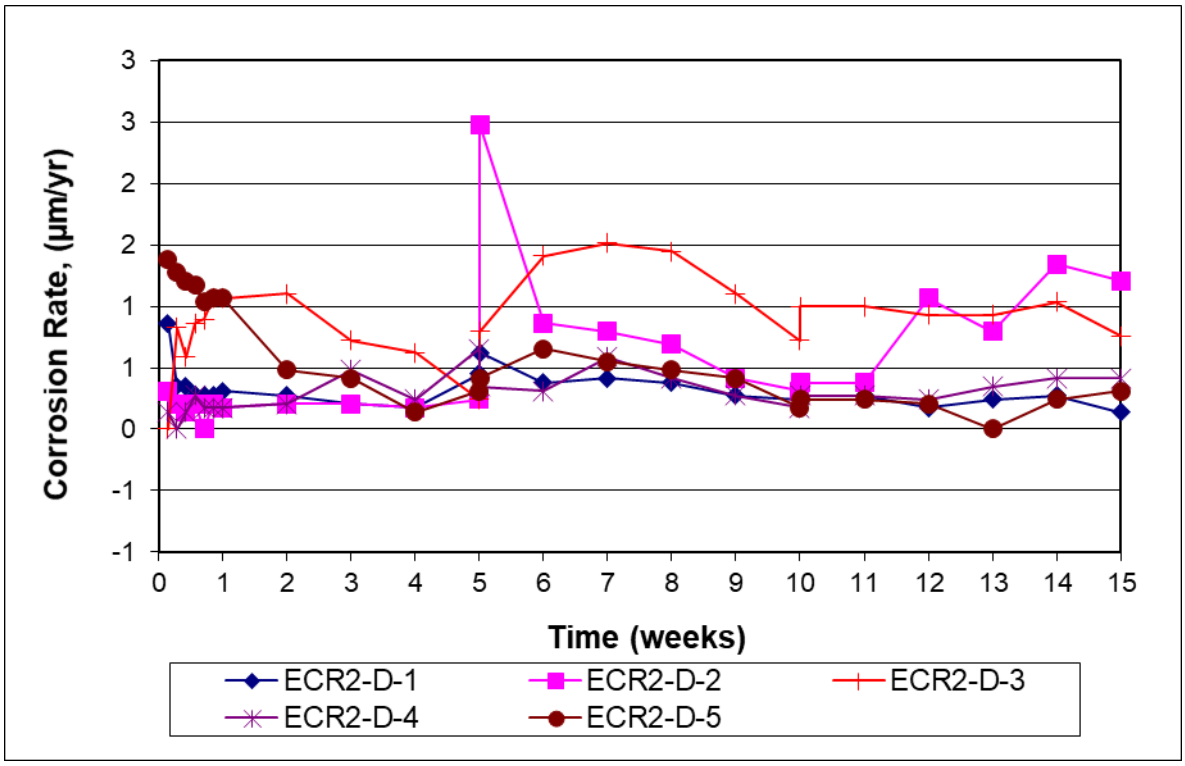

Figure C.19: Corrosion rate of ECR2 reinforcement in the rapid macrocell test

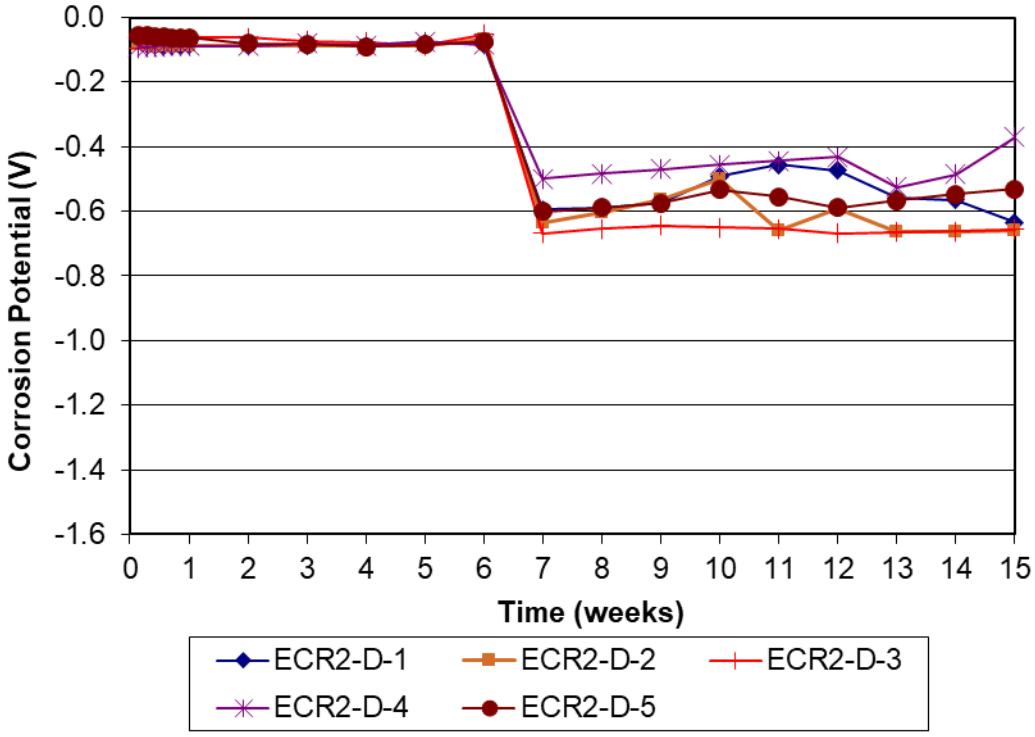

Figure C.20: Corrosion potenital of ECR2 reinforcement in the rapid macrocell test

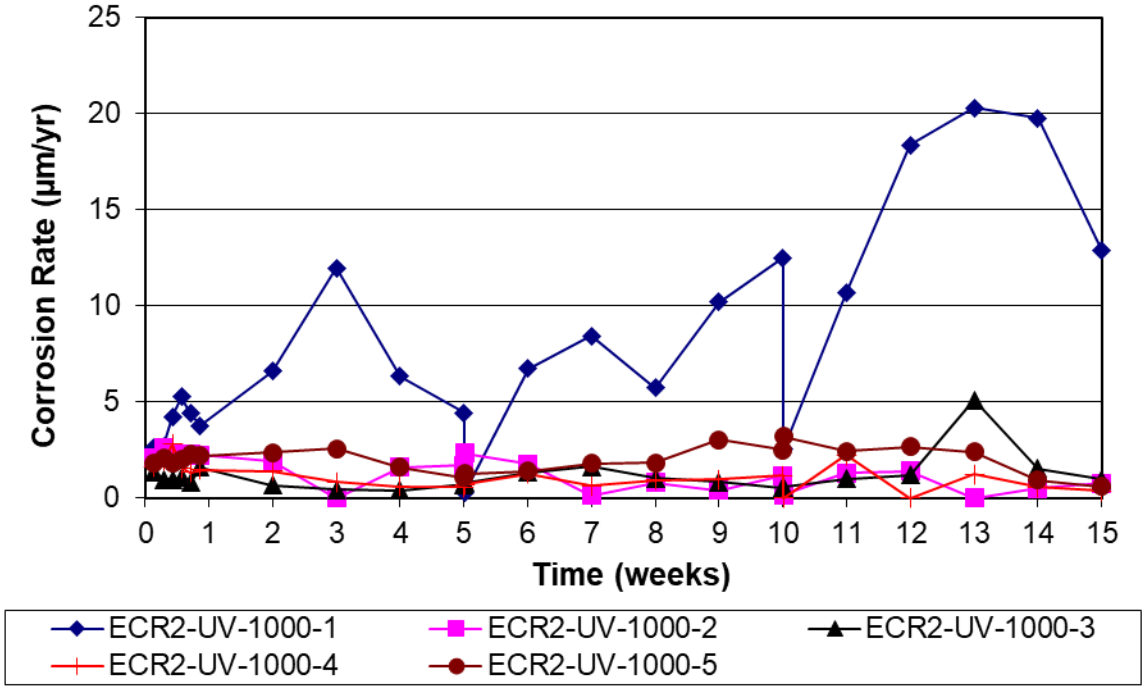

Figure C.21: Corrosion rate of ECR2-UV-1000 reinforcement in the rapid macrocell test

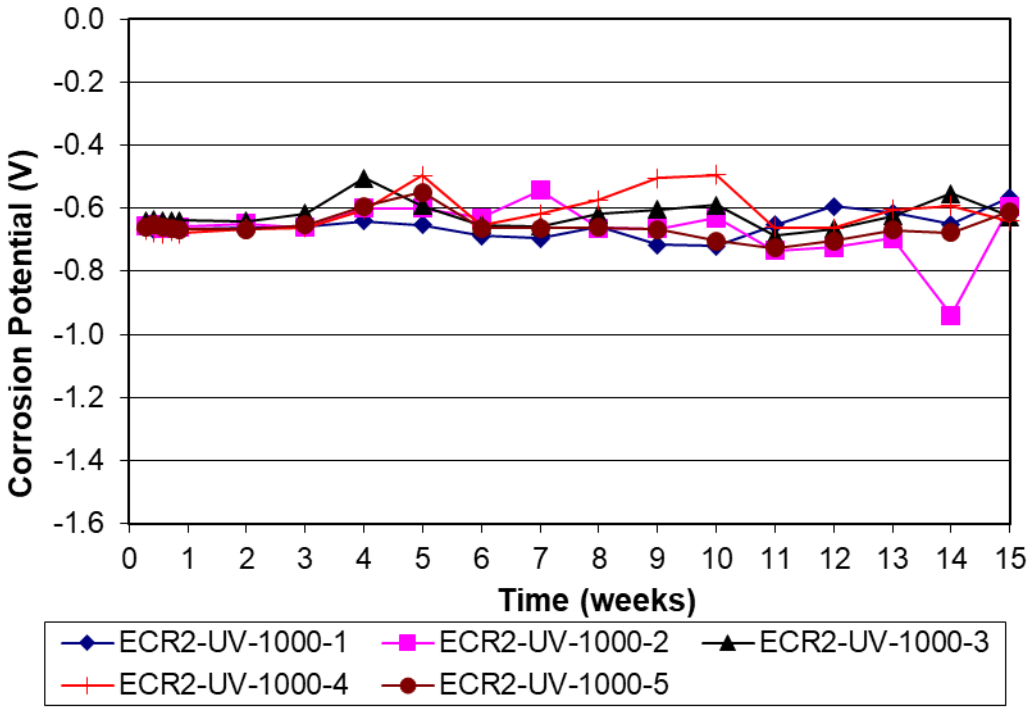

Figure C.22: Corrosion potential of ECR2-UV-1000 reinforcement in the rapid macrocell test

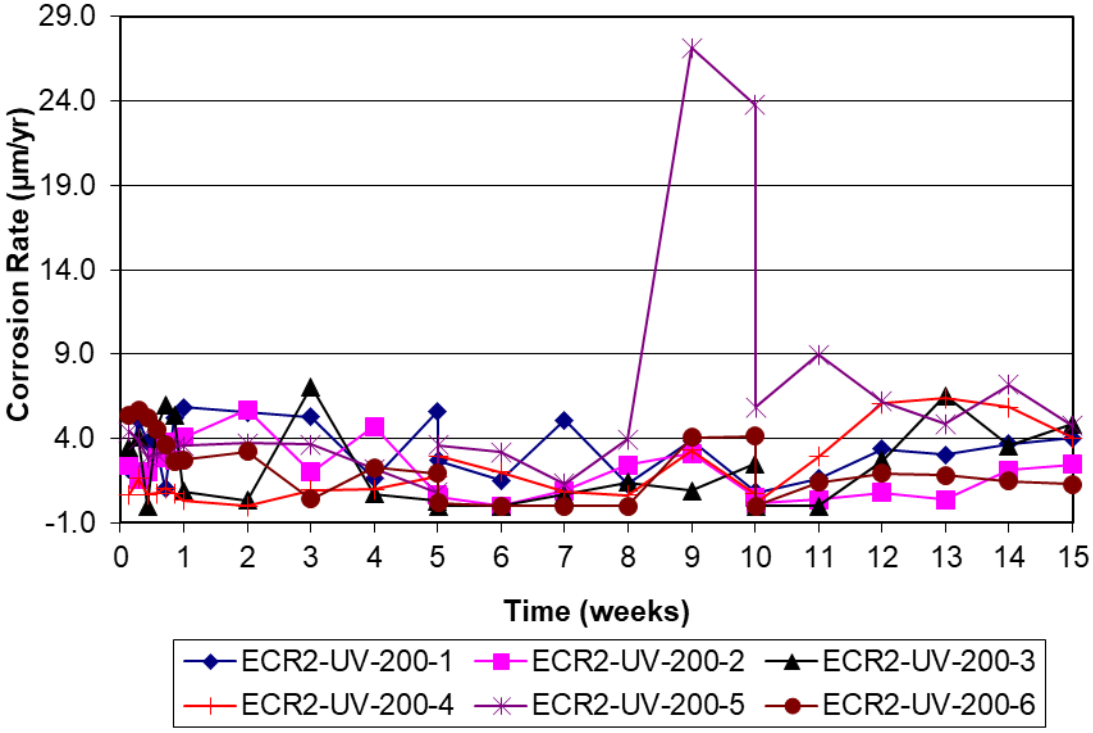

Figure C.23: Corrosion rate of ECR2-UV-200 reinforcement in the rapid macrocell test

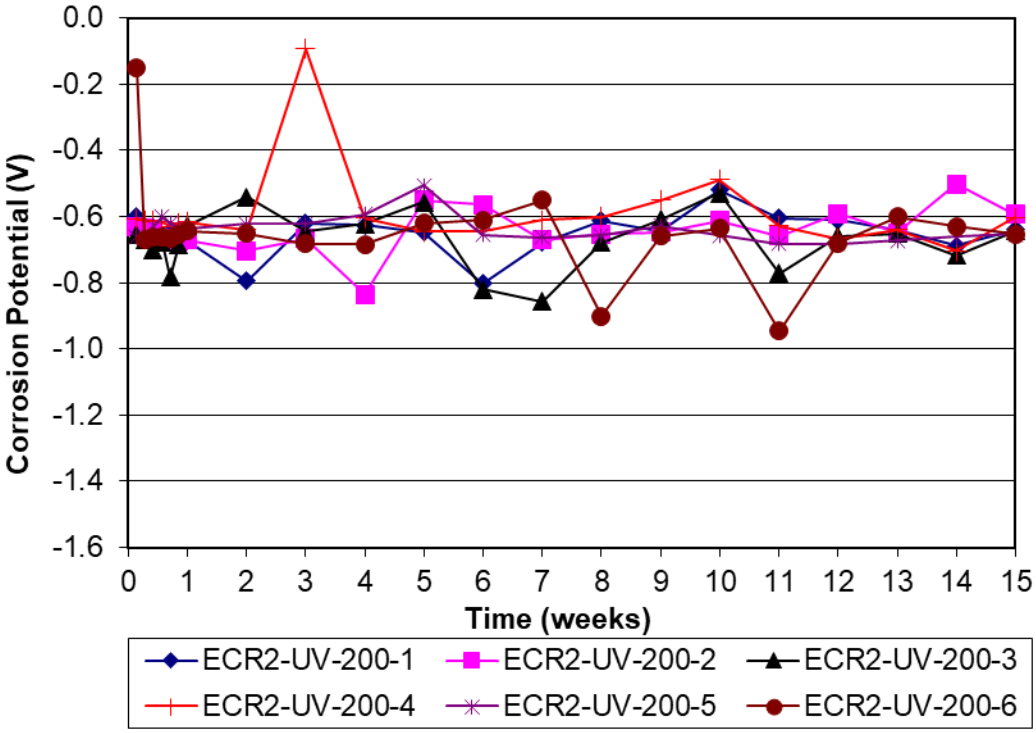

Figure C.24: Corrosion potential of ECR2-UV-200 reinforcement in the rapid macrocell test

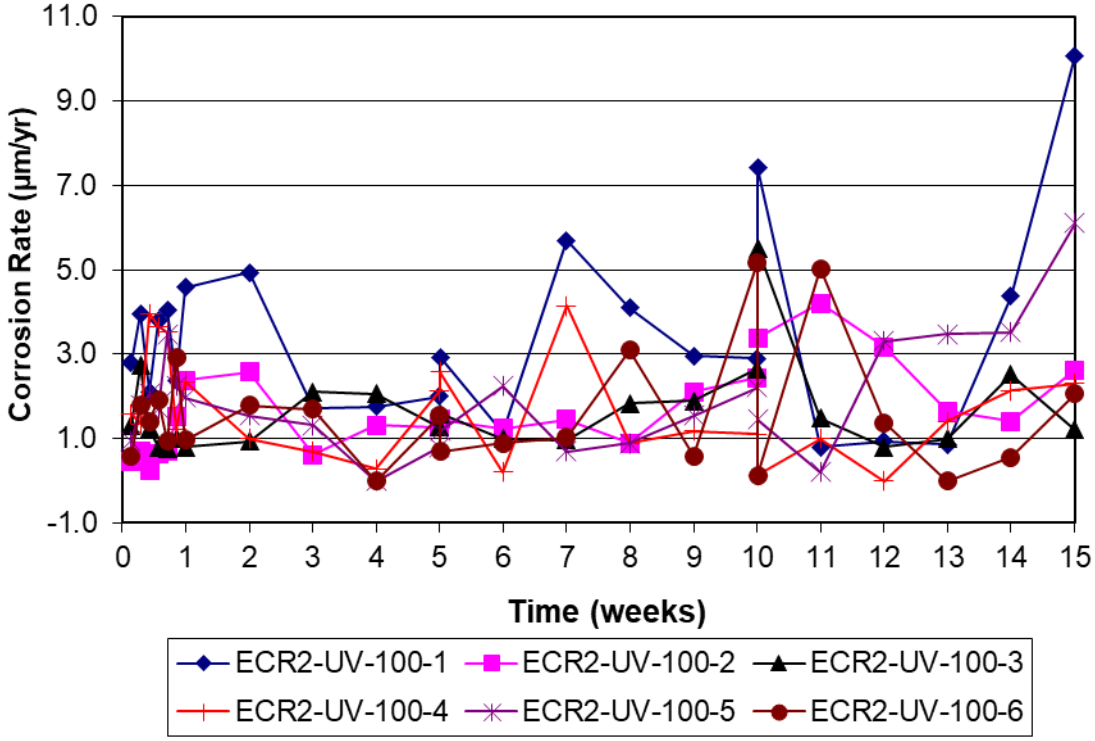

Figure C.25: Corrosion rate of ECR2-UV-100 reinforcement in the rapid macrocell test

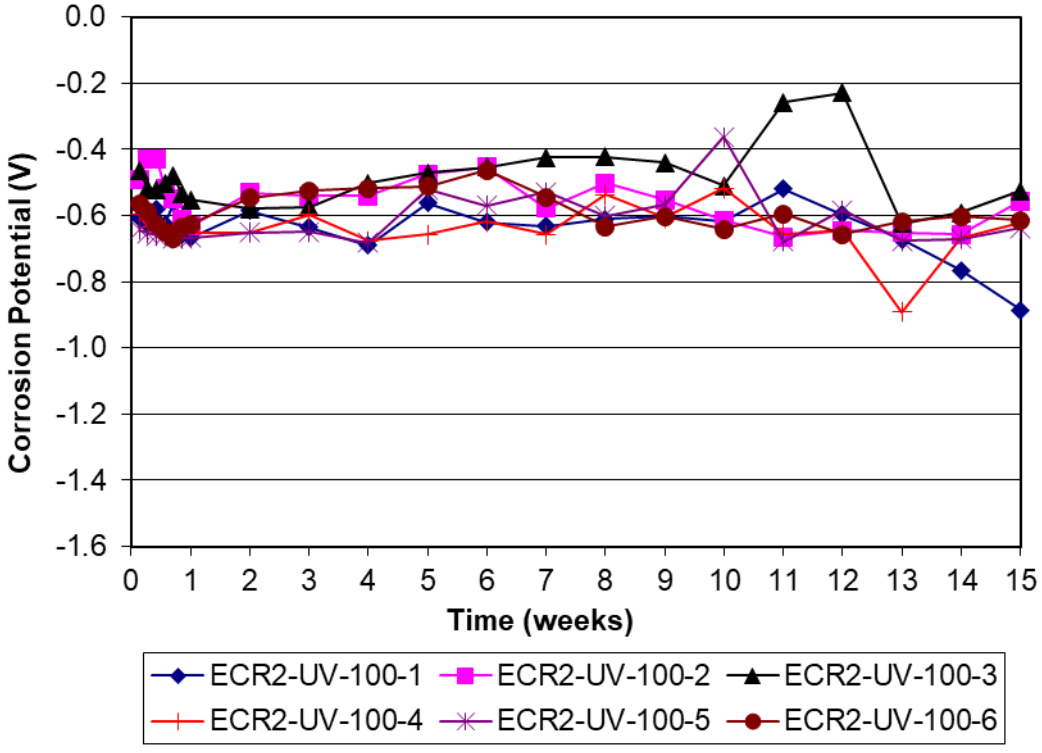

Figure C.26: Corrosion potential of ECR2-UV-100 reinforcement in the rapid macrocell test

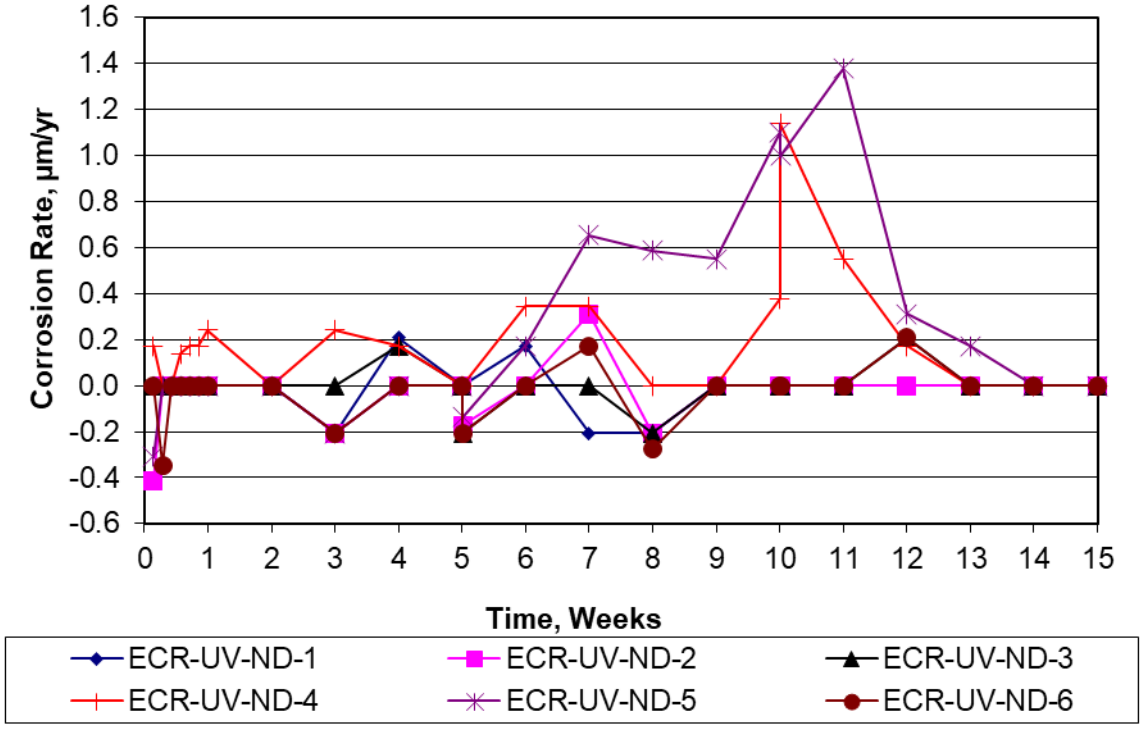

Figure C.27: Corrosion rate of ECR2-UV-ND reinforcement in the rapid macrocell test

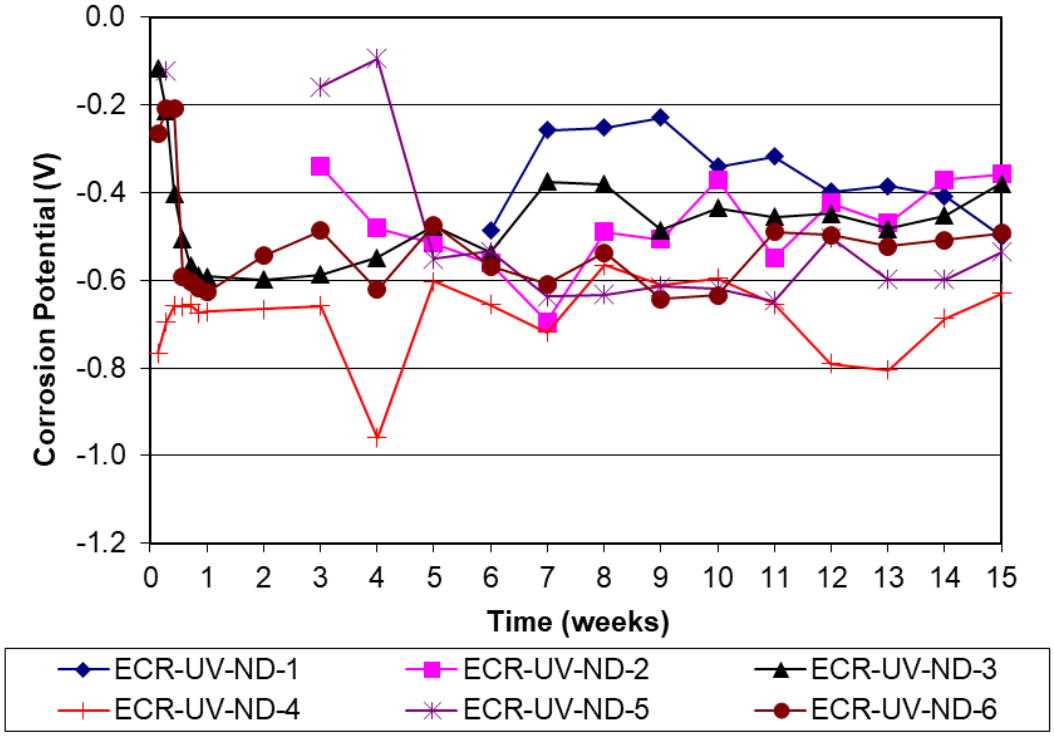

Figure C.28: Corrosion potential of ECR2-UV-ND reinforcement in the rapid macrocell test

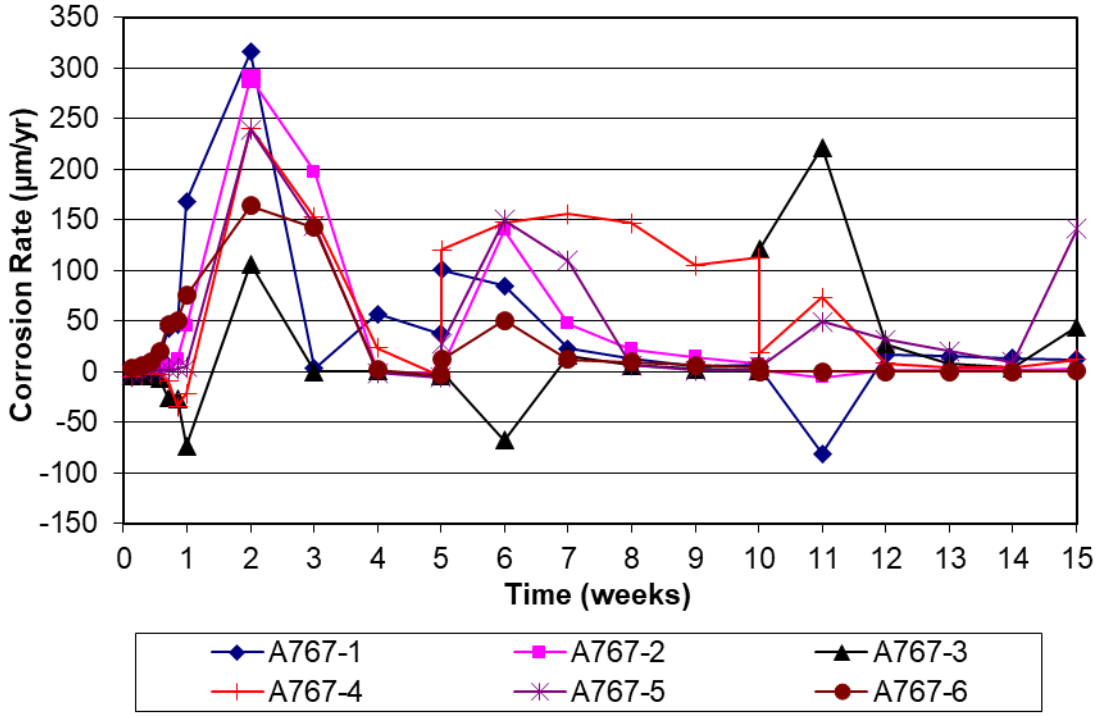

Figure C.29: Corrosion rate of A767 reinforcement in the rapid macrocell test

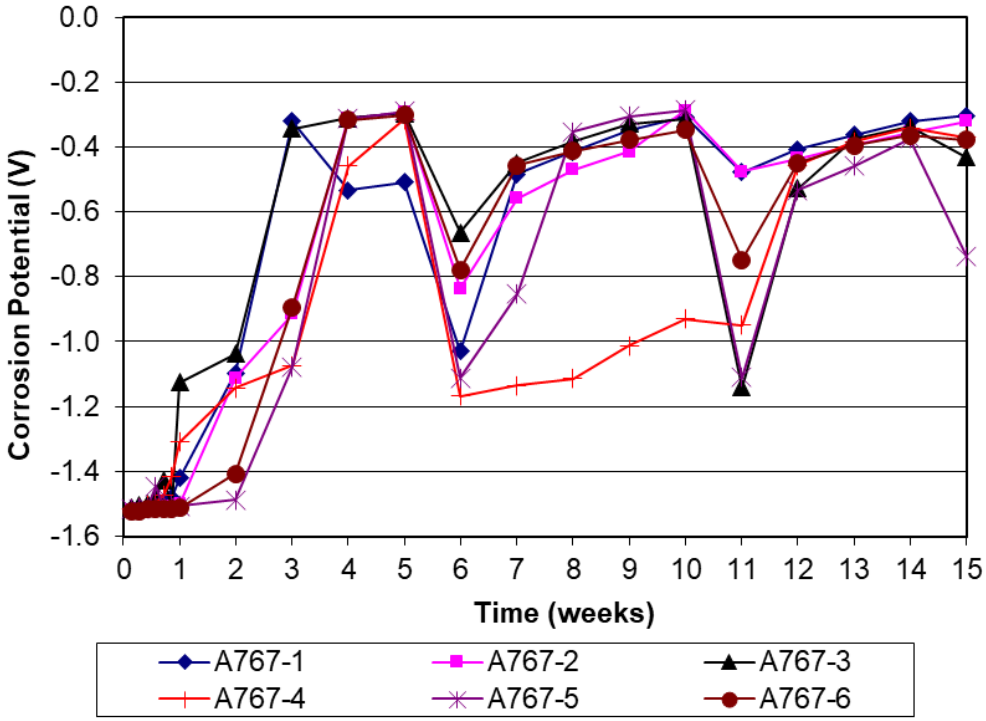

Figure C.30: Corrosion potential of A767 reinforcement in the rapid macrocell test

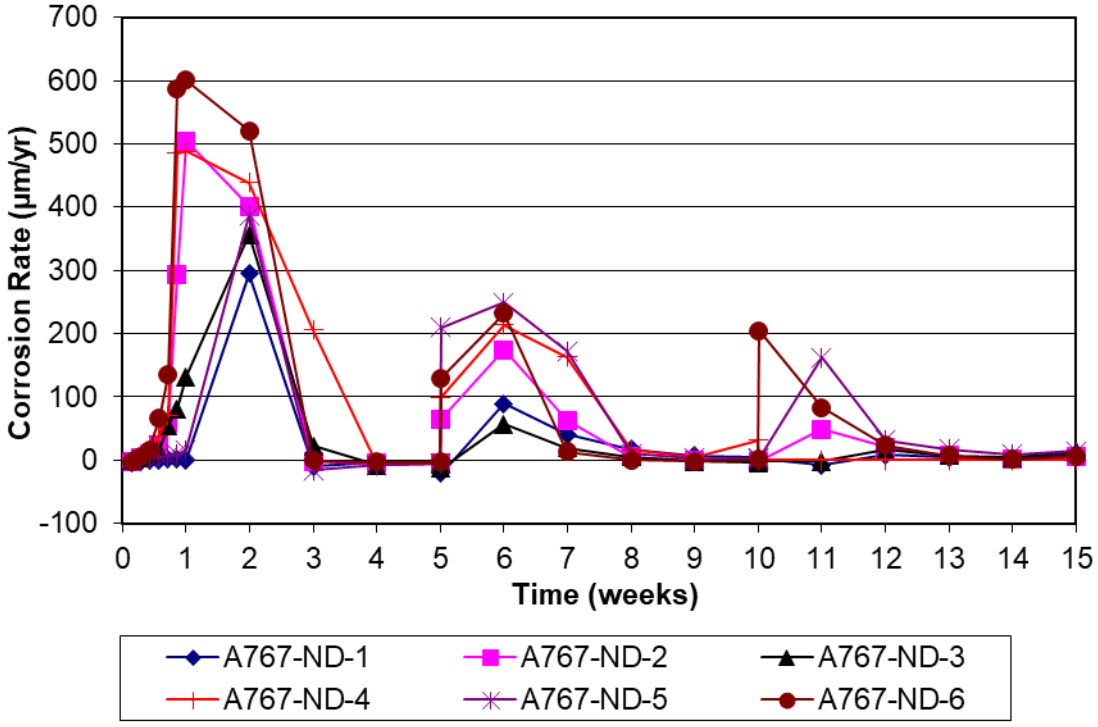

Figure C.31: Corrosion rate of A767-ND reinforcement in the rapid macrocell test

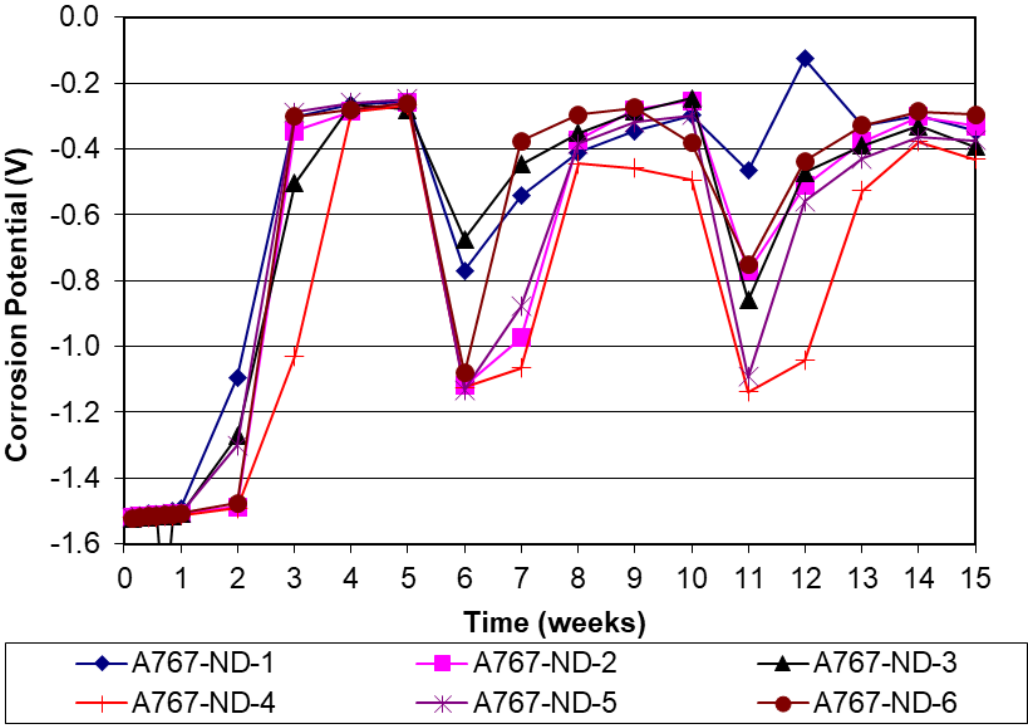

Figure C.32: Corrosion rate of A767-ND reinforcement in the rapid macrocell test

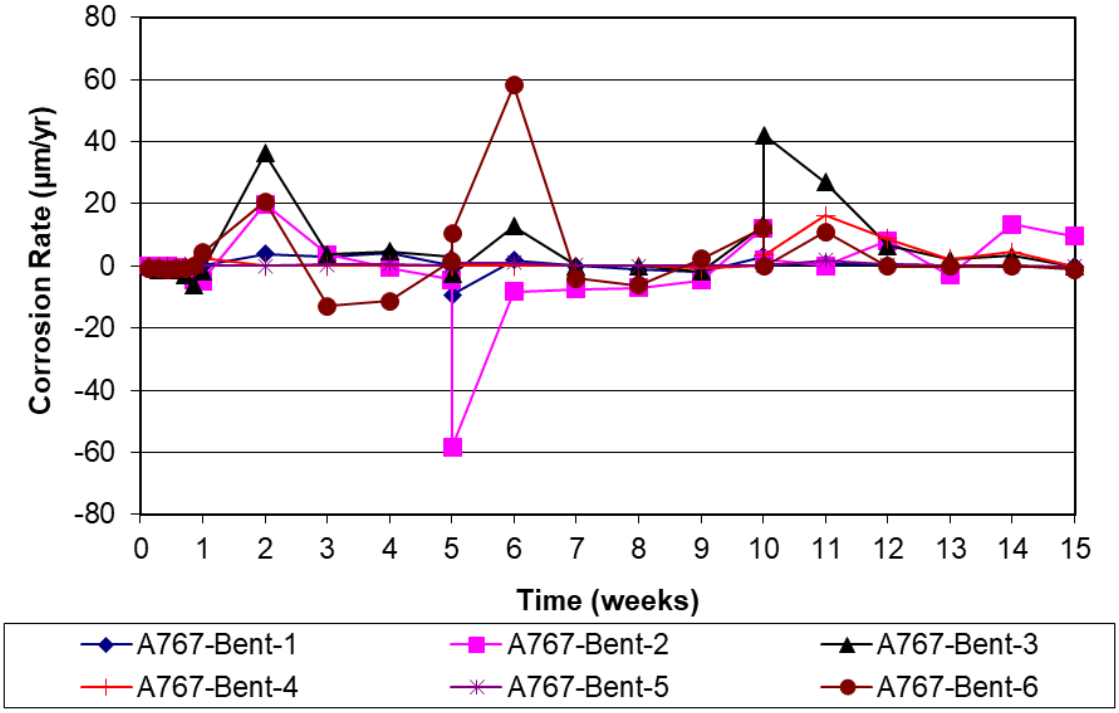

Figure C.33: Corrosion rate of A767-Bent reinforcement in the rapid macrocell test

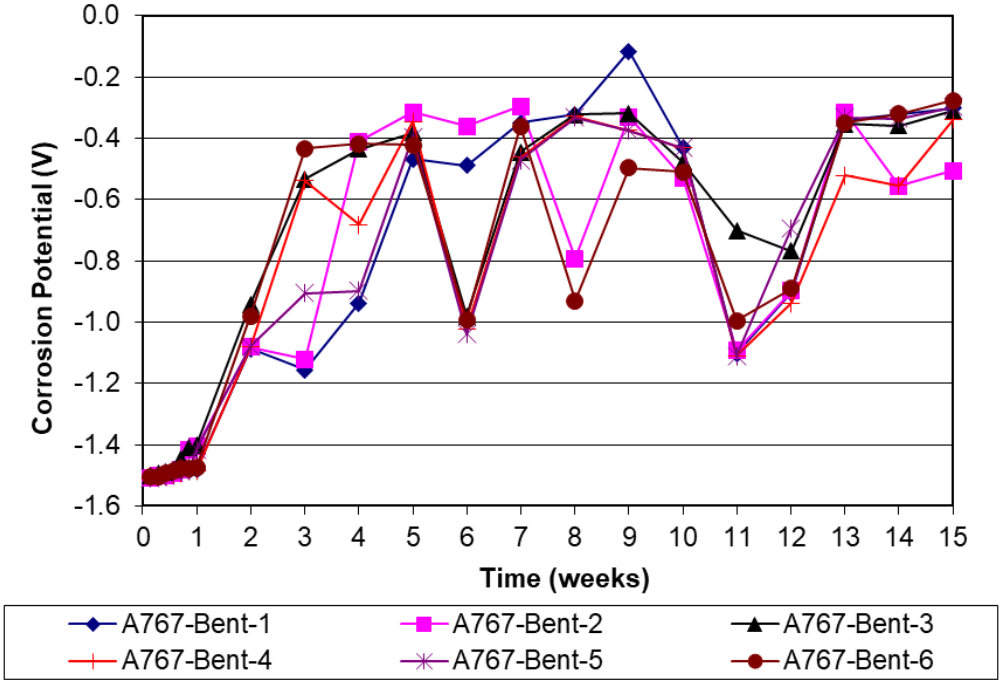

Figure C.34: Corrosion potential of A767-Bent reinforcement in the rapid macrocell test

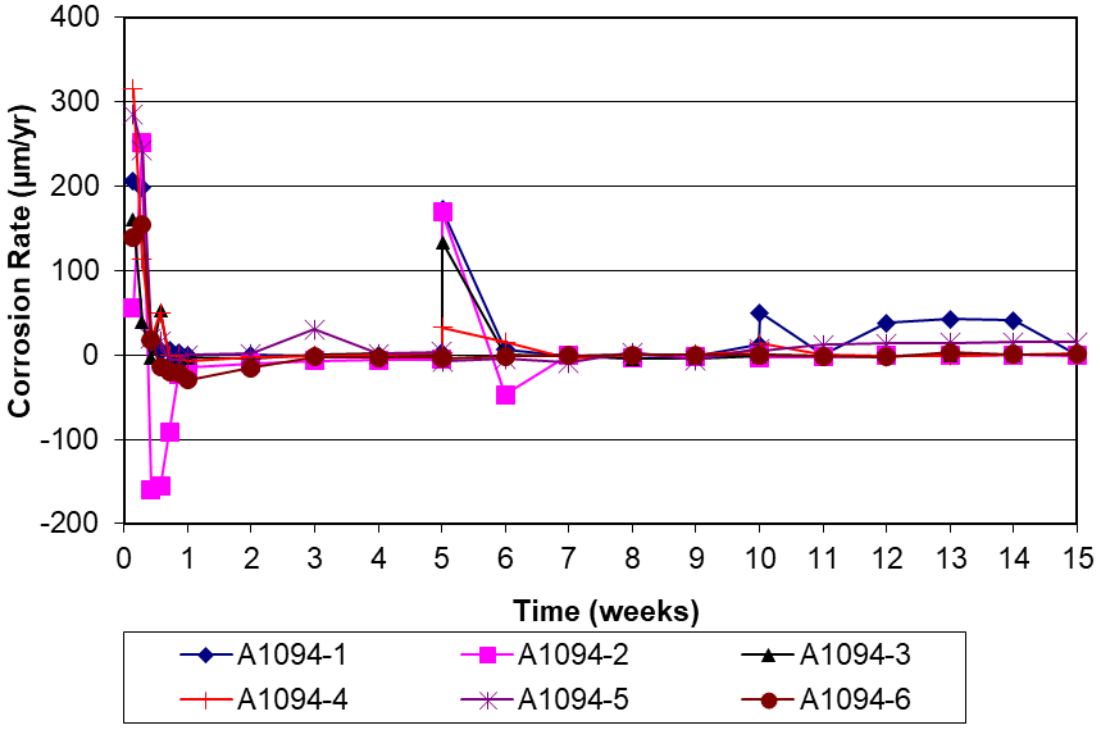

Figure C.35: Corrosion rate of A1094 reinforcement in the rapid macrocell test

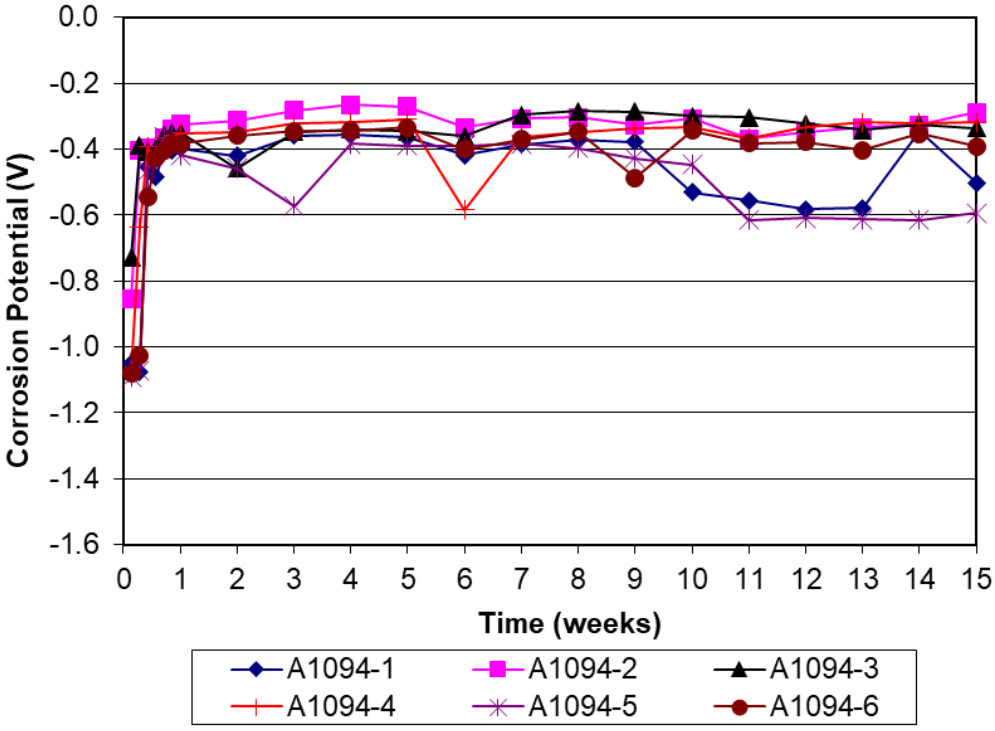

Figure C.36: Corrosion potential of A1094 reinforcement in the rapid macrocell test

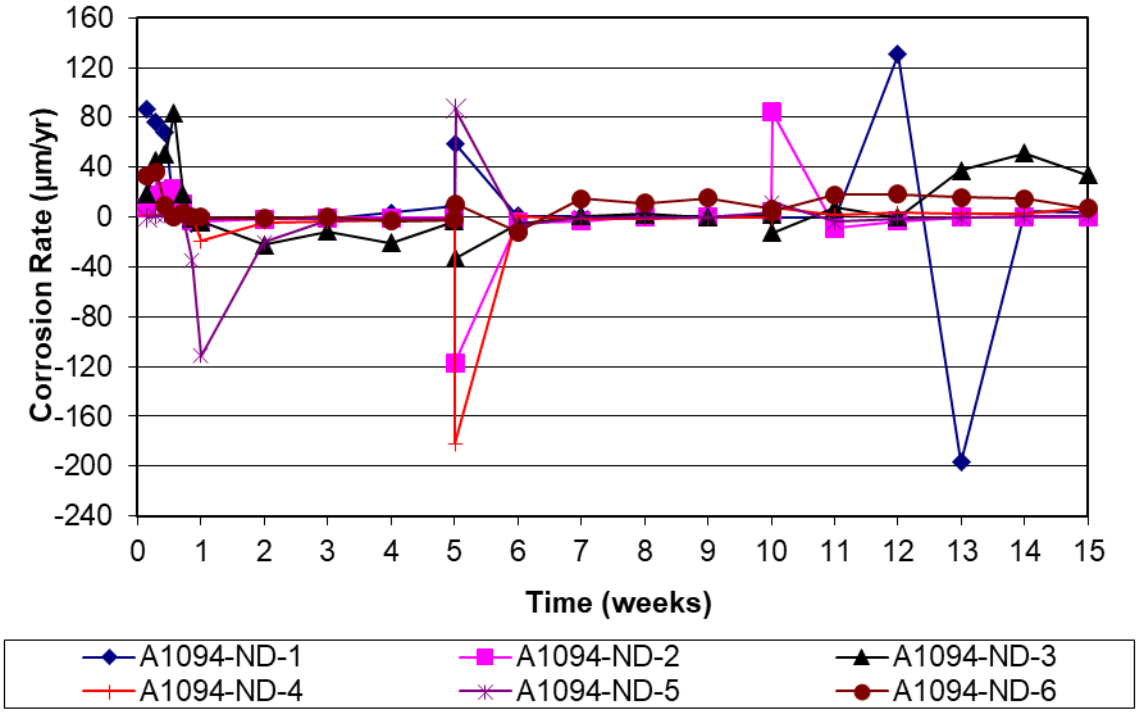

Figure C.37: Corrosion rate of A1094-ND reinforcement in the rapid macrocell test

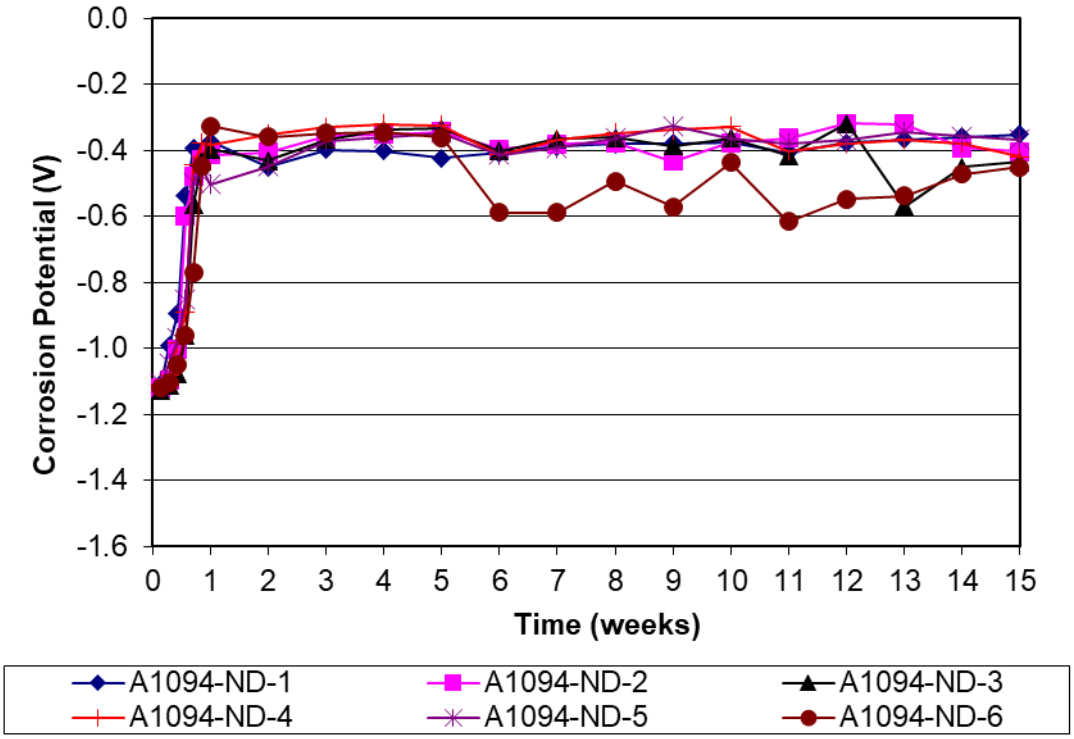

Figure C.38: Corrosion potential of A1094-ND reinforcement in the rapid macrocell test

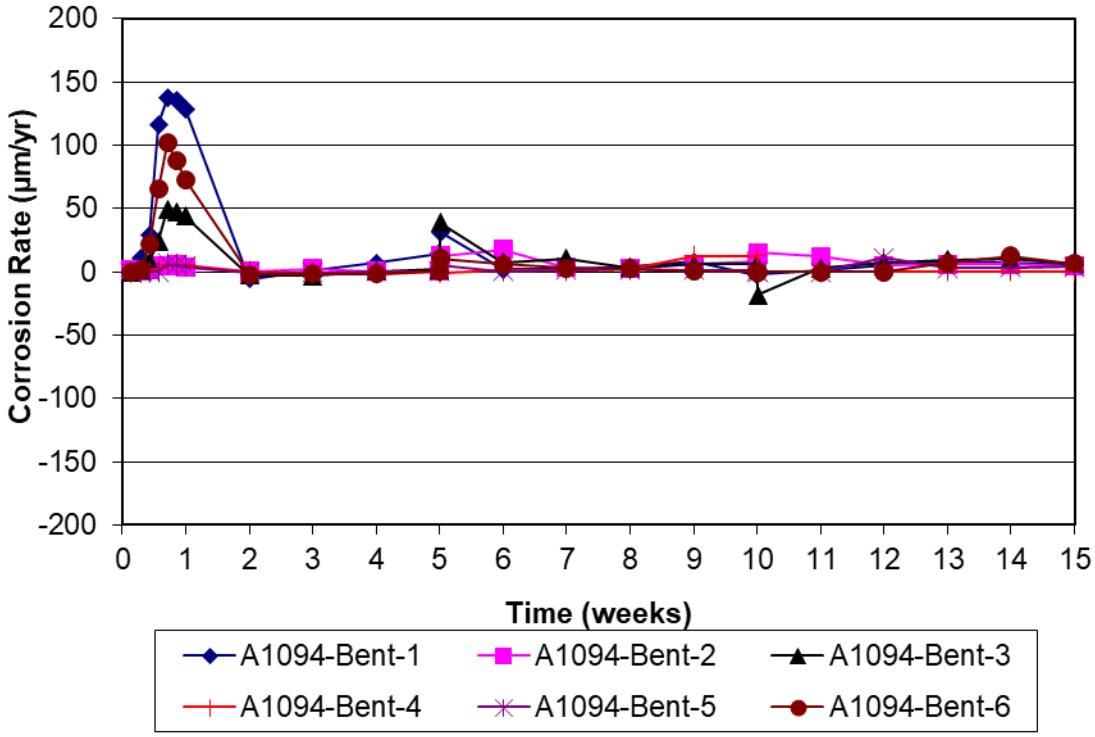

Figure C.39: Corrosion rate of A1094-Bent reinforcement in the rapid macrocell test

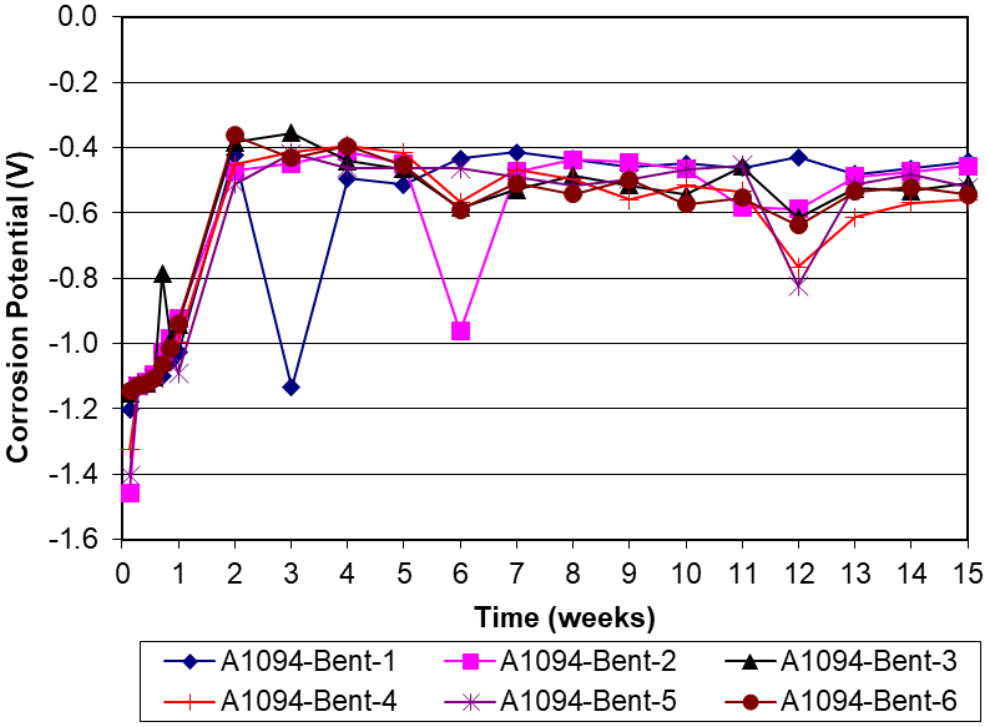

Figure C.40: Corrosion rate of A1094-Bent reinforcement in the rapid macrocell test

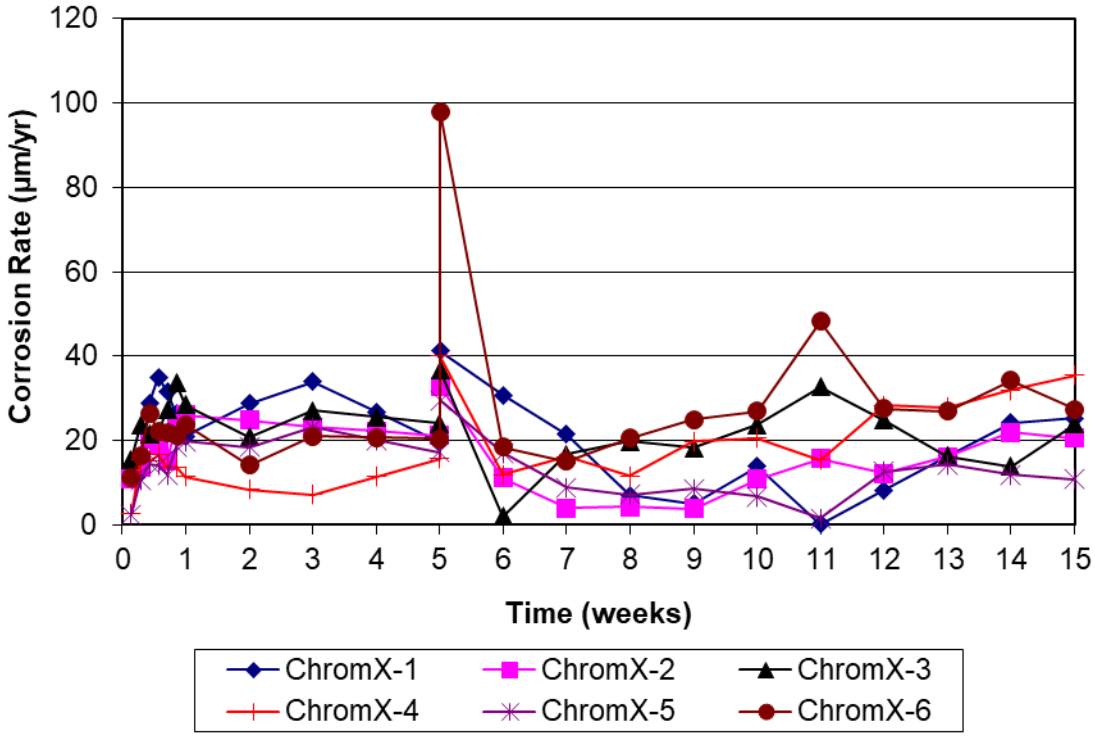

Figure C.41: Corrosion rate of ChromX reinforcement in the rapid macrocell test

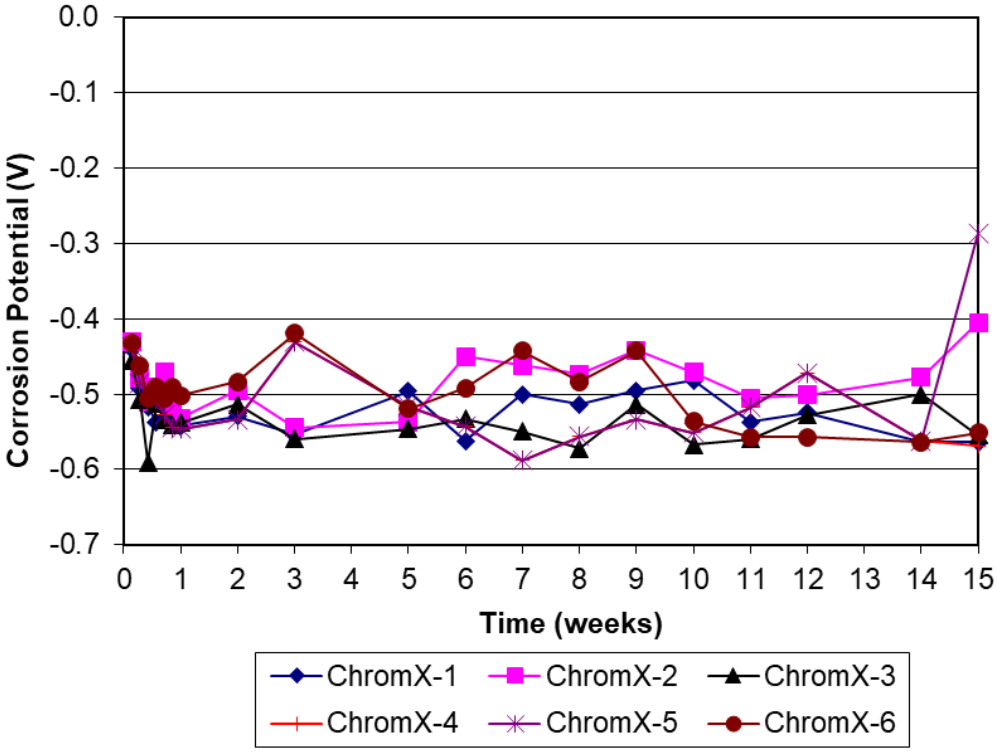

Figure C.42: Corrosion potential of ChromX reinforcement in the rapid macrocell test

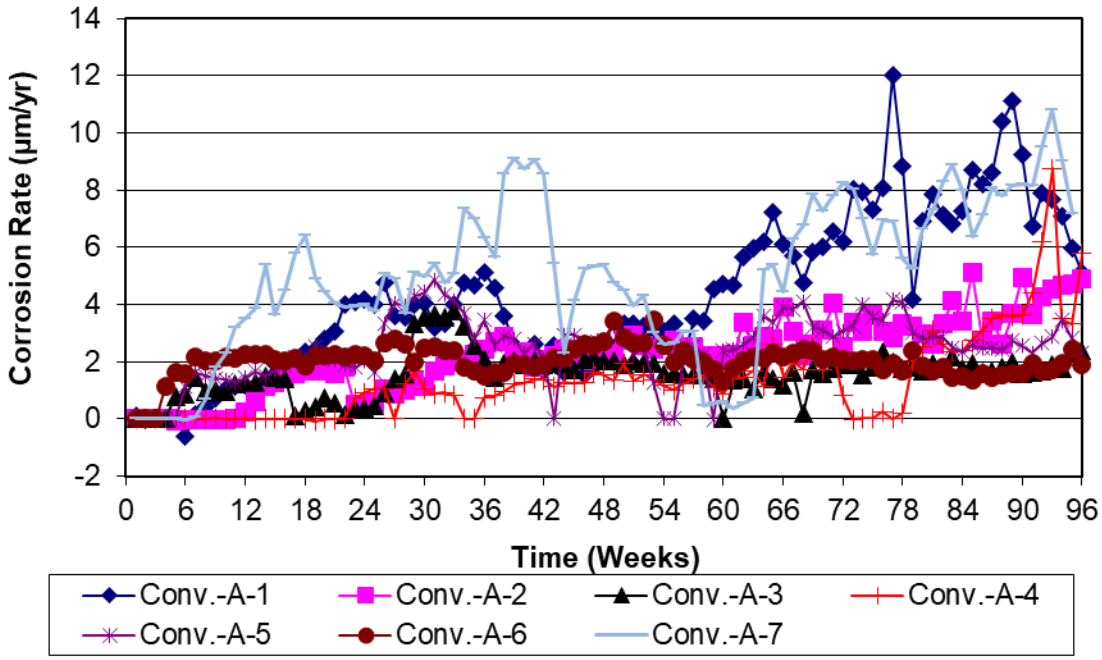

Figure C.43: Corrosion rate of Conv-A reinforcement in the Southern Exposure test

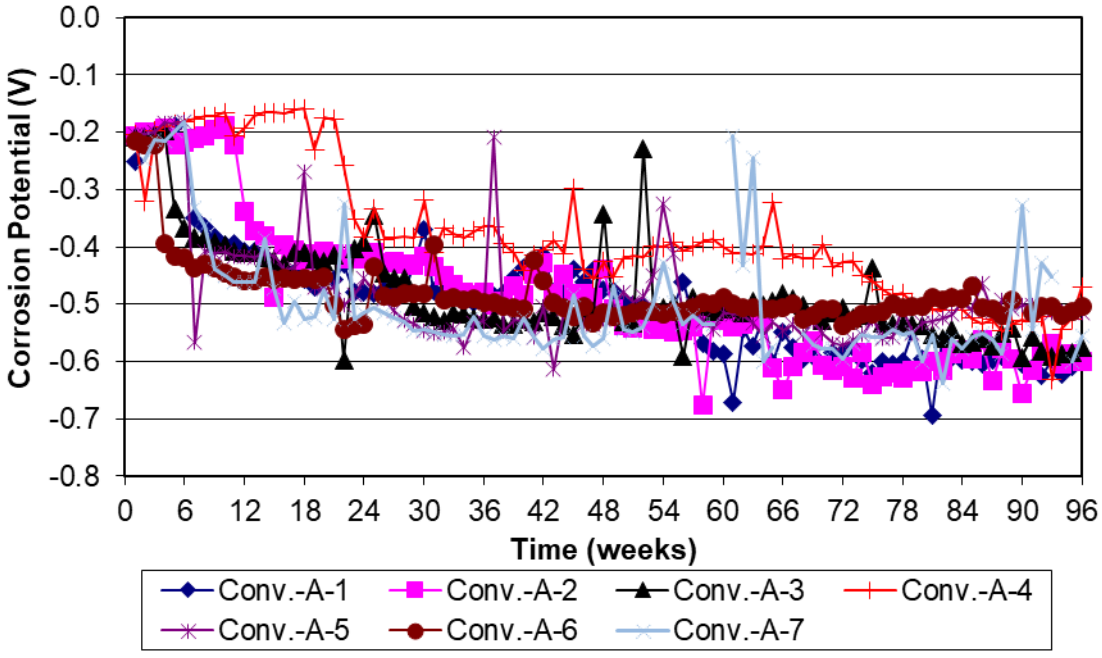

Figure C.44: Corrosion potential of Conv-A reinforcement in the Southern Exposure test

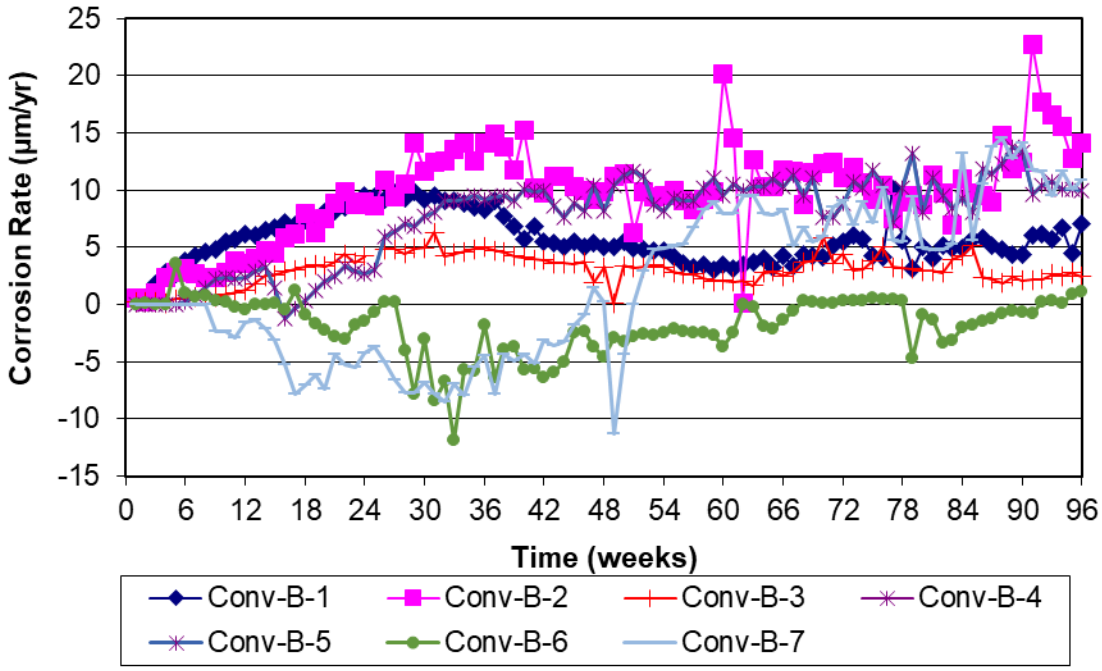

Figure C.45: Corrosion rate of Conv-B reinforcement in the Southern Exposure test

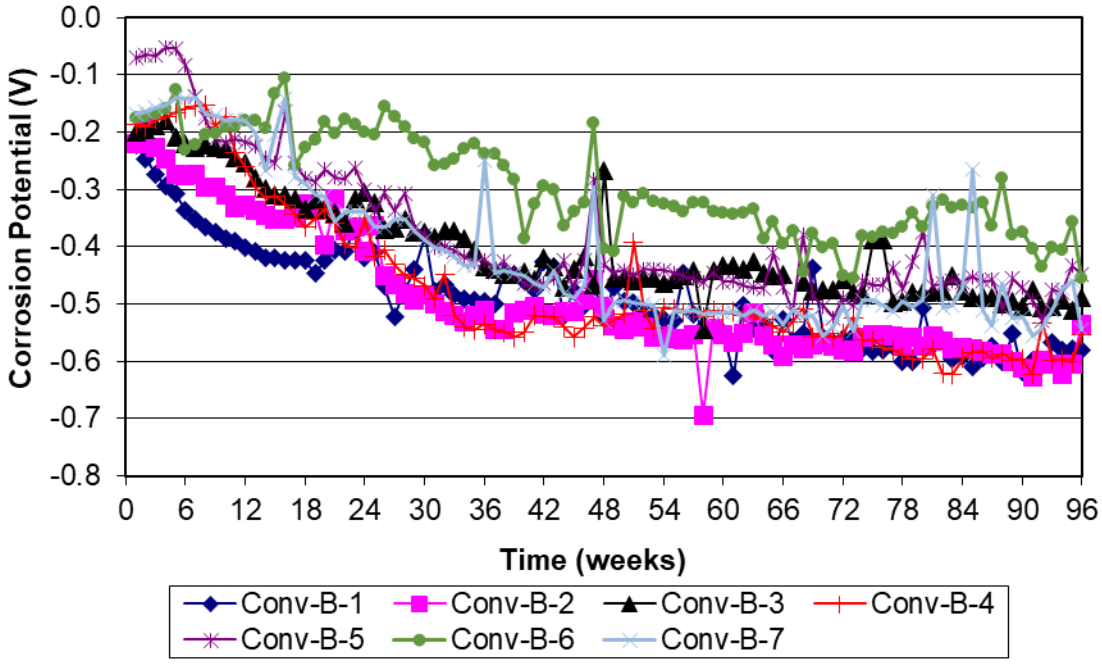

Figure C.46: Corrosion potential of Conv-B reinforcement in the Southern Exposure test

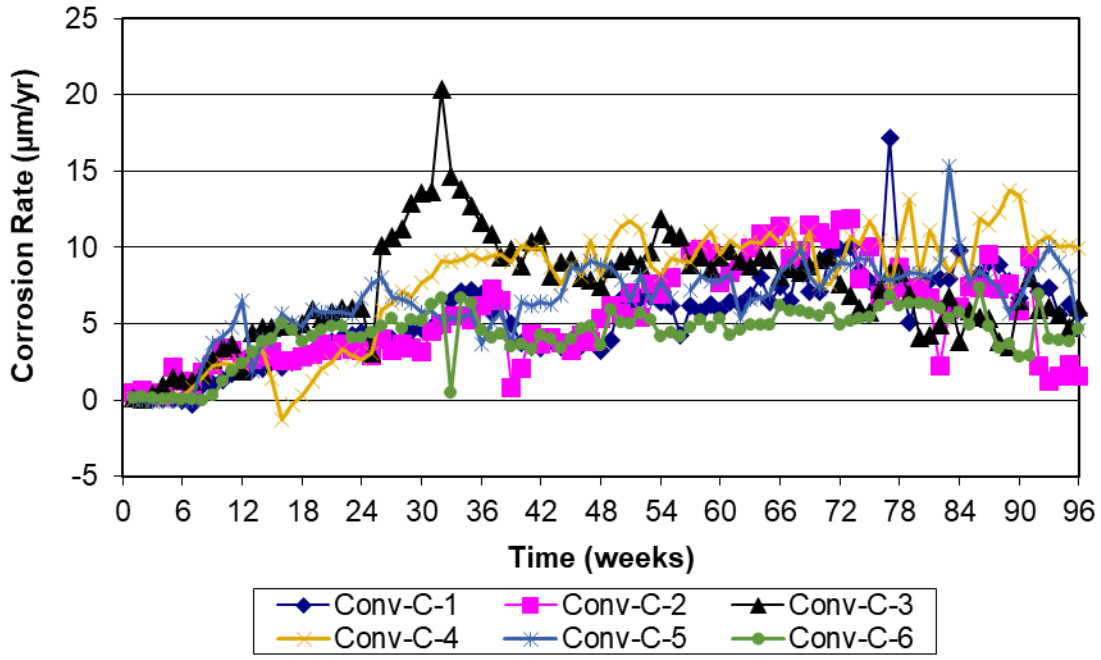

Figure C.47: Corrosion rate of Conv-C reinforcement in the Southern Exposure test

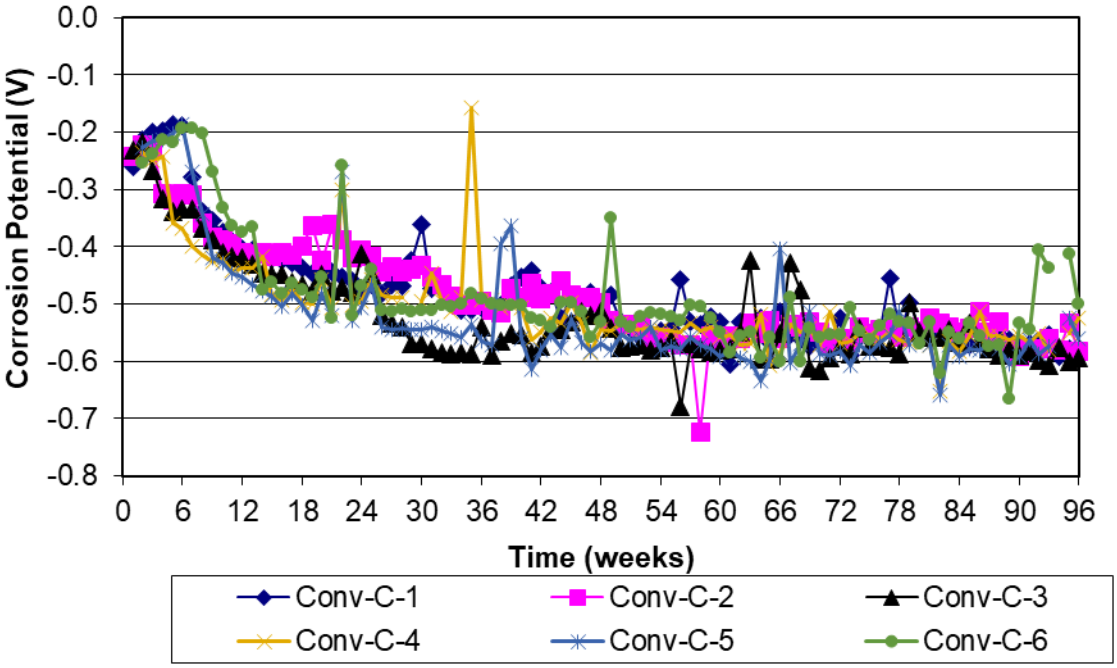

Figure C.48: Corrosion potential of Conv-C reinforcement in the Southern Exposure test

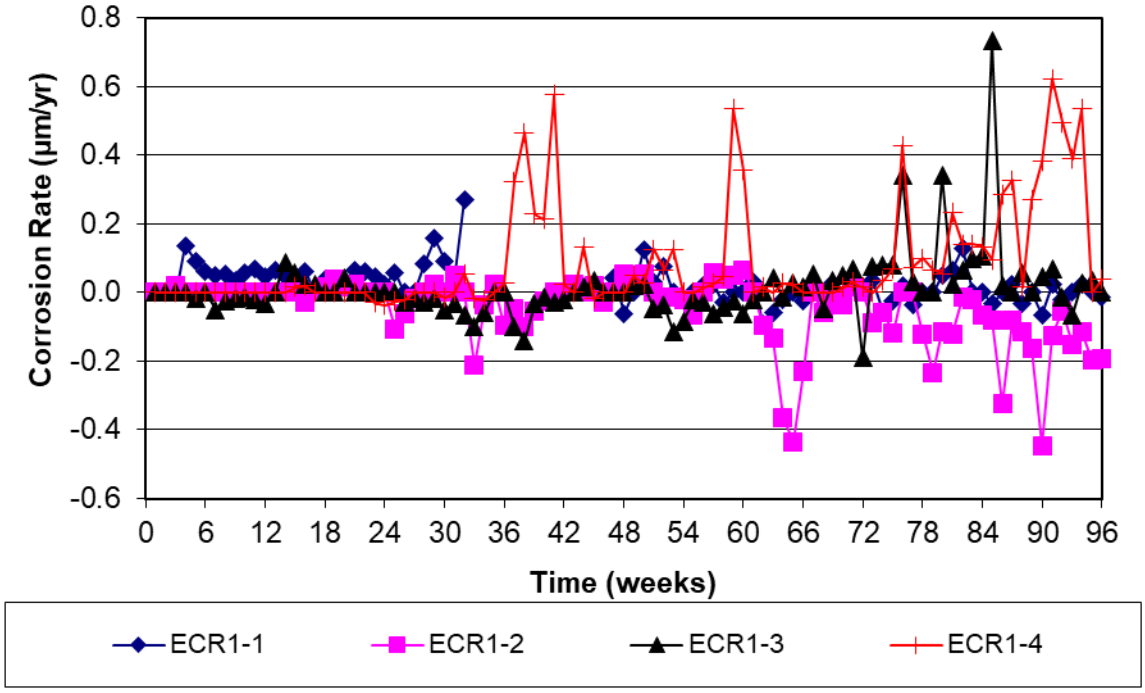

Figure C.49: Corrosion rate of ECR1 reinforcement in the Southern Exposure test

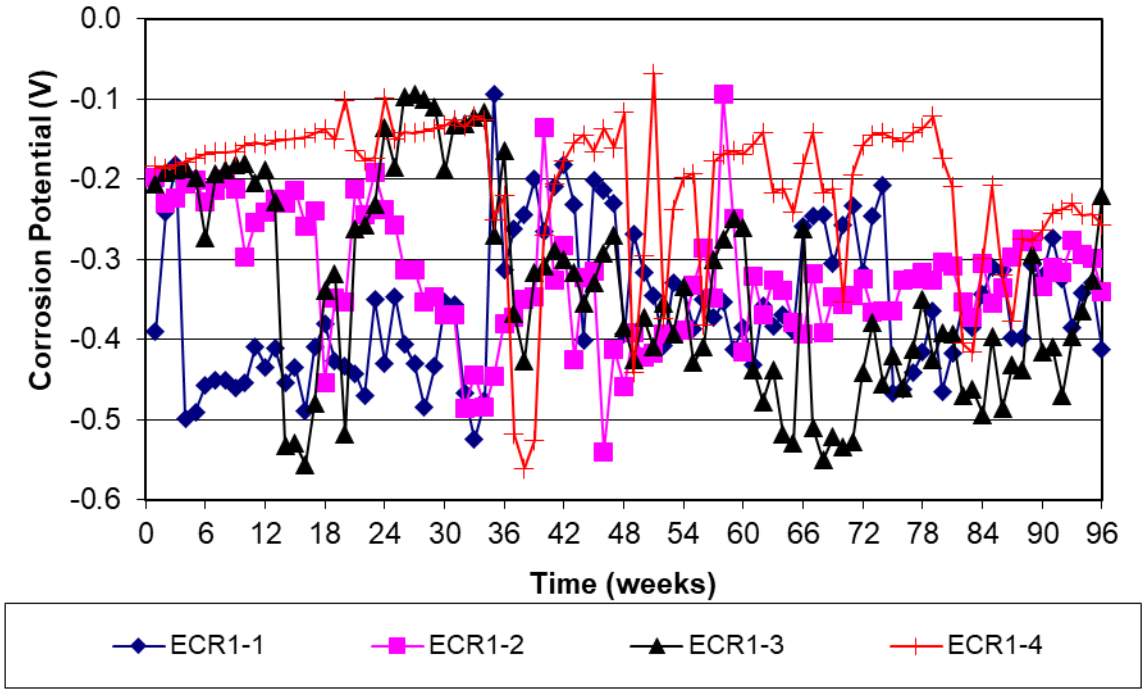

Figure C.50: Corrosion rate of ECR1 reinforcement in the Southern Exposure test

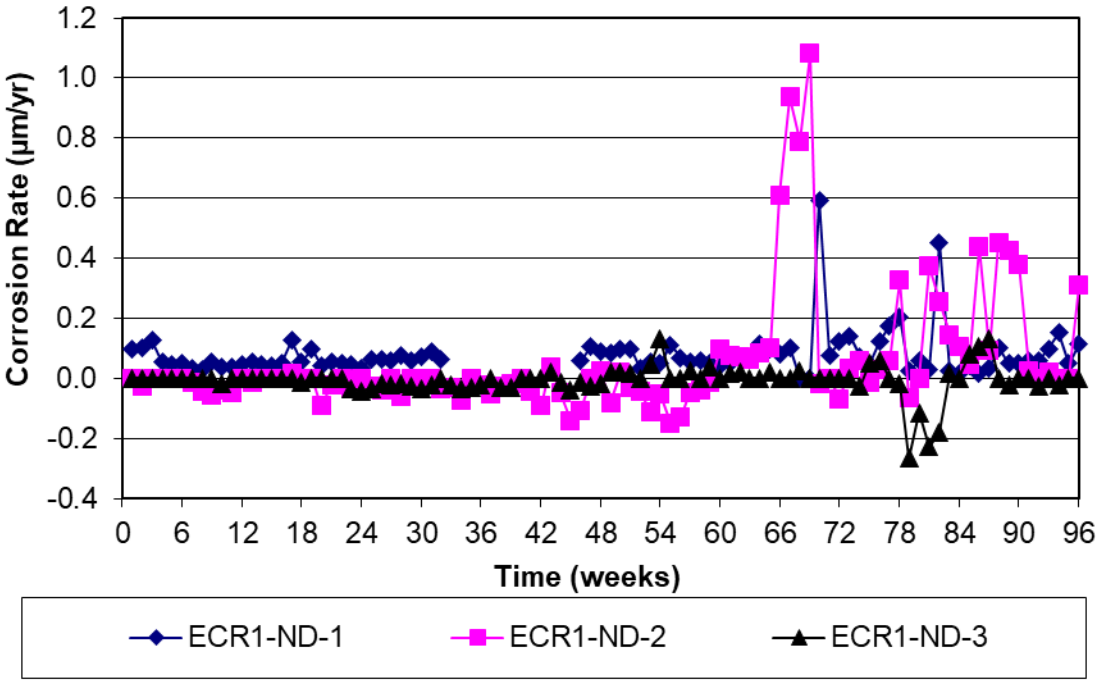

Figure C.51: Corrosion rate of ECR1-ND reinforcement in the Southern Exposure test

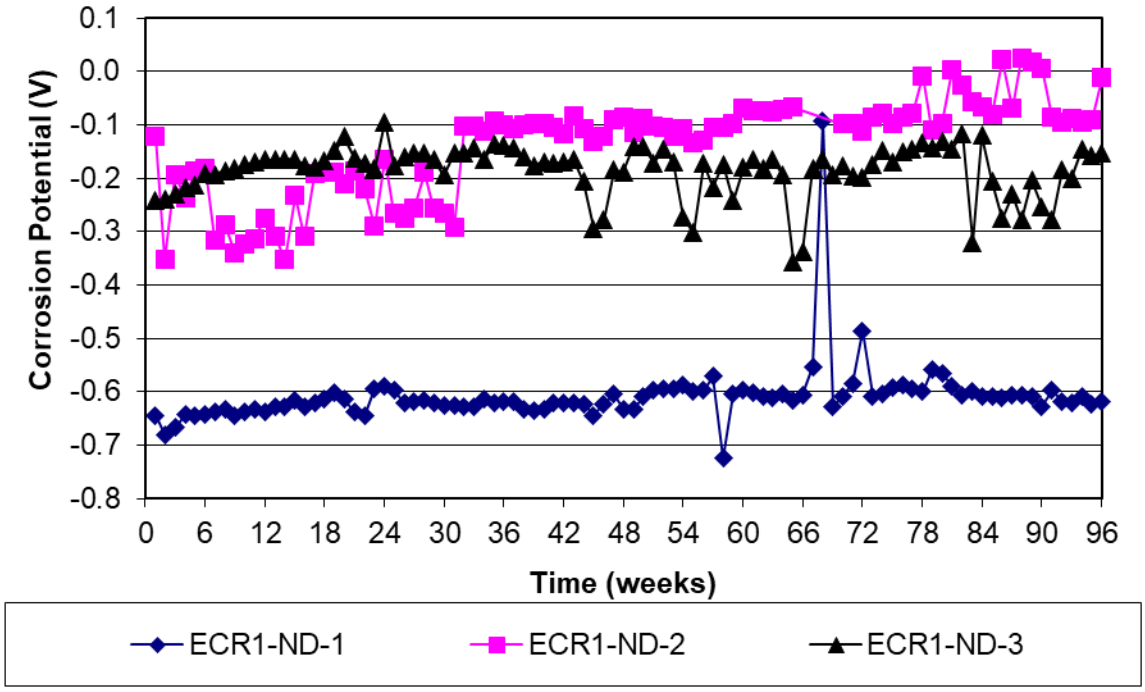

Figure C.52: Corrosion potential of ECR1-ND reinforcement in the Southern Exposure test

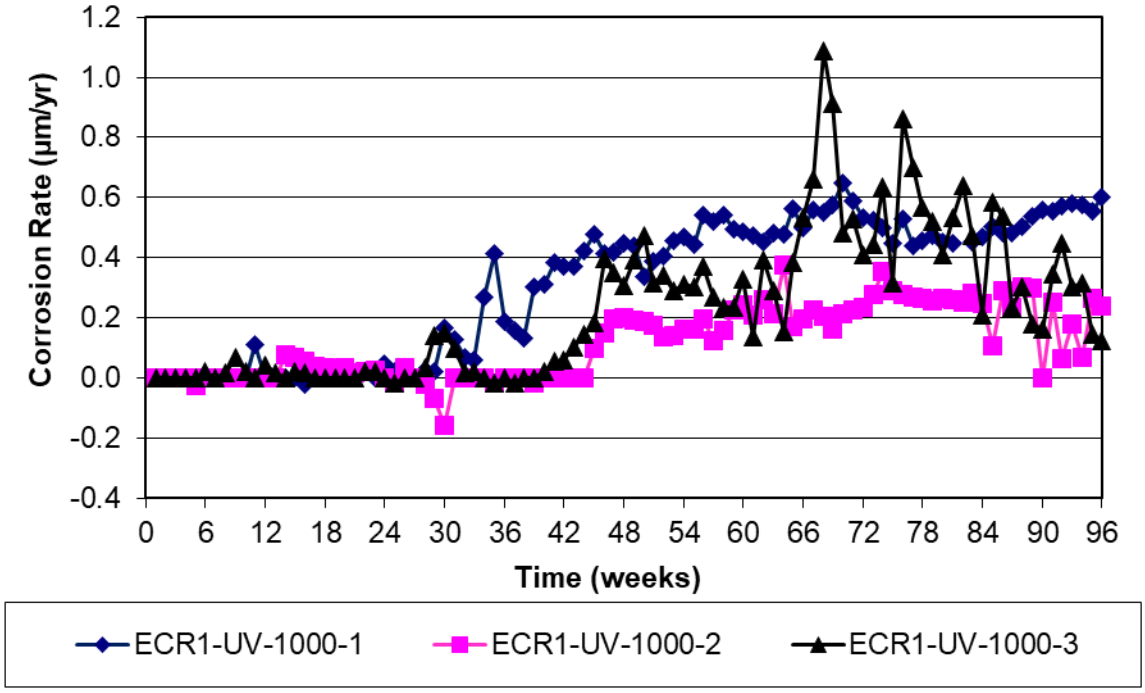

Figure C.53: Corrosion rate of ECR1-UV-1000 reinforcement in the Southern Exposure test

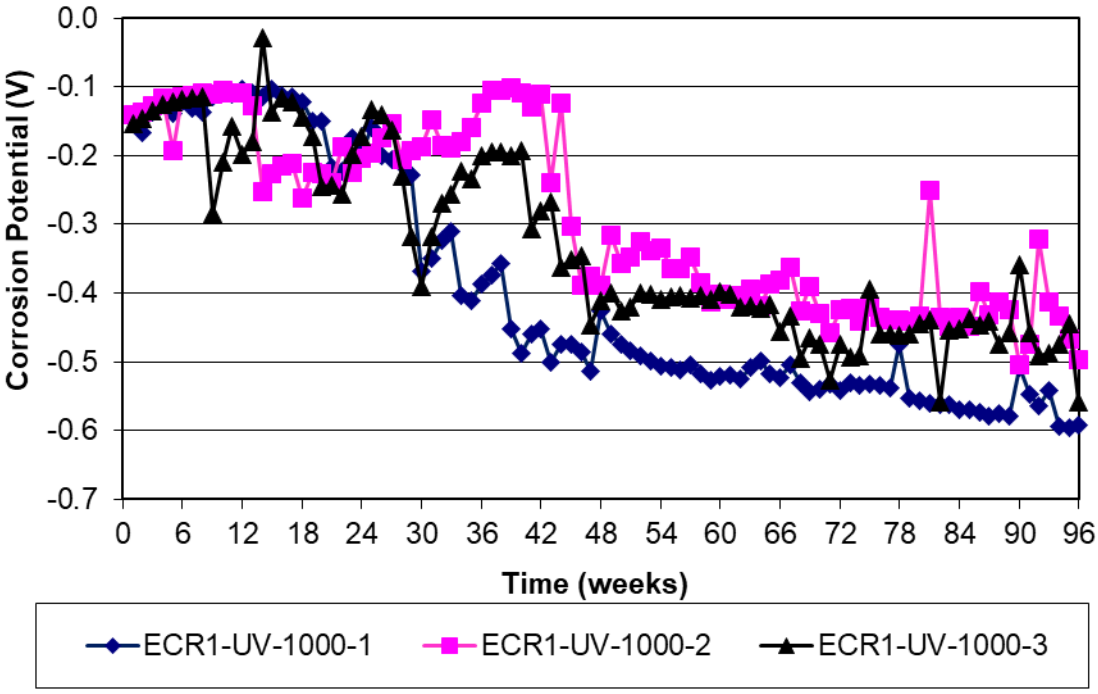

Figure C.54: Corrosion rate of ECR1-UV-1000 reinforcement in the Southern Exposure test

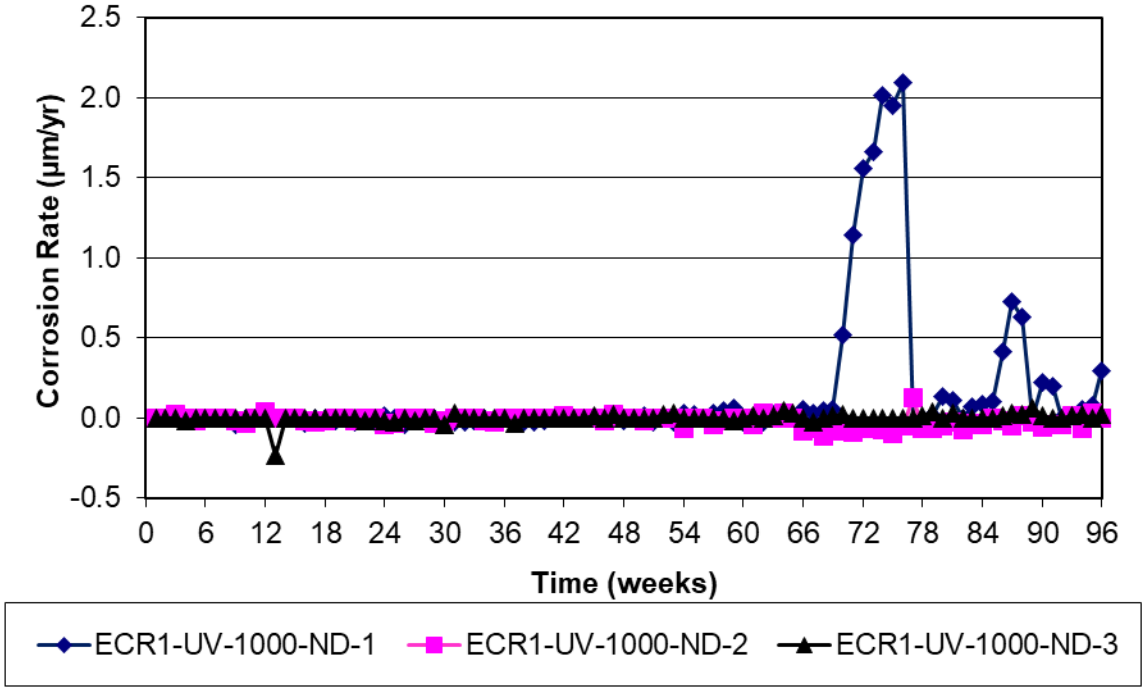

Figure C.55: Corrosion rate of ECR1-UV-ND-1000 reinforcement in the Southern Exposure test

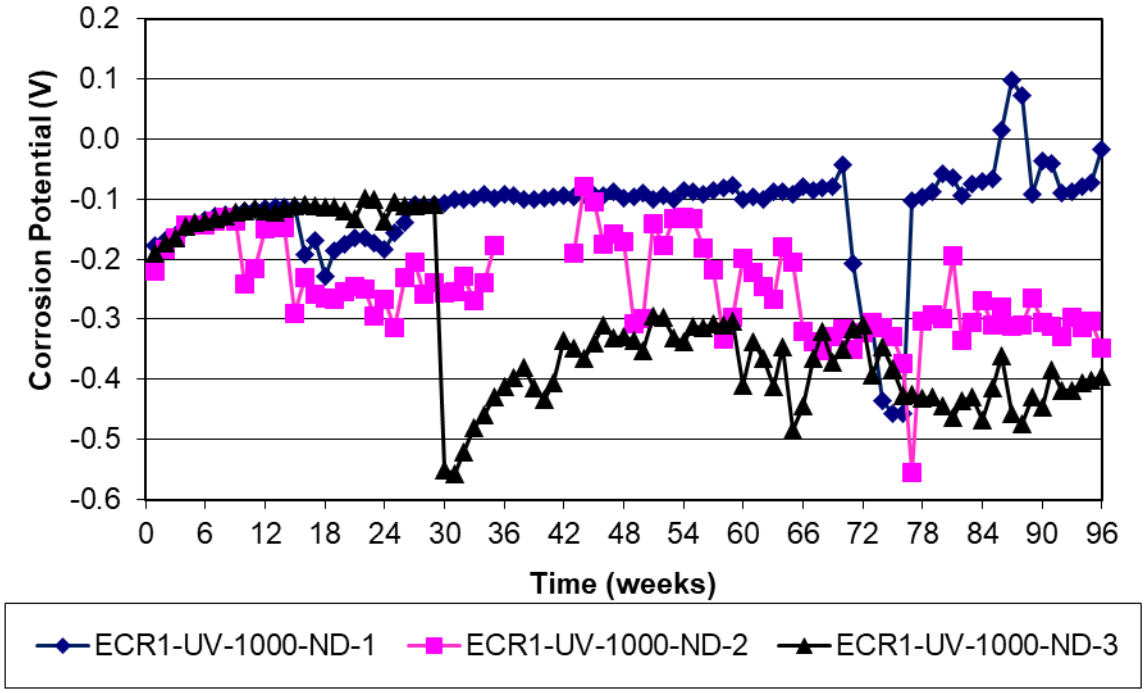

Figure C.56: Corrosion potential of ECR1-UV-ND-1000 reinforcement in the Southern Exposure test

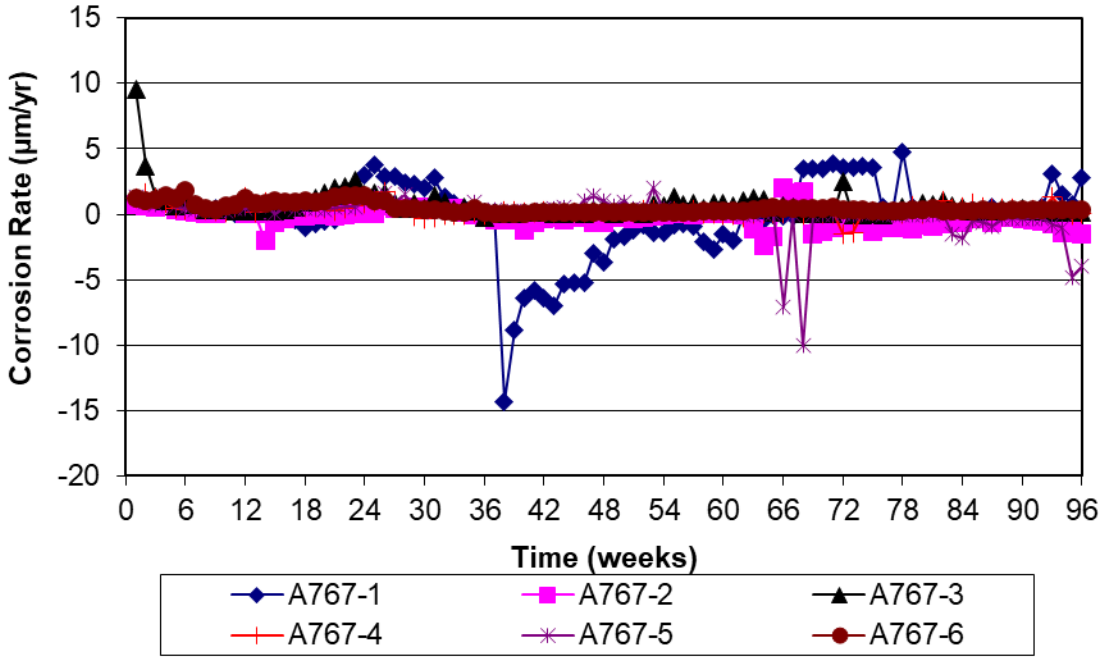

Figure C.57: Corrosion rate of A767 reinforcement in the Southern Exposure test

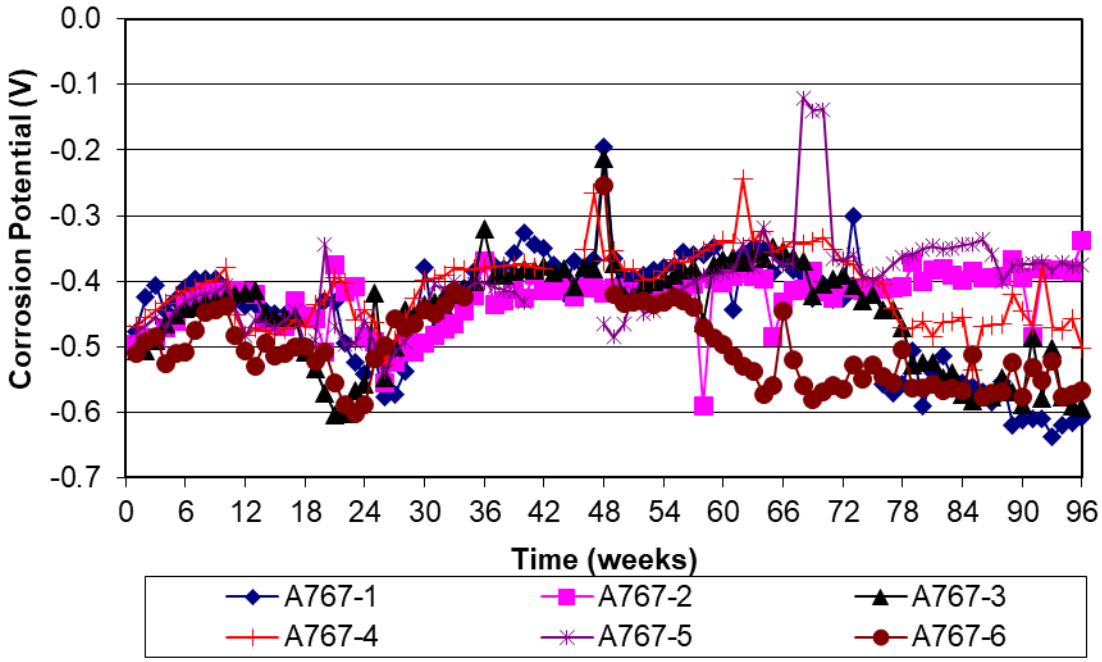

Figure C.58: Corrosion potential of A767 reinforcement in the Southern Exposure test

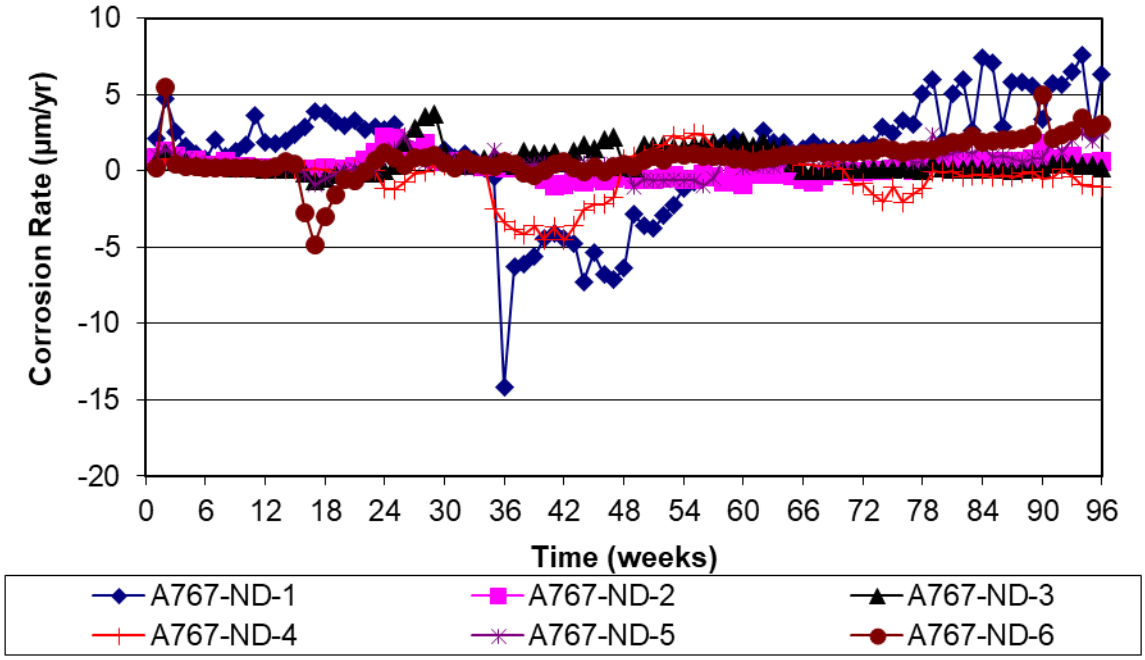

Figure C.59: Corrosion rate of A767-ND reinforcement in the Southern Exposure test

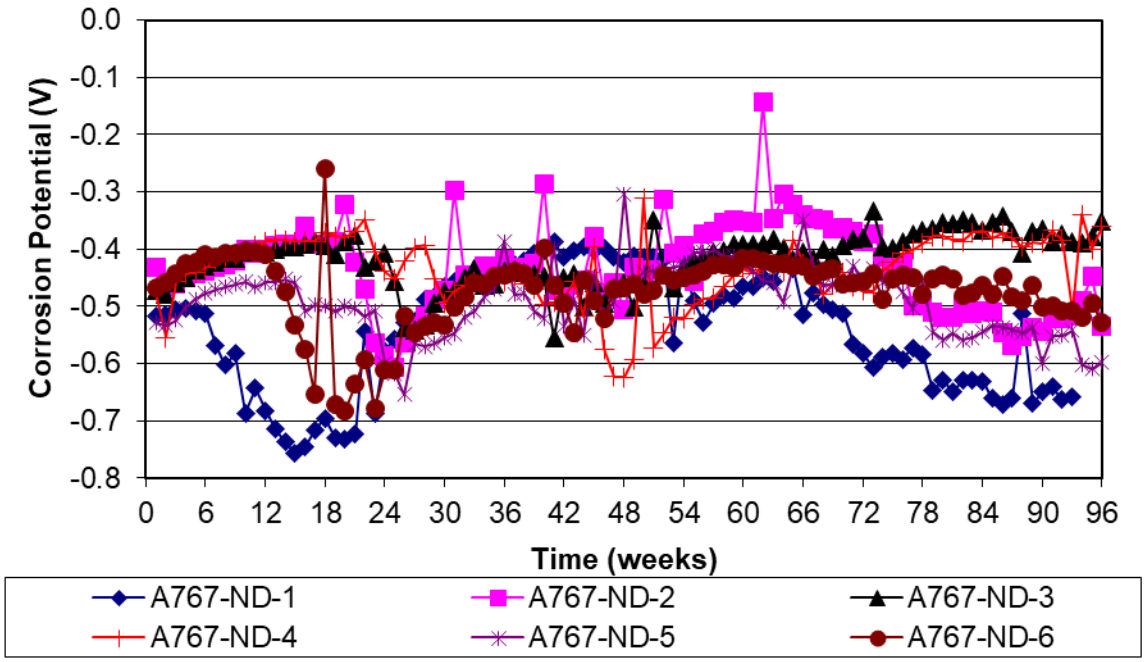

Figure C.60: Corrosion potential of A767-ND reinforcement in the Southern Exposure test

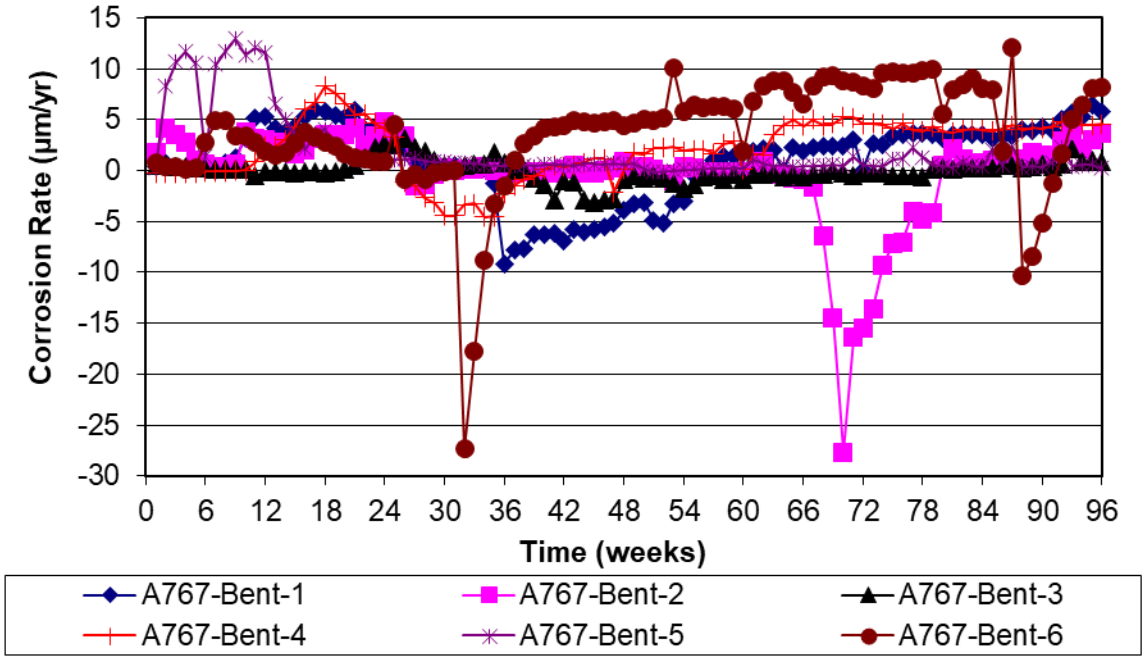

Figure C.61: Corrosion rate of A767-Bent reinforcement in the Southern Exposure test

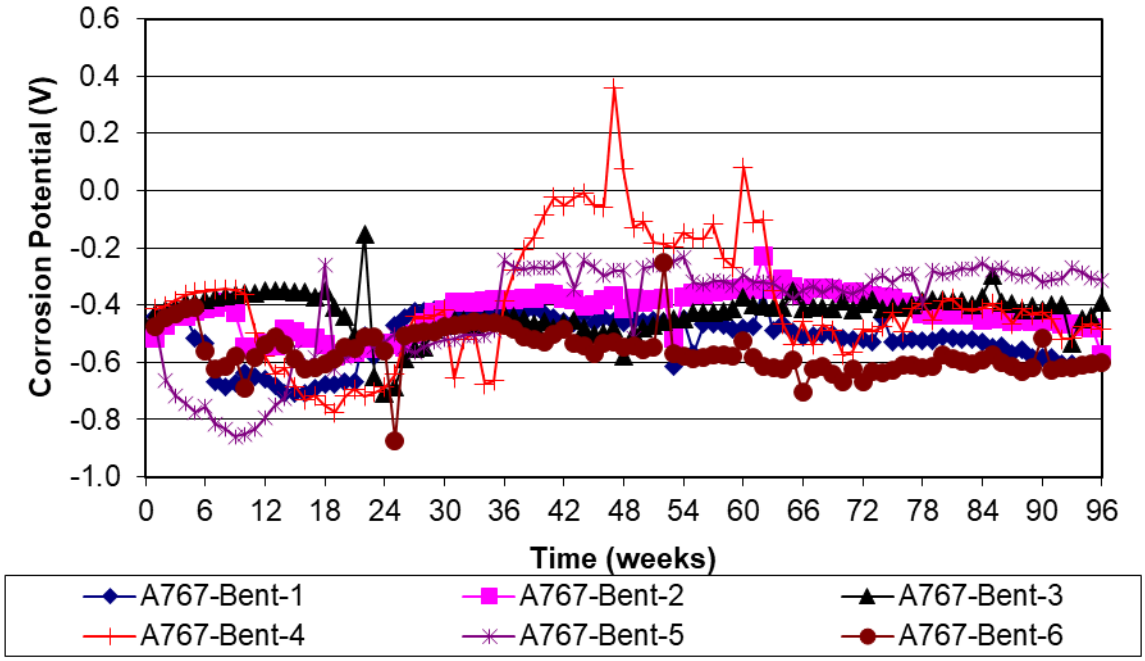

Figure C.62: Corrosion potential of A767-Bent reinforcement in the Southern Exposure test

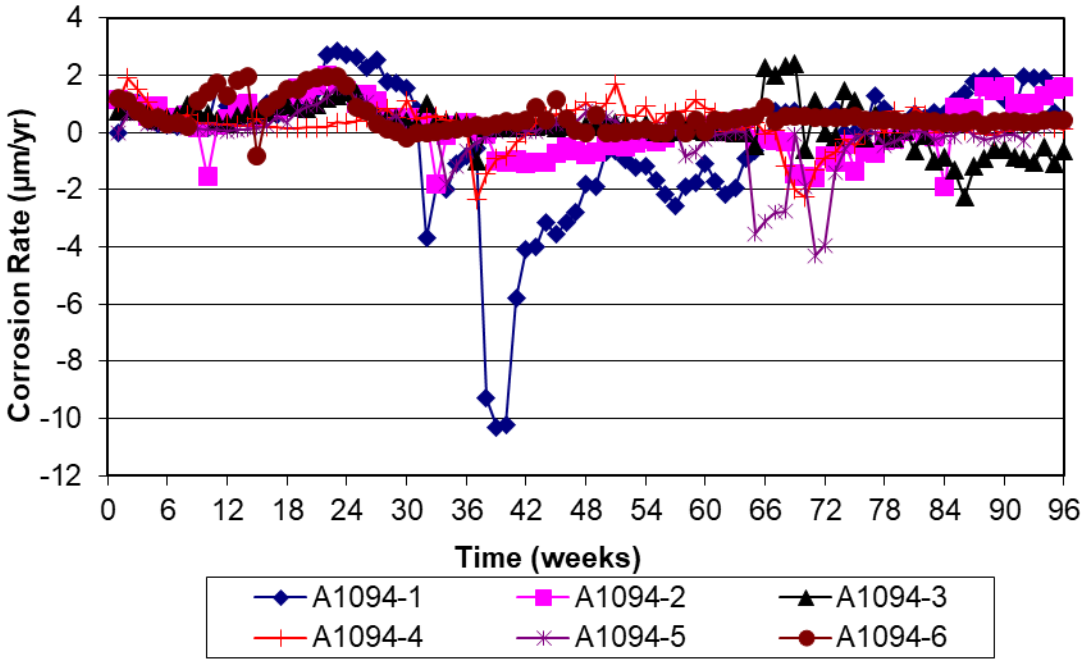

Figure C.63: Corrosion rate of A1094 reinforcement in the Southern Exposure test

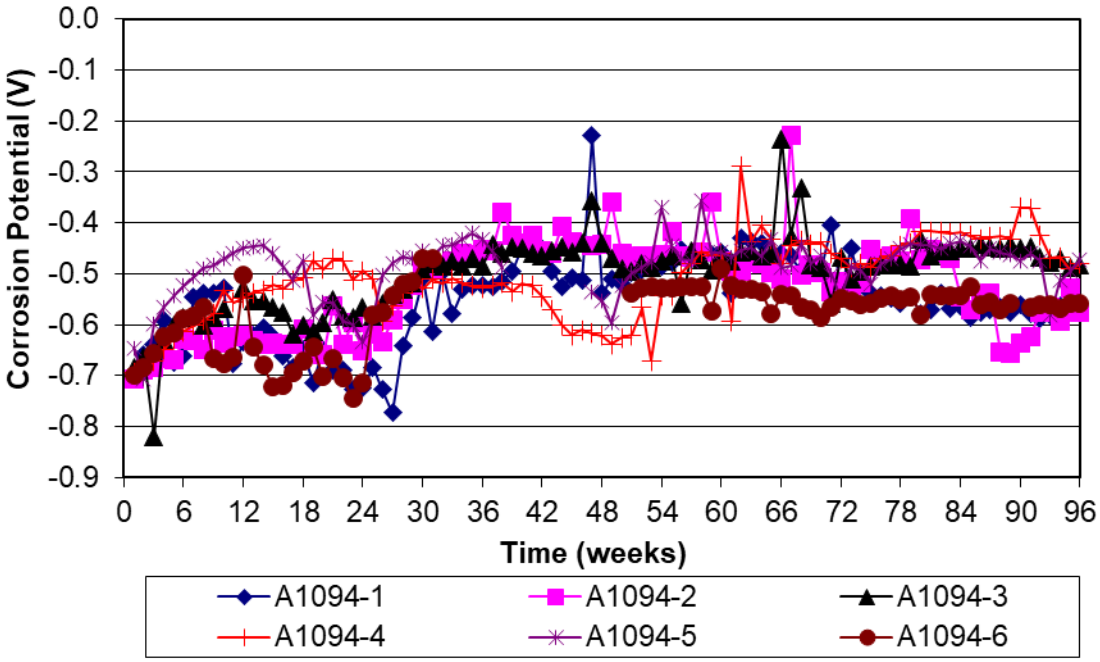

Figure C.64: Corrosion potential of A1094 reinforcement in the Southern Exposure test

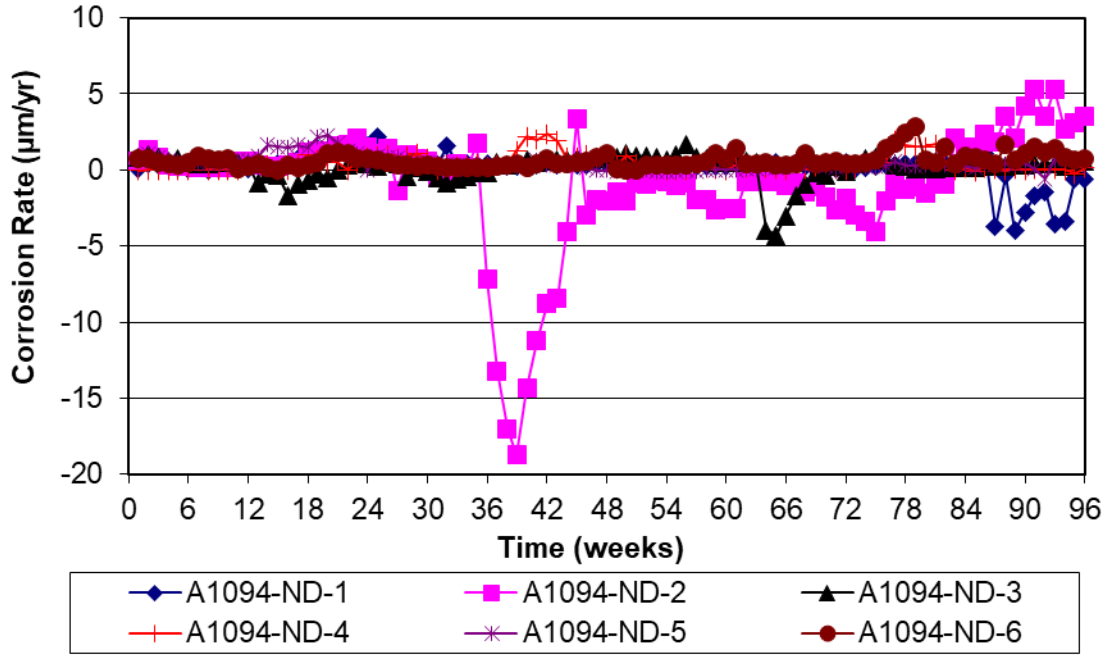

Figure C.65: Corrosion rate of A1094-ND reinforcement in the Southern Exposure test

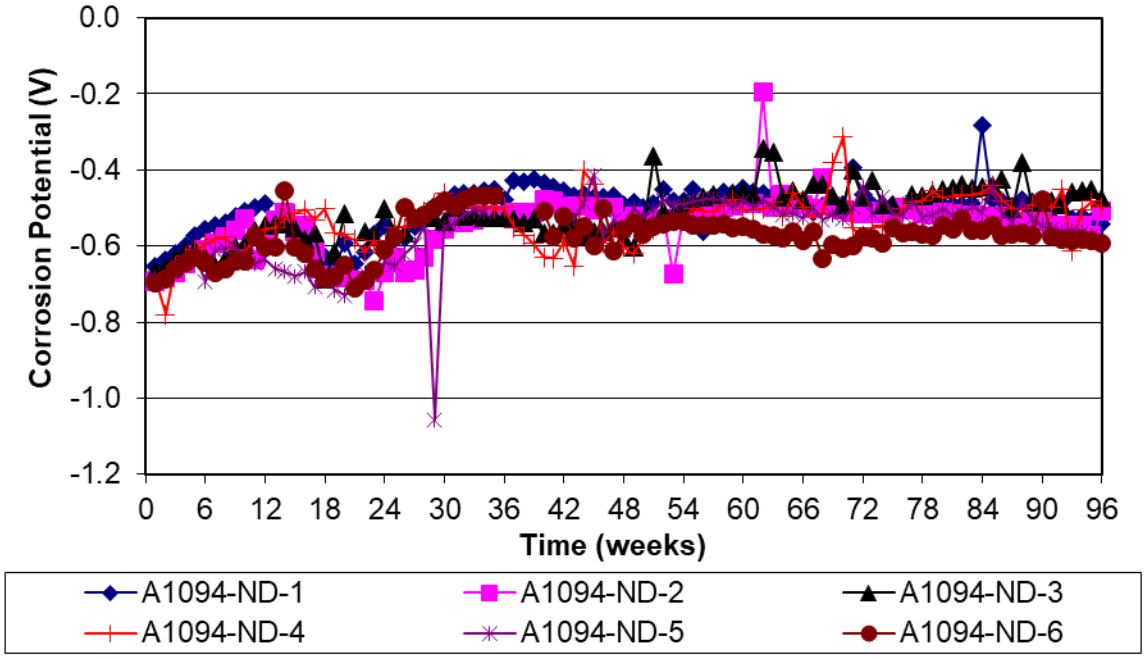

Figure C.66: Corrosion potential of A1094-ND reinforcement in the Southern Exposure test

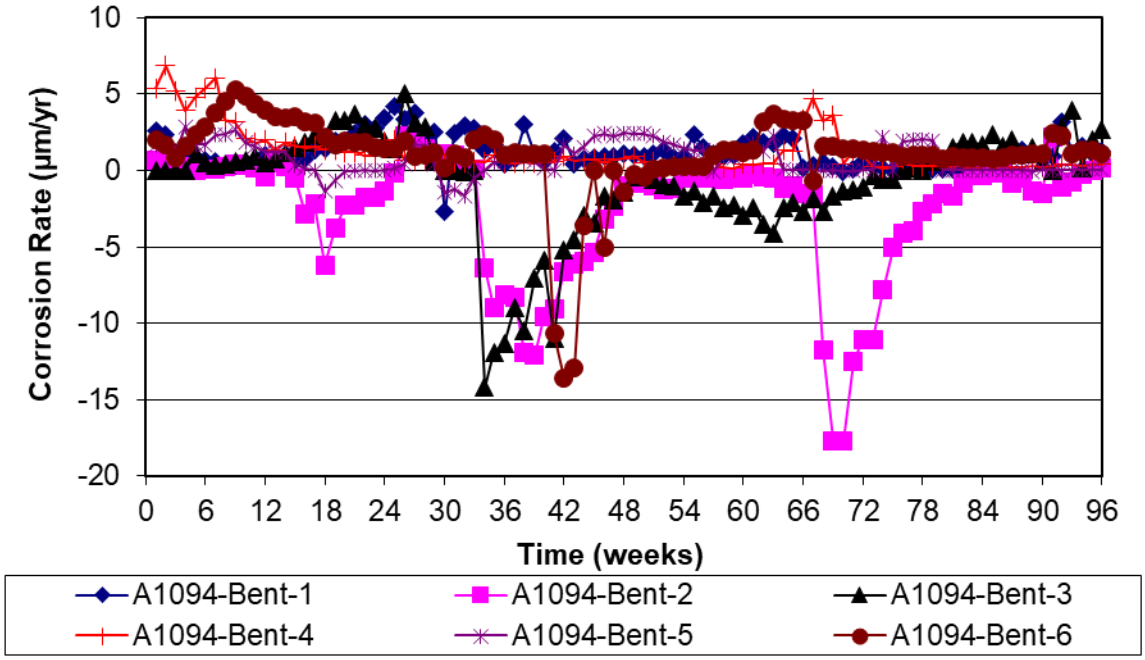

Figure C.67: Corrosion rate of A1094-Bent reinforcement in the Southern Exposure test

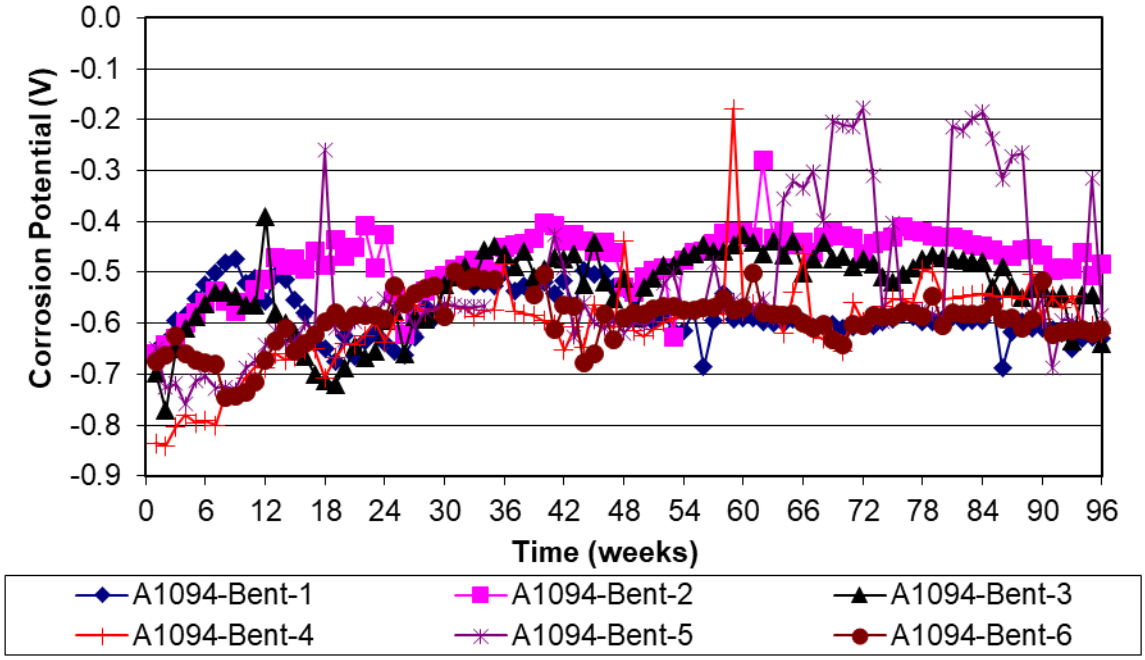

Figure C.68: Corrosion potential of A1094-Bent reinforcement in the Southern Exposure test

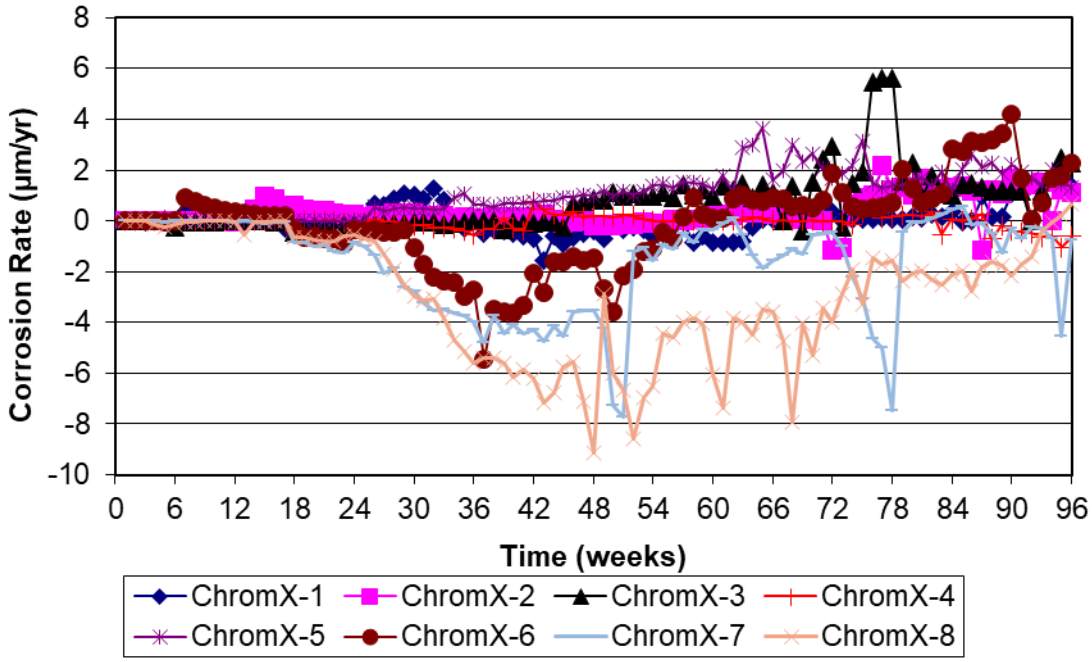

Figure C.69: Corrosion rate of ChromX reinforcement in the Southern Exposure test

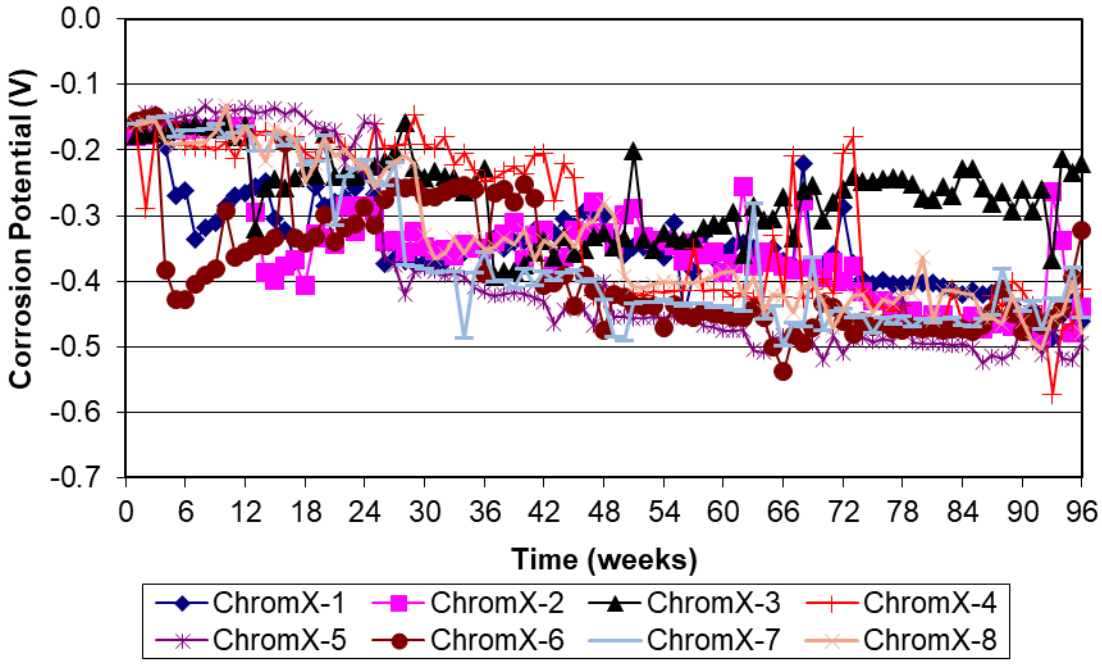

Figure C.70: Corrosion potential of ChromX reinforcement in the Southern Exposure test

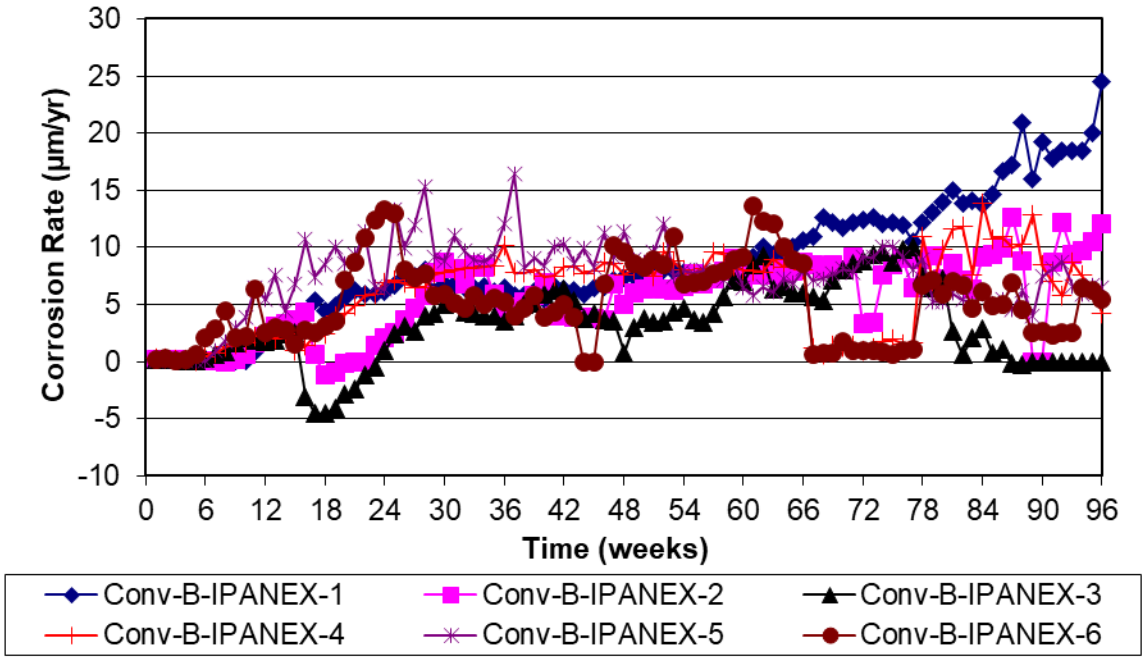

Figure C.71: Corrosion rate of Conv-B-IPANEX reinforcement in the Southern Exposure test

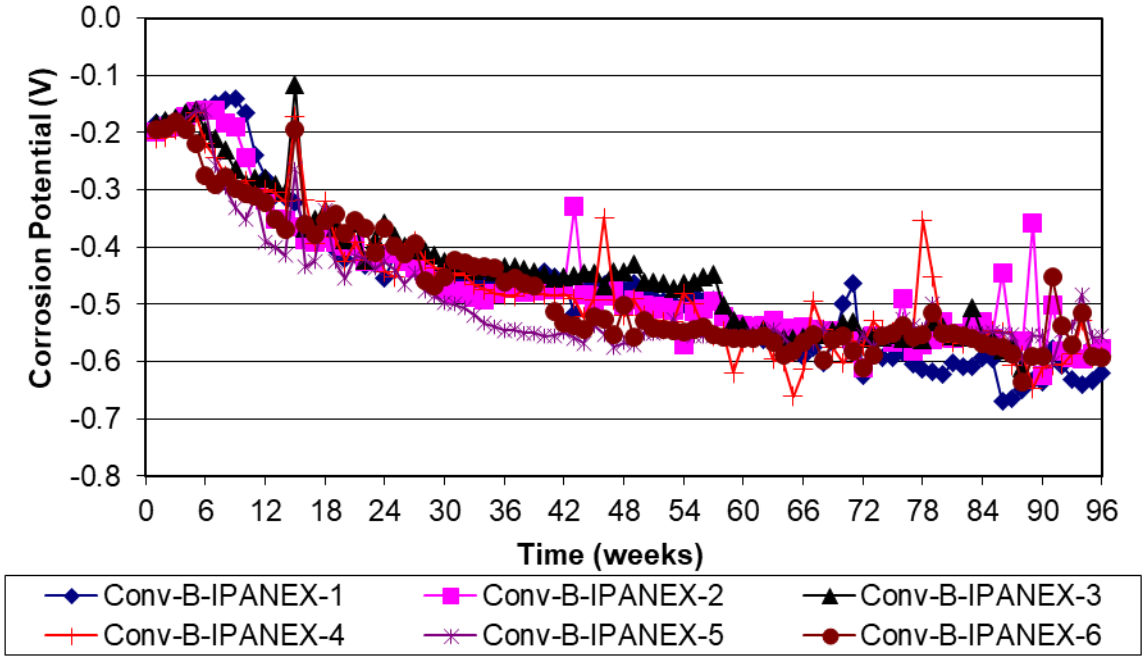

Figure C.72: Corrosion potential of Conv-B-IPANEX reinforcement in the Southern Exposure test

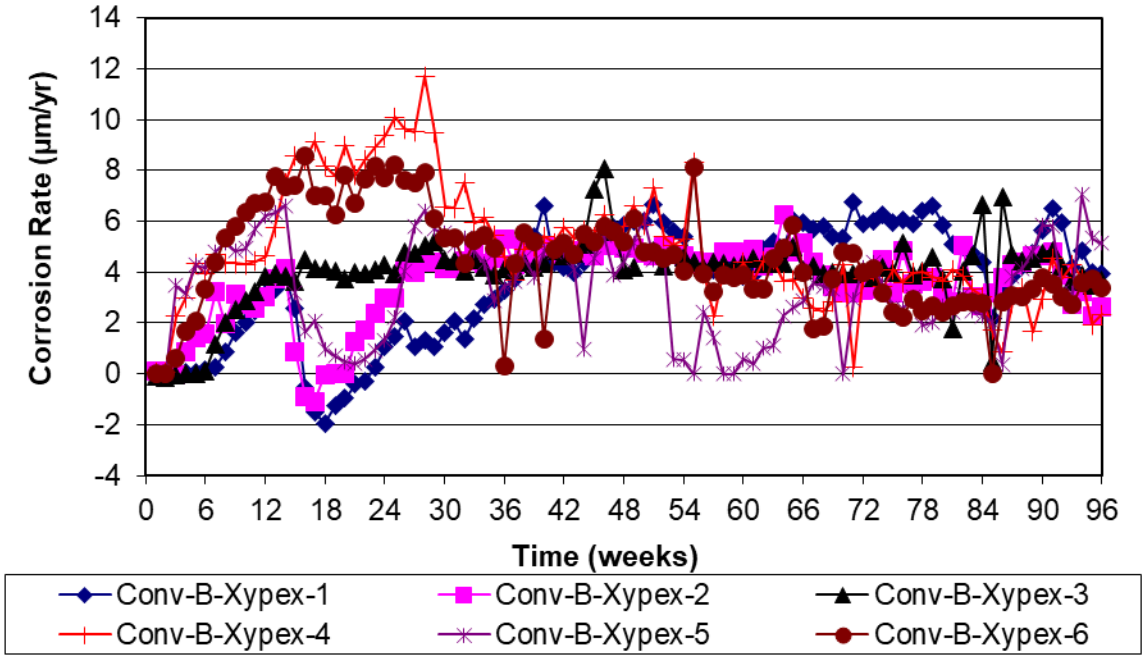

Figure C.73: Corrosion rate of Conv-B-Xypex reinforcement in the Southern Exposure test

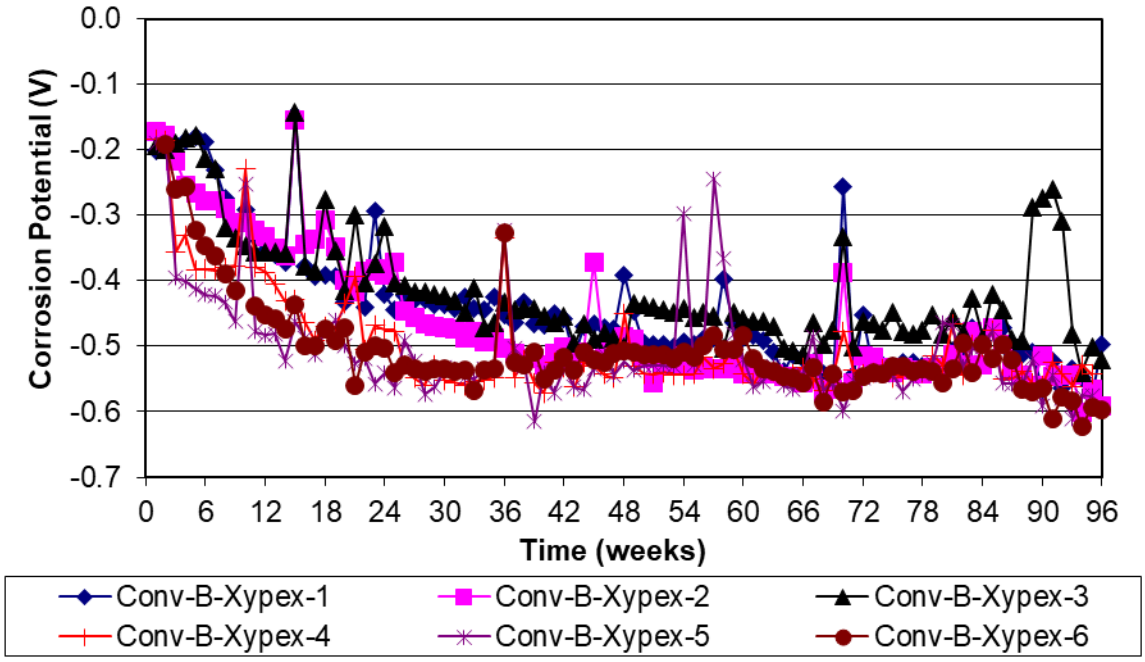

Figure C.74: Corrosion potential of Conv-B-Xypex reinforcement in the Southern Exposure test

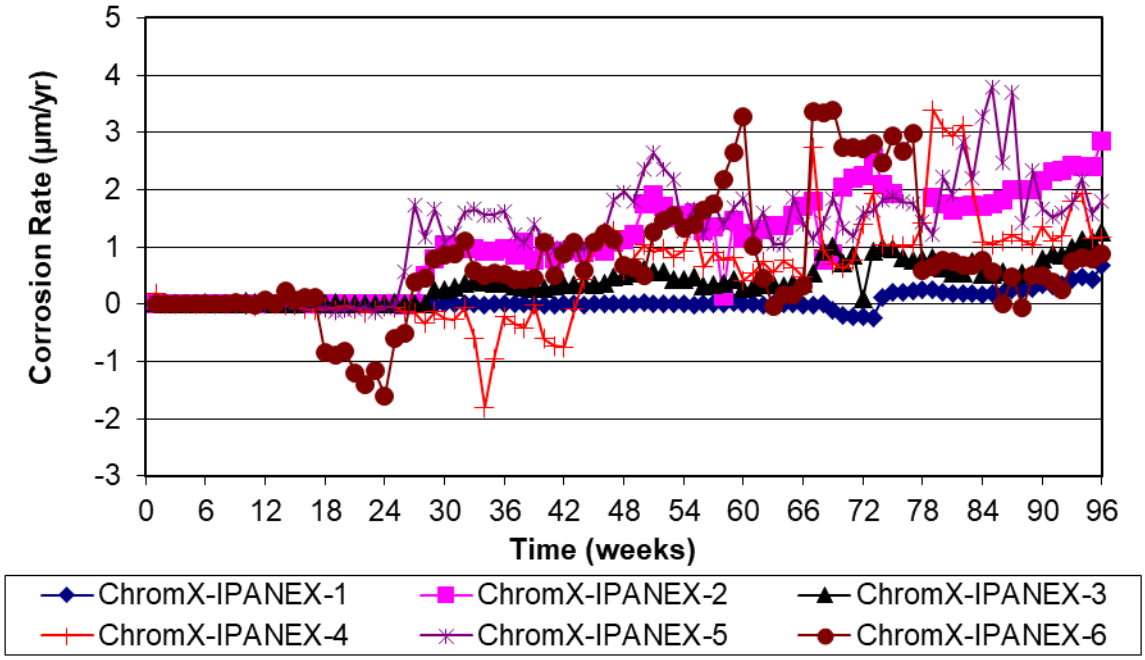

Figure C.75: Corrosion rate of ChromX-IPANEX reinforcement in the Southern Exposure test

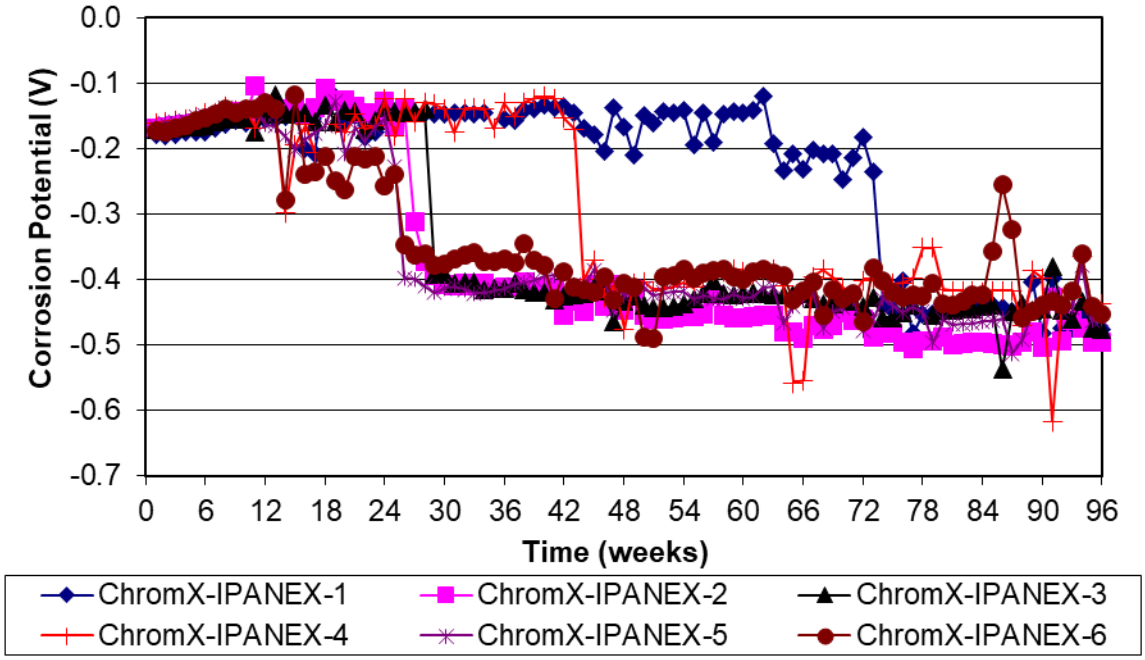

Figure C.76: Corrosion potential of ChromX-IPANEX reinforcement in the Southern Exposure test

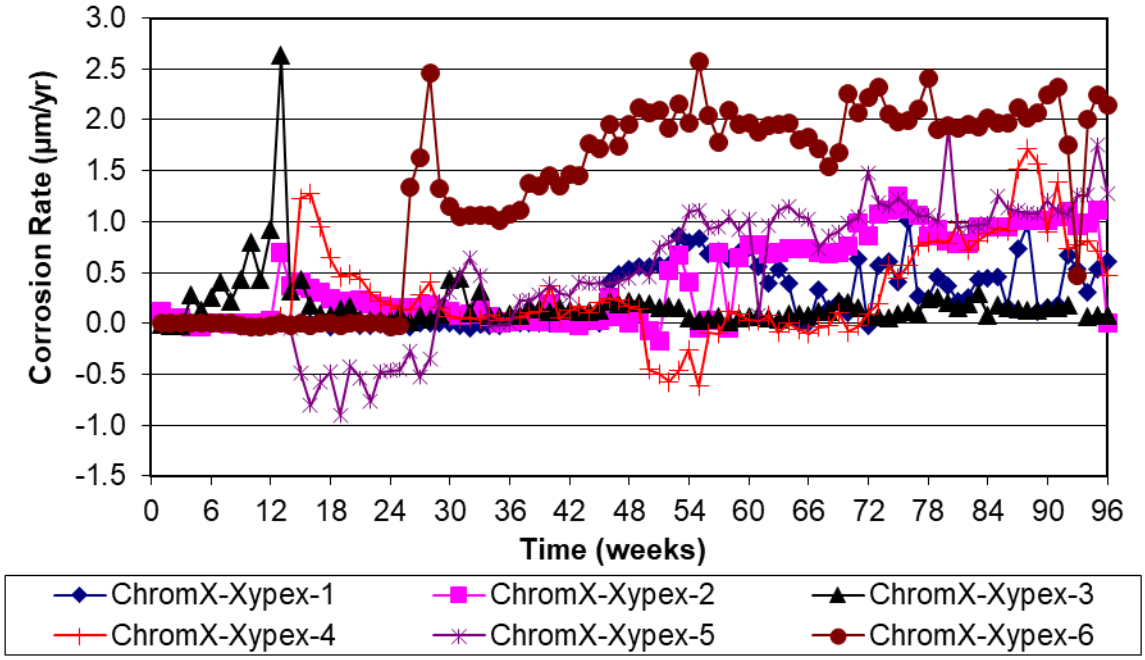

Figure C.77: Corrosion rate of ChromX-Xypex reinforcement in the Southern Exposure test

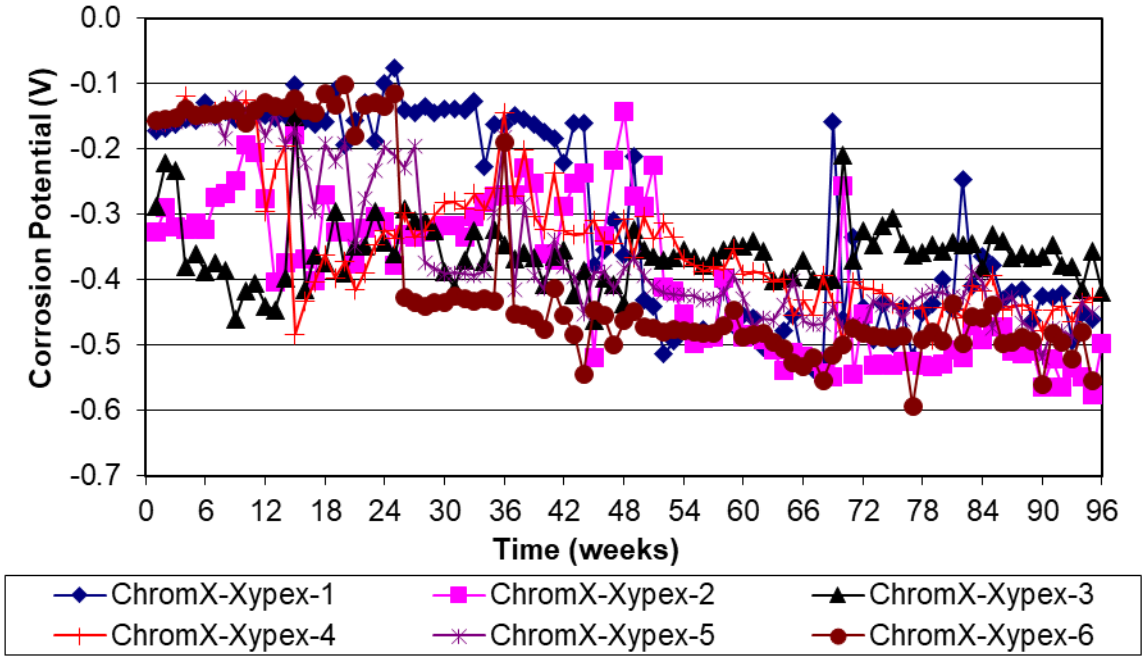

Figure C.78: Corrosion potential of ChromX-Xypex reinforcement in the Southern Exposure test

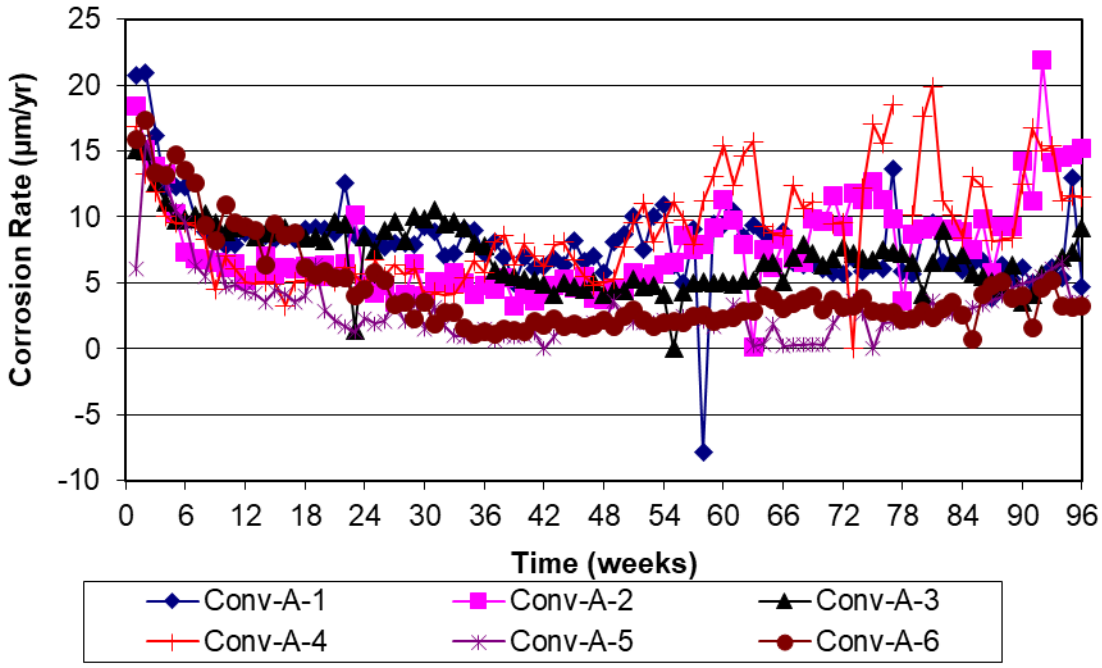

Figure C.79: Corrosion rate of Conv-A reinforcement in the cracked beam test

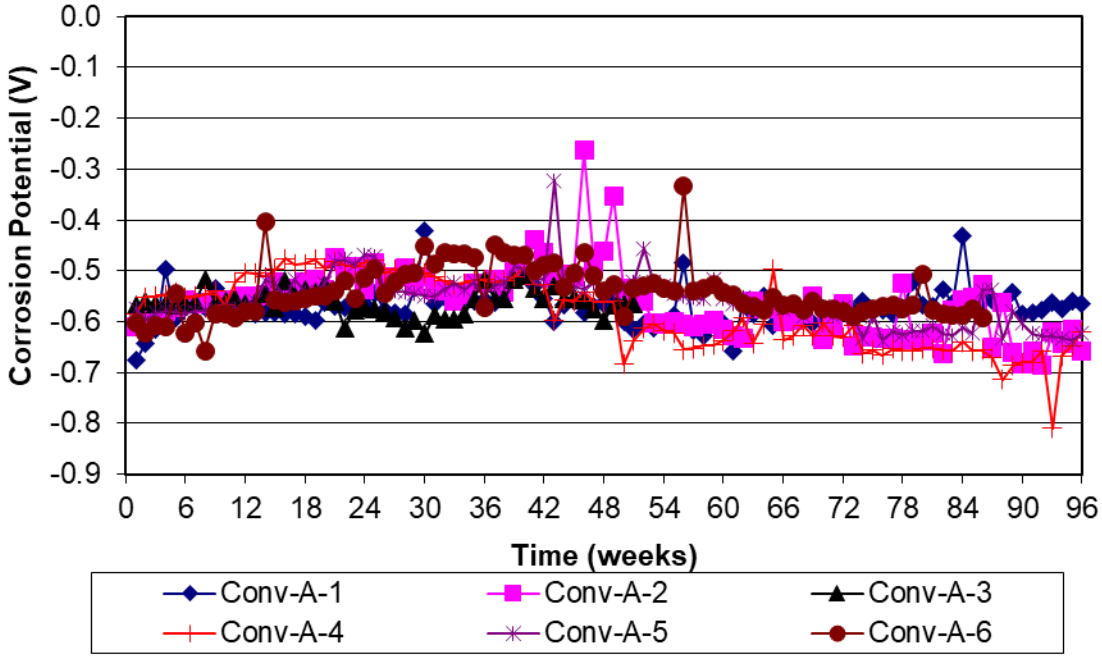

Figure C.80: Corrosion potential of Conv-A reinforcement in the cracked beam test

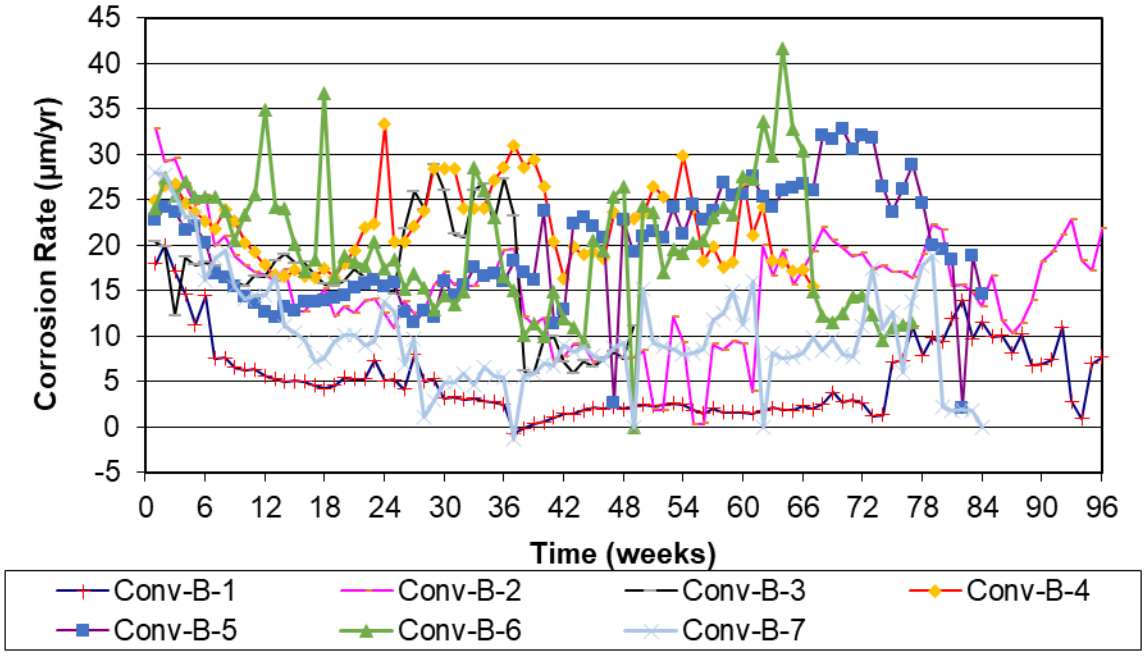

Figure C.81: Corrosion rate of Conv-B reinforcement in the cracked beam test

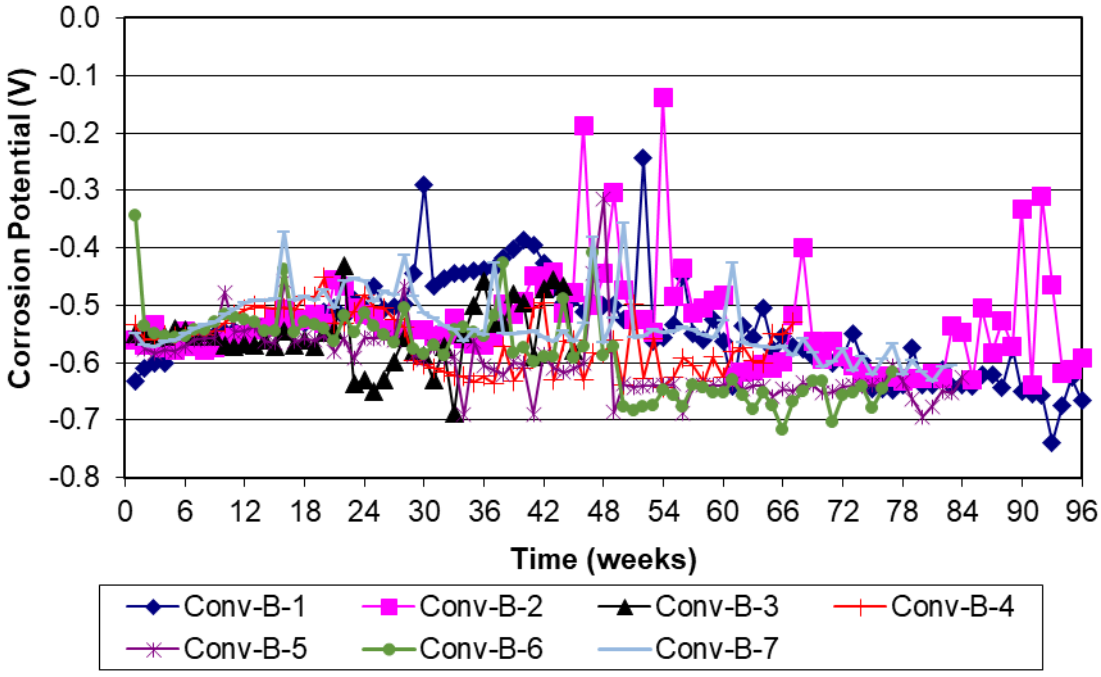

Figure C.82: Corrosion potential of Conv-B reinforcement in the cracked beam test

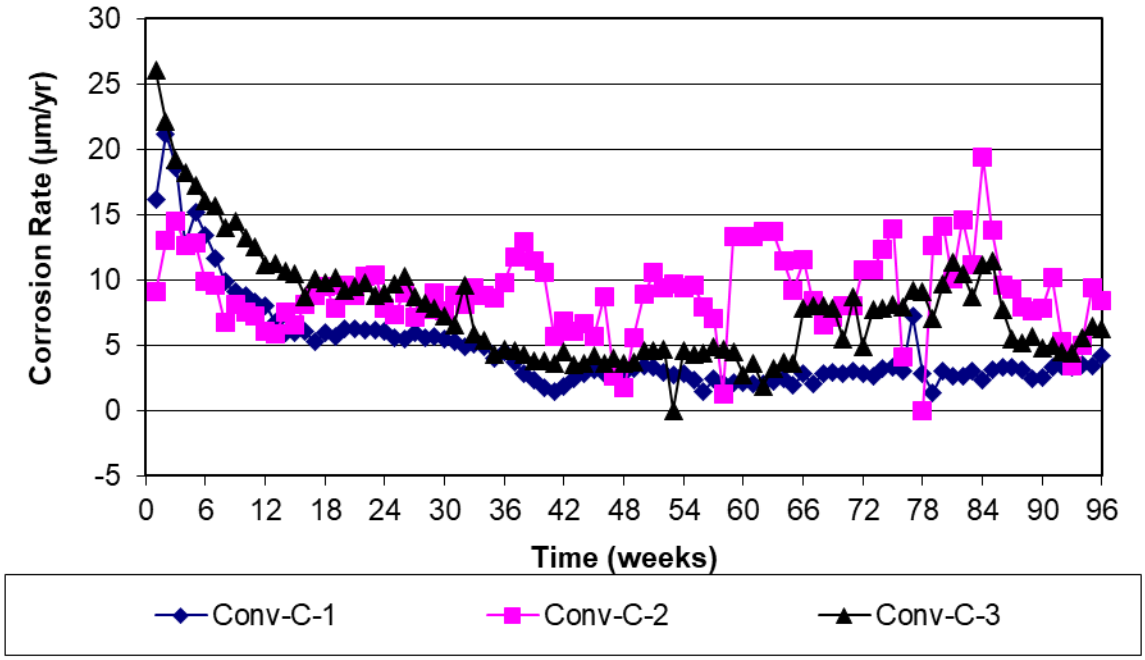

Figure C.83: Corrosion rate of Conv-C reinforcement in the cracked beam test

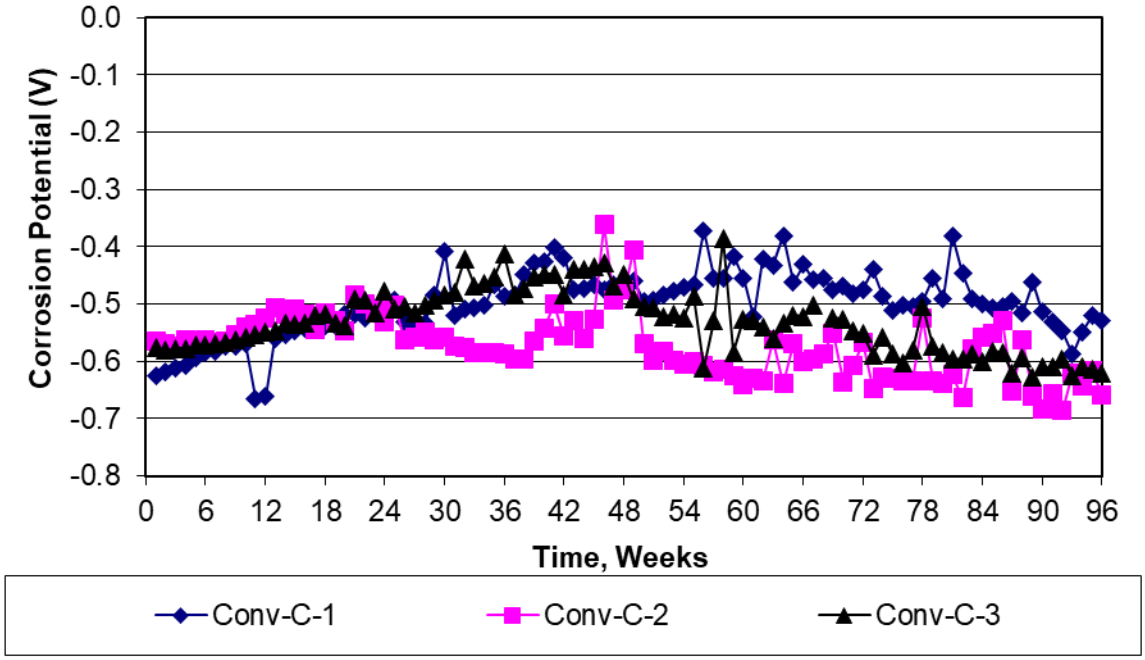

Figure C.84: Corrosion potential of Conv-C reinforcement in the cracked beam test

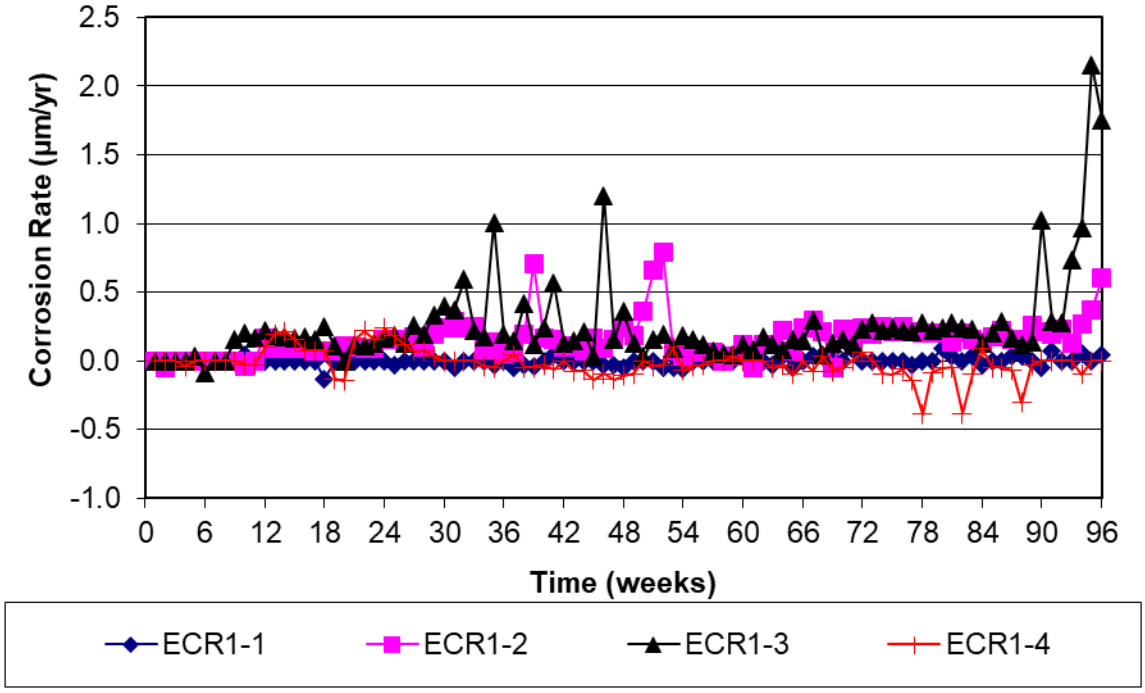

Figure C.85: Corrosion rate of ECR1 reinforcement in the cracked beam test

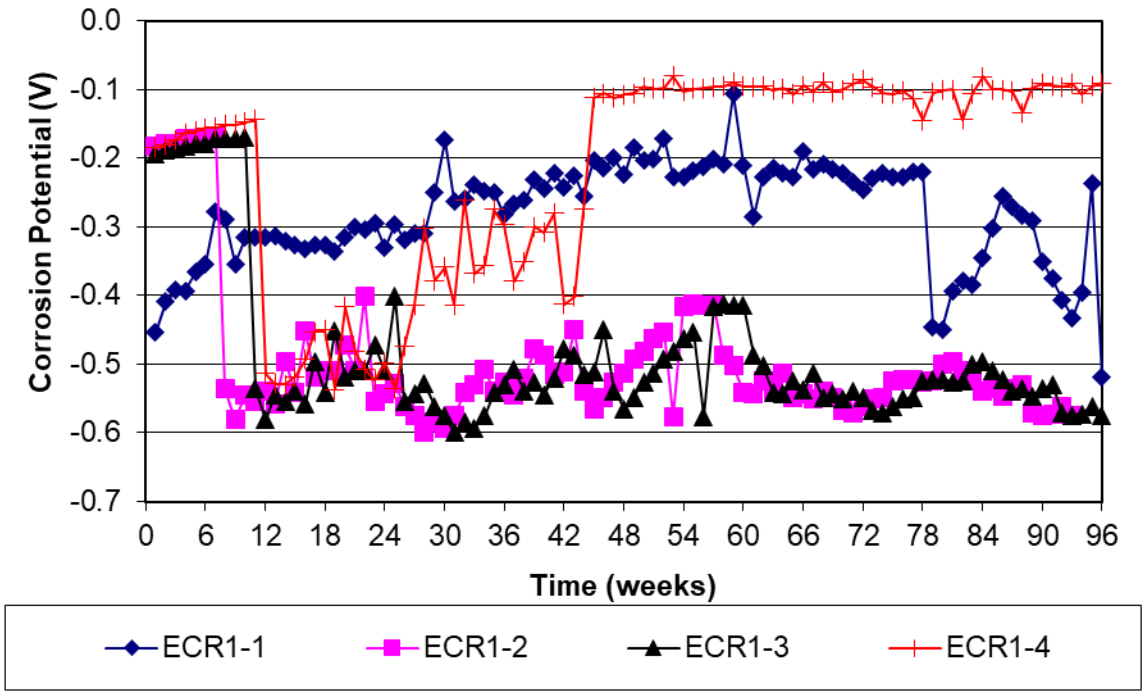

Figure C.86: Corrosion rate of ECR reinforcement in the cracked beam test

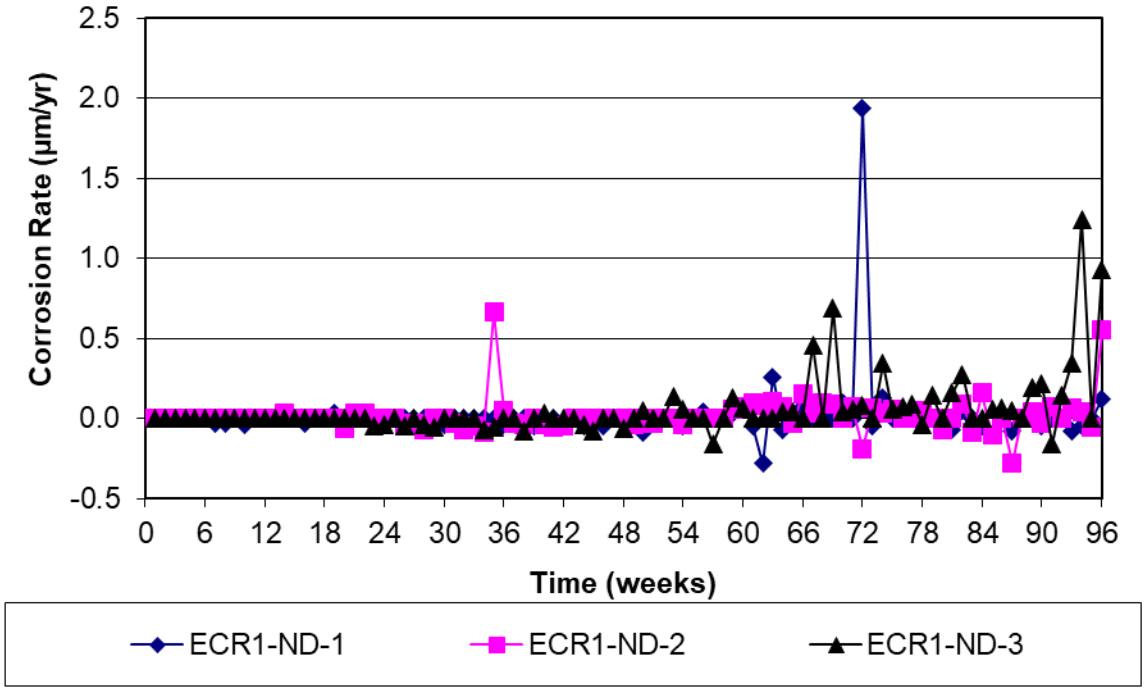

Figure C.87: Corrosion rate of ECR1-ND reinforcement in the cracked beam test

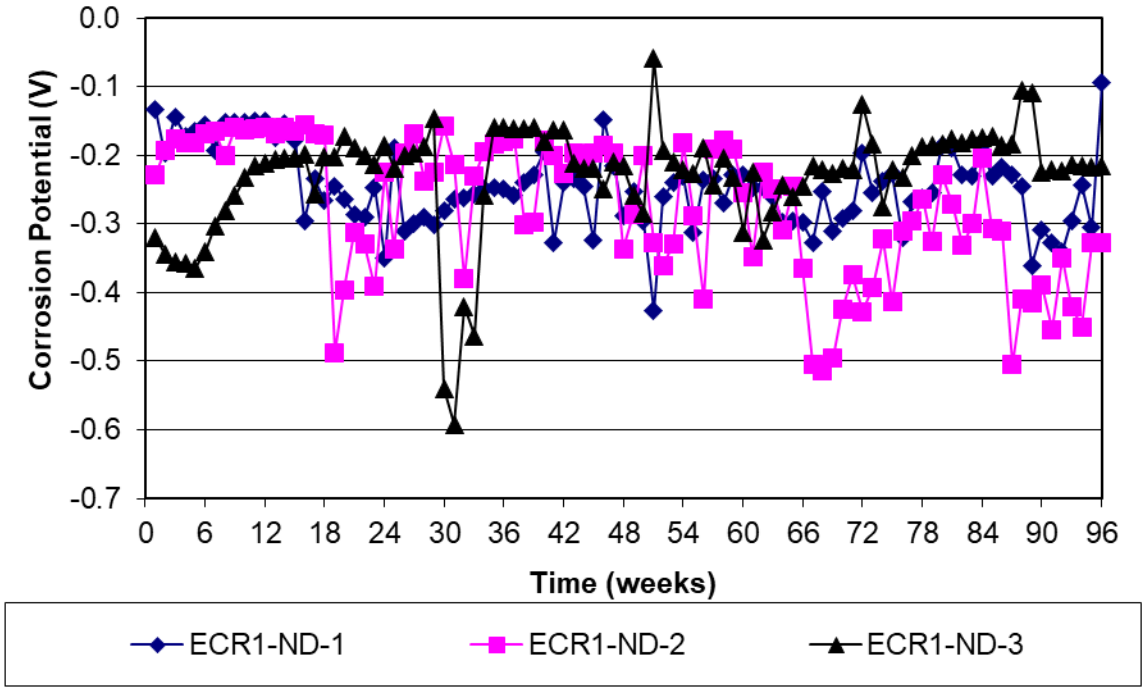

Figure C.88: Corrosion potential of ECR1-ND reinforcement in the cracked beam test

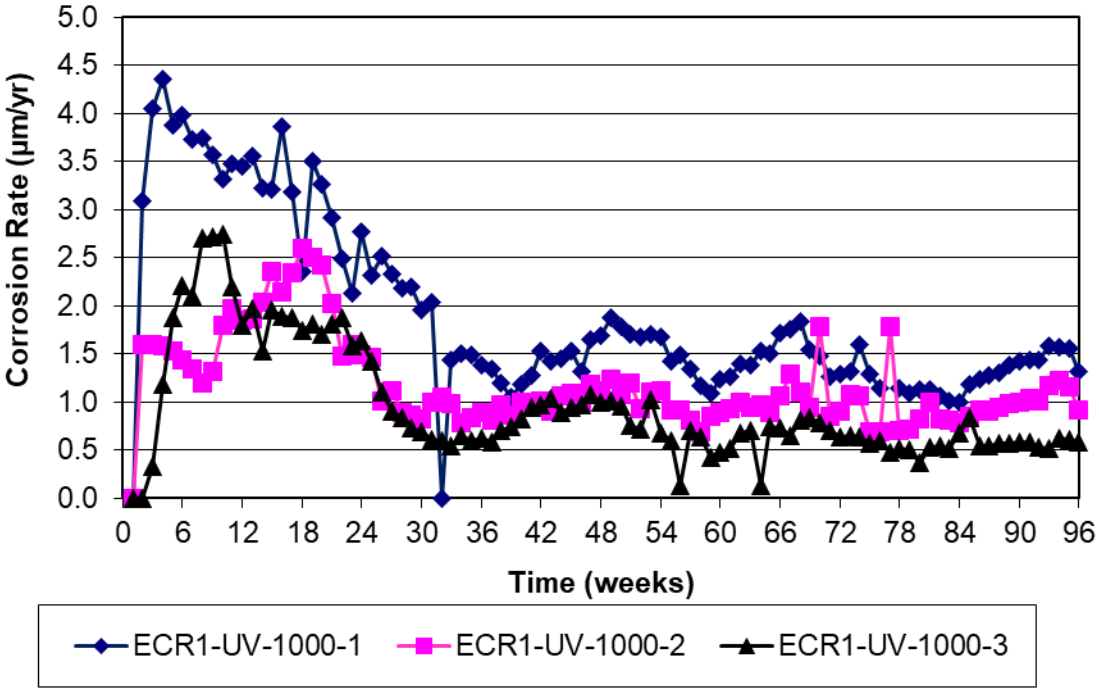

Figure C.89: Corrosion rate of ECR1-UV-1000 reinforcement in the cracked beam test

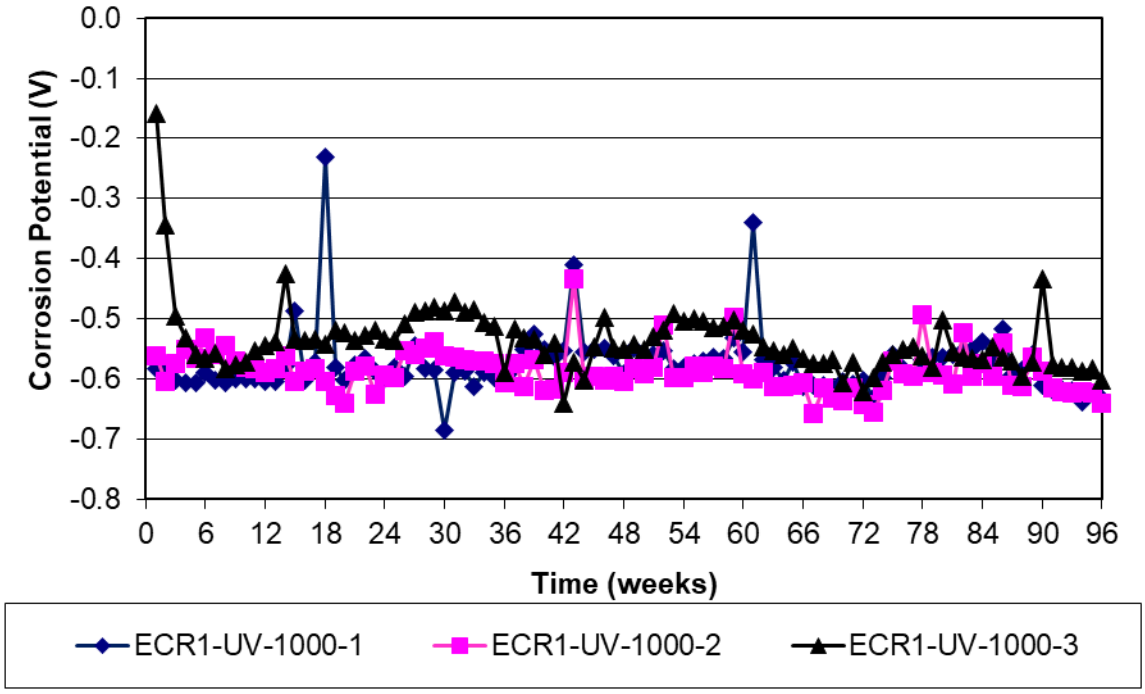

Figure C.90: Corrosion rate of ECR1-UV-1000 reinforcement in the cracked beam test

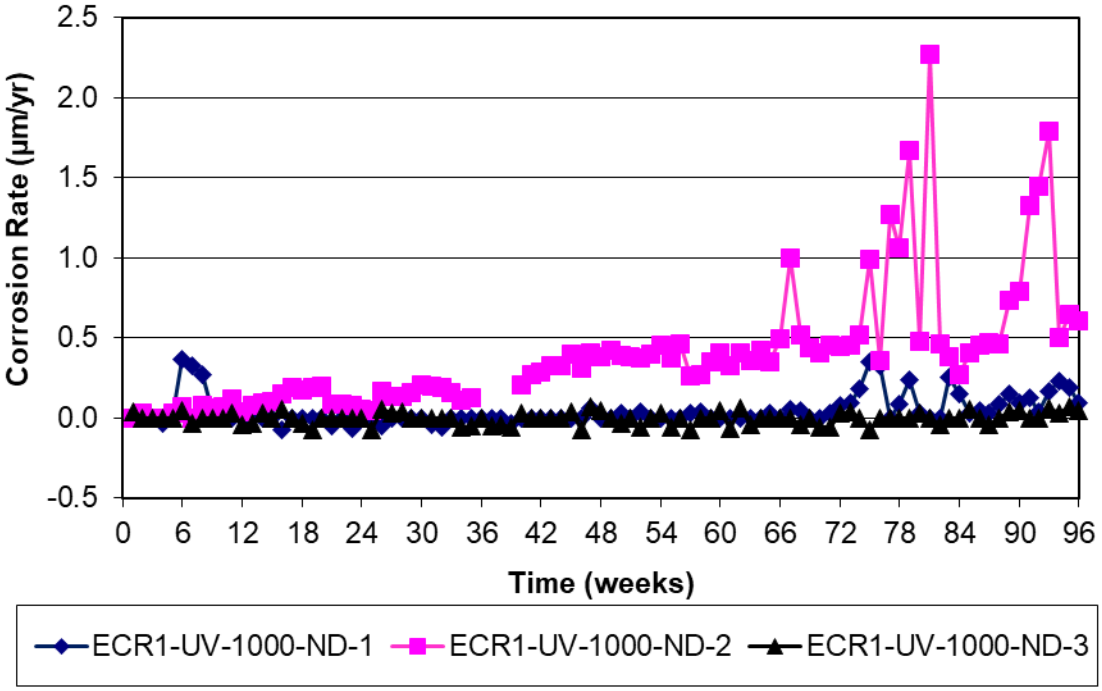

Figure C.91: Corrosion rate of ECR1-UV-ND-1000 reinforcement in the cracked beam test

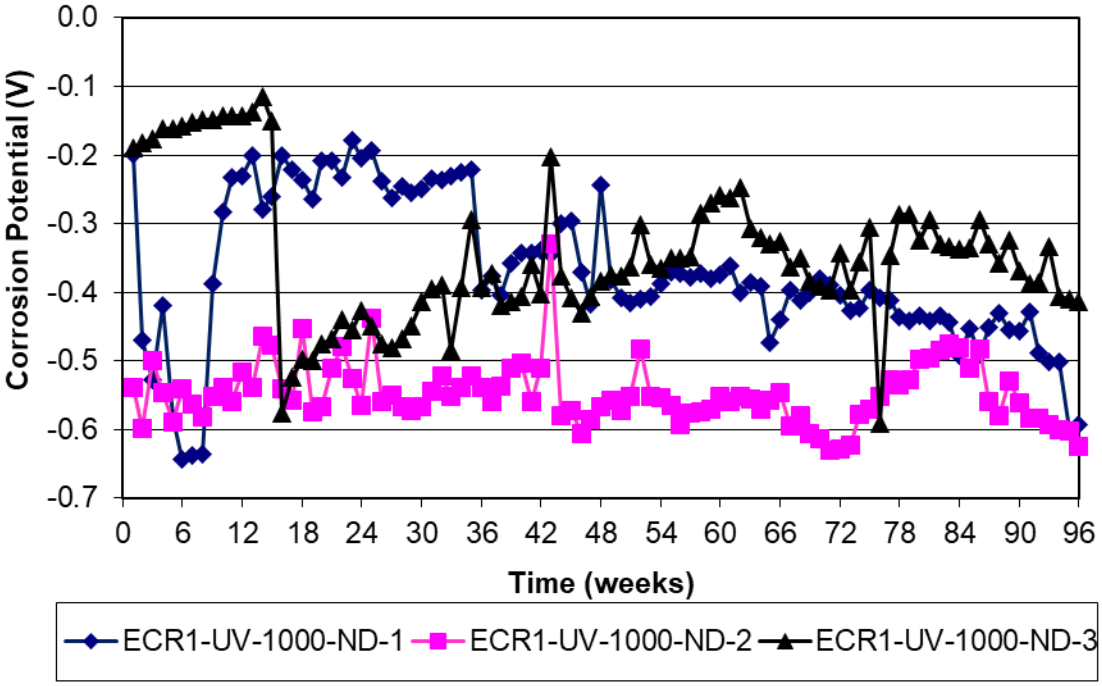

Figure C.92: Corrosion potential of ECR1-UV-ND-1000 reinforcement in the cracked beam test

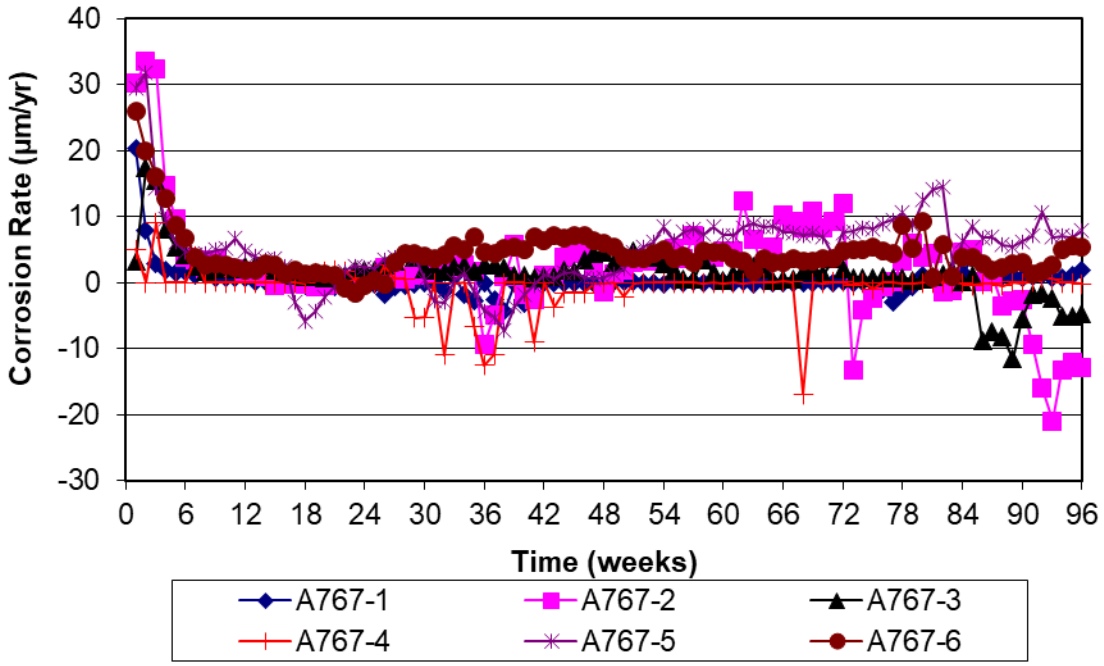

Figure C.93: Corrosion rate of A767 reinforcement in the cracked beam test

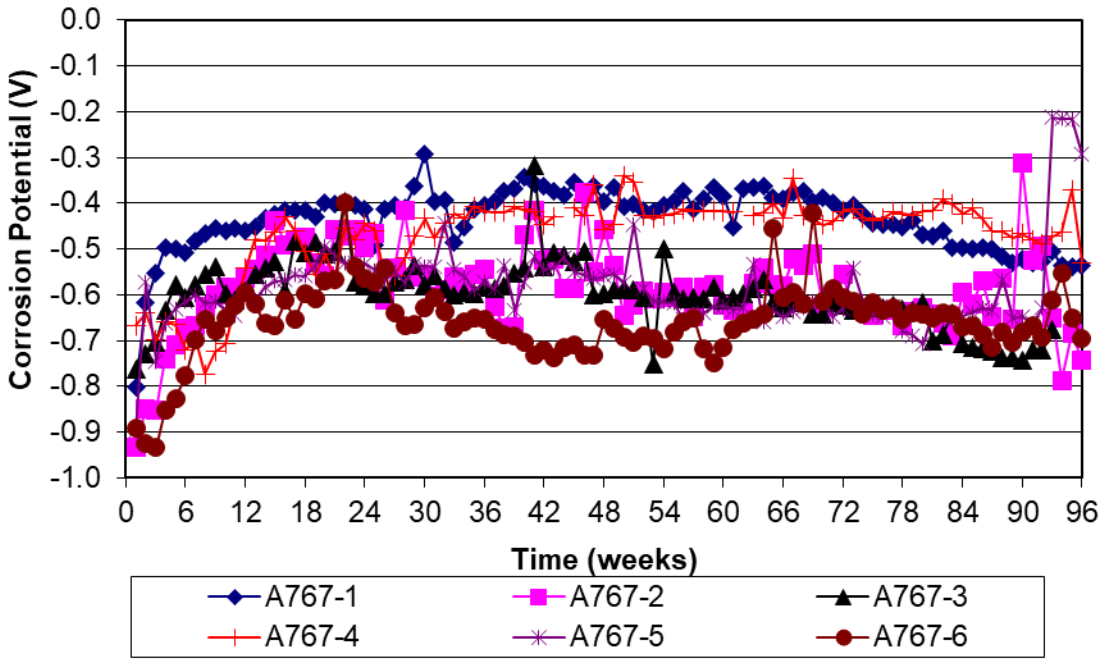

Figure C.94: Corrosion potential of A767 reinforcement in the cracked beam test

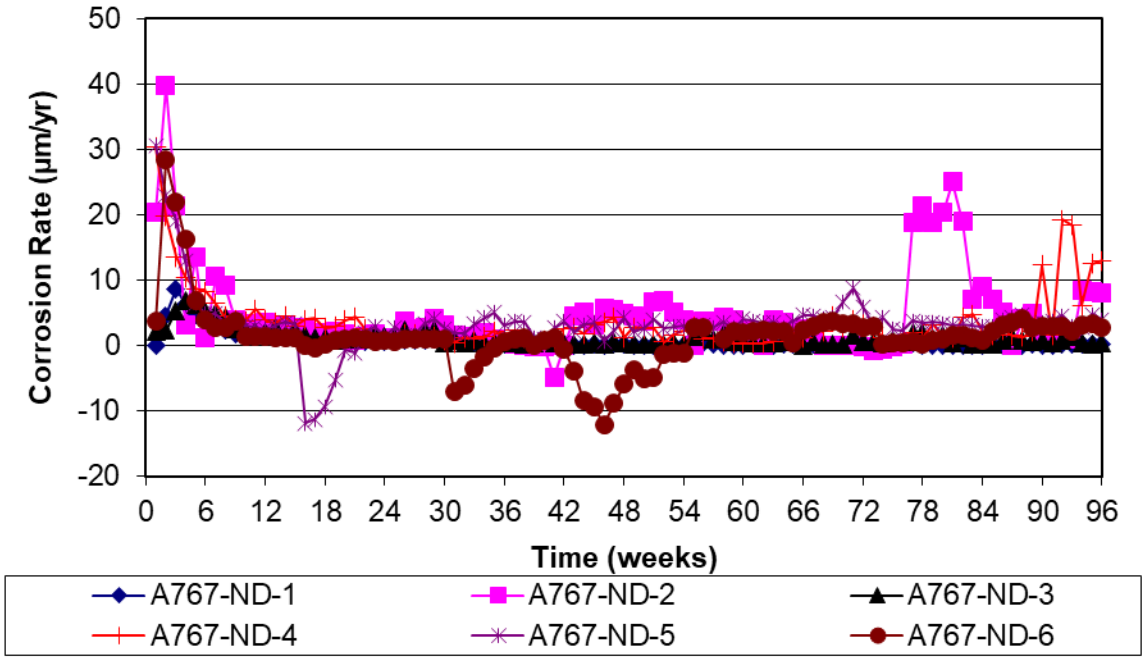

Figure C.95: Corrosion rate of A767-ND reinforcement in the cracked beam test

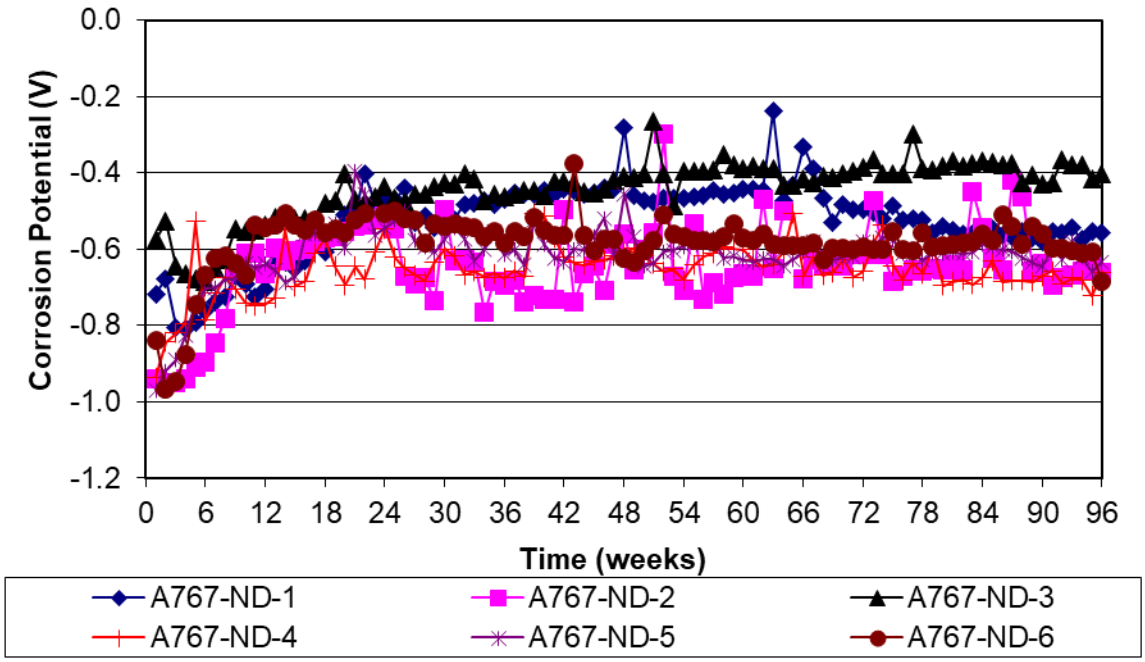

Figure C.96: Corrosion potential of A767-ND reinforcement in the cracked beam test

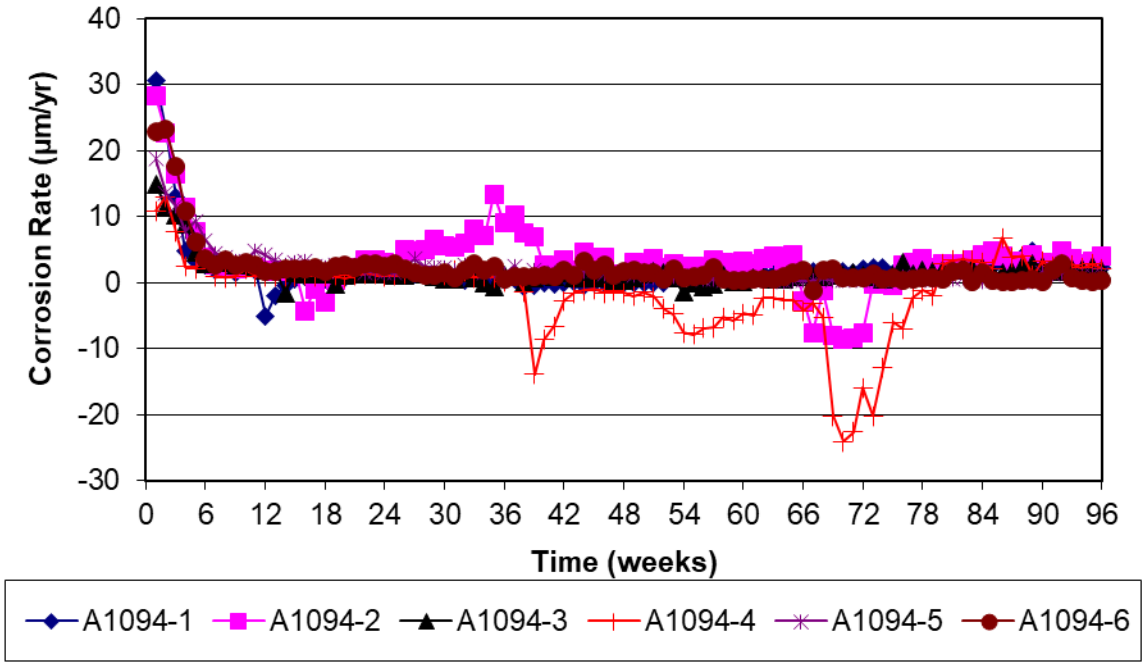

Figure C.97: Corrosion rate of A1094 reinforcement in the cracked beam test

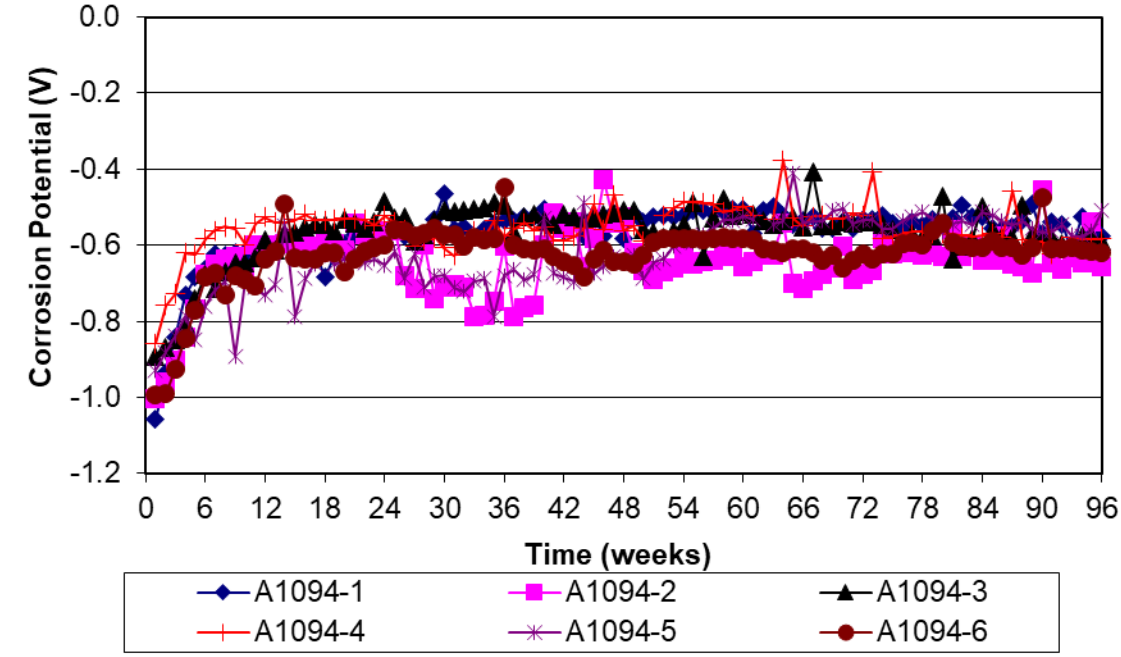

Figure C.98: Corrosion potential of A1094 reinforcement in the cracked beam test

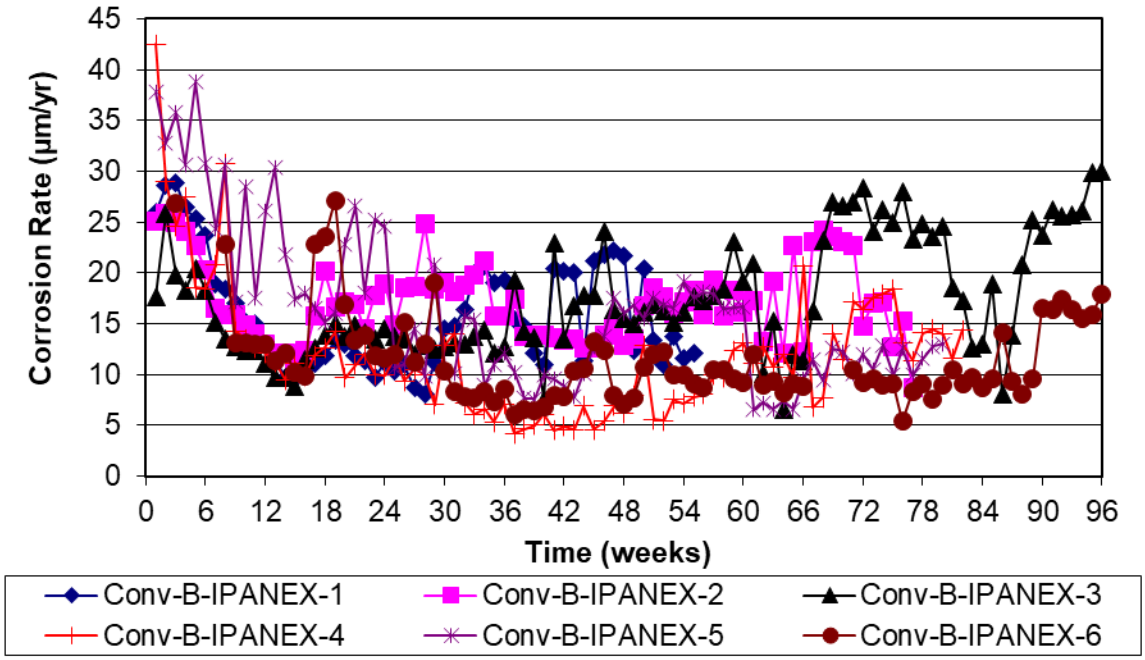

Figure C.99: Corrosion rate of A1094-ND reinforcement in the cracked beam test

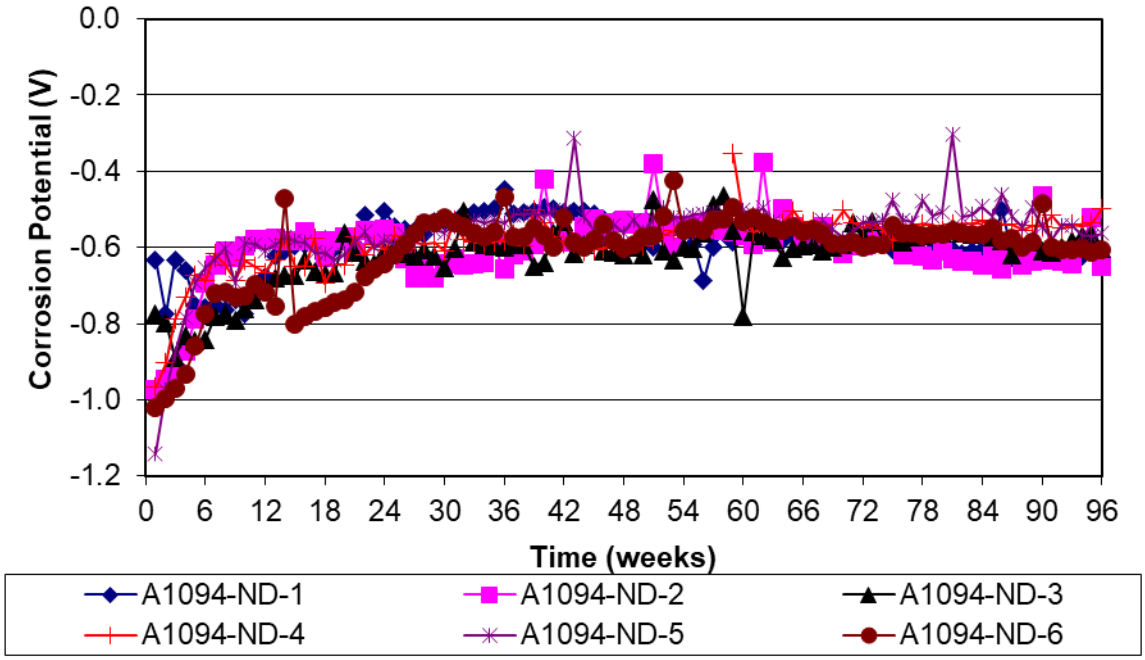

Figure C.100: Corrosion potential of A1094-ND reinforcement in the cracked beam test

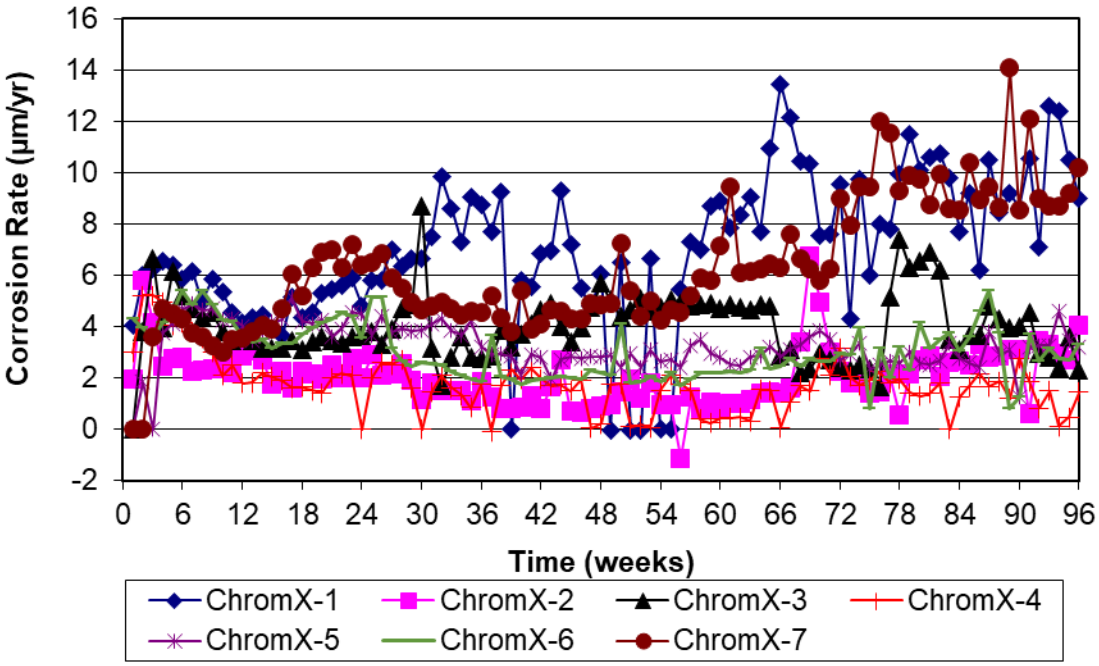

Figure C.101: Corrosion rate of ChromX reinforcement in the cracked beam test

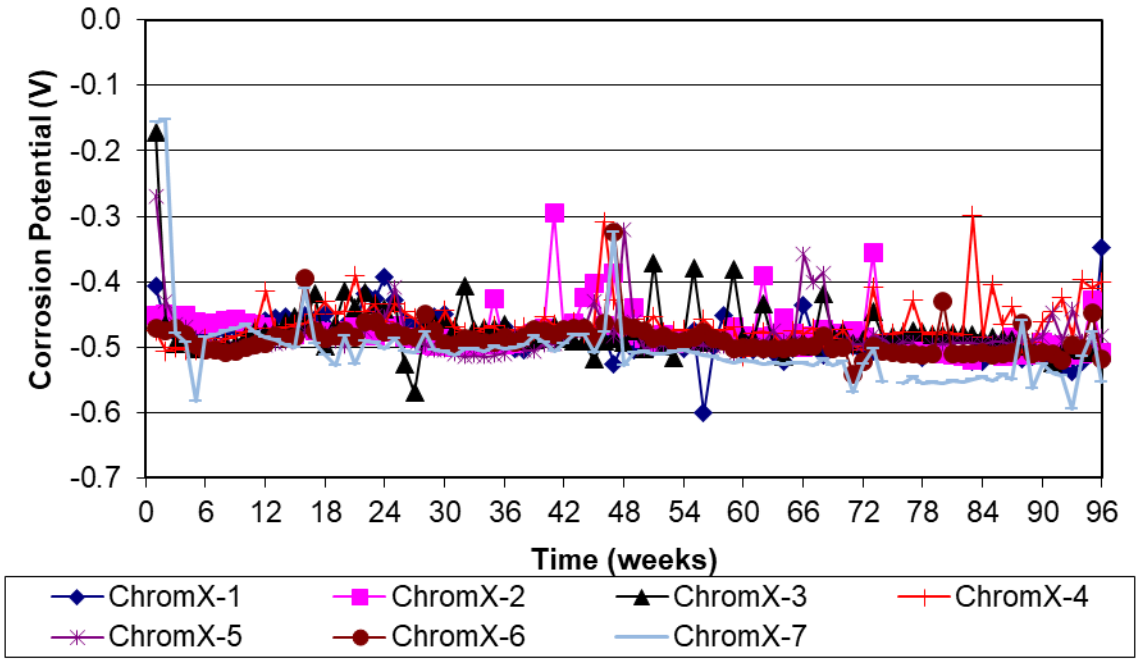

Figure C.102: Corrosion potential of ChromX reinforcement in the cracked beam test

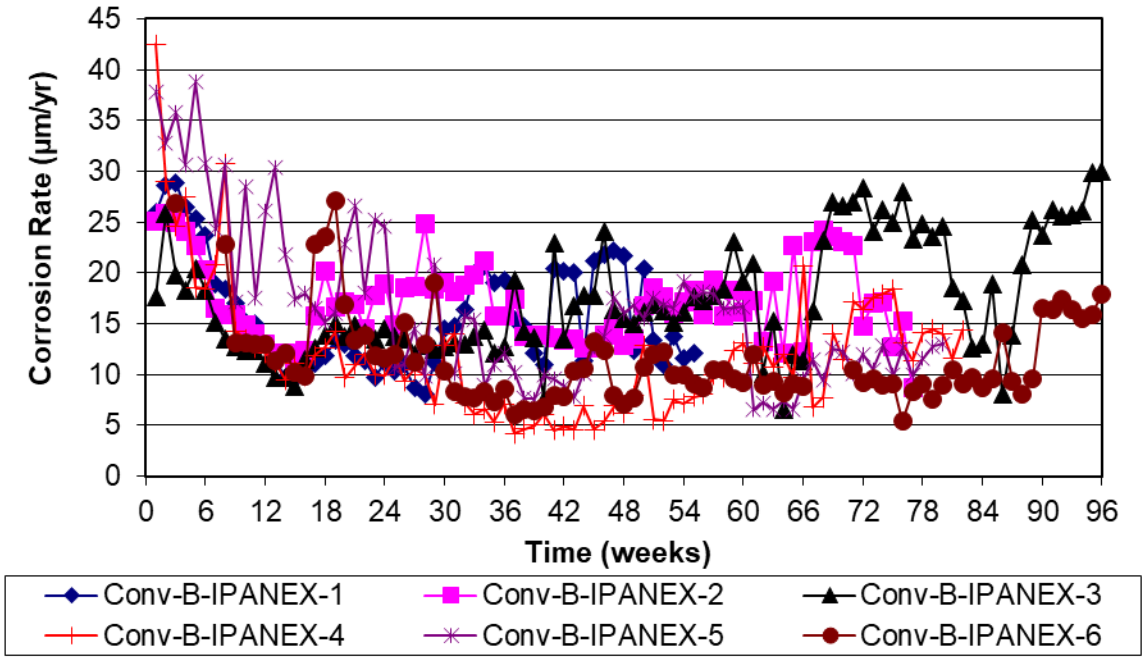

Figure C.103: Corrosion rate of Conv-B-IPANEX reinforcement in the cracked beam test

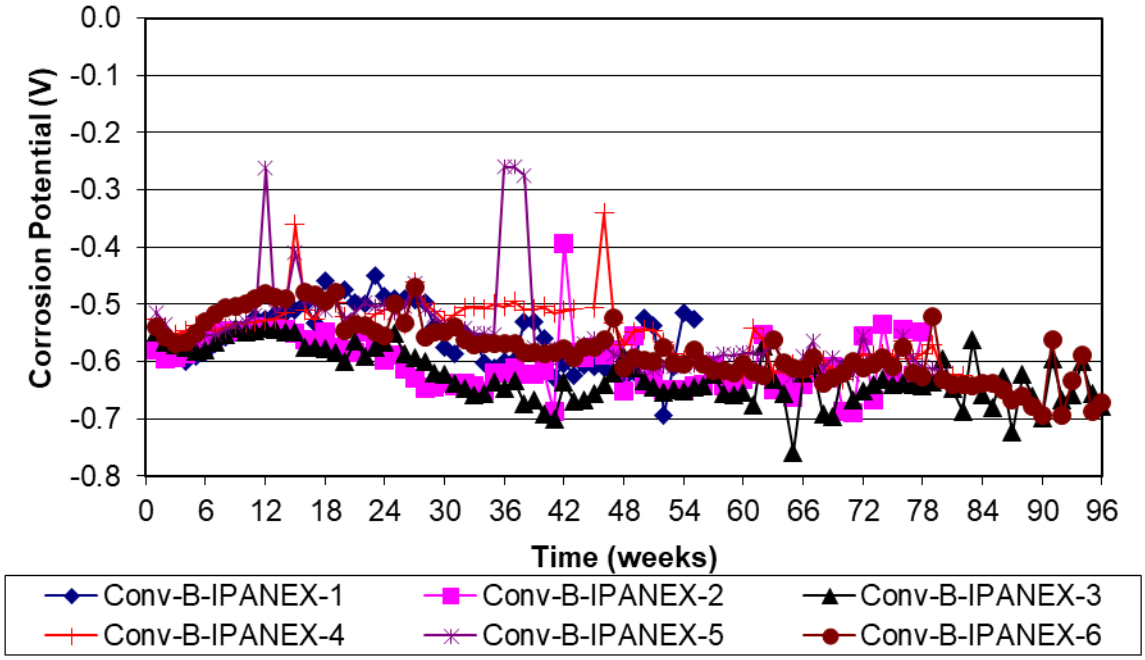

Figure C.104: Corrosion potential of Conv-B-IPANEX reinforcement in the cracked beam test

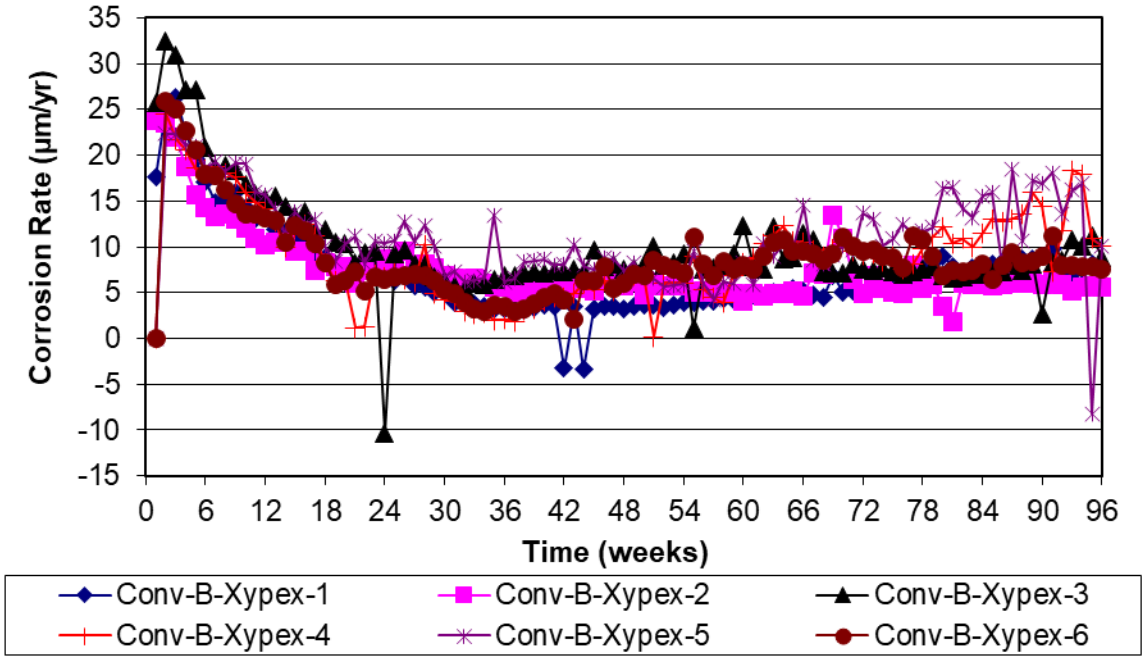

Figure C.105: Corrosion rate of Conv-B-Xypex reinforcement in the cracked beam test

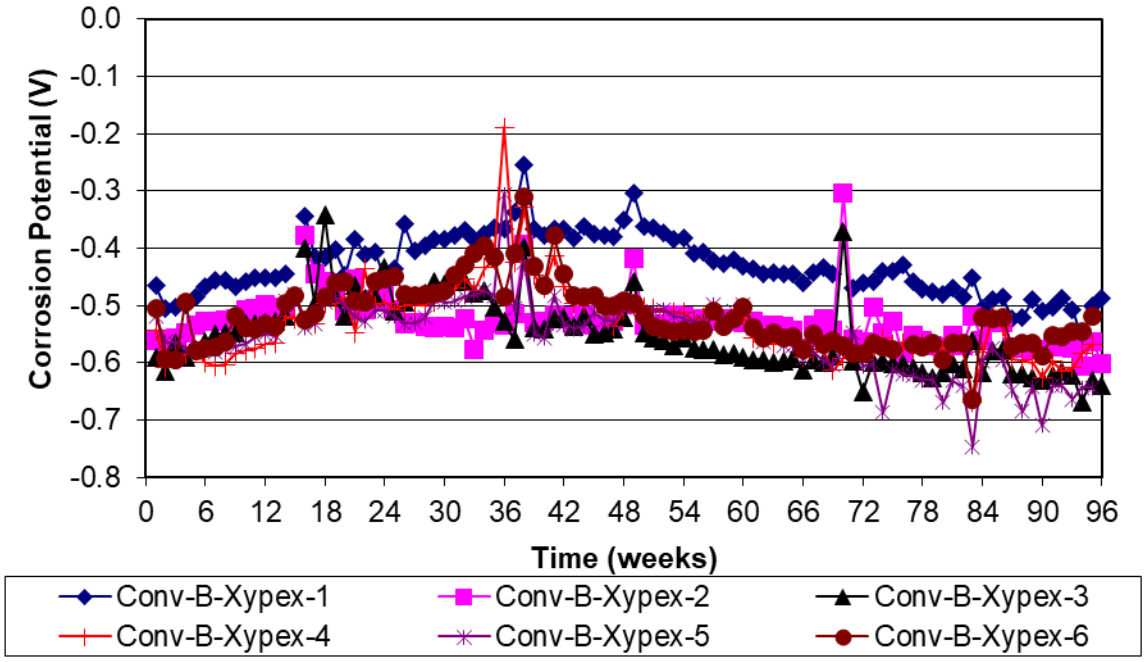

Figure C.106: Corrosion potential of Conv-B-Xypex reinforcement in the cracked beam test

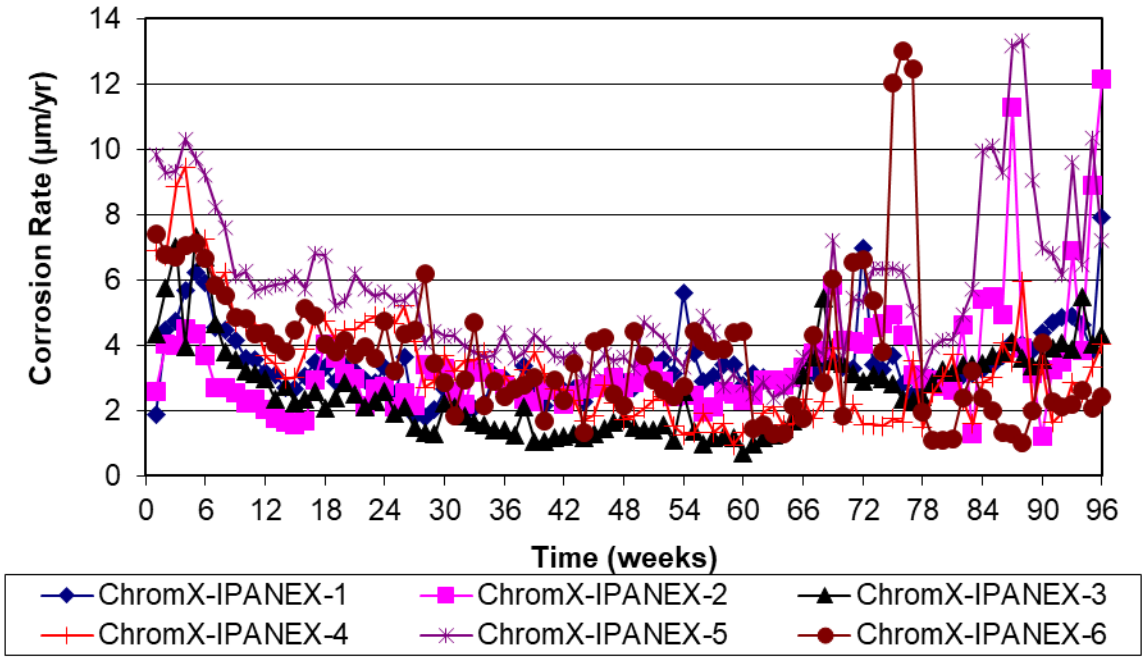

Figure C.107: Corrosion rate of ChromX-IPANEX reinforcement in the cracked beam test

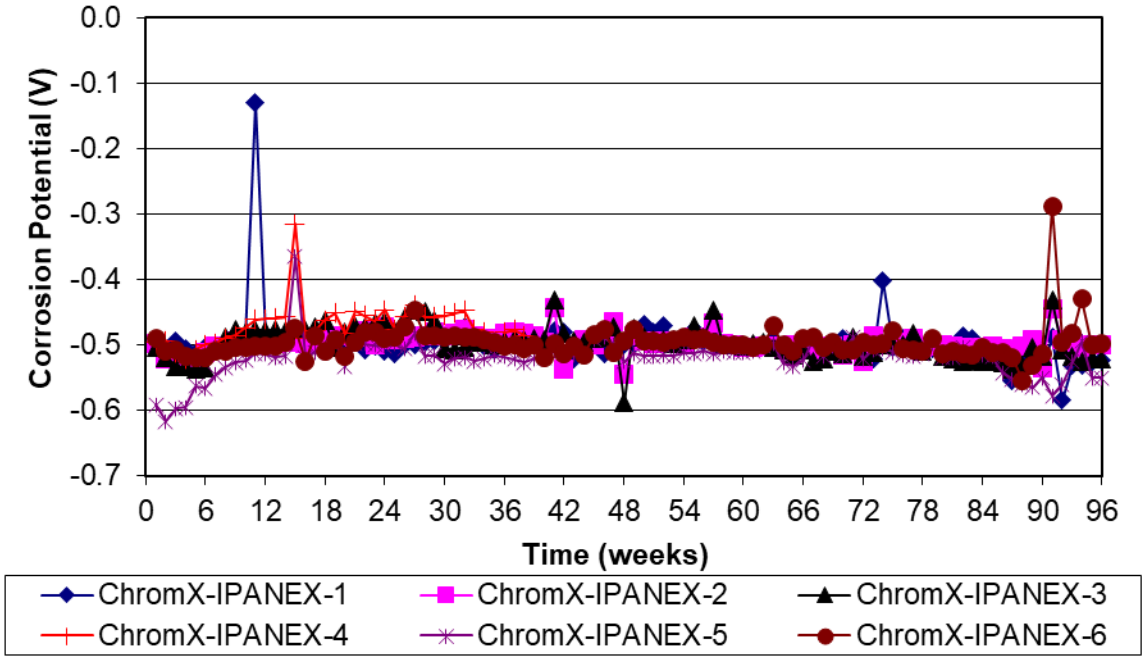

Figure C.108: Corrosion potential of ChromX-IPANEX reinforcement in the cracked beam test

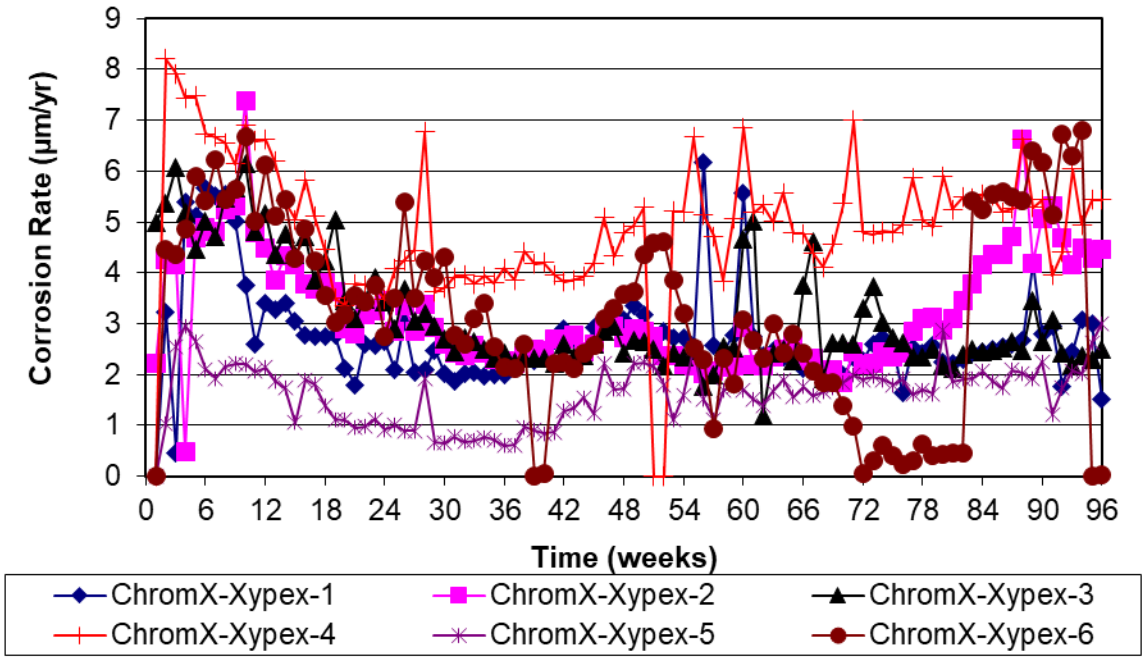

Figure C.109: Corrosion rate of ChromX-Xypex reinforcement in the cracked beam test

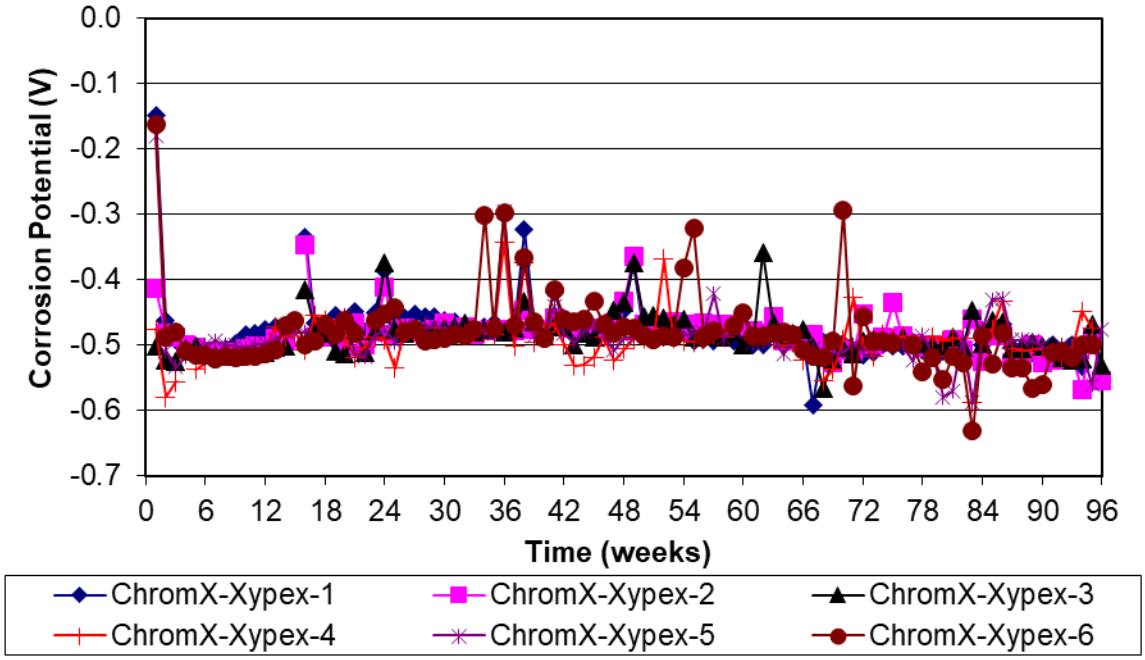

Figure C.110: Corrosion potential of ChromX-Xypex reinforcement in the cracked beam test

APPENDIX D: STUDENT'S T-TEST COMPARISONS

Table D.1: Student's T-Test comparisons for macrocell corrosion losses at 15 weeks based on total area for rapid macrocell specimens

	Conv-A	Conv-B	Conv-C	ECR1	ECR2	ECR1-ND	ECR2-ND	ECR1-UV-1000	ECR1-UV-1000 (b)	ECR1-UV-500	ECR1-UV-250	ECR2-UV-1000	ECR2-UV-200	ECR2-UV-100	ECR1-UV-1000-ND	ECR1-Bent	A767	A767-Bent	A767-ND	A1094	A1094-Bent	A1094-ND	ChromX
Conv-A	1.00	0.02	0.01	0.00	0.00	0.00	0.00	0.00	0.00	0.00	0.00	0.00	0.00	0.00	0.00	0.00	0.00	0.00	0.00	0.04	1.00	0.02	0.01
Conv-B	0.02	1.00	0.85	0.00	0.00	0.00	0.00	0.00	0.00	0.00	0.00	0.00	0.00	0.00	0.00	0.00	0.04	0.00	0.00	0.00	0.02	1.00	0.85
Conv-C	0.01	0.85	1.00	0.00	0.00	0.00	0.00	0.00	0.00	0.00	0.00	0.00	0.00	0.00	0.00	0.00	0.04	0.00	0.00	0.00	0.01	0.85	1.00
ECR1	0.00	0.00	0.00	1.00	0.96	0.05	0.07	0.00	0.01	0.00	0.00	0.00	0.00	0.00	0.10	0.09	0.00	0.06	0.00	0.27	0.00	0.00	0.00
ECR2	0.00	0.00	0.00	0.96	1.00	0.00	0.00	0.00	0.01	0.00	0.00	0.00	0.00	0.00	0.01	0.00	0.00	0.08	0.00	0.31	0.00	0.00	0.00
ECR1-ND	0.00	0.00	0.00	0.05	0.00	1.00	0.10	0.00	0.00	0.00	0.00	0.09	0.00	0.00	0.28	0.01	0.00	0.02	0.00	0.21	0.00	0.00	0.00
ECR2-ND	0.00	0.00	0.00	0.07	0.00	0.10	1.00	0.00	0.00	0.00	0.00	0.10	0.00	0.00	0.59	0.02	0.00	0.02	0.00	0.21	0.00	0.00	0.00
ECR1-UV-1000	0.00	0.00	0.00	0.00	0.00	0.00	0.00	1.00	0.05	0.84	0.06	0.94	0.74	0.04	0.00	0.00	0.00	1.00	0.00	0.68	0.00	0.00	0.00
ECR1-UV-1000 (b)	0.00	0.00	0.00	0.01	0.01	0.00	0.00	0.05	1.00	0.07	0.00	0.57	0.16	0.83	0.00	0.00	0.00	0.38	0.00	0.47	0.00	0.00	0.00
ECR1-UV-500	0.00	0.00	0.00	0.00	0.00	0.00	0.00	0.84	0.07	1.00	0.04	0.99	0.66	0.07	0.00	0.00	0.00	0.94	0.00	0.66	0.00	0.00	0.00
ECR1-UV-250	0.00	0.00	0.00	0.00	0.00	0.00	0.00	0.06	0.00	0.04	1.00	0.51	0.48	0.00	0.00	0.00	0.00	0.42	0.00	0.90	0.00	0.00	0.00
ECR2-UV-1000	0.01	0.00	0.00	0.17	0.20	0.09	0.10	0.94	0.57	0.99	0.51	1.00	0.81	0.60	0.10	0.10	0.00	0.95	0.00	0.71	0.01	0.00	0.00
ECR2-UV-200	0.00	0.00	0.00	0.01	0.02	0.00	0.00	0.74	0.16	0.66	0.48	0.81	1.00	0.18	0.00	0.00	0.00	0.83	0.00	0.76	0.00	0.00	0.00
ECR2-UV-100	0.00	0.00	0.00	0.00	0.00	0.00	0.00	0.04	0.83	0.07	0.00	0.60	0.18	1.00	0.00	0.00	0.00	0.42	0.00	0.49	0.00	0.00	0.00
ECR1-UV-1000-ND	0.00	0.00	0.00	0.10	0.01	0.28	0.59	0.00	0.00	0.00	0.00	0.10	0.00	0.00	1.00	1.00	0.00	0.02	0.00	0.22	0.00	0.00	0.00
ECR1-Bent	0.00	0.00	0.00	0.09	0.00	0.01	0.02	0.00	0.00	0.00	0.00	0.10	0.00	0.00	1.00	1.00	0.00	0.02	0.00	0.22	0.00	0.00	0.00
A767	0.00	0.04	0.04	0.00	0.00	0.00	0.00	0.00	0.00	0.00	0.00	0.00	0.00	0.00	0.00	0.00	1.00	0.00	0.36	0.00	0.00	0.04	0.04
A767-Bent	0.00	0.00	0.00	0.06	0.08	0.02	0.02	1.00	0.38	0.94	0.42	0.95	0.83	0.42	0.02	0.02	0.00	1.00	0.00	0.70	0.00	0.00	0.00
A767-ND	0.00	0.00	0.00	0.00	0.00	0.00	0.00	0.00	0.00	0.00	0.00	0.00	0.00	0.00	0.00	0.00	0.00	0.00	1.00	0.00	0.00	0.00	0.00
A1094	0.04	0.00	0.00	0.27	0.31	0.21	0.21	0.68	0.47	0.66	0.90	0.71	0.76	0.49	0.22	0.22	0.00	0.70	0.00	1.00	0.04	0.00	0.00
A1094-Bent	0.01	0.00	0.00	0.00	0.01	0.00	0.00	0.10	0.02	0.09	0.33	0.28	0.22	0.02	0.00	0.00	0.00	0.20	0.00	0.82	0.01	0.00	0.00
A1094-ND	0.00	0.00	0.00	0.58	0.61	0.41	0.42	0.51	0.89	0.54	0.27	0.65	0.45	0.85	0.43	0.43	0.00	0.56	0.00	0.49	0.00	0.00	0.00
ChromX	0.14	0.11	0.03	0.00	0.00	0.00	0.00	0.00	0.00	0.00	0.00	0.00	0.00	0.00	0.00	0.00	0.01	0.00	0.00	0.00	0.14	0.11	0.03

Table D.2: Student's T-Test comparisons for LPR corrosion losses at 15 weeks based on total area for rapid macrocell specimens

	Conv-A	Conv-B	Conv-C	ECR1	ECR2	ECR1-ND	ECR2-ND	ECR1-UV-1000	ECR1-UV-1000 (b)	ECR1-UV-500	ECR1-UV-250	ECR2-UV-1000	ECR2-UV-200	ECR2-UV-100	ECR1-UV-1000-ND	ECR1-Bent	A767	A767-Bent	A767-ND	A1094	A1094-Bent	A1094-ND	ChromX
Conv-A	1.00	0.07	0.04	0.00	0.00	0.00	0.00	0.05	0.00	0.00	0.00	0.00	0.00	0.00	0.00	0.00	0.00	0.00	0.04	0.06	0.44	0.00	0.00
Conv-B	0.07	1.00	0.16	0.01	0.01	0.00	0.00	0.02	0.00	0.00	0.00	0.00	0.00	0.00	0.00	0.00	0.00	0.00	0.04	0.03	0.05	0.01	0.01
Conv-C	0.04	0.16	1.00	0.00	0.00	0.00	0.00	0.01	0.00	0.00	0.00	0.00	0.00	0.00	0.00	0.00	0.00	0.00	0.04	0.00	0.12	0.00	0.00
ECR1	0.00	0.01	0.00	1.00	0.58	0.03	0.03	0.14	0.00	0.01	0.14	0.02	0.20	0.35	0.51	0.91	0.00	0.00	0.06	0.00	0.06	0.01	0.00
ECR2	0.00	0.01	0.00	0.58	1.00	0.08	0.08	0.16	0.00	0.04	0.43	0.27	0.65	0.74	0.31	0.55	0.00	0.00	0.06	0.00	0.07	0.02	0.00
ECR1-ND	0.00	0.00	0.00	0.03	0.08	1.00	0.34	0.08	0.00	0.00	0.01	0.00	0.01	0.04	0.06	0.18	0.00	0.00	0.04	0.00	0.03	0.00	0.00
ECR2-ND	0.00	0.00	0.00	0.03	0.08	0.34	-	0.07	0.00	0.00	0.01	0.00	0.01	0.03	0.05	0.17	0.00	0.00	0.04	0.00	0.03	0.00	0.00
ECR1-UV-1000	0.05	0.02	0.01	0.14	0.16	0.08	0.07	1.00	0.34	0.33	0.16	0.21	0.14	0.14	0.09	0.10	0.00	0.00	0.04	0.36	0.43	0.67	0.82
ECR1-UV-1000 (b)	0.00	0.00	0.00	0.00	0.00	0.00	0.00	0.34	1.00	0.90	0.01	0.00	0.00	0.00	0.00	0.00	0.00	0.00	0.04	0.00	0.10	0.18	0.01
ECR1-UV-500	0.00	0.00	0.00	0.01	0.04	0.00	0.00	0.33	0.90	1.00	0.09	0.09	0.04	0.05	0.00	0.01	0.00	0.00	0.04	0.00	0.10	0.21	0.03
ECR1-UV-250	0.00	0.00	0.00	0.14	0.43	0.01	0.01	0.16	0.01	0.09	1.00	0.89	0.62	0.63	0.05	0.14	0.00	0.00	0.04	0.00	0.05	0.02	0.00
ECR2-UV-1000	0.00	0.01	0.00	0.02	0.27	0.00	0.00	0.21	0.00	0.09	0.89	1.00	0.40	0.48	0.00	0.05	0.00	0.00	0.06	0.00	0.08	0.04	0.00
ECR2-UV-200	0.00	0.00	0.00	0.20	0.65	0.01	0.01	0.14	0.00	0.04	0.62	0.40	1.00	0.94	0.06	0.21	0.00	0.00	0.04	0.00	0.05	0.01	0.00
ECR2-UV-100	0.00	0.00	0.00	0.35	0.74	0.04	0.03	0.14	0.00	0.05	0.63	0.48	0.94	1.00	0.16	0.32	0.00	0.00	0.04	0.00	0.05	0.02	0.00
ECR1-UV-1000-ND	0.00	0.00	0.00	0.51	0.31	0.06	0.05	0.09	0.00	0.00	0.05	0.00	0.06	0.16	1.00	0.72	0.00	0.00	0.04	0.00	0.03	0.00	0.00
ECR1-Bent	0.00	0.00	0.00	0.91	0.55	0.18	0.17	0.10	0.00	0.01	0.14	0.05	0.21	0.32	0.72	1.00	0.00	0.00	0.04	0.00	0.04	0.01	0.00
A767	0.00	0.00	0.00	0.00	0.00	0.00	0.00	0.00	0.00	0.00	0.00	0.00	0.00	0.00	0.00	0.00	1.00	0.00	0.50	0.00	0.00	0.00	0.00
A767-Bent	0.00	0.00	0.00	0.00	0.00	0.00	0.00	0.00	0.00	0.00	0.00	0.00	0.00	0.00	0.00	0.00	0.00	1.00	0.06	0.00	0.00	0.00	0.00
A767-ND	0.04	0.04	0.04	0.06	0.06	0.04	0.04	0.04	0.04	0.04	0.04	0.06	0.04	0.04	0.04	0.04	0.50	0.06	1.00	0.04	0.04	0.04	0.04
A1094	0.06	0.03	0.00	0.00	0.00	0.00	0.00	0.36	0.00	0.00	0.00	0.00	0.00	0.00	0.00	0.00	0.00	0.00	0.04	1.00	0.84	0.04	0.04
A1094-Bent	0.44	0.05	0.12	0.06	0.07	0.03	0.03	0.43	0.10	0.10	0.05	0.08	0.05	0.05	0.03	0.04	0.00	0.00	0.04	0.84	1.00	0.21	0.26
A1094-ND	0.00	0.01	0.00	0.01	0.02	0.00	0.00	0.67	0.18	0.21	0.02	0.04	0.01	0.02	0.00	0.01	0.00	0.00	0.04	0.04	0.21	1.00	0.61
ChromX	0.00	0.01	0.00	0.00	0.00	0.00	0.00	0.82	0.01	0.03	0.00	0.00	0.00	0.00	0.00	0.00	0.00	0.00	0.04	0.04	0.26	0.61	1.00

Table D.3: Student's T-Test comparisons for corrosion initiation age in Southern Exposure specimens

	Conv-A	Conv-B	Conv-C	ECR1	ECR1-ND	ECR1-UV-1000	ECR1-UV-1000-ND	A767	A767-ND	A767-Bent	A1094	A1094-ND	A1094-Bent	ChromX	Conv-B-IPANEX	ChromX-IPANEX	Conv-B-Xypex	ChromX-Xypex
Conv-A	1.00	0.83	0.07	0.10	-	0.14	-	0.02	0.00	0.00	0.00	0.04	0.04	0.03	0.68	0.01	0.15	0.06
Conv-B	0.83	1.00	0.30	0.13	-	0.19	-	0.03	0.00	0.00	0.00	0.05	0.04	0.09	0.70	0.02	0.43	0.18
Conv-C	0.07	0.30	1.00	0.06	-	0.08	-	0.00	0.00	0.00	0.00	0.03	0.03	0.01	0.02	0.01	0.30	0.02
ECR1	0.10	0.13	0.06	1.00	-	0.86	-	0.22	0.05	0.03	0.05	0.29	0.30	0.96	0.10	0.38	0.08	0.69
ECR1-ND	-	-	-	-	-	-	-	-	-	-	-	-	-	-	-	-	-	-
ECR1-UV-1000	0.14	0.19	0.08	0.86	-	1.00	-	0.19	0.05	0.03	0.04	0.25	0.26	0.81	0.13	0.31	0.10	0.85
ECR1-UV-1000-ND	-	-	-	-	-	-	-	-	-	-	-	-	-	-	-	-	-	-
A767	0.02	0.03	0.00	0.22	-	0.19	-	1.00	0.60	0.37	0.50	0.95	0.81	0.22	0.02	0.58	0.01	0.13
A767-ND	0.00	0.00	0.00	0.05	-	0.05	-	0.60	1.00	0.61	0.83	0.58	0.41	0.03	0.00	0.18	0.00	0.01
A767-Bent	0.00	0.00	0.00	0.03	-	0.03	-	0.37	0.61	1.00	0.79	0.38	0.24	0.01	0.00	0.09	0.00	0.01
A1094	0.00	0.00	0.00	0.05	-	0.04	-	0.50	0.83	0.79	1.00	0.49	0.34	0.03	0.00	0.16	0.00	0.02
A1094-ND	0.04	0.05	0.03	0.29	-	0.25	-	0.95	0.58	0.38	0.49	1.00	0.87	0.29	0.04	0.66	0.03	0.18
A1094-Bent	0.04	0.04	0.03	0.30	-	0.26	-	0.81	0.41	0.24	0.34	0.87	1.00	0.30	0.04	0.76	0.03	0.18
ChromX	0.03	0.09	0.01	0.96	-	0.81	-	0.22	0.03	0.01	0.03	0.29	0.30	1.00	0.02	0.37	0.01	0.63
Conv-B-IPANEX	0.68	0.70	0.02	0.10	-	0.13	-	0.02	0.00	0.00	0.00	0.04	0.04	0.02	1.00	0.01	0.03	0.05
ChromX-IPANEX	0.01	0.02	0.01	0.38	-	0.31	-	0.58	0.18	0.09	0.16	0.66	0.76	0.37	0.01	1.00	0.01	0.19
Conv-B-Xypex	0.15	0.43	0.30	0.08	-	0.10	-	0.01	0.00	0.00	0.00	0.03	0.03	0.01	0.03	0.01	1.00	0.02
ChromX-Xypex	0.06	0.18	0.02	0.69	-	0.85	-	0.13	0.01	0.01	0.02	0.18	0.18	0.63	0.05	0.19	0.02	1.00

Table D.4: Student's T-Test comparisons for critical chloride corrosion threshold in Southern Exposure specimens

	Conv-A	Conv-B	Conv-C	ECR1	ECR1-ND	ECR1-UV-1000	ECR1-UV-1000-ND	A767	A767-ND	A767-Bent	A1094	A1094-ND	A1094-Bent	ChromX	Conv-B-IPANEX	ChromX-IPANEX	Conv-B-Xypex	ChromX-Xypex
Conv-A	1.00	0.76	0.71	0.43	-	-	-	0.22			0.71			0.58	0.40	0.40	0.50	0.21
Conv-B	0.76	1.00	0.96	0.41	-	-	-	0.61			0.57			0.48	0.81	0.34	0.88	0.18
Conv-C	0.71	0.96	1.00	0.40	-	-	-	0.65			0.51			0.43	0.86	0.31	0.93	0.18
ECR1	0.43	0.41	0.40	1.00	-	-	-	0.37			0.46			0.47	0.39	0.54	0.40	0.84
ECR1-ND	-	-	-	-	-	-	-	-			-			-	-	-	-	-
ECR1-UV-1000	-	-	-	-	-	-	-	-			-			-	-	-	-	-
ECR1-UV-1000-ND	-	-	-	-	-	-	-	-			-			-	-	-	-	-
A767																		
A767-ND	0.22	0.61	0.65	0.37	-	-	-	1.00			0.03			0.09	0.45	0.19	0.46	0.14
A767-Bent																		
A1094																		
A1094-ND	0.71	0.57	0.51	0.46	-	-	-	0.03			1.00			0.78	0.11	0.50	0.21	0.24
A1094-Bent																		
ChromX	0.58	0.48	0.43	0.47	-	-	-	0.09			0.78			1.00	0.16	0.63	0.22	0.27
Conv-B-IPANEX	0.40	0.81	0.86	0.39	-	-	-	0.45			0.11			0.16	1.00	0.23	0.87	0.16
ChromX-IPANEX	0.40	0.34	0.31	0.54	-	-	-	0.19			0.50			0.63	0.23	1.00	0.25	0.39
Conv-B-Xypex	0.50	0.88	0.93	0.40	-	-	-	0.46			0.21			0.22	0.87	0.25	1.00	0.16
ChromX-Xypex	0.21	0.18	0.18	0.84	-	-	-	0.14			0.24			0.27	0.16	0.39	0.16	1.00

Table D.5: Student's T-Test comparisons for macrocell corrosion losses at 96 weeks based on total area for Southern Exposure specimens

	Conv-A	Conv-B	Conv-C	ECR1	ECR1-ND	ECR1-UV-1000	ECR1-UV-1000-ND	A767	A767-ND	A767-Bent	A1094	A1094-ND	A1094-Bent	ChromX	ChromX-IPANEX	ChromX-Xypex	Conv-B-IPANEX	Conv-B-Xypex
Conv-A	1.00	0.03	0.00	0.00	0.01	0.02	0.01	0.00	0.00	0.13	0.00	0.00	0.01	0.01	0.01	0.00	0.00	0.21
Conv-B	0.03	1.00	0.98	0.01	0.01	0.02	0.01	0.00	0.00	0.01	0.00	0.00	0.00	0.00	0.00	0.00	0.56	0.14
Conv-C	0.00	0.98	1.00	0.00	0.00	0.00	0.00	0.00	0.00	0.00	0.00	0.00	0.00	0.00	0.00	0.00	0.29	0.01
ECR1	0.00	0.01	0.00	1.00	0.51	0.02	0.64	0.36	0.09	0.11	0.97	0.65	0.87	0.10	0.02	0.06	0.00	0.00
ECR1-ND	0.01	0.01	0.00	0.51	1.00	0.05	0.99	0.50	0.16	0.18	0.87	0.76	0.92	0.17	0.04	0.12	0.00	0.00
ECR1-UV-1000	0.02	0.02	0.00	0.02	0.05	1.00	0.08	0.94	0.35	0.23	0.36	0.87	0.94	0.39	0.12	0.32	0.00	0.00
ECR1-UV-1000-ND	0.01	0.01	0.00	0.64	0.99	0.08	1.00	0.50	0.16	0.18	0.87	0.75	0.92	0.18	0.05	0.12	0.00	0.00
A767	0.00	0.00	0.00	0.36	0.50	0.94	0.50	1.00	0.23	0.09	0.38	0.88	0.93	0.29	0.06	0.23	0.00	0.00
A767-ND	0.00	0.00	0.00	0.09	0.16	0.35	0.16	0.23	1.00	0.21	0.07	0.27	0.57	0.88	0.59	0.91	0.00	0.00
A767-Bent	0.13	0.01	0.00	0.11	0.18	0.23	0.18	0.09	0.21	1.00	0.05	0.09	0.19	0.23	0.29	0.19	0.00	0.02
A1094	0.00	0.00	0.00	0.97	0.87	0.36	0.87	0.38	0.07	0.05	1.00	0.60	0.84	0.09	0.02	0.06	0.00	0.00
A1094-ND	0.00	0.00	0.00	0.65	0.76	0.87	0.75	0.88	0.27	0.09	0.60	1.00	0.98	0.35	0.11	0.28	0.00	0.00
A1094-Bent	0.01	0.00	0.00	0.87	0.92	0.94	0.92	0.93	0.57	0.19	0.84	0.98	1.00	0.65	0.43	0.60	0.00	0.00
ChromX	0.01	0.00	0.00	0.10	0.17	0.39	0.18	0.29	0.88	0.23	0.09	0.35	0.65	1.00	0.49	0.96	0.00	0.00
ChromX-IPANEX	0.01	0.00	0.00	0.02	0.04	0.12	0.05	0.06	0.59	0.29	0.02	0.11	0.43	0.49	1.00	0.47	0.00	0.00
ChromX-Xypex	0.00	0.00	0.00	0.06	0.12	0.32	0.12	0.23	0.91	0.19	0.06	0.28	0.60	0.96	0.47	1.00	0.00	0.00
Conv-B-IPANEX	0.00	0.56	0.29	0.00	0.00	0.00	0.00	0.00	0.00	0.00	0.00	0.00	0.00	0.00	0.00	0.00	1.00	0.01
Conv-B-Xypex	0.21	0.14	0.01	0.00	0.00	0.00	0.00	0.00	0.00	0.02	0.00	0.00	0.00	0.00	0.00	0.00	0.01	1.00

Table D.6: Student's T-Test comparisons for macrocell corrosion losses at 96 weeks based on total area for cracked beam specimens

	Conv-A	Conv-B	Conv-C	ECR1	ECR1-ND	ECR1-UV-1000	ECR1-UV-1000-ND	A767	A767-ND	A1094	A1094-ND	ChromX	ChromX-IPANEX	ChromX-Xypex	Conv-B-IPANEX	Conv-B-Xypex
Conv-A	1.00	0.27	0.79	0.00	0.00	0.00	0.00	0.01	0.01	0.00	0.00	0.05	0.02	0.01	0.02	0.01
Conv-B	0.27	1.00	0.48	0.03	0.07	0.00	0.00	0.03	0.03	0.02	0.01	0.05	0.04	0.03	0.59	0.03
Conv-C	0.79	0.48	1.00	0.00	0.00	0.00	0.00	0.01	0.01	0.00	0.00	0.05	0.01	0.01	0.10	0.01
ECR1	0.00	0.03	0.00	1.00	0.28	0.00	0.74	0.11	0.02	0.10	0.00	0.01	0.00	0.00	0.00	0.00
ECR1-ND	0.00	0.07	0.00	0.28	1.00	0.00	0.32	0.15	0.04	0.13	0.00	0.01	0.00	0.00	0.01	0.00
ECR1-UV-1000	0.00	0.00	0.00	0.00	0.00	1.00	0.00	0.34	0.09	0.63	0.00	0.01	0.00	0.00	0.00	0.00
ECR1-UV-1000-ND	0.00	0.07	0.00	0.74	0.32	0.00	1.00	0.18	0.05	0.17	0.00	0.01	0.00	0.00	0.01	0.00
A767	0.01	0.03	0.01	0.11	0.15	0.34	0.18	1.00	0.75	0.64	0.00	0.17	0.17	0.31	0.00	0.28
A767-ND	0.01	0.03	0.01	0.02	0.04	0.09	0.05	0.75	1.00	0.36	0.00	0.22	0.19	0.41	0.00	0.36
A1094	0.00	0.02	0.00	0.10	0.13	0.63	0.17	0.64	0.36	1.00	0.00	0.05	0.02	0.07	0.00	0.06
A1094-ND	0.00	0.01	0.00	0.00	0.00	0.32	0.01	0.57	0.23	0.98	1.00	0.02	0.00	0.01	0.00	0.01
ChromX	0.05	0.05	0.05	0.01	0.01	0.01	0.01	0.17	0.22	0.05	0.02	1.00	0.79	0.49	0.00	0.55
ChromX-IPANEX	0.02	0.04	0.01	0.00	0.00	0.00	0.00	0.17	0.19	0.02	0.00	0.79	1.00	0.51	0.00	0.60
ChromX-Xypex	0.01	0.03	0.01	0.00	0.00	0.00	0.00	0.31	0.41	0.07	0.01	0.49	0.51	1.00	0.00	0.90
Conv-B-IPANEX	0.02	0.59	0.10	0.00	0.01	0.00	0.01	0.00	0.00	0.00	0.00	0.00	0.00	0.00	1.00	0.00
Conv-B-Xypex	0.01	0.03	0.01	0.00	0.00	0.00	0.00	0.28	0.36	0.06	0.01	0.55	0.60	0.90	0.00	1.00

Table D.7: Student's T-Test comparisons for LPR corrosion losses at 96 weeks based on total area for Southern Exposure specimens

	Conv-A	Conv-B	Conv-C	ECR1	ECR1-ND	ECR1-UV-1000	ECR1-UV-1000-ND	A767	A767-ND	A767-Bent	A1094	A1094-ND	A1094-Bent	ChromX	ChromX-IPANEX	ChromX-Xypex	Conv-B-IPANEX	Conv-B-Xypex
Conv-A	1.00	0.01	0.01	0.00	0.00	0.00	0.00	0.76	0.03	0.16	0.42	0.32	0.30	0.00	0.00	0.00	0.04	0.01
Conv-B	0.01	1.00	0.87	0.00	0.00	0.00	0.00	0.06	0.00	0.95	0.02	0.01	0.46	0.00	0.00	0.00	0.55	0.43
Conv-C	0.01	0.87	1.00	0.00	0.00	0.00	0.00	0.05	0.00	0.98	0.02	0.01	0.41	0.00	0.00	0.00	0.50	0.55
ECR1	0.00	0.00	0.00	1.00	0.51	0.02	0.24	0.03	0.00	0.01	0.03	0.03	0.00	0.09	0.01	0.02	0.00	0.00
ECR1-ND	0.00	0.00	0.00	0.51	1.00	0.07	0.99	0.05	0.01	0.02	0.06	0.06	0.01	0.15	0.02	0.05	0.00	0.00
ECR1-UV-1000	0.00	0.00	0.00	0.02	0.07	1.00	0.06	0.07	0.01	0.02	0.08	0.09	0.02	0.26	0.08	0.11	0.00	0.00
ECR1-UV-1000-ND	0.00	0.00	0.00	0.24	0.99	0.06	1.00	0.05	0.01	0.02	0.06	0.06	0.01	0.15	0.02	0.05	0.00	0.00
A767	0.74	0.05	0.05	0.03	0.05	0.07	0.05	1.00	0.34	0.15	0.72	0.63	0.29	0.11	0.07	0.09	0.11	0.03
A767-ND	0.04	0.00	0.00	0.00	0.01	0.01	0.01	0.34	1.00	0.03	0.55	0.66	0.05	0.14	0.03	0.08	0.00	0.00
A767-Bent	0.11	0.94	0.98	0.01	0.02	0.02	0.02	0.15	0.03	1.00	0.09	0.07	0.56	0.01	0.01	0.02	0.70	0.67
A1094	0.39	0.01	0.02	0.03	0.06	0.08	0.06	0.72	0.55	0.09	1.00	0.89	0.15	0.15	0.09	0.12	0.04	0.01
A1094-ND	0.29	0.01	0.01	0.03	0.06	0.09	0.06	0.63	0.66	0.07	0.89	1.00	0.12	0.18	0.11	0.15	0.03	0.01
A1094-Bent	0.26	0.45	0.41	0.00	0.01	0.02	0.01	0.29	0.05	0.56	0.15	0.12	1.00	0.01	0.01	0.01	0.72	0.22
ChromX	0.00	0.00	0.00	0.09	0.15	0.26	0.15	0.11	0.14	0.01	0.15	0.18	0.01	1.00	0.80	0.98	0.00	0.00
ChromX-IPANEX	0.00	0.00	0.00	0.01	0.02	0.08	0.02	0.07	0.03	0.01	0.09	0.11	0.01	0.80	1.00	0.70	0.00	0.00
ChromX-Xypex	0.00	0.00	0.00	0.02	0.05	0.11	0.05	0.09	0.08	0.02	0.12	0.15	0.01	0.98	0.70	1.00	0.00	0.00
Conv-B-IPANEX	0.04	0.55	0.50	0.00	0.00	0.00	0.00	0.11	0.00	0.70	0.04	0.03	0.72	0.00	0.00	0.00	1.00	0.22
Conv-B-Xypex	0.01	0.43	0.55	0.00	0.00	0.00	0.00	0.03	0.00	0.67	0.01	0.01	0.22	0.00	0.00	0.00	0.22	1.00

Table D.8: Student's T-Test comparisons for LPR corrosion losses at 96 weeks based on total area for cracked beam specimens

	Conv-A	Conv-B	Conv-C	ECR	ECR-ND	ECR-UV-1000	ECR-UV-1000-ND	A767	A767-ND	A1094	A1094-ND	ChromX	ChromX-IPANEX	ChromX-Xypex	Conv-B-IPANEX	Conv-B-Xypex
Conv-A	1.00	0.48	0.22	0.00	0.00	0.00	0.00	0.02	0.01	0.01	0.00	0.00	0.00	0.00	0.26	0.01
Conv-B	0.48	1.00	0.15	0.00	0.00	0.00	0.00	0.02	0.01	0.01	0.00	0.00	0.00	0.00	0.55	0.00
Conv-C	0.22	0.15	1.00	0.00	0.01	0.02	0.01	0.39	0.25	0.28	0.08	0.05	0.17	0.02	0.11	0.31
ECR	0.00	0.00	0.00	1.00	0.17	0.00	1.00	0.00	0.00	0.00	0.00	0.00	0.00	0.00	0.00	0.00
ECR-ND	0.00	0.00	0.01	0.17	1.00	0.00	0.15	0.01	0.00	0.01	0.00	0.00	0.00	0.00	0.00	0.00
ECR-UV-1000	0.00	0.00	0.02	0.00	0.00	1.00	0.00	0.03	0.01	0.03	0.00	0.01	0.00	0.00	0.00	0.00
ECR-UV-1000-ND	0.00	0.00	0.01	0.00	0.15	0.00	1.00	0.01	0.00	0.01	0.00	0.00	0.00	0.00	0.00	0.00
A767	0.02	0.02	0.39	0.00	0.01	0.03	0.01	1.00	0.82	0.79	0.43	0.30	0.96	0.13	0.01	0.61
A767-ND	0.01	0.01	0.25	0.00	0.00	0.01	0.00	0.82	1.00	0.96	0.53	0.36	0.77	0.13	0.00	0.33
A1094	0.01	0.01	0.28	0.00	0.01	0.03	0.01	0.79	0.96	1.00	0.62	0.45	0.75	0.20	0.01	0.36
A1094-ND	0.00	0.00	0.08	0.00	0.00	0.00	0.00	0.43	0.53	0.62	1.00	0.72	0.16	0.17	0.00	0.01
ChromX	0.00	0.00	0.05	0.00	0.00	0.01	0.00	0.30	0.36	0.45	0.72	1.00	0.09	0.37	0.00	0.01
ChromX-IPANEX	0.00	0.00	0.17	0.00	0.00	0.00	0.00	0.96	0.77	0.75	0.16	0.09	1.00	0.00	0.00	0.11
ChromX-Xypex	0.00	0.00	0.02	0.00	0.00	0.00	0.00	0.13	0.13	0.20	0.17	0.37	0.00	1.00	0.00	0.00
Conv-B-IPANEX	0.26	0.55	0.11	0.00	0.00	0.00	0.00	0.01	0.00	0.01	0.00	0.00	0.00	0.00	1.00	0.00
Conv-B-Xypex	0.01	0.00	0.31	0.00	0.00	0.00	0.00	0.61	0.33	0.36	0.01	0.01	0.11	0.00	0.00	1.00

Table D.9: Student's T-Test comparisons for corrosion rates based on LPR corrosion losses at 96 weeks based on total area for cracked beam specimens

	Conv-A	Conv-B	Conv-C	ECR	ECR-UV	A767	A1094	ChromX	IPANEX-ChromX	Xypex-ChromX	IPANEX-Conv-B	Xypex-Conv-B
Conv-A	1.00	0.14	0.22	0.00	0.00	0.02	0.01	0.00	0.00	0.00	0.18	0.01
Conv-B	0.14	1.00	0.04	0.00	0.00	0.00	0.00	0.00	0.00	0.00	0.85	0.00
Conv-C	0.22	0.04	1.00	0.00	0.00	0.38	0.27	0.03	0.17	0.02	0.04	0.30
ECR	0.00	0.00	0.00	1.00	0.00	0.00	0.00	0.00	0.00	0.00	0.00	0.00
ECR-UV	0.00	0.00	0.00	0.00	1.00	0.00	0.00	0.00	0.00	0.00	0.00	0.00
A767	0.02	0.00	0.38	0.00	0.00	1.00	0.79	0.18	0.96	0.13	0.00	0.61
A1094	0.01	0.00	0.27	0.00	0.00	0.79	1.00	0.29	0.75	0.20	0.00	0.35
ChromX	0.00	0.00	0.03	0.00	0.00	0.18	0.29	1.00	0.05	0.79	0.00	0.01
IPANEX-ChromX	0.00	0.00	0.17	0.00	0.00	0.96	0.75	0.05	1.00	0.00	0.00	0.11
Xypex-ChromX	0.00	0.00	0.02	0.00	0.00	0.13	0.20	0.79	0.00	1.00	0.00	0.00
IPANEX-Conv-B	0.18	0.85	0.04	0.00	0.00	0.00	0.00	0.00	0.00	0.00	1.00	0.00
Xypex-Conv-B	0.01	0.00	0.30	0.00	0.00	0.61	0.35	0.01	0.11	0.00	0.00	1.00

APPENDIX E: LPR CORROSION RATES OF RAPID MACROCELL SPECIMENS

Table E.1: LPR corrosion rate (um/yr) in the rapid macrocell test for Conv-A

Week	Specimen 1	Specimen 2	Specimen 3	Specimen 4	Specimen 5	Specimen 6
3	9.98	12.46	17.76	31.92	14.69	14.69
6	12.41	47.91	30.11	16.60	23.20	12.53
9	35.55	4.89	17.98	38.98	34.03	35.44
12	16.39	37.63	12.45	15.53	22.23	33.79
15	59.28	120.64	58.71	60.32	110.84	57.58

Table E.2: LPR corrosion rate (um/yr) in the rapid macrocell test for Conv-B

Week	Specimen 1	Specimen 2	Specimen 3	Specimen 4	Specimen 5	Specimen 6
3	39.39	50.69	60.69	66.71	32.54	0.00
6	54.52	54.02	63.24	79.46	68.92	119.25
9	63.00	33.08	62.73	85.75	76.21	69.30
12	6.43	10.16	3.45	333.85	9.68	280.72
15	51.84	42.25	17.92	105.07	55.94	57.50

Table E.3: LPR corrosion rate (um/yr) in the rapid macrocell test for Conv-C

Week	Specimen 1	Specimen 2	Specimen 3	Specimen 4	Specimen 5	Specimen 6
3	36.99	43.41	41.02	39.16	39.16	41.40
6	25.96	32.22	17.81	25.35	25.35	20.06
9	35.19	59.48	35.96	37.98	37.98	31.56
12	90.49	59.10	46.99	43.07	43.07	63.70
15	74.52	46.72	42.04	50.78	50.78	57.41

Table E.4: LPR corrosion rate (um/yr) in the rapid macrocell test for ECR1

Week	Specimen 1	Specimen 2	Specimen 3	Specimen 4	Specimen 5	Specimen 6
3	0.50	1.58	0.28	4.34	0.35	2.08
6	0.54	3.25	0.23	0.03	1.74	0.00
9	0.53	3.76	0.15	0.06	2.97	0.00
12	0.50	4.06	0.12	0.03	2.33	0.00
15	0.50	4.65	0.16	0.00	3.11	-

- Bad reading

Table E.5: LPR corrosion rate (um/yr) in the rapid macrocell test for ECR2

Week	Specimen 1	Specimen 2	Specimen 3	Specimen 4	Specimen 5
3	0.12	0.79	10.90	0.49	0.38
6	0.39	1.22	2.58	6.79	0.71
9	0.27	0.61	17.63	0.38	0.39
12	0.49	2.13	0.83	0.15	0.63
15	0.62	2.88	2.89	0.53	0.42

ECR1-ND and ECR2-ND show corrosion rates near zero.

Table E.6: LPR corrosion rate (um/yr) in the rapid macrocell test for ECR1-UV-1000

Week	Specimen 1	Specimen 2	Specimen 3	Specimen 4	Specimen 5	Specimen 6
3	4.67	5.19	4.13	4.02	4.99	3.66
6	24.06	258.13	4.32	8.63	8.13	5.98
9	1.25	0.67	2.04	10.25	10.01	7.21
12	1.26	0.88	7.76	12.55	11.95	8.90
15	1.24	0.74	5.45	13.91	13.91	9.56

Table E.7: LPR corrosion rate (um/yr) in the rapid macrocell test for ECR1-UV-1000(b)

Week	Specimen 1	Specimen 2	Specimen 3	Specimen 4	Specimen 5	Specimen 6
3	3.92	6.03	5.53	5.54	1.25	4.86
6	7.70	8.62	4.18	31.16	4.00	5.59
9	9.70	6.66	6.90	1.82	5.96	6.73
12	9.69	6.73	9.27	5.32	7.13	8.53
15	12.98	5.02	8.69	4.31	10.06	9.95

Table E.8: LPR corrosion rate (um/yr) in the rapid macrocell test for ECR1-UV-500

Week	Specimen 1	Specimen 2	Specimen 3	Specimen 4	Specimen 5	Specimen 6
3	6.02	6.79	5.26	4.35	2.00	2.21
6	6.37	0.00	12.39	6.86	3.37	8.82
9	6.42	8.86	6.81	26.97	4.47	4.99
12	2.67	0.00	18.00	10.79	0.00	0.91
15	11.73	15.65	10.11	16.99	0.01	7.57

Table E.9: LPR corrosion rate (um/yr) in the rapid macrocell test for ECR1-UV-250

Week	Specimen 1	Specimen 2	Specimen 3	Specimen 4	Specimen 5	Specimen 6
3	0.74	1.96	2.92	0.41	0.41	1.08
6	1.68	3.56	4.96	4.24	4.24	1.00
9	5.85	6.46	24.68	3.54	3.54	1.13
15	3.03	7.71	11.74	3.79	3.79	4.60

Table E.10: LPR corrosion rate (um/yr) in the rapid macrocell test for ECR2-UV-1000

Week	Specimen 1	Specimen 2	Specimen 3	Specimen 4	Specimen 5
3	1.42	1.85	0.97	0.99	2.11
6	1.34	0.00	1.23	1.00	1.47
9	3.92	7.94	1.58	1.00	6.02
12	3.20	0.03	4.60	4.60	6.14
15	3.76	6.05	8.10	20.03	4.56

Table E.11: LPR corrosion rate (um/yr) in the rapid macrocell test for ECR2-UV-200

Week	Specimen 1	Specimen 2	Specimen 3	Specimen 4	Specimen 5	Specimen 6
3	1.68	1.84	1.51	0.35	0.91	3.96
6	1.30	1.33	8.65	0.94	1.03	14.88
9	1.16	1.29	1.60	0.69	1.47	2.37
12	1.21	0.92	1.40	1.18	1.27	1.71
15	8.21	0.74	5.53	4.72	3.32	9.18

Table E.12: LPR corrosion rate (um/yr) in the rapid macrocell test for ECR2-UV-100

Week	Specimen 1	Specimen 2	Specimen 3	Specimen 4	Specimen 5	Specimen 6
3	26.80	0.26	0.43	0.56	1.11	0.12
6	1.55	0.17	0.16	1.01	0.82	0.12
9	2.75	0.77	0.20	1.25	1.61	1.07
12	6.75	1.11	0.74	11.91	4.12	11.37
15	1.91	0.93	0.42	0.65	1.36	1.20

Table E.13: LPR corrosion rate (um/yr) in the rapid macrocell test for ECR1-UV-1000-ND

Week	Specimen 1	Specimen 2	Specimen 3	Specimen 4	Specimen 5	Specimen 6
3	0.00	0.00	0.03	0.18	0.00	0.00
6	0.00	0.01	0.05	0.34	0.01	0.05
9	0.00	0.01	0.07	0.47	0.04	0.22
12	0.04	0.01	0.11	2.58	0.06	0.31
15	0.04	11.44	0.08	1.86	9.82	0.31

Table E.14: LPR corrosion rate (um/yr) in the rapid macrocell test for A767-D

Week	Specimen 1	Specimen 2	Specimen 3	Specimen 4	Specimen 5	Specimen 6
3	6.78	446.40	3.12	581.10	664.50	29.22
6	315.75	51.39	22.23	316.95	531.00	20.40
9	12.02	30.41	4.40	217.50	15.44	7.93
12	13078.50	9.44	46.67	12.65	41.81	13.49
15	3.88	85.50	18435.00	12375.00	8019.00	16050.00

Table E.15: LPR corrosion rate (um/yr) in the rapid macrocell test for A767-ND

Week	Specimen 1	Specimen 2	Specimen 3	Specimen 4	Specimen 5	Specimen 6
3	10.93	24.74	16.74	447.15	15.00	26.18
6	42.62	44.51	33.38	588.75	525.90	537.30
9	10.31	9.49	8.27	90.62	8.62	17.58
12	2848.50	15.63	157.20	231.15	26.70	50.04
15	9388.50	11817.00	13608.00	4719.00	6151.50	52560.00

Table E.16: LPR corrosion rate (um/yr) in the rapid macrocell test for A767-Bent

Week	Specimen 1	Specimen 2	Specimen 3	Specimen 4	Specimen 5	Specimen 6
3	24.89	25.68	513.30	543.60	728.70	404.70
6	24.89	25.68	513.30	543.60	728.70	404.70
9	164.69	262.82	325.12	526.95	398.29	510.38
12	304.50	499.95	136.94	510.30	67.88	616.05
15	304.50	499.95	136.94	510.30	67.88	616.05

Table E.17: LPR corrosion rate (um/yr) in the rapid macrocell test for A1094-D

Week	Specimen 1	Specimen 2	Specimen 3	Specimen 4	Specimen 5	Specimen 6
3	0.03	7.67	10.50	5.65	0.05	9.95
6	15.50	13.80	32.42	20.25	15.05	10.86
9	5.50	5.38	8.13	3.84	17.55	5.85
12	59.31	7.10	56.22	59.61	65.78	98.70
15	37.76	6.29	15.18	4.13	89.42	13.65

Table E.18: LPR corrosion rate (um/yr) in the rapid macrocell test for A1094-ND

Week	Specimen 1	Specimen 2	Specimen 3	Specimen 4	Specimen 5	Specimen 6
3	8.30	6.88	14.31	5.63	6.77	9.06
6	15.48	8.10	21.44	9.33	10.41	36.89
9	4.71	10.22	9.64	4.52	6.33	32.19
12	0.69	10.07	27.57	5.14	6.48	3.68
15	7.02	0.00	23.37	10.63	6.05	26.60

Table E.19: LPR corrosion rate (um/yr) in the rapid macrocell test for A1094-Bent

Week	Specimen 1	Specimen 2	Specimen 3	Specimen 4	Specimen 5	Specimen 6
3	11.44	133.07	16.11	3.71	12.38	9.59
6	11.44	133.07	16.11	3.71	12.38	9.59
9	24.97	72.00	11.27	4.30	28.94	11.83
12	38.49	10.93	6.44	4.89	45.51	14.06
15	38.49	10.93	6.44	4.89	45.51	14.06

Table E.20: LPR corrosion rate (um/yr) in the rapid macrocell test for ChromX

Week	Specimen 1	Specimen 2	Specimen 3	Specimen 4	Specimen 5	Specimen 6
3	5.34	18.53	21.96	11.04	8.51	6.29
6	7.47	4.04	10.64	6.68	15.97	16.15
9	4.58	3.82	9.84	0.00	18.58	18.76
12	13.15	8.73	0.00	22.88	16.14	27.41
15	17.90	7.36	24.06	24.06	17.32	32.33

APPENDIX F: LPR CORROSION LOSS OF INDIVIDUAL BENCH-SCALE SPECIMENS

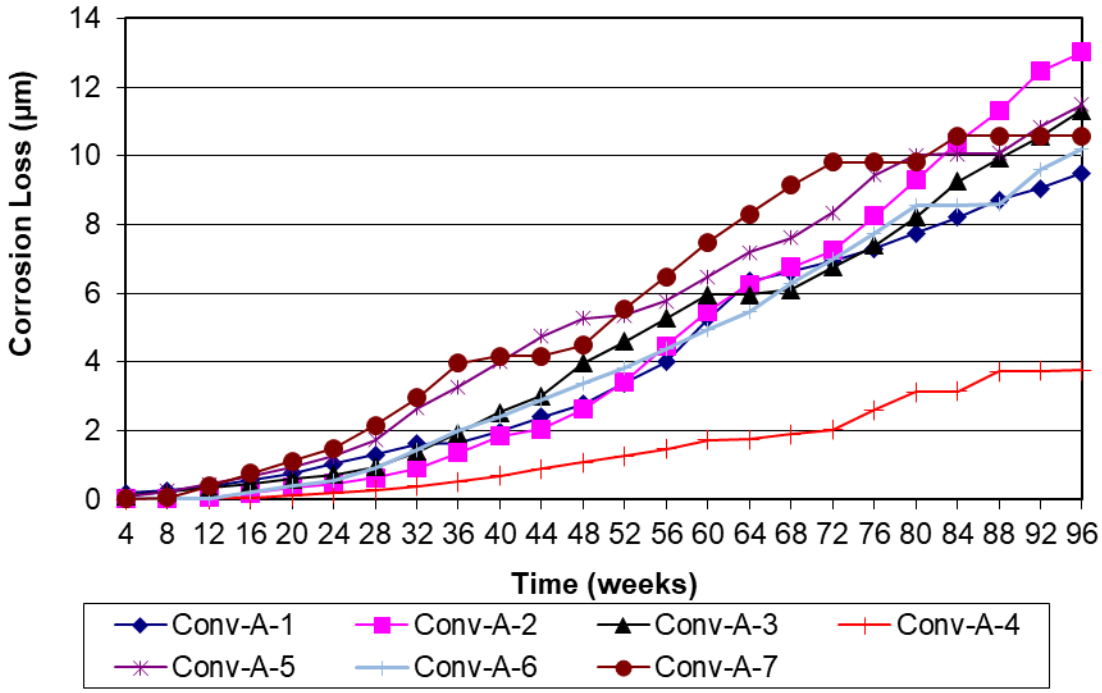

Figure F.1: LPR corrosion losses of Conv-A reinforcement in the Southern Exposure test

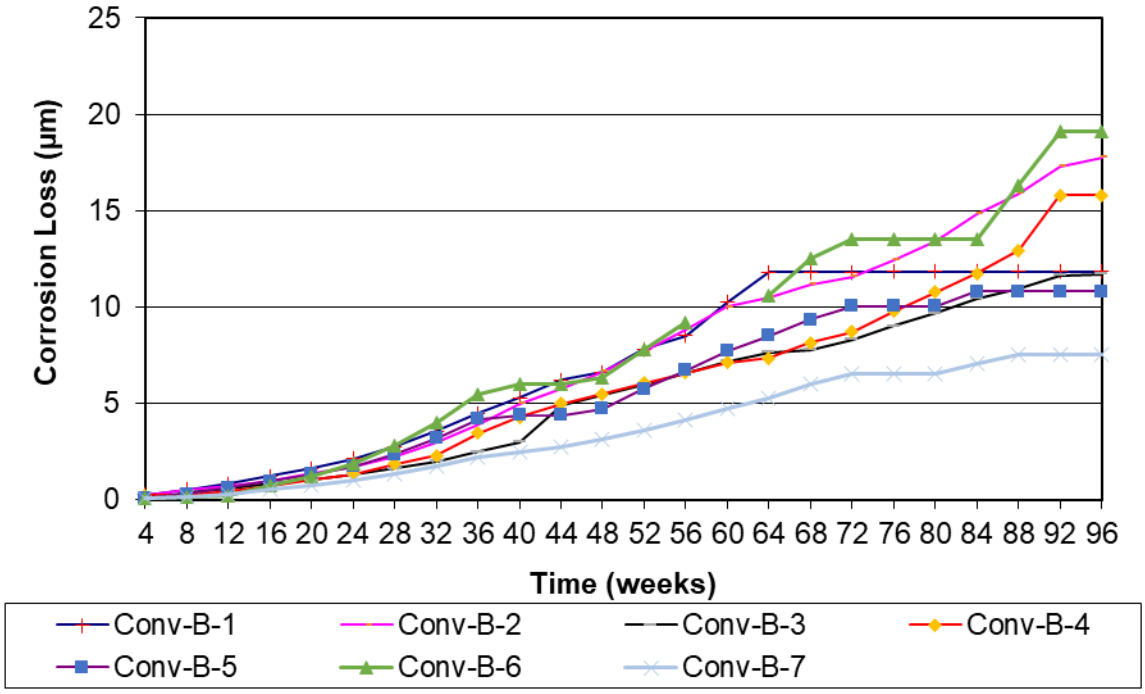

Figure F.2: LPR corrosion losses of Conv-B reinforcement in the Southern Exposure test

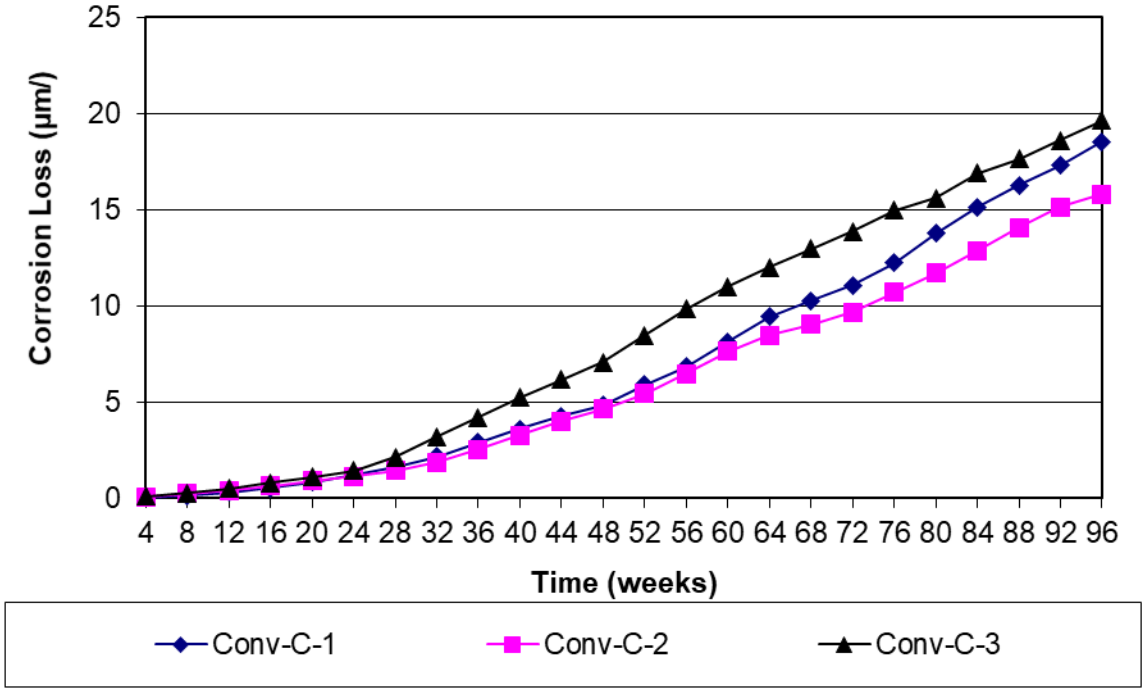

Figure F.3: LPR corrosion losses of Conv-C reinforcement in the Southern Exposure test

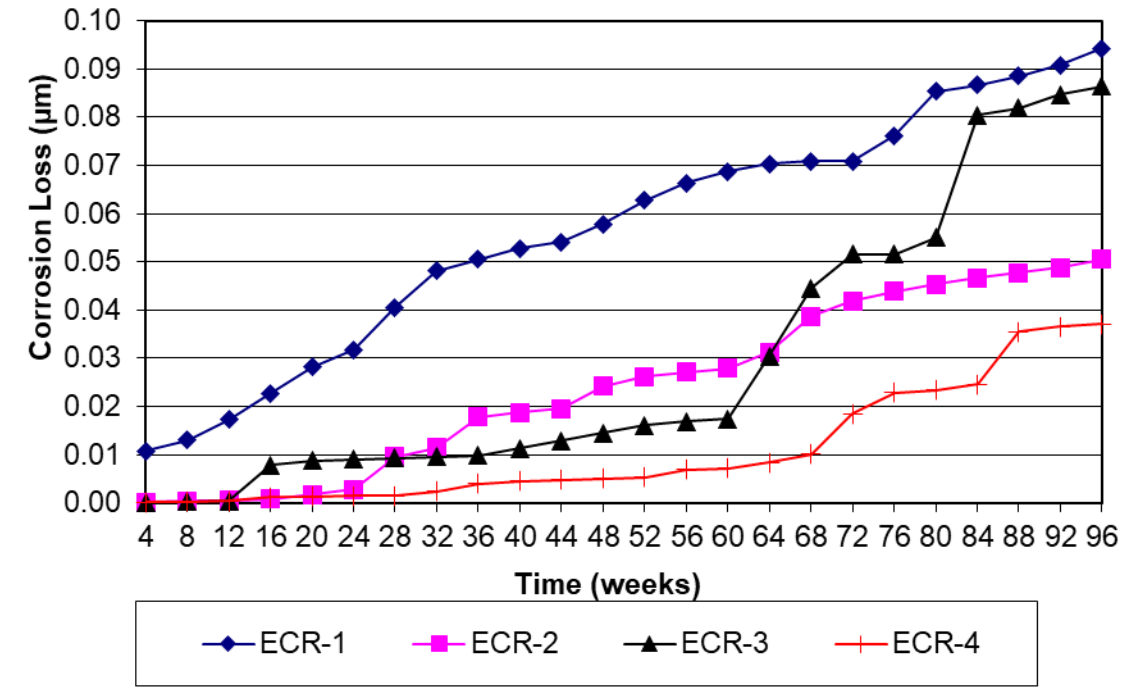

Figure F.4: LPR corrosion losses of ECR1 reinforcement in the Southern Exposure test

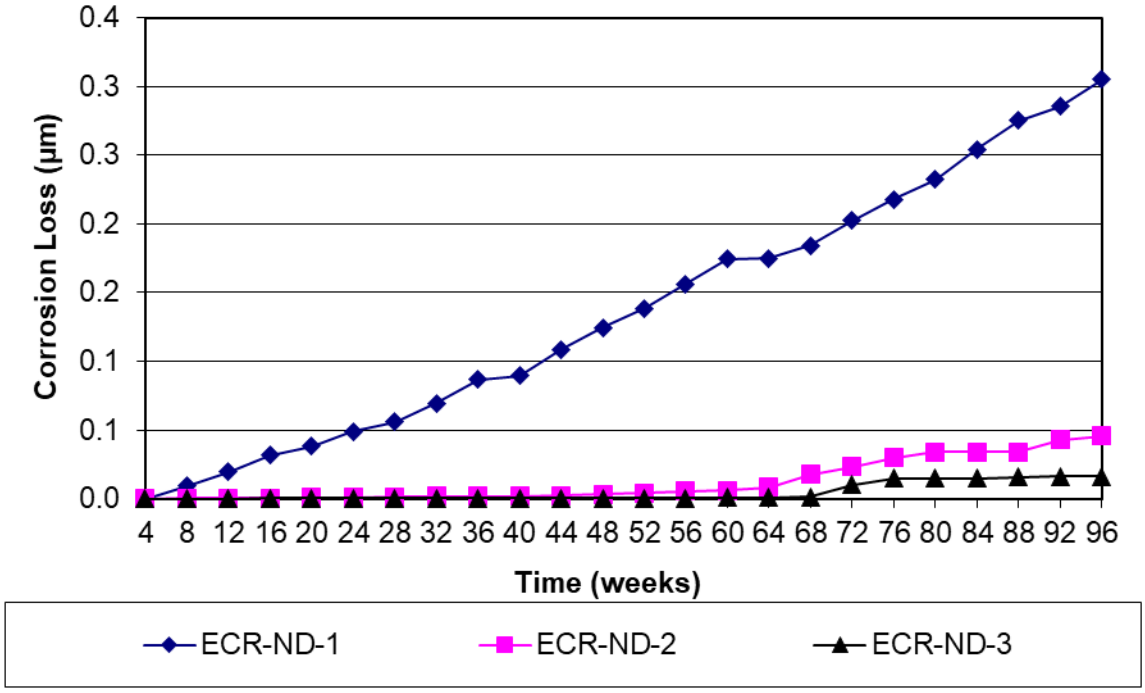

Figure F.5: LPR corrosion losses of ECR1-ND reinforcement in the Southern Exposure test

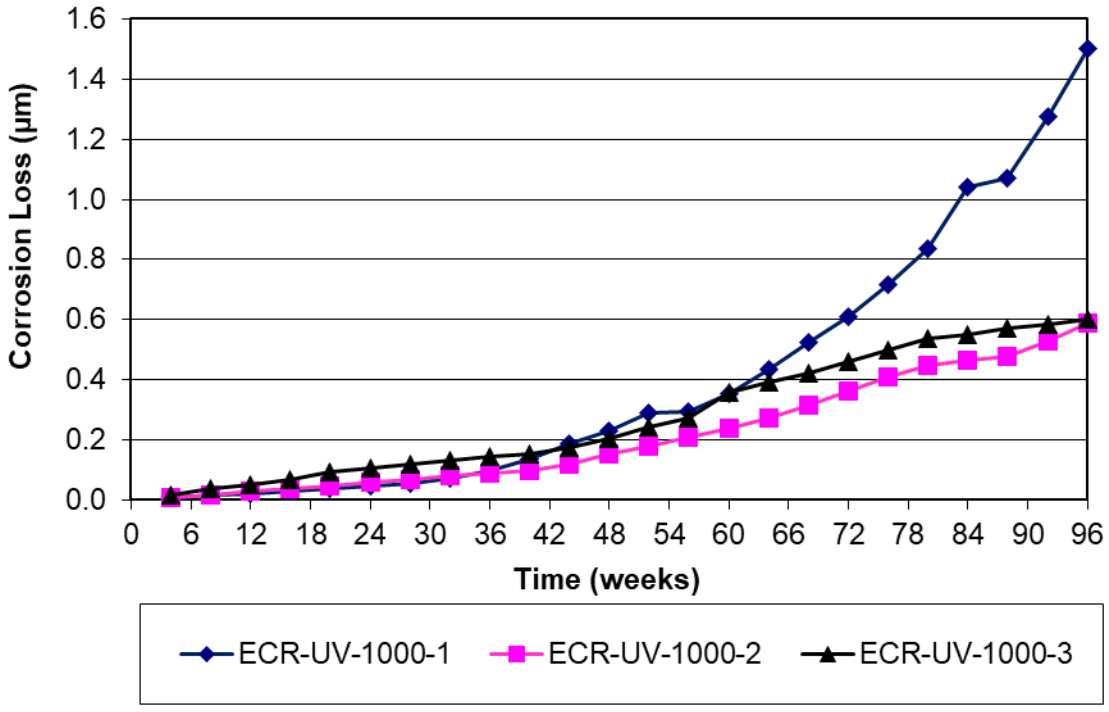

Figure F.6: LPR corrosion losses of ECR1-UV-1000 reinforcement in the Southern Exposure test

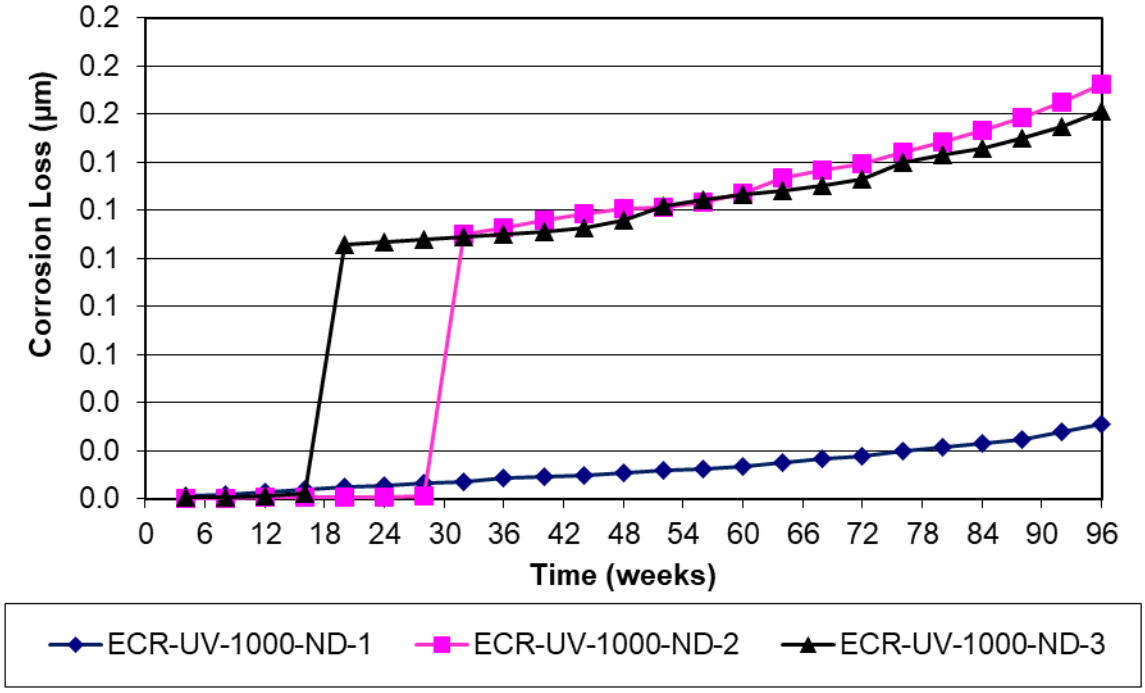

Figure F.7: LPR corrosion losses of ECR1-UV-ND-1000 reinforcement in the Southern Exposure test

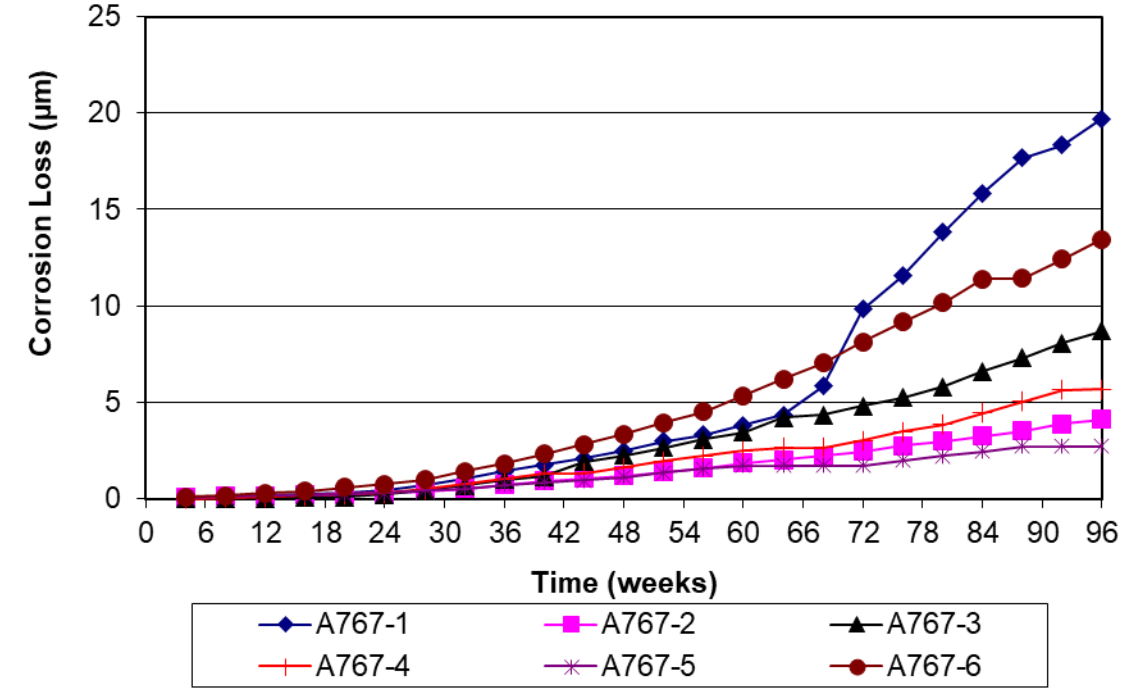

Figure F.8: LPR corrosion losses of A767 reinforcement in the Southern Exposure test

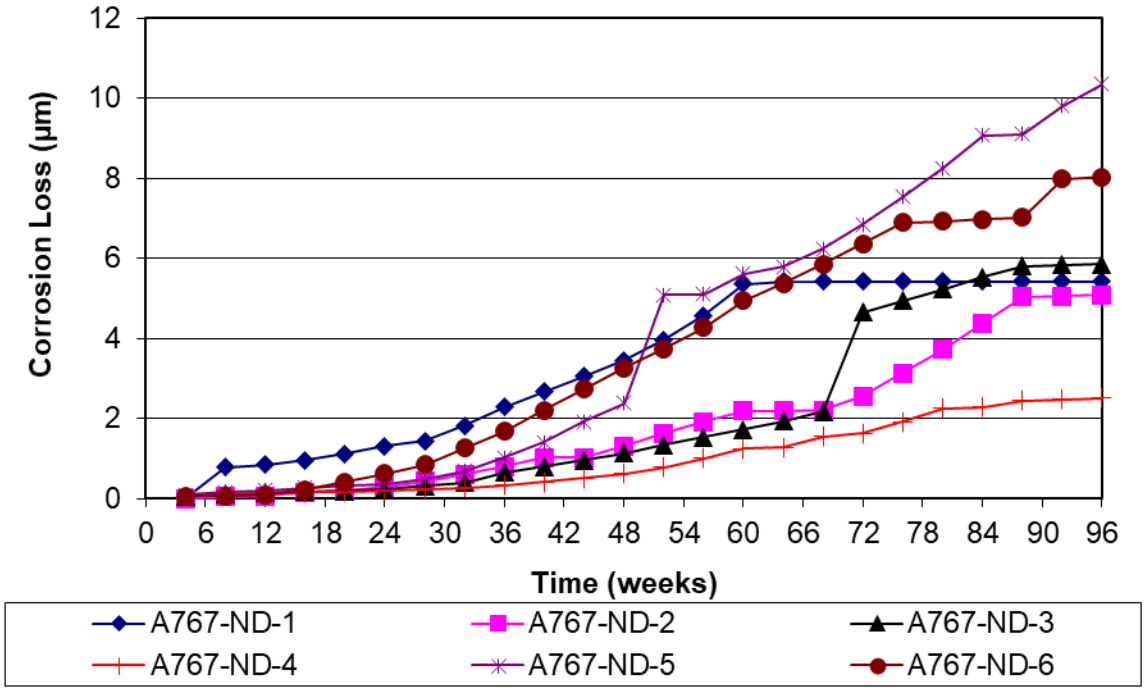

Figure F.9: LPR corrosion losses of A767-ND reinforcement in the Southern Exposure test

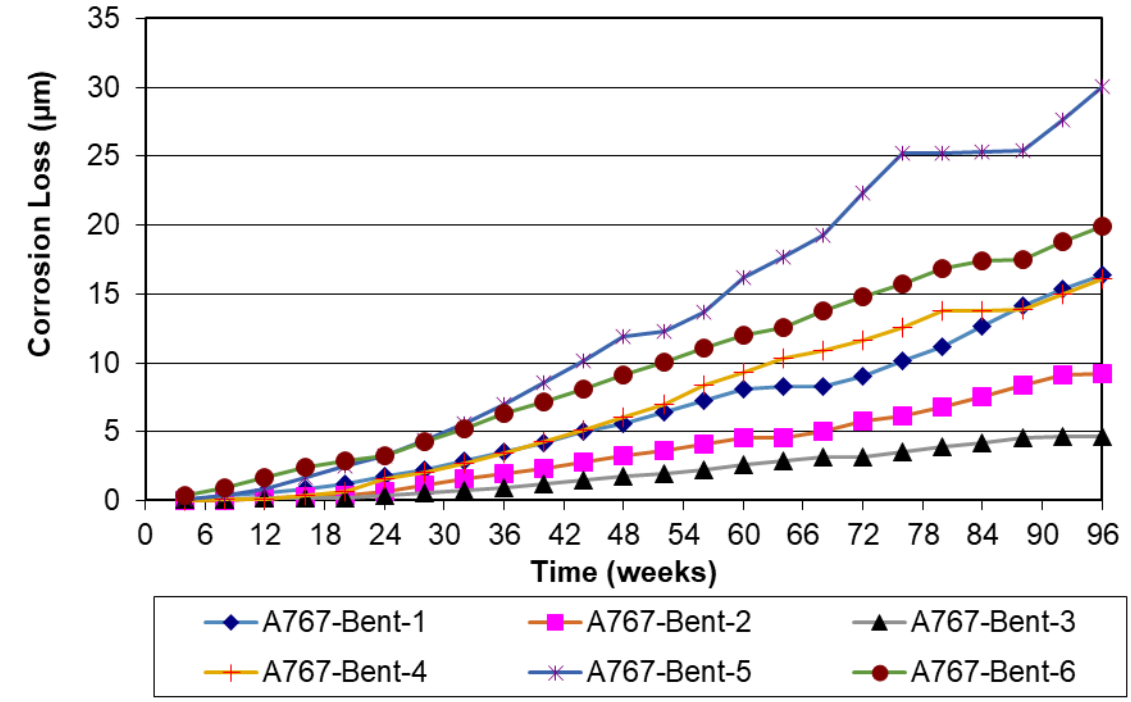

Figure F.10: LPR corrosion losses of A767-Bent reinforcement in the Southern Exposure test

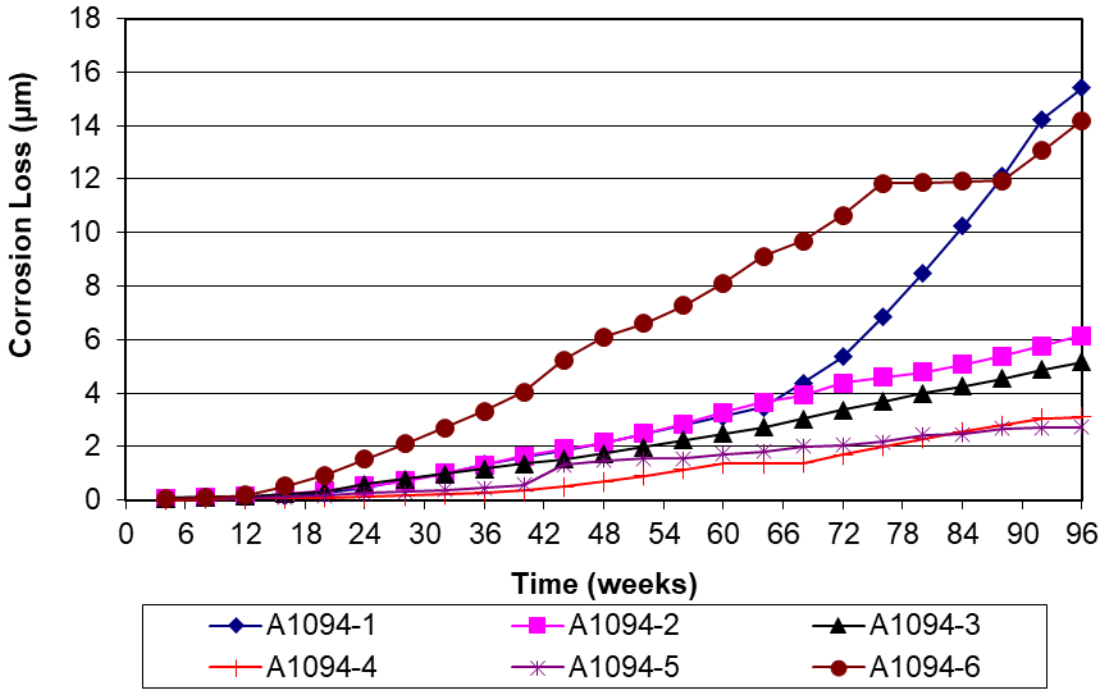

Figure F.11: LPR corrosion losses of A1094 reinforcement in the Southern Exposure test

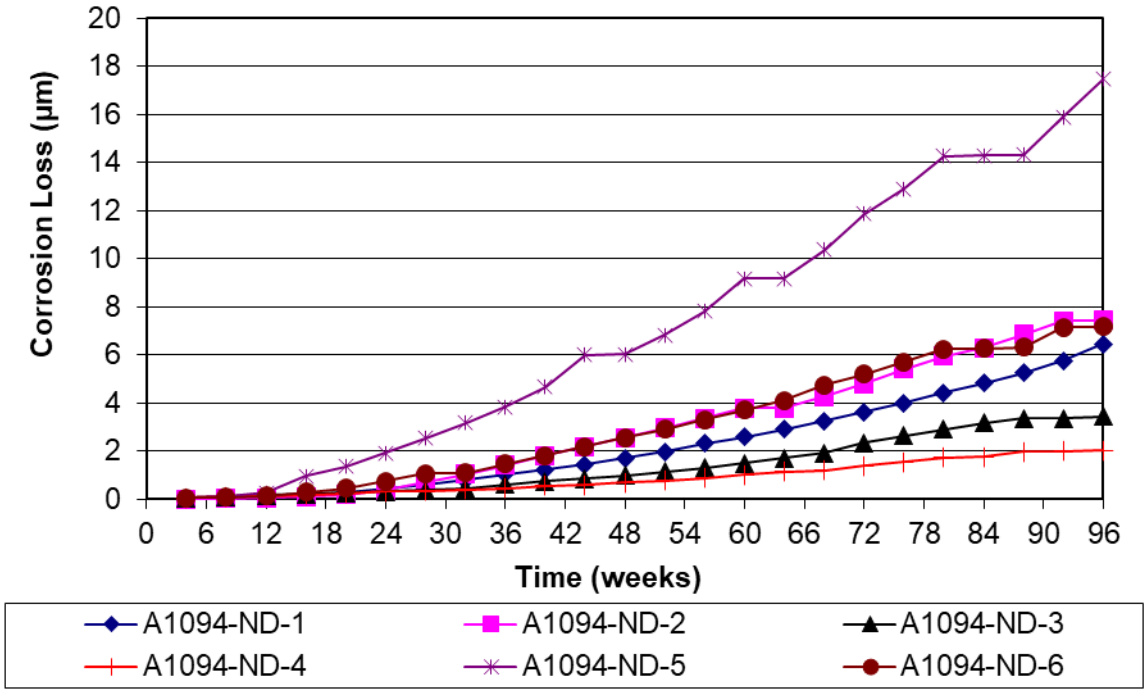

Figure F.9: LPR corrosion losses of A767-ND reinforcement in the Southern Exposure test

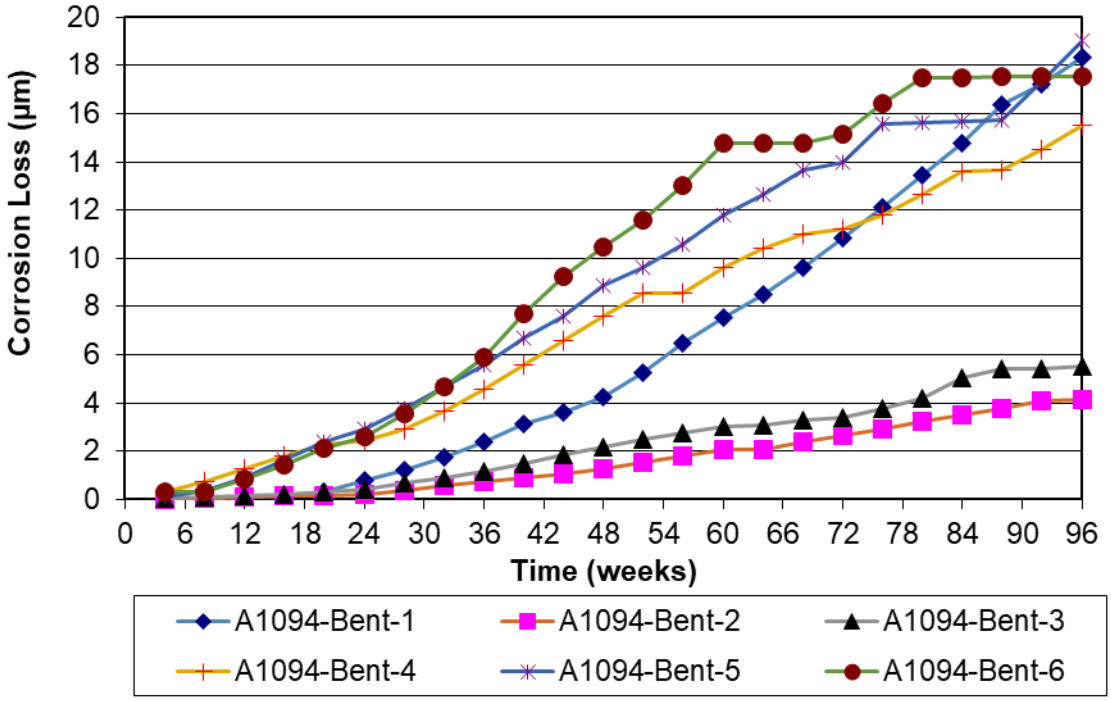

Figure F.9: LPR corrosion losses of A767-Bent reinforcement in the Southern Exposure test

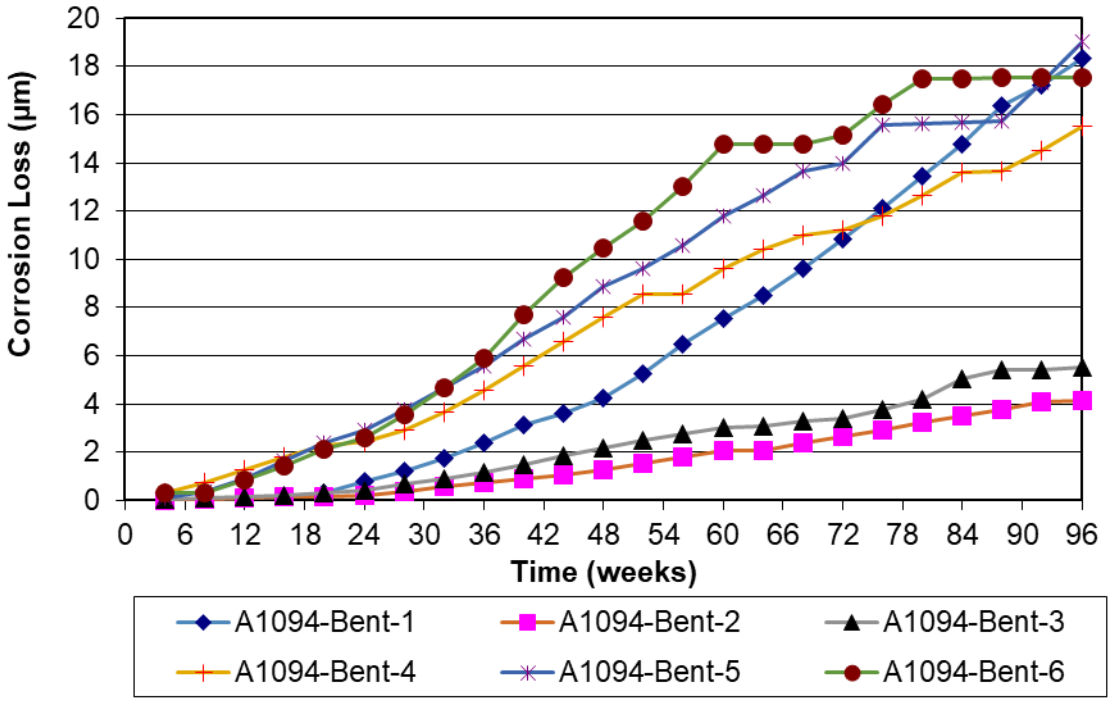

Figure F.14: LPR corrosion losses of ChromX reinforcement in the Southern Exposure test

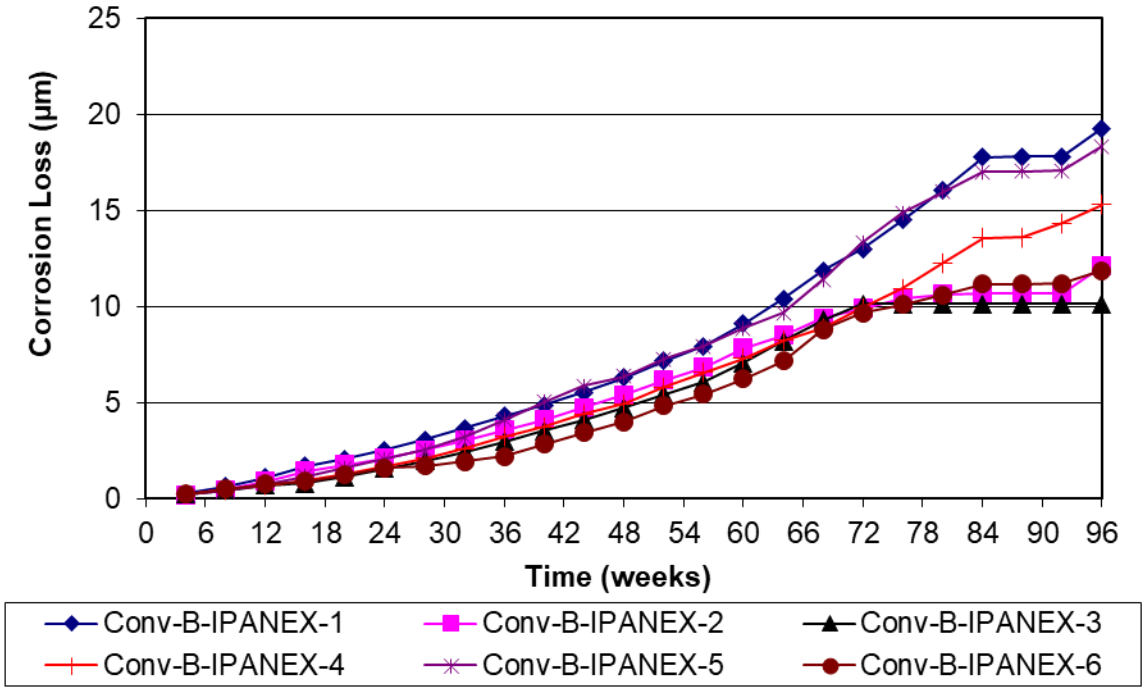

Figure F.15: LPR corrosion losses of Conv-B-IPANEX reinforcement in the Southern Exposure test

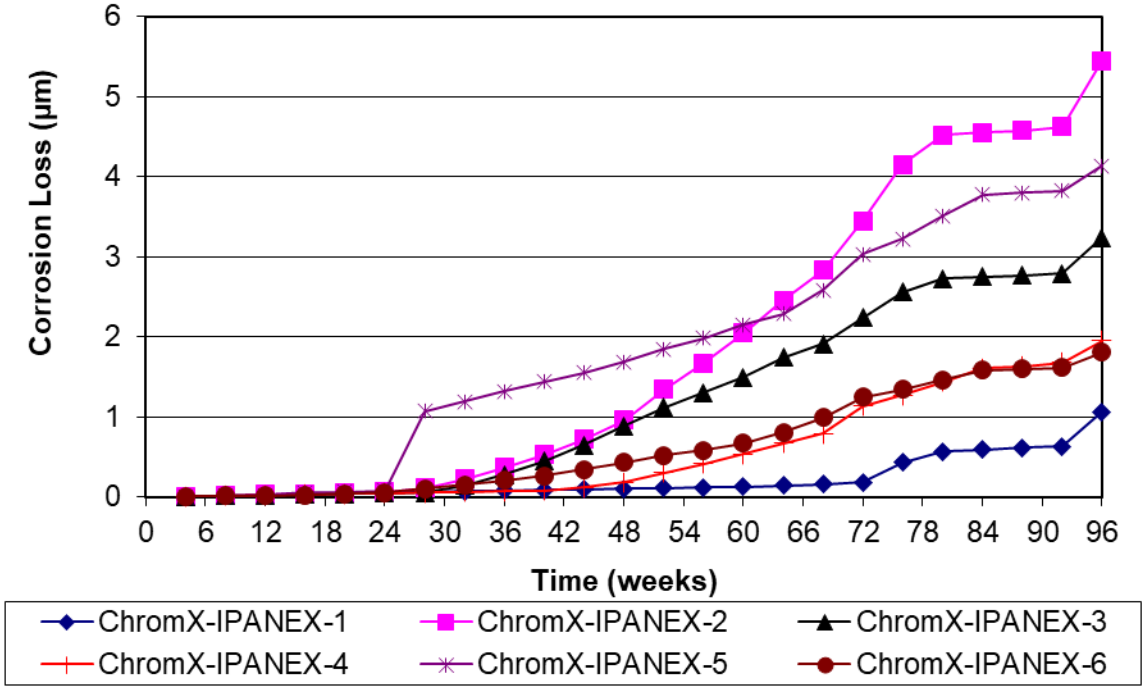

Figure F.16: LPR corrosion losses of Conv-B-Xypex reinforcement in the Southern Exposure test

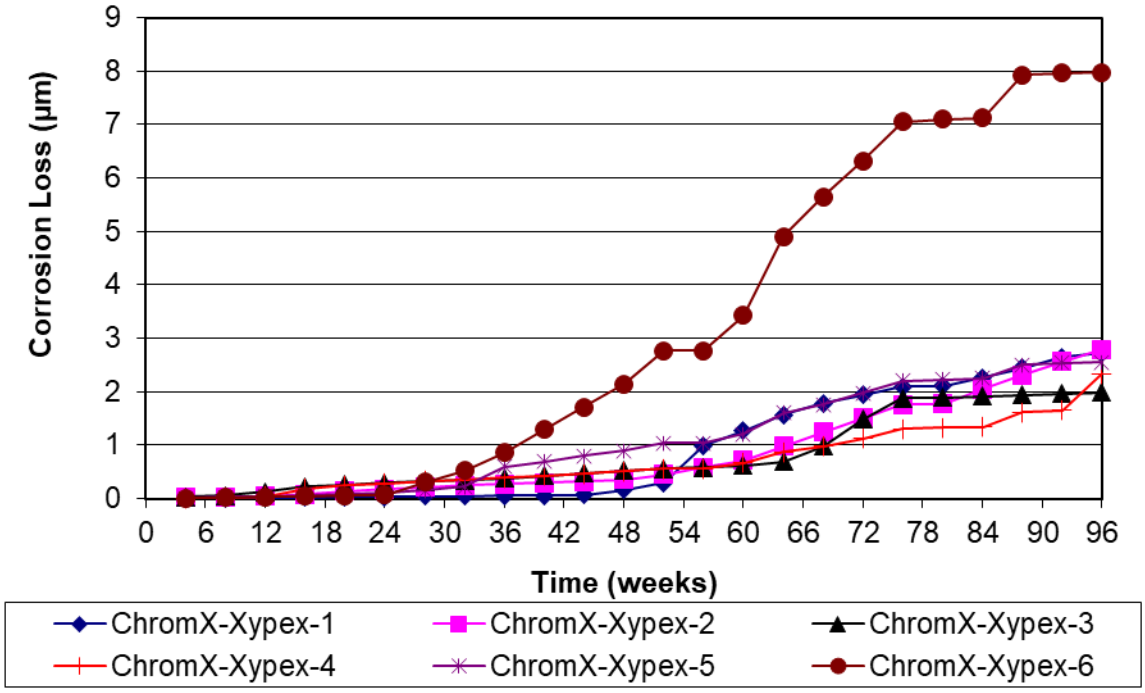

Figure F.17: LPR corrosion losses of ChromX-IPANEX reinforcement in the Southern Exposure test

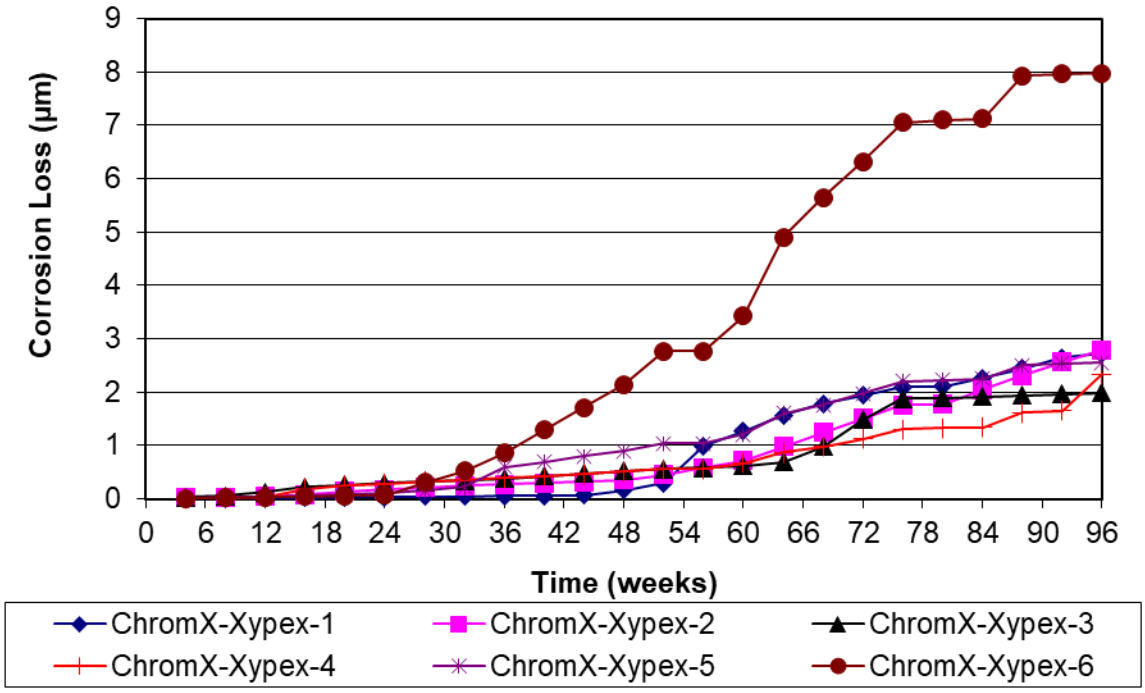

Figure F.18: LPR corrosion losses of ChromX-Xypex reinforcement in the Southern Exposure test

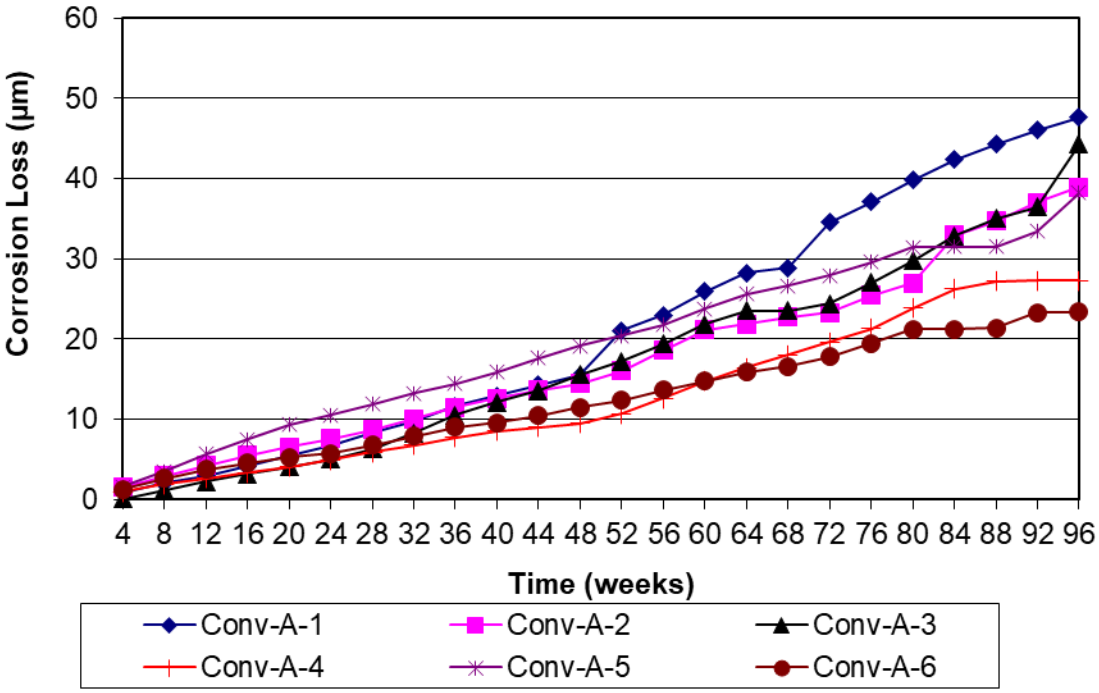

Figure F.19: LPR corrosion losses of Conv-A reinforcement in the cracked beam test

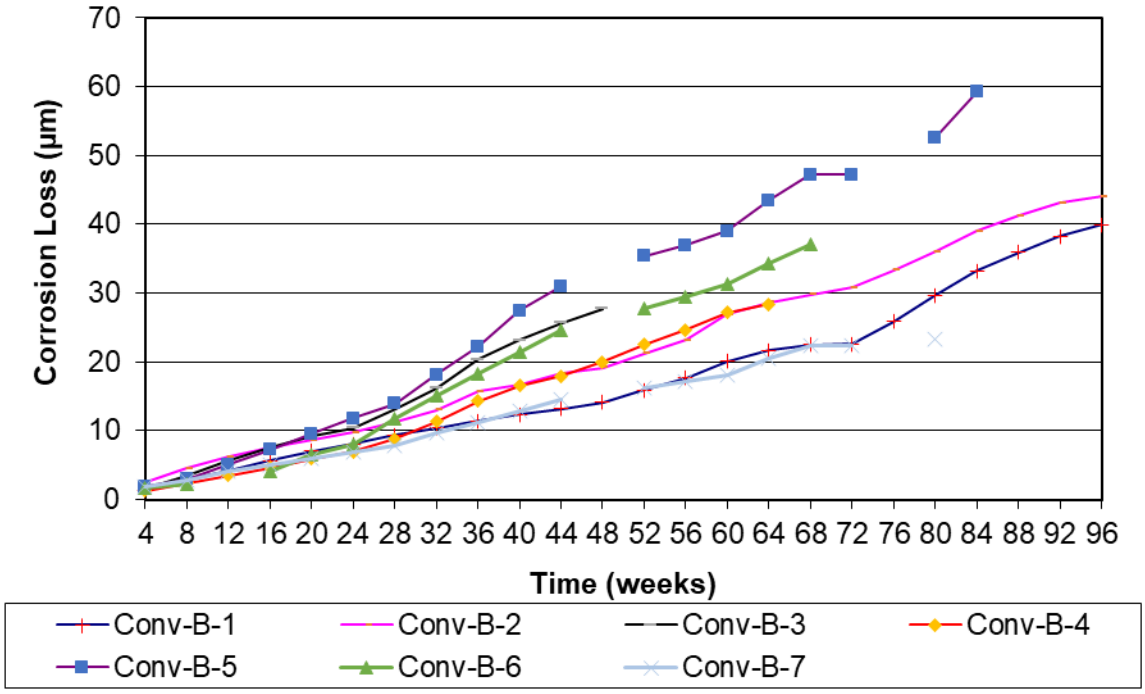

Figure F.20: LPR corrosion losses of Conv-B reinforcement in the cracked beam test

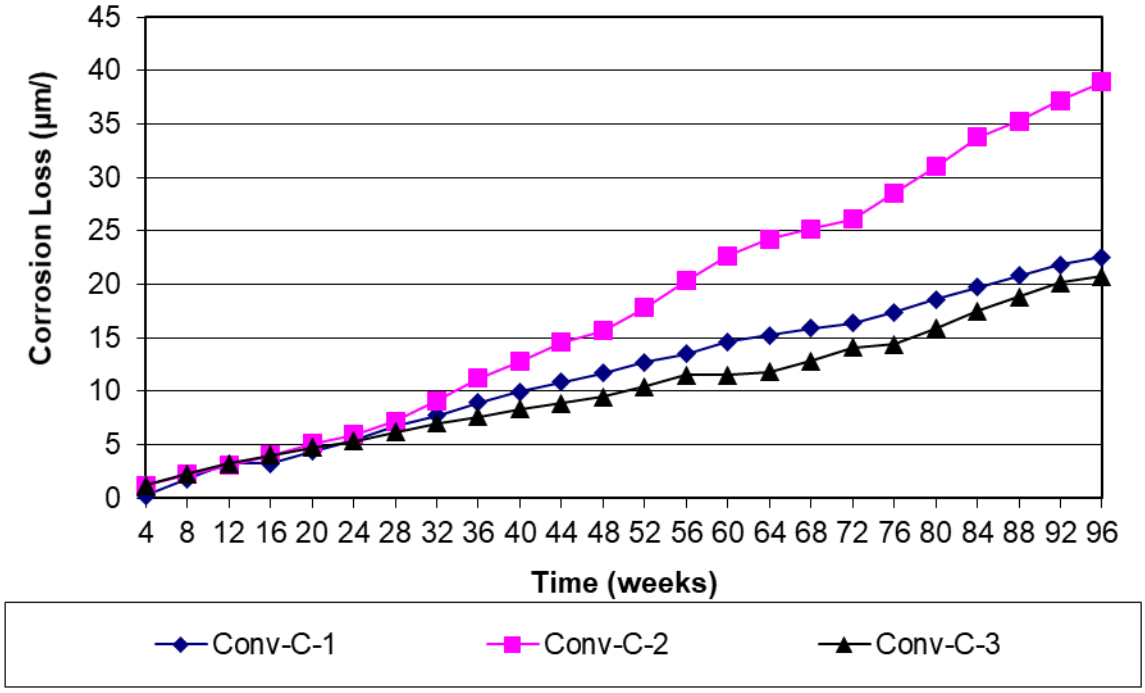

Figure F.21: LPR corrosion losses of Conv-C reinforcement in the cracked beam test

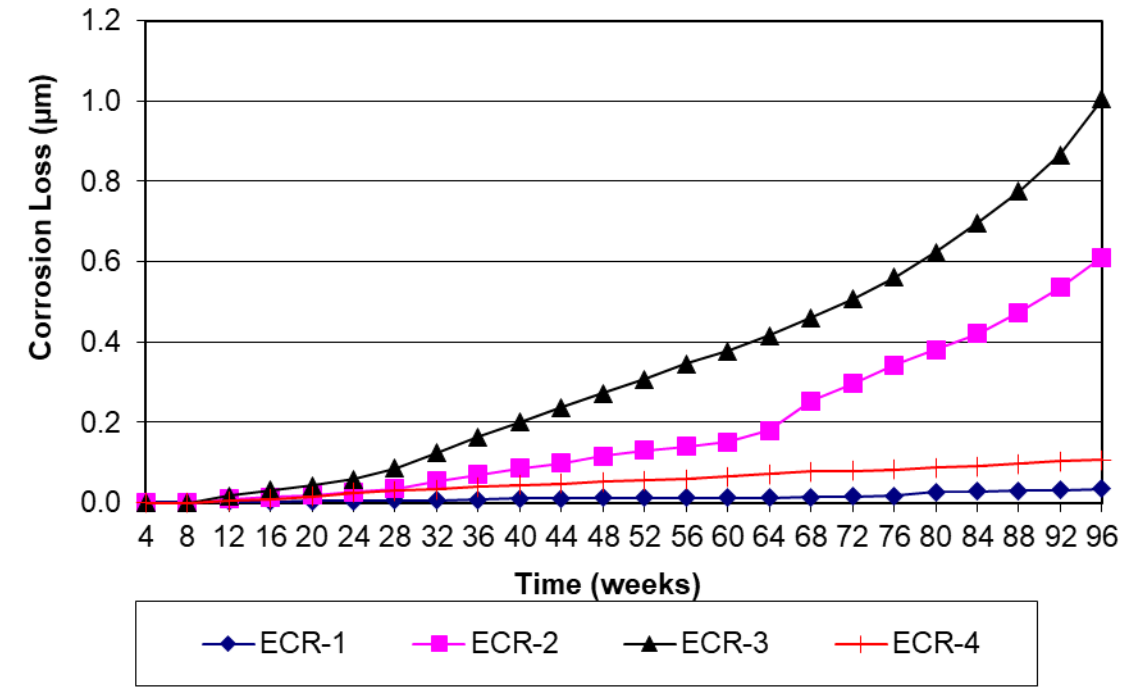

Figure F.22: LPR corrosion losses of ECR1 reinforcement in the cracked beam test

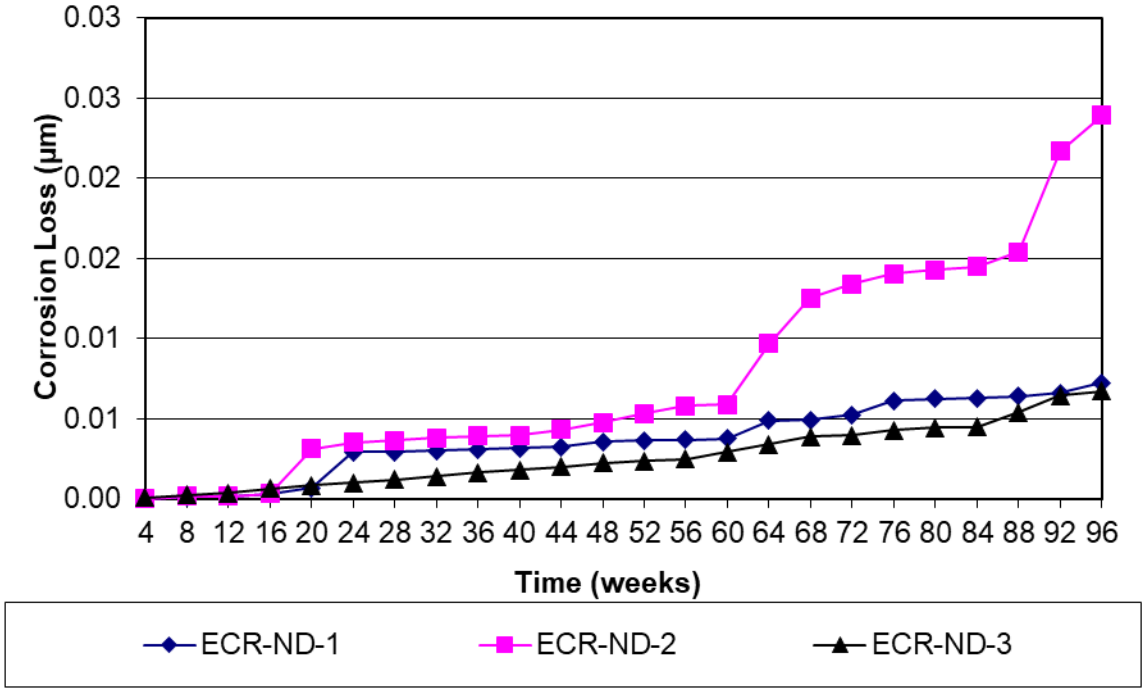

Figure F.23: LPR corrosion losses of ECR1-ND reinforcement in the cracked beam test

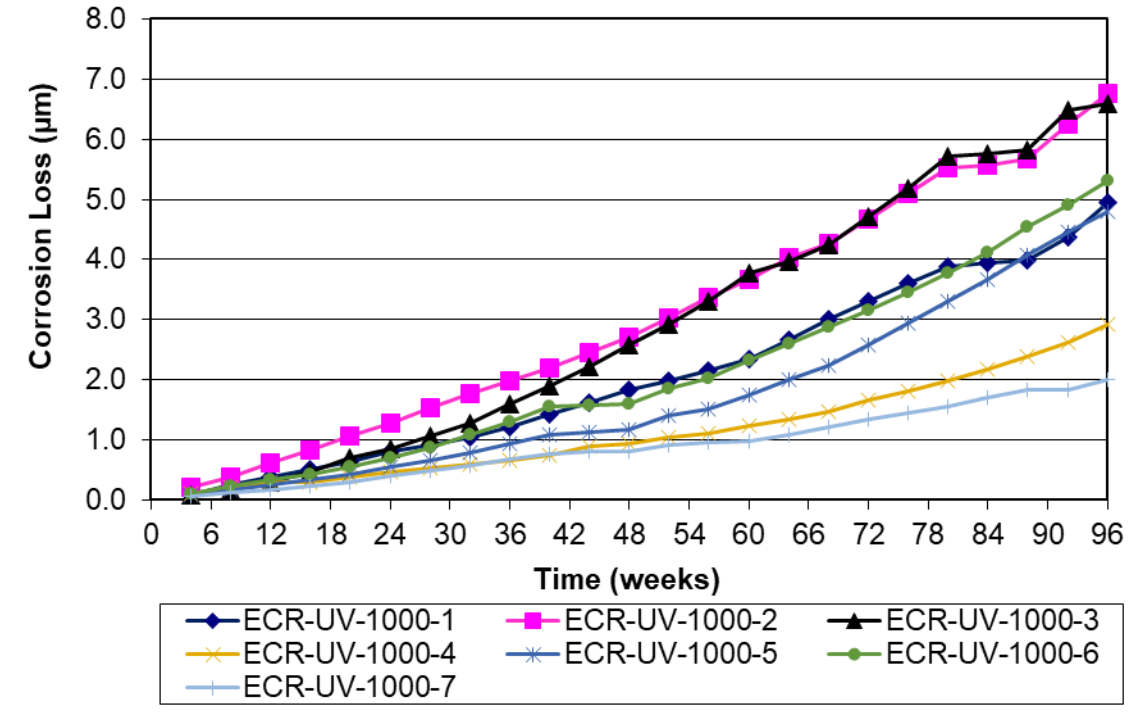

Figure F.24: LPR corrosion losses of ECR1-UV-1000 reinforcement in the cracked beam test

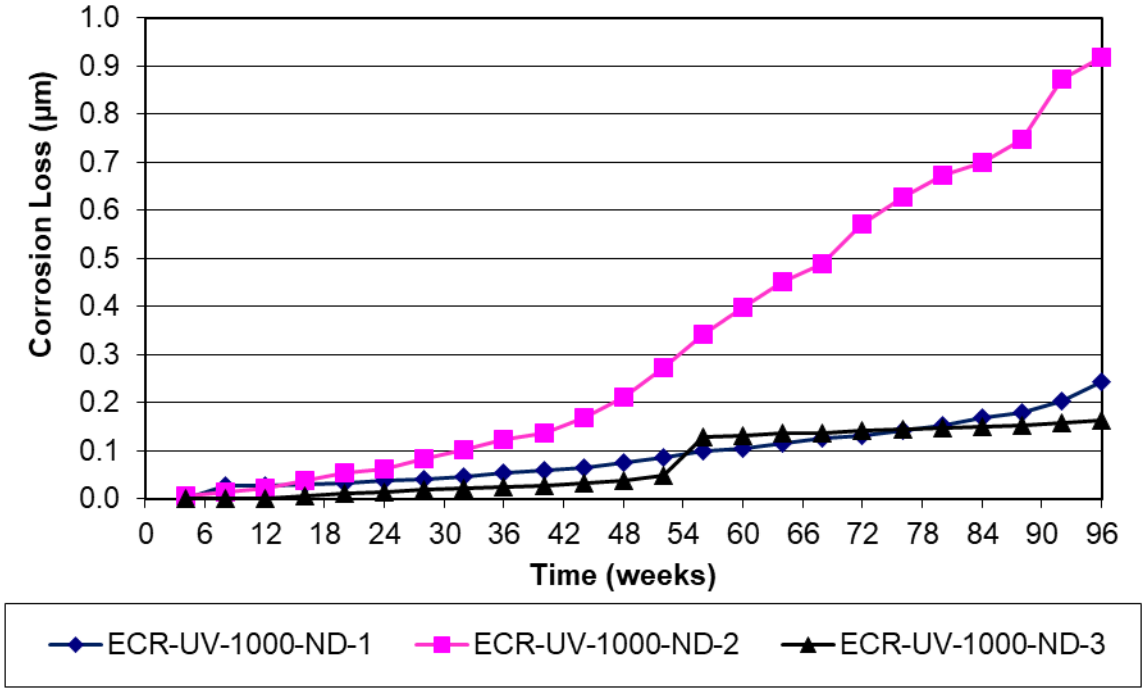

Figure F.25: LPR corrosion losses of ECR1-UV-ND-1000 reinforcement in the cracked beam test

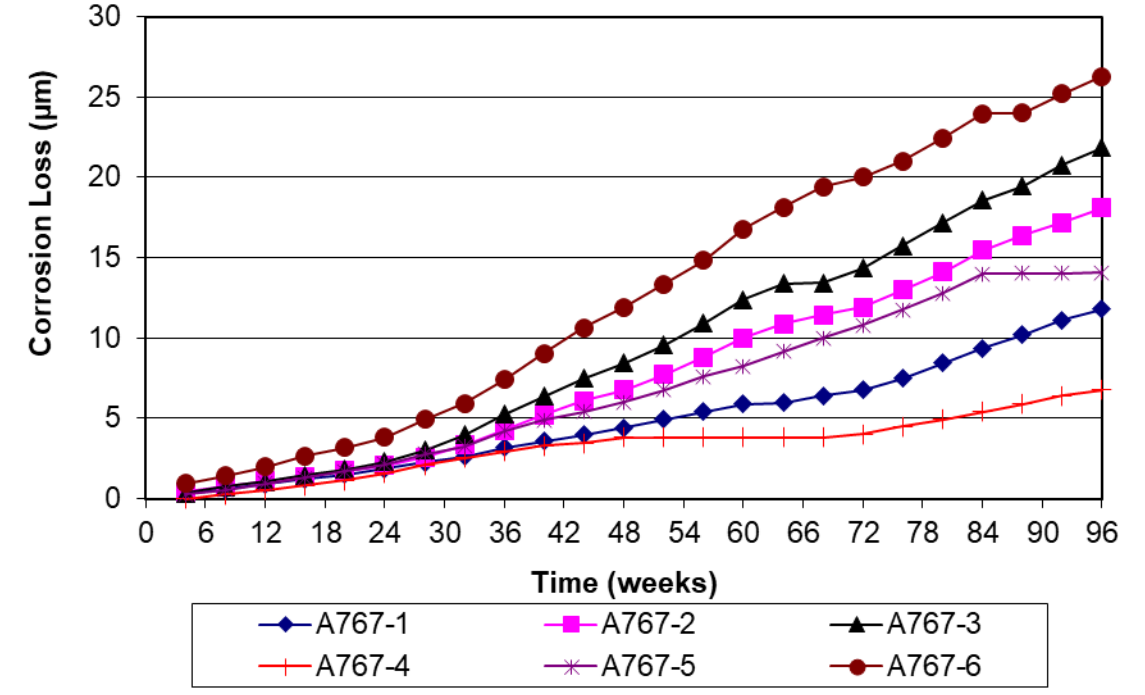

Figure F.26: LPR corrosion losses of A767 reinforcement in the cracked beam test

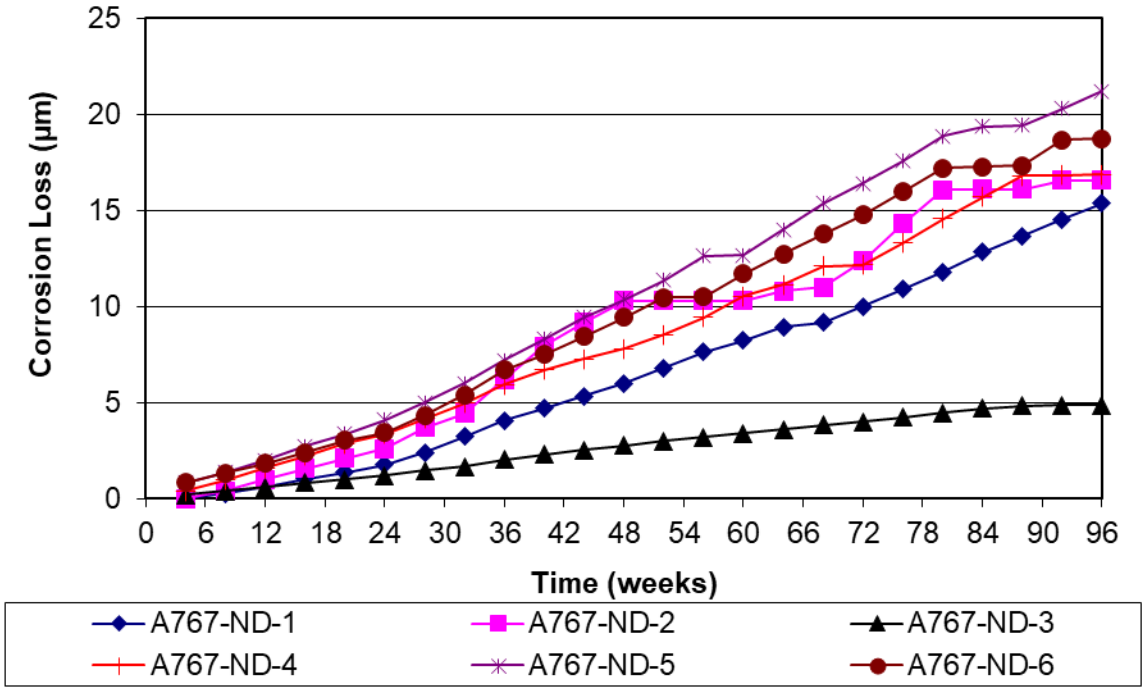

Figure F.27: LPR corrosion losses of A767-ND reinforcement in the cracked beam test

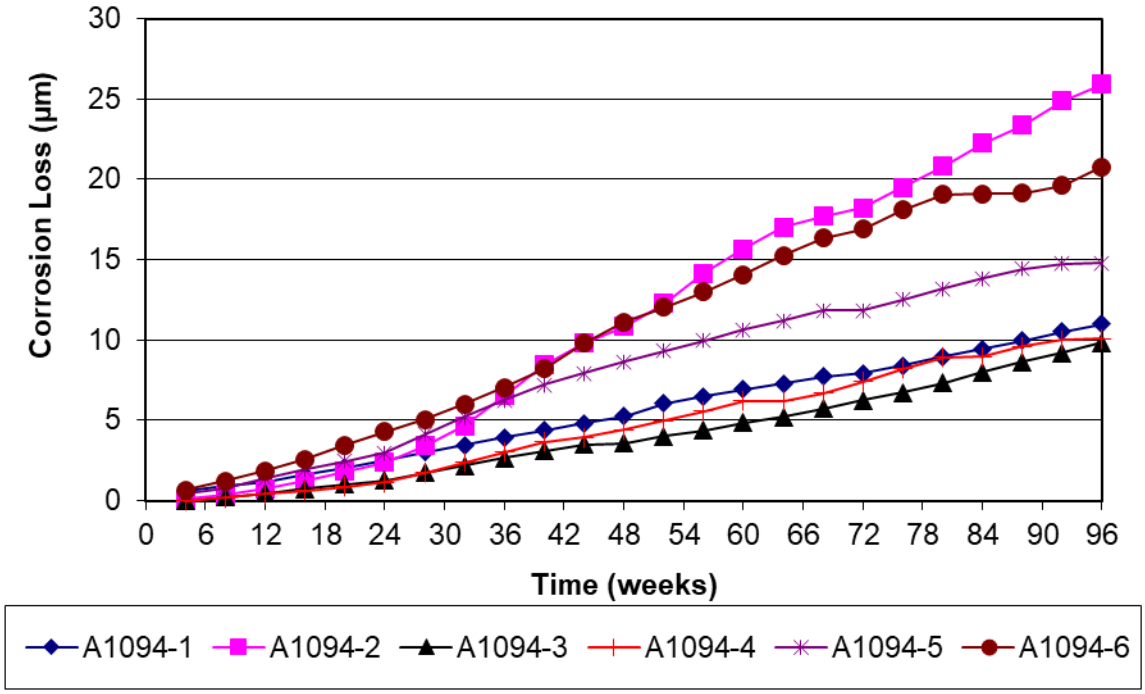

Figure F.28: LPR corrosion losses of A1094 reinforcement in the cracked beam test

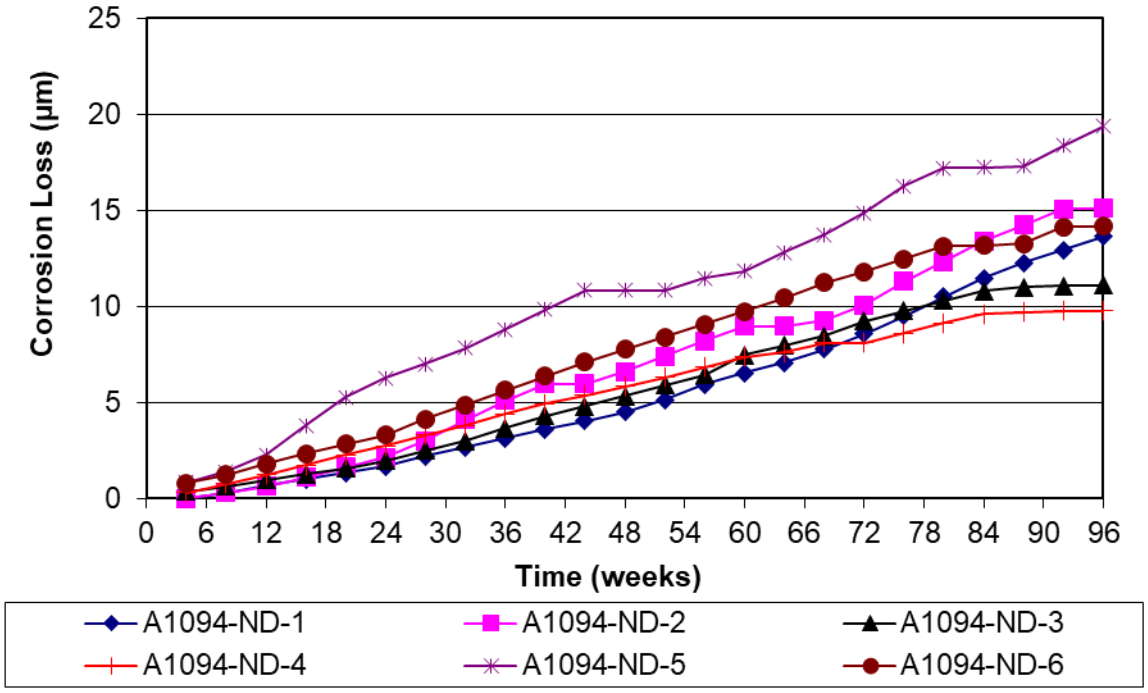

Figure F.29: LPR corrosion losses of A1094-ND reinforcement in the cracked beam test

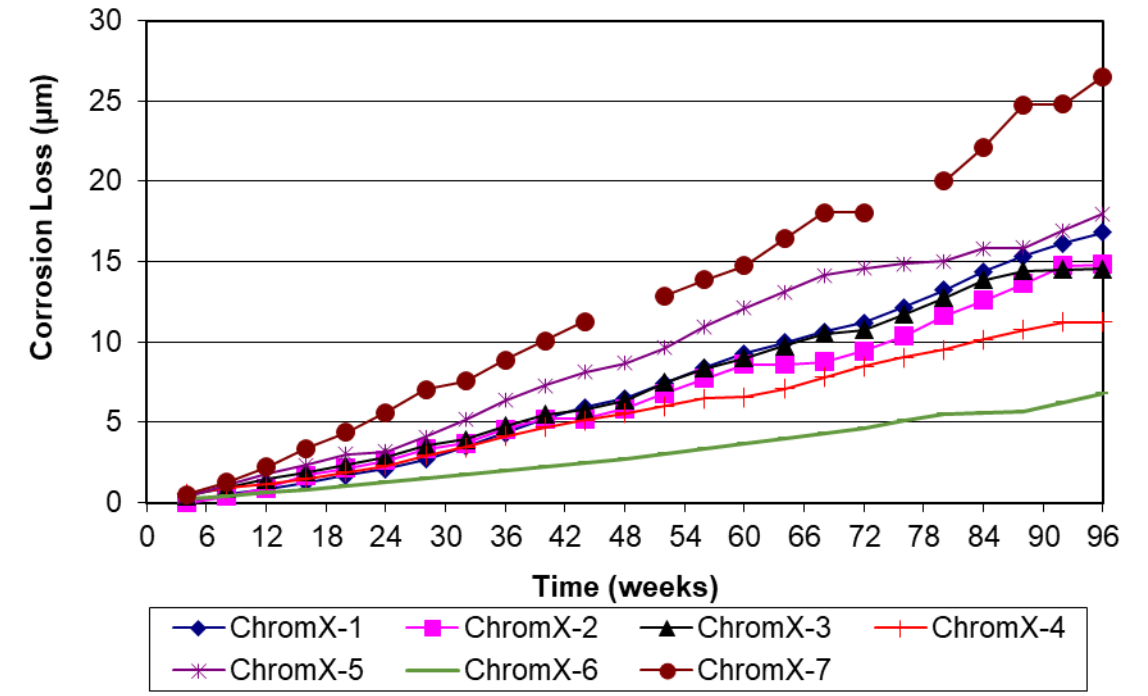

Figure F.30: LPR corrosion losses of ChromX reinforcement in the cracked beam test

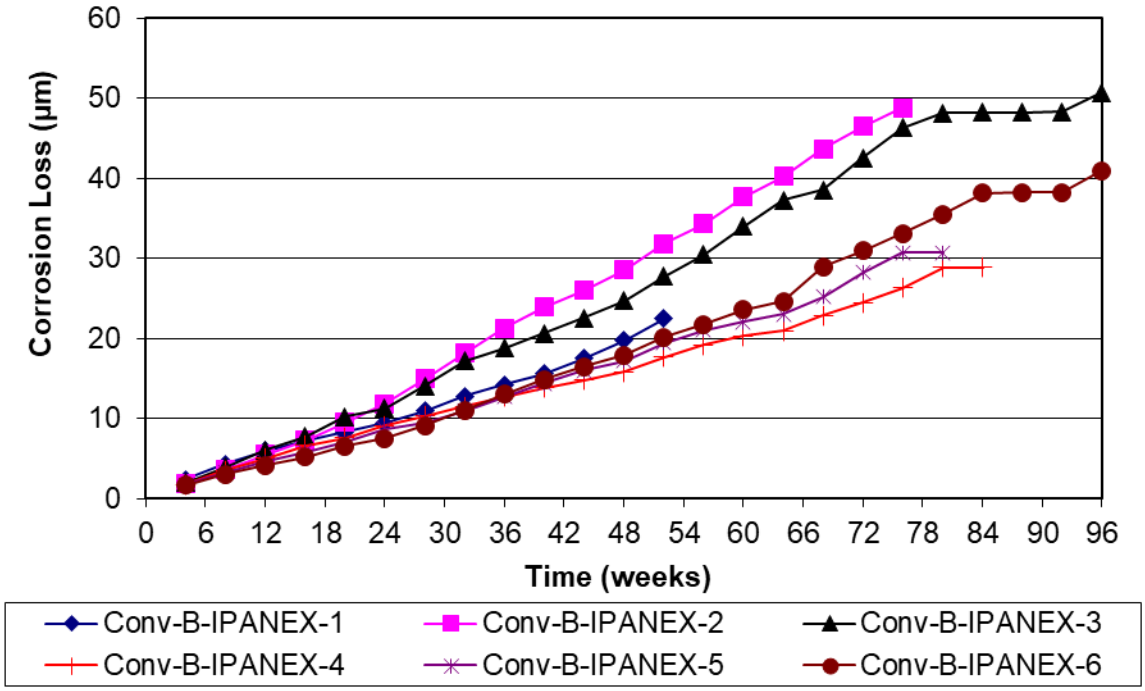

Figure F.31: LPR corrosion losses of Conv-B-IPANEX reinforcement in the cracked beam test

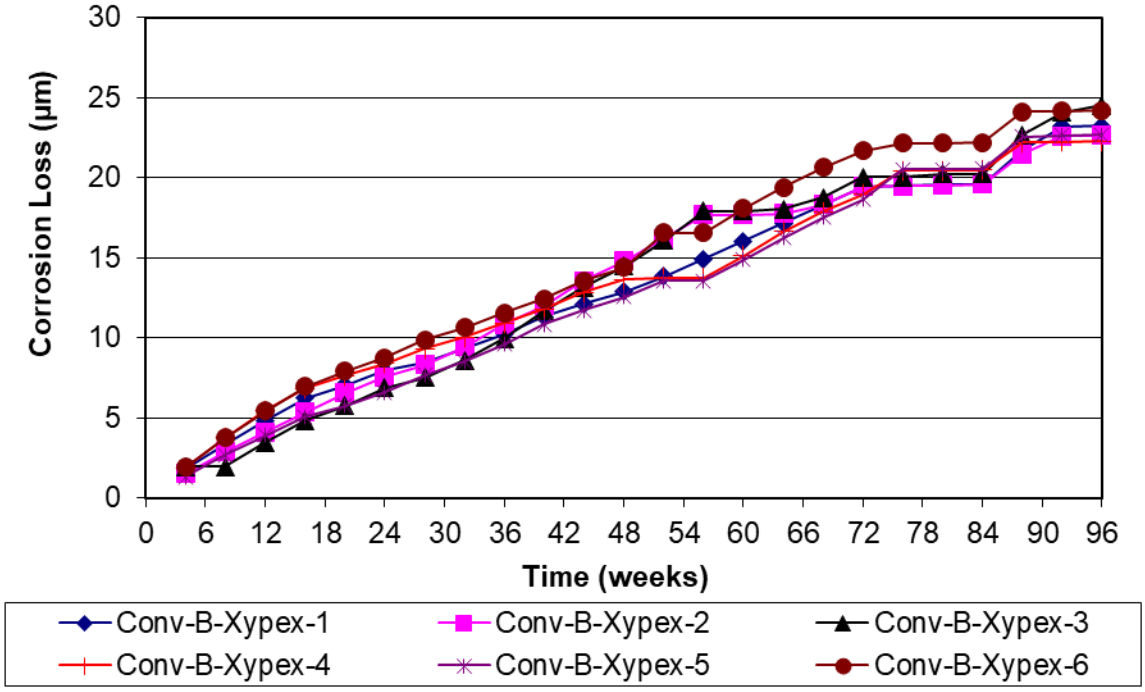

Figure F.32: LPR corrosion losses of Conv-B-Xypex reinforcement in the cracked beam test

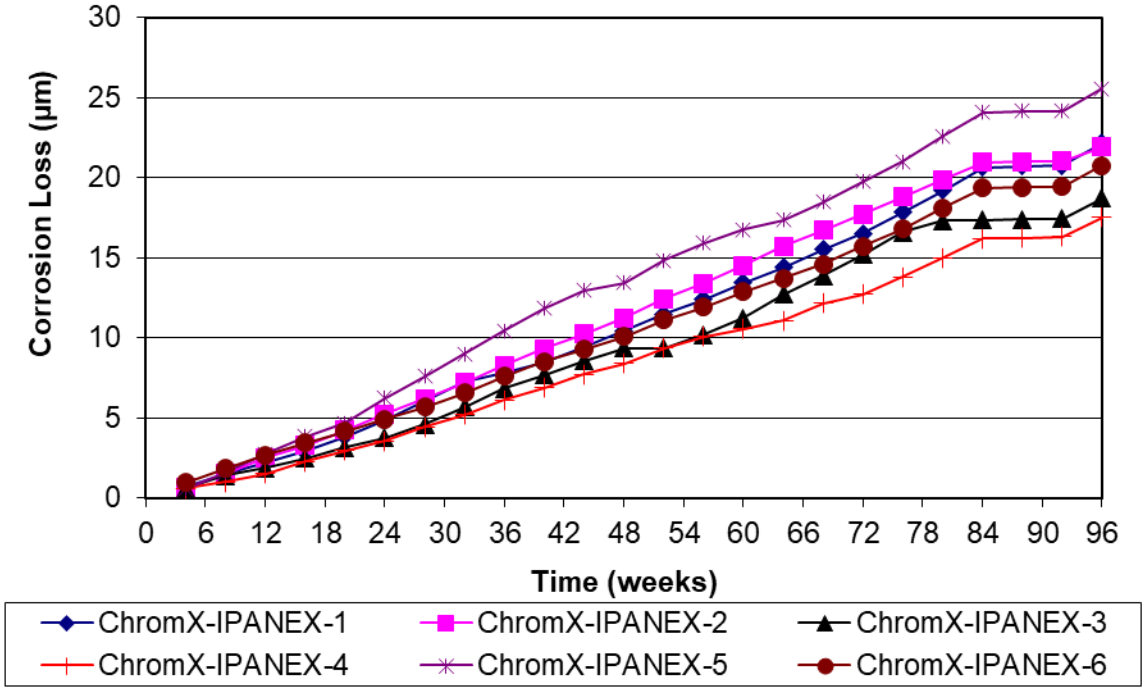

Figure F.33: LPR corrosion losses of ChromX-IPANEX reinforcement in the cracked beam test

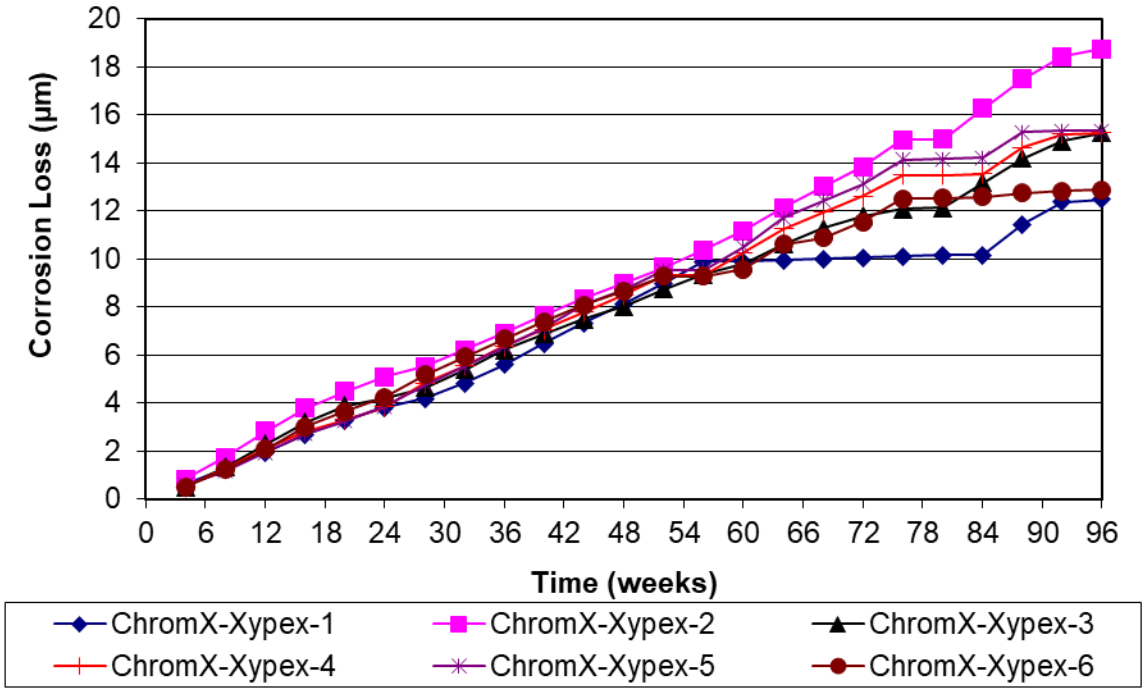

Figure F.34: LPR corrosion losses of ChromX-Xypex reinforcement in the cracked beam test

APPENDIX G: LPR CORROSION LOSS AND CRITICAL CHLORIDE CORROSION THRESHOLD FROM PREVIOUS RESEARCH

Table G.1: Individual LPR corrosion loss (um) and derived average corrosion rate (um/year) for conventional reinforcement in the cracked beam test (Darwin et al. 2013)

	Specimen					
Week	1	2	3	4	5	6
4	3.06	1.28	2.09	2.76	4.76	0.04
8	9.09	2.82	3.42	3.86	9.46	6.24
12	12.03	8.00	7.15	7.55	14.04	11.33
16	18.39	13.12	10.22	11.95	20.95	15.05
20	23.57	20.51	13.17	15.64	22.37	16.03
24	28.10	24.48	15.68	18.20	24.31	17.42
28	37.20	29.65	18.25	23.95	27.94	18.70
32	39.78	37.33	19.49	25.91	28.88	20.05
36	42.15	39.29	20.42	27.23	29.80	21.07
40	43.40	41.15	21.39	28.67	31.01	22.15
44	44.65	42.88	22.43	29.53	31.72	23.27
48	46.21	44.29	23.55	30.72	31.78	24.53
52	47.93	45.99	24.32	31.97	33.06	26.79
56	50.41	48.02	25.49	32.98	34.03	28.75
60	52.91	50.42	26.23	34.27	35.25	30.86
64	54.58	52.84	27.70	35.41	36.35	32.55
68	55.72	54.04	28.91	36.36	38.44	33.15
72	56.42	55.62	29.64	37.86	40.76	34.31
76	57.51	58.23	31.60	39.72	50.40	36.55
80	60.56	60.77	33.61	41.91	52.91	40.04
84	63.46	63.59	35.29	44.61	54.86	42.90
88	66.31	67.35	37.25	46.47	57.65	45.30
92	69.01	69.57	37.61	47.03	58.72	46.04
96	70.69	71.29	41.59	47.83	60.08	46.82
Rate	38.29	38.61	22.53	25.91	32.54	25.36

Table G.2: Individual LPR corrosion loss (um) and derived average corrosion rate (um/year) for conventional reinforcement in the cracked beam test (Darwin et al. 2011)

	Specimen		
Week	1	2	3
4		0.00	1.81
8		0.08	3.30
12		0.16	5.63
16	6.97	0.23	6.73
20	8.43	0.23	7.13
24	9.71	1.44	8.49
28	12.59	1.44	11.87
32	15.54	4.19	14.02
36	19.95	7.82	18.06
40	24.56	10.32	22.13
44	28.90	12.91	24.13
48	33.06	14.85	25.58
52	38.39	17.98	27.12
56	47.67	21.11	28.42
60	56.51	24.35	30.37
64	75.57	26.85	31.49
68	104.41	27.98	31.93
72	113.69	30.98	33.24
76	120.09	33.75	35.25
80	122.46	38.08	36.92
84	133.94	42.16	38.31
88	146.29	43.70	39.73
92	159.15	45.30	40.85
96	166.80	49.16	42.36
Rate	103.88	30.33	19.30

Table G.3: Individual LPR corrosion loss (um) and derived average corrosion rate (um/year) for conventional reinforcement in the cracked beam test (Farshadfar et al. 2017)

	Specimen					
Week	1	2	3	4	5	6
4	0.02	0.03	0.02	0.03	0.02	0.02
8	0.05	0.05	0.04	0.05	0.04	0.02
12	0.07	0.08	0.13	0.29	0.06	0.02
16	0.09	0.21	0.32	0.66	0.42	0.04
20	0.11	0.58	0.55	1.27	0.89	0.34
24	0.40	1.10	0.88	1.95	1.47	0.91
28	0.79	1.71	1.41	2.60	2.05	1.79
32	1.34	2.59	2.07	3.67	2.75	2.58
36	1.91	3.56	2.92	4.96	3.52	3.55
40	2.65	4.68	4.06	5.90	4.61	4.67
44	3.39	5.63	5.16	6.96	5.67	5.70
48	4.49	6.94	6.44	8.11	6.85	6.73
52	5.40	8.30	7.82	9.41	8.13	7.98
56	6.45	9.73	9.27	10.74	9.46	9.19
60	7.34	10.88	10.38	11.74	10.43	10.10
64	8.83	12.48	11.87	13.19	11.73	11.28
68	9.96	13.85	13.44	14.74	13.27	12.46
72	10.97	15.44	15.34	16.06	15.01	13.55
76	12.33	17.26	16.83	17.50	15.79	14.67
80	13.99	19.39	18.76	19.34	17.42	16.18
84	15.70	22.06	20.73	20.98	18.79	17.88
88	16.42	22.99	21.82	21.79	20.01	18.57
92	16.69	24.40	24.56	22.95	21.72	19.51
96	16.78	25.00	25.70	24.42	22.73	20.17
Rate	9.09	13.54	13.92	13.23	12.31	10.93

Table G.4: Individual LPR corrosion loss (um) and derived average corrosion rate (um/year) for ECR in the cracked beam test (Darwin et al. 2013)

	Specimen					
Week	1	2	3	4	5	6
4	0.04	0.03	0.00	0.04	0.06	0.04
8	0.12	0.05	0.01	0.07	0.17	0.13
12	0.25	0.10	0.01	0.11	0.34	0.21
16	0.41	0.14	0.03	4.47	0.55	0.34
20	0.57	0.19	0.04	4.52	0.64	0.34
24	0.67	0.24	0.05	4.56	0.72	0.36
28	0.94	0.41	0.09	4.60	0.82	0.45
32	1.09	0.51	0.12	4.64	0.92	0.59
36	1.24	0.56	0.16	4.65	1.06	0.72
40	1.37	0.69	0.20	4.74	1.18	0.84
44	1.50	0.76	0.23	4.82	1.27	0.98
48	1.65	0.86	0.27	4.89	1.36	1.10
52	1.82	0.93	0.37	4.95	1.46	1.26
56	1.99	1.02	0.42	5.03	1.55	1.41
60	3.87	1.11	0.51	5.14	1.66	1.61
64	3.91	1.21	0.58	5.27	1.77	1.65
68	4.06	1.30	0.63	5.40	1.88	1.78
72	4.21	1.39	0.70	5.47	1.99	1.95
76	4.32	1.53	0.76	5.61	2.13	2.22
80	4.48	1.65	0.85	5.77	2.25	2.46
84	4.87	1.76	1.02	5.92	2.39	2.85
88	5.22	1.87	1.11	6.10	2.51	3.36
92	5.52	1.97	1.25	6.24	2.52	3.74
96	5.76	2.08	1.32	6.41	2.67	4.03
Rate	3.33	1.23	0.97	1.27	1.48	2.30

Table G.5: Individual LPR corrosion loss (um) and derived average corrosion rate (um/year) for ECR in the cracked beam test (Darwin et al. 2011)

Week	Specimen	
4		0.79
8	0.01	0.87
12	0.02	1.01
16	0.02	1.26
20	0.03	1.34
24	0.04	1.52
28	0.09	1.81
32	0.09	2.10
36	0.09	2.39
40	0.11	2.69
44	0.13	3.09
48	0.18	3.22
52	0.19	3.35
56	0.21	3.48
60	0.22	3.62
64	0.24	3.78
68	0.26	3.93
72	0.27	4.03
76	0.29	4.23
80	0.32	4.42
84	0.35	4.56
88	0.40	4.70
92	0.44	4.93
96	0.47	5.19
Rate	0.29	2.49

Table G.6: Individual LPR corrosion loss (um) and derived average corrosion rate (um/year) for ECR in the cracked beam test (Farshadfar et al. 2017)

	Specimen					
Week	1	2	3	4	5	6
4	0.00	0.00	0.00	0.00	0.00	0.00
8	0.00	0.00	0.00	0.00	0.00	0.00
12	0.00	0.00	0.00	0.00	0.00	0.00
16	0.00	0.00	0.00	0.00	0.00	0.00
20	0.00	0.00	0.00	0.00	0.00	0.00
24	0.00	0.00	0.00	0.00	0.00	0.00
28	0.00	0.00	0.00	0.00	0.01	0.00
32	0.00	0.00	0.00	0.00	0.01	0.00
36	0.00	0.00	0.00	0.00	0.01	0.00
40	0.00	0.01	0.00	0.00	0.01	0.00
44	0.01	0.01	0.01	0.01	0.02	0.01
48	0.01	0.03	0.01	0.03	0.03	0.02
52	0.01	0.04	0.02	0.03	0.03	0.04
56	0.02	0.05	0.02	0.05	0.04	0.05
60	0.02	0.05	0.03	0.06	0.05	0.06
64	0.03	0.07	0.03	0.07	0.05	0.08
68	0.04	0.08	0.04	0.07	0.07	0.09
72	0.06	0.09	0.07	0.08	0.10	0.11
76	0.07	0.11	0.08	0.09	0.12	0.12
80	0.09	0.13	0.10	0.10	0.14	0.13
84	0.09	0.15	0.12	0.17	0.16	0.14
88	0.11	0.18	0.14	0.18	0.17	0.15
92	0.15	0.22	0.15	0.20	0.22	0.16
96	0.21	0.28	0.18	0.22	0.28	0.18
Rate	0.23	0.29	0.19	0.21	0.26	0.17

Table G.7: Individual LPR corrosion loss (um) and derived average corrosion rate (um/year) for ChromX reinforcement in the cracked beam test (Farshadfar et al. 2017)

Week	1	2	3	4	5	6
4	0.68	0.71	0.79	0.68	0.55	0.80
8	1.41	1.43	1.73	1.77	1.34	1.52
12	2.50	2.39	2.71	2.92	2.10	2.18
16	3.61	3.30	3.71	4.11	2.80	2.79
20	4.39	4.05	4.75	5.22	3.46	3.49
24	6.43	4.83	5.74	5.35	4.05	4.18
28	7.80	5.76	6.35	6.60	4.78	4.75
32	9.27	6.79	7.28	7.83	5.17	5.38
36	10.87	7.67	8.11	8.79	5.81	5.98
40	12.26	8.61	9.08	9.92	6.29	6.58
44	13.37	9.28	10.02	11.02	6.68	7.13
48	14.43	9.99	10.46	11.87	6.98	7.75
52	16.20	10.88	11.45	13.14	7.44	8.30
56	17.81	11.63	12.26	14.11	7.90	8.91
60	19.74	12.50	13.11	14.95	8.36	9.39
64	21.66	13.26	13.74	17.05	8.91	10.01
68	25.19	14.01	14.00	17.28	9.30	10.52
72	25.92	14.59	15.01	18.87	9.75	10.98
76	27.60	15.61	16.05	20.41	10.07	11.44
80	29.26	16.68	17.11	22.05	10.28	11.64
84	30.29	17.33	17.63	22.70	10.63	12.01
88	31.80	17.92	18.14	23.39	11.20	12.47
92	32.96	18.72	18.58	23.81	11.22	13.02
96	33.63	19.02	19.41	24.97	11.73	13.45
Rate	18.21	10.30	10.51	13.52	6.35	7.28

Table G.7: Critical chloride corrosion threshold (lb/yd^3) in uncracked concrete

Conventional	
Darwin et al. 2013	2.45
	1.33
	1.15
	1.53
	1.44
	2.78
Darwin et al. 2011	2.07
	1.57
	1.41
	2.44
	0.91
Darwin et al. 2011	1.09
	1.79
	0.64
	2.31
	0.66
	1.12
Darwin et al. 2011	2.52
	1.11
	0.8
Farshadfar et al. 2017	1.06
	2.18
	0.86
	2.5
	0.7
Ji et al. 2005	2.01
	2.07
	2.07
Ji et al. 2005	1.55
	2.21
	1.2
	1.99
	0.91
	1.05
	1.53
	0.89

	2.07
	1.97
Draper 2009	3.96
	1.15
	1.01
	4.21
	3.73
	3.96
	1.15
	1.01
	4.21
	3.73
Darwin et al. 2007	1.56
	1.56
	1.32
	0.98
	1.22
	2.02
	1.88
	1.94
	1.97
O'Reilly et al. 2011	2.53
	1.11
	0.81
O'Reilly et al. 2011	2.07
	1.57
	1.42
	2.44
	0.91
	2.07
	1.57
	1.42
	2.44
	0.91
ECR	
Darwin et al. 2013	2.97
	4.06
	6.37

	2.14
	4.05
Darwin et al. 2011	5.76
	15.55
	14.04
Farshadfar et al. 2017	8.48
	7.93
	7.51
	5.76
	7.20
	5.44
Draper 2009	5.76
	15.56
	14.04
ChromX	
Farshadfar et al. 2017	4.24
	5.59
	2.76
	4.12
	1.87
	1.59
	5.45
	10.70
Ji et al. 2005	5.77
	1.90
	2.36
	2.33
O'Reilly et al. 2021	5.60
	4.38
	5.29
	4.50
	0.46
Ji et al. 2005	9.03
	4.99
	6.56
Ji et al. 2005	9.00
	5.07
	8.09
	9.15
	5.44

	5.01
	4.48
	4.64
	5.24
Darwin et al. 2007	6.53
	8.49
	5.45
	4.69
	6.99
Darwin et al. 2007	5.56
	6.54
	6.22